DOUTORAMENTO

BIOTECNOLOGIA MOLECULAR E CELULAR APLICADA ÀS CIÊNCIAS DA SAÚDE

Staphylococcus aureus implant-associated biofilms: Development of a novel nanoparticle-based drug delivery system

Ana Rita Oliveira Macedo Pinto

PhD Thesis Co-Supervision between the University of Porto and the KU Leuven

D

2021



Ana Rita Oliveira Macedo Pinto

Staphylococcus aureus implant-associated biofilms: Development of a novel nanoparticle-based drug delivery system

Tese de Candidatura ao grau de Doutor em Biotecnologia Molecular e Celular Aplicada às Ciências da Saúde; Programa Doutoral da Universidade do Porto (Instituto de Ciências Biomédicas de Abel Salazar e Faculdade de Farmácia) e ao grau de Doctor of Science pela Katholieke Universiteit Leuven, ao abrigo do acordo de Doutoramento em regime de Cotutela Internacional. PhD Thesis Co-Supervision between the University of Porto and KU Leuven.

Orientador – Doutora Cláudia Daniela Oliveira de Lacerda Nunes Pinho

Categoria – Investigador auxiliar FCT

Afiliação – LAQV, REQUIMTE, Faculdade de Farmácia da Universidade do Porto

Orientador – Prof. Patrick Van Dijck

Categoria – Professor Catedrático

Afiliação – Faculty of Science, KU Leuven and VIB KU Leuven Center for Microbiology Leuven

Co-orientador – Prof. Maria Cristina Teixeira Lopes da Costa Pinto Lopes Martins

Categoria – Professor Associado Convidado

Afiliação – i3S - Instituto de Investigação e Inovação em Saúde, INEB - Instituto de Engenharia Biomédica, ICBAS - Instituto de Ciências Biomédicas Abel Salazar da Universidade do Porto

Acknowledgments

Neste percurso de aprendizagem, quer científica quer pessoal, nunca caminhei sozinha. Tive comigo pessoas extraordinárias que sempre me incentivaram e apoiaram. Foi um caminho com alguns altos e baixos, mas aqueles que me rodeiam ajudaram-me a chegar até aqui. A muito lhes devo a amizade, companheirismo e bons momentos. Esta etapa não se resume ao que está escrito nesta tese, mas ficam também as minhas pessoas e tudo o que aprendi sobre mim mesma.

Em primeiro agradeço do fundo do coração à Cláudia, por não se limitar a ser a minha orientadora, mas também por toda a amizade e preocupação que sempre demonstrou. Sei que por vezes fui persistente (ou chata!) e os últimos meses desta etapa foram particularmente intensos. Obrigada por toda a paciência e por veres sempre o lado positivo quando eu só vejo o lado negativo. Se não fosse por ti, sei que nunca teria conseguido ultrapassar certas barreiras. Sempre foste e continuas a ser uma inspiração não só como cientista, mas como pessoa. Esta tese é mérito teu também! Obrigada pelo apoio incondicional durante estes anos!

À Professora Salette também não poderia deixar de agradecer a oportunidade que me deu em integrar o seu grupo de investigação. Obrigada por todo o apoio que sempre me deu, em especial nas alturas mais difíceis. Pela sua forma prática de ver as situações e pelas suas palavras apaziguadoras perante os desafios que fui encontrando nesta caminhada.

To Patrick, I acknowledge your availability to always listen to my problems and for trying to help me fix them. I also thank you for your enthusiasm about the work and for giving me so many resources and opportunities to achieve our goals for this project. I am also grateful for our talks about Portugal and for being so welcoming.

À Cristina Martins pela orientação e pelo apoio durante este doutoramento. Agradeço ainda por me ter proporcionado todos os recursos para que fosse possível a realização de parte deste trabalho no i3s.

A todos aqueles que contribuíram diretamente para este projeto. À Catarina Seabra, um muito obrigado pela contribuição para este projeto, mas também pelas conversas, pelo apoio e preocupação. À Sofia agradeço a ajuda com as culturas celulares e também todo o apoio. À Filipa Soares, obrigada pela colaboração e por todo o teu empenho em escrever o nosso artigo de revisão. À Prof. Susana Casal e à Rebeca pela preciosa ajuda no HPLC e por serem incansáveis a resolver os diversos percalços que tive. À Cláudia Monteiro, por

me teres ensinado tanto sobre biofilmes e pela tua preocupação. To Sruthi, my master student, thank you for your enthusiasm and for always accepting the challenges I proposed to you. I feel that we both learned a lot with this challenge. To Martine and Saleh, for not only the help with the experiments, but also for all the talks and good moments. Thank you both for your patience with me and for being so kind and concern. Celia, I am also so grateful for everything you taught me. To Koen Schouteden for the availability and for allow me to use the DLS and ELS whenever I needed. Lastly, thank you to Prof. Stefaan and Mukaddes for all the help with the *in vivo* experiments.

Um muito especial agradecimento aos meus colegas e amigos do MB^2 por tornarem os meus dias tão especiais e divertidos. Acredito que ao vosso lado tive alguns dos momentos mais felizes da minha vida. Às minhas compinchas de doutoramento Andreia Granja, Andreia Marinho e Ana Isabel. Obrigada por todos os dias em que me fizeram mais felizes, por me ajudarem sempre que precisei e por todos os bons momentos. A todos os elementos do MB^2, que fazem deste um grupo espetacular. Às minhas tias da França, Joaninha, Tânia, Marina e Andreia G, obrigada por todos os almoços e lanches que fizeram os meus dias muito mais solarengos. A outros antigos colegas do MB^2 que marcaram estes últimos anos da minha vida e que guardo com carinho no coração: João, Daniela Resende, José, Virgínia, Catarina Pereira Leite, Yong, Nini. Um muito especial agradecimento à minha eterna Pris, por toda a inspiração e por todos os ensinamentos. Nunca me esquecerei dos bons momentos que passámos juntas.

Agradeço também aos vizinhos de laboratório, em especial à Sara Marques, Inês Ramos e Ana Marta pelas conversas que sempre me animaram. A todos os restantes colegas e aos professores do Laboratório de Química Aplicada muito obrigada pela boa disposição e pela bondade de sempre mostrarem disponibilidade em ajudar-me. À D. Manuela e à Vânia, agradeço todo o apoio que recebi sempre que precisava. Para além disso agradeço a boa disposição e as conversas animadas que tivemos ao longo destes anos.

Aos meus colegas e amigos do BioEngineered Surfaces que tão bem me acolheram, especialmente à Bruna, Pedro, Bia, Luís, Mónica, Sara, Patrícia e Andreia pelos momentos animados que passamos e também por favores que me fizeram sempre que precisei. Às minhas compinchas do “Brunch Party”, Diana, Rute e Sofia, pelos maravilhosos encontros presenciais e online que tornaram os meus dias mais doces e agradáveis. Obrigada pela vossa amizade.

To all my colleagues from the MBC lab that were always available to help me. A special thanks to the ones I shared the small candida lab with, Siebe, Dimi and Hans. Also, to Katrien, Ona and Leni for their help and patience.

Aos meus colegas e amigos do BiotechHealth, os “Internationals”, por todos os bons momentos que passámos juntos, quer a rir, quer a procrastinar. Sem dúvida que tivemos uma grande aventura juntos e foi um gosto percorrer este caminho com vocês. Aos professores do BiotechHealth agradeço a oportunidade de me terem deixado integrar este programa doutoral e por sempre se mostrarem interessados em ouvir a nossa opinião e quererem melhorar o programa com base nas nossas sugestões. Agradeço também à Helena Martins por toda a disponibilidade em me ajudar com problemas administrativos, sempre com uma palavra tranquilizadora e uma eficiência notável.

To my KU Leuven supervisory committee, Liesbeth and Prof. Hans Steenackers for the constructive critics and for the interesting discussions we had about the work. Thank you for your availability and interest in my project. I also thank to Graziella Del Salvio for all the help with administrative issues.

Às minhas “Nenas” com quem continuo a partilhar muitos bons momentos e também desabafos da vida. Obrigada pelos “cafés online” que fizemos quando estava longe e pela nossa tradição do Jantar de Natal.

Às meninas do grupo “Unidas pelo senhor” por me fazerem recordar bons velhos tempos de secundário. É tão bom ter crescido convosco e continuar a acompanhar os vossos percursos e todas as nossas vitórias!

À minha eterna amiga Helena, com quem partilhei mais de 20 anos da minha vida!! Obrigada pelos jantares, pelas conversas e pelas gargalhadas.

À minha Twin, Andreia, por ser muito mais do que uma amiga. Desde o primeiro momento que caminhámos juntas este percurso, com momentos bons e menos bons. Partilhámos frustrações e momentos de vitória. Obrigada por todos os nossos almoços quando as coisas corriam menos bem, pelas horas ao telefone e por estares sempre ao meu lado. Tudo isto foi muito mais divertido e maravilhoso por te ter tido ao meu lado. Não há palavras para descrever o quão importante é a tua amizade para mim.

À minha família, em especial aos meus pais, avó e irmão, por sempre me apoiarem e por terem sempre tanto orgulho em mim. Se tive a oportunidade de chegar aqui foi por vossa causa, pelos vossos sacrifícios e pela educação que me deram.

To Eddy and Renilde for all the support and for making me feel always at home. To Oma, Pépé, Bomma and the rest of the family for all the good moments and for always being so kind to me.

To my Thomas, that supported so much during these years. I apologize for all the times I arrived home with my work problems. Thank you for always listening and for always trying to make me feel better. Thank you also for all the sacrifices you made so I could embrace this adventure and for your tremendous patience. I am sure that we will have many more adventures together, wherever we are.

I am thankful to Fundação para a Ciência e Tecnologia (FCT) for the Research Grant (PD/BI/128326/2017) and the PhD Grant (SFRH/BD/130319/2017). I also acknowledge the Programa Operacional Capital Humano (POCH), specifically the BiotechHealth Programme (Doctoral Programme on Cellular and Molecular Biotechnology Applied to Health Sciences). This work also received financial support from FCT/MCTES e FEDER through Programa Operacional Competitividade e Internacionalização - COMPETE 2020 (project PTDC/NANMAT/31444/2017).



Publicações

Ao abrigo do disposto do número 2, alínea a) do artigo 31º do Decreto-Lei no 115/2013 de 7 de Agosto, fazem parte integrante desta tese de doutoramento as seguintes publicações:

Pinto RM, Monteiro C, Lima SAC, Casal S, Van Dijck P, M. Martins MCL, Nunes C, Reis S. *N*-Acetyl-L-cysteine-Loaded Nanosystems as a Promising Therapeutic Approach Toward the Eradication of *Pseudomonas aeruginosa* Biofilms. *ACS Appl. Mater. Interfaces*. 2021. https://doi.org/10.1021/acsami.1c05124.

Van Dyck K, **Pinto RM**, Pully D, Van Dijck P. Microbial Interkingdom Biofilms and the Quest for Novel Therapeutic Strategies. *Microorganisms*. 2021. doi: 10.3390/microorganisms9020412.

Pinto RM, Soares FA, Reis S, Nunes C, Van Dijck P. Innovative Strategies Toward the Disassembly of the EPS Matrix in Bacterial Biofilms. *Front Microbiol*. 2020. https://doi.org/10.3389/fmicb.2020.00952.

Pinto RM, Lopes-de-Campos D, Martins MCL, Dijck PV, Nunes C, Reis S, Impact of nanosystems in *Staphylococcus aureus* biofilms treatment, *FEMS Microbiology Reviews*. 2019. https://doi.org/10.1093/femsre/fuz021.

Abstract

Bacterial biofilms are currently an increasing concern for modern medicine due to the escalating figures of antimicrobial resistance and the high demand for implantable medical devices. When a medical device enters the human body, it is prone to infection and, eventually, to biofilm formation. The current therapy to treat bacterial biofilms is solely focused on the administration of conventional antibiotics, which fails to target the extracellular polymeric substances (EPS) matrix. The EPS matrix is the first barrier that antibiotics encounter. This structure protects bacterial cells within the biofilm by hindrance the diffusion of antibiotics into deeper layers of the structure. Hence, current therapies to treat implant-associated biofilms commonly fail, and the removal of the device is frequently required.

Several bacterial species are associated with biofilms formed on implantable medical devices, such as *Pseudomonas aeruginosa* and *Staphylococcus* spp. Amongst these, *Staphylococcus aureus* biofilms are being highlighted due to their high prevalence and high mortality and morbidity rates.

In the present work, we proposed innovative strategies based on the encapsulation of matrix-disruptive agents (*N*-acetyl-L-cysteine and caspofungin) and bactericidal agents (moxifloxacin and farnesol) into lipid nanoparticles. The nanoparticles were functionalized with D-amino acids to target and disrupt the biofilms. The developed nanosystems were studied alone and in combination, as a multi-target strategy, to target both the EPS matrix and the bacterial cells within the biofilms. The formulations developed in this thesis were evaluated according to their physical characterization, biocompatibility and antibiofilm efficacy. *In vitro* and *in vivo* studies revealed the potential of the developed nanosystems to improve current therapies toward the eradication of clinically relevant bacterial biofilms.

Resumo

Os biofilmes bacterianos são atualmente uma preocupação na medicina moderna devido ao aumento dos casos de resistência a antibióticos e à necessidade de dispositivos médicos implantáveis. Quando um dispositivo médico é introduzido no corpo humano há risco de infeção e eventualmente, formação de um biofilme. A terapia atual para tratar biofilmes bacterianos é focada na administração de antibióticos convencionais que, frequentemente, não têm como alvo a matriz de substâncias poliméricas extracelulares. A matriz de sustâncias poliméricas extracelulares constitui a primeira barreira aos antibióticos. Esta estrutura protege as células bacterianas através do impedimento da difusão de antibióticos para camadas mais profundas do biofilme. Consequentemente, as terapias atuais para tratar biofilmes associados a implantes frequentemente falham, levando à necessidade de remover o dispositivo.

Diversas espécies de bactérias estão associadas a biofilmes formados em dispositivos médicos implantáveis, como *Pseudomonas aeruginosa* e *Staphylococcus* spp. Entre estas, os biofilmes de *Staphylococcus aureus* destacam-se devido à sua prevalência e aos elevados números de mortalidade e morbidade associados.

No presente trabalho, propomos estratégias inovadoras baseadas na encapsulação de agentes promotores da disrupção da matriz (*N*-acetilcisteína e caspofungina) e agentes bactericidas (moxifloxacina e farnesol) em nanopartículas lipídicas. As nanopartículas foram funcionalizadas com D-amino ácidos para atingir e desestruturar os biofilmes. Os nanosistemas desenvolvidos foram estudados separadamente ou em combinação, como uma estratégia multi-alvo, focada tanto na matriz de substância poliméricas extracelulares, como nas células bacterianas que compõem o biofilme. As formulações desenvolvidas nesta tese foram avaliadas de acordo com as suas características físicas, biocompatibilidade e eficácia anti-biofilmes. Estudos *in vitro* e *in vivo* revelaram o potencial dos nanosistemas desenvolvidos para melhorar as terapias atuais com vista à erradicação de biofilmes bacterianos clinicamente relevantes.

Table of contents

List of abbreviations…….. X

List of symbols…….. XII

List of figures…….. XIII

List of tables…….. XXI

Chapter 1 – Thesis structure……..1

Chapter 2 – Theoretical background……5

Chapter 2.1. Introduction…….5

Chapter 2.2. Innovative Strategies Toward the Disassembly of the EPS Matrix in Bacterial Biofilms……..10

Chapter 2.3. Impact of nanosystems in *Staphylococcus aureus* biofilms treatment……..... 31

Chapter 3 – Motivation and goals……53

Chapter 4 – Rational behind the proposed nano-based strategy……57

Chapter 5 – Methodologies to develop and characterize the nanodelivery systems……..63

Chapter 6 – Progress beyond the state of the art…….....79

Chapter 6.1. – *N*-Acetyl-L-cysteine-Loaded Nanosystems as a Promising Therapeutic Approach Toward the Eradication of *Pseudomonas aeruginosa* Biofilms……..81

Chapter 6.2. – Antibiofilm combinatory strategy towards *S. aureus*: novel moxifloxacin-loaded nanosystems joint with encapsulated N-acetyl-L-cysteine……..….105

Chapter 6.3. – Caspofungin-loaded nanoparticles as an adjuvant to improve nanoantibiotics activity in a multi-target strategy against *Staphylococcus aureus* biofilms……..…....145

Chapter 6.4. – Farnesol-loaded lipid nanoparticles as a non-antibiotic alternative therapy to eradicate *S. aureus* biofilms……185

Chapter 7 – Concluding remarks and future perspectives……...203

Appendix……209

List of abbreviations

BBD	Box-Behnken design
BLI	Bioluminescence imaging
CAS	Caspofungin
CFU	Colony forming unit
CLSM	Confocal laser scanning microscopy
CoNS	Coagulase-negative staphylococci
CV	Crystal violet
Cy7	Cyanine7
DLS	Dynamic light scattering
DoE	Design of experiments
D-Phe	D-Phenylalanine
D-Pro	D-Proline
D-Tyr	D-Tyrosine
DSPE-PEG2000-NH_2	1,2-distearoyl-sn-glycero-3-phosphoethanolamine-N-[amino(polyethylene glycol)-2000
eDNA	Extracellular DNA
EE	Encapsulation efficiency
ELS	Electrophoretic light scattering
EPS	Extracellular polymeric substances
Farn	Farnesol
FTIR	Fourier-transform infrared spectroscopy
HPLC	High performance liquid chromatography
LC	Loading capacity
LDH	Lactate dehydrogenase
LNP	Lipid nanoparticle
MBC	Minimum bactericidal concentration
MDR	Multidrug-resistant
MIC	Minimum inhibitory concentration
MLN	Multiple lipid nanoparticles
MOX	Moxifloxacin
MSCRAMM	Microbial surface components recognizing adhesive matrix molecule
MRSA	Methicillin-resistant *Staphylococcus aureus*
MSSA	Methicillin-susceptible *Staphylococcus aureus*
MTT	3-(4,5-dimethylthiazol-2-yl)-2,5-diphenyltetrazolium bromide

NAC	*N*-acetyl cysteine
NLC	Nanostructured lipid carriers
NPs	Nanoparticles
OVAT	One variable at the time
P. aeruginosa	*Pseudomonas aeruginosa*
PDI	Polydispersity index
PEG	Poly (ethylene glycol)
PGA	Poly-γ-glutamic acid
PIA	Polysaccharide intercellular adhesin
PNAG	Poly-*N*-acetyl-glucosamine
RBC	Red blood cell
RPLC	Reversed phase liquid chromatography
S. aureus	*Staphylococcus aureus*
SEM	Scanning electron microscopy
S. epidermidis	*Staphylococcus epidermidis*
SLN	Solid lipid nanoparticles
TEM	Transmission electron microscopy
USA	United States of America
UV-Vis	Ultraviolet visible
VBNC	Viable but not-culturable
VISA	Vancomycin-intermediate *Staphylococcus aureus*
VRSA	Vancomycin-resistant *Staphylococcus aureus*
XTT	2,3-Bis-(2-Methoxy-4-Nitro-5-Sulfophenyl)-2H-Tetrazolium-5-Carboxanilide

List of symbols

k_B	Boltzmann constant
R_H	Hydrodynamic radius
T	temperature
η	Coefficient of viscosity

List of Figures

Chapter 2 - Theoretical background

Chapter 2.2. Innovative Strategies Toward the Disassembly of the EPS Matrix in Bacterial Biofilms

FIGURE 1 Composition of the EPS matrix and the functions of its major constituents: polyssacharides, enzymes, structural proteins, eDNA, lipids, and biosurfactants. Adapted from Flemming and Wingender (2010), Koo et al. (2017)…… 13

FIGURE 2 Biofilms associated to medical devices and chronic diseases and the most prevalent microorganisms for each device or disease (Donlan and Costerton, 2002; Stoica et al., 2017; Del Pozo, 2018)..... 14

FIGURE 3 Innovative therapeutic strategies to disrupt the biofilm matrix…….. 15

Chapter 2.3. Impact of nanosystems in *Staphylococcus aureus* biofilms treatment

Figure 1. The development of a biofilm involves three main phases: initial attachment, maturation and final detachment. The initial attachment is mediated by host matrix proteins that cover the implant surface immediately after its insertion (Otto 2008). Thus, microbial surface components are able to recognize and bind to these matrix proteins, enabling bacterial colonization. Subsequently, the biofilm grows until it reaches a phase of maturation, adopting a 3D appearance, mainly due to intercellular aggregation mediated by adhesive proteins and exopolymers. Finally, detachment of single cells or cell clusters from the biofilm structure occurs, allowing dissemination and colonization of other sites of the host (Otto 2008)…….. 33

Figure 2. Medical devices associated to biofilm infections and the most prevalent bacterial species for each device (Nafee 2015; Srivastava and Bhargava 2016)…… 34

Figure 3. Schematic representation of *in vitro* biofilm models and the most common assays performed to evaluate the efficiency of antimicrobial agents against bacterial biofilms (Chen et al. 2012; Siala et al. 2016)…… 36

Figure 4. Schematic representation of *ex vivo* and *in vivo* biofilm models and respective examples of assays to evaluate the efficiency of antimicrobial agents against bacterial biofilms (Siala et al. 2016; Fang et al. 2017)…….. 36

Chapter 4 – Rational behind the proposed nano-based strategy

Figure 1: Schematic overview of the overall proposed work towards bacterial biofilm eradication, using lipid NPs as nanocarriers. Strategy 1 consisted in the combination of encapsulated NAC with free antibiotic. Strategy 2 was based on the combination of encapsulated matrix disruptive agents (NAC or CAS) with encapsulated antibiotic (MOX). Strategy 3 was an antibiotic-free strategy based on encapsulation of farnesol…… 57

Chapter 5 – Methodologies to develop and characterize the nanodelivery systems

Figure 1: Schematic overview of the methodologies used for the physical characterization, *in vitro* biocompatibility and antibiofilm assessment, and *in vivo* biodistribution and efficacy of the developed NPs…… 63

Figure 2: Double emulsion technique for production of lipid NPs as carriers of hydrophilic drugs. Adapted from [6]…… 64

Figure 3: Production of multiple lipid nanoparticles (MLNs) as carriers of hydrophilic drugs…… 65

Figure 4: Scheme of the Calgary biofilm device model. Adapted from [27]…… 70

Figure 5: Schematic representation of the murine subcutaneous biofilm model. Firstly, catheter pieces are incubated with a bacterial suspension for 90 mins to promote adhesion of cells to the surface of the material. After several washing steps, the catheter pieces are implanted subcutaneously in the back of the animal to allow biofilm growth in *in vivo* conditions…… 74

Chapter 6 – Progress beyond the state of the art

Figure 1: Composition and production details of the nanosystems developed to encapsulate *N*-acetyl cysteine, moxifloxacin, caspofungin, and farnesol. CAS, caspofungin; DSPE, 1,2-distearoyl-sn-glycero-3-phosphoethanolamine-N-[amino(polyethylene glycol)-2000; Farn, farnesol; MOX, moxifloxacin; NAC, *N*-acetyl cysteine; Phe, phenylalanine; Pro, proline; Tyr, tyrosine……80

Chapter 6.1. *N*-Acetyl-L-cysteine-Loaded Nanosystems as a Promising Therapeutic Approach Toward the Eradication of *Pseudomonas aeruginosa* Biofilms

Figure 1. Schematic overview of the LNPs developed to further combine with MOX in an innovative therapeutic approach to eradicate bacterial biofilms. The designed LNPs were produced by the double emulsion method. The LNPs are composed of cetyl palmitate and Tween 80. The functionalized LNPs were coated with DSPE-PEG_{2000}-NH_2-D-amino acid (D-Phenylalanine, D-Proline, and D-Tyrosine) conjugates..... 83

Figure 2. Infrared spectra of the three D-amino acid conjugates: DSPE-PEG_{2000}-NH_2-Phe, DSPE-PEG_{2000}-NH_2-Pro, and DSPE-PEG_{2000}-NH_2-Tyr. The spectra of DSPE-PEG_{2000}-NH_2, D-phenylalanine, D-proline, and D-tyrosine are also represented..... 86

Figure 3. TEM images of the nonfunctionalized formulations (LNPs and NAC LNPs) and functionalized formulations (Phe_Pro_Tyr LNPs and Phe_Pro_Tyr NAC LNPs)..... 88

Figure 4. Characterization of the LNP suspensions over 24 weeks, stored at 4 °C. (A) Hydrodynamic diameter and PDI. Bars represent the hydrodynamic diameter (left y-axis), and dots represent the PDI (right y-axis). (B) LC. (C) Zeta potential. The parameters were evaluated over time (0, 4, 12, and 24 weeks)..... 89

Figure 5. *In vitro* toxicity studies. (A) MTT assay using the L929 cell line. Different concentrations of the solid lipid were evaluated (0, 0.5, 1.0, 2.0, and 3.0 mg mL^{-1}). The DMEM medium was used as a control. (B) Hemolysis assay. The LNP suspensions were tested at a concentration of 2 mg mL^{-1}, and the corresponding amount of NAC (0.9 mg mL^{-1}) was used for free NAC. Saline solution and Triton-X100 were used as negative and positive controls, respectively..... 90

Figure 6. Quantification of biofilm biomass by crystal violet staining after a 24 h treatment with LNPs or free NAC for (A) *S. epidermidis* and (B) *P. aeruginosa*. The LNP suspensions were tested at a solid lipid concentration of 2 mg mL^{-1}. Free NAC was tested at a concentration of 0.9 mg mL^{-1} (amount of NAC corresponding to 2 mg mL^{-1} of solid lipid in the LNPs)..... 90

Figure 7. Log_{10} biofilm viable count of the *P. aeruginosa* biofilms untreated (control) and treated with LNPs or free NAC for 24 h. The LNP suspensions were tested at a solid lipid concentration of 2 mg mL^{-1}. Free NAC was tested at a concentration of 0.9 mg mL^{-1} (amount of NAC corresponding to 2 mg mL^{-1} of solid lipid in the LNPs)..... 91

Figure 8. Representative SEM images of untreated (control) and treated *P. aeruginosa* biofilms. The LNP suspensions were tested at a solid lipid concentration of 2 mg mL^{-1}. Free NAC was tested at a concentration of 0.9 mg mL^{-1} (amount of NAC corresponding to 2 mg mL^{-1} of solid lipid in the LNPs)..... 91

Figure 9. Quantification of *P. aeruginosa* biofilm biomass by crystal violet staining after a 24 h treatment with LNPs or free NAC in combination with MOX at a concentration of (A) 2 µg mL^{-1}, (B) 4 µg mL^{-1}, and (C) 8 µg mL^{-1}. The LNP suspensions were tested at a solid lipid concentration of 2 mg mL^{-1}. Free NAC was tested at a concentration of 0.9 mg mL^{-1} (amount of NAC corresponding to 2 mg mL^{-1} of solid lipid in the LNPs)..... 92

Figure 10. Log_{10} *P. aeruginosa* biofilm viable count of the biofilms untreated (control) and treated for 24 h with LNPs or free NAC in combination with MOX at a concentration of (A) 2 μg mL^{-1}, (B) 4 μg mL^{-1}, and (C) 8 μg mL^{-1}. The LNP suspensions were tested at a solid lipid concentration of 2 mg mL^{-1}. Free NAC was tested at a concentration of 0.9 mg mL^{-1} (amount of NAC corresponding to 2 mg mL^{-1} of solid lipid in the LNPs)…… 93

Figure S1. Correlation between predicted and measured A) LNPs hydrodynamic diameter, B) LNPs PDI, C) LNPs LC and the correspondent R^2 values for the quadratic model…… 98

Figure S2. Two-dimension response surface plots for each dependent variable: hydrodynamic diameter, PDI and LC…….. 101

Figure S3. Representative SEM images of untreated (control) and treated *P. aeruginosa* biofilms. The LNPs suspensions were tested at a solid lipid concentration of 2 mg ml^{-1}. Free NAC was tested at a concentration of 0.9 mg ml^{-1} (amount of NAC corresponding to 2 mg ml^{-1} of solid lipid in the LNPs)…… 102

Chapter 6.2. Antibiofilm combinatory strategy towards *S. aureus*: novel moxifloxacin-loaded nanosystems joint with encapsulated N-acetyl-L-cysteine

Figure 1: Schematic overview of the antibacterial and antibiofilm components of the nanosystems used for the proposed combinatory strategy. MOX-loaded MLNs were produced by an adapted protocol previously described by Cavalcanti *et al.* (2017), while NAC-loaded nanosystems were produced by the double emulsion method [10]. The MLNs were composed by cetyl palmitate (solid lipid), Miglyol 812 (liquid lipid), farnesol, and the surfactants Tween 80 and Span 80. The LNPs were composed by cetyl palmitate and Tween 80. The surface of the nanoparticles was functionalized with DSPE-PEG-D-amino acid conjugates…… 109

Figure 2: Characterization of the MLNs suspensions over 24 weeks, stored at room temperature. A) Hydrodynamic diameter and PDI. The bars represent the hydrodynamic diameter (left y-axis) and the dots represent the PDI (left y-axis). B) Zeta potential. C) EE. D) LC. The parameters were evaluated at different time points (0, 2, 4, 12, and 24 weeks)…… 118

Figure 3: *In vitro* cytocompatibility studies. A) MTT and B) LDH assays using the fibroblasts L929 cell line. In these assays, different concentrations of encapsulated and free MOX were assessed (2.0, 1.0, 0.5, 0.25, and 0.125 μg ml^{-1}). Triton-100 (1%, v/v) and DMEM were used as negative and positive controls, respectively. C) Hemolysis assay. Encapsulated and free MOX at a concentration of 512 μg ml^{-1} were tested. For positive and negative controls, saline solution (0.85%, m/v) and triton-100 (1%, v/v) were used, respectively…… 120

Figure 4: Quantification of (A-C) biofilm viability (XTT assay) and (D-F) biomass (crystal violet staining) after a 24h treatment with MLNs and free MOX at the concentrations of 0, 0.125, 0.25, 0.5, 1, and 2 μg ml^{-1} of MOX. Unloaded MLNs were tested at the same concentration. The biofilms of (A, D) MRSA (ATCC 33591), (B, E) *S. aureus* (ATCC 6538), and (C, F) the bioluminescent strain *Xen36* were grown in 96-well plates for 24h prior to the treatment. Untreated biofilms (0 μg ml^{-1} of MOX) were used as a positive control…… 123

Figure 5: Quantification of (A-C) biofilm viability (XTT assay) and (D-F) biomass (crystal violet staining) after a 24h treatment with LNPs suspensions at the solid lipid concentrations of 0, 1, and 2 mg ml^{-1}. Free NAC was tested at the concentrations of 0, 0.45, and 0.9 mg ml^{-1}. The biofilms of (A, D) MRSA (ATCC 33591), (B, E) *S. aureus* (ATCC 6538), and (C, F) the bioluminescent strain *Xen36* were grown in 96-well plates for 24h prior the treatment. Untreated biofilms (0 mg ml^{-1} of solid lipid) were used as a positive control…… 125

Figure 6: Three-dimensional CLSM images of untreated (control) and treated *Xen36* biofilms. The developed MLNs and free MOX were tested at a MOX concentration of 0.5 μg ml^{-1}. For the biofilms treated with unloaded and NAC-loaded LNPs, a solid lipid concentration of 2 mg ml^{-1} (0.9 mg ml^{-1} of NAC) was used. Free NAC was used at the same concentration. The biofilms were stained with the LIVE/DEATH kit, where viable and death cells are visualized in green and red, respectively. Untreated biofilms were used as a positive control. …… 127

Figure 7: Biofilm viable count of the strains MRSA (ATCC 33591), *S. aureus* (ATCC 6538), and *Xen36* grown *in vitro* for 24h in catheters, after a 24h treatment with different nanosystems. (A) The unloaded and NAC-loaded LNPs were tested at a concentration of 2 mg ml^{-1} (corresponding to a NAC concentration of 0.9 mg ml^{-1}). Free NAC was tested at the same concentration. (B) The developed MLNs and free MOX were tested at a MOX concentration of 0.5 μg ml^{-1}. Untreated biofilms were used as a positive control…… 129

Figure 8: Biofilm viable count of (A-B) MRSA (ATCC 33591), (C-D) *S. aureus* (ATCC 6538), and (E-F) *Xen36* biofilms grown *in vitro* in catheters after treatment with the combined nano therapy. (A, C, D) Heat maps represent the effect of the combination of MOX- and NAC-loaded nanosystems on the biofilm viable count. The treatment combinations with lower viable count are highlighted (black squares). (B, E, F) F-MOX-MLNs (dark grey) and free MOX (light grey) (0.5 μg ml^{-1}) alone and in combination with NAC-loaded nanosystems (comb uLNPs, comb NAC-LNPs, comb F-uLNPs, and comb F-NAC-LNPs) or free NAC (comb NAC) at a solid lipid concentration of 2 mg ml^{-1} (corresponding to a NAC concentration of 0.9 mg ml^{-1}). Untreated biofilms were used as a positive control…… 131

Figure S1: Cumulative MOX release profile of the non-functionalized (MOX-MLNs) and the functionalized (F-MOX-MLNs) formulations. The profile of the free MOX is also represented. The release was assessed in PBS (pH 7.4), at 37ºC. The values are represented as the mean ± SD…140

Figure S2: Quantification of (A, B) biofilm viability (XTT assay) and (C, D) biomass (crystal violet staining) after a 24h treatment of *S. aureus* (ATCC 25923) biofilms. (A, C) The biofilms were treated

with unloaded and NAC-loaded LNPs at the solid lipid concentrations of 0, 1, and 2 mg ml^{-1}, which corresponds to 0, 0.45, and 0.9 mg ml^{-1} of NAC, respectively. Free NAC was tested at the same concentrations. (B, D) The biofilms were treated with the developed MLNs and free MOX at the concentrations of 0, 0.125, 0.25, 0.5, 1, and 2 µg ml^{-1} of MOX. Untreated biofilms (0 µg ml^{-1}) were used as a positive control…….....143

Chapter 6.3. Caspofungin-loaded nanoparticles as an adjuvant to improve nanoantibiotics activity in a multi-target strategy against *Staphylococcus aureus* biofilms

Figure 1: Schematic overview of the CAS-loaded and MOX-loaded nanosystems, and respective unloaded formulations. CAS-loaded LNPs, composed of cetyl palmitate (solid lipid) and Tween 80, were produced by the double emulsion method [16]. The MOX-loaded multiple lipid nanoparticles (MLNs) were composed by cetyl palmitate, Mglyol 812 (liquid lipid), farnesol, and the surfactants, Tween 80 and Span 80 (chapter 6.22 – section 2.3). The surface of the nanoparticles was functionalized with DSPE-PEG-D-amino acid conjugates (D-Phenylalanine, D-Proline, and D-Tyrosine) …….... 149

Figure 2: A) TEM images of the CAS-LNPs and the F-CAS-LNPs. CAS-LNPs images were acquired at the magnifications of 25 000× (left) ,50 000× (middle), and 100 000× (right), while F-CAS-LNPs image at 50 000×. **(B–E)** Characterization of the LNPs suspensions over 8 weeks, stored at 4ºC. **B)** Hydrodynamic diameter and PDI. The bars represent the hydrodynamic diameter (left y-axis) and the dots represent the PDI (left y-axis). **C)** Zeta potential. **D)** EE. **E)** LC. The parameters were evaluated at different time points (0, 1, 2, 4, and 8 weeks). ..…….... 160

Figure 3: *In vitro* cytocompatibility studies. A) MTT and B) LDH assays using the fibroblasts L929 cell line. In these assays, different concentrations of encapsulated and free CAS were assessed (0, 4, 8, 16, 32, and 64 µg ml^{-1}). Triton-100 (1% v/v) and DMEM were used as negative and positive controls, respectively. C) Hemolysis assay. Encapsulated and free CAS at the CAS concentrations 4, 8, and 16 µg ml^{-1} were tested. For positive and negative controls, saline solution (0.85%, m/v) and triton-100 (1%, v/v) were used, respectively…… 163

Figure 4: Quantification of biofilm viability by the XTT assay, after a 24h treatment with LNPs or free CAS at the CAS concentrations of 0, 4, 8, 16, 32, and 64 µg ml^{-1}. Prior to the treatment, the biofilms of A) MRSA ATCC 33591, B) *S. aureus* ATCC 25923, C) *S. aureus* ATCC 6538, and D) the bioluminescent strain *Xen36*, were grown in 96-well plates for 24h. Untreated biofilms (0 µg ml^{-1} of CAS) were used as a positive control…….... 165

Figure 5: Biofilm viable count of (A-B) MRSA ATCC 33591, (C-D) *S. aureus* ATCC 6538, and (E-F) *Xen36* biofilms grown *in vitro* in catheters after treatment with the combination of lipid nanosystems. (A, C, D) Heat maps represent the effect of the combination of CAS- and MOX-loaded nanosystems on the biofilm viable count (represented as Log_{10} CFUs/catheter). The treatment combinations with

lower viable count are highlighted (black squares). (B, F) F-MOX-MLNs and F-CAS-LNPs alone and in combination (comb). D) F-MOX-MLNs alone and in combination with F-CAS-LNPs (comb F-CAS-LNPs) or CAS (comb CAS). F-CAS-LNPs and CAS alone are also represented. The developed LNPs were assessed at a CAS concentration of 8 µg ml^{-1}. MOX-loaded nanosystems were tested at a MOX concentration of 0.5 µg ml^{-1}, except for the *S. aureus* ATCC 6538 (1 µg ml^{-1} of MOX). Untreated biofilms were used as a positive control…… 167

Figure 6: *In vivo* biodistribution study. A) Real-time imaging of whole body animals at different time-points (1h and 24h) after intraperitoneal administration of Cy7-loaded LNPs or Cy7-loaded MLNs (non-functionalized or functionalized). Graph of fluorescence signal intensity expressed as n-fold increase with respect to 0h (prior administration) at 1h and 24h post-administration of B) Cy7-loaded LNPs (Cy7-LNPs and F-Cy7-MLNs) and C) Cy7-loaded MLNs (Cy7-MLNs and F-Cy7-MLNs). D) Fluorescence signal intensity of the implanted catheters acquired *ex vivo* at 24h post-administration of the Cy7-loaded formulations. Fluorescent signals are expressed in photons per second (p s^{-1}) …….. 170

Figure 7: *In vivo* antibiofilm activity of the combination of CAS-loaded and MOX-loaded nanosystems against the bioluminescent strain *Xen36*. Infected catheters were implanted at day 0 in the back of mice treated 24h after implantation and for the following 7 days. **A)** Representative bioluminescence images at different time points (1, 2, 5, 7, and 8 days after implantation) of the group treated with the combination of F-CAS-LNPs with F-MOX-MLNs. At day 1, mice were imaged prior treatment. **B)** Graph of bioluminescence signal intensity expressed as n-fold increase with respect to day 1 after implantation (prior treatment) at different time points (2, 5, 7, and 8 days after implantation). The values are represented as the mean ± SEM for four animals. **C)** Biofilm viable count retrieved from implanted catheters after 7 days of treatment. The catheters were recovered after sacrifice on day 8 after implantation. The values are represented as the mean ± SEM for four animals (each implanted with four catheters). Bacterial viable count in **D)** spleen, **E)** kidneys, and **F)** liver of mice. The organs were collected at day 8 after implantation. …… 172

Figure S1: Cumulative CAS release profile of the non-functionalized (CAS-LNPs) and the functionalized (F-CAS-LNPs) formulations. The profile of the free CAS is also represented. The release was assessed in PBS (pH 7.4), at 37ºC. The values are represented as the mean ± SD…180

Figure S2: Evaluation of the hemolytic activity of the developed LNPs and free CAS. The LNPs and free compound at the CAS concentrations 4, 8, 16, 32, and 64 µg ml^{-1} were tested. For positive and negative controls, saline solution (0.85%, m/v) and triton-100 (1%, v/v) were used, respectively…… 181

Figure S3: Quantification of biofilm biomass (crystal violet staining) after a 24h treatment with LNPs or free CAS at the CAS concentrations of 0, 4, 8, 16, 32 and 64 µg ml^{-1}. Prior the treatment, the biofilms of A) MRSA ATCC 33591, B) *S. aureus* ATCC 25923, C) *S. aureus* ATCC 6538, and D) the bioluminescent strain *Xen36*, were grown in 96-well plates for 24h. Untreated biofilms (0 µg ml^{-1}) were used as a positive control…… 182

Figure S4: *In vivo* biodistribution study. Fluorescence signal intensity of A) spleen and B) kidneys and liver. The organs were acquired *ex vivo* at 24h post-administration of the Cy7-loaded formulations. Fluorescent signals are expressed in photons per second (p s^{-1})…… 183

Figure S5: Representative bioluminescence images of *Xen36* biofilms at different timepoints (1, 2, 5, 7, and 8 days after implantation) for the groups untreated and treated with the combination of F-CAS-LNPs with F-MOX-MLNs. At day 1, mice were imaged prior to the treatment…… 184

Chapter 6.4. Farnesol-loaded lipid nanoparticles as a non-antibiotic alternative therapy to eradicate *S. aureus* biofilms

Figure 1: Characterization of the SLNs suspensions over 20 weeks at storage conditions (4ºC). A) Hydrodynamic diameter and PDI. The bars represent the hydrodynamic diameter (left y-axis) and the dots represent the PDI (left y-axis). B) Zeta potential. The parameters were evaluated over time (0, 4, 8, 12, and 20 weeks)…… 193

Figure 2: *In vitro* cell viability and cytotoxicity studies. A) MTT and B) LDH assays using the fibroblasts L929 cell line. The cells were treated with the developed SLNs or free Farn, at the Farn concentrations 0, 12.5, 25, 50, 100, and 200 µM. DMEM and 1% (v/v) Triton-100 were used as controls…….. 194

Figure 3: Quantification of biofilm biomass removal by the crystal violet assay for A) MRSA ATCC 33591, B) *S. aureus* ATCC 6538, and C) *Xen36*. The biofilms were grown for 24h and then treated with the developed formulations or free Farn at the Farn concentrations of 12.5, 25, 50, 100, and 200 µM. Untreated biofilms were used as a positive control…… 196

Figure 4: Assessment of biofilm eradication for 24h-old biofilms of A) MRSA ATCC 33591, B) *S. aureus* ATCC 6538, and C) *Xen36*. The biofilm viability was quantified using the XTT assay. The biofilms were treated with the developed SLNs or free Farn at 12.5, 25, 50, 100, and 200 µM of Farn. Untreated biofilms were used as a positive control…… 197

Figure 5: Biofilm viable count for three strains tested: MRSA ATCC 33591, *S. aureus* ATCC 6538, and *Xen36*. The biofilms were grown *in vitro* in catheters and after treated with the developed formulations or free Farn (25 µM of Farn). Untreated biofilms were used as a positive control…… 198

List of Tables

Chapter 2 – Theoretical background

Chapter 2.2. Innovative Strategies Toward the Disassembly of the EPS Matrix in Bacterial Biofilms

TABLE 1 Biofilm disruptive strategies based on matrix disruptive agents…… 16

TABLE 2 Biofilm disruptive strategies based on nanodelivery systems…… 19

TABLE 3 Biofilm disruptive strategies based on magnetic field…… 21

TABLE 4 Biofilm disruptive strategies based on photodynamic therapy…… 23

TABLE 5 Biofilm disruptive strategies based on ultrasounds and laser-induced microbubbles… 26

Chapter 2.3. Impact of nanosystems in *Staphylococcus aureus* biofilms treatment

Table 1: Lipid-based formulations developed to eradicate *S. aureus* biofilms…… 38

Table 2: Polymeric-based formulations developed to eradicate *S. aureus* biofilms…… 41

Table 3: Metallic-based formulations developed to eradicate *S. aureus* biofilms…… 43

Table 4: Silica-based formulations developed to eradicate *S. aureus* biofilms…… 47

Chapter 6 – Progress beyond the state of the art

Chapter 6.1. *N*-Acetyl-L-cysteine-Loaded Nanosystems as a Promising Therapeutic Approach Toward the Eradication of *Pseudomonas aeruginosa* Biofilms

Table 1. Composition and the Respective Predicted and Observed Values for the Optimal Formulation (NAC LNPs)…… 87

Table 2. Composition and Physical Characterization of Unloaded and NAC-Loaded LNPs According to Their Hydrodynamic Diameter, PDI, Zeta Potential, and LC…… 87

Table 3. Activity of MOX Against Planktonic Bacteria (MIC and MBC Values) and Mature Biofilms of *S. epidermidis* and *P. aeruginosa* (MBEC Values)…… 91

Table S1. Independent variables (solid lipid, surfactant and NAC mass) and their corresponding levels. Dependent variables (hydrodynamic diameter, PDI and LC) and their levels of desirability (low, medium, and high)…… 99

Table S2. Summary of the regression analysis for the hydrodynamic diameter, PDI and LC. The values highlighted (grey shade) are statistically significant, with a $P< 0.05$. X_1, X_2 and X_3 represent the solid lipid, surfactant and NAC mass, respectively…… 100

Chapter 6.2. Antibiofilm combinatory strategy towards *S. aureus*: novel moxifloxacin-loaded nanosystems joint with encapsulated N-acetyl-L-cysteine

Table S1: Activity of the developed MLNs and free MOX against planktonic *S. aureus* strains. MIC and MBC values are expressed in µg ml^{-1} of MOX…… 141

Chapter 6.4. Farnesol-loaded lipid nanoparticles as a non-antibiotic alternative therapy to eradicate *S. aureus* biofilms

Table 1: Antibacterial activity of the unloaded and Farn-loaded SLNs against planktonic *S. aureus*. Free Farn was tested at the same conditions. MIC and MBC values are expressed in µM of Farn…… 195

Chapter 1 – Thesis structure

This thesis contains 7 chapters, based on the manuscripts originated from this work.

Chapter 1 – Thesis structure

This section presents a brief description of the chapters that compose this thesis.

Chapter 2 – Theoretical background

This chapter provides an overview of the current state of the art on bacterial biofilms and the developed strategies toward their eradication. Firstly, this chapter presents a brief description on the impact of implant-associated biofilms and the bacterial prevalence on these medical devices. A detailed description of the emergent therapies reported in the literature to fight bacterial biofilms is presented in two review papers:

1- **Innovative Strategies Toward the Disassembly of the EPS Matrix in Bacterial Biofilms** (Front Microbiol. 2020; 11: 952)

This review paper is focused on innovative strategies reported in the literature to surpass the extracellular polymeric substances (EPS) matrix, which is considered the first barrier in bacterial biofilms.

2- **Impact of nanosystems in *Staphylococcus aureus* biofilms treatment** (FEMS Microbiol Rev. 2019; 43(6): 622-641)

This review paper describes the nanosystems developed to eradicate *Staphylococcus aureus* biofilms and the available biofilm models for their preclinical validation.

Chapter 3 – Motivation and goals

This section presents the motivation and the research goals to pursue the development of innovative therapies toward the eradication of bacterial biofilms.

Chapter 4 – Rational behind the proposed nano-based strategy

This chapter provides an overview of the strategies developed in this thesis and the role of key components selected for the design of the lipid nanoparticles.

Chapter 5 – Methodologies to develop and characterize the nanodelivery systems

This chapter presents a theoretical background of the techniques used to produce, optimize, and characterize the developed nanosystems.

Chapter 6 – Progress beyond the state of art

This section comprises the progress beyond the state of art and is presented in the format of 4 original research papers:

1- ***N*-Acetyl-L-cysteine-Loaded Nanosystems as a Promising Therapeutic Approach Toward the Eradication of *Pseudomonas aeruginosa* Biofilms** (ACS Appl. Mater. Interfaces. 2021; 13(36): 42329–42343)

2- **Antibiofilm combinatory strategy towards *S. aureus*: novel moxifloxacin-loaded nanosystems joint with encapsulated N-acetyl-L-cysteine** (to be submitted)

3- **Caspofungin-loaded nanoparticles as an adjuvant to improve nanoantibiotics activity in a multi-target strategy against *Staphylococcus aureus* biofilms** (to be submitted)

4- **Farnesol-loaded lipid nanoparticles as a non-antibiotic alternative therapy to eradicate *S. aureus* biofilms** (to be submitted)

Chapter 7 – Concluding remarks and future perspectives

In this chapter, the main finding and conclusions of this work are drawn. Furthermore, future perspectives for the research work are discussed.

Appendix

A review paper entitled "**Microbial Interkingdom Biofilms and the Quest for Novel Therapeutic Strategies**" (Microorganisms. 2021; 9(2): 412) is provided in this section. This review is focused on bacterial-fungal interactions in polymicrobial biofilms and potential therapeutic approaches to target these biofilms, including nanotechnology. Overall, this review explores a potential future application for the nanosystems developed in the context of this thesis.

Chapter 2 – Theoretical background

Chapter 2.1.

Introduction

1. Biofilm formation on implantable medical devices

Nowadays, implantable medical devices have a massive impact on our society, in the order of hundreds of millions of devices used every year at a worldwide level. Despite revolutionized medicine, these devices are prone to infection due to bacterial colonization [1]. In the USA alone, device-related infections are responsible for 45% of nosocomial infections, with around one million cases per year [2]. Due to their high demand, infections related to central venous and urinary catheters are the most common cause of nosocomially acquired bloodstream infections [3]. In particular, central venous catheter-associated bloodstream infections are highlighted due to high risk of complications, leading to an increased hospital stay, mortality, and healthcare costs [4].

After implantation of a medical device, host proteins immediately adhere to the surface of the material. These proteins mediate attachment of bacterial cells that will further initiate the production of extracellular polymeric substances (EPS), leading to the formation of a bacterial biofilm. Over time, the biofilm grows until it reaches a mature state where bacterial cells are protected by a three-dimensional matrix [5]. The biofilm complex structure plays a key role in antimicrobial tolerance since its EPS matrix constitutes a diffusion barrier to antibacterial agents. In addition, bacteria in the deeper regions of the biofilm adopt a dorment lifestyle, being metabolically less active than planktonic cells, which leads to reduced susceptibility to most antibiotics [6]. These persister cells are non-dividing and exhibit multidrug tolerance and survival, being commonly responsible for the repopulation of a biofilm after treatment [7].

Once a biofilm implant-associated infection is established, physical removal of the implant and the surrounding tissue combined with antibiotic therapy is usually required [8]. Although this strategy is currently vastly used in the clinic, it often fails to fully eradicate the infection, leading to hospitalization. Thus, biofilm implant-associated infections represent an economical burden for healthcare systems [8].

2. Bacterial prevalence on implantable medical devices

Most implant-associated infections are caused by Sta*phylococcus aureus* and coagulase-negative *Staphylococcus*, such as *Staphylococcus epidermidis* [5]. *S. aureus* accounts for about 31.7% prevalence in medical infections, 21.1% in knee arthroplasty infections, 22.2% in hip arthroplasty infections, and 47.8% in infections involving internal fixation, while *S. epidermidis* is responsible for 39.0%, 52.6%, 48.1%, and 26.1% in the same categories [9]. Besides these gram-positive bacteria, gram-negative bacterial species are also commonly found in implantable medical devices, such as *Pseudomonas aeruginosa* [10]. All these bacteria have the potential to produce a biofilm structure when in contact with implants, leading from clinical complications to mortality.

Staphylococcus aureus

S. aureus are gram-positive bacteria characterized by individual cocci with diameters between 0.5 to 1.5 mm and agglomerate to form grape-like clusters [1]. These bacteria are commonly part of the human skin microbiota, being mainly found in the anterior nares and the axillae [11]. However, these opportunistic pathogens can lead to life-threatening infections when cutaneous or mucous barriers are breached [1].

Several virulence factors of *S. aureus* promote bacterial colonization of human tissues or implants. Amongst these, microbial surface components recognizing adhesive matrix molecules (MSCRAMMs) play a key role in the attachment to implants. MSCRAMMs consist of a family of adhesins able to bind to human matrix proteins, such as fibrinogen and fibronectin, allowing colonization and biofilm formation. The polysaccharide intercellular adhesin (PIA), also referred as poly-*N*-acetyl-glucosamine (PNAG), has been also highlighted as an essential virulent factor of *S. aureus*. This polymer is a major component of the EPS matrix of *S. aureus* biofilms, being essential for its formation and to protect bacterial cells from external factors [5]. Thus, virulent factors secreted by bacteria are crucial for their survival and to avoid the host immune system and antibiotics, leading to antimicrobial resistance phenomena.

Due to the emergence of strains resistant to commercially available antibiotics, infections caused by *S. aureus* are a global health concern. Methicillin-resistant *Staphylococcus aureus* (MRSA) was firstly reported in the 1960s and it is characterized by its resistance to β-lactam antibiotics. In 2016, the European Union reported that at least 25% of *S. aureus* invasive isolates were MRSA [12]. The treatment of MRSA infections consists primarily in

the administration of glycopeptide antibiotics, such as vancomycin and teicoplanin. Consequently, some *S. aureus* strains resistant to vancomycin emerged, namely vancomycin-intermediate and vancomycin-resistant *S. aureus* (VISA and VRSA, respectively). Besides vancomycin, several VISA isolates also showed resistance to teicoplanin [11].

Staphylococcus epidermidis

S. epidermidis is a bacterium commonly found in skin and mucous membranes of humans, maintaining a commensal lifestyle. Contrarily to *S. aureus*, this bacterium belongs to the group of coagulase-negative staphylococci (CoNS), which are characterize by lacking the enzyme coagulase [13]. Amongst all members from this group, *S. epidermidis* is the most frequently isolated from implant-associated infections, compromising patients health [1].

The pathogenesis of *S. epidermidis* is characterized by the potential colonization of tissues or implants. This process is initiated by MSCRAMMs with potential to adhere to host proteins, leading to the growth of a multilayered biofilm. Like in *S. aureus*, PNAG is a major component of *S. epidermidis* biofilms. This molecule is responsible for not only the protection of bacterial cells against external factors, but also to avoid phagocytosis by host immune cells [1, 13]. Besides PNAG, the exopolymer poly-γ-glutamic acid (PGA) also plays a key role in protecting bacteria from the host immune system [13].

Similar to *S. aureus*, several clinical isolates of *S. epidermidis* showed resistance to antibiotics. For instance, between 75 – 90% of all hospital isolates of *S. epidermidis* contain the methicillin resistant gene *mecA*. Besides methicillin, *S. epidermidis* strains resistant to other antibiotics, such as rifamycin, gentamicin, and clindamycin, have also been reported [13].

Pseudomonas aeruginosa

Contrarily to *S. aureus* and *S. epidermidis*, *P. aeruginosa* is a gram-negative, rod-shaped, bacterium. This opportunistic pathogen is the leading cause of gram-negative nosocomial infections. *P. aeruginosa* efficiently colonizes the surface of medical devices by using a flagellum and proteinaceous appendages (pili), promoting the initial attachment and formation of a biofilm [11]. *P. aeruginosa* biofilms are rich in the exopolysaccharides Ps1, Pe1, and alginate. These exopolysaccharides are essential for biofilm formation and maturation processes. Moreover, these matrix components protect cells from the host

immune system and the effect of antibiotics, contributing to the achievement of a persistent infection [14]. Besides the exopolysaccharides, extracellular DNA (eDNA) is also a crucial component of *P. aeruginosa* biofilms, being involved in several processes that promote biofilm survival under harsh environmental conditions [14]. Hence, the components of the EPS matrix highly contribute to the increasing resistance of *P. aeruginosa* to antimicrobials. Besides, the outer membrane of *P. aeruginosa* also contributes to increase antimicrobial resistant phenomena due to its low permeability to compounds above 500 Da. The inherent resistance of *P. aeruginosa* cells and the increased protection provided by the biofilm structure led to the emergence of several multidrug-resistant (MDR) strains [11].

Considering the high impact of the previously described pathogens in implant-associated infections it is urgently needed to develop innovative therapeutic strategies to eradicate bacterial biofilms.

3. Emergent therapies to fight bacterial biofilms

The lack of efficiency and the limitations of the current therapy to eradicate bacterial biofilms associated to implants is an increasing concern for healthcare systems. Thus, research has been focusing on alternative antibiofilm therapeutic strategies. The first challenge to eradicate bacterial biofilms is the EPS matrix, which represents a physical barrier against antimicrobial agents. Due to the complex role of the EPS matrix in the antimicrobial resistance phenomenon, several approaches to promote the disassembly of this matrix have been developed (**Chapter 2.2**). Amongst these strategies, nanotechnology emerges as a promising tool to fight bacterial biofilms as nanocarriers of antibiofilm and antibacterial agents. Nanoparticles (NPs) efficiently carry antimicrobial drugs, increasing their concentration at the biofilm. In addition, NPs can be designed to incorporate matrix disruptive agents that target and disrupt the EPS matrix. Several NPs have been engineered as a therapeutic approach against bacterial biofilms. In particular, nanosystems against *S. aureus* biofilms have been highlighted due to the high prevalence of this pathogen in numerous implantable medical devices (**Chapter 2.3**).

References

1. Ribeiro, M., F.J. Monteiro, and M.P. Ferraz, *Infection of orthopedic implants with emphasis on bacterial adhesion process and techniques used in studying bacterial-material interactions.* Biomatter, 2012. **2**(4): p. 176-194, 10.4161/biom.22905

2. Tran, H.M., et al., *Nanomaterials for treating bacterial biofilms on implantable medical devices.* Nanomaterials, 2020. **10**(11): p. 2253,

3. Trautner, B.W. and R.O. Darouiche, *Catheter-associated infections: pathogenesis affects prevention.* Archives of internal medicine, 2004. **164**(8): p. 842-850, 10.1001/archinte.164.8.842

4. Francolini, I. and G. Donelli, *Prevention and control of biofilm-based medical-device-related infections.* FEMS Immunology & Medical Microbiology, 2010. **59**(3): p. 227-238, 10.1111/j.1574-695X.2010.00665.x

5. Otto, M., *Staphylococcal biofilms.* Curr. Top. Microbiol. Immunol., 2008. **322**: p. 207-28,

6. Anderson, G.G. and G.A. O'Toole, *Innate and induced resistance mechanisms of bacterial biofilms.* Curr Top Microbiol Immunol, 2008. **322**: p. 85-105,

7. Lewis, K., *Persister cells, dormancy and infectious disease.* Nat Rev Microbiol, 2007. **5**(1): p. 48-56, 10.1038/nrmicro1557

8. Bhattacharya, M., et al., *Prevention and treatment of Staphylococcus aureus biofilms.* Expert Rev. Anti-infect. Ther., 2015. **13**(12): p. 1499-516, 10.1586/14787210.2015.1100533

9. Montanaro, L., et al., *Scenery of Staphylococcus implant infections in orthopedics.* Future Microbiol, 2011. **6**(11): p. 1329-1349, 10.2217/fmb.11.117

10. Srivastava, S. and A. Bhargava, *Biofilms and human health.* Biotechnol Lett, 2016. **38**(1): p. 1-22, 10.1007/s10529-015-1960-8

11. Pendleton, J.N., S.P. Gorman, and B.F. Gilmore, *Clinical relevance of the ESKAPE pathogens.* Expert Rev Anti Infect Ther, 2013. **11**(3): p. 297-308, 10.1586/eri.13.12

12. Hassoun, A., P.K. Linden, and B. Friedman, *Incidence, prevalence, and management of MRSA bacteremia across patient populations -a review of recent developments in MRSA management and treatment.* Crit Care, 2017. **21**(1): p. 211, 10.1186/s13054-017-1801-3

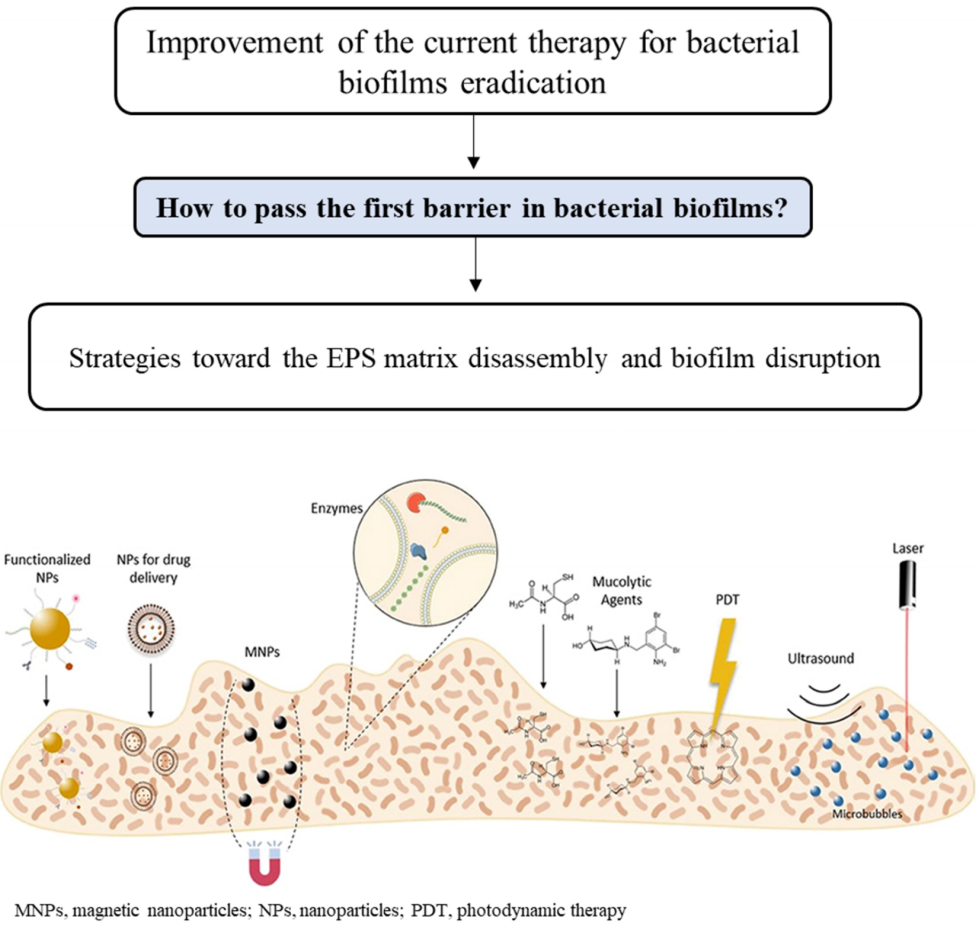
13. Otto, M., *Staphylococcus epidermidis - the 'accidental' pathogen.* Nat Rev Microbiol, 2009. **7**(8): p. 555-567, 10.1038/nrmicro2182

14. Thi, M.T.T., D. Wibowo, and B.H.A. Rehm, *Pseudomonas aeruginosa Biofilms.* International journal of molecular sciences, 2020. **21**(22): p. 8671, 10.3390/ijms21228671

Chapter 2.2.

Innovative Strategies Toward the Disassembly of the EPS Matrix in Bacterial Biofilms

The current standard therapy to treat bacterial biofilms is mainly focused on the administration of antibiotics, which target bacterial cells. However, biofilms are complex structures where the first encountered barrier is the EPS matrix. The relevance of this matrix for antimicrobial resistance prompted research towards innovative strategies for its disruption, facilitating the access of antimicrobials to the bacterial cells within the biofilm structure. This review is focused on several matrix disruptive agents and technologies, including nanocarriers, with potential to disassemble the EPS matrix.



MNPs, magnetic nanoparticles; NPs, nanoparticles; PDT, photodynamic therapy

frontiers in Microbiology

REVIEW
published: 26 May 2020
doi: 10.3389/fmicb.2020.00952

Innovative Strategies Toward the Disassembly of the EPS Matrix in Bacterial Biofilms

Rita M. Pinto[1,2,3], *Filipa A. Soares*[1], *Salette Reis*[1], *Cláudia Nunes*[1] *and Patrick Van Dijck*[2,3]*

[1] LAQV, REQUIMTE, Departamento de Ciências Químicas, Faculdade de Farmácia, Universidade Do Porto, Porto, Portugal, [2] Laboratory of Molecular Cell Biology, Institute of Botany and Microbiology, KU Leuven, Leuven, Belgium, [3] Center for Microbiology, VIB-KU Leuven, Leuven, Belgium

Bacterial biofilms represent a major concern at a worldwide level due to the high demand for implantable medical devices and the rising numbers of bacterial resistance. The complex structure of the extracellular polymeric substances (EPS) matrix plays a major role in this phenomenon, since it protects bacteria from antibiotics, avoiding drug penetration at bactericidal concentrations. Besides, this structure promotes bacterial cells to adopt a dormant lifestyle, becoming less susceptible to antibacterial agents. Currently, the available treatment for biofilm-related infections consists in the administration of conventional antibiotics at high doses for a long-term period. However, this treatment lacks efficiency against mature biofilms and for implant-associated biofilms it may be necessary to remove the medical device. Thus, biofilm-related infections represent an economical burden for the healthcare systems. New strategies focusing on the matrix are being highlighted as alternative therapies to eradicate biofilms. Here, we outline reported matrix disruptive agents, nanocarriers, and technologies, such as application of magnetic fields, photodynamic therapy, and ultrasounds, that have been under investigation to disrupt the EPS matrix of clinically relevant bacterial biofilms. In an ideal therapy, a synergistic effect between antibiotics and the explored innovated strategies is aimed to completely eradicate biofilms and avoid antimicrobial resistance phenomena.

Keywords: bacterial resistance, matrix disruptive agents, nanocarriers, photodynamic therapy, ultrasounds, magnetic nanoparticles

OPEN ACCESS

Edited by:
Luis Cláudio Nascimento da Silva, Universidade Ceuma, Brazil

Reviewed by:
Rosalia Cavaliere, University of Technology Sydney, Australia
Maria José Saavedra, Universidade de Trás os Montes e Alto Douro, Portugal

***Correspondence:**
Patrick Van Dijck
patrick.vandijck@kuleuven.vib.be

Specialty section:
This article was submitted to Antimicrobials, Resistance and Chemotherapy, a section of the journal Frontiers in Microbiology

Received: *15 February 2020*
Accepted: *21 April 2020*
Published: *26 May 2020*

Citation:
Pinto RM, Soares FA, Reis S, Nunes C and Van Dijck P (2020) Innovative Strategies Toward the Disassembly of the EPS Matrix in Bacterial Biofilms. Front. Microbiol. 11:952. doi: 10.3389/fmicb.2020.00952

INTRODUCTION

A post-antibiotic era is now emerging due to the increasing figures of antimicrobial resistance cases at a worldwide level. This phenomenon occurs naturally, however the use and misuse of antimicrobial agents in humans and animals promoted its acceleration in the last decades (WHO, 2014).

Bacterial biofilms are key players in the development of antimicrobial resistance. Biofilms are formed when bacterial cells attach to a substratum or to other cells embedded in a protective polymeric extracellular matrix (Pinto et al., 2019). The biofilm formation process can be divided in three main stages: attachment, maturation, and detachment. As soon as a medical device is implanted in the human body, host matrix proteins immediately adhere to the implant surface. Bacterial cells are able to recognize and attach to these proteins, promoting bacterial colonization.

From this point, the biofilm grows by formation of a matrix of extracellular polymeric substances (EPS) around bacterial cells until it reaches a phase of maturation, adopting a three-dimension structure (Pinto et al., 2019). Eventually, environmental stimuli may lead to the detachment of single cells or cell clusters from the biofilm, promoting dissemination and colonization on other sites of the host (Beitelshees et al., 2018; Pinto et al., 2019).

In biofilm communities, the EPS matrix is responsible for intercellular interactions and protection of bacterial cells from hostile environment. Thus, this matrix mainly contributes to the increased antibiotic tolerance and resistance of biofilms compared with planktonic cells (Flemming et al., 2016; Fulaz et al., 2019). This review provides an overview of the characteristics of the EPS matrix and its role in antibiotic resistance. Besides, biofilm-associated diseases and innovative therapeutic strategies to disrupt the biofilm matrix are also outlined.

THE BIOFILM MATRIX AND ANTIMICROBIAL RESISTANCE

The formation of the biofilm matrix is a dynamic process with high energetic cost for bacteria since it requires production and secretion of extracellular material. In exchange, the EPS matrix provides mechanical stability to the biofilms and mediates interactions between cells (Flemming et al., 2016). In most cases, the biofilm matrix represents around 90% of the total biofilm biomass and is mainly composed by polysaccharides, lipids, proteins and extracellular DNA (eDNA) (Fulaz et al., 2019) (**Figure 1**). Extensive reviews regarding biofilm matrix and antimicrobial resistance can be found elsewhere (Donlan and Costerton, 2002; Flemming and Wingender, 2010).

Polysaccharides are one of the main constituents of the EPS matrix and they attach to cell surfaces forming a complex network. Most of these molecules are heteropolysaccharides composed by a mixture of neutral and charged sugar residues. Additionally, they can contain organic and inorganic substituents, which contributes to their polyanionic or polycationic nature. The exopolysaccharides composition may differ between species and even between strains from the same species (Flemming and Wingender, 2010). Despite the heterogeneity among biofilms, exopolysaccharides are indispensable to biofilm formation and constitute the protective barrier of the EPS matrix (Flemming and Wingender, 2010; Fulaz et al., 2019). Besides, they are also responsible for water retention within the biofilm (Fulaz et al., 2019). Due to the high amount of water, the biofilm provides a highly hydrated environment that protects cells from fluctuations in water potential. In addition, the presence of water confers the biofilm a non-rigid structure with different viscosities that allow movement of the cells in the matrix (Flemming et al., 2016). As a result, a biofilm is a porous structure with macrocolonies surrounded by water-filled voids (Donlan, 2001a).

Extracellular proteins, such as structural proteins and enzymes, are also critical components of the matrix and can even be present in a higher amount than polysaccharides. Structural proteins are mainly involved in stabilization of the biofilm architecture, by connecting cells to the EPS (Fong and Yildiz, 2015). Enzymes are essentially involved in the degradation of other matrix components such as polysaccharides (e.g., dispersin B), matrix proteins (e.g., proteases), and eDNA (e.g., DNases). Thus, enzymatic activity within the biofilm provides nutrients to bacterial cells and promotes biofilm reorganization and dispersal (Fong and Yildiz, 2015).

Besides polysaccharides and proteins, eDNA also contributes for the structural integrity of the matrix (Fulaz et al., 2019). The contribution of this component for the three-dimensional structure of the biofilm differs greatly among species (Beitelshees et al., 2018). For instance, eDNA is a major component of *Pseudomonas aeruginosa* (*P. aeruginosa*) biofilms, while it is found in very low amounts in *Staphylococcus epidermidis* (*S. epidermidis*) biofilms (Beitelshees et al., 2018). Besides supporting the biofilm structure, eDNA facilitates exchange of genetic information between bacterial cells within the biofilm (Flemming and Wingender, 2010).

The complex nature of the matrix represents a diffusion barrier for antimicrobial agents, since it limits their penetration into deeper layers of the biofilm (Donlan and Costerton, 2002; Srivastava and Bhargava, 2016). Besides, within the matrix, antibiotics can interact with EPS components, leading to a decrease of their activity due to enzymatic degradation, complex formation owing to chelation, among other reactions (Flemming et al., 2016). The existence of various biofilm microenvironments, with different physical features such as low oxygen and pH, also influence the efficiency of antibacterial agents (Srivastava and Bhargava, 2016). Therefore, antimicrobial agents usually reach bacteria at sublethal concentrations, which boosts selection of antimicrobial resistance in the biofilm cells (Flemming et al., 2016).

In addition, bacterial cells embedded in the biofilm structure behave differently than in the planktonic state (Donlan and Costerton, 2002). In the lower regions of the biofilm, bacteria adopt a dormant lifestyle, since they have reduced access to nutrients and gaseous exchange (Flemming et al., 2016). These cells are metabolically less active than planktonic cells, leading to their reduced susceptibility to antibiotics (Anderson and

Abbreviations: AC, altering current; AgNPs, silver nanoparticles; ALA, 5-aminolevulinic acid; APTES, 3-aminopropyltriethoxysilane; C_2DA, *Cis*-2-decenoic acid; CES, carboxyethylsilanetriol; CLSM, confocal laser scanning microscopy; CS, chitosan; DC, direct current; DNAse I, deoxyribonuclease I; *E. coli*, *Escherichia coli*; eDNA, extracellular DNA; EDTA, ethylenediaminetetraacetic acid; *E. faecalis*, *Enterococcus faecalis*; *E. faecium*, *Enterococcus faecium*; EOs, essential oils; EPS, extracellular polymeric substances; MBEC, minimum biofilm eliminating concentration; MIC, minimun inhibitory concentration; MNPs, magnetic nanoparticles; MOFs, metal organic frameworks; MRPA, multidrug-resistant *Pseudomonas aeruginosa*; MRSA, methicillin-resistant *Staphylococcus aureus*; NAC, *N*-acetyl cysteine; NPs, nanoparticles; PAE, poly(β-amino ester); *P. aeruginosa*, *Pseudomonas aeruginosa*; PAO1, *Pseudomonas aeruginosa* O1; PDT, photodynamic therapy; PEG, polyethylene glycol; PNAG, poly-*N*-acetylglucosamine; PS, photosensitizer; PTT, photothermal therapy; ROS, reactive oxygen species; SEM, scanning electron microscopy; SPIONs, superparamagnetic iron oxide nanoparticles; *S. epidermidis*, *Staphylococcus epidermidis*; *S. aureus*, *Staphylococcus aureus*; TMP, tetra-substituted *N*-methyl-pyridyl-porphine; USMB, ultrasound-targeted microbubble.

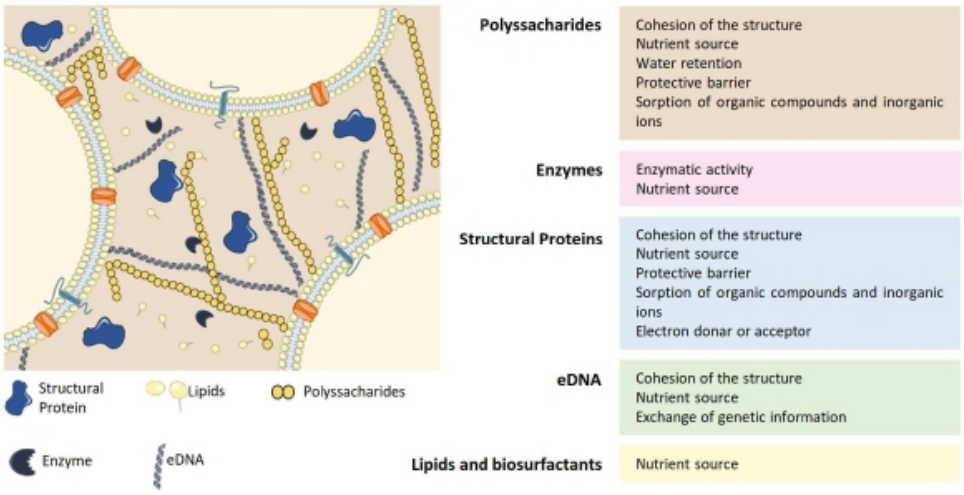


FIGURE 1 | Composition of the EPS matrix and the functions of its major constituents: polyssacharides, enzymes, structural proteins, eDNA, lipids, and biosurfactants. Adapted from Flemming and Wingender (2010), Koo et al. (2017). eDNA, extracellular DNA.

O'Toole, 2008). This resistance may lead to gene modification that can be transferred to other bacteria, through the facilitated intercellular communication promoted by the EPS matrix (Flemming et al., 2016). Thus, this phenomenon also contributes to the enhanced antibacterial resistance of biofilms.

Due to its complex composition and structure, the EPS matrix has a major role in the biofilm formation, development and survival. It is not only a protective barrier against external factors, but also a source of nutrients and enzymes, and an intercellular connector. Ultimately, the unique characteristics of the matrix contributes to the high antimicrobial tolerance and/or resistance of biofilms.

BIOFILMS IN MEDICAL DEVICES AND IN DISEASE

Nowadays, biofilms represent an enormous concern for healthcare systems due to the escalating figures of antimicrobial resistance events and the high demand for implantable medical devices (Archer et al., 2011). Several biofilm forming organisms are commonly associated to medical devices or to chronic infections such as cystic fibrosis, otitis media, and wounds. In **Figure 2** there is a detailed list of the most common medical devices and chronic infections and a list of the most prevalent microorganisms for each medical case.

Medical devices are known to increase the life quality of patients at a world level, but they are frequently associated to infections. When a medical device is implanted in the human body, colonization by bacteria occurs and a biofilm community may be established (Del Pozo, 2018). Several devices currently in medical use are prone to biofilm development by single or multiple microorganisms (Del Pozo, 2018). Some of the concerning examples will be further explored.

The number of orthopedic implants for bone fixation and joint replacement have been increasing in the last decades (Zimmerli, 2014). These implants are crucial to improve the life quality of patients, however, they are frequently associated to infections with devastating consequences, such as chronic pain and immobility (Ribeiro et al., 2012). According to Trampuz and Widmer, nearly 5% of orthopedic implants are infected and the susceptibility for infection increases by 5–40% in the case of a further surgery (Trampuz and Widmer, 2006). The infection may be caused by direct contamination of the device or from the contaminated wound and is frequently associated to opportunistic microorganisms (Stoica et al., 2017). For instance, studies show that periprosthetic joint infections are mainly associated to *Staphylococcus aureus* (*S. aureus*) and coagulase-negative staphylococci, such as *S. epidermidis* (Ribeiro et al., 2012; Zimmerli and Sendi, 2017). Most of these infections are caused by a single species, with only 16% of the cases being prompted by a mixed community (Stoica et al., 2017). Unfortunately, infections related to orthopedic implants are difficult to treat and usually require debridement and eventually removal of the device (Pinto et al., 2019). Extensive reviews addressing orthopedic implant-associated infections can be found in the literature (Ribeiro et al., 2012; Zimmerli, 2014; Zimmerli and Sendi, 2017).

Catheters are also extensively used in medical practice. Among these, urinary catheters-associated infections are the most common to occur and are predominantly caused by *Escherichia coli* (*E. coli*) and species of the genera *Pseudomonas*, *Klebsiella*, *Enterobacter*, and *Candida* (Stoica et al., 2017). On the other hand, coagulase-negative staphylococci (e.g., *S. epidermidis*) and *S. aureus* are the bacterial species mainly found in central venous catheters (Donlan, 2001b).

Less common medical devices-associated infections are verified in cardiovascular implants, such as cardiac prosthetic

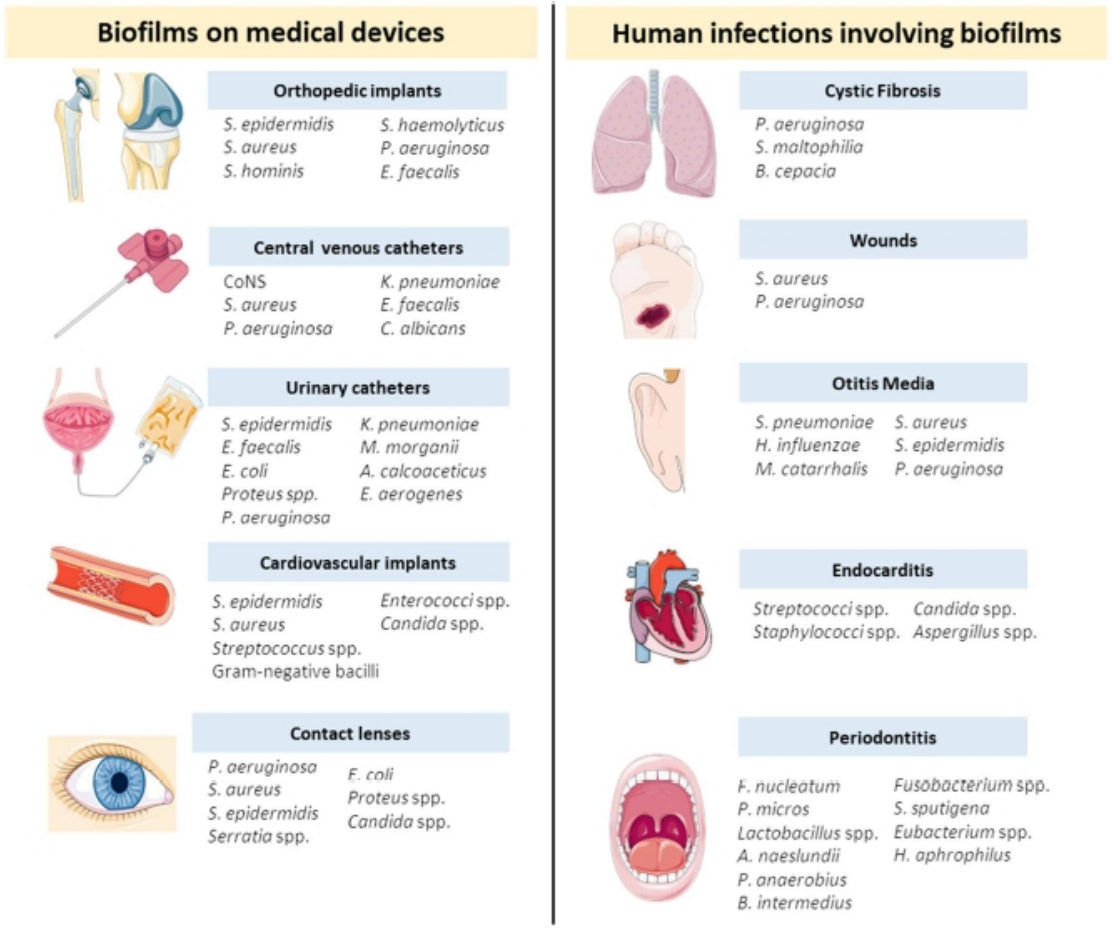


FIGURE 2 | Biofilms associated to medical devices and chronic diseases and the most prevalent microorganisms for each device or disease (Donlan and Costerton, 2002; Stoica et al., 2017; Del Pozo, 2018). *A. calcoaceticus*, *Acinetobacter calcoaceticus*; *A. naeslundii*, *Actinomyces naeslundii*; *B. cepacia*, *Burkholderia cepacia*; *B. intermedius*, *Byrrhodes intermedius*; *C. albicans*, *Candida albicans*; CoNS, Coagulase-negative staphylococci; *E. coli*, *Escherichia coli*; *E. aerogenes*, *Enterobacter aerogenes*; *E. faecalis*, *Enterococcus faecalis*; *F. nucleatum*, *Fusobacterium nucleatum*; *H. aphrophilus*, *Haemophilus aphrophilus*; *H. influenzae*, *Haemophilus influenzae*; *K. pneumoniae*, *Klebsiella pneumoniae*; *M. catarrhalis*, *Moraxella catarrhalis*; *M. morganii*, *Morganella morganii*; *P. aeruginosa*, *Pseudomonas aeruginosa*; *P. anaerobius*, *Peptostreptococcus anaerobius*; *P. micros*, *Peptostreptococcus micros*; *S. aureus*, *Staphylococcus aureus*; *S. epidermidis*, *Staphylococcus epidermidis*; *S. haemolyticus*, *Staphylococcus haemolyticus*; *S. hominis*, *Staphylococcus hominis*; *S. maltophilia*, *Stenotrophomonas maltophilia*; *S. pneumoniae*, *Streptococcus pneumoniae*; *S. sputigena*, *Selenomonas sputigena*.

valves and stents (Stoica et al., 2017). Despite less frequent, these infections are a huge concern due to the high mortality rate that can reach 30% of the patients (Darouiche, 2004).

Besides implant-related infections, biofilms also play a role in chronic diseases in the oral cavity, ear, gastrointestinal, and urinary tracts, wounds and airways, among others (Del Pozo, 2018). For instance, the colonization of the lower respiratory tract by *P. aeruginosa* may lead to a chronic disease, cystic fibrosis, which is characterized by the accumulation of pulmonary secretions. Biofilms associated to chronic wounds, such as diabetic foot ulcers, are currently a clinical burden to patients since it delays the healing process (Del Pozo, 2018). Infections in the middle ear are also very common, especially in childhood (Donlan and Costerton, 2002). Otitis media involves inflammation of the mucoperiosteal lining and the associated biofilms are difficult to treat due to the low penetration of antibiotics into the middle ear fluid. Another frequent condition involving biofilms is endocarditis, which develops when damaged endothelium interacts with bacteria or fungi in the bloodstream (Donlan and Costerton, 2002).

When a biofilm is established, cells or cell clusters may detach from the structure and colonize other sites, leading to new infections (Donlan and Costerton, 2002). Moreover, bacteria within biofilms produce endotoxins and are more resistant to

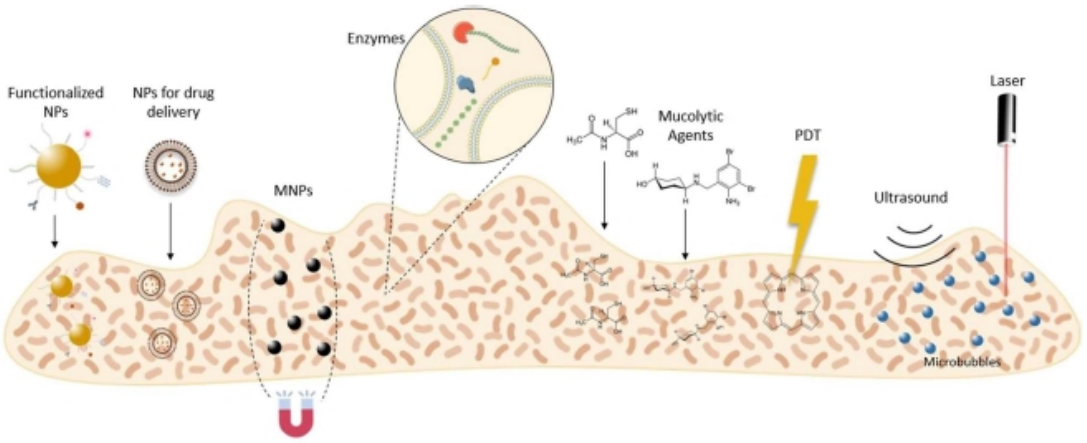


FIGURE 3 | Innovative therapeutic strategies to disrupt the biofilm matrix. MNPs, magnetic nanoparticles; NPs, nanoparticles; PDT, photodynamic therapy.

the host immune system (Donlan and Costerton, 2002). Despite the high complexity of biofilm-associated infections, current therapies still consist in the administration of conventional antimicrobial agents at high doses for a long-term period (Koo et al., 2017; Pinto et al., 2019). Ultimately, these therapies lack efficiency since they fail to approach combinatory strategies that target more than one component of the biofilm microenvironment (Koo et al., 2017).

NEW STRATEGIES TO ERADICATE BACTERIAL BIOFILMS

The EPS matrix remains a critical challenge for bacterial biofilm eradicating strategies, due to its complexity and variability (Fulaz et al., 2019). Nevertheless, many research works are emerging in this field. Thus, this review is focused on innovative strategies to disrupt the EPS matrix of mature biofilms. Here, we outline reported disruptive agents, nanocarriers, and technologies for matrix disassembly (**Figure 3**).

Matrix Disruptive Agents

The increasing resistance to antibiotics in combination with their lack of efficiency on biofilms are leading researchers to focus on the EPS matrix as a barrier to overcome. Thus, many studies in the literature highlight several antibiofilm agents capable of disrupting the EPS matrix in mature biofilms (**Table 1**).

Enzymes

In a biofilm community, enzymes are naturally secreted by bacterial cells and retained within the matrix. Among other functions, enzymes are essential for the remodeling process of the biofilm. During this process, specific enzymes degrade components of the EPS matrix, leading to active dispersal of the biofilm. Consequently, the dispersed cells are able to recolonize other sites of the host (Flemming et al., 2016).

Despite being considered a biofilm virulence factor, these enzymes may be engineered to be used in strategies for biofilm disassembly. For instance, recombinant dispersin B was produced by cloning in *E. coli* a synthetic gene encoding the protein from *Aggregatibacter actinomycetemcomitans* (Dobrynina et al., 2015). After purification, the enzyme was tested against biofilms of *S. epidermidis*, *Burkholderia cenocepacia*, and *Achromobacter xylosoxidans*. Dispersin B actively disrupted mature *S. epidermidis* biofilms at low concentrations (lower than 0.3 μg per sample). However, for the other two strains, a dispersin B concentration above 5 μg per sample was required to reduce the biofilm biomass (Dobrynina et al., 2015). Dispersin B is a glycosyl hydrolase able to specifically disrupt poly-*N*-acetylglucosamine (PNAG), which is the main exopolysaccharide of *S. epidermidis* biofilms (Chaignon et al., 2007). Contrarily, PNAG is not a predominant component of *Burkholderia cenocepacia* and *Achromobacter xylosoxidans* biofilms, which may explain their higher resistance to the recombinant enzyme (Yakandawala et al., 2011; Dobrynina et al., 2015). In a more complex approach, Chen et al. conjugated recombinant dispersin B with a silver-binding peptide, which promotes *in situ* formation of silver nanoparticles (AgNPs) in the presence of silver ions (Lee et al., 2008; Chen and Lee, 2018). In this combinatory strategy, the recombinant enzyme disrupts the matrix and the AgNPs kills the dispersed cells (Chen and Lee, 2018). Comparing to dispersin B alone, the enzyme-peptide conjugate showed at least a 2-fold higher activity against 48 h-old *S. epidermidis* biofilms (Chen and Lee, 2018).

Besides dispersin B, deoxyribonuclease I (DNase I) has also been highlighted for antibiofilm purposes. The effects of DNase I in combination with several antibiotics were evaluated on 24 h-old biofilms (Tetz et al., 2009). The enzyme alone showed a 40% reduction in biofilm biomass for all tested strains. However, it did not compromise the number of viable cells. Antibiotics in combination with DNase I showed a decrease of 2- to 15-fold in the number of colony forming units (CFUs) in comparison

TABLE 1 | Biofilm disruptive strategies based on matrix disruptive agents.

Strategy	Agent	Associated compound	Mechanism of action	Bacterial strains	Disease model	References
Enzymes	**Dispersin B** (0–20 μg/sample)	-	Disrupt PNAG	*S. epidermidis* (strain 210) *B.cenocepacia* (*SCCH2:Bcn33-1220 ST709*) *A. xylosoxidans* (*SCCH3:Ach 33-1365 git allele 2*)	-	Dobrynina et al., 2015
	Dispersin B (0.03 U ml^{-1})	Ag-BP2 peptide	Disrupt PNAG	*S. epidermidis* (ATCC 35984)	-	Chen and Lee, 2018
	DNase I (5.0 μg ml^{-1})	Ampicillin Cefotaxime Rifampin Levofloxacin Azithromycin (50 × MIC)	Disrupt eDNA Antibacterial activity	*E. coli* (ATCC 25922) *H. influenzae* (VT 450-2006) *K. pneumoniae* (VT 1367) *P. aeruginosa* (ATCC 27853) *S. aureus* (ATCC 29213) *S. pyogenes* (VT 59) *A. baumannii* (VT 126)	-	Tetz et al., 2009
	Alginate lyase (15 U) DNase I (100 mg l^{-1})	Vancomycin (0.25 g l^{-1})	Disrupt EPS Antibacterial activity	*E. faecalis* (clinical isolates) *E. faecium* (clinical isolates)	Urinary tract infections	Torelli et al., 2017
	DNase I (0.5 μg ml^{-1}) Marine bacterial DNase (0.5 μg ml^{-1})	**Essential oils from:** *Pogostemon heyneanus* *Cinnamomum tamala* 1 and 1.5% (v/v)	Target eDNA Antibacterial activity	MRSA (ATCC 33591)	-	Rubini et al., 2018
	Esperase® (8.3 × 10^{-4} U ml^{-1})	Prontosan® (10%) EDTA (10 mM)	Proteins cleavage Matrix disruption Antibacterial activity	*P. aeruginosa* (CIP 103.467) *S. aureus* (CIP 4.83)	Chronic wounds	Lefebvre et al., 2016
Mucolytic agent	Ambroxol (1.07 mg ml-1)	Ciprofloxacin (4.0 mg l^{-1})	Disrupt alginate Antibacterial activity	*P. aeruginosa* (PAO1)	Acute lung infection	Cheng et al., 2015
	Ambroxol (1.875 mg ml^{-1})	Vancomycin (2.0 and 5.0 mg ml^{-1})	Reduce EPS Antibacterial activity	*S. epidermidis* (ATCC 35984)	Catheter-related bloodstream infections	Zhang et al., 2015
	N-acetyl cysteine (12.5 mg ml^{-1})	-	Disrupt EPS	*S. epidermidis* (ATCC 12228) *P. acnes* (ATCC 6919) *M. smegmatis* (mc^2 155)	-	Eroshenko et al., 2017
	N-acetyl cysteine (0 – 100 mg ml^{-1})	-	Disrupt EPS	MRSA (clinical isolates) QRPA (clinical isolates)	Post-tympanostomy tube otorrhea	Jun et al., 2019
	N-acetyl cysteine (40 mg ml^{-1})	Linezolid (1.0 μg ml^{-1})	Disrupt EPS	*S. epidermidis* (clinical isolates: 9142 and 1457)	-	Leite et al., 2013

A. baumannii, Acinetobacter baumannii; A. xylosoxidans, Achromobacter xylosoxidans; B.cenocepacia, Burkholderia cenocepacia; DNAse I, deoxyribonuclease I; E. coli, Escherichia coli; eDNA, extracellular DNA; EDTA, Ethylenediamine tetraacetic acid; E. faecalis, Enterococcus faecalis; E. faecium, Enterococcus faecium; EPS, extracellular polymeric substances; H. influenzae, Haemophilus influenzae; K. pneumoniae, Klebsiella pneumoniae; MIC, minimum inhibitory concentration; MRSA, Methicillin-resistant Staphylococcus aureus; M. smegmatis, Mycobacterium smegmatis; P. acnes, Propionibacterium acnes; P. aeruginosa, Pseudomonas aeruginosa; PNAG, poly-β(1-6)-N-acetylglucosamine; QRPA, quinolone-resistant Pseudomonas aeruginosa; S. aureus, Staphylococcus aureus; S. epidermidis, Staphylococcus epidermidis; S. pyogenes, Streptococcus pyogenes; U, unit.

with antibiotics alone. According to the authors, the disruption of eDNA by DNase I leads to a decrease of matrix material and, consequently, increases the efficiency of antibiotics (Tetz et al., 2009). Torelli et al. also reported the synergistic effect of matrix degrading enzymes and antibiotics. In this study, the efficacy of vancomycin in combination with DNase I or alginate lyase against 48 h-old biofilms was assessed (Torelli et al., 2017). For this purpose, three clinical isolates of *Enterococcus faecalis* (*E. faecalis*) and *Enterococcus faecium* (*E. faecium*) derived from catheter-associated urinary tract infections were

used. In planktonic cells, both enzymes did not change the minimun inhibitory concentration (MIC) values of vancomycin. In *E. faecalis* biofilms, vancomycin alone, and vancomycin in combination with DNase I showed minimum biofilm eliminating concentration (MBEC) values of ∼16 and 4 mg l^{-1}, respectively. On the other hand, alginate lyase showed more potential than DNase I against *E. faecium* biofilms, with a MBEC reduction from ∼16 mg l^{-1} (antibiotic alone) to 2 mg l^{-1} (vancomycin and alginate lyase).

In alternative to antibiotics, essential oils (EOs) derived from plants were also combined with DNases to promote the eradication of established biofilms (Rubini et al., 2018). EOs from *Pogostemon heyneanus* and *Cinnamomum tamala* were tested against mature methicillin-resistant *Staphylococcus aureus* (MRSA) biofilms alone and in combination with DNase I or marine bacterial DNase extracted from marine bacterium *Vibrio alginolyticus*. In *in vitro* efficacy studies, both DNase I and marine bacterial DNase in combination with EOs showed a percentage of inhibition around 85%. Through scanning electron microscopy (SEM) and an EPS quantification assay it was possible to verify a great reduction of EPS matrix after treatment with the EOs (Rubini et al., 2018). Hence, the combination of EOs with enzymes seems a promising strategy for biofilm eradication.

In a more complex approach, proteases were combined with antiseptics and ethylenediamine tetra-acetic acid (EDTA) for eradication of *S. aureus* and *P. aeruginosa* biofilms in chronic wounds (Lefebvre et al., 2016). EDTA is reported to destabilize the biofilm through cation chelation and inhibition of matrix metalloprotease activity (Raad et al., 2002; Percival et al., 2005). EDTA and enzymes can potentiate antiseptics activity, allowing the administration of lower doses (Lefebvre et al., 2016). Unlike the previous mentioned studies, Lefebvre et al. tested non-specific enzymes, with a broad-spectrum effect for several bacterial strains. The combinatory treatment revealed synergistic effects for both strains, with a significant reduction on bacterial viability. Nevertheless, the authors highlighted the need to develop a system able to efficiently deliver these molecules to the biofilm (Lefebvre et al., 2016).

Other enzymes, such as proteinase K (Kumar Shukla and Rao, 2013), glycoside hydrolases $PelA_h$, and $PslG_h$ (Baker et al., 2016), α-amylase (Kalpana et al., 2012; Watters et al., 2016), bromelain (Watters et al., 2016), lysostaphin (Watters et al., 2016), papain (Watters et al., 2016), and NucB (Shields et al., 2013) were investigated in a lesser extent for their ability to disrupt matrix components. Despite the promising *in vitro* efficacy of these enzymes, further studies in animal models are still required for validation purposes.

Compounds

Contrarily to enzymes, only few compounds have been reported to have active matrix disruptive properties. Among these, mucolytic agents, such as ambroxol and *N*-acetyl cysteine (NAC), are being highlighted for antibiofilm purposes.

Ambroxol is a frequently used mucolytic agent with antioxidant and anti-inflammatory effects in patients with pulmonary infections (Beeh et al., 2008; Paleari et al., 2011). Cheng et al. studied the combined effect of ambroxol with ciprofloxacin in a rat model of acute lung infection. With this aim, 3-days old biofilms of the mucoid strain *Pseudomonas aeruginosa* O1 (PAO1) were grown in the inner surface of inoculation tubes and further intubated in rats by intratracheal placement (Cheng et al., 2015). The rats were then treated once a day by inhalatory administration of antibiotic and ambroxol, for a total period of 7 days. The combination of ambroxol with ciprofloxacin showed lower bacterial counts compared to treatments with the antibiotic or the mucolytic agent alone. The biofilm morphology was assessed by SEM, where it was possible to observe thinner and less fibrous biofilms after treatment with the combination of ambroxol and the antibiotic. These results indicate that ambroxol has a synergistic effect with ciprofloxacin on mucoid biofilms. The authors speculate that this effect is a consequence of ambroxol enzymatic activity against alginate, which is the main component of these biofilms (Cheng et al., 2015). Ambroxol antibiofilm activity was also assessed against *S. epidermidis* biofilms in catheter-related bloodstream infections (Zhang et al., 2015). *In vitro* efficacy studies showed that ambroxol in combination with vancomycin significantly reduced bacterial viability and biofilm thickness, when compared with ambroxol or the antibiotic alone. By confocal laser scanning microscopy (CLSM) analysis, it was observable larger pore channels in the biofilm structure after treatment with ambroxol. Hence, these changes in the EPS matrix facilitates antibiotics penetration. Further *in vivo* studies in a rabbit infection model confirmed a synergistic effect between ambroxol and vancomycin, with disruption of mature biofilms and reduced inflammatory response (Zhang et al., 2015).

NAC is also a mucolytic agent with potential to eradicate bacterial biofilms. This synthetic agent is an antioxidant that disrupts disulfide bonds in mucus and inhibits cysteine use, by competition. Regarding to biofilms, NAC reduces production of EPS matrix and promotes disruption of mature structures (Romano et al., 2013). Several studies of NAC alone or in combination with antibiotics have been reported in the literature. For instance, Eroshenko et al. studied the effect of NAC on *S. epidermidis*, *Propionibacterium acnes*, and *Mycobacterium smegmatis* biofilms. The results showed that NAC has a high disruptive effect on a mixed biofilm of *S. epidermidis* and *Propionibacterium acnes*, with a 61% biomass reduction compared to the control. However, an insignificant reduction of biofilm biomass was verified when both strains were cultured alone, after a 4 h treatment with NAC (Eroshenko et al., 2017). More recently, the efficacy of NAC alone as an antibiofilm agent was evaluated in MRSA and quinolone-resistant *P. aeruginosa* biofilms, which are common in tympanostomy-tube infections (Jun et al., 2019). For both biofilm types, NAC showed a decrease of biofilm biomass comparing to the control group. The antibiofilm activity of NAC was further confirmed by a decrease in bacterial colonies and by a decrease in observable biofilm structure in SEM images (Jun et al., 2019). Some other studies also shown the synergy between NAC and antibiotics, such as fosfomycin and linezolid (Marchese et al., 2003; Leite et al., 2013).

Some compounds able to inhibit the production of EPS components, have also been reported. For instance, Siala et al.

outlined the activity of the antifungal caspofungin acetate against MRSA biofilms. This lipopeptide acts in bacterial biofilms by inhibiting the PNAG synthesis. In combination with antibiotics, caspofungin acetate showed potential synergistic effects, both *in vitro* and in an animal model system for catheter-based infections (Siala et al., 2016). Besides this compound, other non-disruptive agents such as chitosan, *Cis*-2-decenoic acid (C_2DA), nitric oxide, and rhamnolipids, may also trigger cell dispersion in bacterial biofilm (Chung and Toh, 2014; Fleming and Rumbaugh, 2017).

Although the promising results of the reported matrix disruptive agents, their therapeutic use still presents several limitations such as low bioavailability and non-specific biodistribution, which leads to adverse side effects and low concentrations at the target site (Poznansky, 1984). Hence, innovative vehicles for efficient delivery of enzymes and drugs to the target biofilms are a step forward in the design of new antibiofilm therapies.

Nanocarriers

Nanosystems may play a critical role in both targeting and disruption of the EPS matrix. In the past few years, many researchers engineered sophisticated nanocarriers to increase penetration within the biofilm matrix and release their contents, such as antibiotics, closer to bacterial cells. This non-specific targeting is based on electrostatic interactions between the nanoparticles (NPs) and the matrix components (Fulaz et al., 2019).

The surface charge of NPs has an important role in the destruction of biofilms. The EPS matrix is manly composed by substances with a negative charge, including the bacterial cell wall. Thus, the EPS matrix is more likely to interact with positively charged NPs, which may lead to increased diffusion within the matrix comparing to neutral or negatively charged NPs (Fulaz et al., 2019). Several studies reported that lipid and polymer-based NPs showed increased efficacy against biofilms when positively charged (Lin et al., 2017; Thomsen et al., 2017; Wang et al., 2019). For instance, positively charged polymeric NPs were designed to bind and efficiently deliver nitric oxide to MRSA biofilms, for the treatment of diabetic wounds (Hasan et al., 2019). Gold NPs and nanotubes were also engineered to promote electrostatic interactions with the biofilm, by immobilizing the cationic polymer chitosan at the particles surface (Laskar et al., 2017; Lu et al., 2018; Khan et al., 2019). However, cationic NPs are considered more cytotoxic than neutral and negatively charged particles, which is a consequence of an enhanced cellular uptake (Frohlich, 2012; Hühn et al., 2013). Thus, Su et al. developed polymeric micelles containing polyurethanes with surface charge switchable properties due to protonation and deprotonation of tertiary amine groups in acidic and basic environments, respectively. Consequently, at the acidic pH of the biofilm, the micelles were able to switch to a positively charged surface, increasing their interaction with the matrix (Su et al., 2018). Mixed-shell polymeric micelles composed of the polyethylene glycol (PEG) and poly(β-amino ester) (PAE) were also developed for a pH-triggered switch of the surface charge (Liu et al., 2016). Electrostatic interactions may also be manipulated through the co-administration of negatively charged NPs with a penetration enhancer. Harper et al. observed that the co-administration of anionic alpha-tocopherol phosphate liposomes with a cationic electrolyte, Tris((hydroxymethyl)aminomethane), increased their penetration into the EPS matrix and interaction with bacteria. This phenomenon occurred due to ability of the cationic electrolyte to decrease the electrostatic interactions between the negatively charged liposomes and the biofilm components (Harper et al., 2019).

Targeting bacterial biofilms through electrostatic interactions and pH-triggered release, may offer appealing results for delivery of antimicrobial agents in higher concentrations to deeper layers of the biofilm. However, a complete physical removal of the biofilm is difficult to occur in biofilms of limited access (e.g., implant-related biofilms) (Flemming, 2011). Consequently, the remaining biofilm structures may provide an ideal site for colonization of other microbial cells. Additionally, mature biofilms contain dormant cells with higher resistance to antimicrobials, that may survive and recolonize the matrix (Flemming et al., 2016). Thus, a promising innovative approach consists in the addition of matrix disruptive enzymes and/or compounds, to the design of nanocarriers, in order to promote EPS disruption and dispersal of dormant cells (**Table 2**).

With the purpose to combine antibacterial and antibiofilm agents in a nanocarrier, Tan et al. developed positively charged chitosan NPs co-encapsulating oxacillin and DNase I to eradicate 24 h-old *S. aureus* mature biofilms. A repeated treatment during 48 h revealed that NPs loading both the DNAse I and oxacillin exhibited higher antibiofilm activity than oxacillin-loaded NPs, with a 98.4% biofilm reduction. In addition, their positively charged surface facilitated penetration within the biofilm, without observable cytotoxicity effects against a human immortalized keratinocytes (HaCaT) cell line (Tan et al., 2018a). In a similar study, ciprofloxacin-loaded polymeric NPs were coated with DNase I covalently grafted to the cationic poly-L-lysine (Baelo et al., 2015). The results after a repeated treatment of 48 h-old *P. aeruginosa* biofilms for 3 days showed an eradication higher than 99.8%. The NPs safety profile was confirmed *in vitro* against J774 murine macrophages (Baelo et al., 2015). More recently, Tan et al. co-immobilized DNase I and cellobiose dehydrogenase in chitosan NPs to treat monomicrobial and polymicrobial biofilms of *Candida albicans* and *S. aureus*. Cellobiose dehydrogenase was selected as an antimicrobial agent since it uses cello-oligomers as a substrate to produce hydrogen peroxidase, which generates free radicals that promote oxidation of biofilm matrix components and has bactericidal effects (Henriksson et al., 2000; Gao et al., 2014; Tan et al., 2020). The efficiency of the developed NPs was tested in 24 h-old biofilms. The NPs revealed a high activity by reducing biofilm percentage more than 80% on both mono- and polymicrobial biofilms (Tan et al., 2020). NPs immobilizing only DNase I were also tested and showed no significant effect on the biofilms. According to the authors, this result is a consequence of the absence of a bactericidal agent, which allows dispersed bacterial cells to form a new biofilm. However, the co-immobilization with cellobiose dehydrogenase indicates a synergistic effect with DNase I (Tan et al., 2020).

TABLE 2 | Biofilm disruptive strategies based on nanodelivery systems.

Strategy	Composition of the material	Physicochemical characteristics	Mechanism of action	Bacterial strains	Disease model	References
Polymeric NPs	Chitosan TPP **Encapsulated compound:** Oxacillin **Functionalization:** DNase	**Size:** 166.7 nm **PDI:** 0.179 **Z. Potential:** +8.3 mV **LC:** 6.65%	Disrupt eDNA Electrostatic interactions Antibiotic controlled release	*S. aureus* (ATCC 6538)	-	Tan et al., 2018a
	PLGA PVA poly-L-lysine **Encapsulated compound:** Ciprofloxacin **Functionalization:** DNase I	**Size:** 251.9 nm **PDI:** 0.122 **Z. Potential:** + 28.9 ± 1.43 mV **Ciprofloxacin content:** 0.17 (w/w) (%)	Disrupt eDNA Antibiotic controlled release	*P. aeruginosa* (ATCC 15692) *S. aureus* (ATCC 12600)	Cystic fibrosis	Baelo et al., 2015
	Chitosan TPP **Functionalization:** DNase Cellobiose dehydrogenase	**Size:** 164.73 nm **Z. Potential:** + 13.07 mV	Disrupt eDNA Electrostatic interactions Antibacterial activity	*S. aureus* (ATCC 6538) *C. albicans* (DAY185)	-	Tan et al., 2020
	Chitosan TPP **Encapsulated compound:** Ciprofloxacin **Functionalization:** Alginate lyase	**Size:** 205.5 ± 9.0 nm **PDI:** 0.302 ± 0.031 **Z. Potential:** 12.2 ± 2.1 mV **EE:** 51.8 ± 2.1%	Disrupt extracellular alginate Antibacterial activity	*P. aeruginosa* (clinical isolate)	Cystic fibrosis	Patel et al., 2019
	Carboxymethyl chitosan Linolenic acid **Functionalization:** Dispersin B	**LE:** 51.14 ± 0.93% **LC:** 767.08 ± 13.90 mg g^{-1}	Disrupt PNAG Electrostatic interactions	*S. aureus* (RN6390;15981; 8325; Col) *S. epidermidis* (QY301; RP62A; M187; 1457) *A. actinomycete mcomitans* (HK1651)	-	Tan et al., 2015
Gold NPs	Citrate-capped gold NPs **Functionalization:** Proteinase-K	**Size:** 27.17 ± 0.61 nm **PDI:** 0.238 ± 0.022 **Z. Potential:** −3.79 ± 0.21 mV	Disrupt extracellular proteins Antibacterial activity	*P. fluorescens* (PCL 1701)	-	Habimana et al., 2018
MOFs	gold MIL-88B (Fe) Cerium (IV) complexes	**LC:** 11.14 μ mol g^{-1}	Target eDNA Peroxidase-like activity	*S. aureus* (ATCC 25923)	Topical wound	Liu et al., 2019

A. actinomycetemcomitans, Actinobacillus actinomycetemcomitans; C. albicans, Candida albicans; DNase I, deoxyribonuclease I; eDNA, extracellular DNA; EE, encapsulation efficiency; LC, loading capacity; LE, loading efficiency; MOFs, Metal–organic frameworks; NPs, nanoparticles; P. aeruginosa, Pseudomonas aeruginosa; PDI, polydispersity index; P. fluorescens, Pseudomonas fluorescens; PLGA, poly(lactic-co-glycolic acid); PNAG, poly-β(1-6)-N-acetylglucosamine; PVA, poly(vinyl alcohol); S. aureus, Staphylococcus aureus; S. epidermidis, Staphylococcus epidermidis; TPP, Tri-poly phosphate; Z. Potential, Zeta Potential.

The enzyme alginate lyase was also immobilized in polymeric NPs for matrix disruption purposes. Patel et al. designed ciprofloxacin-loaded NPs functionalized with alginate lyase for the treatment of biofilm-associated *P. aeruginosa* infection in cystic fibrosis. The *in vitro* efficacy assay against 48 h-old biofilms showed a complete disruption of the EPS matrix and no viable bacteria after repeated treatment for 72 h (Patel et al., 2019). This effect was not verified with antibiotic alone or in combination with alginate lyase and with non-functionalized NPs. Further, microscopy assessment of the biofilm confirmed the low biomass and biofilm thickness after treatment with the functionalized NPs. Additionally, *in vitro* and *in vivo* toxicity studies indicated a good biocompatibility of the developed nanosystem (Patel et al., 2019). In another study, Tan et al. designed chitosan NPs for immobilization of dispersin B from *Aggregatibacter actinomycetemcomitans* HK1651. The *in vitro* antibiofilm efficacy of this formulation was evaluated on *S. aureus*, *S. epidermidis*, and *Aggregatibacter actinomycetemcomitans* 24 h-old biofilms (Tan et al., 2015). For all tested strains, free and immobilized dispersin B showed a similar disruptive effect on the biofilms. Thus, the

immobilization of the enzyme into polymeric NPs did not seem to compromise its activity (Tan et al., 2015).

Besides polymeric-based NPs, gold NPs were also functionalized with enzymes. Habimana et al. reported the synthesis of gold NPs functionalized with proteinase-K, combining bactericidal and matrix-degrading activities. The particles were tested against *Pseudomonas fluorescens* mature biofilms, showing a 78% thickness decrease comparing to the control (Habimana et al., 2018). However, this effect was similar to the non-functionalized particles (72% biofilm reduction).

Although the previous studies show a high potential of enzymes as antibiofilm therapies, their use is limited by high cost and poor stability (Wu et al., 2019). To overcome these issues, Liu et al. designed nanoenzymes based on metal organic frameworks (MOFs) and cerium (IV) complexes. In this system, MOFs have a peroxidase-like activity, which leads to bacterial cell death. On the other hand, cerium (IV) complexes mimic the DNase activity by hydrolyzing eDNA from 12 h-old *S. aureus* biofilms (Liu et al., 2019). *In vitro* efficacy studies showed the dispersal potential of the nanoenzyme. Nevertheless, the nanoenzyme alone was not able to have bactericidal activity. Hence, nanoenzymes were assessed in combination with free hydrogen peroxidase. In this condition, bacteria dispersed from the biofilm were efficiently killed. This result was further confirmed in *in vivo* studies using a subcutaneous model. Besides the antibiofilm effects, the treatment with the nanoenzyme and free hydrogen peroxidase revealed a significantly reduction of inflammation and negligible toxicity (Liu et al., 2019).

Technologies for Biofilm Physical Removal

In the past few years, several technologies have been optimized to disrupt bacterial biofilms. These technologies are mainly based on magnetic field in association with NPs, phototherapy and ultrasounds.

Magnetic Field

Early studies based on the success of using magnetic and electric fields to affect other physiological processes triggered the hypothesis that this strategy could be effective in bacterial biofilm control, when in combination with appropriate antibiotics (Grosman et al., 1992; Khoury et al., 1992; Sinisterra, 1992; Benson et al., 1994). Therefore, in the last decades, association of magnetic fields with magnetic nanoparticles (MNPs), namely superparamagnetic iron-oxide nanoparticles (SPIONs) began to emerge. Among these, various magnetic field-based strategies to disrupt bacterial biofilms were reported (**Table 3**).

Several studies showed that, besides the good biocompatibility and low cytotoxicity, MNPs can be controlled and concentrated close to a target, through the application of an external magnetic field. This allows a deeper penetration into the biofilm and interferes in the organization of the matrix (Subbiahdoss et al., 2012; Bandara et al., 2015; Li J. et al., 2019; Quan et al., 2019). Consequently, possible elimination of the target biofilm is achieved through its breakup, along with cell detachment. Bandara et al. aimed to investigate the efficacy of different application modes of magnetic fields (static one-sided, static switched, oscillating, static + oscillating) in eliminating *in vitro* mature *P. aeruginosa* biofilms. These biofilms were treated with an aerosolized formulation containing different combinations of MNPs, ciprofloxacin and spray dried lactose (Bandara et al., 2015). Magnetic fields alone were able to disrupt the biofilms, negatively affecting the EPS matrix, either by interfering in its production or by direct disruption. Also, it was observed that the highest suppression of viability and biomass was achieved in biofilms exposed to a static switched field. The combination of static switched magnetic field with MNP/ciprofloxacin/MNP + ciprofloxacin showed the most promising results regarding the biofilm matrix disruption, which enables an easier penetration of the antibiotic to deeper layers of the biofilm (Bandara et al., 2015).

Besides magnetic targeting, MNPs also allow the increase in temperature by magnetic hyperthermia induction, through the application of alternating magnetic fields. Considering this additional effect, Li J. et al. compared the eradication efficiency of MNPs, with different sizes and concentrations, under AC and DC applied magnetic fields against MRSA biofilms. Greater cell detachment and matrix damage were observed for both 8 and 11 nm MNPs, exposed either to AC or DC magnetic fields. Considering all three tested sizes (8, 11, and 70 nm), although the application of AC fields allowed a local heating of the biofilms, DC fields showed to be the most effective strategy to break the EPS matrix and kill the bacteria. A 4.71 $\log_{10}$ reduction was achieved in biofilm bacteria after the treatment with 30 mg ml^{-1} of 11 nm NPs, under DC magnetic field (Li J. et al., 2019).

Although the type of the applied magnetic field and the size of MNPs are relevant, surface functionalities have also been suggested to be crucial in the interaction process with the EPS matrix and bacteria. Considering this, Subbiahdoss et al. showed that no differences in the antibiofilm efficacy were found between bare, carboxyethylsilanetriol(CES)-grafted and 3-aminopropyltriethoxysilane(APTED)-grafted SPIONs, against 24 h-old *S. epidermidis* biofilms. However, PEGylated SPIONs showed to be ineffective against staphylococcal biofilms. Optical cross-sections obtained using CLSM in the presence of magnetically concentrated CES-grafted SPIONs showed not only dead bacteria in the biofilm but also the formation of some channels across all the biofilm thickness (Subbiahdoss et al., 2012). In line with the previous findings, Quan et al. explored the mechanism behind the physical disruption of the biofilm matrix, responsible for the enhancement of the antimicrobial penetration. Similar to the results obtained by Subbiahdoss et al. (2012), formation of artificial channels, with around 1.4 µm of width, were observed in treated 24 h-old *S. aureus* biofilms. In addition, incubation of these biofilms with gentamicin caused a significant enhancement (4–6-fold) in staphylococcal killing, due to the improved penetration allowed by the non-biotical channels (Quan et al., 2019).

Other NPs have been added to this strategy in order to improve the antibiofilm effects of the magnetic field associated to MNPs. For instance, Wang et al. produced highly efficient nanoplatforms, consisting of gentamicin, tannic acid and AgNPs coated on MNPs, to test against established biofilms of *S. aureus*. Additionally to the MNPs expected effect, the presence of AgNPs caused the production of reactive oxygen species (ROS), which enhanced decomposition of polysaccharides and

TABLE 3 | Biofilm disruptive strategies based on magnetic field.

Strategy	Method of exposure	NPs	Additional compound	Physicochemical characteristics	Bacterial strains	Mechanism of action	References
External magnetic field	Static one-sided, Static switched, Oscillating,Static +oscillating	SPIONs (FluidMAGC-MX)	Ciprofloxacin loaded in spray-dried lactose particles	**Size:** 150 nm	*P. aeruginosa* (PAO1)	Disruption of the EPS matrix	Bandara et al., 2015
	AC and DC	Fe-oxide NPs coated with SiO_2	–	**Sizes:** 8 nm, 11 nm, 70 nm	MRSA (ATCC 33592)	Damage and detachment of the matrix Magnetic hyperthermia	Li J. et al., 2019
	Static one-sided	Surface-modified SPIONs (CES, APTES, PEG functionalities)	-	*Bare*: **Size:** 13.7 ± 2.1 nm **-Zeta potential:** +43.7 ± 1.7 mV *CES-grafted*: **Size:** 13.8 ± 2.1 nm **Zeta potential:** −15.4 ± 0.5 mV *PEGylated*: **Size:** 14.9 ± 1.8 nm **Zeta potential:** −7.71 ± 0.9 mV *APTES- grafted*: **Size:** 17.8 ± 2.6 nm **Zeta potential:** +32.6 ± 0.3 mV	*S. aureus* (ATCC 12600) *S. epidermidis* (ATCC 35984)	Enhanced biofilm penetration Improved antibiotic efficacy	Subbiahdoss et al., 2012
	Static one-sided	SPIONs (Fe_3O_4)	Free Gentamicin	**Size:** 278 ± 61 nm	*S. aureus* (ATCC 12600; ATCC 5298)	Creation of Artificial Channels in the matrix	Quan et al., 2019
	Static one-sided	Fe_3O_4@Ag@HA	Gentamicin	**Zeta potential:** −19.4 mV **Saturation magnetization value:** 45.3 emu g^{-1}	*S. aureus* (ATCC 25922)	ROS production Disruption and decomposition of the matrix Enhanced antimicrobial efficiency	Wang et al., 2018a
	Static one-sided	IOPs (Encapsulated SPIONs)	Encapsulated methicillin	*SPIONs* **Size:** 5 ± 2.5 nm *IOPs* **Size:** 83 ± 6 nm **Zeta Potential:** −1 ± 3 mV	*S. epidermidis* (RP62a)	Enhanced biofilm penetration Targeted delivery	Geilich et al., 2017
	Static one-sided	Fe_3O_4@CS-PEG-Gent NPs	Gentamicin (loaded on the surface)	**Size:** ~40 nm **Zeta potential:** 8.7 mV	*S. aureus* (ATCC 5922)	Enhanced biofilm penetration Improved antibiotic efficacy	Wang et al., 2018b
	AC	SPIONs (Fe_3O_4)	Vancomycin	**Size:** 16 nm	*S. aureus* (BCRC10451)	Hyperthermia Improve antibiotic efficacy	Fang et al., 2017

AC, alternative current; APTES, 3-aminopropyltriethoxysilane; CES, carboxyethylsilanetriol; CS, chitosan; DC, direct current; EPS, extracellular polymeric substances; Gent, gentamicin; HA, hyaluronic acid; IOPs, iron oxide polymersomes; MRSA, methicillin-resistant Staphylococcus aureus; NPs, nanoparticles; P. aeruginosa, Pseudomonas aeruginosa; PEG, polyethylene glycol; ROS, reactive oxygen species; S. aureus, Staphylococcus aureus; S. epidermidis, Staphylococcus epidermidis; SPIONs, superparamagnetic iron oxide nanoparticles.

proteins of the EPS matrix (Wang et al., 2018a). Iron oxide-encapsulating polymersomes, containing both hydrophobic SPIONs and the hydrophilic antibiotic methicillin, were also developed to eradicate antibiotic-resistant infections associated with 24 h-old *S. epidermidis* biofilms (Geilich et al., 2017). It was proved that this formulation was able to completely eradicate all bacteria throughout the biofilm thickness, while not being toxic toward mammalian cells. Extensive bacterial death was observed within the boundaries of the magnetic field and SEM images of the biofilm ultrastructure showed both bacterial death and decoherence of the EPS matrix (Geilich et al., 2017). Wang et al. designed biocompatible Fe_3O_4/chitosan/PEG/Gentamicin MNPs

aiming to eradicate mature *S. aureus* biofilms. This strategy combined the inner magnetic core and the loaded antibiotic, allowing the improvement of the effectiveness and bioavailability of gentamicin at acidic media, through the application of an external magnetic field. CLSM images showed that, just by applying the NPs to the biofilms, the biofilm structure starts to disrupt, and the number of dead bacteria significantly increases (Wang et al., 2018b). The proposed explanation for this phenomenon is the existence of electrostatic interactions between the positively charged MNPs and the negatively charged EPS matrix. Adding the external magnetic field, the biofilm matrix was found to be completely compromised, with an extensive bacterial death observed (Wang et al., 2018b). Also, dual-catalytic iron oxide MNPs have recently demonstrated to controllably kill, degrade, and remove biofilms. These NPs generate free radicals with bactericidal activity and promote EPS matrix degradation. Besides, a subsequent removal of the fragmented biofilm debris is achieved via magnetically forced nanoparticle movement (Hwang et al., 2019).

To evaluate the effect of MNPs-induced hyperthermia associated with antibiotics to treat osteomyelitis, Fang et al. mimicked a clinical situation of a chronic infection in an animal model. A metallic needle was implanted into the bone marrow cavity of distal femur of male Wistar rats, after the injection of *S. aureus*. The temperature increase, achieved through magnetic hyperthermia, led to biofilm destruction, without any significant damage on the surrounding tissues (Fang et al., 2017). The subsequent local administration of vancomycin into the femoral canal allowed biofilm eradication. Consistently with *in vitro* results, *in vivo* efficacy studies showed that MNPs under AC fields were able to compromise the protection barrier of biofilms through MNPs-induced hyperthermia, affecting their structure and enhancing the therapeutic effect of antibiotics (Fang et al., 2017).

Photodynamic Therapy and Ultrasounds

Photodynamic therapy (PDT) and ultrasound mediated therapies are also examples of technologies with growing interest due to their noninvasiveness, relatively low cost, flexibility, and minimal risk of inducing microbial resistance (Briggs et al., 2018). Both strategies, while being effective carried out separately, have already been combined, as further explored. PDT involves the use of nontoxic dyes, called photosensitizers (PS), which in the presence of molecular oxygen and visible light of appropriate wavelength can be excited, leading to the production of ROS (Hu et al., 2018). As a multiple target strategy, the generated ROS can not only oxidize several cellular components (e.g., lipids and DNA), leading to cell inactivation, but can also attack EPS molecules, causing the degradation of matrix structure (de Melo et al., 2013; Hu et al., 2018). Usually, highly conjugated, unsaturated organic molecules with large absorption coefficient in the visible spectrum can behave as PS (Hu et al., 2018). Considering these properties, a wide range of compounds of remarkably different structures have already been used as PS to target different types of biofilms (**Table 4**).

Di Poto et al. demonstrated the efficiency of tetra-substituted (N-methyl-pyridyl) porphine (TMP) as a PS on *S. aureus* mature biofilms. A TMP concentration of 10 μM and light doses of 150–200 J cm^{-2} allowed a significant decrease in survival of the biofilms (up to 2 log), with evident dispersion of the matrix and significant reduction in the number of adherent bacteria. Combining PDT with vancomycin resulted in 10^3-10^4 times lower counts than biofilm inhibitory concentrations used to kill untreated biofilms, showing that the detached and dispersed bacteria became more susceptible to antibiotics (Di Poto et al., 2009). Later, Li et al. revealed that 5-aminolevulinic acid (ALA) had potential to eliminate 24 h-old biofilms of MRSA and methicillin-resistant *S. epidermidis*. An increase of light dosage led to a gradual decrease in the survival as well as a decrease in the number of adherent bacteria in the biofilms of both strains (Li et al., 2013). After the highest dosage irradiation (300 J cm^{-2}), SEM images showed a greater disruption of both biofilms, only with few aggregated colonies remaining. The mechanism of action could be associated with the loss of cell-to-cell and cell-to-matrix interactions, which led to dispersion of the bacterial cells, comprising the biofilm structure (Li et al., 2013). The same mechanism can also be used to explain the morphological damages observed in *S. aureus* and multidrug-resistant *S. aureus* biofilms, after a treatment with porphin sodium (Jia et al., 2019). For both strains, when a light dose of 15 J cm^{-2} was applied, a typical biofilm structure was no longer observed, being the adhesion between bacteria completely compromised (Jia et al., 2019).

Tan et al. also reported the effect of ALA-PDT but on 48 h-old *P. aeruginosa* biofilms. Regarding the biofilm structure, SEM images showed that, for 20 mM ALA complemented with a 108 J cm^{-2} light source treatment, the biofilm was visibly sparse, with bacteria presenting cracks, breaks, and different sizes (Tan et al., 2018b). In another study, phenothiazinium dyes (Toluidine blue O, Azure A, and New methylene blue) were tested against 24 h-old *E. faecalis* and *Klebsiella pneumoniae* preformed biofilms (Misba et al., 2017). A clear disruption of the EPS matrix was observed, comparing to the control groups, with $8\log_{10}$ and $3\log_{10}$ reductions in bacterial count achieved for *E. faecalis* and *Klebsiella pneumoniae*, respectively. Besides the disruptive effect on preformed biofilms, the results also showed an inhibition of EPS production in both species (Misba et al., 2017).

As previously referred, EPS matrix and specifically polysaccharides represent a huge portion of a biofilm. Thus, considering the reported effects of PDT on the matrix, Beirão et al. investigated the influence of a Tetra-Py^+-Me-induced PDT on the extracellular polysaccharides of 24 h-old *P. aeruginosa* biofilms. In fact, a reduction of 81% on the polysaccharides was observed, which shows that these EPS components may be a primary target of photodynamic damage (Beirao et al., 2014).

Nevertheless, like other compounds, PS are also limited in their effectiveness due to the difficulty to penetrate the biofilm matrix as well as possible rapid degradation. Additionally, it is reported that some PS tend to aggregate in water, which also limits an effective therapy (Huang et al., 2010). To overcome these issues, different types of nanocarriers and nanostructures, such as chitosan NPs, gold NPs, carbon nanotubes, and silica NPs, have been developed to deliver and protect PS (Darabpour et al., 2016, 2017; Anju et al., 2019a; Paramanantham et al., 2019;

TABLE 4 | Biofilm disruptive strategies based on photodynamic therapy.

Strategy	PS and associated compounds	Light Parameters	Time of exposure	Bacterial strains	Mechanism of action	References
PDT	TMP (10 μM) Vancomycin	*Tungsten lamp* **WL:** 400–800 nm (white light) **Power density:** 166 mW cm^{-2} **Fluence:** 150–200 J cm^{-2}	~15–20 min	*S. aureus* (SA113, V329) MRSA (BH1C)	Bacteria dispersion Increased susceptibility to antibiotic	Di Poto et al., 2009
	ALA (40 mM)	*HPG5000 semiconductor laser* **WL:** 635 nm (red light) **Fluence:** 0–300 J cm^{-2}	-	MRSA (ATCC 43300) MRSE (287)	Dose-dependent phototoxicity Interference in cell-to-cell and cell-to-matrix interactions	Li et al., 2013
	S-PS (0.5, 1, and 2 μg ml^{-1}) EPIs	**WL:** 650 nm **Fluences:** 5, 10, 15 J cm^{-2}	1 h	*S. aureus* (CMCC 260003) MDR *S. aureus* (ATCC 29213)	Morphological damage caused by ROS Enhanced antimicrobial efficiency	Jia et al., 2019
	ALA (10 or 20 mM)	*LED* **WL:** 630 nm (red light) **Power density:** 90 mW cm^{-2} **Fluence:** 108 J cm^{-2}	20 min	*P. aeruginosa* (PAO1)	Dose-dependent growth inhibition and bacterial death Dispersion of the matrix	Tan et al., 2018b
	TBO, Azure A, and New MetB (10 μM)	**WL:** 630 nm **Power:** 100 mW **Power density:** 0.130 W cm^{-2} **Fluence:** 100 J cm^{-2}	Maximum time exposure 13 min	*Enterococcus faecalis* (MTCC 2729) *Klebsiella pneumonia* (ATCC700603)	EPS disruption Reduction of EPS production	Misba et al., 2017
	Tetra-Py^{+}-Me (20 μg)	*13 parallel OSRAM 2' 18 W/840 lamps* **WL:** 380–700 nm (white light) **Fluence:** Maximum of 64.8 J cm^{-2} **Power density:** 4.0 mW cm^{-2}	Maximum time exposure 270 min	*S. aureus* (ATCC 700699) *P. aeruginosa* (57) *Candida albicans* (ATCC 10231)	Matrix decomposition (decrease of polysaccharides content)	Beirao et al., 2014
	TBO encapsulated in microemulsion (50 – 100 ppm) EDTA (100–500 ppm)	*LED lamps* **WL:** 610 – 630 nm (Red light) **Fluence:** 0.607 J cm^{-2}	15 min	*S. aureus* (ATCC 35556) *S. epidermidis* (ATCC 35984)	EPS disruption by EDTA chelating effect Enhanced penetration of the PS	Rout et al., 2018
	ICG and EDTA (2 mM or 5 mM) Vancomycin for MRSA Amikacin for MRPA	*Diode laser* **WL:** 808 nm **Power density:** 1.5 W cm^{-2} **Fluence:** 135 J cm^{-2}	90s	*S. aureus* (ATCC 25923) MRSA (10485) *P. aeruginosa* (ATCC 27853) MRPA (10911)	Formation of bacteria-free voids Bacterial death	Li X. et al., 2019
	Malachite green conjugated to carboxyl-functionalized multi-walled carbon nanotubes (50 μg ml^{-1})	*Red Laser* **WL:** 660 nm **Fluence:** 58.49 J cm^{-2}	3 min	*P. aeruginosa* (PAO1) *S. aureus* (MCC 2408)	Improved biofilm inhibition EPS inhibition Reduced cell viability	Anju et al., 2019b
	Surface Coating: IR780 (0.02 mg ml^{-1}) MoS2 and arginine-glycine-aspartic acid-cysteine	**WL:** 808 nm **Power density:** 0.5 W cm^{-2}	30 s intervals for 10 min	*S. aureus* (ATCC 29213)	Synergistic PDT/PTT effect (ROS generation/ local hyperthermia)	Li M. et al., 2019

(Continued)

TABLE 4 | Continued

Strategy	PS and associated compounds	Light Parameters	Time of exposure	Bacterial strains	Mechanism of action	References
	ICG loaded into mesoporous polydopamine NPs	*Laser* **WL:** 808 nm **Power density:** 0.75 W cm^{-2} **Diameter:** 15.6 mm	600 s	*S. aureus* (ATCC 29213)	Synergistic PDT/PTT effect (ROS generation/local hyperthermia)	Yuan et al., 2019
	RLP068/Cl (50 μM)	*Diode laser* **WL:** 689 nm **Power density:** 120 mW cm^{-2} **Fluence:** 60 J cm^{-2}	~8 min	MRSA (SAUMRBP2) *P. aeruginosa* (PAE2)	Decrease in biomass Decrease in the number of viable cells	Vassena et al., 2014
	MetB (0.3 mM)	*Laser* **WL:** 665 nm **Fluence:** 35 J cm^{-2} **Power density:** 35 mW cm^{-2}	16 min	*S. aureus* MRSA *S. epidermidis* *P. aeruginosa* *A. baumannii* (sourced from NCTC and ATCC)	Bactericidal effect Total (or partial) eradication of formed biofilms	Briggs et al., 2018

A. baumannii, Acinetobacter baumannii; ALA, 5-aminolevulinic acid; EDTA, ethylenediaminetetraacetic acid; EPIs, efflux pump inhibitors; EPS, extracellular polymeric substances; ICG, indocyanine green; LED, light-emitting diode; MDR S. aureus, multidrug-resistant Staphylococcus aureus; MetB, methylene blue; MRPA, multidrug-resistant Pseudomonas aeruginosa; MRSA, methicillin-resistant Staphylococcus aureus; MRSE, methicillin-resistant Staphylococcus epidermidis; NPs, nanoparticles; P. aeruginosa, Pseudomonas aeruginosa; PDT, photodynamic therapy; PS, photosensitizer; PTT, photothermal therapy; ROS, reactive oxygen species; S. aureus, Staphylococcus aureus; S. epidermidis, Staphylococcus epidermidis; S-PS, S-porphin sodium; TBO, toluidine blue O; TMP, tetra-substituted N-methyl-pyridyl-porphine; WL, wavelength.

Parasuraman et al., 2019; Mirzahosseinipour et al., 2020). Rout et al. studied the potential of Toluidine blue O in solution and in microemulsion, as well as Toluidine blue O in microemulsion with EDTA, in 16 h-old *S. aureus* and *S. epidermidis* biofilms. SEM and fluorescence microscopy results showed that the most effective treatment was the one done with encapsulated Toluidine blue O, with higher biofilm damaged, regarding its EPS matrix as well as bacteria viability (Rout et al., 2018). The combination of this formulation with EDTA resulted in an enhanced inhibition of bacterial biofilms, being ~100% for *S. aureus* biofilms and 80% for *S. epidermidis* biofilms. Surfactants and EDTA combined were able to penetrate deeper into the biofilms, due to the smaller microemulsion size achieved with the encapsulation of Toluidine blue O. Additionally, the chelating effect of EDTA allowed EPS matrix disruption, through sequestration of Ca^{2+} and Mg^{2+} ions, leading to an easier penetration (Rout et al., 2018). Considering this effect, recent studies also proposed a combination of PDT, EDTA, and antibiotics as an efficient approach to disrupt the matrix of 24 h-old MRSA and multidrug-resistant *Pseudomonas aeruginosa* (MRPA) biofilms (Li X. et al., 2019). Consistently with the previous study, Li X. et al. showed that PDT mediated by EDTA promoted the formation of bacteria-free voids. In combination with antibiotics, a higher evidence of biofilm destruction was observed, with dead cells present throughout the entire thickness of the treated biofilms and decreased metabolic activities of 8.29% and 7.75% for MRSA and MRPA, respectively (Li X. et al., 2019). Applying a nanotechnological perspective, Darabpour et al. investigated the potentiality of a mixture of polycationic chitosan NPs and methylene blue on the PDT antibiofilm efficiency against 24 h-old *S. aureus* and *P. aeruginosa*. The high affinity of the polycationic chitosan NPs to the negatively charged EPS compromised the adhesion, leading to the disruption of the biofilm (Darabpour et al., 2016). Using carbon nanotubes as a support nanostructure for cationic dye malachite green, Anju et al. proved that exopolysaccharide inhibition (57.84% for *S. aureus* and 37.25% for *P. aeruginosa*) and considerable biofilm reduction can also be achieved in *P. aeruginosa* and *S. aureus* biofilms (Anju et al., 2019b).

As known, bacteria tend to colonize and adhere to several medical devices, such as implants, which represents a huge concern. Considering this, great efforts have been made to design biocompatible and non-invasive phototherapeutic strategies, for instance, based on the coating of titanium implants and near-infrared light (Li M. et al., 2019; Yuan et al., 2019). Promising eradication results have been achieved for *S. aureus* biofilms by taking advantage of the synergistic effect of the ROS produced by PDT and the thermal effect of the photothermal therapy (PTT), without showing noticeable toxicity (Li M. et al., 2019; Yuan et al., 2019). PDT was also studied for prosthetic joint infections, as a mean to target the biofilms that cause these infections (Vassena et al., 2014; Briggs et al., 2018). Vassena et al. studied the application of RLP068/Cl as a PS in biofilms of mature MRSA and *P. aeruginosa*. This study revealed that besides the antimicrobial activity, the tested PS also promoted some biofilm disruption along with an estimated decrease of 45% and 38% in *S. aureus* and *P. aeruginosa* biomass, respectively (Vassena et al., 2014). Briggs et al. explored the effectiveness of methylene blue as a PS, growing bacteria on both polished titanium alloy and hydroxyapatite-coated disk for 3 days. *S. aureus*, MRSA, *S. epidermidis*, and *P. aeruginosa* biofilms were investigated on the polished surface, while only *P. aeruginosa* was tested in the hydroxyapatite-coated disk. PDT treatment presented significant effect on MRSA and *P. aeruginosa* biofilms and completely eradicated *S. aureus* and *S. epidermidis* biofilms.

They also showed that PDT was less effective when eradicating mature bacterial biofilms grown on hydroxyapatite-coated disk. However, with higher laser power, light intensity and exposure time, greater antibiofilm activity can be achieved (Briggs et al., 2018).

As an alternative to PDT, the use of ultrasounds to induce mechanical disruption of the biofilm structure has been also investigated (**Table 5**). Since the 90's, therapeutic ultrasounds combined with antibiotics have been showing promising results, both *in vitro* and *in vivo*, using low intensity (up to 3 W cm^{-2}) and low-frequency (a few 100 kHz–1 MHz) (Qian et al., 1997, 1999; Johnson et al., 1998; Carmen et al., 2004, 2005; Ensing et al., 2005). Even recently, the effect of low-intensity and low-frequency ultrasounds is still under investigation, for instance in combination with tobramycin, against beta-lactamases *E. coli* biofilms. It was found that the morphology of the biofilms subjected to the treatment was seriously affected, presenting reduced thickness and a loosened structure. As a consequence, the penetration of the antibiotic increased, which led to an increased antibacterial effect (Hou et al., 2019).

With the aim to achieve greater effects, gas-filled particles, called microbubbles have been associated with ultrasounds. Microbubbles provide nuclei for inertial cavitation and lower the threshold for ultrasounds-induced cavitation, resulting in a substantial effect with a reduced exposure time (He et al., 2011; Dong et al., 2017). He et al. showed that the application of ultrasound-targeted microbubbles (USMB) destruction could significantly improve vancomycin activity against 12 h-old *S. epidermidis* biofilms. Ultrasounds-activated sulfur hexafluoride microbubbles and vancomycin created micropores within the biofilm architecture, which facilitated the vancomycin penetration (He et al., 2011). Besides, a significant decrease in the number of viable cells (7.17 log_{10} CFU ml^{-1}) was observed, compared to an untreated control (10.51 log_{10} CFU ml^{-1}). *In vivo S. epidermidis* biofilms were grown on polyethylene disks and further subcutaneously implanted in rabbit models. The results revealed a significant decrease of the log_{10} numbers of viable CFU cm^{-2} in biofilms treated with vancomycin and ultrasounds, alone or in combination with microbubbles. It is worth to note that the lowest number of viable cells was observed when microbubbles were added to the treatment (He et al., 2011).

The effect of USMB was also investigated by Dong et al. In this study, low-frequency ultrasounds (300 kHz) combined with vancomycin and microbubbles were evaluated in 24 h-old *S. epidermidis* biofilms. Once more, a reduction of the biofilm thickness was observed, which allowed vancomycin to reach inner layers (Dong et al., 2013). Although the biophysical effect of acoustically activated microbubbles is evident, the underlying mechanisms of interaction between the bubbles and the biofilm has not been elucidated yet (Dong et al., 2017). Therefore, besides the mechanical effects of the USMB treatment in combination with vancomycin, Dong et al. showed that ultrasonic energy could also present biochemical effects on extracellular matrix of *S. epidermidis* biofilms. An ultrasounds treatment (1 MHz, 0.5 W cm^{-2}, 50% duty cycle, for 5 min) combined with microbubbles interfered with *quorum sensing* regulator genes and reduced the expression level of icaA, which is one of the encoding genes to polysaccharide intercellular adhesin, a major component of *S. epidermidis* EPS matrix. Although biochemical effects could not be completely distinguished from the mechanical effects of ultrasounds, the combination of all mechanisms resulted in a reduction of the biomass and an enhanced antibiotic activity, through fragilization of the matrix (Dong et al., 2017). As a continuum of the previous studies and with the aim of facilitate the translation of this technology, Dong et al. further explored this same synergistic effect in an *in vivo* rabbit model (Dong et al., 2018). Consistently, SEM images showed that when treated with USMB in combination with vancomycin, biofilms presented the greatest reduction in terms of thickness as well as bacterial density, compared to the other treatment groups. The susceptibility to the antibiotic significantly increased, since the reduction of bacterial counts with USMB + vancomycin treatment was close to three orders of magnitude compared with the control. Also, histopathologic examinations showed no damage to the skin and organs, as a consequence of ultrasounds alone or USMB, which indicates that these technologies may be well tolerated by the body and have the potential to be safely applied (Dong et al., 2018).

Other conventional antibiotics, such as gentamicin and streptomycin, have also been tested in association with USMB (Ronan et al., 2016). It was found that exposing 72 h-old *P. aeruginosa* biofilms to USMB alone caused significant structural damage to the biofilm, through the formation of voids and 5–20 μm diameter craters. The ultrasonic disruption of the microbubbles enables the resulting shockwaves and microjets to act nearby the biofilm, affecting not only the permeability of the cells but also the EPS matrix integrity. The additional action with the antibiotics led to a significant reduction in overall biomass and thickness of the treated biofilms as well as a reduction in the metabolic activity of the bacteria, detected by CO_2 production rate quantification (Ronan et al., 2016).

Besides ultrasounds, laser light can also be used to induce the vaporization of nanobubbles, producing similar damage on the matrix and potentiating antibiotic effects (Teirlinck et al., 2019). Teirlinck et al. tested this approach against *P. aeruginosa* and *S. aureus* biofilms, in conjugation with small gold NPs. When short laser pulses were applied to the biofilms, these NPs could absorb the energy of high intensity, heating the water surrounding of the particles that quickly evaporated, resulting in expanding and imploding water vapor nanobubbles (Teirlinck et al., 2019). The organized structure of the biofilm was compromised by the generated pressure waves, enabling a better diffusion of the drug molecules deep into the biofilm. In fact, the treatment with vapor nanobubbles enhanced the antibacterial effects of the tested compounds, achieving results comparable with the ones obtained for forced disrupted biofilms, by sonication and vortexing (Teirlinck et al., 2019).

Throughout this section, it was shown that both PDT and ultrasounds are efficient technologies for the eradication of biofilms. Niavarzi et al. recently considered the hypothesis of combining these two strategies, by using ultrasounds to activate a PS (methylene blue), followed by PDT. In fact, ultrasonic activation of PS in conjugation with the PDT increased the

TABLE 5 | Biofilm disruptive strategies based on ultrasounds and laser-induced microbubbles.

Strategy	MB/NB characteristics	Additional compounds	Parameters	Bacterial strains	Mechanism of action	References
Low-intensity and low-frequency ultrasound	-	Vancomycin (50 mg kg^{-1})	**Frequency**: 28.5 kHz **Duty cycle**: 1:3 **Power density**: 500 mW cm^{-2} **Time of exposure**: 24 or 48 h	*S. epidermidis* (ATCC 35984)	*In vivo* enhancement of antibiotic action	Carmen et al., 2004
	-	Gentamicin (8 mg kg^{-1})	**Frequency:** 28.5 kHz **Duty cycle:** 1:3 **Power density:** 500 mW cm^{-2} **Time of exposure:** 24 or 48 h	*E. coli* (ATCC 10798) *P. aeruginosa* (ATCC 27853)	*In vivo* enhancement of antibiotic action	Carmen et al., 2005
	-	Gentamicin (8 mg kg^{-1})	**Frequency:** 28.48 kHz **Power density:** 500 mW cm^{-2} **Time of exposure:** 24 to 72 h	*E. coli* (ATCC 10798)	*In vivo* enhancement of antibiotic action (applied locally or systemically)	Ensing et al., 2005
	-	Tobramycin (8 and 80 µg ml^{-1})	**Frequency:** 42 kHz **Power density:** 0.66 W cm^{-2} **Time of exposure:** 30 min	ESBLs *E.coli* (Clinic isolates)	Reduction of the biofilm thickness Loss of structure Enhanced of antibiotic penetration	Hou et al., 2019
USMB	SonoVue 30% (v/v)	Vancomycin (100 µg ml^{-1})	**Frequency:** 0.08 MHz **Power density:** 1.0 W cm^{-2} **Duty cycle:** 50% **Time of exposure:** 10 min	*S. epidermidis* (ATCC 35984)	Formation of micropores Reduction of the biofilm density Increased antibiotic penetration	He et al., 2011
	1% and 4% (v/v)	Vancomycin (32 mg l^{-1})	**Frequency:** 300 kHz **Power density:** 0.5 W cm^{-2} **Duty cycle:** 50% **Time of exposure:** 5 min	*S. epidermidis* (ATCC 35984)	Formation of micropores Reduction of biofilm thickness Enhancement of susceptibility	Dong et al., 2013
	1% and 4% (v/v)	Vancomycin (32 mg l^{-1})	**Frequency:** 1 MHz pulsed US waves **Power density:** 0.5 W cm^{-2} **Duty cycle:** 50% **Time of exposure:** 5 min	*S. epidermidis* (ATCC 35984)	Downregulation of the expression of icaA Interference with *quorum sensing* regulator genes	Dong et al., 2017
	1% (v/v) 4–6 µm	Vancomycin (25 mg kg^{-1})	**Frequency**: 300 kHz **Power density**: 0.5 W cm^{-2} **Duty cycle**: 50% **Time of exposure**: 24 to 72 h after surgery; 5 min, 2 times a day	*S. epidermidis* (ATCC 35984)	*In vivo:* Reduction of biofilm thickness Enhancement of susceptibility	Dong et al., 2018
	Perflutren lipid-coated microspheres filled with octafluoropropane gas (mean diameter: 1.1–3.3 µm)	Gentamicin sulfate (50 mg l^{-1}); Streptomycin sulfate (50 mg l^{-1})	500 kHz at a peak negative pressure of 1.1 MPa; 16 cycle tone burst; **Frequency:** 1 kHz pulse repetition **Time of exposure:** 5 min	*P. aeruginosa* (PAO1)	Formation of craters Synergistic effect with the antibiotics	Ronan et al., 2016
Laser-induced vapor nanobubbles	NB produced by the laser thermal effect on 70 nm AuNP (1.4 × 10^{10} AuNP ml^{-1})	Pvp-I (0.01%) Chx (0.04%), BzCl (0.06%); Cetr (0.15%), Mupi (0.01%)	**WL:** 561 nm **Fluence:** 1.7 J cm^{-2} **Laser beam diameter:** ~150 µm **Time of exposure:** 1 or 2 laser pulses for 7 ns	*P. aeruginosa* (LMG 27622) *S. aureus* (Mu50)	Enhanced penetration of antibiotics Biofilm disruption	Teirlinck et al., 2019

AuNP, silver nanoparticles; BzCl, benzalkonium chloride; Cetr, cetrimonium bromide; Chx, chlorhexidine; E. coli, Escherichia coli; ESBLs, extended-spectrum beta-lactamases; MB, microbubbles; Mupi, mupirocin; NB, nanobubbles; P. aeruginosa, Pseudomonas aeruginosa; Pvp-I, povidone-iodine; S. aureus, Staphylococcus aureus; S. epidermidis, Staphylococcus epidermidis; US, ultrasound; USMB, ultrasound and microbubbles; WL, wavelenght.

penetration depth into *E. faecalis* biofilms, leading to greater antibiofilm activity of the PS compared to the use of PDT alone, with reduction bacterial counts of ~98%, comparing to the control group (Niavarzi et al., 2019).

FUTURE PERSPECTIVES

Biofilm-associated infections are nowadays a major concern for the healthcare systems. At a clinical level, the current therapies available are mainly focused only on a biocidal approach. Strategies focusing on targeting and disruption of the EPS matrix may be a promising approach to increase cell susceptibility to antibacterial agents (Fulaz et al., 2019). Antibiofilm agents have been reported in the literature to potentiate the activity of antibiotics due to their ability to disassemble the matrix. In a more complex strategy, NPs as carriers of antibiofilm agents have been developed. However, these nanocarriers are mostly focused on the immobilization of matrix disruptive enzymes, such as DNase I, dispersin B, and alginate lyase. To the best of our knowledge, nanocarriers for delivery of mucolytic agents with antibiofilm potential have not been developed.

Regarding the explored innovative technologies, it was shown that physical disturbance of the EPS matrix is also achieved, through generation of ROS, interference with matrix polysaccharides or creation of voids and craters in the biofilm structure. Although these mechanisms can efficiently disrupt biofilms without development of bacterial resistance, cell detachment can increase the risk of reinfection. Thus, a synergistic effect between the antibacterial effect of antibiotics and the mechanical disruption caused by these technologies is aimed in most reported studies.

In conclusion, the ideal strategy for biofilm eradication would consider the combination of antibacterial agents with strategies for EPS disassembly. In this scenario, the EPS would be disrupted, and the dispersed bacterial cells would be further killed by a bactericidal agent. Hence, this innovative therapy would decrease bacterial resistance and prevent biofilm recurrence.

AUTHOR CONTRIBUTIONS

RP and FS drafted the manuscript. SR, CN, and PV reviewed and edited the manuscript. All authors read and approved the final version.

FUNDING

This work was supported by the project PTDC/NAN-MAT/31444/2017, financed by FCT/MCTES e FEDER through Programa Operacional Competitividade e Internacionalização - COMPETE 2020.

ACKNOWLEDGMENTS

RP and CN are thankful to Fundação para a Ciência e Tecnologia (FCT) for the Ph.D. Grant [SFRH/BD/130319/2017] and the investigator Grant [IF/00293/2015], respectively. PV is thankful to the Fund for Scientific Research Flanders (FWO grant WO.009.16N). FS is thankful for the grant [ICETA 2019-81]. The authors RP, FS, CN, and SR acknowledge to the institution LAQV - Laboratório Associado para a Química Verde (UIDB/50006/2020). RP also acknowledges the Programa Operacional Capital Humano (POCH), specifically the BiotechHealth Programme (Doctoral Programme on Cellular and Molecular Biotechnology Applied to Health Sciences). The authors acknowledge Servier Laboratories for permission for adaptation of figures.

REFERENCES

Anderson, G. G., and O'Toole, G. A. (2008). Innate and induced resistance mechanisms of bacterial biofilms. *Curr. Top Microbiol. Immunol.* 322, 85–105. doi: 10.1007/978-3-540-75418-3_5

Anju, V. T., Paramanantham, P., S, B.S., Sharan, A., Syed, A., Bahkali, N. A., et al. (2019a). Antimicrobial photodynamic activity of toluidine blue-carbon nanotube conjugate against *Pseudomonas aeruginosa* and *Staphylococcus aureus* - understanding the mechanism of action. *Photodiagnosis Photodyn. Ther.* 27, 305–316. doi: 10.1016/j.pdpdt.2019.06.014

Anju, V. T., Paramanantham, P., Siddhardha, B., Sruthil Lal, S. B., Sharan, A., Alyousef, A. A., et al. (2019b). Malachite green-conjugated multi-walled carbon nanotubes potentiate antimicrobial photodynamic inactivation of planktonic cells and biofilms of *Pseudomonas aeruginosa* and *Staphylococcus aureus*. *Int. J. Nanomed.* 14, 3861–3874. doi: 10.2147/ijn.S202734

Archer, N. K., Mazaitis, M. J., Costerton, J. W., Leid, J. G., Powers, M. E., and Shirtliff, M. E. (2011). *Staphylococcus aureus* biofilms: properties, regulation, and roles in human disease. *Virulence* 2, 445–459. doi: 10.4161/viru.2.5.17724

Baelo, A., Levato, R., Julian, E., Crespo, A., Astola, J., Gavalda, J., et al. (2015). Disassembling bacterial extracellular matrix with DNase-coated nanoparticles to enhance antibiotic delivery in biofilm infections. *J. Control Release* 209, 150–158. doi: 10.1016/j.jconrel.2015.04.028

Baker, P., Hill, P. J., Snarr, B. D., Alnabelseya, N., Pestrak, M. J., Lee, M. J., et al. (2016). Exopolysaccharide biosynthetic glycoside hydrolases can be utilized to disrupt and prevent *Pseudomonas aeruginosa* biofilms. *Sci. Adv.* 2:e1501632. doi: 10.1126/sciadv.1501632

Bandara, H. M., Nguyen, D., Mogarala, S., Osinski, M., and Smyth, H. D. (2015). Magnetic fields suppress *Pseudomonas aeruginosa* biofilms and enhance ciprofloxacin activity. *Biofouling* 31, 443–457. doi: 10.1080/08927014.2015.1055326

Beeh, K. M., Beier, J., Esperester, A., and Paul, L. D. (2008). Antiinflammatory properties of ambroxol. *Eur. J. Med. Res.* 13, 557–562.

Beirao, S., Fernandes, S., Coelho, J., Faustino, M. A., Tome, J. P., Neves, M. G., et al. (2014). Photodynamic inactivation of bacterial and yeast biofilms with a cationic porphyrin. *Photochem. Photobiol.* 90, 1387–1396. doi: 10.1111/php.12331

Beitelshees, M., Hill, A., Jones, C. H., and Pfeifer, B. A. (2018). Phenotypic variation during biofilm formation: implications for anti-biofilm therapeutic design. *Materials* 11:1086. doi: 10.3390/ma11071086

Benson, D. E., Grissom, C. B., Burns, G. L., and Mohammad, S. F. (1994). Magnetic field enhancement of antibiotic activity in biofilm forming *Pseudomonas aeruginosa*. *Asaio J.* 40, M371–M376. doi: 10.1097/00002480-199407000-00025

Briggs, T., Blunn, G., Hislop, S., Ramalhete, R., Bagley, C., McKenna, D., et al. (2018). Antimicrobial photodynamic therapy - a promising treatment for prosthetic joint infections. *Lasers Med. Sci.* 33, 523–532. doi: 10.1007/s10103-017-2394-4

Carmen, J. C., Roeder, B. L., Nelson, J. L., Beckstead, B. L., Runyan, C. M., Schaalje, G. B., et al. (2004). Ultrasonically enhanced vancomycin activity against *Staphylococcus epidermidis* biofilms *in vivo*. *J. Biomater. Appl.* 18, 237–245. doi: 10.1177/0885328204040540

Carmen, J. C., Roeder, B. L., Nelson, J. L., Ogilvie, R. L., Robison, R. A., Schaalje, G. B., et al. (2005). Treatment of biofilm infections on implants with

low-frequency ultrasound and antibiotics. *Am. J. Infect. Control.* 33, 78–82. doi: 10.1016/j.ajic.2004.08.002

Chaignon, P., Sadovskaya, I., Ragunah, C., Ramasubbu, N., Kaplan, J. B., and Jabbouri, S. (2007). Susceptibility of staphylococcal biofilms to enzymatic treatments depends on their chemical composition. *Appl. Microbiol. Biotechnol.* 75, 125–132. doi: 10.1007/s00253-006-0790-y

Chen, K. J., and Lee, C. K. (2018). Twofold enhanced dispersin B activity by N-terminal fusion to silver-binding peptide for biofilm eradication. *Int. J. Biol. Macromol.* 118, 419–426. doi: 10.1016/j.ijbiomac.2018.06.066

Cheng, C., Du, L., Yu, J., Lu, Q., He, Y., and Ran, T. (2015). Ciprofloxacin plus erythromycin or ambroxol ameliorates endotracheal tube-associated *Pseudomonas aeruginosa* biofilms in a rat model. *Pathol. Res. Pract.* 211, 982–988. doi: 10.1016/j.prp.2015.10.003

Chung, P. Y., and Toh, Y. S. (2014). Anti-biofilm agents: recent breakthrough against multi-drug resistant *Staphylococcus aureus*. *Pathog. Dis.* 70, 231–239. doi: 10.1111/2049-632x.12141

Darabpour, E., Kashef, N., Amini, S. M., Kharrazi, S., and Djavid, G. E. (2017). Fast and effective photodynamic inactivation of 4-day-old biofilm of methicillin-resistant *Staphylococcus aureus* using methylene blue-conjugated gold nanoparticles. *J. Drug Deliv. Sci. Technol.* 37, 134–140. doi: 10.1016/j.jddst.2016.12.007

Darabpour, E., Kashef, N., and Mashayekhan, S. (2016). Chitosan nanoparticles enhance the efficiency of methylene blue-mediated antimicrobial photodynamic inactivation of bacterial biofilms: an *in vitro* study. *Photodiagnosis Photodyn. Ther.* 14, 211–217. doi: 10.1016/j.pdpdt.2016.04.009

Darouiche, R. O. (2004). Treatment of infections associated with surgical implants. *N. Engl. J. Med.* 350, 1422–1429. doi: 10.1056/NEJMra035415

de Melo, W. C., Avci, P., de Oliveira, M. N., Gupta, A., Vecchio, D., Sadasivam, M., et al. (2013). Photodynamic inactivation of biofilm: taking a lightly colored approach to stubborn infection. *Expert Rev. Anti. Infect. Ther.* 11, 669–693. doi: 10.1586/14787210.2013.811861

Del Pozo, J. L. (2018). Biofilm-related disease. *Expert Rev. Anti Infect. Ther.* 16, 51–65. doi: 10.1080/14787210.2018.1417036

Di Poto, A., Sbarra, M. S., Provenza, G., Visai, L., and Speziale, P. (2009). The effect of photodynamic treatment combined with antibiotic action or host defence mechanisms on *Staphylococcus aureus* biofilms. *Biomaterials* 30, 3158–3166. doi: 10.1016/j.biomaterials.2009.02.038

Dobrynina, O. Y., Bolshakova, T. N., Umyarov, A. M., Boksha, I. S., Lavrova, N. V., Grishin, A. V., et al. (2015). Disruption of bacterial biofilms using recombinant dispersin B. *Microbiology* 84, 498–501. doi: 10.1134/S0026261715040062

Dong, Y., Chen, S., Wang, Z., Peng, N., and Yu, J. (2013). Synergy of ultrasound microbubbles and vancomycin against *Staphylococcus epidermidis* biofilm. *J. Antimicrob. Chemother.* 68, 816–826. doi: 10.1093/jac/dks490

Dong, Y., Li, J., Li, P., and Yu, J. (2018). Ultrasound microbubbles enhance the activity of vancomycin against *Staphylococcus epidermidis* biofilms *in vivo*. *J. Ultrasound Med.* 37, 1379–1387. doi: 10.1002/jum.14475

Dong, Y., Xu, Y., Li, P., Wang, C., Cao, Y., and Yu, J. (2017). Antibiofilm effect of ultrasound combined with microbubbles against *Staphylococcus epidermidis* biofilm. *Int. J. Med. Microbiol.* 307, 321–328. doi: 10.1016/j.ijmm.2017.06.001

Donlan, R. M. (2001a). Biofilm formation: a clinically relevant microbiological process. *Clin. Infect. Dis.* 33, 1387–1392. doi: 10.1086/322972

Donlan, R. M. (2001b). Biofilms and device-associated infections. *Emerging Infect. Dis.* 7, 277–281. doi: 10.3201/eid0702.010226

Donlan, R. M., and Costerton, J. W. (2002). Biofilms: survival mechanisms of clinically relevant microorganisms. *Clin. Microbiol. Rev.* 15, 167–193. doi: 10.1128/CMR.15.2.167-193.2002

Ensing, G. T., Roeder, B. L., Nelson, J. L., van Horn, J. R., van der Mei, H. C., Busscher, H. J., et al. (2005). Effect of pulsed ultrasound in combination with gentamicin on bacterial viability in biofilms on bone cements *in vivo*. *J. Appl. Microbiol.* 99, 443–448. doi: 10.1111/j.1365-2672.2005.02643.x

Eroshenko, D., Polyudova, T., and Korobov, V. (2017). N-acetylcysteine inhibits growth, adhesion and biofilm formation of Gram-positive skin pathogens. *Microb. Pathog.* 105, 145–152. doi: 10.1016/j.micpath.2017.02.030

Fang, C. H., Tsai, P. I., Huang, S. W., Sun, J. S., Chang, J. Z., Shen, H. H., et al. (2017). Magnetic hyperthermia enhance the treatment efficacy of peri-implant osteomyelitis. *BMC Infect. Dis.* 17, 516. doi: 10.1186/s12879-017-2621-4

Fleming, D., and Rumbaugh, K. P. (2017). Approaches to dispersing medical biofilms. *Microorganisms* 5:15. doi: 10.3390/microorganisms5020015

Flemming, H.-C. (2011). "Microbial biofouling: unsolved problems, insufficient approaches, and possible solutions," in *Biofilm highlights*, eds F. Hans-Curt, W. Jost, and S. Ulrich (Berlin; Heidelberg: Springer), 81–109.

Flemming, H. C., and Wingender, J. (2010). The biofilm matrix. *Nat. Rev. Microbiol.* 8, 623–633. doi: 10.1038/nrmicro2415

Flemming, H. C., Wingender, J., Szewzyk, U., Steinberg, P., Rice, S. A., and Kjelleberg, S. (2016). Biofilms: an emergent form of bacterial life. *Nat. Rev. Microbiol.* 14, 563–575. doi: 10.1038/nrmicro.2016.94

Fong, J. N. C., and Yildiz, F. H. (2015). Biofilm matrix proteins. *Microbiol. Spectr.* 3, 1–16. doi: 10.1128/microbiolspec.MB-0004-2014

Frohlich, E. (2012). The role of surface charge in cellular uptake and cytotoxicity of medical nanoparticles. *Int. J. Nanomedicine.* 7, 5577–5591. doi: 10.2147/ijn.S36111

Fulaz, S., Vitale, S., Quinn, L., and Casey, E. (2019). Nanoparticle-biofilm interactions: the role of the EPS matrix. *Trends Microbiol.* 27, 915–926. doi: 10.1016/j.tim.2019.07.004

Gao, L., Giglio, K. M., Nelson, J. L., Sondermann, H., and Travis, A. J. (2014). Ferromagnetic nanoparticles with peroxidase-like activity enhance the cleavage of biological macromolecules for biofilm elimination. *Nanoscale* 6, 2588–2593. doi: 10.1039/c3nr05422e

Geilich, B. M., Gelfat, I., Sridhar, S., van de Ven, A. L., and Webster, T. J. (2017). Superparamagnetic iron oxide-encapsulating polymersome nanocarriers for biofilm eradication. *Biomaterials* 119, 78–85. doi: 10.1016/j.biomaterials.2016.12.011

Grosman, Z., Kolar, M., and Tesarikova, E. (1992). Effects of static magnetic field on some pathogenic microorganisms. *Acta Univ. Palacki. Olomuc. Fac. Med.* 134, 7–9.

Habimana, O., Zanoni, M., Vitale, S., O'Neill, T., Scholz, D., Xu, B., et al. (2018). One particle, two targets: a combined action of functionalised gold nanoparticles, against *Pseudomonas fluorescens* biofilms. *J. Colloid Interface Sci.* 526, 419–428. doi: 10.1016/j.jcis.2018.05.014

Harper, R. A., Carpenter, G. H., Proctor, G. B., Harvey, R. D., Gambogi, R. J., Geonnotti, A. R., et al. (2019). Diminishing biofilm resistance to antimicrobial nanomaterials through electrolyte screening of electrostatic interactions. *Colloids Surf. B* 173, 392–399. doi: 10.1016/j.colsurfb.2018.09.018

Hasan, N., Cao, J., Lee, J., Naeem, M., Hlaing, S. P., Kim, J., et al. (2019). PEI/NONOates-doped PLGA nanoparticles for eradicating methicillin-resistant *Staphylococcus aureus* biofilm in diabetic wounds via binding to the biofilm matrix. *Mater. Sci. Eng. C* 103:109741. doi: 10.1016/j.msec.2019.109741

He, N., Hu, J., Liu, H., Zhu, T., Huang, B., Wang, X., et al. (2011). Enhancement of vancomycin activity against biofilms by using ultrasound-targeted microbubble destruction. *Antimicrob. Agents Chemother.* 55, 5331–5337. doi: 10.1128/aac.00542-11

Henriksson, G., Johansson, G., and Pettersson, G. (2000). A critical review of cellobiose dehydrogenases. *J. Biotechnol.* 78, 93–113. doi: 10.1016/S0168-1656(00)00206-6

Hou, Y., Yang, M., Jiang, H., Li, D., and Du, Y. (2019). Effects of low-intensity and low-frequency ultrasound combined with tobramycin on biofilms of extended-spectrum beta-lactamases (ESBLs) *Escherichia coli*. *FEMS Microbiol. Lett.* 366:fnz026. doi: 10.1093/femsle/fnz026

Hu, X., Huang, Y. Y., Wang, Y., Wang, X., and Hamblin, M. R. (2018). Antimicrobial photodynamic therapy to control clinically relevant biofilm infections. *Front. Microbiol.* 9:1299. doi: 10.3389/fmicb.2018.01299

Huang, L., Dai, T., and Hamblin, M. R. (2010). Antimicrobial photodynamic inactivation and photodynamic therapy for infections. *Methods Mol. Biol.* 635, 155–173. doi: 10.1007/978-1-60761-697-9_12

Hühn, D., Kantner, K., Geidel, C., Brandholt, S., De Cock, I., Soenen, S. J. H., et al. (2013). Polymer-coated nanoparticles interacting with proteins and cells: focusing on the sign of the net charge. *ACS Nano* 7, 3253–3263. doi: 10.1021/nn3059295

Hwang, G., Paula, A. J., Hunter, E. E., Liu, Y., Babeer, A., Karabucak, B., et al. (2019). Catalytic antimicrobial robots for biofilm eradication. *Sci. Robot.* 4:aaw2388. doi: 10.1126/scirobotics.aaw2388

Jia, M., Mai, B., Liu, S., Li, Z., Liu, Q., and Wang, P. (2019). Antibacterial effect of S-Porphin sodium photodynamic therapy on *Staphylococcus aureus* and

multiple drug resistance *Staphylococcus aureus*. *Photodiagnosis Photodyn. Ther.* 28, 80–87. doi: 10.1016/j.pdpdt.2019.08.031

Johnson, L. L., Peterson, R. V., and Pitt, W. G. (1998). Treatment of bacterial biofilms on polymeric biomaterials using antibiotics and ultrasound. *J. Biomater. Sci. Polym. Ed.* 9, 1177–1185. doi: 10.1163/156856298x00712

Jun, Y., Youn, C. K., Jo, E. R., and Cho, S. I. (2019). *In vitro* inhibitory activity of N-acetylcysteine on tympanostomy tube biofilms from methicillin-resistant *Staphylococcus aureus* and quinolone-resistant *Pseudomonas aeruginosa*. *Int. J. Pediatr. Otorhinolaryngol.* 126:109622. doi: 10.1016/j.ijporl.2019.109622

Kalpana, B. J., Aarthy, S., and Pandian, S. K. (2012). Antibiofilm activity of alpha-amylase from *Bacillus subtilis* S8-18 against biofilm forming human bacterial pathogens. *Appl. Biochem. Biotechnol.* 167, 1778–1794. doi: 10.1007/s12010-011-9526-2

Khan, F., Lee, J. W., Manivasagan, P., Pham, D. T. N., Oh, J., and Kim, Y. M. (2019). Synthesis and characterization of chitosan oligosaccharide-capped gold nanoparticles as an effective antibiofilm drug against the *Pseudomonas aeruginosa* PAO1. *Microb. Pathog.* 135:103623. doi: 10.1016/j.micpath.2019.103623

Khoury, A. E., Lam, K., Ellis, B., and Costerton, J. W. (1992). Prevention and control of bacterial infections associated with medical devices. *ASAIO J.* 38, M174–M178. doi: 10.1097/00002480-199207000-00013

Koo, H., Allan, R. N., Howlin, R. P., Stoodley, P., and Hall-Stoodley, L. (2017). Targeting microbial biofilms: current and prospective therapeutic strategies. *Nat. Rev. Microbiol.* 15, 740–755. doi: 10.1038/nrmicro.2017.99

Kumar Shukla, S., and Rao, T. S. (2013). Dispersal of Bap-mediated *Staphylococcus aureus* biofilm by proteinase K. *J. Antibiot.* 66, 55–60. doi: 10.1038/ja.2012.98

Laskar, K., Faisal, S. M., Rauf, A., Ahmed, A., and Owais, M. (2017). Undec-10-enoic acid functionalized chitosan based novel nano-conjugate: an enhanced anti-bacterial/biofilm and anti-cancer potential. *Carbohydr. Polym.* 166, 14–23. doi: 10.1016/j.carbpol.2017.02.082

Lee, E., Kim, D. H., Woo, Y., Hur, H. G., and Lim, Y. (2008). Solution structure of peptide AG4 used to form silver nanoparticles. *Biochem. Biophys. Res. Commun.* 376, 595–598. doi: 10.1016/j.bbrc.2008.09.042

Lefebvre, E., Vighetto, C., Di Martino, P., Larreta Garde, V., and Seyer, D. (2016). Synergistic antibiofilm efficacy of various commercial antiseptics, enzymes and EDTA: a study of *Pseudomonas aeruginosa* and *Staphylococcus aureus* biofilms. *Int. J. Antimicrob. Agents.* 48, 181–188. doi: 10.1016/j.ijantimicag.2016.05.008

Leite, B., Gomes, F., Teixeira, P., Souza, C., Pizzolitto, E., and Oliveira, R. (2013). Combined effect of linezolid and N-acetylcysteine against *Staphylococcus epidermidis* biofilms. *Enferm. Infecc. Microbiol. Clin.* 31, 655–659. doi: 10.1016/j.eimc.2012.11.011

Li, J., Nickel, R., Wu, J., Lin, F., van Lierop, J., and Liu, S. (2019). A new tool to attack biofilms: driving magnetic iron-oxide nanoparticles to disrupt the matrix. *Nanoscale* 11, 6905–6915. doi: 10.1039/c8nr09802f

Li, M., Li, L., Su, K., Liu, X., Zhang, T., Liang, Y., et al. (2019). Highly effective and noninvasive near-infrared eradication of a *Staphylococcus aureus* biofilm on implants by a photoresponsive coating within 20 min. *Adv. Sci.* 6:1900599. doi: 10.1002/advs.201900599

Li, X., Guo, H., Tian, Q., Zheng, G., Hu, Y., Fu, Y., et al. (2013). Effects of 5-aminolevulinic acid-mediated photodynamic therapy on antibiotic-resistant staphylococcal biofilm: an *in vitro* study. *J. Surg. Res.* 184, 1013–1021. doi: 10.1016/j.jss.2013.03.094

Li, X., Huang, W., Zheng, X., Chang, S., Liu, C., Cheng, Q., et al. (2019). Synergistic *in vitro* effects of indocyanine green and ethylenediamine tetraacetate-mediated antimicrobial photodynamic therapy combined with antibiotics for resistant bacterial biofilms in diabetic foot infection. *Photodiagnosis Photodyn. Ther.* 25, 300–308. doi: 10.1016/j.pdpdt.2019.01.010

Lin, M. H., Hung, C. F., Aljuffali, I. A., Sung, C. T., Huang, C. T., and Fang, J. Y. (2017). Cationic amphiphile in phospholipid bilayer or oil-water interface of nanocarriers affects planktonic and biofilm bacteria killing. *Nanomedicine* 13, 353–361. doi: 10.1016/j.nano.2016.08.011

Liu, Y., Busscher, H. J., Zhao, B., Li, Y., Zhang, Z., van der Mei, H. C., et al. (2016). Surface-adaptive, antimicrobially loaded, micellar nanocarriers with enhanced penetration and killing efficiency in staphylococcal biofilms. *ACS Nano* 10, 4779–4789. doi: 10.1021/acsnano.6b01370

Liu, Z., Wang, F., Ren, J., and Qu, X. (2019). A series of MOF/Ce-based nanozymes with dual enzyme-like activity disrupting biofilms and hindering recolonization of bacteria. *Biomaterials* 208, 21–31. doi: 10.1016/j.biomaterials.2019.04.007

Lu, B., Lu, F., Ran, L., Yu, K., Xiao, Y., Li, Z., et al. (2018). Imidazole-molecule-capped chitosan-gold nanocomposites with enhanced antimicrobial activity for treating biofilm-related infections. *J. Colloid Interface Sci.* 531, 269–281. doi: 10.1016/j.jcis.2018.07.058

Marchese, A., Bozzolasco, M., Gualco, L., Debbia, E. A., Schito, G. C., and Schito, A. M. (2003). Effect of fosfomycin alone and in combination with N-acetylcysteine on *E. coli* biofilms. *Int. J. Antimicrob. Agents* 22(Suppl.2), 95–100. doi: 10.1016/s0924-8579(03)00232-2

Mirzahosseinipour, M., Khorsandi, K., Hosseinzadeh, R., Ghazaeian, M., and Shahidi, F. K. (2020). Antimicrobial photodynamic and wound healing activity of curcumin encapsulated in silica nanoparticles. *Photodiagnosis Photodyn. Ther.* 29:101639. doi: 10.1016/j.pdpdt.2019.101639

Misba, L., Zaidi, S., and Khan, A. U. (2017). A comparison of antibacterial and antibiofilm efficacy of phenothiazinium dyes between Gram positive and Gram negative bacterial biofilm. *Photodiagnosis Photodyn. Ther.* 18, 24–33. doi: 10.1016/j.pdpdt.2017.01.177

Niavarzi, S., Pourhajibagher, M., Khedmat, S., Ghabraei, S., Chiniforush, N., and Bahador, A. (2019). Effect of ultrasonic activation on the efficacy of antimicrobial photodynamic therapy: evaluation of penetration depth of photosensitizer and elimination of *Enterococcus faecalis* biofilms. *Photodiagnosis Photodyn. Ther.* 27, 362–366. doi: 10.1016/j.pdpdt.2019.06.001

Paleari, D., Rossi, G. A., Nicolini, G., and Olivieri, D. (2011). Ambroxol: a multifaceted molecule with additional therapeutic potentials in respiratory disorders of childhood. *Expert Opin. Drug Discov.* 6, 1203–1214. doi: 10.1517/17460441.2011.629646

Paramanantham, P., Siddhardha, B., Lal Sb, S., Sharan, A., Alyousef, A. A., Al Dosary, M. S., et al. (2019). Antimicrobial photodynamic therapy on *Staphylococcus aureus* and *Escherichia coli* using malachite green encapsulated mesoporous silica nanoparticles: an *in vitro* study. *PeerJ.* 7:e7454. doi: 10.7717/peerj.7454

Parasuraman, P., Antony, A. P., Sharan, A., Siddhardha, B., Kasinathan, K., Bahkali, N. A., et al. (2019). Antimicrobial photodynamic activity of toluidine blue encapsulated in mesoporous silica nanoparticles against *Pseudomonas aeruginosa* and *Staphylococcus aureus*. *Biofouling* 35, 89–103. doi: 10.1080/08927014.2019.1570501

Patel, K. K., Tripathi, M., Pandey, N., Agrawal, A. K., Gade, S., Anjum, M. M., et al. (2019). Alginate lyase immobilized chitosan nanoparticles of ciprofloxacin for the improved antimicrobial activity against the biofilm associated mucoid *P. aeruginosa* infection in cystic fibrosis. *Int. J. Pharm.* 563, 30–42. doi: 10.1016/j.ijpharm.2019.03.051

Percival, S. L., Kite, P., Eastwood, K., Murga, R., Carr, J., Arduino, M. J., et al. (2005). Tetrasodium EDTA as a novel central venous catheter lock solution against biofilm. *Infect. Control Hosp. Epidemiol.* 26, 515–519. doi: 10.1086/502577

Pinto, R. M., Lopes-de-Campos, D., Martins, M. C. L., Van Dijck, P., Nunes, C., and Reis, S. (2019). Impact of nanosystems in *Staphylococcus aureus* biofilms treatment. *FEMS Microbiol. Rev.* 43, 622–641. doi: 10.1093/femsre/fuz021

Poznansky, M. J. (1984). Enzyme-albumin polymers. new approaches to the use of enzymes in medicine. *Appl. Biochem. Biotechnol.* 10, 41–56. doi: 10.1007/bf02783734

Qian, Z., Sagers, R. D., and Pitt, W. G. (1997). The effect of ultrasonic frequency upon enhanced killing of *P. aeruginosa* biofilms. *Ann. Biomed. Eng.* 25, 69–76. doi: 10.1007/bf02738539

Qian, Z., Sagers, R. D., and Pitt, W. G. (1999). Investigation of the mechanism of the bioacoustic effect. *J. Biomed. Mater. Res.* 44, 198–205. doi: 10.1002/(sici)1097-4636(199902)44:2<198::aid-jbm10>3.0.co;2-p

Quan, K., Zhang, Z., Chen, H., Ren, X., Ren, Y., Peterson, B. W., et al. (2019). Artificial channels in an infectious biofilm created by magnetic nanoparticles enhanced bacterial killing by antibiotics. *Small* 15:e1902313. doi: 10.1002/smll.201902313

Raad, I., Hachem, R., Tcholakian, R. K., and Sherertz, R. (2002). Efficacy of minocycline and EDTA lock solution in preventing catheter-related bacteremia, septic phlebitis, and endocarditis in rabbits. *Antimicrob. Agents Chemother.* 46, 327–332. doi: 10.1128/aac.46.2.327-332.2002

Ribeiro, M., Monteiro, F. J., and Ferraz, M. P. (2012). Infection of orthopedic implants with emphasis on bacterial adhesion process and techniques used in studying bacterial-material interactions. *Biomatter* 2, 176–194. doi: 10.4161/biom.22905

Romano, C. L., Toscano, M., Romano, D., and Drago, L. (2013). Antibiofilm agents and implant-related infections in orthopaedics: where are we? *J. Chemother.* 25, 67–80. doi: 10.1179/1973947812y.0000000045

Ronan, E., Edjiu, N., Kroukamp, O., Wolfaardt, G., and Karshafian, R. (2016). USMB-induced synergistic enhancement of aminoglycoside antibiotics in biofilms. *Ultrasonics* 69, 182–190. doi: 10.1016/j.ultras.2016.03.017

Rout, B., Liu, C. H., and Wu, W. C. (2018). Increased anti-biofilm efficacy of toluidine blue on *Staphylococcus* species after nano-encapsulation. *Photodiagnosis Photodyn. Ther.* 21, 190–200. doi: 10.1016/j.pdpdt.2017.12.007

Rubini, D., Banu, S. F., Nisha, P., Murugan, R., Thamotharan, S., Percino, M. J., et al. (2018). Essential oils from unexplored aromatic plants quench biofilm formation and virulence of Methicillin resistant *Staphylococcus aureus*. *Microb. Pathog.* 122, 162–173. doi: 10.1016/j.micpath.2018.06.028

Shields, R. C., Mokhtar, N., Ford, M., Hall, M. J., Burgess, J. G., ElBadawey, M. R., et al. (2013). Efficacy of a marine bacterial nuclease against biofilm forming microorganisms isolated from chronic rhinosinusitis. *PLoS ONE* 8:e55339. doi: 10.1371/journal.pone.0055339

Siala, W., Kucharikova, S., Braem, A., Vleugels, J., Tulkens, P. M., Mingeot-Leclercq, M. P., et al. (2016). The antifungal caspofungin increases fluoroquinolone activity against *Staphylococcus aureus* biofilms by inhibiting N-acetylglucosamine transferase. *Nat. Commun.* 7, 1–15. doi: 10.1038/ncomms13286

Sinisterra, J. V. (1992). Application of ultrasound to biotechnology: an overview. *Ultrasonics* 30, 180–185. doi: 10.1016/0041-624X(92)90070-3

Srivastava, S., and Bhargava, A. (2016). Biofilms and human health. *Biotechnol. Lett.* 38, 1–22. doi: 10.1007/s10529-015-1960-8

Stoica, P., Chifiriuc, M. C., Rapa, M., and Lazăr, V. (2017). "Overview of biofilm-related problems in medical devices," in *Biofilms and Implantable Medical Devices*, eds Y. Deng, and W. Lv (Cambridge, UK: Woodhead Publishing), 3–23.

Su, Y., Zhao, L., Meng, F., Qiao, Z., Yao, Y., and Luo, J. (2018). Triclosan loaded polyurethane micelles with pH and lipase sensitive properties for antibacterial applications and treatment of biofilms. *Mater. Sci. Eng. C Mater. Biol. Appl.* 93, 921–930. doi: 10.1016/j.msec.2018.08.063

Subbiahdoss, G., Sharifi, S., Grijpma, D. W., Laurent, S., van der Mei, H. C., Mahmoudi, M., et al. (2012). Magnetic targeting of surface-modified superparamagnetic iron oxide nanoparticles yields antibacterial efficacy against biofilms of gentamicin-resistant staphylococci. *Acta Biomater.* 8, 2047–2055. doi: 10.1016/j.actbio.2012.03.002

Tan, Y., Cheng, Q., Yang, H., Li, H., Gong, N., Liu, D., et al. (2018b). Effects of ALA-PDT on biofilm structure, virulence factor secretion, and QS in *Pseudomonas aeruginosa*. *Photodiagnosis Photodyn. Ther.* 24, 88–94. doi: 10.1016/j.pdpdt.2018.07.005

Tan, Y., Ma, S., Leonhard, M., Moser, D., Haselmann, G. M., Wang, J., et al. (2018a). Enhancing antibiofilm activity with functional chitosan nanoparticles targeting biofilm cells and biofilm matrix. *Carbohydr. Polym.* 200, 35–42. doi: 10.1016/j.carbpol.2018.07.072

Tan, Y., Ma, S., Leonhard, M., Moser, D., Ludwig, R., and Schneider-Stickler, B. (2020). Co-immobilization of cellobiose dehydrogenase and deoxyribonuclease I on chitosan nanoparticles against fungal/bacterial polymicrobial biofilms targeting both biofilm matrix and microorganisms. *Mater. Sci. Eng. C Mater. Biol. Appl.* 108:110499. doi: 10.1016/j.msec.2019.110499

Tan, Y., Ma, S., Liu, C., Yu, W., and Han, F. (2015). Enhancing the stability and antibiofilm activity of DspB by immobilization on carboxymethyl chitosan nanoparticles. *Microbiol. Res.* 178, 35–41. doi: 10.1016/j.micres.2015.06.001

Teirlinck, E., Fraire, J. C., Van Acker, H., Wille, J., Swimberghe, R., Brans, T., et al. (2019). Laser-induced vapor nanobubbles improve diffusion in biofilms of antimicrobial agents for wound care. *Biofilm* 1:100004. doi: 10.1016/j.bioflm.2019.100004

Tetz, G. V., Artemenko, N. K., and Tetz, V. V. (2009). Effect of DNase and antibiotics on biofilm characteristics. *Antimicrob. Agents Chemother.* 53, 1204–1209. doi: 10.1128/aac.00471-08

Thomsen, H., Benkovics, G., Fenyvesi, E., Farewell, A., Malanga, M., and Ericson, M. B. (2017). Delivery of cyclodextrin polymers to bacterial biofilms - an exploratory study using rhodamine labelled cyclodextrins and multiphoton microscopy. *Int. J. Pharm.* 531, 650–657. doi: 10.1016/j.ijpharm.2017.06.011

Torelli, R., Cacaci, M., Papi, M., Paroni Sterbini, F., Martini, C., Posteraro, B., et al. (2017). Different effects of matrix degrading enzymes towards biofilms formed by *E. faecalis* and *E. faecium* clinical isolates. *Colloids Surf. B* 158, 349–355. doi: 10.1016/j.colsurfb.2017.07.010

Trampuz, A., and Widmer, A. F. (2006). Infections associated with orthopedic implants. *Curr. Opin. Infect. Dis.* 19, 349–356. doi: 10.1097/01.qco.0000235161.85925.e8

Vassena, C., Fenu, S., Giuliani, F., Fantetti, L., Roncucci, G., Simonutti, G., et al. (2014). Photodynamic antibacterial and antibiofilm activity of RLP068/Cl against *Staphylococcus aureus* and *Pseudomonas aeruginosa* forming biofilms on prosthetic material. *Int. J. Antimicrob. Agents.* 44, 47–55. doi: 10.1016/j.ijantimicag.2014.03.012

Wang, X., Deng, A., Cao, W., Li, Q., Wang, L., Zhou, J., et al. (2018b). Synthesis of chitosan/poly (ethylene glycol)-modified magnetic nanoparticles for antibiotic delivery and their enhanced anti-biofilm activity in the presence of magnetic field. *J. Mater. Sci.* 53, 6433–6449. doi: 10.1007/s10853-018-1998-9

Wang, X., Wu, J., Li, P., Wang, L., Zhou, J., Zhang, G., et al. (2018a). Microenvironment-responsive magnetic nanocomposites based on silver nanoparticles/gentamicin for enhanced biofilm disruption by magnetic field. *ACS Appl. Mater. Interfaces* 10, 34905–34915. doi: 10.1021/acsami.8b10972

Wang, Z., Bai, H., Lu, C., Hou, C., Qiu, Y., Zhang, P., et al. (2019). Light controllable chitosan micelles with ROS generation and essential oil release for the treatment of bacterial biofilm. *Carbohydr. Polym.* 205, 533–539. doi: 10.1016/j.carbpol.2018.10.095

Watters, C. M., Burton, T., Kirui, D. K., and Millenbaugh, N. J. (2016). Enzymatic degradation of *in vitro Staphylococcus aureus* biofilms supplemented with human plasma. *Infect. Drug Resist.* 9, 71–78. doi: 10.2147/idr.S103101

WHO (2014). *Antimicrobial Resistance: Global Report on Surveillance*. France: World Health Organization.

Wu, J., Wang, X., Wang, Q., Lou, Z., Li, S., Zhu, Y., et al. (2019). Nanomaterials with enzyme-like characteristics (nanozymes): next-generation artificial enzymes (II). *Chem. Soc. Rev.* 48, 1004–1076. doi: 10.1039/C8CS00457A

Yakandawala, N., Gawande, P. V., LoVetri, K., Cardona, S. T., Romeo, T., Nitz, M., et al. (2011). Characterization of the poly-beta-1,6-N-acetylglucosamine polysaccharide component of *Burkholderia* biofilms. *Appl. Environ. Microbiol.* 77, 8303–8309. doi: 10.1128/aem.05814-11

Yuan, Z., Tao, B., He, Y., Mu, C., Liu, G., Zhang, J., et al. (2019). Remote eradication of biofilm on titanium implant via near-infrared light triggered photothermal/photodynamic therapy strategy. *Biomaterials* 223:119479. doi: 10.1016/j.biomaterials.2019.119479

Zhang, Y., Fu, Y., Yu, J., Ai, Q., Li, J., Peng, N., et al. (2015). Synergy of ambroxol with vancomycin in elimination of catheter-related *Staphylococcus epidermidis* biofilm *in vitro* and *in vivo*. *J. Infect. Chemother.* 21, 808–815. doi: 10.1016/j.jiac.2015.08.017

Zimmerli, W. (2014). Clinical presentation and treatment of orthopaedic implant-associated infection. *J. Intern. Med.* 276, 111–119. doi: 10.1111/joim.12233

Zimmerli, W., and Sendi, P. (2017). Orthopaedic biofilm infections. *APMIS.* 125, 353–364. doi: 10.1111/apm.12687

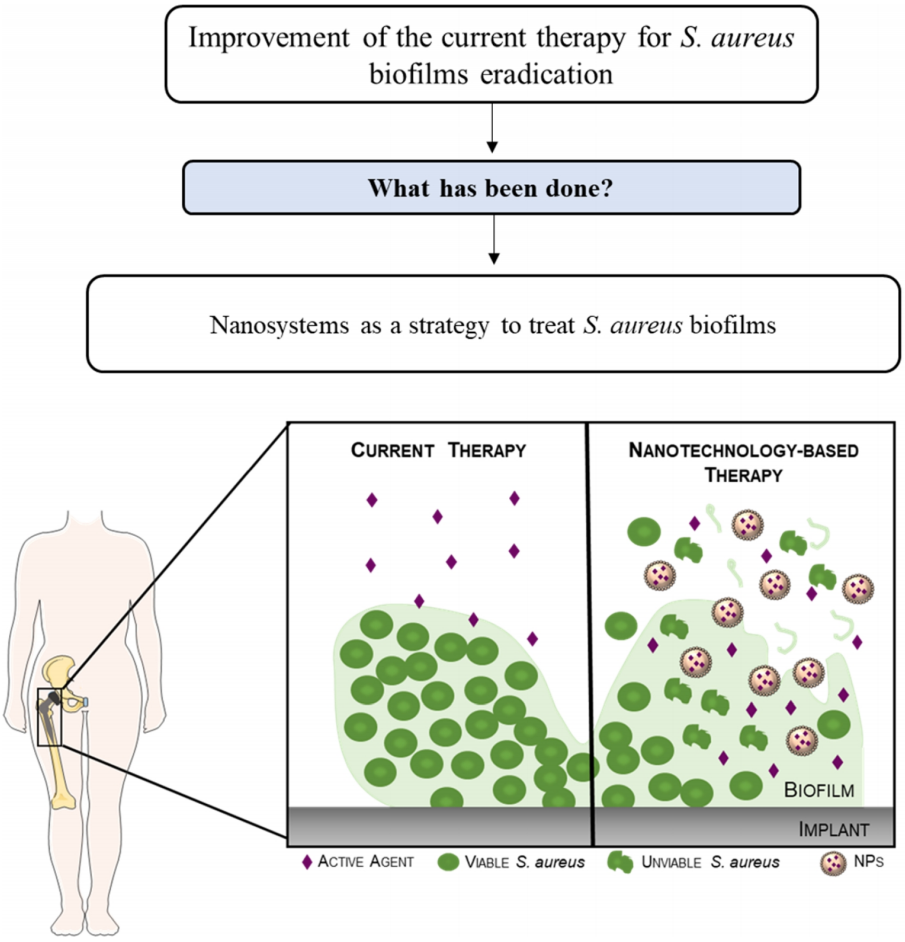
Conflict of Interest: The authors declare that the research was conducted in the absence of any commercial or financial relationships that could be construed as a potential conflict of interest.

Copyright © 2020 Pinto, Soares, Reis, Nunes and Van Dijck. This is an open-access article distributed under the terms of the Creative Commons Attribution License (CC BY). The use, distribution or reproduction in other forums is permitted, provided the original author(s) and the copyright owner(s) are credited and that the original publication in this journal is cited, in accordance with accepted academic practice. No use, distribution or reproduction is permitted which does not comply with these terms.

Chapter 2.3.

Impact of nanosystems in *Staphylococcus aureus* biofilms treatment

Nanotechnology has been emerging as a promising tool to fight bacterial biofilms. NPs have intrinsic characteristics (e.g., charge and size) that facilitates their diffusion through the EPS matrix, promoting the delivery of encapsulated compounds to deeper regions of the biofilm. Thus, nanocarriers encapsulating antibiofilm compounds can greatly improve the current treatment against bacterial biofilms. Several nanosystems have been engineered with the aim of eradicating *S. aureus* biofilms. This high priority pathogen is commonly found in numerous implantable medical devices, being the main responsible for nosocomial infections. This review provides an overview of the nanosystems developed to eradicate implant-associated *S. aureus* biofilms and the available biofilm models for their preclinical validation.



FEMS Microbiology Reviews, fuz021, 1–20

doi: 10.1093/femsre/fuz021
Advance Access Publication Date: 17 August 2019
Review Article

Downloaded from https://academic.oup.com/femsre/advance-article-abstract/doi/10.1093/femsre/fuz021/5550945 by Universidade do Porto user on 14 October 2019

REVIEW ARTICLE

Impact of nanosystems in *Staphylococcus aureus* biofilms treatment

Rita M. Pinto[1,2,3,4], Daniela Lopes-de-Campos[1], M. Cristina L. Martins[4,5], Patrick Van Dijck[2,3,†], Cláudia Nunes[1,*] and Salette Reis[1]

[1]LAQV, REQUIMTE, Departamento de Ciências Químicas, Faculdade de Farmácia, Universidade do Porto, Rua de Jorge Viterbo Ferreira, 228, 4050-313 Porto, Portugal, [2]Laboratory of Molecular Cell Biology, Institute of Botany and Microbiology, KU Leuven, B-3001 Leuven, Belgium, [3]VIB-KU Leuven, Center for Microbiology, B-3001 Leuven, Belgium, [4]i3S, Instituto de Investigação e Inovação em Saúde, Universidade do Porto; INEB, Instituto de Engenharia Biomédica, Universidade do Porto, Rua Alfredo Allen, 208, 4200-135 Porto, Portugal and [5]ICBAS, Instituto de Ciências Biomédicas Abel Salazar, Universidade do Porto, Rua de Jorge Viterbo Ferreira, 228, 4050-313 Porto, Portugal

*Corresponding author: Rua de Jorge Viterbo Ferreira, 228, 4050-313 Porto, Portugal. Tel: +351 220428500; E-mail: cdnunes@ff.up.pt

One sentence summary: *Staphylococcus aureus* biofilms are a major cause for implant-associated infections. The lack of an effective treatment and the escalating numbers of antibiotic-resistance events are prompting the research toward alternative nano-based strategies.

Editor: Ehud Banin

†Patrick Van Dijck, http://orcid.org/0000-0002-1542-897X

ABSTRACT

Staphylococcus aureus (*S. aureus*) is considered by the World Health Organization as a high priority pathogen for which new therapies are needed. This is particularly important for biofilm implant-associated infections once the only available treatment option implies a surgical procedure combined with antibiotic therapy. Consequently, these infections represent an economic burden for Healthcare Systems. A new strategy has emerged to tackle this problem: for small bugs, small particles. Here, we describe how nanotechnology-based systems have been studied to treat *S. aureus* biofilms. Their features, drawbacks and potentialities to impact the treatment of these infections are highlighted. Furthermore, we also outline biofilm models and assays required for preclinical validation of those nanosystems to smooth the process of clinical translation.

Keywords: nanotechnology; nanomedicine; drug delivery; antibacterial activity; biofilm eradication

INTRODUCTION

Staphylococcus aureus is a Gram-positive commensal bacterium mostly present in the normal bacterial flora of the human skin and mucous membranes (WHO 2014). This bacterium is able to establish a mature 3D biofilm, where bacterial cells attached to a surface or to other cells are embedded within a protective polymeric extracellular matrix (Donlan and Costerton 2002; Lister and Horswill 2014) (Fig. 1). After the implantation of a medical device into the human body, proteins, which are present at the surgical wound site (e.g. fibronectin), adhere to the implants

Received: 20 December 2018; **Accepted:** 15 August 2019

© FEMS 2019. This is an Open Access article distributed under the terms of the Creative Commons Attribution-NonCommercial-NoDerivs licence (http://creativecommons.org/licenses/by-nc-nd/4.0/), which permits non-commercial reproduction and distribution of the work, in any medium, provided the original work is not altered or transformed in any way, and that the work is properly cited. For commercial re-use, please contact journals.permissions@oup.com

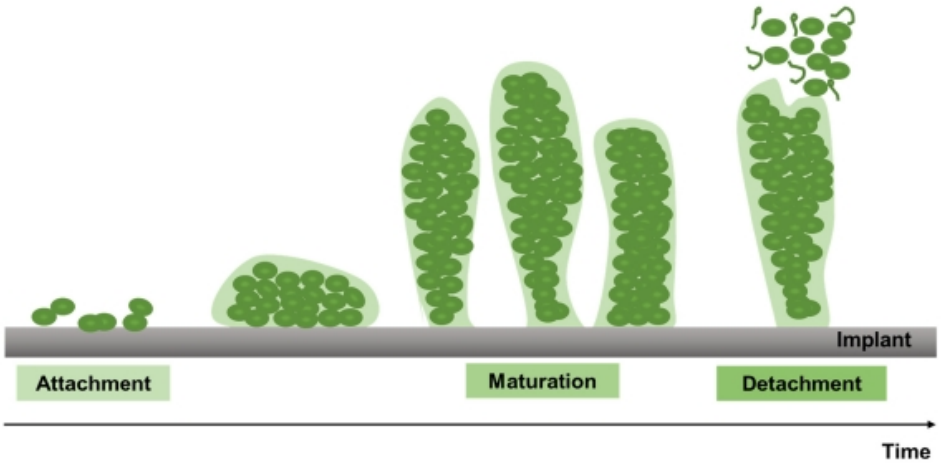


Figure 1. The development of a biofilm involves three main phases: initial attachment, maturation and final detachment. The initial attachment is mediated by host matrix proteins that cover the implant surface immediately after its insertion (Otto 2008). Thus, microbial surface components are able to recognize and bind to these matrix proteins, enabling bacterial colonization. Subsequently, the biofilm grows until it reaches a phase of maturation, adopting a 3D appearance, mainly due to intercellular aggregation mediated by adhesive proteins and exopolymers. Finally, detachment of single cells or cell clusters from the biofilm structure occurs, allowing dissemination and colonization of other sites of the host (Otto 2008).

surface (Bhattacharya *et al.* 2015). These proteins are easily recognized by microbial surface components as adhesive matrix molecules, providing an opportunity for bacteria to establish a biofilm. This mode of bacterial growth plays a key role in antibiotic resistance, mainly due to an insufficient drug penetration into the biofilms matrix (Anderson and O'Toole 2008). Besides, the bacteria within the biofilm adopt a dormant lifestyle, contributing to a poor response to antibiotics (Anderson and O'Toole 2008). The complex structure of biofilms provides a unique opportunity to the survival and virulence of bacteria in the human body and ultimately to severe pathological conditions (Parsek and Singh 2003). Biofilms have a high genetic and phenotypic diversity, with less metabolically active bacterial cells in the lower regions of the structure that are well adapted to persist in hostile environments (Srivastava and Bhargava 2016). In the biofilm matrix, antibiotics are mostly restrained to the surface of the biofilm and are unable to reach the bacterial cells in the deeper layers of the structure (Srivastava and Bhargava 2016). Additionally, altered microenvironments, such as low pH and low oxygen, may compromise the efficacy of antibacterial agents (del Pozo and Patel 2007). Enzymes embedded in the biofilm matrix are also capable of destroying antibacterial agents, contributing to a low efficacy of these agents. At a genetic level, biofilms structure facilitates horizontal gene transfer, which promotes the spread of antimicrobial resistance (del Pozo and Patel 2007). Due to these factors, biofilms can be up to 1000 times more tolerant to antibiotics compared to planktonic bacteria (Srivastava and Bhargava 2016). The biofilm matrix also protects bacteria from the immune system by hindering the recognizable antigens present in bacterial cells (Parsek and Singh 2003). The detachment of single cells or clusters from the biofilm structure also contributes to the dissemination of bacterial cells, which may lead to infections in other parts of the body (Srivastava and Bhargava 2016).

Implantable medical devices have a massive global impact, in the order of hundreds of millions (Arciola, Campoccia and Montanaro 2018). Each year, more than a million cardiovascular electronic devices are implanted worldwide (McIntyre and Healey 2017). In the USA alone, >1 million knee and hip arthroplasty procedures are performed annually (Andersen *et al.* 2013). Despite the high use in the clinic, there are still complications associated to these devices, leading to their failure. In the past decades, different bacterial biofilms have been found to be a major cause of several infections associated to medical devices, such as orthopedic implants, catheters and pacemakers (Fig. 2). Among the most common biofilm-associated infections are osteomyelitis, endocarditis and urinary tract infections (Del Pozo 2018). These infections represent an economic burden for Healthcare Systems, leading to an increase in hospital stays as well as hospital-associated mortality (Bhattacharya *et al.* 2015). Onche *et al.* (2011)) estimated the costs associated with the removal of infected orthopedic implants to be $613.15 (USD) per patient, considering hospital costs and loss of work days. More recently, Otto (2014) reported that device-related biofilm infections add >$1 billion (USD) to hospitalization costs in the USA each year.

Nowadays, *S. aureus* is recognized by the Nosocomial Infections Surveillance System as one of the most frequent causes of nosocomial and community-acquired infections (Otto 2008; Lister and Horswill 2014). Among these, implant-associated infections are being highlighted due to the increasing number of multiple-antibiotic resistance cases and the high demand for indwelling prosthetic devices (Archer *et al.* 2011).

The global health and economic impact of *S. aureus* biofilm implant-associated infections represent a critical concern due to the current lack of an effective treatment and the increasing numbers of antibiotic-resistance bacterial strains. Thus, the World Health Organization considers *S. aureus* as a high priority pathogen for which new therapies should be developed (Tacconelli *et al.* 2018). This review provides an overview of the current therapy and its limitations, biofilm models available for preclinical validation of new therapeutic approaches and nanosystems as tools for the treatment of *S. aureus* biofilm implant-associated infections.

Downloaded from https://academic.oup.com/femsre/advance-article-abstract/doi/10.1093/femsre/fuz021/5550945 by Universidade do Porto user on 14 October 2019

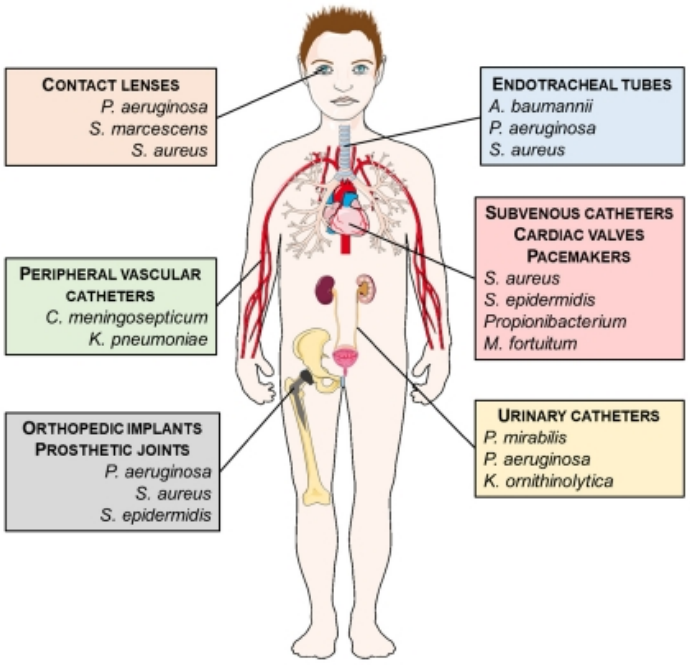


Figure 2. Medical devices associated to biofilm infections and the most prevalent bacterial species for each device (Nafee 2015; Srivastava and Bhargava 2016). *A. baumannii*, *Acinetobacter baumannii*; *C. meningosepticum*, *Chryseobacterium meningosepticum*; *K. ornithinolytica*, *Klebsiella ornithinolytica*; *K. pneumoniae*, *Klebsiella pneumoniae*; *M. fortuitum*, *Mycobacterium fortuitum*; *P. aeruginosa*, *Pseudomonas aeruginosa*; *P. mirabilis*, *Proteus mirabilis*; *S. aureus*, *Staphylococcus aureus*; *S. epidermidis*, *Staphylococcus epidermidis*; *S. marcescens*, *Serratia marcescens*. Figure adapted with the permission of Servier Laboratories.

CURRENT TREATMENT OF IMPLANT-ASSOCIATED *S. AUREUS* BIOFILM

Once a mature *S. aureus* biofilm is established at the surface of an implant, only a few treatment alternatives exist. The solution for these infections usually requires physical removal of the implant and surrounding infected tissue combined with antibiotic therapy (Bhattacharya *et al.* 2015).

The treatment of biofilm implant-associated infections commonly implies a surgical procedure, ranging from debridement with implant retention to implant removal (Bhattacharya *et al.* 2015). The first procedure is less invasive and less time-consuming than surgical removal of the implant. Unfortunately, retention of implants frequently leads to failure, requiring revision surgery combined with antibiotic therapy to solve the infection (Bhattacharya *et al.* 2015). Thus, replacement of the infected implant by a new one is currently the best option to eradicate a long-lasting mature biofilm.

Nowadays, due to the increasing impact of bacterial resistance, there is no consensus on the antibiotic that should be used (Sousa *et al.* 2010). Thus, the guidelines for antibiotic therapy are specific for the type of infection and depend on the antibiotic susceptibility of the *S. aureus* strains (Osmon *et al.* 2013).

Methicillin-resistant *S. aureus* (MRSA) has evolved from methicillin-susceptible *S. aureus* (MSSA) by acquisition of the gene *mecA* (WHO 2014). This gene mediates the production of a beta-lactamase enzyme that inactivates both beta-lactamase-stable drugs (e.g. methicillin and cloxacillin) and beta-lactamase inhibitors (e.g. sulbactam). Since its discovery, MRSA strains widely spread through all regions of the world. In 2014, the World Health Organization reported that 86% of the clinical isolates of *S. aureus* were resistant to methicillin (MRSA). Patients infected with MRSA have an increased mortality rate and require more healthcare resources than MSSA-infected patients, representing a high health and economic burden (WHO 2014). Furthermore, the treatment of MRSA infections may require second-line antibiotics, which are more expensive and have higher toxicity at a systemic level. Currently, antibiotics such as vancomycin and daptomycin are among the most commonly used drugs to treat MRSA infections (WHO 2014).

Vancomycin is a widely administered glycopeptide antibiotic for both MRSA and *S. aureus* biofilm-associated infections (Foster 2017). However, recent cases of vancomycin-intermediate and vancomycin-resistant *S. aureus* strains led to the need of combining vancomycin with other drugs, such as rifampicin or linezolid (Bhattacharya *et al.* 2015). More recently, antibiotics such as daptomycin are being suggested for the treatment of biofilm-associated infections once only few nonsusceptible bacterial isolates were reported (Gonzalez-Ruiz, Seaton and Hamed 2016). Daptomycin is a cyclic lipopeptide molecule characterized by a fast bactericidal effect against a wide range of Gram-positive pathogens, including multiresistant staphylococci isolates (Sader *et al.* 2014; Bhattacharya *et al.* 2015; Gonzalez-Ruiz, Seaton and Hamed 2016). The mechanism of action of daptomycin involves calcium-dependent insertion of the compound into the bacterial cytoplasmic membrane, promoting a fast disruption of the bacterial membrane (Gonzalez-Ruiz, Seaton and Hamed 2016; Foster 2017). However, the use of this antibiotic to eradicate bacterial biofilms requires several high-dose administrations (Gonzalez-Ruiz, Seaton and Hamed

Downloaded from https://academic.oup.com/femsre/advance-article-abstract/doi/10.1093/femsre/fuz021/5550945 by Universidade do Porto user on 14 October 2019

2016). Similar to other antibiotics, daptomycin faces the challenge of efficiently penetrating the biofilms matrix and reaching the bacterial cells. Consequently, the antibiotic is unable to reach bacterial cells deep within the biofilm structure at therapeutic concentrations, which may lead to antibiotic resistance phenomena. A detailed overview of the mechanisms of resistance to currently used antibiotics can be found elsewhere (Foster 2017).

To overcome the challenge of poor antibiotic penetration within the biofilms matrix, some research has been focusing on matrix disrupting agents. For instance, Siala *et al.* (2016) suggests the combination of an antifungal as a matrix inhibitor with antibiotics for an innovative approach to treat bacterial biofilms. However, the use of antifungals might affect the human fungal flora, which may limit the clinical use of this therapeutic approach.

Besides bacterial resistance, other drawbacks are also associated to the treatment against bacterial biofilms. Antimicrobial drugs are commonly administered through the oral route, with a poor bioavailability and efficacy of drugs (Pinto *et al.* 2017). Additionally, the systemic distribution of antibiotics leads to a lower concentration at the target site. Consequently, the treatment of bacterial infections usually requires high and repetitive doses, which may lead to adverse side effects. The efficacy of antimicrobial drugs can also be compromised by intrinsic factors, such as poor cellular penetration, limited intracellular retention, decreased intracellular activity and inefficient subcellular distribution (Pinto *et al.* 2017).

Overall and considering the high costs and discomfort of removal surgery and the increasing numbers of antibiotic resistance, the current available treatments are far from being ideal. Thus, novel effective therapies are urgently needed.

NANOTECHNOLOGY AS A NOVEL APPROACH FOR THE TREATMENT OF S. AUREUS BIOFILMS

The limitations and the inefficiency of the current therapy available against *S. aureus* biofilm implant-associated infections are prompting the research toward alternative strategies. Nanotechnology is a promising approach to treat biofilm-associated infections. Nanoparticles (NPs) are emerging as potential drug delivery systems due to their ability to maintain a sustained drug release at the target site, minimizing side effects and improving the therapeutic efficacy (Lopes *et al.* 2015; Nafee 2015). Additionally, some nanoparticles are being extensively studied for their intrinsic antimicrobial activity (Nafee 2015). Due to the characteristics of NPs, the use of nanotechnology in antimicrobial therapy decreases the potential development of bacterial resistance (Lopes *et al.* 2015).

In the last few decades, several nanosystems have been approved for clinical use in a variety of diseases, while many other nanoparticle formulations are under clinical trials (Zhang *et al.* 2010). A market analysis revealed that 67 nanodevices were identified in the market by January 2012, out of which 33 were associated to nanotherapeutics (Etheridge *et al.* 2013). In this analysis, 11 approved nanosystems with antimicrobial properties were reported (Etheridge *et al.* 2013). According to the BCC Research report, the market value of the worldwide nanomedicine industry was $214.2 billion (USD) in 2013 and $248.3 billion (USD) in 2014 (Evers 2015). By the year 2019, it is projected that the global market of nanomedicine reach $528 billion (USD) (Evers 2015).

NANOSYSTEMS PRECLINICAL VALIDATION: BIOFILM MODELS

The preclinical validation of nanosystems is a crucial step for further clinical trials and commercialization. Biofilm models are an important tool to evaluate the antibiofilm activity of nanosystems. Several *in vitro*, *ex vivo* and *in vivo* biofilm models have been developed for that purpose. Extensive reviews about biofilm models can be found in the literature (Peterson *et al.* 2011; Lebeaux *et al.* 2013).

In vitro biofilm models are widely used in research due to their simplicity and low cost (Fig. 3). These models mimic important characteristics of biofilms, such as gradients of nutrients and production and release of extracellular matrix (Lebeaux *et al.* 2013). Static systems (e.g. colony biofilm and calgary biofilm device) are fast and simple methods, amenable to high throughput screening. However, these models have limited nutrient flow and aeration. On the other hand, dynamic systems (e.g. flow cells) have constant replacement of nutrients and removal of dead cells and metabolic byproducts (Lebeaux *et al.* 2013). Additionally, it is possible to control environmental parameters of the systems and to perform nondestructive visualization of the biofilms by microscopy (Heydorn *et al.* 2000; Lebeaux *et al.* 2013). Nevertheless, dynamic systems are not well adapted for high throughput analysis and require specialized equipment and technical support (Lebeaux *et al.* 2013). More recently, complex systems based on the interactions between bacteria and the host were developed. These systems, microcosms, consider the complexity and heterogeneity of the *in vivo* environment.

Several *in vitro* assays based on pharmacodynamic parameters, biofilm morphology and biomass, cell viability and NPs–biofilm interactions have been extensively used on biofilm models (Fig. 3). The determination of the minimum inhibitory concentration (MIC) and of the minimum bactericidal concentration (MBC) are key pharmacodynamic parameters to study the efficiency of nanosystems against planktonic bacteria (Pinto *et al.* 2017). On the other hand, to assess the efficacy of nanosystems against bacteria within a biofilm structure, minimum biofilm inhibitory concentration (MBIC) and the minimum biofilm eradication concentration (MBEC) are used (Macia, Rojo-Molinero and Oliver 2014).

Besides these parameters, other *in vitro* studies can be performed to elucidate the potential of nanosystems for eradication of biofilms. For instance, biofilm morphological changes can be detected by microscopy techniques, namely, scanning electron microscopy (Meng *et al.* 2016; Siala *et al.* 2016), atomic force microscopy (Salunke *et al.* 2014) and fluorescence microscopy (Hou *et al.* 2017). The biofilm biomass can also be determined by *in vitro* assays, such as the crystal violet staining method (Boda *et al.* 2015; Thomas *et al.* 2015). Despite the importance of evaluating morphological changes and biofilm biomass, it is also essential to assess bacterial cell viability within the biofilm structure. For that purpose, a live/dead staining (Boda *et al.* 2015) or a resazurin assay (Guo *et al.* 2017a) can be performed. Additionally, epifluorescence studies are commonly used to evaluate the interactions between nanosystems and biofilms (Rivero Berti *et al.* 2016). The penetration of nanosystems within the biofilm can also be examined by confocal laser scanning microscopy (Siala *et al.* 2016).

In an effort to consider the complex environment of *in vivo* models in a controlled experimental condition, *ex vivo* models were developed (Fig. 4). *Ex vivo* models consist on extracting tissues or organs from an organism and place them in an artificial environment for further procedures (Lebeaux *et al.* 2013). These

Downloaded from https://academic.oup.com/femsre/advance-article-abstract/doi/10.1093/femsre/fuz021/5550945 by Universidade do Porto user on 14 October 2019

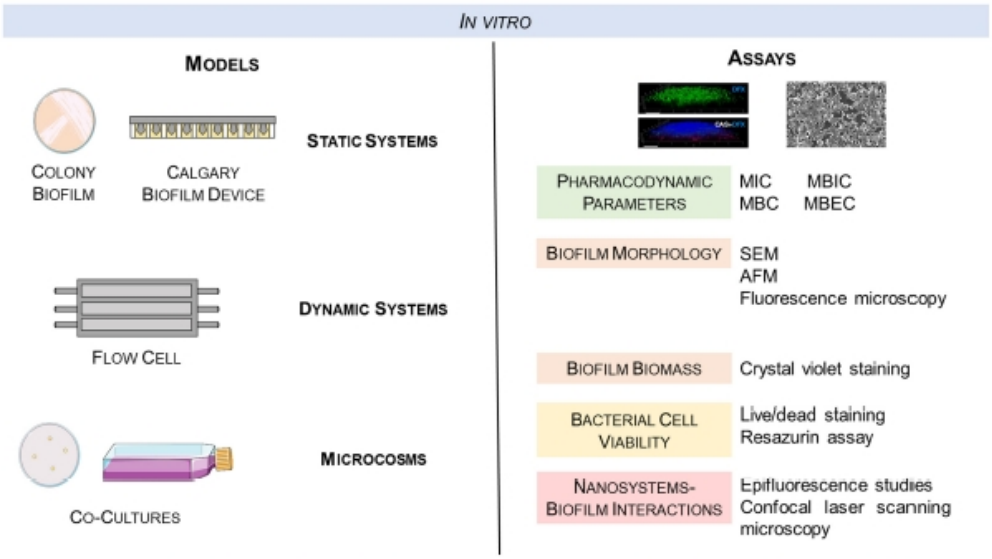


Figure 3. Schematic representation of *in vitro* biofilm models and the most common assays performed to evaluate the efficiency of antimicrobial agents against bacterial biofilms (Chen *et al.* 2012; Siala *et al.* 2016). AFM, atomic force microscopy; MBC, minimum bactericidal concentration; MBEC, minimum biofilm eradication concentration; MBIC, minimum biofilm inhibitory concentration; MIC, minimum inhibitory concentration; SEM, scanning electron microscopy. Microscopic images were reprinted with permission from Siala *et al.* 2016 (left) and Chen *et al.* 2012, American Chemical Society (right).

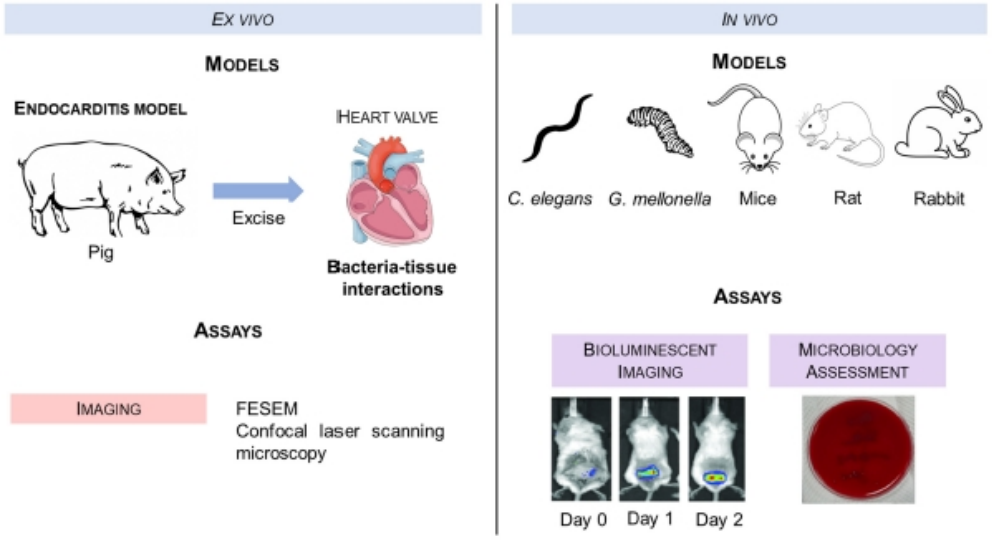


Figure 4. Schematic representation of *ex vivo* and *in vivo* biofilm models and respective examples of assays to evaluate the efficiency of antimicrobial agents against bacterial biofilms (Siala *et al.* 2016; Fang *et al.* 2017). *C. elegans*, *Caenorhabditis elegans*; FESEM, field emission scanning electron microscopy; *G. mellonela*, *Galleria mellonela*. Images from experimental assays were reprinted with permission from Siala *et al.* 2016 (left) and Fang *et al.* 2017 (right).

models are extremely useful for imaging and analysis of bacterial colonization of the organ or tissue of interest (Lebeaux *et al.* 2013).

Although *in vitro* and *ex vivo* studies are useful tools, they are still far from mimicking the *in vivo* conditions. Several *in vivo* models have been developed to study the toxicity and efficacy of antibacterial agents against biofilms. The most commonly used are mice (Meng *et al.* 2016) and rat (Sharma, Gupta and Gupta 2016). However, lower eukaryotes, such as *Caenorhabditis elegans* (Mizdal *et al.* 2018; Kannappan *et al.* 2019) and *Galleria mellonela* (Souza dos Santos *et al.* 2019), are attractive alternative biofilm infection models due to their simple methodology, which is an advantage for high throughput screenings. Thus, *in vivo* efficiency assays are required to validate the *in vitro* outcome. For instance, Siala *et al.* (2016) used *in vivo* bioluminescent live imaging to evaluate the activity of antimicrobial agents in mice for 7

Downloaded from https://academic.oup.com/femsre/advance-article-abstract/doi/10.1093/femsre/fuz021/5550945 by Universidade do Porto user on 14 October 2019

days. Additionally, microbiology assessment can be performed after sacrificing the *in vivo* models (Fang *et al.* 2017).

In the past decades, several nanotechnology-based systems that aimed to eradicate *S. aureus* biofilm-associated infections were studied using the previously mentioned *in vitro* and *in vivo* models. These novel nanosystems, their advantages and their limitations are going to be detailed in this review. An overview of the lipid, polymeric, metallic, magnetic, silica-based and quantum dots (QDs) systems that have been reported in the literature is provided.

LIPID-BASED NANOSYSTEMS

Liposomes

Liposomes are vesicles composed of a phospholipid bi- or multilayer with an aqueous core (Huh and Kwon 2011; Lopes *et al.* 2014). These vesicles are widely used delivery systems for antimicrobial agents due to their lipid bilayer structure that mimics the cell membrane (Huh and Kwon 2011). Consequently, they are able to easily fuse with infectious microbes, such as *S. aureus* (Huh and Kwon 2011). Additionally, both hydrophobic and hydrophilic drugs can be encapsulated within the biocompatible and biodegradable structure of liposomes (Lopes *et al.* 2014). Due to their advantages, liposomes are, by far, the main delivery system in the market (Huh and Kwon 2011). In this context, several studies are being developed with these carriers for *S. aureus* biofilms eradication (see Table 1).

Despite the promising results of liposomes as delivery systems to eradicate bacterial biofilms, their poor stability is still a concern. To overcome this limitation, surface modification of liposomes with stabilizer ligands is being investigated. For instance, calcium phosphate was used as a coating to improve the delivery capacity and the mechanical stability of liposomes (Rivero Berti *et al.* 2016). In this study, two dyes, acridine orange and 5,10,15,20-tetrakis(1-methyl-4-pyridinio)porphyrin (TMP), were loaded into the aqueous core of liposomes. Furthermore, the interaction of the calcium phosphate-coated liposomes and *S. aureus* was evaluated. Microscopy images showed that the calcium phosphate-coated vesicles remained adhered to the bacterial cell walls, even after intense washing treatment. Epifluorescence studies showed stained biofilms after a 2 h incubation with the liposomes. According to the authors, this indicates that upon contact of *S. aureus* biofilms and calcium phosphate-coated liposomes, there is a controlled release of the fluorophores (Rivero Berti *et al.* 2016). More recently, Hou *et al.* (2017) designed a gentamicin-loaded liposomal formulation with lysozyme surface functionalization. The cationic lysozyme was associated to the negatively charged liposome through electrostatic attraction. Besides stabilizing the vesicle, the functionalization also facilitated the interactions of the liposomes with the negatively charged matrix of the bacterial biofilm. The functionalization with lysozyme led to a zeta potential change from −54.5 to 17.5 mV. Additionally, it prevented undesirable drug release during storage. Besides, lysozyme-associated liposomes showed higher efficiency at preventing biofilm formation and disrupting preformed biofilms, when compared with gentamicin or lysozyme alone (Hou *et al.* 2017).

In the past few years, several ligands were used at the surface of liposomes to promote a targeted delivery of antimicrobial agents to biofilms. Hydrophobic derivates of mannan, such as cholesteryl mannan and sialo-mannan, were investigated by Vyas *et al.* (2007) when anchored at the surface of metronidazole-loaded liposomes. These ligands were obtained from the conjugation of mannan (hydrophilic) with hydrophobic anchors, which enables the polysaccharide to interact with the vesicle membrane. The main purpose of using mannan as ligands was to promote receptor-mediated uptake of liposomal contents into the vicinity of the biofilms. When tested against *S. aureus* biofilms, the mannosylated liposomes showed a percentage of bacterial growth inhibition of 98% for sialo-mannan-anchored, 86% for cholesteryl mannan-anchored and 70% for plain liposomes (Vyas, Sihorkar and Jain 2007). Similarly, *in vivo* results using a carboxymethylcellulose pouch infection model showed a higher efficiency of sialo-mannan-anchored liposomes (>3 log10 reduction) when compared with other formulations (Vyas, Sihorkar and Jain 2007). These findings suggest that sialo-mannan ligand mediates the interactions between the liposomes and the biofilm, leading to the release of the encapsulated drug, metronidazole, at the target site (Vyas, Sihorkar and Jain 2007).

In addition to the importance of targeting to increase drug release near the biofilm, ligands can simultaneously be used to promote an immune response. For instance, liposomes can be modified with wheat germ agglutinin (WGA) (Meng *et al.* 2016). WGA recognizes N-acetylglucosamine present in the biofilm matrix, promoting the interaction of liposomes with the bacterial cell walls and subsequent drug release (Cerca *et al.* 2006; Meng *et al.* 2016). Moreover, WGA contributes for an enhanced antibacterial activity of the immune system by binding to the surface of macrophages (Corradin, Buchmuller-Rouiller and Mauel 1991; Meng *et al.* 2016). This leads to enhanced phagocytosis of bacterial cells and upregulated expression of several cytokines (Corradin, Buchmuller-Rouiller and Mauel 1991; Meng *et al.* 2016). Nonmodified were compared with WGA-modified liposomal clarithromycin for antibiofilm activity against MRSA biofilms (Meng *et al.* 2016). The MIC values of the plain drug and the drug-loaded nonmodified liposomes were 64 $\mu g\ mL^{-1}$. This result shows that the entrapped drug in nonmodified liposomes could not enhance the antibacterial activity against MRSA, when compared to the free drug. However, drug-loaded WGA-modified liposomes showed a significant lower MIC value (16 $\mu g\ mL^{-1}$). Regarding eradication of *in vitro* preformed biofilm, only WGA-modified liposomes led to a significant decrease of biofilm, compared to the negative control (Meng *et al.* 2016). *In vivo* assays, where mice were injected intraperitoneally with 1×10^7 CFU, revealed a decrease of 16- to 24-fold of the viable bacteria that remained in the kidneys and the spleens of infected animals after being treated with WGA-modified liposomes, compared to the control group (Meng *et al.* 2016). Additionally, *in vitro* cellular uptake studies showed that phagocytosis of MRSA treated with WGA-modified liposomes was significantly higher than with the nonmodified vesicles. The targeted efficiency of WGA was further confirmed by *in vivo* biodistribution studies, in which the modified liposomes revealed a high affinity to the abdominal cavity. Therefore, liposomes modified with WGA showed an enhanced targeted delivery and immune response for therapeutic applications of abdominal infections (Meng *et al.* 2016).

Although several reports in the literature are focused on antibiotics encapsulation, natural compounds have recently been highlighted as promising alternatives to conventional antibacterial drugs, due to the increasing bacterial resistance phenomenon observed for the latter ones. Cui *et al.* (2016) designed liposomes to encapsulate cinnamon oil, a natural essential oil with antibacterial properties obtained from a plant resource. This compound interacts with microbial membranes due to its hydrophobicity, leading to their destruction (Mathew and Abraham 2006). Nevertheless, the chemical instability of

Downloaded from https://academic.oup.com/femsre/advance-article-abstract/doi/10.1093/femsre/fuz021/5550945 by Universidade do Porto user on 14 October 2019

Table 1: Lipid-based formulations developed to eradicate *S. aureus* biofilms.

Type of formulation	Formulation composition	Encapsulated compound	Physicochemical characteristics		Mechanism of action	Bacterial species/strains	Ref.
Liposomes	DOPA **Coating:** CaP	AO TMP	**Size (nm):** **EE (%):** AO liposomes TMP liposomes	200-400 18 -	Controlled drug release Enhanced liposomal stability	*S. aureus*	(Rivero Berti *et al.*, 2016)
	DPPC DPPG **Functionalization:** Lysozyme	Gentamicin	**Size (nm):** **Z. Potential (mV):**	~100 17.5	Enhanced liposomal stability Controlled drug release	*P. aeruginosa* *S. aureus*	(Hou *et al.*, 2017)
	Egg phosphatidylcholine, cholesterol, stearylamine **Functionalization:** CHM or SM	Metronidazole	**Size (nm):** CHM- anchored SM-anchored **PDI:** CHM- anchored SM-anchored **EE (%):** CHM- anchored SM-anchored	 454 ± 42 467 ± 51 0.124 0.143 31.7 ± 2.5 30.9 ± 3.1	Targeted delivery	*S. aureus*	(Vyas *et al.*, 2007)
	Soy phosphatidylcholine, cholesterol, DC-Chol, DSPE-PEG2000 **Functionalization:** wheat germ agglutinin	Clarithromycin	**Size (nm):** **PDI:** **Z. Potential (mV):** **EE (%):** **LC (%):**	112.9 ± 0.49 0.184 ± 0.011 23.9 ± 2.7 97.8 ± 7.1 1.23 ± 0.12	Targeted delivery Enhanced phagocytosis of microbial cells	MRSA	(Meng *et al.*, 2016)
	Soy lecithin, cholesterol	Cinnamon oil	**Size (nm):** **PDI:** **Z. Potential (mV):** **EE (%):**	144.3 ± 1.08 0.230 ± 0.0012 -54.7 ± 2.01 29.20 ± 1.45	Enhanced chemical stability Enhanced antimicrobial activity	MRSA	(Cui *et al.*, 2016)
Quatsomes	Cholesterol CPC	-	**Size (nm):** **PDI:** **Z. Potential (mV):**	90-100 < 0.3 70-80	Enhanced antimicrobial activity	*S. aureus*	(Thomas *et al.*, 2015)
Solid lipid Nanoparticles	Stearic acid Tristearin Soya lecithin **Surfactant:** Poloxamer 188	Cefuroxime axetil	**Size (nm):** **PDI:** **Z. Potential (mV):** **EE (%):**	279.2 ± 28.5 0.107 ± 0.07 -23.58 70.62 ± 0.82	Enhanced bioavailability Enhanced antimicrobial activity	*S. aureus*	(Singh *et al.*, 2014)
	Stearic acid Tristearin Soya lecithin **Surfactant:** Pluronic F-68	Clarithromycin	**Size (nm):** **PDI:** **Z. Potential (mV):** **EE (%):** **LC (%):**	307 ± 23 0.21 ± 0.04 -29 ± 5 84 ± 9 6.5 ± 0.9	Enhanced oral bioavailability Controlled release	*S. aureus*	(Sharma *et al.*, 2016)
Micelles	Biosurfactant from *Corynebacterium zerosis* NS5	-	**CMC (mg L^{-1}):** **Emulsification index (%):**	25 61	Enhanced biocompatibility Enhanced antimicrobial activity	*E. coli* *P. aeruginosa* *S. aureus* *S. mutans*	(Dalili *et al.*, 2015)
Nanodroplets	DPPC DSPE-PEG2000 Perfluoropentane	-	**Size (nm):** **PDI:** **Z. Potential (mV):**	309 ± 67 0.18 ± 0.09 -16.0 ± 3.6	Enhanced antimicrobial activity	MRSA	(Guo *et al.*, 2017)

Abbreviations: 1,2-dioleoyl-*sn*-glycero-3-phosphate (DOPA), 1,2-dipalmitoyl-*sn*-glycero-3-phosphocholine (DPPC), 1,2-dipalmitoyl-*sn*-glycero-3-phosphor-(10-rac-glycerol) (DPPG), 1,2-distearoyl-*sn*-glycero-3-phosphoethanolamine-N- [methoxy(polyethylene glycol)-2000] (DSPE-PEG2000), 5,10,15,20-tetrakis(1-methyl-4-pyridinio)porphyrin (TMP), acridine orange (AO), calcium phosphate (CaP), cetylpyridinium chloride (CPC), cholesteryl 3β-N-di-methyl-amino-ethyl-carbamate hydrochloride (DC-Chol), cholesteryl mannan (CHM), critical micelle concentration (CMC), encapsulation efficiency (EE), *Escherichia coli* (*E. coli*), loading capacity (LC), methicillin-resistant *Staphylococcus aureus* (MRSA), polydispersity index (PDI), *Pseudomonas aeruginosa* (*P. aeruginosa*), sialo-mannan (SM), *Staphylococcus aureus* (*S. aureus*), *Streptococcus mutans* (*S. mutans*), zeta potential (Z. Potential).

cinnamon oil hinders its application for health purposes (Cui *et al.* 2016). Thus, cinnamon oil was encapsulated into liposomes to reduce its chemical instability and to improve its antibacterial activity. To assess its *in vitro* antibiofilm efficiency, the liposomal formulation was incubated for 24 h with MRSA biofilms previously established on different material surfaces (stainless steel, gauze, nylon membrane and nonwoven fabrics). In all tested materials, a significant reduction of MRSA was observed when compared with free cinnamon oil. Specifically, the treatment of biofilms formed on stainless steel with free cinnamon

Downloaded from https://academic.oup.com/femsre/advance-article-abstract/doi/10.1093/femsre/fuz021/5550945 by Universidade do Porto user on 14 October 2019

oil reduced the amount of MRSA viable cells by 1.49 logs, while the treatment with loaded liposomes reduced this number by 2.45 logs (Cui *et al.* 2016). Microscopic analysis showed reduced thickness and sizes of MRSA biofilms after treatment with the liposomal formulation (Cui *et al.* 2016). Thus, the improved chemical stability of cinnamon oil after encapsulation into liposomes led to an enhancement of its antibiofilm activity.

Quatsomes

Inspired by liposomes, other structures, such as quatsomes, were developed for delivery purposes. Quatsomes are unilamellar vesicles composed of quaternary ammonium surfactants and sterols (Grimaldi *et al.* 2016). These structures are stable during a long storage time and homogenous regarding size, lamellarity and membrane organization. Similar to liposomes, both hydrophilic and hydrophobic drugs can be encapsulated within quatsomes structure. Thus, these novel systems are a promising alternative to overcome the low stability of structures such as liposomes (Grimaldi *et al.* 2016).

Quatsomes obtained from the self-assembly of equimolar ratios of cetylpyridinium chloride (CPC) and cholesterol were developed by Thomas *et al.* (2015) aiming the eradication of *S. aureus* biofilms (see Table 1). CPC is an antiseptic quaternary ammonium compound, composed of a lipophilic tail and a positively charged head group (Gilbert and Moore 2005). This composition facilitates the interaction of CPC with the negatively charged bacterial surface, leading to bacterial cell lysis (Gilbert and Moore 2005). In this study, the CPC quatsomes were compared with CPC micelles for their antibacterial activity (Thomas *et al.* 2015). CPC quatsomes showed *in vitro* a dose-dependent antibacterial effect, with >99% biofilm killing at the CPC concentration of 0.5% (Thomas *et al.* 2015). At lower concentrations, CPC quatsomes revealed a significantly lower efficiency than CPC micelles. In fact, CPC micelles showed 80–90% of efficiency against *S. aureus* biofilms at a CPC concentration of 0.05% and 0.1%. Higher CPC concentrations resulted in almost complete bacteria killing within the biofilm. The authors suggest that this effect may result from the penetration of the micellar formulation into the biofilm, while CPC quatsomes are mostly present at the surface of the biofilm. To evaluate the safety of the both CPC micelles and quatsomes, epithelial toxicity studies using lactate dehydrogenase were performed. At all CPC concentrations tested (from 0.05% to 1.0%), both formulations showed no cytotoxicity on the NuLi-1 human airway epithelial cell line. In conclusion, the main goal of this research work is to highlight the potentiality of quatsomes as a safe new drug delivery system (Thomas *et al.* 2015). Despite their potential, further research to optimize quatsomes for drug delivery purposes is required.

Solid lipid nanoparticles

Lipid nanoparticles have been recently highlighted due to their ability to enable a controlled drug release and to be cost effective and easily scaled-up (Battaglia and Gallarate 2012; Severino *et al.* 2012). Lipid NPs are usually composed of a matrix of physiological or physiologically related lipids characterized by their versatility, biocompatibility and biodegradability (Pardeike, Hommoss and Müller 2009; Das and Chaudhury 2011; Battaglia and Gallarate 2012). In addition, these NPs are able to incorporate either hydrophobic or hydrophilic drugs (Abed and Couvreur 2014). Different types of lipid NPs have been engineered, such as solid lipid nanoparticles (SLNs) and nanostructured lipid carriers (Ali Khan *et al.* 2013). Until this moment, in the context of biofilm treatment, only SLNs studies have yet been reported. SLNs are composed of a matrix of lipids in a solid state at both room and body temperatures (Severino *et al.* 2012).

Nowadays, antibiotics such as clarithromycin and cefuroxime axetil have been widely used against a vast variety of pathogens, including *S. aureus*. However, both antimicrobial agents have a poor systemic bioavailability (Singh *et al.* 2014; Sharma, Gupta and Gupta 2016). To overcome this drawback, SLNs have been engineered (see Table 1).

Singh *et al.* (2014) developed cefuroxime-loaded SLNs to treat *S. aureus* biofilms. The SLNs were produced and optimized to achieve a small particle size, a narrow polydispersity index and a high encapsulation efficiency (see Table 1). *In vitro* drug release studies at pH 6.8 indicated a prolonged and sustained release, since the lipid formulation showed 54% of drug diffusion in 2 h and 96% in 12 h. Under the same experimental conditions, 99% of free drug was released in the first 2 h. The optimal formulation showed an MBIC of 40 $\mu g\ mL^{-1}$, whereas the free drug had an MBIC of 80 $\mu g\ mL^{-1}$ (Singh *et al.* 2014). According to the authors, the lower MBIC suggests a superior antibiofilm activity of the drug when encapsulated into SLNs, which may be due to the nanoscale effect combined with the enhanced biofilm penetration of lipid NPs (Singh *et al.* 2014). Despite the promising findings, this work lacks *in vivo* studies for further elucidation of the formulation potential for a therapeutic application.

With the same purpose, Sharma, Gupta and Gupta (2016) designed SLNs encapsulating clarithromycin. For the formulation optimization, three different surfactants were tested: poly vinyl alcohol, Pluronic F-68 and Tween 80. The formulation containing Pluronic F-68 showed the smaller particle size with higher encapsulation efficiency. These findings support the hypothesis that Pluronic F-68 provides a higher mechanical and thermodynamic stability than poly vinyl alcohol and Tween 80, which prevents the coalescence of the particles (Lee, Choi and Park 2008; Peltonen and Hirvonen 2010; Sharma, Gupta and Gupta 2016). Consequently, Pluronic F-68 was selected for the optimization process (Sharma, Gupta and Gupta 2016). Additionally, stearic acid with tristearin was used to enhance the encapsulation efficiency during the optimization process. The optimized formulation (see Table 1) exhibited a controlled drug release behavior, with only 34% of drug diffusion after 3.5 h, while 99% of free drug was released in the same conditions. Furthermore, the optimized formulation showed to be 12 times more effective than the free drug against a *S. aureus* strain (MTCC86), *in vitro*. The efficiency of the formulation was also verified against *S. aureus* biofilms. Complete *in vitro* biofilm eradication was obtained at a drug concentration of 40 $\mu g\ mL^{-1}$ for the optimized formulation, whereas 140 $\mu g\ mL^{-1}$ of free drug was required to achieve the same effect (Sharma, Gupta and Gupta 2016). According to the authors, the higher efficiency of the SLNs is probably due to a sustained drug delivery profile and the adherence/adsorption of these particles to the bacterial cell walls (Sharma, Gupta and Gupta 2016). To evaluate the *in vitro* cytotoxicity of the SLNs, a macrophage (J774A.1) cell line was used and the SLNs showed no cytotoxicity at a drug concentration of 48 $\mu g\ mL^{-1}$, which is higher than the MBIC of the formulation. *In vivo* studies in wistar rats showed that a dose equivalent to 10 mg per kg of body weight did not cause toxic effects after an oral administration. Moreover, the *in vivo* pharmacokinetic profile of the SLNs revealed an almost 5-fold improvement of clarithromycin oral bioavailability comparing to the free drug (Sharma, Gupta and Gupta 2016). The superior antibacterial activity and oral bioavailability of clarithromycin encapsulated into SLNs combined with the safety of the nanosystem may lead

Downloaded from https://academic.oup.com/femsre/advance-article-abstract/doi/10.1093/femsre/fuz021/5550945 by Universidade do Porto user on 14 October 2019

to an improved drug efficiency. Overall, these studies support the evidence of lipid NPs as delivery systems with potential to enhance the therapeutic effect of drugs for the treatment of bacterial biofilms.

Micelles

Micelles are structures composed of amphiphilic molecules (Letchford and Burt 2007). When in an aqueous solution, these molecules self-assemble into micelles above a specific concentration, the critical micelle concentration. In a micelle, amphiphilic molecules organize their hydrophobic regions to create an inner core, where lipophilic drugs can be loaded (Letchford and Burt 2007). Dalili *et al.* (2015) isolated a novel cyclic lipopeptide from *Corynebacterium xerosis* NS5, named coryxin which consists of a heptapeptide and a β-hydroxy fatty acid with 11 carbon atoms (see Table 1). The low critical micelle concentration of coryxin (25 mg L^{-1}) revealed the high efficiency of this biosurfactant. Furthermore, the antibacterial and the antibiofilm efficacy of the isolated coryxin was evaluated through *in vitro* studies against *Pseudomonas aeruginosa*, *Escherichia coli*, *S. aureus* and *Streptococcus mutans*. The biosurfactant exhibited antimicrobial activity against all strains, with MIC values of 0.19 mg mL^{-1} against *S. aureus* and *S. mutans* and MIC values of 3.12 and 100 mg mL^{-1} for *E. coli* and *P. aeruginosa*, respectively (Dalili *et al.* 2015). Regarding its antibiofilm activity, coryxin (100 mg mL^{-1}) was able to disrupt 1-day old biofilms from all tested strains, by 83%, 80%, 66% and 30% for *S. aureus*, *Streptococcus mutans*, *E. coli* and *P. aeruginosa*, respectively. According to these results, Gram-positive bacteria were more sensitive to the biosurfactant effect than Gram-negative bacteria, which the authors claim is probably due to the differences in the bacterial membrane structure (Dalili *et al.* 2015). Due to its nature, coryxin and other biosurfactants are biocompatible and nontoxic, contrary to chemically synthesized surfactants (Dusane *et al.* 2011; Dalili *et al.* 2015). Besides being a lipopeptide, coryxin easily modifies the bacterial surface hydrophobicity and, consequently, interferes with the bacterial adhesion to medical devices (Pecci *et al.* 2010; Dalili *et al.* 2015). Thus, the use of biosurfactants to treat *S. aureus* biofilms adhered to medical devices may be a promising, effective and safe alternative to the current therapy.

Nanodroplets

Besides the well-known NPs previously described, other nanotechnology-based structures have been researched. Recently, Guo *et al.* (2017a) designed novel stimulated phase-shift acoustic nanodroplets (NDs) in combination with vancomycin for an efficient MRSA biofilm eradication. The lipid phase-shift NDs consisted of a lipid shell of 1,2-dipalmitoyl-*sn*-glycero-3-phosphocholine (DPPC) and 1,2-distearoyl-*sn*-glycero-3-phosphoethanolamine-*N*-[methoxy(polyethylene glycol)-2000] (DSPE-PEG2000) and a liquid core of condensed perfluoropentane (Guo *et al.* 2017a). NDs undergo a phase transition to gaseous bubbles (acoustic droplet vaporization) when they are exposed to an ultrasound or thermal energy threshold (Kripfgans *et al.* 2000; Rapoport *et al.* 2009). It is hypothesized that the generated bubbles may cause mechanical effects in tissues or cells after cavitation (Pajek *et al.* 2014). The NDs treated sequentially with low-intensity pulsed ultrasound and heating (37°C) achieved vaporization and cavitation (Guo *et al.* 2017a). Furthermore, the combined effect of NDs and vancomycin was evaluated against established MRSA biofilms. This combined effect promoted a stronger destruction on the biofilm structure and a higher bacterial death than NDs or vancomycin alone, which was verified by microscopy and a resazurin assay. The authors suggest that NDs detach the biofilm structure, which promotes a closer contact of vancomycin with the bacteria (Guo *et al.* 2017a). Thus, stimulated phase-shift acoustic NDs are a potential antibiofilm strategy, when combined with traditional antibacterial agents.

POLYMERIC-BASED NANOSYSTEMS

Polymeric nanoparticles

Polymeric NPs are composed of biodegradable polymers and are characterized by a high structural integrity. Hence, they can increase the stability of any volatile drug, promoting its controlled release (Kayser, Lemke and Hernandez-Trejo 2005). Besides, they are easy to scale-up, are cost effective and have a high stability during storage (Kayser, Lemke and Hernandez-Trejo 2005, El-Say and El-Sawy 2017).

Among a wide range of polymers, poly(lactic-*co*-glycolic acid) (PLGA) is the most commonly used for drug delivery purposes due to its biocompatibility and biodegradability (Huh and Kwon 2011). Several studies reported the use of PLGA micro- and nanoparticles for antibiotic delivery to bacterial biofilms. In the study performed by Thomas *et al.* (2016), micro- and nanoparticles encapsulating ciprofloxacin were designed to overcome the low bioavailability of this drug and its tolerance by biofilms. The different surface areas of micro- and nanoparticles led to a significant difference in the loading capacity values (see Table 2). The lower loading capacity of NPs can also be associated to a high energy input required to produce these particles, which may facilitate drug leakage (Thomas *et al.* 2016). Both micro- and nanoparticles showed identical release profiles, with 50–60% of ciprofloxacin release in the first 24 h and complete drug release within 5 days. The MBEC was evaluated using 5-day old *S. aureus* and *P. aeruginosa* biofilms and was lower for the free drug compared to the MBEC of both micro- and nanoparticles, after 24 h incubation at 37°C (Thomas *et al.* 2016). For *S. aureus*, the MBEC values were 128 and >256 μg mL^{-1} for free drug and encapsulated drug, respectively. This result was expected as the particles showed a time-dependent drug release, with an incomplete release within 24 h (Thomas *et al.* 2016). The antibiofilm performance of free drug and encapsulated drug during a treatment of 6 days was also evaluated. The sustained drug release by both micro- and nanoparticles contributed to a higher efficiency in the eradication of *S. aureus* biofilms, compared to the repeated administration of free drug under the same conditions. Based on these results, the authors claim that both types of particles revealed a high potential to a local treatment of biofilms once sustained antibiotic concentrations are locally achieved and, consequently, systemic adverse effects are expected to be minimized, although this was not studied (Thomas *et al.* 2016).

Despite that several studies reported successful eradication of bacterial biofilms using uncoated polymeric NPs, evidence shows that functionalization of their surfaces with specific ligands, making them targeted delivery systems or promoting a faster recovery from the infection, increases their efficiency (Huh and Kwon 2011). For instance, Bastari *et al.* (2014) showed the potential of a ceramic–polymer hybrid system for osteomyelitis, by providing a controlled drug release and promoting bone regeneration. In this study, biodegradable PLGA NPs coated with calcium phosphate to accelerate the bone healing process were developed and loaded with either nafcillin or levofloxacin (see Table 2). Due to the higher potency of levofloxacin

Downloaded from https://academic.oup.com/femsre/advance-article-abstract/doi/10.1093/femsre/fuz021/5550945 by Universidade do Porto user on 14 October 2019

Table 2: Polymeric-based formulations developed to eradicate *S. aureus* biofilms.

Type of formulation	Formulation composition	Encapsulated compound	Physicochemical characteristics		Mechanism of action	Bacterial species/strains	Ref.
Polymeric Nanoparticles	PLGA PVA	Ciprofloxacin	**Size:** NPs (nm) MPs (μm) **PDI:** NPs MPs **Z Potential (mV):** NPs MPs **EE (%):** NPs MPs **LC (%):** NPs MPs	 300 ± 0.06 12 ± 1.7 0.14 0.40 -4.1 ± 0.4 -4.5 ± 0.1 96 55 4.3 ± 0.3 7.5 ± 0.6	Enhance drug bioavailability Reduction of side effects Controlled release	*P. aeruginosa* *S. aureus*	(Thomas *et al.*, 2016)
	PLGA PEMA **Coating:** CaP	Nafcillin Levofloxacin	**Size (μm):** **EE (%):** Nafcillin Levofloxacin	25 – 50 59.4 ± 6.2 49.2 ± 7.6	Controlled drug release Promote bone regeneration	*S. aureus*	(Bastari *et al.*, 2014)
	Chitosan TPP	Oxacillin DNase I	**Size (nm):** **PDI:** **Z Potential (mV):** **LC (%):**	166.7 0.179 +8.3 6.65	Enhance antibiofilm activity by targeting the biofilm's matrix Enhance antimicrobial activity Controlled drug release	*S. aureus*	(Tan *et al.*, 2018)
Dendrimers	PAMAM **Functionalization:** C_{16}-DABCO Mannoside	-	**Z Potential (mV):**	Positive	Enhanced antimicrobial activity	*B. cereus* *E. coli* *P. aeruginosa* *S. aureus* *S. oralis*	(VanKoten *et al.*, 2016)
	PAMAM **Functionalization:** Epoxybutane or epoxyhexane	Nitric oxide	**Payload (μmol mg^{-1}):**	~1.0	Enhanced antibiofilm activity	MRSA *P. aeruginosa* *S. aureus*	(Worley *et al.*, 2015)

Abbreviations: 4-aza-1-hexadecyl-azoniabicylo-[2.2.2]octane (C_{16}-DABCO), *Bacillus cereus* (*B. cereus*), calcium phosphate (CaP), deoxyribonuclease I (DNase I), encapsulation efficiency (EE), *Escherichia coli* (*E. coli*), loading capacity (LC), methicillin-resistant *Staphylococcus aureus* (MRSA), microparticles (MPs), nanoparticles (NPs), poly (amidoamine) (PAMAM), poly (ethylene-alt-maleic anhydride) (PEMA), poly(lactic-co-glycolic acid) (PLGA), polyanionic sodium triphosphate (TPP), polydispersity index (PDI), polyvinyl alcohol (PVA), *Pseudomonas aeruginosa* (*P. aeruginosa*), *Staphylococcus aureus* (*S. aureus*), *Streptococcus oralis* (*S. oralis*), zeta potential (Z. Potential).

against *S. aureus* and the superior loading capacity and controlled drug release of levofloxacin than nafcillin, the first formulation was used for biofilm inhibition and deterioration studies (Bastari *et al.* 2014). Both coated and uncoated levofloxacin-loaded NPs prevented biofilm formation for >4 weeks and completely eradicated an established biofilm after 7 days of treatment. Thus, levofloxacin-loaded NPs have a high potential for both prevention and eradication of *S. aureus* biofilms associated to osteomyelitis.

Besides PLGA, other polymers such as chitosan are widely used in pharmaceutical and medical applications. Chitosan is a derivate of chitin and presents biocompatible and biodegradable properties and it has been reported that chitosan also shows antibacterial activity itself (Jayakumar *et al.* 2010). Due to these properties, Tan *et al.* (2018) produced chitosan NPs for the co-delivery of an antibacterial agent (oxacillin) and a biofilm matrix disruptive agent (Deoxyribonuclease I). Deoxyribonuclease I (DNase I) was selected for this purpose since it breaks the extracellular DNA, which is one of the key components of the biofilm's matrix (Montanaro *et al.* 2011). The antibacterial and antibiofilm activities of the DNase-oxacillin NPs against *S. aureus* were evaluated. This formulation revealed an MIC value of 1 μg mL^{-1}, while free oxacillin showed an MIC value of 0.5 μg mL^{-1} (Tan *et al.* 2018). The authors claim that this result is probably due to a controlled drug release from the NPs. However, DNase-oxacillin NPs exhibited higher antibiofilm activity than the free drug against mature biofilms. The antibiofilm effect with repeated treatment for 2 days was also assessed and the higher concentration of free drug and DNase-oxacillin NPs revealed a biofilm reduction of 92.3% and 100%, respectively. Additionally, the DNase-oxacillin NPs did not show any cytotoxic effects against a human immortalized keratinocytes (HaCaT) cell line (Tan *et al.* 2018).

Dendrimers

Dendrimers are hyperbranched polymers synthetized layer-by-layer around a core unit (Huh and Kwon 2011). Consequently, these structures have a high surface area to size ratio, leading to great reactivity to bacteria *in vivo*. Both hydrophilic

Downloaded from https://academic.oup.com/femsre/advance-article-abstract/doi/10.1093/femsre/fuz021/5550945 by Universidade do Porto user on 14 October 2019

and hydrophobic drugs can be loaded within the dendrimers structure. Besides, a high density of functional groups can be added to these structures for a targeted delivery (Huh and Kwon 2011).

In an attempt to inhibit and eradicate bacterial biofilms, fourth-generation poly(amidoamine) (PAMAM) dendrimers were developed by VanKoten *et al.* (2016) (see Table 2). These dendrimers were decorated with a quaternary ammonium compound, 4-aza-1-hexadecylazoniabicylo-[2.2.2]octane (C_{16}-DABCO), which is a cationic surfactant with antibacterial activity (McDonnell and Russell 1999). Additionally, mannoside end groups were added to the dendrimeric structure to promote interactions with the bacterial cell wall (VanKoten *et al.* 2016). The antibacterial activity of these dendrimers was compared with the C_{16}-DABCO monomer to evaluate the effect of multivalency on the MIC values. For all tested Gram-positive (*Streptococcus oralis*, *S. aureus* and *Bacillus cereus*) and Gram-negative (*P. aeruginosa* and *E. coli*) strains, the MIC value is at least 10-fold higher for the monomer than for the dendrimeric structure. The authors claim that this discrepancy is probably due to the dendrimers native cations that interact with surface-associated adhesion molecules from bacteria (VanKoten *et al.* 2016). Despite the promising results against planktonic bacteria, disruption was not observed when the dendrimers were evaluated in previously established biofilms. According to the authors, the lack of efficiency against mature biofilms is possibly due to the dendrimers' large size, which hinders their penetration into the matrix of the biofilm and are restricted to the biofilm surface (VanKoten *et al.* 2016). Besides, the dendrimers showed toxicity in hemolysis assays and in a cytotoxic assay using the A549 human lung carcinoma cell line, at concentrations within the same order of magnitude as the MIC values assessed for the studied bacterial strains (VanKoten *et al.* 2016). The authors believe that this result indicates a broad activity of the dendrimers on both bacterial and mammalian cells. Despite the antibacterial activity of these dendrimers, their safety and antibiofilm activity need to be improved for therapeutic applications.

To overcome the low penetration efficiency of dendrimers into bacterial biofilms, nitric oxide (NO)-releasing PAMAM dendrimers were designed by Worley, Schilly and Schoenfisch (2015) (see Table 2). NO free radical has a wide range of antibacterial activity due to the production of reactive products that promote bacterial membrane disruption (Fang 1997). The designed NO-releasing PAMAM dendrimers were functionalized with butyl and hexyl chains (Worley, Schilly and Schoenfisch 2015). The efficiency of the dendrimers was evaluated against bacterial biofilms, namely of *P. aeruginosa*, *S. aureus* and MRSA. The biofilms were grown on medical-grade silicon rubber substrates and further exposed to the dendrimers for 24 h. Hexyl-modified dendrimers were undoubtedly more effective at biofilm eradication than the butyl systems. Thus, it is hypothesized by the authors that the hexyl-modified dendrimers penetrate deeper into the biofilm at a faster rate and promote higher cell membrane damage due to a longer alkyl chain (Worley, Schilly and Schoenfisch 2015). The NO release from hexyl-modified dendrimers did not show an improvement in antibiofilm efficacy. This result suggests that a significant membrane damage promoted by the hexyl chains precludes the achievement of intracellular NO to bactericidal concentrations (Worley, Schilly and Schoenfisch 2015). In the case of butyl-modified dendrimers, NO-releasing dendrimers have a higher biocidal action than those without NO. Additionally, it was verified that increasing the dendrimer generation from G1 to G2 or G3 increases the eradication efficiency of the butyl-modified dendrimers due to a higher functional group density. Regarding the bacterial strains, hexyl-modified dendrimers exhibited a higher activity against *P. aeruginosa* biofilms, disregarding of the dendrimer generation. Both types of dendrimers revealed similar bactericidal action against MRSA biofilms, requiring higher eradication concentrations than nonresistant *S. aureus* (Worley, Schilly and Schoenfisch 2015). Thus, the efficacy of the dendrimers depends on their alkyl chain length, the dendrimer generation and the bacterial strain. Nevertheless, only the G3 hexyl dendrimer system efficiently eradicated biofilms at concentrations below the inhibitory concentration at 50% viability (IC_{50}) against L929 mouse fibroblasts cell line (Worley, Schilly and Schoenfisch 2015). Due to its efficiency and safety, this dendrimer is the most promising option for biomedical applications.

METALLIC-BASED NANOSYSTEMS

Metallic nanoparticles

Metallic NPs can be applied as drug delivery systems once they can protect the drugs until their target site and avoid the immune system activation with low cytotoxicity (Lopes *et al.* 2014). Additionally, many metallic NPs have been studied for their intrinsic antimicrobial effect and the unlikely development of bacterial resistance to these type of NPs (Lopes *et al.* 2014). A summary of the metallic NPs developed for *S. aureus* biofilm eradication is shown in Table 3.

Gold and silver NPs are among the most commonly researched types of metallic NPs, with several literature articles focusing on their antimicrobial activity against planktonic and biofilm bacteria. Additionally, these NPs are easily functionalized with ligands, which contributes in enhancing their biocompatibility and chemical stability.

Boda *et al.* (2015) developed ultrasmall AuNPs functionalized with triphenylphosphine-monosulfonate. The triphenylphosphine-monosulfonate shell was added to the Au core of the NPs to improve their stability. The AuNPs with core diameters of 0.8 and 1.4 nm (Au0.8MS and Au1.4MS) were evaluated against *S. aureus*, *Staphylococcus epidermidis*, *E. coli* and *P. aeruginosa in vitro*. The AuNPs caused acute toxicity to planktonic bacteria, with a 5-log reduction in viable cells after 5 h of exposure (Boda *et al.* 2015). Regarding staphylococci, AuNPs caused membrane blebbing and cell swelling, which was observed by scanning electron microscopy, suggesting membrane damage and eventual cell lysis. Mature staphylococci biofilms of 48 h were treated with Au0.8MS and Au1.4MS, showing 80% reduction in bacterial viability when compared with the untreated bacteria (Boda *et al.* 2015). However, *Staphylococcus epidermidis* biofilms were less sensitive to the toxicity of AuNPs than *S. aureus* biofilms since no significant biomass reduction was obtained when such biofilms were treated. In this context, further studies regarding the efficiency of AuNPs against staphylococcal biofilms are needed.

Despite their potential for biomedical applications, chemical synthesis of metallic NPs is a concern due to the use of organic solvents, toxic compounds and the existence of hazardous by-products (Abou El-Nour *et al.* 2010; Singh *et al.* 2016). To overcome these limitations, a simple, rapid and eco-friendly methodology has emerged. The green synthesis relies on the use of compounds from microorganisms and plant extracts to reduce and to stabilize the NPs during their preparation, acting as reducing and capping agents (Abou El-Nour *et al.* 2010; Singh *et al.* 2016).

Downloaded from https://academic.oup.com/femsre/advance-article-abstract/doi/10.1093/femsre/fuz021/5550945 by Universidade do Porto user on 14 October 2019

Table 3: Metallic-based formulations developed to eradicate *S. aureus* biofilms.

Type of formulation	Formulation composition	Encapsulated compound	Physicochemical characteristics		Mechanism of action	Bacterial species/strains	Ref.
Metallic Nanoparticles	Gold **Coating:** TPPMS	-	**Size (nm):** Au0.8MS Au1.4MS	0.8 1.4	Enhanced antimicrobial activity	*S. aureus* *S. epidermidis*	(Boda *et al.*, 2015)
	Silver *Bombyx mori* silk fibroin	-	**Size (nm):**	12 ± 2	Enhanced chemical stability	MRSA	(Fei *et al.*, 2013)
	Silver Tea (*Camelia sinensis* L.) leaf extract	-	**Size (nm):**	20	Enhanced chemical stability	*E. coli* *S. aureus*	(Goswami *et al.*, 2015)
	Silver Leaves extract of *Convolvulus arvensis*	-	**Size (nm):** **PDI:**	28 0.2	Enhanced chemical stability	*P. aeruginosa* *S. aureus*	(Hamedi *et al.*, 2017)
	Gold or Silver Root extract of Korean red ginseng	-	**Size (nm):** Ag NPs Au NPs **PDI:** Ag NPs Au NPs	83 183 0.190 0.159	Enhanced chemical stability	*P. aeruginosa* *S. aureus*	(Singh *et al.*, 2016)
	Gold Silver Root extract of *Plumbago zeylanica*	-	**Size (nm):** **Z. Potential (mV):**	93.04 93.04 -21	Enhanced antimicrobial activity	*A. baumannii* *E. coli* *S. aureus*	(Salunke *et al.*, 2014)
	Silver **Coating:** silica **Functionalization:** B vitamins (biotin, pantothenate, nicotinamide)	-	**Size (nm):** **PDI:**	311 0.371	Enhanced antimicrobial activity Enhanced stability	*B. subtilis* *E. coli* *P. aeruginosa* *S. aureus*	(Tudose *et al.*, 2015)
	Silver **Coating:** silica **Functionalization:** antibiotics (penicillin G, ampicillin, isoniazide)	-	**Size (nm):** **PDI:**	311 0.371	Enhanced antimicrobial activity Enhanced stability	*B. subtilis* *E. coli* *P. aeruginosa* *S. aureus*	(Tudose *et al.*, 2015)
	Magnesium fluoride	-	**Size (nm):**	26 ± 0.8	Enhanced antimicrobial activity	*E. coli* *S. aureus*	(Lellouche *et al.*, 2012)
	Zinc oxide **Functionalization:** Ethylene glycol, gelatin, PVA	-	**Size (nm):** **Z. Potential (mV):**	65 ± 1.2 -8	Enhanced chemical stability Enhanced antimicrobial activity	*P. aeruginosa* *S. aureus*	(Akhil *et al.*, 2016)
	Zinc oxide **Coating:** *Phβ*-GBP extracted from *Paratelphusa hydrodromus*	-	**Size (nm):**	20-50	Enhanced antimicrobial activity Targeting	*P. vulgaris* *S. aureus*	(Iswarya *et al.*, 2017)
	Silver DMAEMA PAGA		**Size (nm):** **Z. Potential (mV):**	34.1 ± 1.26 20	Enhanced stability Enhanced biocompatibility Enhanced antimicrobial activity	*B. amyloliquefaciens* *E. coli* *P. aeruginosa* *S. aureus*	(Guo *et al.*, 2017)
Magnetic Nanoparticles	Iron oxide **Coating:** CMCS	-	**Size (nm):** **Z. Potential (mV):**	268.9 ± 5.3 -40.4 ± 5.8	Enhanced antimicrobial activity Enhanced biocompatibility	*E. coli* *S. aureus*	(Chen *et al.*, 2012)
	Bayoxide E 8706 **Functionalization:** Silver NPs **Coating:** CMCS	-	**Size (nm):**	250	Enhanced delivery of AgNPs Enhanced antimicrobial activity	*S. aureus*	(Vo *et al.*, 2017)

Downloaded from https://academic.oup.com/femsre/advance-article-abstract/doi/10.1093/femsre/fuz021/5550945 by Universidade do Porto user on 14 October 2019

Iron oxide **Functionalization/coating:** OA APTMS	-	**Z. Potential (mV):** OA NPs ATPMS NPs	 -29 ± 4 24 ± 5	Enhanced antimicrobial activity	*E. coli* *S. aureus*	(Shebl *et al.*, 2017)
Iron oxide	-	**Size (nm):**	16	Enhanced antimicrobial activity Promote bone regeneration Controlled delivery Targeting	*S. aureus*	(Fang *et al.*, 2017)
Iron oxide Silver	-	**Size (nm):**	176.5 ± 27	Enhanced antimicrobial activity Targeted delivery	MRSA	(Durmus & Webster, 2013)

Abbreviations: 2-(Dimethylamino)ethyl methacrylate (DMAEMA), *Acinetobacter baumannii* (*A. baumannii*), amino-propyl trimethoxy silane (APTMS), *Bacillus amyloliquefaciens* (*B. amyloliquefaciens*), *Bacillus subtilis* (*B. subtilis*), carboxymethyl chitosan (CMCS), *Escherichia coli* (*E. coli*), methicillin-resistant *Staphylococcus aureus* (MRSA), nanoparticles (NPs), oleic acid (OA), poly(2-(acrylamido) glucopyranose) (PAGA), polydispersity index (PDI), polyvinyl alcohol (PVA), *Proteus vulgaris* (*P. vulgaris*), *Pseudomonas aeruginosa* (*P. aeruginosa*), triphenylphosphine-monosulfonate (TPPMS), *Staphylococcus aureus* (*S. aureus*), *Staphylococcus epidermidis* (*S. epidermidis*), zeta potential (Z. Potential), β-1, 3- glucan binding protein (Phβ-GBP).

In this process, a plant extract or microorganism-derived compound is added to the solvent and to the metal solution during the process (Kalpana and Devi Rajeswari 2018). Several naturally synthetized Au and Ag NPs with antibiofilm activity are reported in the literature. For instance, Fei *et al.* (2013) prepared AgNPs *in situ* using the natural polymer *Bombyx mori* silk fibroin as a reducing agent of Ag. Additionally, silk fibroin chains were connected to the surface of the AgNPs, which improved their stability in aqueous dispersions due to the nonionic nature of the silk fibroin (Kvitek *et al.* 2008; Fei *et al.* 2013). After their preparation, AgNPs were tested against mature MRSA biofilms obtained from a clinical isolate. At the concentration of 76.8 μg mL^{-1}, AgNPs were able to partially disrupt the biofilm structure with a significant decrease in bacterial viability, revealing the strong bactericidal activity of these particles. A 5-fold increase of the NPs concentration resulted in a complete destruction of the bacterial biofilm (Fei *et al.* 2013). Similarly, Goswami *et al.* (2015) developed AgNPs from tea extract (*Camelia sinensis* L.) and evaluated their potential against bacterial biofilms. *S. aureus* and *E. coli* biofilms grew at the surface of silicone tubes and polystyrene coverslips for 24 h and were then incubated during 48 h with AgNPs, at room temperature. At the concentration of 15 μg mL^{-1}, the AgNPs showed an inhibition rate of 89% and 75% for *S. aureus* and *E. coli*, respectively. In addition, the release of cellular contents after the treatment with AgNPs confirmed the impairment of bacterial cell–cell adhesion due to membrane damage (Goswami *et al.* 2015). To evaluate the biocompatibility and safety of the designed AgNPs, a hemolytic assay was conducted using goat erythrocytes. The results revealed that AgNPs induced insignificant hemolysis, being a potentially safe nanosystem for drug formulation and coating on medical devices. Nevertheless, cytotoxic studies using animal cell lines to assess NPs biocompatibility are lacking (Goswami *et al.* 2015). Hamedi, Shojaosadati and Mohammadi (2017) also reported the potential of green synthesis of AgNPs against *S. aureus* biofilms. In this study, leave extracts of *Convolvulus arvensis* were used. Most bacteria of the biofilm were inactivated when exposed to 20 μg mL^{-1} of AgNPs (Hamedi, Shojaosadati and Mohammadi 2017). AgNPs and AuNPs were also produced by Singh *et al.* (2016) using root extracts of the herbal medicinal plant Korean red ginseng. The developed NPs did not aggregate, revealing a long-term stability at room temperature, in aqueous solution. However, only AgNPs were tested to determine their activity against *S. aureus* and *P. aeruginosa* biofilms. For both biofilm types, a maximum biofilm degradation was observed at 4 μg mL^{-1} of AgNPs (Singh *et al.* 2016).

Bimetallic NPs (AgAuNPs) synthesized using a green methodology have also been studied for their superior antimicrobial properties. AgAuNPs synthesized using the medicinal plant *Plumbago zeylanica* reported a higher antibacterial effect than AgAuNPs chemically synthesized, with a biofilm disruption activity of 61–77% for all tested biofilms (*Acinetobacter baumannii*, *E. coli* and *S. aureus*) (Salunke *et al.* 2014). Despite the scientific progress, the poor disruption activity of these AgAuNPs emphasizes the need of optimization of these nanosystems for a potential therapeutic application.

An alternative strategy to stabilize metallic NPs, such as AgNPs, consists in using a silica matrix to avoid coagulation and oxidation (Ravindran, Chandran and Khan 2013; Tudose *et al.* 2015a; Tudose *et al.* 2015b). Tudose *et al.* (2015a) developed AgNPs coated with silica (Ag-SiO_2NPs) and functionalized with vitamins B (biotin, pantothenate and nicotinamide). Ag-SiO_2-biotin and Ag-SiO_2-nicotinamide exhibited very low MBEC values (0.97 and 1.95 μg mL^{-1}, respectively) against *S. aureus* biofilms *in vitro*, revealing a higher antibiofilm activity than nonfunctionalized Ag-SiO_2NPs. Thus, it is hypothesized by the authors that the vitamins promoted the release of Ag ions and their intracellular accumulation and facilitated the penetration of Ag-SiO_2NPs into the biofilm matrix (Tudose *et al.* 2015a). Furthermore, Ag-SiO_2NPs were also functionalized with antibiotics (ampicillin, penicillin G and isoniazide) (Tudose *et al.* 2015b). Despite being a promising approach, *in vitro* efficacy assays showed that nonfunctionalized Ag-SiO_2NPs had a similar or even higher antibiofilm activity than the ones functionalized with penicillin G and isoniazide (Tudose *et al.* 2015b). The authors claim that a chemical modification of the antibiotics occurred, leading to a decrease of their antibacterial efficiency. On the contrary, a synergistic effect between ampicillin and Ag-SiO_2NPs was confirmed by the lower MBEC values against *S. aureus* and *P. aeruginosa* biofilms, when compared with the nonfunctionalized Ag-SiO_2NPs (Tudose *et al.* 2015b).

Besides AuNPs and AgNPs, other types of metallic NPs are also reported in the literature for their potential antibacterial and antibiofilm activity. Lellouche *et al.* (2012) produced magnesium fluoride NPs and evaluated their efficiency against established *S. aureus* and *E. coli* biofilms. Biofilms 1- to 7-day old

Downloaded from https://academic.oup.com/femsre/advance-article-abstract/doi/10.1093/femsre/fuz021/5550945 by Universidade do Porto user on 14 October 2019

were exposed to the magnesium fluoride NPs in a concentration of 1 mg mL^{-1} for 24 h. The NPs promoted an 87% and 44% decrease in *E. coli* biofilm viability for a 1- and 7-day old biofilm, respectively. Under the same experimental conditions, *S. aureus* biofilm viability decreased 92% (1-day old) and 69% (7-day old) after treatment with magnesium fluoride NPs (Lellouche *et al.* 2012). In another example, zinc oxide NPs were synthetized by co-precipitation and evaluated for their antibacterial and antibiofilm activity against *S. aureus* and *P. aeruginosa* (Akhil *et al.* 2016). For both species, zinc oxide NPs showed a higher efficiency against established biofilms in the presence of light than in dark conditions. According to the authors, these results are probably due to reactive oxygen species production in the presence of light (Akhil *et al.* 2016). A more complex system involving zinc oxide NPs was recently reported by Iswarya *et al.* (2017). Zinc oxide NPs were coated with crustacean immune molecule β-1,3-glucan binding protein (*Ph*β-GBP) purified from the rice field crab *Paratelphusa hydrodromus*. The coated zinc oxide NPs exhibited antibiofilm activity against a *S. aureus* established biofilm by disrupting bacterial membranes and destroying the biofilm structure. The biofilm thickness was significantly reduced from 40 (control) to 10 μm after treatment with 75 μg mL^{-1} of NPs (Iswarya *et al.* 2017). The strong antibiofilm activity of these particles suggests a combinatory effect of the *Ph*β-GBP coat, which specifically binds to the surface of bacteria, and zinc oxide NPs, that induces reactive oxygen species release from bacterial cells (Goncalves *et al.* 2012; Iswarya *et al.* 2017).

The previously mentioned studies show highly promising alternative therapies to treat bacterial biofilms, including from *S. aureus* strains. Nonetheless, there is a lack of *in vivo* studies to further confirm the *in vitro* antibiofilm efficacy of the NPs. Guo *et al.* (2017b) studied the antibiofilm activity of polymer functional silver nanocomposites both *in vitro* and *in vivo*. In these nanocomposites, the biocompatible carbohydrate polymer poly(2-(acrylamido) glucopyranose) (PAGA) and the membrane-disrupting cationic polymer quaternizated poly(2-dimethylaminoethyl methacrylate) (PDMAEMA-C_4) were used as ligands. The safety of this nanosystem was evaluated by *in vitro* hemolysis and cytotoxicity assays. The NPs revealed no toxic effects on red blood cells at all polymer concentrations tested (until 10 μmol L^{-1}). On NIH3T3 cells, the nanocomposites did not induce significant cytotoxic effects below a polymer concentration of 2.5 μmol L^{-1}. The efficacy of these nanocomposites was evaluated against several biofilms, including *S. aureus* (Guo *et al.* 2017b). For the *in vivo* efficiency assay, implants coated with biofilms were introduced into the mouse peritoneum and then locally treated with the nanocomposites (5 μmol L^{-1}). After 24 h incubation, it was observed a reduced bacterial colonization on the implant, compared with the control group (Guo *et al.* 2017b). Although the developed nanocomposites have potential to eradicate *in vivo* biofilms previously established on implantable medical devices, the polymer concentration used for this study showed cytotoxicity effects on mammalian cells. Thus, the safety of this nanosystem needs to be improved for therapeutic purposes.

In the past few decades, the magnetic properties of iron oxide NPs have been studied for their diagnostic and therapeutic properties (Pankhurst *et al.* 2003; Wu *et al.* 2015). Thus, magnetic NPs (MNPs) are a potential targeted nanosystem as they can be directed or guided by a magnetic field gradient toward biological targets (Pankhurst *et al.* 2003). Additionally, these particles are cost effective, physically and chemically stable, biocompatible and eco-friendly (Wu *et al.* 2015).

Chen *et al.* (2012) produced MNPs coated with carboxymethyl chitosan (CMCS) to effectively eradicate bacterial biofilms applying an external magnetic field. The CMCS was selected due to its enhanced aqueous solubility and antimicrobial activity, when compared with chitosan (Chen and Park 2003). The strong bactericidal action of CMCS is a consequence of the lysis and the inhibition of the nutrients transport into bacteria (Gu *et al.* 2007; Eldin *et al.* 2008; Du *et al.* 2009). The designed CMCS MNPs were evaluated *in vitro* against *S. aureus* and *E. coli* both in planktonic and biofilm forms (Chen *et al.* 2012). A decrease of 26% and 30% of viable *S. aureus* were found after 2 h treatment with CMCS and CMCS MNPs, respectively. The viability dropped to 1% after 10 h of treatment with CMCS and CMCS MNPs. Further, both CMCS and CMCS MNPs were evaluated regarding their antibiofilm activity at concentrations that showed no cytotoxic effects on 3T3 fibroblast cells. After a 48 h incubation period, CMCS (0.34 mg mL^{-1}) and CMCS MNPs (1.0 and 2.0 mg mL^{-1}) did not show significant decrease in *S. aureus* cell viability within the biofilms in the absence of a magnetic field (Chen *et al.* 2012). However, the number of viable *S. aureus* cells exposed to CMCS MNPs decreased by 84% when an external magnetic field was applied for 5 minutes, revealing a higher penetration of the MNPs into the biofilm structure. Nevertheless, a complete biofilm eradication was not achieved due to the restricted bactericidal activity of CMCS MNPs to bacteria in the immediate surroundings. Thus, the bacteria that are not in direct contact with the particles may survive within the biofilm matrix (Chen *et al.* 2012). To overcome this limitation, Vo, Sabrina and Lee (2017) added AgNPs to the surface of CMCS MNPs (AgNPs-CMCS MNPs). AgNPs are able to release Ag ions and generate reactive oxygen species that effectively kill bacteria (Xu *et al.* 2012). On the other hand, CMCS MNPs may be a good scaffold to avoid AgNPs aggregation (Varma, Deshpande and Kennedy 2004; Huang *et al.* 2008; Laudenslager, Schiffman and Schauer 2008). In this study, when 3-day old *S. aureus* biofilms were exposed to AgNPs-CMCS MNPs for 15 minutes, under an external magnetic field, no live bacteria were observed (Vo, Sabrina and Lee 2017). Hence, a high concentration of Ag ions and reactive oxygen species were released from AgNPs under a magnetic field, which effectively killed the bacteria within the biofilm (Vo, Sabrina and Lee 2017). Therefore, the dual action of AgNPs-CMCS MNPs shows a high potential for a therapeutic application against bacterial biofilms.

The hydrophobicity and the charge modulation are characteristics with a high impact in the antibacterial and the antibiofilm activity of MNPs. Shebl, Farouk and Azzazy (2017) revealed that oleic acid-coated MNPs (hydrophobic) and aminopropyl trimethoxy silane (APTMS)-coated MNPs (positively charged) were able to destroy 94% and 89% of preformed *S. aureus* biofilms, respectively. These findings suggest that the negative charge of bacterial cells and the hydrophobicity of both MNPs and biofilm matrixes play a critical role in their interaction (Pagedar, Singh and Batish 2010; Hajipour *et al.* 2012; Krasowska and Sigler 2014). Despite being a promising strategy for biofilms eradication, both types of MNPs exhibited cytotoxicity effects in human epithelial cells (Shebl, Farouk and Azzazy 2017).

Among all magnetic nanoparticles, superparamagnetic iron oxide particles (SPIONs) have been extensively used for several medical applications, including imaging, biodetection, drug and gene delivery, among others (Hao *et al.* 2010). Fang *et al.* (2017) studied the heating effect of MNP-induced hyperthermia in *in vivo S. aureus* biofilms. For that purpose, an osteomyelitis rat model was stablished by implanting metallic 18 G needle into the bone marrow cavity of distal femur after injecting a

Downloaded from https://academic.oup.com/femsre/advance-article-abstract/doi/10.1093/femsre/fuz021/5550945 by Universidade do Porto user on 14 October 2019

bacterial suspension of *S. aureus*. The inserted implants were further heated to 75°C by magnetic heating, promoting a better distribution of the particles within the biofilm structure. The use of MNPs heated by hyperthermia promoted the destruction of the biofilm and enhanced the efficiency of the plain vancomycin, which was co-administrated with the MNPs. This study highlights the potential of combining antibiotics with hyperthermia to enhance antibiotic penetration within the biofilm matrix and, consequently, to eradicate bacterial biofilms (Fang *et al.* 2017). Besides the combination with antibiotics, SPIONs were also combined with Ag as an alternative to treat bacterial biofilms. The Ag-conjugated SPIONs were tested against MRSA, without using antibiotics (Durmus and Webster 2013). In this study, 24 h old biofilms were exposed to the developed Ag-conjugated SPIONs for 24 h. The Ag-conjugated SPIONs (1 mg mL^{-1}) significantly decreased planktonic MRSA growth to 1.57% within the biofilm structure. Furthermore, they showed a significant biofilm biomass decrease to <47% in the presence of an external magnetic field. Thus, the combination of magnetic (SPIONS) and antibacterial properties (Ag) within the same system increases the potential of this nanosystem as a targeted therapy to eradicate MRSA biofilms, in alternative to antibiotics (Durmus and Webster 2013).

SILICA-BASED NANOSYSTEMS

Mesoporous silica NPs are promising drug delivery systems due to their biocompatibility and their stability that leads to a controlled drug release (Bharti *et al.* 2015). Besides, their large surface area, provided by homogenous pores, enables a high payload and an effective functionalization with a variety of groups for a targeted delivery (Bharti *et al.* 2015). These NPs do not have an intrinsic antimicrobial activity. However, they have a huge potential for antibiotics delivery to multidrug resistant infections once they can be designed to load multiple drugs within their structure (Miller *et al.* 2015). A summary of the silica-based NPs developed to eradicate *S. aureus* biofilms is provided in Table 4. For antibiotic delivery purposes, Gounani *et al.* (2019) produced carboxyl-modified mesoporous silica NPs loaded with polymyxin B and vancomycin. The antibiofilm activity of these NPs was evaluated in both *P. aeruginosa* and *S. aureus* mature biofilms. The MBIC and MBEC values of the studied NPs were surprisingly higher than free antibiotics. According to the authors, these findings suggest that NPs did not penetrate the biofilm probably due to their size and the electrostatic interactions between the NPs and the negatively charged biofilm matrix. The *in vitro* cytotoxicity of the NPs and the free drugs was evaluated using three human cell lines (HEPG2, HEF-2 and HEK-293) (Gounani *et al.* 2019). The results showed a dose-dependent decrease in cell viability and increase of reactive oxygen species production in all cell lines when exposed to the free drugs. For the same drug concentrations, the developed NPs showed no cytotoxicity effects. Additionally, an hemolysis assay confirmed the safety of the nanosystem. Based on this, the authors claim that carboxyl-modified mesoporous silica NPs loading antibiotics may lead to an enhanced biocompatibility of the drugs, reducing their adverse side effects (Gounani *et al.* 2019).

Despite the relevance of antibiotics in this fight, the increasing rates of resistance to these agents leads to the search for alternatives with equal antimicrobial potential. Slomberg *et al.* (2013) designed NO-releasing silica NPs to eradicate *S. aureus* and *P. aeruginosa* biofilms. The particles were evaluated according to their size (14, 50 and 150 nm) and shape (spherical and rod-like). The smaller particles were more effective against planktonic and biofilm *S. aureus*, compared to 50 and 150 nm particles. Regarding their shape, the spherical NPs were significantly less effective than rod-like NPs, requiring a higher concentration to eradicate the biofilms. These findings were further confirmed by confocal microscopy, where it was possible to observe that NO-releasing NPs with decreased size and increased aspect ratio exhibited better NO delivery and, consequently, enhanced bactericidal action (Slomberg *et al.* 2013). Despite their therapeutic potential, the NO-releasing NPs exhibited cytotoxicity effects against L929 fibroblasts at the MBEC values for *S. aureus* and *P. aeruginosa*. Thus, it is crucial to optimize this nanosystem toward lower toxicity to nontarget cells. Additionally, further studies combining NO with other antibacterial agents can be explored to reduce NO to nontoxic levels (Slomberg *et al.* 2013).

Combination of different drugs/compounds within the same nanosystem may lead to a synergistic antibacterial effect against resistant bacteria, such as MRSA. Duan *et al.* (2017) designed pH-responsive metal–carbenicillin framework-coated mesoporous silica nanoparticles (MSNs) to efficiently co-deliver β-lactam antibiotics and β-lactamase inhibitors to MRSA biofilms. Carbenicillin, the selected β-lactam antibiotic, was coordinated with Fe^{3+} to form the metal–carbenicillin framework to block the pores of the MSNs (Duan *et al.* 2017). However, bacteria are rapidly evolving to efficiently evade antibiotics, lowering their antibacterial potential. One of the most important bacterial mechanisms to resist to β-lactam antibiotics is the production of β-lactamases (Fisher Meroueh and Mobashery 2005; O'Connell *et al.* 2013). Thus, to improve the antibacterial efficiency of carbenicillin, the β-lactamase inhibitor sulbactam was encapsulated in the MSNs pores (Duan *et al.* 2017). The developed nanosystem was stable at physiological conditions (Duan *et al.* 2017). At the acidic pH of the bacterial infection site (pH~5.0) there was a controlled release of the active agents due to the sensitivity of the coordination between carbenicillin and Fe^{3+} at low pH. Additionally, cytotoxicity and hemolysis assays confirmed the safety and nontoxic profile of the MSNs *in vitro*. Confocal scanning laser microscopy images showed an effective penetration and diffusion of the designed MSNs within the biofilm matrix. As expected, the enhanced penetration ability of MSNs, associated to the synergistic effects of carbenicillin and sulbactam, lead to an effective destruction of established MRSA biofilms (Duan *et al.* 2017). To further confirm the potential of the system, MRSA intradermally infected mouse were used as an *in vivo* model system. The control group treated with phosphate-buffered saline exhibited an obvious skin infection, while the group treated with the developed MSNs only showed a slight skin infection. Thus, the authors believe that the reported MSNs may be an alternative therapeutic approach for the treatment of biofilm-associated infections (Duan *et al.* 2017).

QUANTUM DOTS

QDs are semiconducting NPs with excellent optical properties and high photostability (Ozkan 2004). These particles have a wide ultraviolet absorption spectrum, while their emission spectrum is very narrow, enabling multiplexed imaging under a single light source. Additionally, QDs are easily functionalized, having a great potential for targeted drug delivery (Ozkan 2004). Singh *et al.* (2017) developed curcumin (Cur) QDs composed of zirconia to enhance Cur aqueous solubility and stability. Cur is a hydrophobic polyphenol compound with a wide spectrum of medical applications, including in antimicrobial

Downloaded from https://academic.oup.com/femsre/advance-article-abstract/doi/10.1093/femsre/fuz021/5550945 by Universidade do Porto user on 14 October 2019

Table 4: Silica-based formulations developed to eradicate *S. aureus* biofilms.

Type of formulation	Formulation composition	Encapsulated compound	Physicochemical characteristics		Mechanism of action	Bacterial species/strains	Ref.
Silica Nanoparticles	CTAB TEOS **Functionalization:** AAPTMS Succinic anhydride	Polymyxin B Vancomycin	**Size (nm):** **Z. Potential (mV):** **Drug loading (μg):**	128.7 ± 7 -52.8 453	Enhance local drug delivery Enhanced biocompatibility	*P. aeruginosa* *S. aureus*	(Gounani *et al.*, 2019)
	TEOS AHAP AEAI	Nitric oxide	**Size (nm):**	14.8 ± 2 56.1 ± 5 139.9 ± 13	Enhanced delivery	*P. aeruginosa* *S. aureus*	(Slomberg *et al.*, 2013)
	CTATos APTES TEOS **Coating:** Metal-carbenicillin framework	Sulbactam	**Size (nm):** **Z. Potential (mV):** **LC (%):**	~ 200 ~ 10 25	Enhanced antimicrobial activity	MRSA	(Duan *et al.*, 2017)

Abbreviations: aminopropyltriethoxysilane (APTES), cetyltrimethylammonium tosylate (CTATos), hexadecyltrimethylammonium bromide (CTAB), loading capacity (LC), methicillin-resistant *Staphylococcus aureus* (MRSA), *N*-(2-aminoethyl)-3-amino-isobutyl-dimethyl-methoxysilane (AEAI), *N*-(2-aminoethyl)-3-aminopropyltrimethoxy-silane (AAPTMS), *N*-(6-aminohexyl)-aminopropyltrimethoxysilane (AHAP), *Pseudomonas aeruginosa* (*P. aeruginosa*), *Staphylococcus aureus* (*S. aureus*), tetraethylorthosilicate (TEOS), zeta potential (Z. Potential).

therapy (Priyadarsini 2014). However, this compound is rapidly degraded and has a poor aqueous solubility, which limits its use for clinical purposes (Wang *et al.* 1997; Priyadarsini 2014). The designed Cur QDs had a particles size, a polydispersity index and a zeta potential of 2.5 nm, 0.172 and −26 mV, respectively (Singh *et al.* 2017). The Cur QDs were also tested for their antibacterial effect against several bacterial strains, including *S. aureus* and MRSA. The MIC values of Cur QDs were in the range of 3.91 to 15.65 μg mL^{-1}, while the MIC values of the free Cur were significantly higher (175 to 350 μg mL^{-1}). Interestingly, Cur QDs revealed a higher biofilm inhibitory activity on the formation of MRSA biofilms comparing to *S. aureus* biofilms. Additionally, the Cur QDs exhibited a strong biofilm degrading activity against *S. aureus* 3-day old biofilms, with disintegration of the biofilm matrix at a concentration of 0.125 μg mL^{-1}. Confocal microscopy was used to validate the antibiofilm effects of Cur QDs, and it was possible to observe that Cur QDs complexes were localized manly at the superficial layers of the biofilm. It was hypothesized by the authors that the strong activity and aqueous solubility of Cur QDs might be related to the small size of these particles, which may lead to a higher penetration and interaction with the biofilm matrix and a higher cellular uptake (Singh *et al.* 2017).

CONCLUDING REMARKS

The high number of infections, the increasing multiple-antibiotic resistance cases, the health and economic burden and the lack of an effective therapy that does not require surgery for *S. aureus* biofilms have boosted the research to improve the available therapies. In this context, several nanosystems were developed to eradicate *S. aureus* biofilms established on the surface of an implant device.

Some systems described above were used to enhance the bioavailability of antibiotics and their controlled release, while reducing their adverse systemic side effects. As an alternative strategy, antibacterial agents such as nitric oxide, enzyme inhibitors and matrix disruptive agents were encapsulated alone or in combination with antibiotics into nanosystems. Additionally, some NPs reported in the literature were functionalized with ligands for a targeted delivery of the antibacterial agents to the biofilm and for increasing chemical stability of the nanosystems.

Research in nanotechnology to fight bacterial biofilms has been also focused on developing systems with intrinsic antibacterial activity such as metallic NPs, to overcome the antibiotic resistance phenomenon. Among these, magnetic NPs are also highlighted for their potential for a targeted delivery to biofilms, when exposed to an external magnetic field.

The studies reported in the literature demonstrated *in vitro* efficiency against *S. aureus* either in its planktonic form or within a biofilm structure. Even though with promising results, only a few studies achieved eradication of the bacteria. Moreover, most of these studies lack *ex vivo* and *in vivo* assays to evaluate biofilm eradication.

Although *in vitro* biofilm models highlight the potential of nanosystems for the eradication of these bacterial structures, they are still far from representing the *in vivo* conditions. The high complexity of biological systems is, usually, not considered in *in vitro* models. In a biological context, the nanosystems interact with biological fluids and bacterial and host cells. These cells produce extracellular polymeric substances and cellular debris that may hamper the efficiency of nanosystems (Buhmann *et al.* 2016). Thus, the use of serum in the biofilm culture medium (Rosman *et al.* 2014) and of the co-culture with host cells (Subbiahdoss *et al.* 2011) is a step forward in the development of *in vitro* biofilms with increasing relevance at a clinical level.

Additionally, reference bacterial strains to conduct *in vitro* studies are currently lacking, which leads to issues of reproducibility and may raise questions regarding the *in vivo* potential of the developed nanosystems (Roberts *et al.* 2015; Buhmann *et al.* 2016).

Perhaps, the major limitation of *in vitro* efficacy studies concerns the use of 24 or 48 h old biofilms. Considering that *in vivo* the biofilm maturation occurs during a much longer period, it is expected that the *in vivo* efficiency of nanosystems will be lower than in *in vitro* assays. In fact, Lellouche *et al.* (2012) compared the efficiency of NPs against 1- and 7-day old biofilms of *S. aureus* and *E. coli*. For both strains, the eradication efficiency of the treatment decreased 20–40% for 7-day old biofilms. Thus, *in vitro* assays based on 1-day old biofilms may overestimate the antimicrobial activity of therapeutic agents.

Downloaded from https://academic.oup.com/femsre/advance-article-abstract/doi/10.1093/femsre/fuz021/5550945 by Universidade do Porto user on 14 October 2019

Besides *in vitro* and *in vivo* efficiency evaluation of nanosystems, it is also necessary to assess their cytotoxicity. Some of the reported studies lack *in vitro* assays to assess the safety and the biocompatibility of the designed systems. However, some *in vivo* mechanisms, such as toxicokinetics, translocation and coordinated response of tissues, are not represented in the current *in vitro* models (Lopes *et al.* 2014). Thus, further research is required to evaluate the *in vivo* toxicity of nanomaterials, regarding biodistribution and interactions with organs and tissues (Arora, Rajwade and Paknikar 2012).

In conclusion, nanotechnology has a tremendous potential to treat biofilm-associated infections caused by pathogens such as *S. aureus*. Despite this potential, no clinical trials using nanotechnology to fight bacterial biofilms are going on. Therefore, it is urgent to focus on the *in vivo* efficacy and safety of the nanosystems, essential to initiate further clinical studies.

FUNDING

RMP, DLC and CN are thankful to Fundaçao para a Ciência e Tecnologia (FCT) for the PhD Grant [SFRH/BD/130319/2017], the PhD Grant [PD/BD/105957/2014] and the investigator Grant [IF/00293/2015], respectively. This work was supported by FCT through the FCT PhD Programmes and by Programa Operacional Capital Humano (POCH), specifically by the BiotechHealth Programme (Doctoral Programme on Cellular and Molecular Biotechnology Applied to Health Sciences). The work was supported by UID/QUI/50006/2019 with funding from FCT/MCTES through national funds as well as from the Fund for Scientific Research Flanders (FWO grant WO.009.16N) to PVD. This work is under the framework of the project POCI-01-0145-FEDER-31444, financed by Fundo Europeu de Desenvolvimento Regional (FEDER) - through the COMPETE 2020 - Operational Programme for Competitiveness and Internationalisation (POCI) - and by national funds through Fundação para a Ciência e Tecnologia (FCT).

Conflict of interests. None declared.

REFERENCES

Abed N, Couvreur P. Nanocarriers for antibiotics: a promising solution to treat intracellular bacterial infections. *Int J Antimicrob Agents* 2014;**43**:485–96.

Abou El-Nour KMM, Eftaiha AA, Al-Warthan A *et al.* Synthesis and applications of silver nanoparticles. *Arabian J Chem* 2010;**3**:135–40.

Akhil K, Jayakumar J, Gayathri G *et al.* Effect of various capping agents on photocatalytic, antibacterial and antibiofilm activities of ZnO nanoparticles. *J Photochem Photobiol B, Biol* 2016;**160**:32–42.

Ali Khan A, Mudassir J, Mohtar N *et al.* Advanced drug delivery to the lymphatic system: lipid-based nanoformulations. *Int J Nanomed* 2013;**8**:2733–44.

Andersen OZ, Offermanns V, Sillassen M *et al.* Accelerated bone ingrowth by local delivery of strontium from surface functionalized titanium implants. *Biomaterials* 2013;**34**:5883–90.

Anderson GG, O'Toole GA. Innate and induced resistance mechanisms of bacterial biofilms. *Curr Top Microbiol Immunol* 2008;**322**:85–105.

Archer NK, Mazaitis MJ, Costerton JW *et al.* *Staphylococcus aureus* biofilms: properties, regulation, and roles in human disease. *Virulence* 2011;**2**:445–59.

Arciola CR, Campoccia D, Montanaro L. Implant infections: adhesion, biofilm formation and immune evasion. *Nat Rev Microbiol* 2018;**16**:397–409.

Arora S, Rajwade JM, Paknikar KM. Nanotoxicology and *in vitro* studies: the need of the hour. *Toxicol Appl Pharmacol* 2012;**258**:151–65.

Bastari K, Arshath M, Ng ZH *et al.* A controlled release of antibiotics from calcium phosphate-coated poly(lactic-co-glycolic acid) particles and their *in vitro* efficacy against *Staphylococcus aureus* biofilm. *J Mater Sci Mater Med* 2014;**25**:747–57.

Battaglia L, Gallarate M. Lipid nanoparticles: state of the art, new preparation methods and challenges in drug delivery. *Expert Opin Drug Deliv* 2012;**9**:497–508.

Bharti C, Nagaich U, Pal AK *et al.* Mesoporous silica nanoparticles in target drug delivery system: a review. *Int J Pharm Investig* 2015;**5**:124–33.

Bhattacharya M, Wozniak DJ, Stoodley P *et al.* Prevention and treatment of *Staphylococcus aureus* biofilms. *Expert Rev Anti-infect Ther* 2015;**13**:1499–516.

Boda SK, Broda J, Schiefer F *et al.* Cytotoxicity of ultrasmall gold nanoparticles on planktonic and biofilm encapsulated gram-positive staphylococci. *Small* 2015;**11**:3183–93.

Buhmann MT, Stiefel P, Maniura-Weber K *et al.* *In vitro* biofilm models for device-related infections. *Trends Biotechnol* 2016;**34**:945–8.

Cerca N, Jefferson KK, Oliveira R *et al.* Comparative antibody-mediated phagocytosis of *Staphylococcus epidermidis* cells grown in a biofilm or in the planktonic state. *Infect Immun* 2006;**74**:4849–55.

Chen T, Wang R, Xu LQ *et al.* Carboxymethyl chitosan-functionalized magnetic nanoparticles for disruption of biofilms of *Staphylococcus aureus* and *Escherichia coli*. *Ind Eng Chem Res* 2012;**51**:13164–72.

Chen X-G, Park H-J. Chemical characteristics of O-carboxymethyl chitosans related to the preparation conditions. *Carbohydr Polym* 2003;**53**:355–9.

Corradin SB, Buchmuller-Rouiller Y, Mauel J. Phagocytosis enhances murine macrophage activation by interferon-gamma and tumor necrosis factor-alpha. *Eur J Immunol* 1991;**21**:2553–8.

Cui H, Li W, Li C *et al.* Liposome containing cinnamon oil with antibacterial activity against methicillin-resistant *Staphylococcus aureus* biofilm. *Biofouling* 2016;**32**:215–25.

Dalili D, Amini M, Faramarzi MA *et al.* Isolation and structural characterization of coryxin, a novel cyclic lipopeptide from *Corynebacterium xerosis* NS5 having emulsifying and antibiofilm activity. *Colloids Surf B* 2015;**135**:425–32.

Das S, Chaudhury A. Recent advances in lipid nanoparticle formulations with solid matrix for oral drug delivery. *AAPS PharmSciTech* 2011;**12**:62–76.

Del Pozo JL, Patel R. The challenge of treating biofilm-associated bacterial infections. *Clin Pharmacol Ther* 2007;**82**:204–9.

Del Pozo JL. Biofilm-related disease. *Expert Rev Anti Infect Ther* 2018;**16**:51–65.

Donlan RM, Costerton JW. Biofilms: survival mechanisms of clinically relevant microorganisms. *Clin Microbiol Rev* 2002;**15**:167–93.

Duan F, Feng X, Jin Y *et al.* Metal–carbenicillin framework-based nanoantibiotics with enhanced penetration and highly efficient inhibition of MRSA. *Biomaterials* 2017;**144**:155–65.

Durmus NG, Webster TJ. Eradicating antibiotic-resistant biofilms with silver-conjugated superparamagnetic iron oxide nanoparticles. *Adv Healthc Mater* 2013;**2**:165–71.

Downloaded from https://academic.oup.com/femsre/advance-article-abstract/doi/10.1093/femsre/fuz021/5550945 by Universidade do Porto user on 14 October 2019

Dusane DH, Pawar VS, Nancharaiah YV *et al.* Anti-biofilm potential of a glycolipid surfactant produced by a tropical marine strain of *Serratia marcescens*. *Biofouling* 2011;**27**:645–54.

Du W-L, Niu S-S, Xu Y-L *et al.* Antibacterial activity of chitosan tripolyphosphate nanoparticles loaded with various metal ions. *Carbohydr Polym* 2009;**75**:385–9.

El-Say KM, El-Sawy HS. Polymeric nanoparticles: promising platform for drug delivery. *Int J Pharm* 2017;**528**:675–91.

Eldin MM, Soliman E, Hashem A *et al.* Antibacterial activity of chitosan chemically modified with new technique. *Trends Biomater Artif Organs* 2008;**22**:121–33.

Etheridge ML, Campbell SA, Erdman AG *et al.* The big picture on nanomedicine: the state of investigational and approved nanomedicine products. *Nanomed-Nanotechnol* 2013;**9**: 1–14.

Evers P. Nanotechnology in medical applications: the global market. BCC Research, Wellesley, MA, 2015.

Fang CH, Tsai PI, Huang SW *et al.* Magnetic hyperthermia enhance the treatment efficacy of peri-implant osteomyelitis. *BMC Infect Dis* 2017;**17**:516.

Fang FC. Perspectives series: host/pathogen interactions. Mechanisms of nitric oxide-related antimicrobial activity. *J Clin Invest* 1997;**99**:2818–25.

Fei X, Jia M, Du X *et al.* Green synthesis of silk fibroin-silver nanoparticle composites with effective antibacterial and biofilm-disrupting properties. *Biomacromolecules* 2013;**14**:4483–8.

Fisher JF, Meroueh SO, Mobashery S. Bacterial resistance to beta-lactam antibiotics: compelling opportunism, compelling opportunity. *Chem Rev* 2005;**105**:395–424.

Foster TJ. Antibiotic resistance in *Staphylococcus aureus*. Current status and future prospects. *FEMS Microbiol Rev* 2017;**41**:430–49.

Gilbert P, Moore LE. Cationic antiseptics: diversity of action under a common epithet. *J Appl Microbiol* 2005;**99**:703–15.

Goncalves P, Vernal J, Rosa RD *et al.* Evidence for a novel biological role for the multifunctional beta-1,3-glucan binding protein in shrimp. *Mol Immunol* 2012;**51**:363–7.

Gonzalez-Ruiz A, Seaton RA, Hamed K. Daptomycin: an evidence-based review of its role in the treatment of Gram-positive infections. *Infect Drug Resist* 2016;**9**:47–58.

Goswami S, Sahareen T, Singh M *et al.* Role of biogenic silver nanoparticles in disruption of cell–cell adhesion in *Staphylococcus aureus* and *Escherichia coli* biofilm. *J Ind Eng Chem* 2015;**26**:73–80.

Gounani Z, Asadollahi MA, Pedersen JN *et al.* Mesoporous silica nanoparticles carrying multiple antibiotics provide enhanced synergistic effect and improved biocompatibility. *Colloids Surf B* 2019;**175**:498–508.

Grimaldi N, Andrade F, Segovia N *et al.* Lipid-based nanovesicles for nanomedicine. *Chem Soc Rev* 2016;**45**:6520–45.

Gu C, Sun B, Wu W *et al.* Synthesis, characterization of copper-loaded carboxymethyl-chitosan nanoparticles with effective antibacterial activity. *Macromol Symp* 2007;**254**:160–6.

Guo H, Wang Z, Du Q *et al.* Stimulated phase-shift acoustic nanodroplets enhance vancomycin efficacy against methicillin-resistant *Staphylococcus aureus* biofilms. *Int J Nanomed* 2017a;**12**:4679–90.

Guo Q, Zhao Y, Dai X *et al.* Functional silver nanocomposites as broad-spectrum antimicrobial and biofilm-disrupting agents. *ACS Appl Mater Interfaces* 2017b;**9**:16834–47.

Hajipour MJ, Fromm KM, Ashkarran AA *et al.* Antibacterial properties of nanoparticles. *Trends Biotechnol* 2012;**30**:499–511.

Hamedi S, Shojaosadati SA, Mohammadi A. Evaluation of the catalytic, antibacterial and anti-biofilm activities of the *Convolvulus arvensis* extract functionalized silver nanoparticles. *J Photochem Photobiol B, Biol* 2017;**167**:36–44.

Hao R, Xing R, Xu Z *et al.* Synthesis, functionalization, and biomedical applications of multifunctional magnetic nanoparticles. *Adv Mater* 2010;**22**:2729–42.

Heydorn A, Nielsen AT, Hentzer M *et al.* Quantification of biofilm structures by the novel computer program COMSTAT. *Microbiology* 2000;**146**:2395–407.

Hou Y, Wang Z, Zhang P *et al.* Lysozyme associated liposomal gentamicin inhibits bacterial biofilm. *Int J Mol Sci* 2017;**18**:784.

Huang L, Zhai ML, Long DW *et al.* UV-induced synthesis, characterization and formation mechanism of silver nanoparticles in alkalic carboxymethylated chitosan solution. *J Nanoparticle Res* 2008;**10**:1193–202.

Huh AJ, Kwon YJ. "Nanoantibiotics": a new paradigm for treating infectious diseases using nanomaterials in the antibiotics resistant era. *J Control Release* 2011;**156**:128–45.

Iswarya A, Vaseeharan B, Anjugam M *et al.* Multipurpose efficacy of ZnO nanoparticles coated by the crustacean immune molecule beta-1,3-glucan binding protein: toxicity on HepG2 liver cancer cells and bacterial pathogens. *Colloids Surf B* 2017;**158**:257–69.

Jayakumar R, Menon D, Manzoor K *et al.* Biomedical applications of chitin and chitosan based nanomaterials—a short review. *Carbohydr Polym* 2010;**82**:227–32.

Kalpana VN, Devi Rajeswari V. A review on green synthesis, biomedical applications, and toxicity studies of ZnO NPs. *Bioinorg Chem Appl* 2018;**2018**:3569758.

Kannappan A, Balasubramaniam B, Ranjitha R *et al.* *In vitro* and *in vivo* biofilm inhibitory efficacy of geraniol-cefotaxime combination against Staphylococcus spp. *Food Chem Toxicol* 2019;**125**:322–32.

Kayser O, Lemke A, Hernandez-Trejo N. The impact of nanobiotechnology on the development of new drug delivery systems. *Curr Pharm Biotechnol* 2005;**6**:3–5.

Krasowska A, Sigler K. How microorganisms use hydrophobicity and what does this mean for human needs? *Front Cell Infect Microbiol* 2014;**4**:112.

Kripfgans OD, Fowlkes JB, Miller DL *et al.* Acoustic droplet vaporization for therapeutic and diagnostic applications. *Ultrasound Med Biol* 2000;**26**:1177–89.

Kvitek L, Panáček A, Soukupova J *et al.* Effect of surfactants and polymers on stability and antibacterial activity of silver nanoparticles (NPs). *J Phys Chem C* 2008;**112**:5825–34.

Laudenslager MJ, Schiffman JD, Schauer CL. Carboxymethyl chitosan as a matrix material for platinum, gold, and silver nanoparticles. *Biomacromolecules* 2008;**9**:2682–5.

Lebeaux D, Chauhan A, Rendueles O *et al.* From *in vitro* to *in vivo* models of bacterial biofilm-related infections. *Pathogens* 2013;**2**:288–356.

Lee J, Choi JY, Park CH. Characteristics of polymers enabling nano-comminution of water-insoluble drugs. *Int J Pharm* 2008;**355**:328–36.

Lellouche J, Friedman A, Lellouche JP *et al.* Improved antibacterial and antibiofilm activity of magnesium fluoride nanoparticles obtained by water-based ultrasound chemistry. *Nanomed-Nanotechnol* 2012;**8**:702–11.

Letchford K, Burt H. A review of the formation and classification of amphiphilic block copolymer nanoparticulate structures: micelles, nanospheres, nanocapsules and polymersomes. *Eur J Pharm Biopharm* 2007;**65**:259–69.

Downloaded from https://academic.oup.com/femsre/advance-article-abstract/doi/10.1093/femsre/fuz021/5550945 by Universidade do Porto user on 14 October 2019

Lister JL, Horswill AR. *Staphylococcus aureus* biofilms: recent developments in biofilm dispersal. *Front Cell Infect Microbiol* 2014;**4**:1–9.

Lopes D, Nunes C, Martins MC *et al.* Eradication of *Helicobacter pylori*: past, present and future. *J Control Release* 2014;**189**:169–86.

Lopes D, Nunes C, Martins MCL *et al.* Targeting strategies for the treatment of *Helicobacter pylori* infections. In: Naik J (ed). *Nano Based Drug Delivery*. Croatia: IAPC Publishing, 2015, 604.

Macia MD, Rojo-Molinero E, Oliver A. Antimicrobial susceptibility testing in biofilm-growing bacteria. *Clin Microbiol Infect* 2014;**20**:981–90.

Mathew S, Abraham TE. *In vitro* antioxidant activity and scavenging effects of *Cinnamomum verum* leaf extract assayed by different methodologies. *Food Chem Toxicol* 2006;**44**:198–206.

McDonnell G, Russell AD. Antiseptics and disinfectants: activity, action, and resistance. *Clin Microbiol Rev* 1999;**12**:147–79.

McIntyre WF, Healey JS. Cardiac implantable electronic device infections: from recognizing risk to prevention. *Heart Rhythm* 2017;**14**:846–7.

Meng Y, Hou X, Lei J *et al.* Multi-functional liposomes enhancing target and antibacterial immunity for antimicrobial and antibiofilm against methicillin-resistant *Staphylococcus aureus*. *Pharm Res* 2016;**33**:763–75.

Miller KP, Wang L, Benicewicz BC *et al.* Inorganic nanoparticles engineered to attack bacteria. *Chem Soc Rev* 2015;**44**:7787–807.

Mizdal CR, Stefanello ST, da Costa Flores V *et al.* The antibacterial and anti-biofilm activity of gold-complexed sulfonamides against methicillin-resistant *Staphylococcus aureus*. *Microb Pathog* 2018;**123**:440–8.

Montanaro L, Poggi A, Visai L *et al.* Extracellular DNA in biofilms. *Int J Artif Organs* 2011;**34**:824–31.

Nafee N. Chapter 11 - Nanocarriers against bacterial biofilms: current status and future perspectives. In: Kon K (ed). *Nanotechnology in Diagnosis, Treatment and Prophylaxis of Infectious Diseases*. Boston: Academic Press, 2015, 167–89.

O'Connell KM, Hodgkinson JT, Sore HF *et al.* Combating multidrug-resistant bacteria: current strategies for the discovery of novel antibacterials. *Angew Chem Int Ed Engl* 2013;**52**:10706–33.

Onche II, Osagie OE, INuhu S. Removal of orthopaedic implants: indications, outcome and economic implications. *J West Afr Coll Surg* 2011;**1**:101–12.

Osmon DR, Berbari EF, Berendt AR *et al.* Diagnosis and management of prosthetic joint infection: clinical practice guidelines by the Infectious Diseases Society of America. *Clin Infect Dis* 2013;**56**:e1–25.

Otto M. Biofilms in disease. In: Rumbaugh KP, Ahmad I (eds). *Antibiofilm agents: from diagnosis to treatment and prevention*. Berlin, Heidelberg: Springer Berlin Heidelberg, 2014, 3–13.

Otto M. Staphylococcal biofilms. *Curr Top Microbiol Immunol* 2008;**322**:207–28.

Ozkan M. Quantum dots and other nanoparticles: what can they offer to drug discovery? *Drug Discov Today* 2004;**9**:1065–71.

Pagedar A, Singh J, Batish VK. Surface hydrophobicity, nutritional contents affect *Staphylococcus aureus* biofilms and temperature influences its survival in preformed biofilms. *J Basic Microbiol* 2010;**50**:98–106.

Pajek D, Burgess A, Huang Y *et al.* High intensity focused ultrasound sonothrombolysis: the use of perfluorocarbon droplets to achieve clot lysis at reduced acoustic powers. *Ultrasound Med Biol* 2014;**40**:2151–61.

Pankhurst QA, Connolly J, Jones S *et al.* Applications of magnetic nanoparticles in biomedicine. *J Phys D: Appl Phys* 2003;**36**:R167.

Pardeike J, Hommoss A, Müller RH. Lipid nanoparticles (SLN, NLC) in cosmetic and pharmaceutical dermal products. *Int J Pharm* 2009;**366**:170–84.

Parsek MR, Singh PK. Bacterial biofilms: an emerging link to disease pathogenesis. *Annu Rev Microbiol* 2003;**57**:677–701.

Pecci Y, Rivardo F, Martinotti MG *et al.* LC/ESI-MS/MS characterisation of lipopeptide biosurfactants produced by the *Bacillus licheniformis* V9T14 strain. *J Mass Spectrom* 2010;**45**:772–8.

Peltonen L, Hirvonen J. Pharmaceutical nanocrystals by nanomilling: critical process parameters, particle fracturing and stabilization methods. *J Pharm Pharmacol* 2010;**62**:1569–79.

Peterson SB, Irie Y, Borlee BR *et al.* Different methods for culturing biofilms *in vitro*. In: Bjarnsholt T, Jensen PØ, Moser C, Høiby N (eds). *Biofilm Infections*. New York, NY: Springer New York, 2011, 251–66.

Pinto RM, Lopes D, Nunes C *et al.* Oral administration of lipid-based delivery systems to combat infectious diseases. *Nanoparticles in the Life Sciences and Biomedicine*. Singapore: Pan Stanford Publishing, 2017, 75–110.

Priyadarsini KI. The chemistry of curcumin: from extraction to therapeutic agent. *Molecules* 2014;**19**:20091–112.

Rapoport NY, Efros AL, Christensen DA *et al.* Microbubble generation in phase-shift nanoemulsions used as anticancer drug carriers. *Bubble Sci Eng Technol* 2009;**1**:31–9.

Ravindran A, Chandran P, Khan SS. Biofunctionalized silver nanoparticles: advances and prospects. *Colloids Surf B* 2013;**105**:342–52.

Rivero Berti I, Dell' Arciprete ML, Dittler ML *et al.* Delivery of fluorophores by calcium phosphate-coated nanoliposomes and interaction with *Staphylococcus aureus* biofilms. *Colloids Surf B* 2016;**142**:214–22.

Roberts AE, Kragh KN, Bjarnsholt T *et al.* The limitations of *in vitro* experimentation in understanding biofilms and chronic infection. *J Mol Biol* 2015;**427**:3646–61.

Rosman BM, Barbosa JA, Passerotti CP *et al.* Evaluation of a novel gel-based ureteral stent with biofilm-resistant characteristics. *Int Urol Nephrol* 2014;**46**:1053–8.

Sader HS, Farrell DJ, Flamm RK *et al.* Daptomycin activity tested against 164457 bacterial isolates from hospitalised patients: summary of 8 years of a Worldwide Surveillance Programme (2005–2012). *Int J Antimicrob Agents* 2014;**43**:465–9.

Salunke GR, Ghosh S, Santosh Kumar RJ *et al.* Rapid efficient synthesis and characterization of silver, gold, and bimetallic nanoparticles from the medicinal plant *Plumbago zeylanica* and their application in biofilm control. *Int J Nanomed* 2014;**9**:2635–53.

Severino P, Andreani T, Macedo AS *et al.* Current state-of-art and new trends on lipid nanoparticles (SLN and NLC) for oral drug delivery. *J Drug Deliv* 2012;**2012**:750891.

Sharma M, Gupta N, Gupta S. Implications of designing clarithromycin loaded solid lipid nanoparticles on their pharmacokinetics, antibacterial activity and safety. *RSC Adv* 2016;**6**:76621–31.

Shebl RI, Farouk F, Azzazy HME-S. Effect of surface charge and hydrophobicity modulation on the antibacterial and

Downloaded from https://academic.oup.com/femsre/advance-article-abstract/doi/10.1093/femsre/fuz021/5550945 by Universidade do Porto user on 14 October 2019

antibiofilm potential of magnetic iron nanoparticles. *J Nanomaterials* 2017;**2017**:1–15.

Siala W, Kucharikova S, Braem A *et al.* The antifungal caspofungin increases fluoroquinolone activity against *Staphylococcus aureus* biofilms by inhibiting N-acetylglucosamine transferase. *Nat Commun* 2016;**7**:1–15.

Singh AK, Prakash P, Singh R *et al.* Curcumin quantum dots mediated degradation of bacterial biofilms. *Front Microbiol* 2017;**8**:1517.

Singh B, Vuddanda PR, M RV *et al.* Cefuroxime axetil loaded solid lipid nanoparticles for enhanced activity against *S. aureus* biofilm. *Colloids Surf B* 2014;**121**:92–8.

Singh P, Kim YJ, Wang C *et al.* Biogenic silver and gold nanoparticles synthesized using red ginseng root extract, and their applications. *Artif Cells Nanomed Biotechnol* 2016;**44**:811–6.

Slomberg DL, Lu Y, Broadnax AD *et al.* Role of size and shape on biofilm eradication for nitric oxide-releasing silica nanoparticles. *ACS Appl Mater Interfaces* 2013;**5**:9322–9.

Sousa R, Pereira A, Massada M *et al.* Empirical antibiotic therapy in prosthetic joint infections. *Acta Orthop Belg* 2010;**76**:254–9.

Souza dos Santos B, Bezerra Filho CM, Alves do Nascimento Junior JA *et al.* Anti-staphylococcal activity of *Syagrus coronata* essential oil: biofilm eradication and *in vivo* action on *Galleria mellonela* infection model. *Microb Pathog* 2019;**131**:150–7.

Srivastava S, Bhargava A. Biofilms and human health. *Biotechnol Lett* 2016;**38**:1–22.

Subbiahdoss G, Fernandez IC, Domingues JF *et al.* *In vitro* interactions between bacteria, osteoblast-like cells and macrophages in the pathogenesis of biomaterial-associated infections. *PLoS One* 2011;**6**:e24827.

Tacconelli E, Carrara E, Savoldi A *et al.* Discovery, research, and development of new antibiotics: the WHO priority list of antibiotic-resistant bacteria and tuberculosis. *Lancet Infect Dis* 2018;**18**:318–27.

Tan Y, Ma S, Leonhard M *et al.* Enhancing antibiofilm activity with functional chitosan nanoparticles targeting biofilm cells and biofilm matrix. *Carbohydr Polym* 2018;**200**:35–42.

Thomas N, Dong D, Richter K *et al.* Quatsomes for the treatment of *Staphylococcus aureus* biofilm. *J Mater Chem B* 2015;**3**:2770–7.

Thomas N, Thorn C, Richter K *et al.* Efficacy of poly-lactic-co-glycolic acid micro- and nanoparticles of ciprofloxacin against bacterial biofilms. *J Pharm Sci* 2016;**105**:3115–22.

Tudose M, Culita DC, Ionita P *et al.* Silver nanoparticles embedded into silica functionalized with vitamins as biological active materials. *Ceram Int* 2015a;**41**:4460–7.

Tudose M, Culita DC, Munteanu C *et al.* Antibacterial activity evaluation of silver nanoparticles entrapped in silica matrix functionalized with antibiotics. *J Inorg Organomet Polym Mater* 2015b;**25**:869–78.

VanKoten HW, Dlakic WM, Engel R *et al.* Synthesis and biological activity of highly cationic dendrimer antibiotics. *Mol Pharm* 2016;**13**:3827–34.

Varma AJ, Deshpande SV, Kennedy JF. Metal complexation by chitosan and its derivatives: a review. *Carbohydr Polym* 2004;**55**:77–93.

Vo DT, Sabrina S, Lee CK. Silver deposited carboxymethyl chitosan-grafted magnetic nanoparticles as dual action deliverable antimicrobial materials. *Mater Sci Eng C: Mater Biol Appl* 2017;**73**:544–51.

Vyas SP, Sihorkar V, Jain S. Mannosylated liposomes for bio-film targeting. *Int J Pharm* 2007;**330**:6–13.

Wang YJ, Pan MH, Cheng AL *et al.* Stability of curcumin in buffer solutions and characterization of its degradation products. *J Pharm Biomed Anal* 1997;**15**:1867–76.

WHO. *Antimicrobial Resistance: Global Report on Surveillance*. World Health Organization 2014.

Worley BV, Schilly KM, Schoenfisch MH. Anti-Biofilm efficacy of dual-action nitric oxide-releasing alkyl chain modified poly(amidoamine) dendrimers. *Mol Pharm* 2015;**12**:1573–83.

Wu W, Wu Z, Yu T *et al.* Recent progress on magnetic iron oxide nanoparticles: synthesis, surface functional strategies and biomedical applications. *Sci Technol Adv Mater* 2015;**16**:023501.

Xu H, Qu F, Xu H *et al.* Role of reactive oxygen species in the antibacterial mechanism of silver nanoparticles on *Escherichia coli* O157:H7. *Biometals* 2012;**25**:45–53.

Zhang L, Pornpattananangku D, Hu CM *et al.* Development of nanoparticles for antimicrobial drug delivery. *Curr Med Chem* 2010;**17**:585–94.

Downloaded from https://academic.oup.com/femsre/advance-article-abstract/doi/10.1093/femsre/fuz021/5550945 by Universidade do Porto user on 14 October 2019

Chapter 3 – Motivation and goals

Bacterial biofilms are nowadays a high concern due to their contribution to the escalating figures of antimicrobial resistant phenomena and the high demand for implantable medical devices. The current therapy to treat implant-associated bacterial biofilm infections consists in the removal of the medical device combined with long-lasting antibiotic administration [1]. Unfortunately, this approach is solely focused on the administration of antibiotics, which target and kill bacterial cells [2]. Thus, this treatment does not address the main challenge of biofilms: the EPS matrix. The EPS matrix represents the first physical barrier of a biofilm and is largely responsible for the inefficiency of antibiotics, since it hinders their diffusion to deeper regions of the biofilm and may even interact with the antimicrobial agents, leading to their inactivation [3-5]. Consequently, the current therapy ultimately fails to completely eradicate the biofilm.

Nanotechnology emerges as a promising approach to overcome the major limitations of the current standard therapy. NPs used as delivery systems may improve the diffusion of both antibiotics and matrix disruptive agents within the biofilm structure. Nanocarriers are well-known to maintain a sustained drug release, while minimizing side effects [6]. Nanocarriers can be designed to have advantageous intrinsic characteristics (e.g., size, charge, and functionalization) that facilitate their penetration within the biofilm, allowing a release of their cargo in deeper regions of the structure [7]. Among these, lipid NPs are appealing systems to efficiently encapsulate drugs due to their high biocompatibility, biodegradability, low cost, and easy scale-up [8, 9]. Besides, these are versatile carriers that can incorporate both lipophilic and hydrophilic compounds, promoting a controlled drug release over time [10].

The lack of an efficient treatment to completely eradicate biofilms on implantable medical devices leads to the main purpose of this thesis, which was to develop **lipid-based nanocarriers as tools to efficiently and synergistically eradicate bacterial biofilms**. To fulfill this aim, lipid nanocarriers encapsulating antimicrobial and matrix disruptive agents were developed. The potential of the lipid NPs was studied in biofilms of *S. epidermidis*, *P. aeruginosa*, and *S. aureus*. A special focus has been given to the latter, since *S. aureus* is the major responsible for nosocomial infections and it can be found associated with infection in several implantable medical devices [4, 11].

To achieve the aim of this work, several research goals were established, namely to:

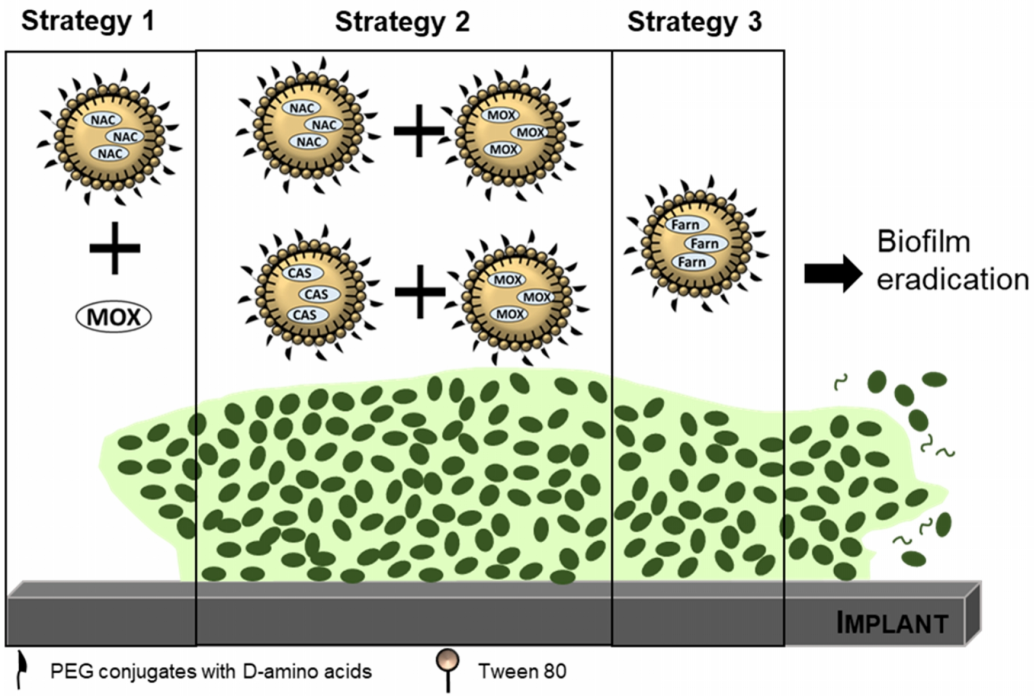
- Design lipid NPs encapsulating matrix disruptive and antimicrobial agents.
- Evaluate the *in vitro* cytocompatibility of the developed nanosystems.
- Evaluate the *in vitro* and *in vivo* antibiofilm potential of the developed nanosystems alone or in a combinatory strategy to eradicate bacterial biofilms.
- Evaluate the *in vivo* distribution of the developed nanosystems.

References

1. Bhattacharya, M., et al., *Prevention and treatment of Staphylococcus aureus biofilms.* Expert Rev. Anti-infect. Ther., 2015. **13**(12): p. 1499-516, 10.1586/14787210.2015.1100533
2. Koo, H., et al., *Targeting microbial biofilms: current and prospective therapeutic strategies.* Nat Rev Microbiol, 2017. **15**(12): p. 740-755, 10.1038/nrmicro.2017.99
3. Donlan, R.M. and J.W. Costerton, *Biofilms: survival mechanisms of clinically relevant microorganisms.* Clin Microbiol Rev, 2002. **15**(2): p. 167-193, 10.1128/CMR.15.2.167-193.2002
4. Srivastava, S. and A. Bhargava, *Biofilms and human health.* Biotechnol Lett, 2016. **38**(1): p. 1-22, 10.1007/s10529-015-1960-8
5. Flemming, H.C., et al., *Biofilms: an emergent form of bacterial life.* Nat Rev Microbiol, 2016. **14**(9): p. 563-575, 10.1038/nrmicro.2016.94
6. Nafee, N., *Nanocarriers Against Bacterial Biofilms: Current Status and Future Perspectives*, in *Nanotechnology in Diagnosis, Treatment and Prophylaxis of Infectious Diseases*, K. Kon, Editor. 2015, Academic Press: Boston. p. 167-189.
7. Fulaz, S., et al., *Nanoparticle-biofilm interactions: the role of the EPS matrix.* Trends Microbiol, 2019. **27**(11): p. 915-926, 10.1016/j.tim.2019.07.004
8. Severino, P., et al., *Current State-of-Art and New Trends on Lipid Nanoparticles (SLN and NLC) for Oral Drug Delivery.* J. Drug Deliv., 2012. **2012**: p. 750891, 10.1155/2012/750891
9. Battaglia, L. and M. Gallarate, *Lipid nanoparticles: state of the art, new preparation methods and challenges in drug delivery.* Expert Opin. Drug Deliv., 2012. **9**(5): p. 497-508, 10.1517/17425247.2012.673278
10. Pinto, R.M., et al., *Oral administration of lipid-based delivery systems to combat infectious diseases*, in *Nanoparticles in the Life Sciences and Biomedicine*, P.S. Publishing, Editor. 2017.
11. Otto, M., *Staphylococcal biofilms.* Curr. Top. Microbiol. Immunol., 2008. **322**: p. 207-28,

Chapter 4 – Rational behind the proposed nano-based strategy

The main goal of this work was to **develop lipid-based nanocarriers to efficiently and synergistically eradicate bacterial biofilms.** Lipid nanoparticles have been recently highlighted for their properties that lead to a controlled drug release, their cost effectiveness, and their easy scale-up [1]. These nanoparticles are highly biocompatible and biodegradable, with a lipid matrix composed of physiologically or physiologically related lipids [2]. Thus, different lipid nanoparticles encapsulating matrix-disruptive agents (*N*-acetyl cysteine and caspofungin) and antimicrobial agents (moxifloxacin and farnesol) were designed and studied alone or in a combinatory strategy. A schematic overview of the strategies developed in this thesis can be found in **Figure 1**. Besides, the role of all encapsulated compounds and some key components of the lipid NPs are briefly described below.



CAS, caspofungin; Farn, farnesol; MOX, moxifloxacin; NAC, *N*-acetyl cysteine.

Figure 1: Schematic overview of the overall proposed work towards bacterial biofilm eradication, using lipid NPs as nanocarriers. **Strategy 1** consisted in the combination of encapsulated NAC with a free antibiotic. **Strategy 2** was based on the combination of encapsulated matrix disruptive agents (NAC or CAS) with an encapsulated antibiotic (MOX). **Strategy 3** was an antibiotic-free strategy based on the encapsulation of farnesol.

1. Encapsulated compounds

1.1 Matrix-disruptive agents

N-acetyl cysteine (NAC)

N-acetyl cysteine (NAC) is a mucolytic agent that disrupts disulfide bonds in mucus and inhibits cysteine use, by competition [3]. NAC has several described clinical applications and has been highlighted by its excellent biocompatible profile [4]. Amongst its potential applications, NAC shows antibiofilm activity by reducing EPS production and promote disruption of mature biofilms [3]. Several reports in the literature show the potential of NAC alone or in combination against *S. epidermidis*, *P. aeruginosa*, and *S. aureus* biofilms [5-8].

Caspofungin (CAS)

Caspofungin (CAS) is an antifungal echinocandin that inhibits the synthesis of the β-(1,3)-D-glucan, which is a component of the fungal cell wall [9]. This antifungal agent acts on *Candida* and *Aspergillus* species [10]. Recently, Siala *et al.* (2016) reported the antibiofilm effect of CAS in *S. aureus* biofilms, by inhibition of the enzymatic activity of IcaA, which shares homology with the fungal the β-(1,3)-D-glucan [11]. In *S. aureus* strains expressing the *ica* operon (IcaA), this plays a critical role in the synthesis of the biofilm matrix component PNAG [12]. Hence, caspofungin revealed a potential synergistic effect with antibiotics, by improving the activity of fluoroquinolones against *S. aureus* biofilms [11].

1.2 Antimicrobial agents

Moxifloxacin (MOX)

Moxifloxacin (MOX) is an approved fourth-generation fluoroquinolone, which prevents bacterial DNA duplication. This antibiotic has a broad spectrum of antibacterial activity, and it is generally well-tolerated [13]. In addition, MOX demonstrated efficiency in reducing biofilms in both Gram-negative and Gram-positive bacteria [14, 15].

Farnesol (Farn)

Farnesol (Farn) is a compound that can be found in the essential oils of some plant species and in yeasts from the genus *Candida* [16, 17]. In *Candida* species, farnesol prevents the transition from yeast to hyphal growth, which deeply compromises the ability to form biofilms [18]. This quorum-sensing molecule exhibits antimicrobial properties and it also showed

potential antibiofilm effect against *S. aureus* strains, both methicillin-resistant and methicillin-susceptible. Farn showed potential in inhibiting biofilm formation by *S. aureus* and has been able to disturb the cell membrane integrity of bacterial cells [19]. Thus, Farn enhances the membrane permeability, which facilitates the entry of antibiotics in the cells [19]. Due to its synergistic effect with antibiotics, Farn is a potential adjuvant therapeutical agent against bacterial biofilms.

2. Antimicrobial components of the lipid nanoparticles

Polysorbate 80 (Tween 80)

Polysorbate 80 (Tween 80) is a well-known non-ionic surfactant, commonly used in the preparation of lipid NPs as a stabilizer [20-22]. Recently, Tween 80 has been highlighted for its antibacterial and antibiofilm properties [20, 23, 24]. Several studies showed the potential of Tween 80 to reduce bacterial adhesion and inhibit biofilm formation of *P. aeruginosa* and *S. aureus* strains [23, 24].

D-amino acids

D-amino acids as promising antibiofilm agents have been investigated by several researchers. D-amino acids are naturally produced by several bacteria, such as *Bacillus subtilis*, and incorporate into the peptidoglycan, triggering the release of the protein component of the matrix [25]. D-amino acids potential to inhibit biofilm formation in *S. aureus*, *S. epidermidis*, and *P. aeruginosa* is also described, however, the mechanism of action remains poorly understood [26-29]. In *S. aureus* biofilms, D-amino acids did not prevent the initial attachment of bacteria to a surface, instead, they inhibited the growth of small microcolonies into larger aggregates, by affecting the protein component of the EPS. In addition, a mixture of three D-amino acids (D-Tyr, D-Pro, and D-Phe) showed the potential to disassemble mature *S. aureus* biofilms [27].

References

1. Severino, P., et al., *Current State-of-Art and New Trends on Lipid Nanoparticles (SLN and NLC) for Oral Drug Delivery.* J. Drug Deliv., 2012. **2012**: p. 750891, 10.1155/2012/750891
2. Battaglia, L. and M. Gallarate, *Lipid nanoparticles: state of the art, new preparation methods and challenges in drug delivery.* Expert Opin. Drug Deliv., 2012. **9**(5): p. 497-508, 10.1517/17425247.2012.673278
3. Romano, C.L., et al., *Antibiofilm agents and implant-related infections in orthopaedics: where are we?* J Chemother, 2013. **25**(2): p. 67-80, 10.1179/1973947812y.0000000045
4. Kao, L.W., et al., *What Is the Rate of Adverse Events After Oral N-Acetylcysteine Administered by the Intravenous Route to Patients with Suspected Acetaminophen Poisoning?* Ann. Emerg. Med., 2003. **42**(6): p. 741-750, 10.1016/s0196-0644(03)00508-0
5. Leite, B., et al., *Combined Effect of Linezolid and N-Acetylcysteine Against Staphylococcus epidermidis Biofilms.* Enferm. Infecc. Microbiol. Clin., 2013. **31**(10): p. 655-659, 10.1016/j.eimc.2012.11.011
6. Zhao, T. and Y. Liu, *N-Acetylcysteine Inhibit Biofilms Produced by Pseudomonas aeruginosa.* BMC Microbiol., 2010. **10**: p. 140, 10.1186/1471-2180-10-140
7. Jun, Y., et al., *In vitro inhibitory activity of N-acetylcysteine on tympanostomy tube biofilms from methicillin-resistant Staphylococcus aureus and quinolone-resistant Pseudomonas aeruginosa.* Int J Pediatr Otorhinolaryngol, 2019. **126**: p. 109622, 10.1016/j.ijporl.2019.109622
8. Manoharan, A., et al., *The effect of N-acetylcysteine in a combined antibiofilm treatment against antibiotic-resistant Staphylococcus aureus.* Journal of Antimicrobial Chemotherapy, 2020. **75**(7): p. 1787-1798, 10.1093/jac/dkaa093
9. McCormack, P.L. and C.M. Perry, *Caspofungin.* Drugs, 2005. **65**(14): p. 2049-2068, 10.2165/00003495-200565140-00009
10. Wiederhold, N.P., et al., *Pharmacodynamics of caspofungin in a murine model of invasive pulmonary aspergillosis: evidence of concentration-dependent activity.* J Infect Dis, 2004. **190**(8): p. 1464-1471, 10.1086/424465
11. Siala, W., et al., *The Antifungal Caspofungin Increases Fluoroquinolone Activity Against Staphylococcus aureus Biofilms by Inhibiting N-Acetylglucosamine Transferase.* Nat. Commun., 2016. **7**: p. 1-15, 10.1038/ncomms13286

12. O'Gara, J.P., *ica and beyond: biofilm mechanisms and regulation in Staphylococcus epidermidis and Staphylococcus aureus.* FEMS Microbiol Lett, 2007. **270**(2): p. 179-188, 10.1111/j.1574-6968.2007.00688.x
13. Keating, G.M. and L.J. Scott, *Moxifloxacin: a review of its use in the management of bacterial infections.* Drugs, 2004. **64**(20): p. 2347-2377, 10.2165/00003495-200464200-00006
14. Bauer, J., et al., *A combined pharmacodynamic quantitative and qualitative model reveals the potent activity of daptomycin and delafloxacin against Staphylococcus aureus biofilms.* Antimicrob Agents Chemother, 2013. **57**(6): p. 2726-37, 10.1128/AAC.00181-13
15. Eick, S. and W. Pfister, *Efficacy of antibiotics against periodontopathogenic bacteria within epithelial cells: an in vitro study.* J Periodontol, 2004. **75**(10): p. 1327-1334, 10.1902/jop.2004.75.10.1327
16. Weber, K., B. Schulz, and M. Ruhnke, *The quorum-sensing molecule E,E-farnesol-its variable secretion and its impact on the growth and metabolism of Candida species.* Yeast, 2010. **27**(9): p. 727-739, 10.1002/yea.1769
17. Langford, M.L., A.L. Atkin, and K.W. Nickerson, *Cellular interactions of farnesol, a quorum-sensing molecule produced by Candida albicans.* Future Microbiol, 2009. **4**(10): p. 1353-1362, 10.2217/fmb.09.98
18. Yu, L.H., et al., *Possible inhibitory molecular mechanism of farnesol on the development of fluconazole resistance in Candida albicans biofilm.* Antimicrob Agents Chemother, 2012. **56**(2): p. 770-775, 10.1128/aac.05290-11
19. Jabra-Rizk, M.A., et al., *Effect of farnesol on Staphylococcus aureus biofilm formation and antimicrobial susceptibility.* Antimicrobial agents and chemotherapy, 2006. **50**(4): p. 1463-1469, 10.1128/AAC.50.4.1463-1469.2006
20. Lopes-de-Campos, D., et al., *Delivering Amoxicillin at the Infection Site - a Rational Design through Lipid Nanoparticles.* Int. J. Nanomedicine, 2019. **14**: p. 2781-2795, 10.2147/ijn.S193992
21. Upadhyay, S.U., et al., *Effect of different lipids and surfactants on formulation of solid lipid nanoparticles incorporating tamoxifen citrate.* Journal of pharmacy & bioallied sciences, 2012. **4**(Suppl 1): p. S112-S113, 10.4103/0975-7406.94161
22. Kaur, P., et al., *Development, optimization and evaluation of surfactant-based pulmonary nanolipid carrier system of paclitaxel for the management of drug resistance lung cancer using Box-Behnken design.* Drug Deliv, 2016. **23**(6): p. 1912-1925, 10.3109/10717544.2014.993486

23. Ueda, Y., et al., *Inhibitory Effects of Polysorbate 80 on MRSA Biofilm Formed on Different Substrates Including Dermal Tissue.* Sci. Rep., 2019. **9**(1): p. 3128, 10.1038/s41598-019-39997-3
24. Toutain-Kidd, C.M., et al., *Polysorbate 80 Inhibition of Pseudomonas aeruginosa Biofilm Formation and its Cleavage by the Secreted Lipase LipA.* Antimicrob. Agents Chemother., 2009. **53**(1): p. 136-145, 10.1128/aac.00500-08
25. Lupoli, T.J., et al., *Transpeptidase-mediated incorporation of D-amino acids into bacterial peptidoglycan.* J Am Chem Soc, 2011. **133**(28): p. 10748-10751, 10.1021/ja2040656
26. Kolodkin-Gal, I., et al., *D-Amino Acids Trigger Biofilm Disassembly.* Science, 2010. **328**(5978): p. 627-629, 10.1126/science.1188628
27. Hochbaum, A.I., et al., *Inhibitory Effects of D-Amino Acids on Staphylococcus aureus Biofilm Development.* J. Bacteriol., 2011. **193**(20): p. 5616-5622, 10.1128/JB.05534-11
28. Rumbo, C., et al., *Assessment of antivirulence activity of several d-amino acids against Acinetobacter baumannii and Pseudomonas aeruginosa.* J Antimicrob Chemother, 2016. **71**(12): p. 3473-3481, 10.1093/jac/dkw342
29. Aliashkevich, A., L. Alvarez, and F. Cava, *New Insights Into the Mechanisms and Biological Roles of D-Amino Acids in Complex Eco-Systems.* Frontiers in Microbiology, 2018. **9**(683), 10.3389/fmicb.2018.00683

Chapter 5 – Methodologies to develop and characterize the nanodelivery systems

This chapter aims to describe the basic theoretical knowledge behind the production, optimization, and characterization of the developed NPs (**Figure 1**). The NPs were optimized and further physically characterized regarding functionalization, size, zeta potential, loading capacity, and morphology. *In vitro* studies to evaluate the cytocompatibility (cell viability, hemolysis) and the efficacy (viability, biomass, morphology) of the NPs were performed. *In vivo* biodistribution and antibiofilm efficacy were also assessed.

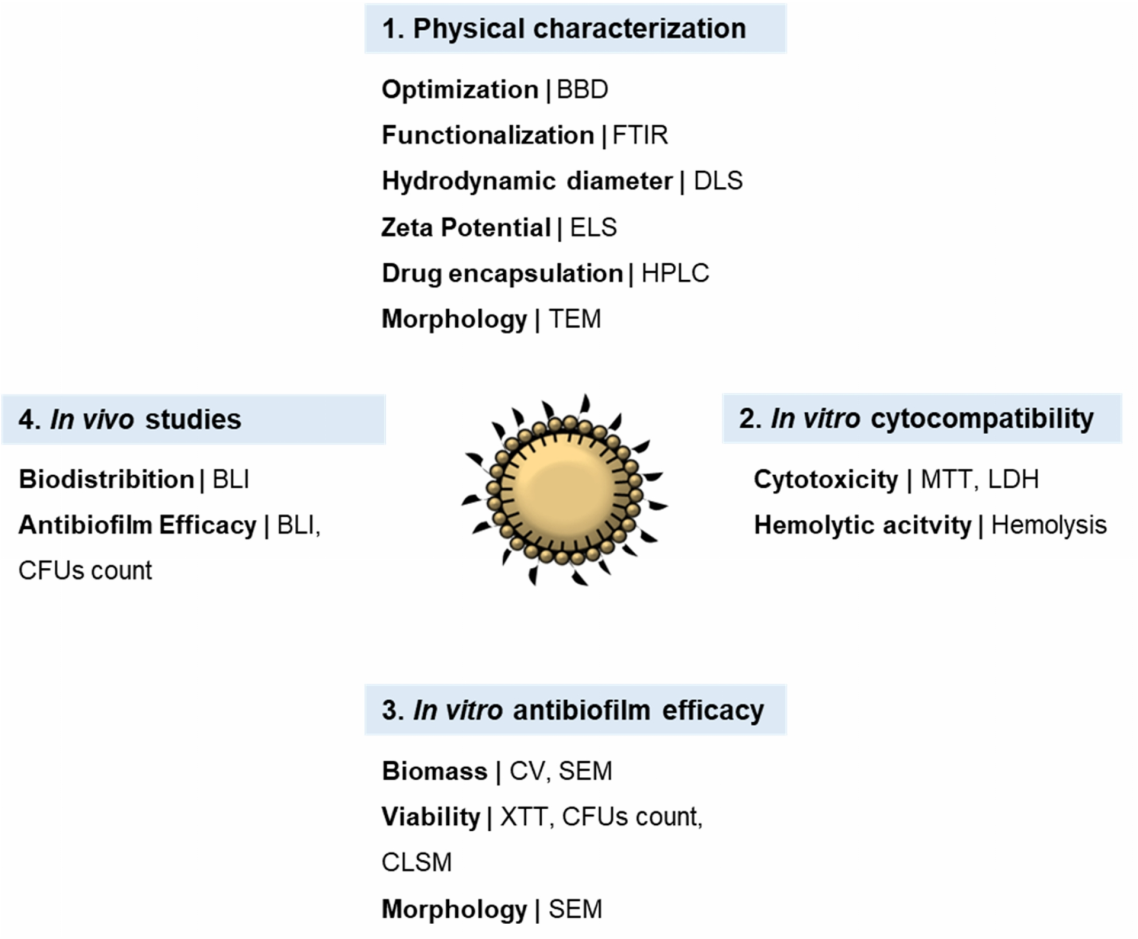


Figure 1: Schematic overview of the methodologies used for the physical characterization, *in vitro* cytocompatibility and antibiofilm assessment, and *in vivo* biodistribution and efficacy of the developed NPs. BBD, Box-Behnken design; BLI, bioluminescence imaging ; CFU, colony forming unit; CLSM, confocal laser scanning microscopy; CV, crystal violet; DLS, dynamic light scattering; ELS, electrophoretic light scattering; FTIR, Fourier-transform infrared spectroscopy; HPLC, high performance liquid chromatography; LDH, lactate dehydrogenase; MTT, 3-(4,5-dimethylthiazol-2-yl)-2,5-diphenyltetrazolium bromide; SEM, scanning electron microscopy; TEM, transmission electron microscopy; XTT, 2,3-Bis-(2-Methoxy-4-Nitro-5-Sulfophenyl)-2H-Tetrazolium-5-Carboxanilide.

Lipid nanoparticles preparation

In the last few decades, lipid NPs have been emerging as potential safe drug delivery systems to incorporate both lipophilic and hydrophilic drugs [1]. These carriers are composed by a matrix of physiological or physiologically related lipids that are easily degraded in the human body. Thus, these carriers usually show good biocompatibility and low cytotoxicity, which led to their extensive study for several applications [2]. Lipid NPs such as solid lipid nanoparticles (SLNs) and nanostructured lipid carriers (NLCs) are extensively described in the literature [1-3]. More recently, a new generation of lipid NPs were described by Cavalcanti *et al.* (2017), multiple lipid nanoparticles (MLNs), which have characteristics of both NLCs and multiple emulsions (W/O/W) [4].

Several methods to produce SLNs are reported, herein these NPs were produced by the double emulsion technique to encapsulate hydrophilic drugs (**Figure 2**). Briefly, in this procedure, hydrophilic drugs are incorporated in the inner aqueous phase. This phase is then added to the lipid phase and homogenized with agitation to form a primary emulsion (W/O). Further, the primary emulsion is emulsified with an outer aqueous phase containing a surfactant to form the double emulsion (W/O/W) under agitation. Lastly, the organic solvent is removed by evaporation under stirring at room temperature [5, 6].

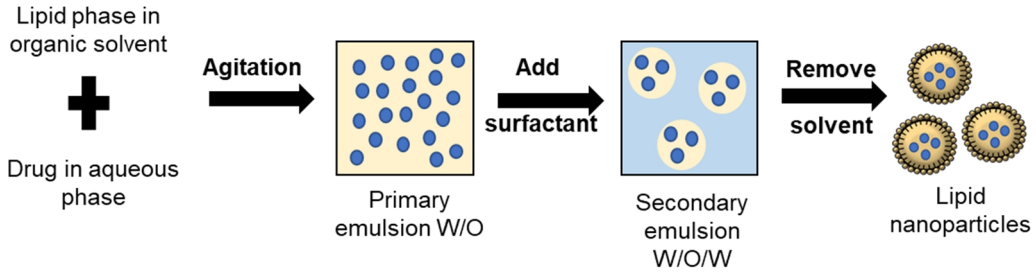


Figure 2: Double emulsion technique for production of lipid NPs as carriers of hydrophilic drugs. Adapted from [6].

The production of MLNs consists in a process based on a hot homogenization method combined with ultrasonication (**Figure 3**). In this thesis, the production method of MLNs reported by Cavalcanti *et al.* (2017) was adapted to obtain smaller particle sizes (around 200-300 nm). Firstly, the lipid phase (solid lipid, lipid liquid, and hydrophobic surfactant) is heated above the phase transition temperature of the solid lipid. Then, the pre-heated drug aqueous phase containing the hydrophilic drug is added to the melted lipid phase and the mixture is ultrasonicated to form the primary emulsion. This emulsion is left to cool down at

room temperature. Further, the hydrophilic surfactant is added, and the mixture is once more ultrasonicated [4].

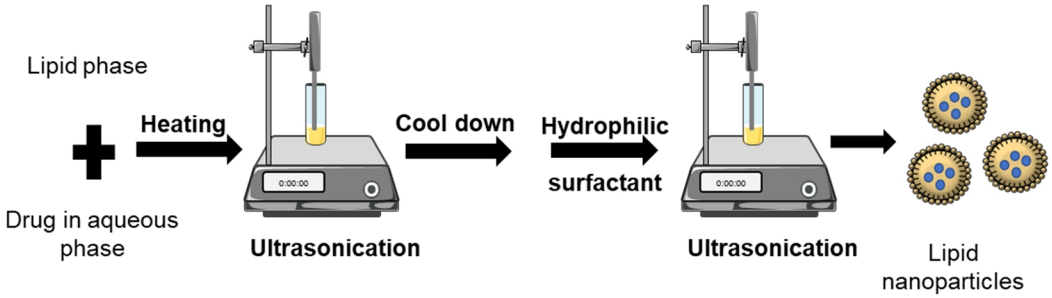


Figure 3: Production of multiple lipid nanoparticles (MLNs) as carriers of hydrophilic drugs.

Lipid nanoparticles optimization and characterization

1. Fourier transform infrared spectroscopy

Fourier transform infrared spectroscopy (FTIR) is a technique that measures the absorption of electromagnetic radiation in the infra-red region (wavelengths between 4000 - 400 cm^{-1}). The FTIR spectrum records the position of bands, according to the strength and nature of the molecular bonds vibrations. By analyzing these bands is possible to identify functional groups present in the sample, providing information regarding the presence of specific ligands at the nanoparticles surface [7].

2. Box-Behnken design

Optimization of NPs is commonly reached by studying the influence of one variable at the time (OVAT), while other variables are kept constant. The optimal formulation obtained by applying this approach is usually sub-optimal, since the interactions between variables are not considered [8].

To overcome the limitations of the OVAT approach, design of experiments (DoE) methodologies emerged. These require fewer experiments to achieve an optimal formulation, therefore lower consumption of reagents and less laborious work [8, 9]. Through experimental designs, it is possible to assess the effect of formulation factors (independent variables) and the interactions between them on the responses (dependent variables) [10].

The Box-Behnken design (BBD) is a widely used approach when several variables are studied simultaneously. In this design, the independent variables are adjusted at three equally distributed levels (-1, 0, +1). For 3 dependent variables, BBD requires 15 experimental runs, which can be represented by a multidimensional cube. The central point of this cube represents three replicates that are used to assess the precision of the design [10]. Additionally, BBD excludes combinations in which all independent variables are simultaneously at their lowest or highest level, avoiding experiments under extreme conditions [9].

3. Dynamic light scattering

Dynamic light scattering (DLS) is a commonly used technique to measure the size and size distribution of NPs in liquids [11]. This technique determines the hydrodynamic size of spherical particles in a colloid dispersion based on the Stokes-Einstein equation (1):

$$\boldsymbol{D_t} = \frac{\boldsymbol{k_B T}}{\boldsymbol{6\pi\eta R_H}} \quad (1)$$

Where k_B is the Boltzmann constant (1.38064852×10^{-23} J/K), T is temperature, η is absolute viscosity, and R_H is the hydrodynamic radius. The hydrodynamic radius considers the particles in a hydrated/solvated state [12].

In the DLS apparatus, the NPs suspension is exposed to an incident laser and the intensity of the scattered light is detected. The continuous movement of particles in the suspension (Brownian movement) causes constructive or destructive interferences on the intensity of the scattered light [12]. This interference is dependent on the particles size, with larger particles showing slower fluctuations of light scattered intensity over time.

This technique is widely used for the characterization of NPs, since it is noninvasive, accurate to determine the size of monodisperse samples, and the samples can be measured after dilution. Nevertheless, it has some limitations regarding samples with heterogeneous size distributions and non-spherical nanomaterials, being unable to accurately determine sizes in these cases. Additionally, dust particles may interfere with the scattering intensity, which leads to inaccuracies in the measurements [13].

4. Electrophoretic light scattering

The surface charge of NPs highly affects their behavior in the body, by influencing biodistribution, opsonization, toxicity, and ultimately the interactions with the biofilm [14, 15].

Both the biofilm matrix and bacterial cell wall are mainly negatively charged, which may lead to a preferential interaction with positively charged NPs, rather than negatively or neutrally charged NPs [15]. However, positively charged NPs usually exhibit a higher *in vivo* toxicity than negatively ones. Besides the influence on biological interactions, surface charge also plays a key role in the stability of a nanosuspension [14].

The zeta potential is a quantitative measure of the particle surface charge [14]. In an aqueous medium, the particles charge is affected by the ion distribution around the NPs. The surface of the particles is strongly bound to opposite charged ions, forming the Stern layer. Surrounding this layer there is an outer diffuse layer, consisting of ions that are loosely associated. Together, the two layers form the electrical double layer. When an external electrical field is applied to the nanosuspension, particles are attracted to the electrode with opposite charge. The equilibrium is reached when particles move at a constant velocity. This electrophoretic mobility allows to determine the zeta potential [13].

An absolute value of the zeta potential greater than 30 mV indicates a stable nanosuspension with no tendency to form aggregates, since individual charged particles repulse each other. However, when the absolute value is below 30 mV, the surface charge of the particles is relatively neutral, with insufficient charge repulsion to avoid aggregation [13, 14]. Consequently, aggregates, coagulation or flocculation may occur in the suspension [13].

The zeta potential measurement is highly sensitive to environmental changes, such as pH and ionic strength. The electroosmotic effect also influences the measurement of zeta potential, which may compromise precision and reproducibility [13].

5. High performance liquid chromatography

High performance liquid chromatography (HPLC) is a highly sensitive analytical method used for separation, analysis and quantification of substances. Regarding nanocarriers, HPLC is a useful technique to quantify the amount of drug encapsulated in the nanoparticles.

This technique is based on the distribution of an analyte (sample) between two different phases. In the process, high-pressure pumps (500 to 20 000 psi) force the liquid eluent (mobile phase) and the injected sample to pass through a column filled with an adsorbent material (stationary phase) [16]. At optimal conditions, the separation process occurs due to specific interactions between the molecules of the sample and the adsorbent material inside the column. Thus, each component of the sample will interact differently with the two

phases, which leads to different retention times in the column. After leaving the column, the sample components are collected by a detector (e.g., UV/VIS or fluorescence). The signals obtained by the detector are further converted into a chromatogram [16, 17]. In general, the HPLC instrument is composed by an injector, pump, column, and detector. In this system, the injector is responsible for adding the sample to the mobile phase [16].

The most popular HPLC mode for separation of substances is the reversed phase liquid chromatography (RPLC), since it is suitable for compounds of a wide range of structures and polarities (e.g., drugs and biomolecules). This mode consists in a nonpolar stationary phase and a polar mobile phase composed by water and a water-miscible organic solvent. Thus, RPLC is compatible with aqueous solutions and allows the separation of nonpolar, polar, and ionic compounds in the same run [18].

6. Transmission electron microscopy

Transmission electron microscopy (TEM) is commonly used to determine size, morphology, and degree of aggregation of NPs. In this microscopy, an incident electron beam is transmitted through the sample. The interaction between the beam and the sample leads to the transformation of the incident electrons into unscattered, elastically scattered, or inelastically scattered electrons. These electrons are focused by electromagnetic lenses and then projected on a screen [13].

This technique has a high spatial resolution, which enhances morphological analysis, however, it also presents several drawbacks. TEM requires high vacuum, which may lead to sample destruction and analysis in non-physiological conditions. Sample damage is also promoted by the intense, high voltage incident electron beam. Moreover, TEM produces two-dimensional images, which is a limitation for three-dimensional samples [13].

Cytocompatibility studies

1. Cell viability

To determine the cytotoxicity of NPs against cell cultures, it is common to use the tetrazolium salt (3-(4,5-dimethylthiazol-2-yl)-2,5-diphenyltetrazolium bromide) (MTT). This salt is able to cross the cell membrane due to its lipophilic side groups and positive net charge. Once inside viable cells, the MTT (weakly colored) is reduced by mitochondrial or cell plasma enzymes into the water-insoluble formazan (dark purple color). The formation

of formazan crystals ultimately compromises the integrity of cells, leading to cell death and stopping the reaction quickly. The formazan is further dissolved by an organic solvent and measured by UV spectroscopy. Despite being easy and rapid, the MTT assay is not suitable for real-time measurements, since the addition of MTT to the cell culture leads to cell death [19]. The lactate dehydrogenase (LDH) assay is also widely used to evaluate the cytotoxicity of nanosystems. LDH is a cytoplasmic enzyme present in most cells. When the cell membrane is damaged, LDH is rapidly released to the cell culture medium. The LDH is quantified through an enzymatic reaction where LDH catalyzes the conversion of lactate to pyruvate with reduction of NAD+ to NADH, followed by reduction of a tetrazolium salt to a red formazan product. Formazan is quantified, being directly proportional to the amount of LDH released from the cells [20].

2. Hemolysis

The cytocompatibility of nanoparticles can be also evaluated through their hemolytic potential when in contact with blood [21, 22].

In this assay, red blood cells (RBCs) are separated from the remaining blood components and further incubated with the NPs. During the incubation period, the amount of hemoglobin released from RBCs is spectrophotometrically quantified as a measure of hemolysis [22, 23]. The results are normalized by a positive control where RBCs are treated with a detergent (e.g., Triton X-100). The amount of hemoglobin released in this control is calibrated to 100% hemolysis. Contrarily, in the negative control (buffer) is not expected to observe significant hemolysis [23].

The hemolysis assay is a very useful, fast, and easy method to evaluate cytocompatibility. However, it is highly susceptible to variations that depend on blood conditions (e.g., presence of anticoagulants), incubation time, wavelength at which the hemoglobin is quantified, among others. Thus, comparison of results from different studies becomes a difficult task [21].

In vitro antibiofilm efficacy studies

1. Biofilm models

Microtiter plate biofilm model

In vitro biofilm models are crucial to evaluate the potential antibiofilm efficacy of nanoparticles prior an *in vivo* assessment. The microtiter plate is widely used as an *in vitro* biofilm model due to being a fast, inexpensive, and simple method, which does not require advanced equipment [24, 25]. On the other hand, a limitation of this model is that the biofilm is commonly loosely attached to the surfaces, which may lead to its detachment during the washing steps [25].

Calgary biofilm device model

In the Calgary biofilm device model, biofilm formation occurs in pegs attached to a coverslip that fits the wells of a microtiter plate containing a bacterial suspension (**Figure 4**) [26]. Similar to the microtiter plate biofilm model, this model is adequate for high-throughput screening. However, the biofilms formed on the pegs of this model do not result from cell sedimentation, but only from sessile development. Despite this advantage, the formation of biofilm on pegs requires sonication for bacterial cell recovery, which typically recovers only a fraction of the microbial community [25].

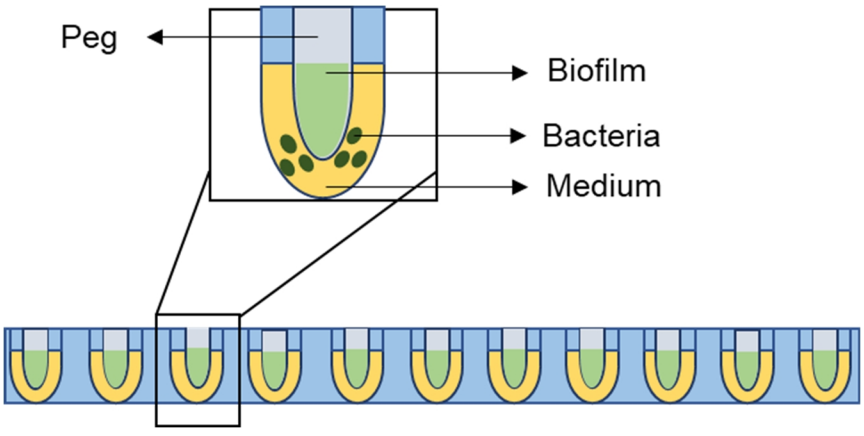


Figure 4: Scheme of the Calgary biofilm device model. Adapted from [27].

Catheter biofilm model

The catheter biofilm model has been previously reported in the literature [28]. In this model, biofilms are formed in polyurethane catheters. The use of catheters allows to mimic the *in vivo* three-dimensional biofilm architecture. The initial microbial adhesion on the surface of catheters is dependent of the physicochemical characteristics of the material, such as roughness, hydrophobicity, and electrostatic interactions [29]. Thus, these properties will determine the formation and growth of biofilm structures. However, quantification of biofilm biomass requires sonication of the catheters, where firmly attached cells may not be removed efficiently [25]. In addition, the washing steps required in this model may promote detachment of loosely attached bacterial cells.

2. Crystal violet (CV)

Crystal violet (CV) staining is widely used as an indirect method for quantification of biofilm biomass [30]. In this staining, a basic trianiline dye permeates both live and dead cells, as well as some components of the biofilm matrix. The CV assay consists in the incubation of the biofilm with the dye and further biofilm washing to remove the unattached cells and the unbound dye [25, 30]. Finally, a decoloring solution is added to dissolve crystal violet and the absorbance is read at 530-600 nm [30].

This method is easy to perform, inexpensive, fast, and versatile, being possible to use with a high range of bacterial species [25, 30]. Besides, it does not require cell detachment from the support, contrarily to plate counts [25].

Despite the advantages, this technique also presents some limitations. The main disadvantage is the nonspecific nature of CV, which unable to distinguish between live and dead cells. Also, the several washing steps may remove attached cells from loose biofilms, leading to bias quantification of biomass [25].

3. Bacterial cell viability

Plate count: colony forming units (CFUs)

The determination of colony forming units (CFUs) on agar media is a widely used technique to quantify the number of viable cells within the biofilm [25]. In this assay, the cells within a mature biofilm are suspended and homogenized in a liquid medium by scraping, vortexing,

or sonication, followed by serial dilution and plating onto agar media. Then, the cells in the agar plates are incubated until it is possible to count colonies [30].

A great advantage of this assay comparing with crystal violet, is that it differentiates viable and dead cells, allowing the quantification of viable cells without the need of applying a dye [30]. Besides, this technique does not require advanced equipment, being easy to perform. However, plate count is time consuming, and it may not detect a common subpopulation of biofilm cells: viable but not-culturable (VBNC) cells. Furthermore, the number of culturable cells can be underestimated due to existence of microbial aggregates (clumps) in suspension [25, 30].

XTT assay

Tetrazolium salts are extensively used to monitor metabolism in *in vitro* conditions. Amongst these, XTT (2,3-Bis-(2-Methoxy-4-Nitro-5-Sulfophenyl)-2H-Tetrazolium-5-Carboxanilide) is commonly used to quantify cellular viability within biofilms [30]. This colorless salt is cleaved by dehydrogenase enzymes of metabolic active cells within the biofilm into formazan, which is detectable by UV-VIS spectroscopy at a wavelength of 490 nm [25, 30].

4. Scanning electron microscopy

Scanning electron microscopy (SEM) is a high-resolution microscopy widely used to evaluate surface topography. Concerning biofilms, SEM images allow to evaluate bacterial interactions, EPS organization, and biofilm morphology [30].

In this technique, an incident electron beam interacts with the sample, which generates the emission of secondary electrons that are detected and converted into a digital image of the sample surface due to their low energy [30].

Due to its high-resolution, SEM reveals in deep detail the biofilm structure and topography. However, since SEM analysis is performed under high vacuum, samples preparation requires fixation and dehydration of the biofilms, which may result in distortions of size and structure. Posteriorly, the biofilms are coated with an ultrathin layer of a conductive metal to allow for dissipation of static charges, which often leads to artifacts [30].

5. Confocal laser scanning microscopy (CLSM)

Confocal laser scanning microscopy (CLSM) is a widely used technique for several applications. In this technique, it is possible to acquire planes at different depths in the sample to build a three-dimensional representation of the biofilm. Thus, parameters such as biofilm bio-volume, thickness, and roughness, are accessed through this microscopy [25, 31]. In addition, it is possible to perform analysis of cell viability within the biofilm. For this purpose, fluorescent dyes that stain live and dead cells are used. The most popular live/dead kit consists in the use of SYTO-9 (green color) in combination with propidium iodide (red color). SYTO-9 is a cell permeant, while propidium iodide is a cell impermeant. Therefore, live bacteria will appear green, while dead bacteria will appear yellow or red. However, the local properties of biofilms and the natural auto-fluorescence of some samples may interfere with the signal of the used dyes [25].

In vivo studies

1. Murine subcutaneous biofilm model

The murine subcutaneous biofilm model is described in detail by Kucharíková *et al.* (2015). In this *in vivo* model, previously infected 1 cm long catheter pieces were implanted subcutaneously in mice (**Figure 5**) [32]. This model has been used to evaluate the efficacy of antibiofilm agents against several microorganisms, such as *Candida albicans* [32, 33], *Candida glabrata* [34], and *S. aureus* [28, 35]. The number of catheter pieces implanted in each animal may vary from 4 to 8 pieces [32, 33, 36]. Comparing with other *in vivo* models, the main advantage of this model consists in the potential to study multiple individual biofilms per animal, by considering the biofilms formed inside the lumen of each catheter piece as independent structures [32].

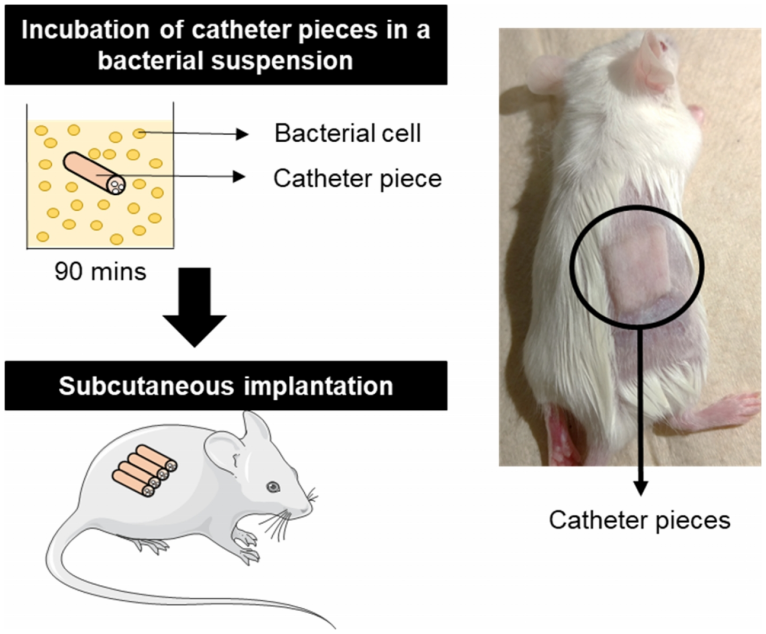


Figure 5: Schematic representation of the murine subcutaneous biofilm model. Firstly, catheter pieces are incubated with a bacterial suspension for 90 mins to promote adhesion of cells to the surface of the material. After several washing steps, the catheter pieces are implanted subcutaneously in the back of the animal to allow biofilm growth in *in vivo* conditions.

2. *In vivo* bioluminescent imaging

Some living organisms have been showing the ability to convert chemical energy into light, a biological process that requires an enzyme (luciferase), a substrate (luciferin), and oxygen. This natural phenomenon has prompted research in the field of bioluminescence imaging (BLI) [37]. The BLI technique is based on the detection of photons emitted from cells or tissues and presents several advantages compared to fluorescence methods [37, 38]. Luminescent reporters are much more sensitive than fluorescent ones, characterized by negligible background levels of bioluminescence. In addition, these reporters do not require exogenous illumination, which in fluorescence methods commonly leads to disturbances in light-sensitive tissues and phototoxic damage to cells. Hence, BLI is a highly sensitive non-toxic technique, ideal for long-term, longitudinal studies in living cells, tissues, or whole animals [38]. This technology has been applied to several fields of research, such as neuroscience, cancer, stem cells, and infectious diseases [37]. In particular, several studies reported the use of BLI to assess biofilm progression and treatment in mice, using bioluminescent strains (e.g., *Xen36*) [28, 33, 34].

References

1. Battaglia, L. and M. Gallarate, *Lipid nanoparticles: state of the art, new preparation methods and challenges in drug delivery.* Expert Opin. Drug Deliv., 2012. **9**(5): p. 497-508, 10.1517/17425247.2012.673278
2. Das, S. and A. Chaudhury, *Recent advances in lipid nanoparticle formulations with solid matrix for oral drug delivery.* AAPS PharmSciTech, 2011. **12**(1): p. 62-76, 10.1208/s12249-010-9563-0
3. Severino, P., et al., *Current State-of-Art and New Trends on Lipid Nanoparticles (SLN and NLC) for Oral Drug Delivery.* J. Drug Deliv., 2012. **2012**: p. 750891, 10.1155/2012/750891
4. Cavalcanti, S.M.T., et al., *Multiple Lipid Nanoparticles (MLN), a New Generation of Lipid Nanoparticles for Drug Delivery Systems: Lamivudine-MLN Experimental Design.* Pharm Res, 2017. **34**(6): p. 1204-1216, 10.1007/s11095-017-2136-0
5. Shah, R., et al., *Lipid nanoparticles: production, characterization and stability*. 2015: Springer.
6. Iqbal, M., et al., *Double Emulsion Solvent Evaporation Techniques Used for Drug Encapsulation.* Int. J. Pharm., 2015. **496**(2): p. 173-190, https://doi.org/10.1016/j.ijpharm.2015.10.057
7. Mourdikoudis, S., R.M. Pallares, and N.T.K. Thanh, *Characterization techniques for nanoparticles: comparison and complementarity upon studying nanoparticle properties.* Nanoscale, 2018. **10**(27): p. 12871-12934, 10.1039/C8NR02278J
8. Singh, B., et al., *Developing Oral Drug Delivery Systems Using Formulation by Design: Vital Precepts, Retrospect and Prospects.* Expert Opin. Drug Deliv., 2011. **8**(10): p. 1341-1360, 10.1517/17425247.2011.605120
9. Ferreira, S.L.C., et al., *Box-Behnken Design: An Alternative for the Optimization of Analytical Methods.* Anal. Chim. Acta, 2007. **597**(2): p. 179-186, https://doi.org/10.1016/j.aca.2007.07.011
10. Marasini, N., et al., *Development and optimization of self-nanoemulsifying drug delivery system with enhanced bioavailability by Box-Behnken design and desirability function.* J Pharm Sci, 2012. **101**(12): p. 4584-4596, 10.1002/jps.23333
11. Pecora, R., *Dynamic light scattering measurement of nanometer particles in liquids.* Journal of nanoparticle research, 2000. **2**(2): p. 123-131,
12. Bhattacharjee, S., *DLS and zeta potential – what they are and what they are not?* J Control Release, 2016. **235**: p. 337-351, https://doi.org/10.1016/j.jconrel.2016.06.017

13. Lin, P.-C., et al., *Techniques for physicochemical characterization of nanomaterials.* Biotechnology Advances, 2014. **32**(4): p. 711-726, https://doi.org/10.1016/j.biotechadv.2013.11.006
14. Kalashnikova, I., et al., *Characterization of drug-loaded nanoparticles*. 2015, IAPC Publishing, Zagreb, Croatia. p. 147-164,
15. Pinto, R.M., et al., *Innovative strategies toward the disassembly of the EPS matrix in bacterial biofilms.* Front. Microbiol., 2020. **11**(952), 10.3389/fmicb.2020.00952
16. LaCourse, M.E. and W.R. LaCourse, *Chapter 17 - General instrumentation in HPLC*, in *Liquid Chromatography (Second Edition)*, S. Fanali, et al., Editors. 2017, Elsevier. p. 417-429.
17. Weston, A. and P.R. Brown, *Chapter 1 - High-Performance Liquid Chromatography*, in *HPLC and CE*, A. Weston and P.R. Brown, Editors. 1997, Academic Press: San Diego. p. 1-23.
18. García-Alvarez-Coque, M.C., J.J. Baeza-Baeza, and G. Ramis-Ramos, *Reversed phase liquid chromatography.* Analytical Separation Science, 2015: p. 159-198,
19. Prabst, K., et al., *Basic colorimetric proliferation assays: MTT, WST, and resazurin.* Methods Mol Biol, 2017. **1601**: p. 1-17, 10.1007/978-1-4939-6960-9_1
20. Decker, T. and M.L. Lohmann-Matthes, *A quick and simple method for the quantitation of lactate dehydrogenase release in measurements of cellular cytotoxicity and tumor necrosis factor (TNF) activity.* J Immunol Methods, 1988. **115**(1): p. 61-69, 10.1016/0022-1759(88)90310-9
21. Dobrovolskaia, M.A., et al., *Method for analysis of nanoparticle hemolytic properties in vitro.* Nano letters, 2008. **8**(8): p. 2180-2187, 10.1021/nl0805615
22. Choi, J., et al., *Physicochemical characterization and in vitro hemolysis evaluation of silver nanoparticles.* Toxicol Sci, 2011. **123**(1): p. 133-43, 10.1093/toxsci/kfr149
23. Evans, B.C., et al., *Ex vivo red blood cell hemolysis assay for the evaluation of pH-responsive endosomolytic agents for cytosolic delivery of biomacromolecular drugs.* J Vis Exp, 2013(73): p. e50166, 10.3791/50166
24. Lebeaux, D., et al., *From in vitro to in vivo models of bacterial biofilm-related infections.* Pathogens, 2013. **2**(2): p. 288-356, 10.3390/pathogens2020288
25. Azeredo, J., et al., *Critical review on biofilm methods.* Crit Rev Microbiol, 2017. **43**(3): p. 313-351, 10.1080/1040841x.2016.1208146
26. Ceri, H., et al., *The Calgary Biofilm Device: new technology for rapid determination of antibiotic susceptibilities of bacterial biofilms.* J. Clin. Microbiol., 1999. **37**(6): p. 1771-1776, 10.1128/jcm.37.6.1771-1776.1999

27. Harrison, J.J., et al., *The use of microscopy and three-dimensional visualization to evaluate the structure of microbial biofilms cultivated in the calgary biofilm device.* Biological Procedures Online, 2006. **8**(1): p. 194-215, 10.1251/bpo127
28. Siala, W., et al., *The Antifungal Caspofungin Increases Fluoroquinolone Activity Against Staphylococcus aureus Biofilms by Inhibiting N-Acetylglucosamine Transferase.* Nat. Commun., 2016. **7**: p. 1-15, 10.1038/ncomms13286
29. Gominet, M., et al., *Central venous catheters and biofilms: where do we stand in 2017?* Apmis, 2017. **125**(4): p. 365-375, 10.1111/apm.12665
30. Wilson, C., et al., *Quantitative and qualitative assessment methods for biofilm growth: a mini-review.* Res Rev J Eng Technol, 2017. **6**(4),
31. Bridier, A., et al., *The biofilm architecture of sixty opportunistic pathogens deciphered using a high throughput CLSM method.* Journal of Microbiological Methods, 2010. **82**(1): p. 64-70, https://doi.org/10.1016/j.mimet.2010.04.006
32. Kucharíková, S., et al., *Candida albicans biofilm development on medically-relevant foreign bodies in a mouse subcutaneous model followed by bioluminescence imaging.* Journal of visualized experiments : JoVE, 2015(95): p. 52239-52239, 10.3791/52239
33. Vande Velde, G., et al., *Bioluminescence imaging increases in vivo screening efficiency for antifungal activity against device-associated Candida albicans biofilms.* Int J Antimicrob Agents, 2018. **52**(1): p. 42-51, 10.1016/j.ijantimicag.2018.03.007
34. Persyn, A., et al., *Monitoring of Fluconazole and Caspofungin Activity against In Vivo Candida glabrata Biofilms by Bioluminescence Imaging.* Antimicrob Agents Chemother, 2019. **63**(2), 10.1128/aac.01555-18
35. Rogiers, O., et al., *Anidulafungin increases the antibacterial activity of tigecycline in polymicrobial Candida albicans/Staphylococcus aureus biofilms on intraperitoneally implanted foreign bodies.* J Antimicrob Chemother, 2018. **73**(10): p. 2806-2814, 10.1093/jac/dky246
36. Vila, T., et al., *Therapeutic implications of C. albicans-S. aureus mixed biofilm in a murine subcutaneous catheter model of polymicrobial infection.* Virulence, 2021. **12**(1): p. 835-851, 10.1080/21505594.2021.1894834
37. Badr, C.E. and B.A. Tannous, *Bioluminescence imaging: progress and applications.* Trends in biotechnology, 2011. **29**(12): p. 624-633, 10.1016/j.tibtech.2011.06.010
38. Welsh, D.K. and S.A. Kay, *Bioluminescence imaging in living organisms.* Curr Opin Biotechnol, 2005. **16**(1): p. 73-78, 10.1016/j.copbio.2004.12.006

Chapter 6. Progress beyond the state of the art

The manuscripts that this thesis has originated will be presented in the following subchapters:

Chapter 6.1. – *N*-Acetyl-L-cysteine-Loaded Nanosystems as a Promising Therapeutic Approach Toward the Eradication of *Pseudomonas aeruginosa* Biofilms (ACS Appl. Mater. Interfaces. 2021; 13(36): 42329–42343)

Chapter 6.2. – Antibiofilm combinatory strategy towards *S. aureus*: novel moxifloxacin-loaded nanosystems joint with encapsulated N-acetyl-L-cysteine

Chapter 6.3. – Caspofungin-loaded nanoparticles as an adjuvant to improve nanoantibiotics activity in a multi-target strategy against *Staphylococcus aureus* biofilms

Chapter 6.4. – Farnesol-loaded lipid nanoparticles as a non-antibiotic alternative therapy to eradicate *S. aureus* biofilms

In this work, four nanosystems were developed by different production methods to encapsulate *N*-acetyl cysteine, moxifloxacin, caspofungin, and farnesol. The composition of the lipid nanoparticles and the production method used for each nanosystem can be found in **Figure 1**.

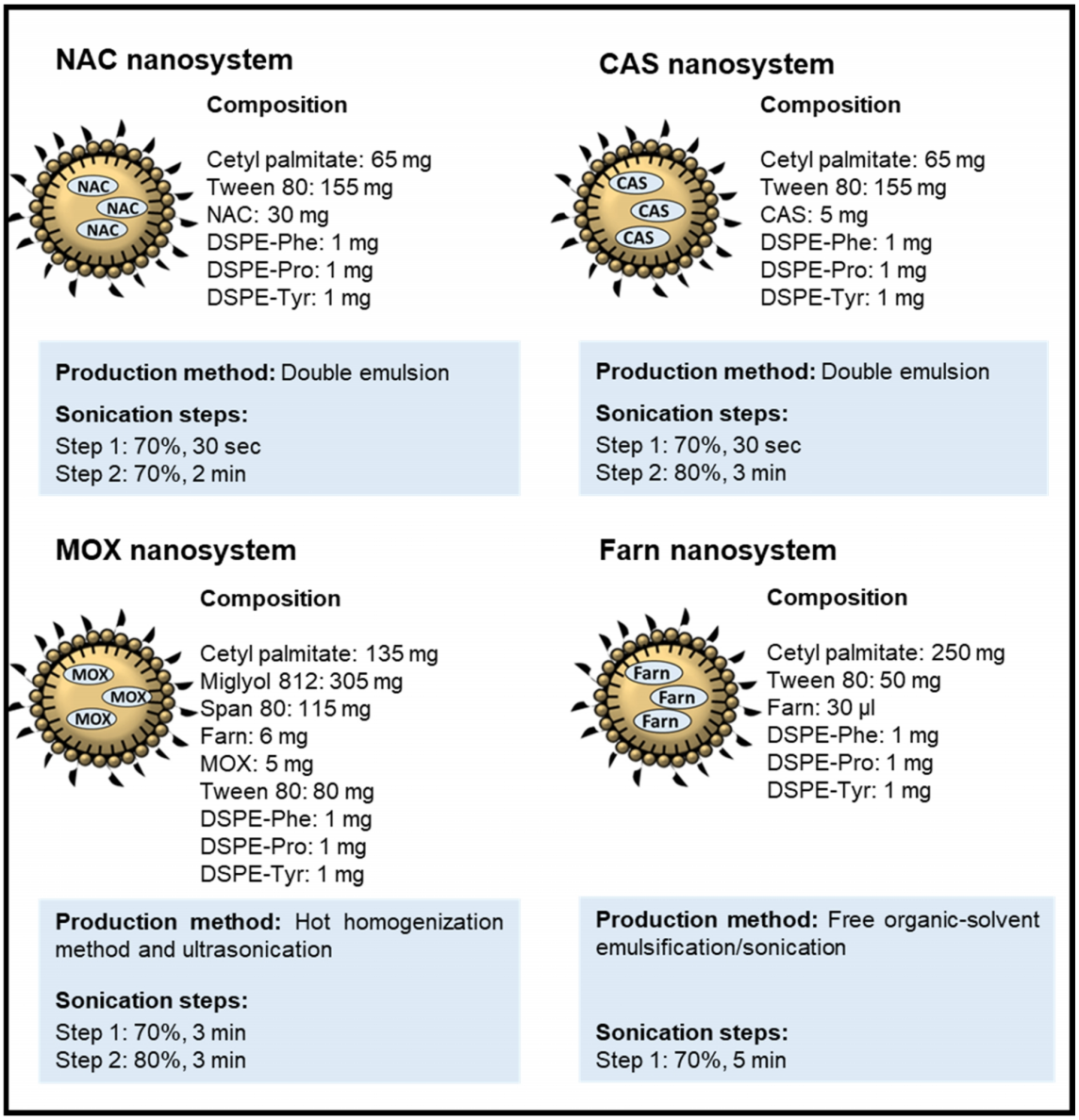
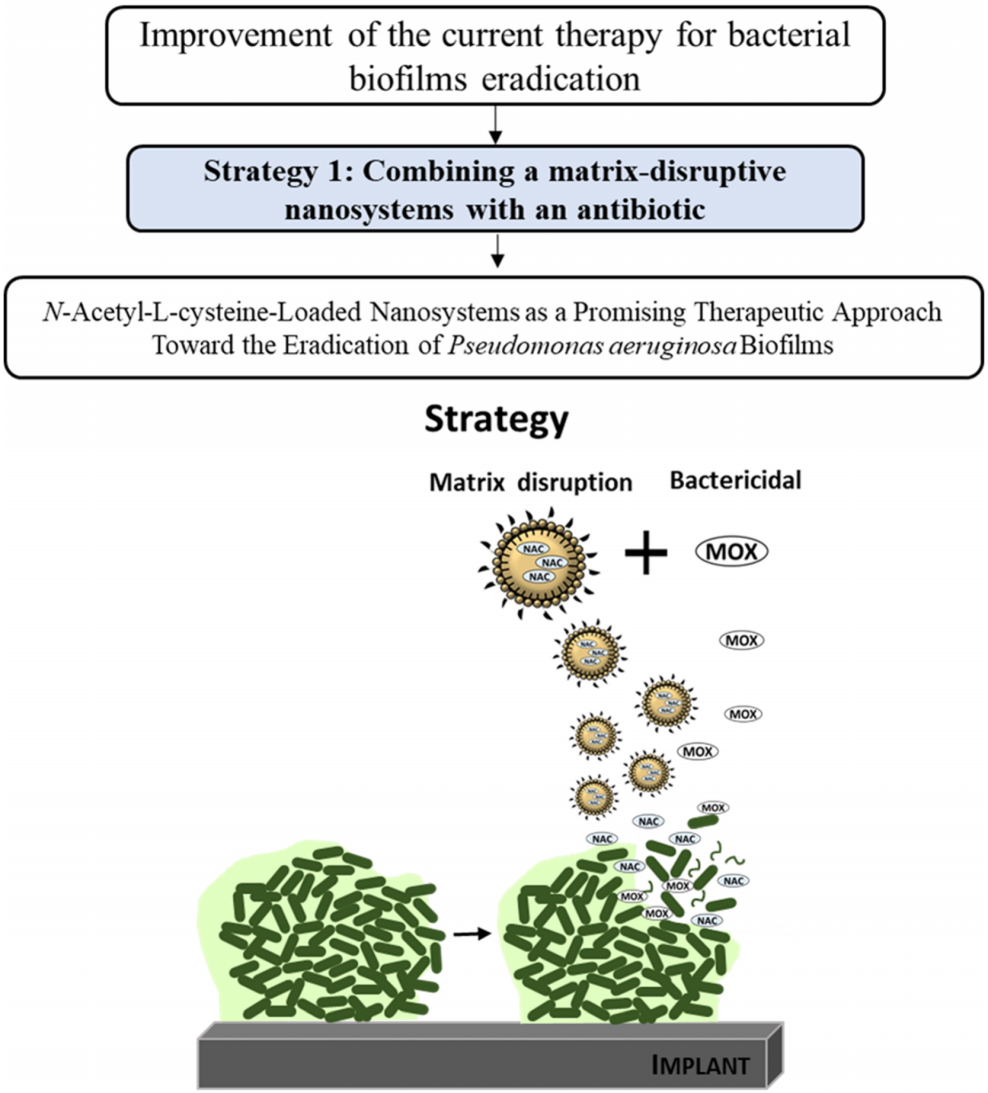


Figure 1: Composition and production details of the nanosystems developed to encapsulate *N*-acetyl cysteine, moxifloxacin, caspofungin, and farnesol. CAS, caspofungin; DSPE, 1,2-distearoyl-sn-glycero-3-phosphoethanolamine-N-[amino(polyethylene glycol)-2000; Farn, farnesol; MOX, moxifloxacin; NAC, *N*-acetyl cysteine; Phe, phenylalanine; Pro, proline; Tyr, tyrosine.

Chapter 6.1.

N-Acetyl-L-cysteine-Loaded Nanosystems as a Promising Therapeutic Approach Toward the Eradication of *Pseudomonas aeruginosa* Biofilms

In this chapter, *N*-acetyl-L-cysteine (NAC)-loaded lipid nanoparticles functionalized with D-amino acids were optimized and characterized. The *in vitro* antibiofilm activity of the formulations was assessed in both gram-positive (*S. epidermidis*) and gram-negative (*P. aeruginosa*) bacteria. The NAC-loaded nanoparticles were ineffective against *S. epidermidis*, however they revealed potential alone or in combination with an antibiotic (moxifloxacin) against *P. aeruginosa* biofilms.



ACS APPLIED MATERIALS & INTERFACES

www.acsami.org Research Article

N-Acetyl-L-cysteine-Loaded Nanosystems as a Promising Therapeutic Approach Toward the Eradication of *Pseudomonas aeruginosa* Biofilms

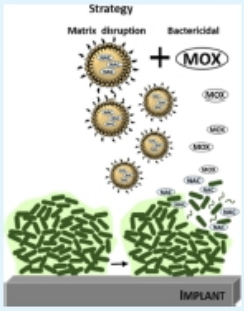
Rita M. Pinto, Claudia Monteiro, Sofia A. Costa Lima, Susana Casal, Patrick Van Dijck, M. Cristina L. Martins, Cláudia Nunes,* and Salette Reis

Cite This: https://doi.org/10.1021/acsami.1c05124 Read Online

ACCESS | Metrics & More | Article Recommendations | Supporting Information

Downloaded via KU LEUVEN on September 1, 2021 at 06:52:31 (UTC).
See https://pubs.acs.org/sharingguidelines for options on how to legitimately share published articles.

ABSTRACT: Bacterial biofilms are a major health concern, mainly due to their contribution to increased bacterial resistance to well-known antibiotics. The conventional treatment of biofilms represents a challenge, and frequently, eradication is not achieved with long-lasting administration of antibiotics. In this context, the present work proposes an innovative therapeutic approach that is focused on the encapsulation of *N*-acetyl-L-cysteine (NAC) into lipid nanoparticles (LNPs) functionalized with D-amino acids to target and disrupt bacterial biofilms. The optimized formulations presented a mean hydrodynamic diameter around 200 nm, a low polydispersity index, and a high loading capacity. These formulations were stable under storage conditions up to 6 months. *In vitro* biocompatibility studies showed a low cytotoxicity effect in fibroblasts and a low hemolytic activity in human red blood cells. Nevertheless, unloaded LNPs showed a higher hemolytic potential than NAC-loaded LNPs, which suggests a safer profile of the latter. The *in vitro* antibiofilm efficacy of the developed formulations was tested against *Staphylococcus epidermidis* (Gram-positive) and *Pseudomonas aeruginosa* (Gram-negative) mature biofilms. The results showed that the NAC-loaded LNPs were ineffective against *S. epidermidis* biofilms, while a significant reduction of biofilm biomass and bacterial viability in *P. aeruginosa* biofilms were observed. In a more complex therapeutic approach, the LNPs were further combined with moxifloxacin, revealing a beneficial effect between the LNPs and the antibiotic against *P. aeruginosa* biofilms. Both alone and in combination with moxifloxacin, unloaded and NAC-loaded LNPs functionalized with D-amino acids showed a great potential to reduce bacterial viability, with no significant differences in the presence or absence of NAC. However, the presence of NAC in NAC-loaded functionalized LNPs shows a safer profile than the unloaded LNPs, which is beneficial for an *in vivo* application. Overall, the developed formulations present a potential therapeutic approach against *P. aeruginosa* biofilms, alone or in combination with antibiotics.



KEYWORDS: *S. epidermidis, P. aeruginosa, D-amino acids, nanoparticles, moxifloxacin*

1. INTRODUCTION

Nowadays, bacterial biofilms are a major health concern at a worldwide level. Particularly, implant-associated biofilms play a key role in the increasing numbers of antibiotic resistance cases due to high demand for indwelling prosthetic devices. When a mature biofilm is established on the surface of the implant, the only available treatment consists of medical device removal and further antibiotic therapy.[1] Thus, the lack of an efficient therapy due to antibiotic resistance phenomena promotes the search for an alternative nonantibiotic treatment.

N-Acetyl-L-cysteine (NAC) is a clinically used drug with a broad number of applications. Among others, this mucolytic agent is commonly used to treat acetaminophen intoxications, chemotherapy-induced toxicity, and psychiatric disorders.[2] Additionally, some studies also report the antibiofilm activity of NAC (alone or in combination with antibiotics) against both Gram-negative and Gram-positive bacteria.[3−5] The antimicrobial mechanism of NAC is still relatively unknown; however, it is suggested that the sulfhydryl group of this compound may react with bacterial proteins and disturb the intracellular redox equilibrium.[6,7] In the biofilms, NAC is able to reduce and prevent biofilm formation on surfaces, reduce extracellular polysaccharide production, and even disrupt mature biofilms.[7,8] However, NAC has low bioavailability (below 5%) and it exchanges redox reactions with proteins in plasma.[2] Thus, the efficiency of NAC by both oral and intravenous administration is compromised.

Nanotechnology is a promising approach for drug delivery purposes because nanoparticles can protect the drug from the

Received: March 18, 2021
Accepted: July 19, 2021

ACS Publications © XXXX The Authors. Published by American Chemical Society

https://doi.org/10.1021/acsami.1c05124
ACS Appl. Mater. Interfaces XXXX, XXX, XXX−XXX

ACS Applied Materials & Interfaces www.acsami.org Research Article

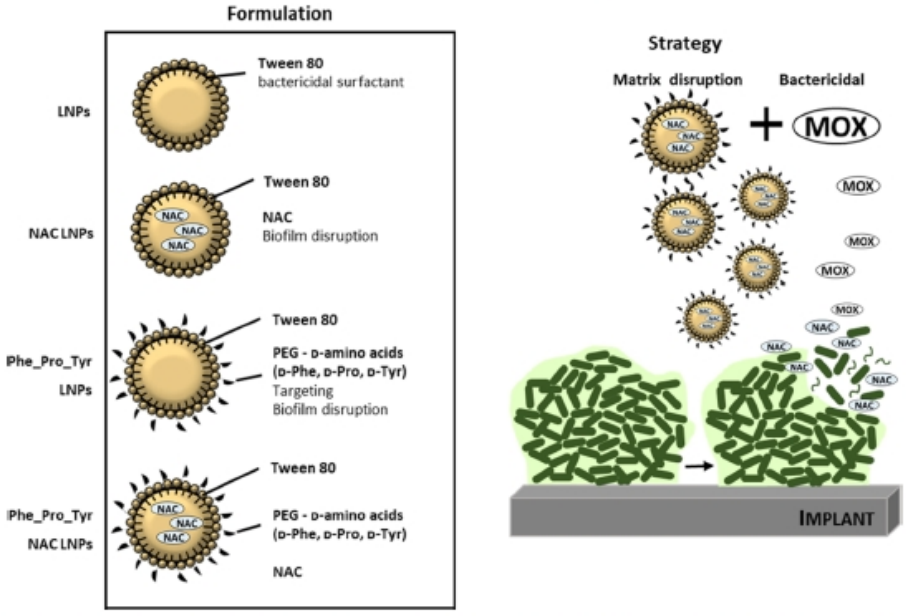


Figure 1. Schematic overview of the LNPs developed to further combine with MOX in an innovative therapeutic approach to eradicate bacterial biofilms. The designed LNPs were produced by the double emulsion method. The LNPs are composed of cetyl palmitate and Tween 80. The functionalized LNPs were coated with DSPE-PEG_{2000}-NH_2-D-amino acid (D-Phenylalanine, D-Proline, and D-Tyrosine) conjugates.

harsh external environment, while targeting it to the site of interest, improving its therapeutic efficiency.[9] Among the several types of nanocarriers, lipid nanoparticles (LNPs) have received some attention not only for their biocompatibility and biodegradability but also for their low-cost and easy scale-up.[10]

The current work aims to design a targeted nanosystem with potential to eradicate mature bacterial biofilms. Due to the potential antibiofilm activity of NAC, this agent was encapsulated into LNPs, aiming to avoid redox reactions between NAC and plasma proteins and renal clearance, therefore increasing its concentration at the target site. The surface of the LNPs was functionalized with poly (ethylene glycol) (PEG) and three D-amino acids: D-phenylalanine (D-Phe), D-proline (D-Pro), and D-tyrosine (D-Tyr). PEG was used to increase the LNP circulation time after an intravenous administration and sustain the release rate of the encapsulated NAC.[11] PEG promotes an increased circulation time of the LNPs mainly by avoiding recognition by the host immune system.[12] The three D-amino acids were selected as functionalization agents due to their ability to target and disassemble bacterial biofilms.[13] According to the literature, these compounds prevent biofilm formation and disrupt existing biofilms by incorporating into the peptide side chains of peptidoglycan, which ultimately triggers the release of amyloid fibers responsible to link cells to the biofilm structure.[13,14] Polysorbate 80 (Tween 80) was chosen as a surfactant due to its reported antibiofilm activity against both Gram-negative and Gram-positive bacteria.[15,16]

Thus, this study encompasses the design, development, and characterization of unloaded and NAC-loaded LNPs for intravenous administration. To optimize the LNP properties, a Box–Behnken design (BBD) was used. This approach is useful when several variables are studied simultaneously in an optimization process, which is more efficient and of lower cost compared to full three-level factorial designs.[17] In this methodology, the effect of independent variables adjusted at three different levels on the response of fixed dependent variables is investigated.[17−20] The LNPs were physically characterized according to the mean hydrodynamic diameter, polydispersity (PDI), zeta potential, and loading capacity (LC). The storage stability and the *in vitro* toxicity of the LNPs to red blood cells and fibroblasts were also evaluated. Moreover, the antibiofilm activity of the unloaded and NAC-loaded LNPs was assessed in both Gram-negative [*Pseudomonas aeruginosa* (*P. aeruginosa*)] and Gram-positive [*Staphylococcus epidermidis* (*S. epidermidis*)] bacteria. Under specific circumstances, these bacteria can lead to serious infections. As pathogens, a key virulent factor of these bacteria is the formation of a biofilm structure. Thus, *P. aeruginosa* and *S. epidermidis* are among the most prevalent species in common biofilm-related infections, which can be associated with medical devices (contact lenses, implants, and catheters) or disease (cystic fibrosis and wounds).[1,21]

In a step forward toward an innovative therapeutic against bacterial biofilms, the developed LNPs were further combined with an antibiotic, moxifloxacin (MOX). In this approach, the encapsulated NAC would disrupt the biofilm matrix, while the antibiotic would kill the dispersed bacterial cells (Figure 1). MOX was selected for this purpose due to a previous report of the synergistic potential of this antibiotic with a matrix-disruptive agent, caspofungin, to eradicate bacterial biofilms.[22] Besides, MOX is a fluoroquinolone with a broad spectrum of activity against both Gram-negative and Gram-positive bacteria.[23]

2. EXPERIMENTAL SECTION

2.1. Materials. The lipid Cetyl palmitate was a kind gift from Gattefossé (Gattefossé, France). DSPE-PEG2000-NH_2 (1,2-distearo-

https://doi.org/10.1021/acsami.1c05124
ACS Appl. Mater. Interfaces XXXX, XXX, XXX−XXX

yl-*sn*-glycero-3-phosphoethanolamine-*N*-[amino(PEG)-2000] (ammonium salt)) was purchased from Avanti Polar Lipids Inc. (Alabaster, Alabama, USA). D-Phenylalanine (Phe), D-proline (Pro), D-tyrosine (Tyr), acetylcysteine impurity C, triethylamine (TEA), dicyclohexylcarbodiimide (DCC), *N*-hydroxysuccinimide (NHS), sodium hydroxide (NaOH), sodium chloride, Polysorbate 80 (Tween 80), Triton X-100, thiazolyl blue tetrazolium (MTT), fumaric acid, trifluoroacetic acid (TFA), tryptic soy agar (TSA), tryptic soy broth (TSB), Müller−Hinton broth (MHB), MHB cation adjusted (MHB−Ca^{2+}), crystal violet dye, glutaraldehyde solution, sodium cacodylate trihydrate buffer, hexamethyldisilazane, and MOX hydrochloride were obtained from Sigma-Aldrich (USA). *N*-Acetyl-L-cysteine (NAC) and TSB were purchased from Merck, Millipore Ltd. (Ireland). Acetonitrile 99%, chloroform, and dimethyl sulfoxide (DMSO) were obtained from VWR International LLC (USA). Dulbecco's Modified Eagle's Medium (DMEM), trypsin−EDTA (1×), Penicillin−Streptomycin (Pen Strep), Dulbecco's phosphate buffered saline 10× pH 7.4 (PBS), and fetal bovine serum (FBS) were purchased from Gibco by Life Technologies (UK). The L929 cell line (ATCC CCL-1TM) was acquired from the American Type Culture Collection (USA). All components were used without further purification. The procedures to obtain human biological samples were in accordance to the principles of the Declaration of Helsinki. Human red blood cells were isolated from surplus blood from healthy blood donors, kindly donated by Serviço de Hematologia do Centro Hospitalar do Porto.

2.2. Bacterial Strains. All bacterial studies were performed with *S. epidermidis* (ATCC 35984) and *P. aeruginosa* (ATCC 27853) strains, acquired from ATCC (USA).

2.3. Synthesis of DSPE-PEG$_{2000}$-NH$_2$-D-Amino Acid Conjugates. The synthesis process of DSPE-PEG$_{2000}$-NH$_2$-D-amino acid (D-phenylalanine, D-proline, and D-tyrosine) conjugates was based on a previously reported protocol.[24] To activate the D-amino acids, 62.5 mg of the respective D-amino acid was added to a mixture of 5 mL of DMSO and 62.5 μL of triethylamine (TEA) and stirred overnight, in the dark, under anhydrous conditions. Afterward, 62.5 mg of dicyclohexylcarbodiimide (DCC) and 65 mg of *N*-hydroxysuccinimide (NHS) were added to the previous mixture and stirred overnight in the dark. The side product dicyclohexylurea was removed using a 0.45 μm filter (Ministart, pore size 450 nm, cellulose acetate membrane, Sartorius Stedim Biotech, Germany). DMSO and TEA were evaporated under vacuum. Activated D-amino acid solution (2 mL) was added to 1 mL of DMSO and 50 mg of DSPE-PEG$_{2000}$-NH$_2$ and stirred ovemight, in the dark, under anhydrous conditions. Afterward, DMSO was evaporated under vacuum and 6 mL of Milli-Q water were added. The conjugate was purified by dialysis (Spectra/Por3 Dialysis Membrane, 3.5 kD, Spectrum Laboratories, Inc., CA, USA) in 1 L of Milli-Q water for 48 h to remove the unconjugated D-amino acids. The conjugates were lyophilized (LyoQuest −85 plus v.407, Telstar) and stored at −20 °C. Conjugates were characterized by Fourier-transform infrared spectroscopy (FTIR) (Frontier TM, PerkinElmer, CA, USA) equipped with a horizontal attenuated total reflectance (ATR) sampling accessory with a diamond crystal. The spectra were recorded between 4000 and 1000 cm^{-1}, with a resolution of 2 cm^{-1}.

2.4. Preparation of the NAC-Loaded LNPs. The LNPs were produced by the double emulsion method using a VCX-130 Vibra-Cell sonicator (Sonics & Materials Inc; USA) with a CV-18 probe (130 W, 20 kHz). In this method, NAC was dissolved in an aqueous solution of NaOH 1 M (400 μL of NaOH 1 M in 600 μL of Milli-Q water). This solution was then added to the solid lipid (cetyl palmitate) previously dissolved in chloroform (2 mL). The mixture was sonicated for 30 s at an amplitude of 70%. D-amino acids (phenylalanine, proline, and tyrosine) dissolved in a small volume of chloroform were added to the emulsion, when applicable. A solution of Tween 80 (different concentrations, 4 mL) was added, and the emulsion was sonicated for 2 min at 70% amplitude. A solution of Tween 80 (13.75 mg mL^{-1}, 4 mL) was added, and the final LNP suspension was placed in a stirring plate at room temperature under agitation until complete evaporation of the chloroform.

2.5. Experimental Design. A BBD was used to optimize the characteristics of the NAC-loaded LNPs.[17] A 15-run, 3-level, 3-factor design was used to maintain a low hydrodynamic diameter (Y_1) and PDI (Y_2) and to maximize the LC (Y_3). In this study, the solid lipid mass (X_1), the surfactant mass (X_2), and the NAC mass (X_3) were defined as independent variables. The concentration of the surfactant in the second addition was kept constant (13.75 mg mL^{-1}), and only the concentration in the first addition was variable. For each factor, the lower (−1), medium (0), and higher (+1) levels were established according to preliminary experiments. The hydrodynamic diameter and PDI were selected as dependent variables due to the relevance of the diameter of the LNPs for an intravenous administration.[25] LC was chosen to maximize the NAC ratio in comparison with the excipients used for the particle production. The model that considers nonlinear quadratic interactions generated by the design is reflected in the following equation

$$Y = A_0 + A_1X_1 + A_2X_2 + A_3X_3 + A_4X_1X_2 + A_5X_2X_3 + A_6X_1X_3 + A_7X_1^2 + A_8X_2^2 + A_9X_3^2 \quad (1)$$

in which Y is the dependent variable; A_0 is the intercept; A_1 to A_3 are the linear coefficients; A_4 to A_6 are the interaction coefficients; A_7 to A_9 are the squared coefficients; and X_1 to X_3 are the coded levels of independent variables. The terms X_1X_2, X_2X_3, and X_1X_3 represent the linear interactions terms, while X_i^2 (i = 1, 2, or 3) represents the quadratic terms.

The experimental design was generated using STATISTICA Software (v12, StatSoft Inc, USA), and the predicted values for the dependent variables were further compared with the experimental values.

2.6. Physical Characterization of LNPs. The hydrodynamic diameter and PDI were determined using a particle size analyzer (Brookhaven Instruments Corporation, Software: Particle Sizing v.5 Brookhaven Instruments, NY, USA). For zeta potential measurements, a Zeta potential analyzer (ZetaPALS, Brookhaven Instruments Corporation, Software: PALS Zeta Potential Analyzer v.5 Brookhaven Instruments, NY, USA) was used. The system was operated with an incidence light angle of 90° at room temperature. The LNPs were diluted (1:100) in Milli-Q water before the measurements.

Transmission electron microscopy (TEM) was used to assess the morphology of LNPs. The suspensions were diluted (1:15) in Milli-Q water. A copper-mesh grid was used to put 10 μL of LNPs for 2 min. The excess of LNPs was then removed, and 10 μL of 0.75% (w/v) uranyl acetate solution was added to the grid for 30 s at room temperature (negative staining). The samples were observed in a JEM-1400 transmission electron microscope (JEOL Ltd., Tokyo, Japan) with an acceleration voltage of 80 kV.

2.7. Encapsulation Efficiency and Loading Capacity. Encapsulation efficiency (EE) and loading capacity (LC) were determined by the HPLC technique and by direct measurement of the entrapped NAC. For separation of unloaded and loaded NAC, a dialysis diffusion method was used under sink conditions. At room temperature, under agitation, 500 μL of LNPs was added to a cellulose dialysis bag (Spectra/Por3 Dialysis Membrane, 6−8 kD, Spectrum Laboratories, Inc., CA, USA). Milli-Q water (80 mL) was used as dissolution medium. After 30 min, 80 μL of LNPs was removed from the dialysis bag and added to 50 μL of fumaric acid solution (0.05 mg mL^{-1}), which was used as an internal standard for HPLC measurements. Acetonitrile (0.5 mL) was added to dissolve the LNPs, followed by centrifugation at 30 000×*g* for 30 min. NAC solubilized in acetonitrile (300 μL) was added to 500 μL of Milli-Q water and 100 μL of TFA 1% (v/v) for further measurements by HPLC.

A Jasco integrated system (Tokyo, Japan) composed of an automated sample injector (AS-4050), two integrated PU-4180 plus high-pressure pumps, and a multiwavelength DAD (MD-4010), set at 215 nm, was used for HPLC. A sample volume of 20 μL was injected. The chromatographic separation was obtained by using a Gemini NX C18 110 Å (150 × 4.60 mm, 5 μm) column from Phenomenex (USA). The chromatographic conditions were optimized based on the

https://doi.org/10.1021/acsami.1c05124
ACS Appl. Mater. Interfaces XXXX, XXX, XXX−XXX

protocol stablished by the Portuguese Pharmacopeia.[26] The isocratic mobile phase consisted of an aqueous solution and acetonitrile with 0.1% (v/v) of TFA at a ratio of 95:5. At a flow rate of 0.7 mL min^{-1}, NAC retention time is 5.9 min, while the *N,N′*-diacetyl-L-cystine (impurity) retention time is 13.1 min. Fumaric acid was used as an internal standard and had a retention time of 4.9 min under the same chromatographic conditions. Calibration curves of NAC (0.01−0.2 mg mL^{-1}) and *N,N′*-diacetyl-L-cystine (impurity) (0.007—0.07 mg mL^{-1}) with fumaric acid solution (50 μL, 0.05 mg mL^{-1}) as an internal standard were used for quantification (data not shown).

The EE was calculated as follows

$$\text{EE (\%)} = \frac{\text{loaded NAC amount}}{\text{total NAC amount}} \times 100 \quad (2)$$

The LC was calculated using the EE as follows

$$\text{LC (\%)} = \frac{\text{EE} \times \text{total NAC amount}}{\text{total solid lipid amount}} \times 100 \quad (3)$$

2.8. Evaluation of the Storage Stability. The LNP formulations were stored at 4 °C for 24 weeks. To evaluate the physicochemical stability, the hydrodynamic diameter, PDI, zeta potential, and LC parameters were measured over time. The measurements were performed using the methods described in the previous sections.

2.9. *In Vitro* Cell Viability Study. For *in vitro* cell viability studies, the L929 fibroblast cell line was used because it is recommended by the ISO international standard 10993−5 for biocompatibility assessment studies.[27] L929 cells were cultured in DMEM supplied with 10% FBS and 1% penicillin−streptomycin at 37 °C, 5% CO_2 atmosphere.

The LNP effect on cell viability was measured using the MTT assay. Briefly, L929 cells were seeded in 96-well plates at a density of 5 × 10^4 cells/well. After adhesion, the cells were incubated with different concentrations of LNPs (0, 0.5, 1.0, 2.0, and 3.0 mg mL^{-1} of solid lipid) for 24 h. Fresh DMEM was used as a positive control. After the incubation time, the medium was replaced by the MTT solution (100 μL, 0.5 mg mL^{-1}) and incubated for 2 h at 37 °C, 5% CO_2. Formazan crystals were then dissolved in 100 μL of DMSO. The absorbance was measured at 590 and 630 nm using a microplate reader (BioTek Instruments Inc., Synergy HT, Software: Gen5 v1.08.4, BioTek Instruments Inc., USA). The latter was used to remove the background interference.

2.10. *In Vitro* Hemolysis Study. The protocol for the hemolysis assay was adapted from the study by Guo *et al.* (2017).[28] Briefly, the blood was centrifuged at 955 *g* for 5 min at 4 °C, and the serum was discarded. The red blood cells were washed three times using saline solution 0.85% (w/v) and further diluted to a volume fraction of 4%. 100 μL of NPs diluted in saline solution 0.85% (w/v) was added to 100 μL of red blood cells to obtain a final LNP concentration of 2 mg mL^{-1} of solid lipid. The samples were incubated at 37 °C for 1 h. The supernatants were collected and read at 540 and 630 nm. The latter was used to remove the background interference. The percentage of hemolysis was calculated according to the following

$$\text{hemolysis (\%)} = \frac{\text{Abs} - \text{Abs}(-)}{\text{Abs}(+) - \text{Abs}(-)} \times 100 \quad (4)$$

where Abs, Abs (−), and Abs (+) are the absorbances of the sample, the negative control (saline solution 0.85%), and the positive control (Triton-X100), respectively. The absorbance was measured using a microplate reader (BioTek Instruments Inc., Cytation, Software: Gen5 v1.08.4, BioTek Instruments Inc., USA).

2.11. MIC and MBC of the LNPs and MOX. Antimicrobial activity of the LNPs and MOX against the bacterial strains was determined using the microbroth dilution assay.[29] To determine the minimal inhibitory concentration (MIC), bacteria were first grown overnight at 37 °C in TSB and further diluted to a concentration of 2.0 × 10^5 CFUs mL^{-1} in MHB and MHB cation adjusted (MHB−Ca^{2+}) for the LNPs and MOX, respectively. The bacterial suspension (75 μL) and LNPs or MOX (25 μL) were added to a 96-well polypropylene microtiter plate (Corning Incorporated, USA) and incubated at 37 °C for 24 h. LNPs were tested at a range of solid lipid concentrations from 0.0625 to 2.0 mg mL^{-1}. Different concentrations of MOX were tested for *S. epidermidis* (0 to 16 μg mL^{-1}) and *P. aeruginosa* (0 to 512 μg mL^{-1}). The MIC was recorded as the lowest concentration, which inhibited the visual growth of bacteria. The minimal bactericidal concentration (MBC) was further determined by plating 10 μL from each well with no visual bacterial growth onto TSA plates (incubation at 37 °C, overnight). MBC was defined as the lowest concentration resulting in the death of 99.9% of the initial inoculum. This procedure was performed in duplicate.

2.12. Biofilm Formation and Exposure to LNPs and MOX. The description of the following protocols for biofilm formation and assessment complies with the minimum information guidelines.[30]

Bacterial biofilms were grown in a MBEC Biofilm Inoculator according to the manufacturer (Innovotech, Canada). First, bacteria were grown overnight at 37 °C on a TSA plate. A total of 5 to 10 bacterial colonies were collected from the plate and dispersed in TSB to grown at 37 °C, overnight, with shaking (150 rpm) (Digital Orbital Shaker, Intertek 5003396, 12 VDC, 1.5 AMPS, 18 W, Heathrow Scientific). Afterward, the bacteria were diluted to a concentration of 10^7 CFUs mL^{-1} and added to the MBEC Biofilm Inoculator (150 μL of bacterial inoculum per well).[31] The plate was incubated at 110 rpm, 37 °C, in a humidified atmosphere. The biofilm growth conditions were optimized to form mature biofilms with a dense matrix. Thus, *S. epidermidis* and *P. aeruginosa* biofilms were grown for 3 and 2 days, respectively, with medium replacement every 24 h.

The biofilms were washed once with PBS 1× and then incubated with the treatment at 60 rpm, 37 °C, during 24 h in a humidified atmosphere. For the treatment, LNPs with a solid lipid concentration of 2 mg mL^{-1} or free NAC (0.9 mg mL^{-1}) were selected. In a combinatory treatment with the LNPs or free NAC, MOX was tested in three different concentrations (2, 4, and 8 μg mL^{-1}). This procedure was used for the following assays.

2.13. Determination of the MBEC of MOX. *S. epidermidis* and *P. aeruginosa* biofilms were grown according to the protocol described in step 2.12. Mature 3-day (*S. epidermidis*) and 2-day (*P. aeruginosa*) biofilms were then washed once with PBS 1× and then incubated in TSB with different concentrations of MOX (0−512 μg mL^{-1}). The biofilms were kept in the dark, at 37 °C, 60 rpm, and a humidified atmosphere, during 24 h. After the treatment, the biofilms were washed twice with PBS 1×, and each peg was transferred to a microcentrifuge tube containing 150 μL of PBS 1× and further placed in a sonication bath with ice for 30 min at 160 W (BactoSonic, Bandelin, Germany) to disperse the biofilms. The bacterial suspensions were serial diluted in PBS 1× and spot-plated (10 μL) on TSA plates. After an overnight incubation of the plates at 37 °C, the CFUs were counted.

2.14. Biofilm Biomass Study. The biofilm biomass of the formed biofilms was evaluated by the crystal violet staining method.[32] After exposure to the treatment, the biofilms were washed twice with PBS 1× and further dried overnight. The biofilms in the pegs were incubated with 200 μL of crystal violet solution 0.4% (w/v) during 10 min at room temperature. The stained pegs were let to dry at room temperature for 10 min and then washed with distilled water, until complete removal of the excess of stain. To dissolve the remaining stain in the pegs, 210 μL of DMSO was added. The absorbance was read at 595 nm using a microplate reader (BioTek Instruments Inc., USA).

2.15. Biofilm Viability Study. The viability of the bacterial cells within the biofilm after treatment was accessed by the colony forming unit (CFU) assay. In this assay, the biofilms were washed twice with PBS 1×, and each peg was transferred to a microcentrifuge tube containing 150 μL of PBS 1× and further placed in a sonication bath with ice for 30 min at 160 W (BactoSonic, Bandelin, Germany) to disperse the biofilms. The bacterial suspensions were serial diluted in PBS 1× and spot-plated (10 μL) on TSA plates. After an overnight incubation of the plates at 37 °C, the CFUs were counted.

2.16. SEM Biofilm Analysis. The biofilms previously treated with LNPs or free NAC were prepared for scanning electron microscopy

https://doi.org/10.1021/acsami.1c05124
ACS Appl. Mater. Interfaces XXXX, XXX, XXX−XXX

(SEM). The protocol to prepare the samples was adapted from ref 33. First, the samples were washed twice with PBS 1× and once with saline solution 0.85%. The adherent bacteria were then fixed with a freshly prepared solution of 1.5% glutaraldehyde in 0.14 M of sodium cacodylate buffer for 30 min at room temperature. After fixation, the samples were rinsed twice with deionized water and dehydrated using a growing ethanol/water gradient (50, 60, 70, 80, 90, and 99%), maintaining the samples in each solution for 10 min. 200 μL of hexamethyldisilazane was added to each sample, and they were let to dry overnight. The samples were placed onto SEM pin stubs (TED PELLA, Inc., USA) using carbon tape and sputtered with an Au/Pd thin film (15 mA, 60 s) to improve their conductivity. The morphology and distribution of the biofilms on the pegs were characterized by SEM using a Quanta 400 FEG ESEM/EDAX Genesis X4M (ThermoFischer, USA).

2.17. Statistical Analysis. Statistical analysis was performed using SPSS Software (version 25; IBM, USA). The data are expressed as mean ± SD, and each assay was performed at least three independent times (three replicates per experiment), with exception of the MIC determination assay (Section 2.11), which was performed in duplicate with two replicates per experiment. Data were analyzed using one-way analysis of variance (ANOVA). A *P*-value under 0.05 was considered statistically significant.

3. RESULTS AND DISCUSSION

3.1. Characterization of the DSPE-PEG$_{2000}$-NH$_2$-D-amino Acid Conjugates. The D-amino acid conjugates (DSPE-PEG$_{2000}$-NH$_2$-Phe, DSPE-PEG$_{2000}$-NH$_2$-Pro, and DSPE-PEG$_{2000}$-NH$_2$-Tyr) synthetized were further analyzed by FTIR spectroscopy (Figure 2). The conjugates present the characteristic vibrations of the DSPE-PEG$_{2000}$-NH$_2$ molecule, like the C=O vibration at 1730 cm^{-1}, a marker for lipids, and the C−C−O stretch of esters at 1160 cm^{-1}. Besides, each conjugate presents vibrations of the corresponding D-amino acid. In the DSPE-PEG$_{2000}$-NH$_2$-Phe spectrum, it is possible to observe a peak at 1494 cm^{-1} corresponding to stretching in aromatic C=C bonds, which is also present at the D-Phenylalanine spectrum. With regard to the DSPE-PEG$_{2000}$-NH$_2$-Pro spectrum, a peak at 1612 cm^{-1} corresponding to bending in N−H bonds of secondary amines is also observed in the spectrum of D-Proline. In the DSPE-PEG$_{2000}$-NH$_2$-Tyr bands, it is possible to distinguish a peak at 1240 cm^{-1} corresponding to the phenolic OH stretch present at the D-tyrosine molecule. Furthermore, the coupling of D-amino acids to DSPE-PEG$_{2000}$-NH$_2$ is established through the formation of a secondary amide. FTIR confirms these new amide II bonds by the presence of new characteristic peaks, namely, related to the N−H stretching vibrations at 3324 cm^{-1} and the N−H in-plane bending at 1533 cm^{-1} in all three synthesized conjugates. Thus, the formation of a new amide linkage is evident between the DSPE-PEG$_{2000}$-NH$_2$ molecule and each D-amino acid (D-phenylalanine, D-proline, and D-tyrosine).

3.2. Experimental Design. Prior to the experimental design, preliminary formulations were prepared and characterized to evaluate which variables were more relevant for the physical characteristics and LC of the LNPs (data not shown). From this knowledge, the amounts of solid lipid, surfactant, and NAC were defined as independent variables and the hydrodynamic diameter, PDI, and LC as dependent variables. The formulation of NAC LNPs (NAC-loaded and unfunctionalized) was selected to be optimized because the functionalization was not expected to change dramatically the characteristics of the LNPs.

The BBD required the production and characterization of fifteen formulations, from which three corresponded to a central point used to estimate the experimental error. To determine which fitting model was suitable for each dependent variable, the R^2 values obtained from the correlation between the predictable and experimental measurements were evaluated. For all dependent variables, the quadratic model (eq 1) revealed a higher R^2 value compared to other models (Figure S1). A detailed description of the results obtained from this design can be found in the Supporting Information.

The levels of desirability for the dependent variables were defined with the aim to have a particle hydrodynamic diameter between 100−270 nm and a low PDI (<0.2) and to maximize the LC (Table S1). According to the selected constraints for each dependent variable, the STATISTICA (v12) software suggested an ideal formulation (NAC LNPs). The composition and predicted values for hydrodynamic diameter, PDI, and LC of this formulation can be found in Table 1. The observed characteristics of the optimal formulation were not statistically different from the predicted values with regard to hydrodynamic diameter, PDI, and LC. Therefore, the experimental

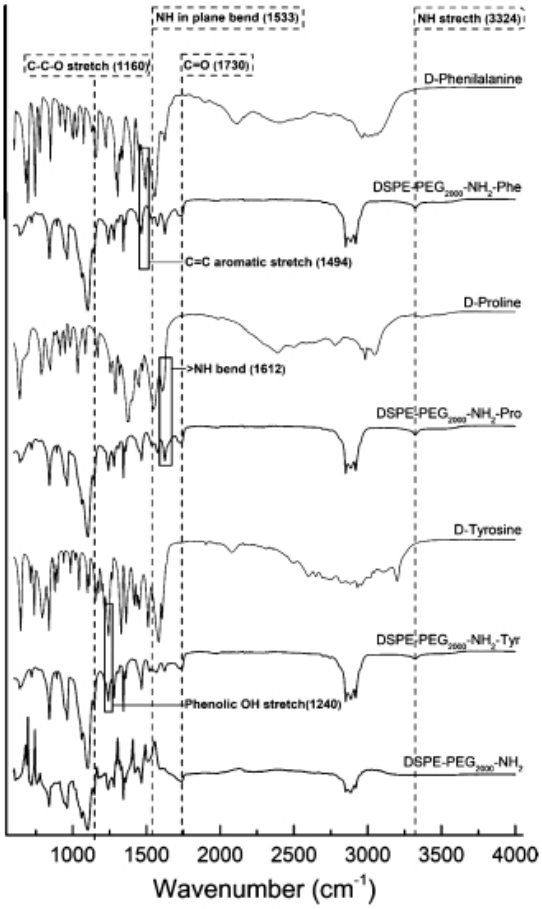


Figure 2. Infrared spectra of the three D-amino acid conjugates: DSPE-PEG$_{2000}$-NH$_2$-Phe, DSPE-PEG$_{2000}$-NH$_2$-Pro, and DSPE-PEG$_{2000}$-NH$_2$-Tyr. The spectra of DSPE-PEG$_{2000}$-NH$_2$, D-phenylalanine, D-proline, and D-tyrosine are also represented.

https://doi.org/10.1021/acsami.1c05124
ACS Appl. Mater. Interfaces XXXX, XXX, XXX−XXX

ACS Applied Materials & Interfaces www.acsami.org Research Article

Table 1. Composition and the Respective Predicted and Observed Values for the Optimal Formulation (NAC LNPs)[a,b]

		predicted			observed		
composition	mg	hydrodynamic diameter (nm)	PDI	LC (%)	hydrodynamic diameter (nm)	PDI	LC (%)
solid lipid	65						
surfactant−1st phase	100	200 ± 26	0.13 ± 0.06	11.8 ± 0.7	216 ± 2	0.13 ± 0.02	11.3 ± 0.4
NAC	30						

[a]The predicted and observed values showed no statistical significance. [b]Values represent the mean ± SD (n = 3).

Table 2. Composition and Physical Characterization of Unloaded and NAC-Loaded LNPs According to Their Hydrodynamic Diameter, PDI, Zeta Potential, and LC[a]

formulation	LNPs	NAC LNPs	Phe NAC LNPs	Pro NAC LNPs	Tyr NAC LNPs	Phe_Pro_Tyr LNPs	Phe_Pro_Tyr NAC LNPs
Cetyl p. (mg)	65	65	65	65	65	65	65
Tween 80 (mg)	155	155	155	155	155	155	155
NAC (mg)		30	30	30	30		30
DSPE-Phe (mg)			1			1	1
DSPE-Pro (mg)				1		1	1
DSPE-Tyr (mg)					1	1	1
hydrodynamic diameter (nm)	225 ± 2	216 ± 2	198 ± 9*	208 ± 8*	209 ± 3*	257 ± 4*	214 ± 2
PDI	0.11 ± 0.01	0.13 ± 0.02	0.14 ± 0.02	0.13 ± 0.02	0.12 ± 0.02	0.11 ± 0.02	0.15 ± 0.02
Zeta P. (mV)	−53 ± 8	−50 ± 2	−49 ± 1	−46 ± 7	−47 ± 7	−45 ± 11	−53 ± 6
LC (%)		11.3 ± 0.4	12 ± 1	11.5 ± 0.5	12 ± 2		9 ± 2

[a]Values represent the mean ± SD (n = 3). *p < 0.05 relative to LNP formulation (placebo).

design showed robustness and the assessed conditions were always used for the following studies.

3.3. Physical Characterization of LNPs. After the optimization process, seven formulations with different compositions were produced. The LNPs were characterized with regard to mean hydrodynamic diameter, PDI, zeta potential, and LC (Table 2). The aim of studying these formulations was to understand the effects of functionalization with phenylalanine (Phe), proline (Pro), and tyrosine (Tyr), alone or in combination. Besides the physical properties, toxicity and efficiency of the LNPs in the absence of NAC were also evaluated.

All formulations appeared white and milky and presented a low viscosity, with no visible aggregation. This appearance was further confirmed by both low PDI (<0.2) and zeta potential below −30 mV, which suggests that the LNP suspensions were stable, with a low tendency to form aggregates.[34]

The entrapment of NAC into the LNPs does not compromise their hydrodynamic diameter because NAC LNP formulation is not significantly different from the unloaded LNPs. Regarding the functionalization, a significant increase in hydrodynamic diameter in the presence of the three conjugates (Phe_Pro_Tyr LNPs) is observed. This may be a consequence of steric effects at the surface of the nanoparticles due to the existence of different D-amino acids. However, this effect is not observable in functionalized NAC-loaded nanoparticles (Phe_Pro_Tyr NAC LNPs), which suggests that NAC stabilizes the nanoparticles. On the contrary, in the presence of only one conjugate, a significant decrease of particle hydrodynamic diameters is observed. According to the chemical structure of DSPE-PEG_{2000}-NH_2-D-amino acid conjugates, it is highly probable that DSPE is entrapped in the lipid matrix, where it can establish hydrophobic interactions. Consequently, the DSPE may increase the packing of lipid molecules, decreasing the hydrodynamic diameter of the LNPs.

The LC values were satisfactorily high for all formulations, with no significant differences between functionalized and nonfunctionalized LNPs. Thus, the conjugates do not seem to interfere with the encapsulation of NAC.

The characteristics of the LNP suspensions are crucial for their *in vivo* biodistribution. Particles administered by an intravenous route must be significantly smaller than 5 μm (diameter of the smallest capillaries in the human body), with no tendency to form aggregates, to avoid embolism.[35] Surface charge also plays a role in prolonging particles half-life in the bloodstream. Neutral and negatively charged particles show less adsorption of serum proteins, increasing their circulation times.[34] Considering these features, the produced formulations are suitable for intravenous administration.

The morphology of the particles was also evaluated by TEM (Figure 3). From the images obtained, it is possible to observe that both unloaded and NAC-loaded LNPs have a spherical shape, with no visible aggregation. Besides, the functionalization with the conjugates does not change the morphology of the particles. These results are consistent with the ones determined by dynamic light scattering. Additionally, TEM images show aqueous vacuoles inside the LNPs, which is a consequence of the double emulsion production method of the formulations.[36]

3.4. Storage Stability. The physical stability of the LNP suspensions under storage conditions was evaluated over 24 weeks, when kept at 4 °C, protected from light. Periodic measurements of the hydrodynamic diameter, PDI, zeta potential, and LC were performed over 24 weeks (Figure 4).

The hydrodynamic diameter and PDI (Figure 4A) of all formulations were shown to be stable over the 24 weeks. During this time, the hydrodynamic diameter of all LNPs remained below 275 nm and the PDI below 0.2. The zeta potential of both LNP and Phe_Pro_Tyr NAC LNP formulations also showed no significant changes during storage. For the remaining formulations, it is possible to

https://doi.org/10.1021/acsami.1c05124
ACS Appl. Mater. Interfaces XXXX, XXX, XXX−XXX

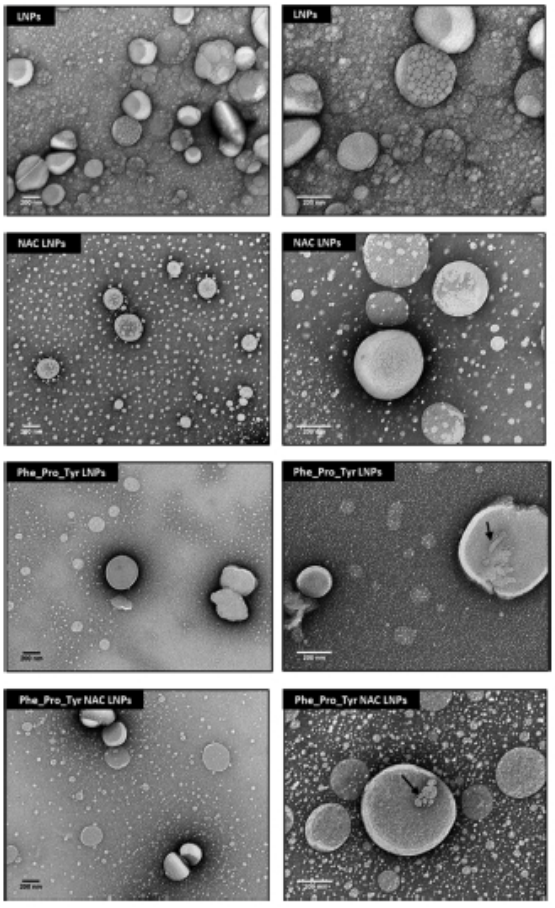


Figure 3. TEM images of the nonfunctionalized formulations (LNPs and NAC LNPs) and functionalized formulations (Phe_Pro_Tyr LNPs and Phe_Pro_Tyr NAC LNPs). Aqueous vacuoles (black arrows) can be observed inside the LNPs. The left images are at a magnification of 50 000×, and right images are at a magnification of 100 000×.

observe a significant change in zeta potential after 12 weeks (NAC LNPs, Phe NAC LNPs, Pro NAC LNPs, and Tyr NAC LNPs) and 24 weeks (Phe_Pro_Tyr LNPs). Nevertheless, for all suspensions, the zeta potential values were always below −30 mV, which suggests a high stability and no tendency to form aggregates.

The LC of the NAC-loaded LNP suspensions was also measured over time. For the NAC LNP formulation, after 12 weeks, there is a significant decrease of LC. This phenomenon was not observed in functionalized particles, except for Tyr NAC LNPs. The latter shows a significant increase in drug release after 24 weeks, which is shown by the decrease of LC. Overall, these results suggest that functionalization of the LNPs seems to delay NAC leakage under storage conditions over the 24 weeks of study.

3.5. *In Vitro* Toxicity Studies. The cytotoxicity of the LNP suspensions was evaluated against the L929 fibroblast cell line. According to the ISO international standard 10993−5, a cell viability lower than 70% of the control presents a cytotoxic potential.[27] For the MTT assay (Figure 5A), different solid lipid concentrations of the LNPs were tested (0, 0.5, 1.0, 2.0, and 3.0 mg mL^{-1}). All LNP suspensions showed viability higher than 70% until 2 mg mL^{-1} of the solid lipid. At a higher concentration (3 mg mL^{-1}), the formulations showed cytotoxic effects toward the tested cells. These results suggest that the developed formulations do not interfere with cell viability until 2 mg mL^{-1} of solid lipid, which corresponds to a NAC concentration of 0.9 mg mL^{-1}, enough to exert its antibiofilm activity.[4]

To evaluate the effects of the LNP suspensions on red blood cells after an intravenous administration, a hemolysis assay was performed. For this assay, a solid lipid concentration of 2 mg mL^{-1}, which corresponds to 0.9 mg mL^{-1} of NAC, was selected. Figure 5B shows that all formulations have a hemolytic activity below 25%, while no activity is verified for free NAC. In fact, all NAC-loaded LNPs have a hemolysis value below 5%. According to some studies in the literature, hemolysis values between 5 and 25% are of no concern.[37,38] Because all LNP suspensions meet this criterion, they have potential to be a safe system for intravenous administration. Nevertheless, the ASTM E2524-08 standard indicates that a hemolysis percentage above 5% causes some damage to the red blood cells. NAC is vastly known for its excellent safety profile, which was previously reported in the literature.[39] Thus, it is likely that this compound is partially adsorbed to the surface of the nanoparticles, leading to an increased biocompatibility of the NAC-loaded LNPs. On the other hand, in the unloaded formulations, a higher amount of Tween 80 is exposed at the surface of the nanoparticles due to the absence of NAC. This nonionic surfactant is commonly used in the pharmaceutical industry; however, studies report adverse side effects of Tween 80 after administration, including hemolysis.[40] Hence, a higher concentration of Tween 80 at the surface of the unloaded LNPs may be responsible for the higher hemolytic effect observed for these formulations. Therefore, NAC-loaded LNPs present a safer profile than the corresponding unloaded LNPs.

3.6. *In Vitro* Efficacy Studies of the LNPs. *3.6.1. Minimal Inhibitory Concentration.* For this assay, nontoxic concentrations of the LNP suspensions were tested (0.065 to 2 mg mL^{-1} of the solid lipid) against both *S. epidermidis* and *P. aeruginosa*. For all formulations, the inhibition of planktonic bacterial growth was not observed even at the higher concentration (2 mg mL^{-1} of the solid lipid), which corresponds to 0.9 mg mL^{-1} of NAC. These results were expected because the MIC values of NAC reported for *S. epidermidis* (ATCC 35984) and *P. aeruginosa* (ATCC 27853) are 5 mg mL^{-1}[41] and 2.5 mg mL^{-1},[4] respectively. Thus, neither the concentration of NAC in the formulations nor the vehicle seem to affect the development of planktonic bacteria.

3.6.2. Biofilm Biomass Quantification. The biofilm biomass was evaluated by the crystal violet staining method, which stains both bacteria and the surrounding matrix within the biofilm.[42] The results for both *S. epidermidis* and *P. aeruginosa* are shown in Figure 6.

A 24 h treatment with unloaded LNPs and unloaded Phe_Pro_Tyr LNPs showed a significant decrease in *S. epidermidis* biofilm biomass compared to the control (untreated biofilm) (Figure 6A). For the remaining formulations, no significant effects were observed at the evaluated concentration (2 mg mL^{-1} of solid lipid). Besides, free NAC at the concentration of 0.9 mg mL^{-1} (amount of NAC corresponding to 2 mg mL^{-1} of solid lipid in the LNPs) showed no effects against mature *S. epidermidis* biofilms. These

https://doi.org/10.1021/acsami.1c05124
ACS Appl. Mater. Interfaces XXXX, XXX, XXX−XXX

ACS Applied Materials & Interfaces www.acsami.org Research Article

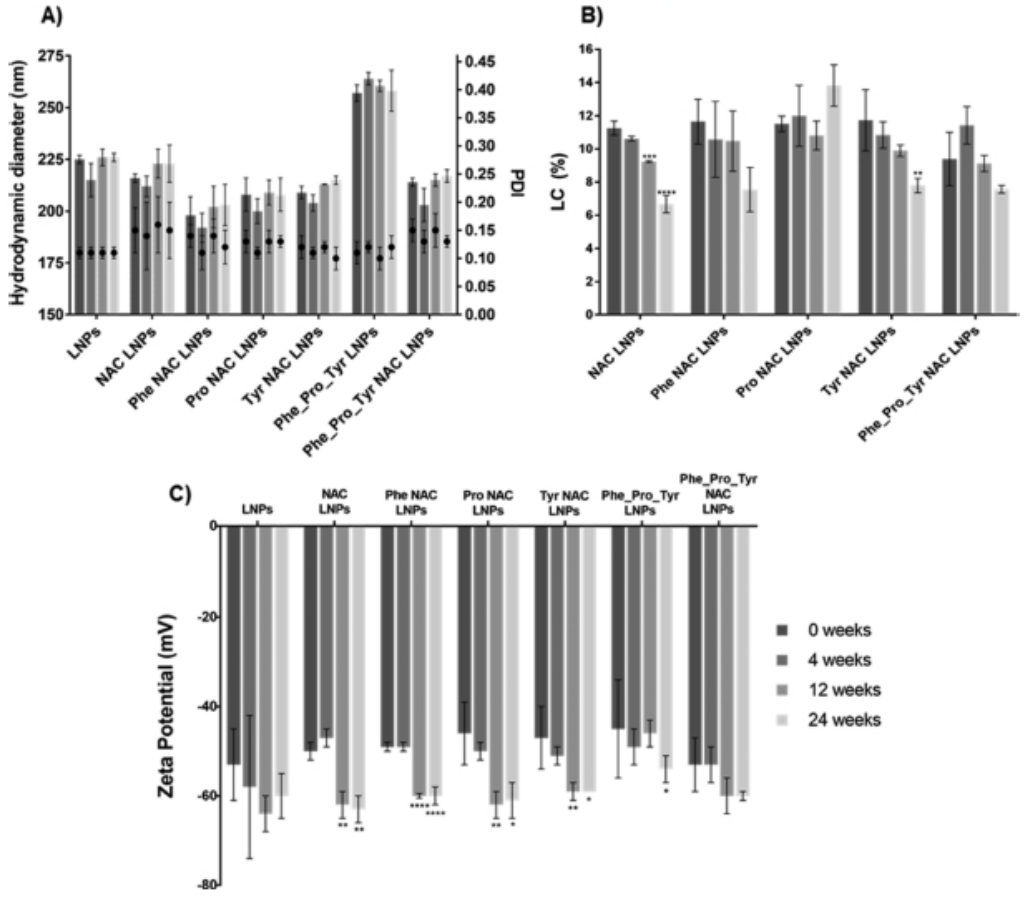


Figure 4. Characterization of the LNP suspensions over 24 weeks, stored at 4 °C. (A) Hydrodynamic diameter and PDI. Bars represent the hydrodynamic diameter (left *y*-axis), and dots represent the PDI (right *y*-axis). (B) LC. (C) Zeta potential. The parameters were evaluated over time (0, 4, 12, and 24 weeks). Values are represented as the mean ± SD ($n = 3$). $^{*}P < 0.05$, $^{**}P < 0.01$, $^{***}P < 0.001$, $^{****}P < 0.0001$ relatively to 0 weeks.

results suggest that both encapsulated and free NAC at the tested concentration do not promote biofilm disruption. The inefficiency of NAC against *S. epidermidis* may be a consequence of the low concentration tested. In the literature, it is reported that NAC shows a significant biofilm biomass reduction at a much higher concentration (40 mg mL^{-1}) for two *S. epidermidis* isolates (9142 and 1457).[3] In fact, the presence of NAC in the formulations seems to neutralize the disruptive potential of the vehicles. This potential of the vehicle is observed in the unloaded formulations (LNPs and Phe_Pro_Tyr LNPs), where Tween 80 is likely exposed in a higher amount at the surface of the nanoparticles. Despite improving the stability of the formulations, this surfactant has antibacterial and antibiofilm properties against several bacterial species.[15,16] Hence, the results obtained suggest that the adsorption of NAC onto the surface of the nanoparticles hinders the exposure of Tween 80, leading to a decreased interaction between the surfactant and the biofilm in NAC-loaded LNPs.

Regarding *P. aeruginosa* biofilms (Figure 6B), all formulations showed a significant reduction of biofilm biomass compared to the control (untreated biofilms), except for Pro NAC LNPs. In fact, LNPs functionalized with only one type of D-amino acids (Phe, Pro, or Tyr) do not show significant reduction in biofilm biomass compared to nonfunctionalized NAC LNPs. However, both unloaded Phe_Pro_Tyr LNPs and Phe_Pro_Tyr NAC LNPs showed higher efficiency in reducing the biofilm content (more than 50% reduction) compared to the remaining formulations. The similar disruptive effect of the Phe_Pro_Tyr LNPs and the corresponding NAC-loaded formulation suggests the targeting effect of the functionalization toward the biofilm. Consequently, a higher efficiency of the vehicle is achieved. Free NAC at the same concentration of the encapsulated NAC (0.9 mg mL^{-1}) also showed significant disruption of the biofilm, which is in agreement with a previous study found in the literature.[4]

3.6.3. Biofilm Viability Study. Due to the high effect of the LNPs on decreasing *P. aeruginosa* biofilm biomass (Figure 6B), the biofilm viability was further evaluated through the plate count. For this study, LNPs functionalized with only one type of D-amino acids (Phe, Pro, or Tyr) were not considered

https://doi.org/10.1021/acsami.1c05124
ACS Appl. Mater. Interfaces XXXX, XXX, XXX−XXX

ACS Applied Materials & Interfaces www.acsami.org Research Article

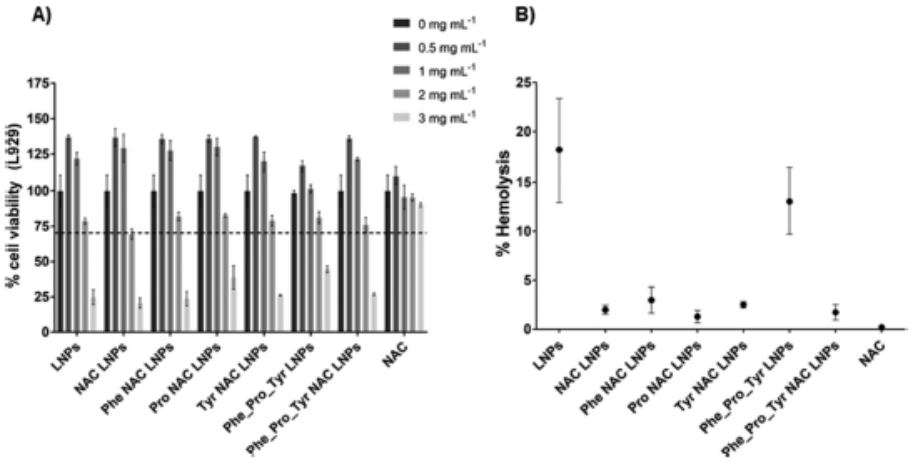


Figure 5. *In vitro* toxicity studies. (A) MTT assay using the L929 cell line. Different concentrations of the solid lipid were evaluated (0, 0.5, 1.0, 2.0, and 3.0 mg mL^{-1}). The DMEM medium was used as a control. (B) Hemolysis assay. The LNP suspensions were tested at a concentration of 2 mg mL^{-1}, and the corresponding amount of NAC (0.9 mg mL^{-1}) was used for free NAC. Saline solution and Triton-X100 were used as negative and positive controls, respectively. All values are represented as mean ± SD (n = 3).

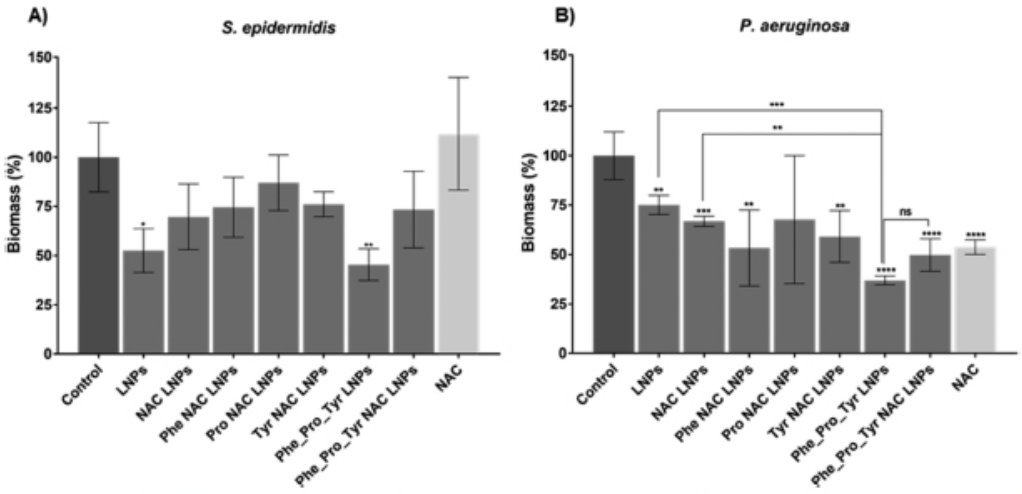


Figure 6. Quantification of biofilm biomass by crystal violet staining after a 24 h treatment with LNPs or free NAC for (A) *S. epidermidis* and (B) *P. aeruginosa*. The LNP suspensions were tested at a solid lipid concentration of 2 mg mL^{-1}. Free NAC was tested at a concentration of 0.9 mg mL^{-1} (amount of NAC corresponding to 2 mg mL^{-1} of solid lipid in the LNPs). Values are represented as the mean ± SD (n = 3). $^{*}P < 0.05$, $^{**}P < 0.01$, $^{***}P < 0.001$, $^{****}P < 0.0001$ relatively to the control (untreated biofilms). ns, not significant; $^{**}P < 0.01$, $^{***}P < 0.001$.

because Phe_Pro_Tyr LNPs and Phe_Pro_Tyr NAC LNPs showed a significantly higher effect on biofilm biomass. In Figure 7, it is possible to observe that all tested formulations significantly decreased biofilm viability when compared to the control (untreated biofilms) ($P < 0.0001$). The functionalized NAC-loaded LNPs (Phe_Pro_Tyr NAC LNPs) show a significant decrease in viable count when compared with LNPs alone and with free NAC at the concentration of 0.9 mg mL^{-1}. Despite that this formulation does not show a statistical significance to NAC LNPs and Phe_Pro_Tyr LNPs, it shows a slight decrease in bacterial viability.

3.6.4. SEM Biofilm Analysis. SEM was used to assess the morphology and integrity of untreated and treated *P. aeruginosa* biofilms (Figures 8 and S3). From Figure 8, it is possible to observe that untreated biofilms are dense and bacteria form aggregates where a thick layer of the biofilm matrix surrounds the bacterial cells for protection and to promote a strong adhesion to the surface of the material. In accordance with the previous results, the biofilms treated with LNPs show a reduction of the biofilm adhered to the material, lacking a dense layer of the matrix surrounding individual bacterial cells and with a visible reduction of aggregates. Additionally, in treated biofilms, it is possible to observe matrix substances adhered to the material in regions without bacterial cells (white arrows), which may suggest that part of the biofilm content in those regions was removed by the effect of the LNPs. Free NAC also seems to reduce the amount of the biofilm adhered to the material when compared with the

https://doi.org/10.1021/acsami.1c05124
ACS Appl. Mater. Interfaces XXXX, XXX, XXX−XXX

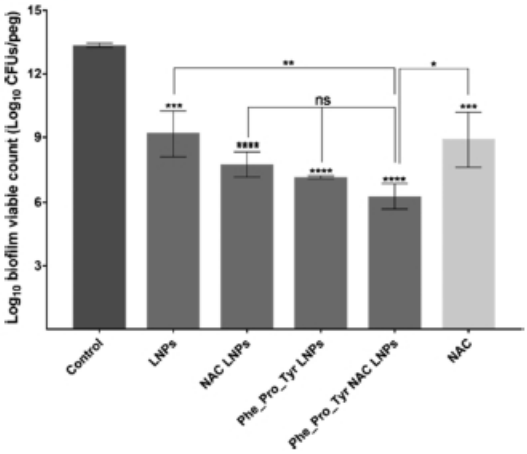


Figure 7. Log_{10} biofilm viable count of the *P. aeruginosa* biofilms untreated (control) and treated with LNPs or free NAC for 24 h. The LNP suspensions were tested at a solid lipid concentration of 2 mg mL^{-1}. Free NAC was tested at a concentration of 0.9 mg mL^{-1} (amount of NAC corresponding to 2 mg mL^{-1} of solid lipid in the LNPs). Values are represented as the mean ± SD ($n = 3$). ****$P < 0.0001$ relatively to the control (untreated biofilms). ns, not significant; *$P < 0.05$, **$P < 0.01$.

untreated biofilms; however, it is still observable large aggregates of bacterial cells and matrix components. SEM images also show that LNPs (unloaded, nonfunctionalized) present some aggregates of bacterial cells, which seems to be considerably reduced in the remaining three formulations (NAC LNPs, Phe_Pro_Tyr LNPs, and Phe_Pro_Tyr NAC LNPs). Between these three formulations, no visible differences in the amount of the adhered material are observed by SEM.

Overall, SEM analysis seems to corroborate the results obtained for biofilm biomass quantified by crystal violet (Figure 6B), by showing the matrix-disruptive potential of the developed LNPs. These findings are in agreement with the observations previously reported, where NAC promoted disruption of the biofilm matrix and reduced the production of extracellular polysaccharides at concentrations as low as 0.5 mg mL^{-1}.[4]

3.7. *In Vitro* Efficacy Studies of the LNPs in a Combined Therapy with MOX. Due to the promising results obtained with the developed formulations, a combined therapy with MOX was further tested to observe possible synergistic effects. In this strategy, the aim of the developed LNPs is to promote disruption of the biofilm matrix to facilitate the interaction between the antibiotic and the bacterial cells released from the biofilm structure.

3.7.1. MIC, MBC, and MBEC of MOX. The antimicrobial activity of MOX alone was tested in planktonic bacteria by determination of the MIC and MBC values (Table 3). The

Table 3. Activity of MOX Against Planktonic Bacteria (MIC and MBC Values) and Mature Biofilms of *S. epidermidis* and *P. aeruginosa* (MBEC Values)

strain	MIC ($\mu g\ mL^{-1}$)	MBC ($\mu g\ mL^{-1}$)	MBEC ($\mu g\ mL^{-1}$)
S. epidermidis (ATCC 35984)	0.06	0.125	0.125
P. aeruginosa (ATCC 27853)	2.00	2.00	16.00

MIC values for *S. epidermidis* (ATCC 35984) and *P. aeruginosa* (ATCC 27853) were 0.06 and 2.00 $\mu g\ mL^{-1}$, respectively. The MBC was further determined for both strains. For *S. epidermidis*, the MBC was higher than the MIC (0.125 $\mu g\ mL^{-1}$), while for *P. aeruginosa*, the MIC and MBC correspond to the same value.

The effect of MOX in mature biofilms from both strains was evaluated by determining the MBEC value (Table 3). The

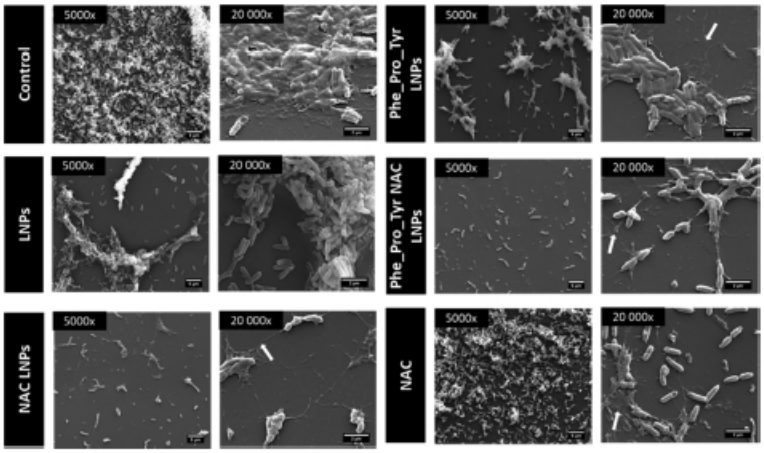


Figure 8. Representative SEM images of untreated (control) and treated *P. aeruginosa* biofilms. The LNP suspensions were tested at a solid lipid concentration of 2 mg mL^{-1}. Free NAC was tested at a concentration of 0.9 mg mL^{-1} (amount of NAC corresponding to 2 mg mL^{-1} of solid lipid in the LNPs). 5000× and 20 000× (at the top left of each image) indicate the magnification used for the respective image. White arrows indicate regions with adhered matrix substances.

https://doi.org/10.1021/acsami.1c05124
ACS Appl. Mater. Interfaces XXXX, XXX, XXX−XXX

ACS Applied Materials & Interfaces www.acsami.org Research Article

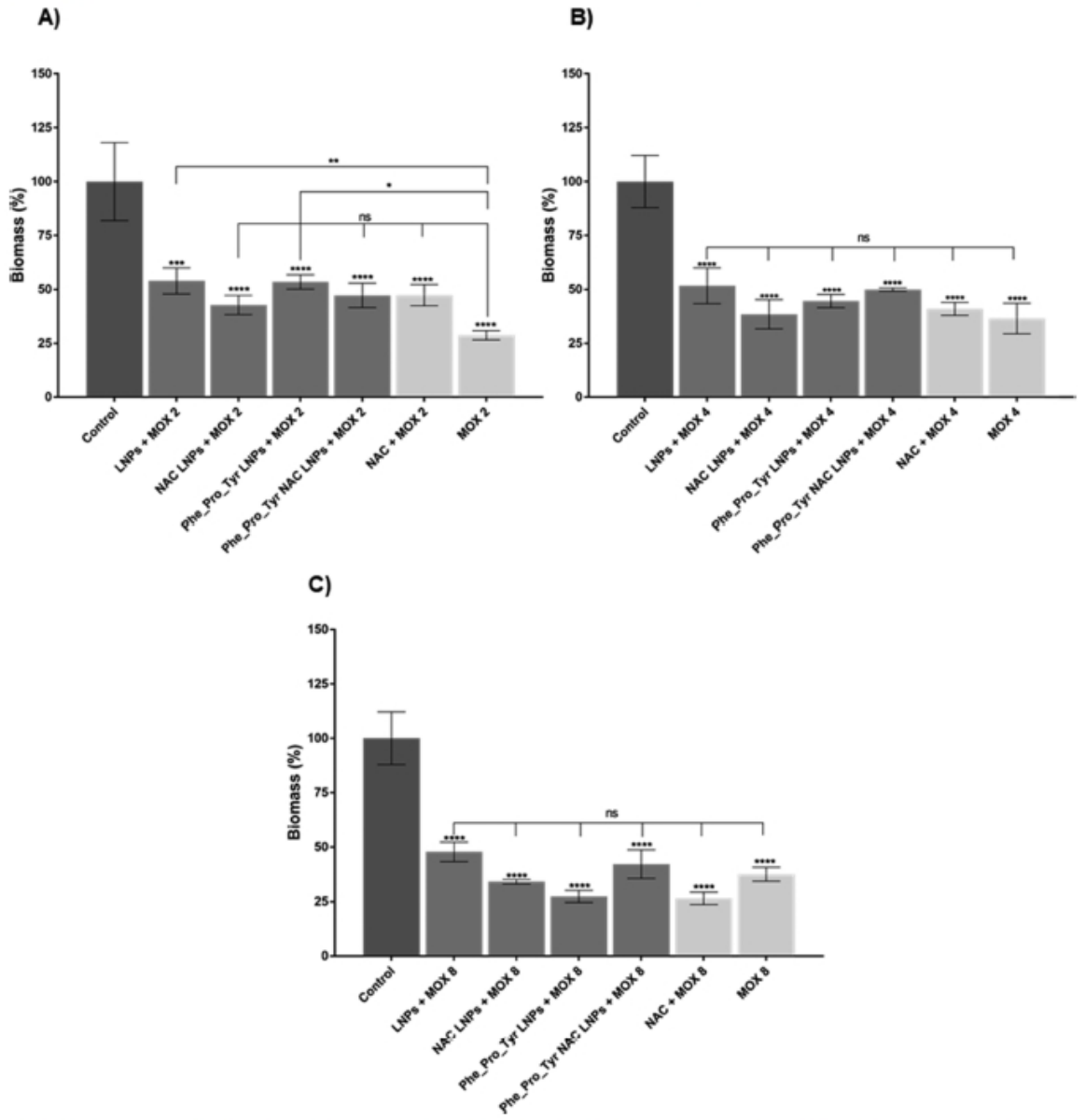


Figure 9. Quantification of *P. aeruginosa* biofilm biomass by crystal violet staining after a 24 h treatment with LNPs or free NAC in combination with MOX at a concentration of (A) 2 μg mL^{-1}, (B) 4 μg mL^{-1}, and (C) 8 μg mL^{-1}. The LNP suspensions were tested at a solid lipid concentration of 2 mg mL^{-1}. Free NAC was tested at a concentration of 0.9 mg mL^{-1} (amount of NAC corresponding to 2 mg mL^{-1} of solid lipid in the LNPs). Values are represented as the mean ± SD (n = 3). ***P < 0.001, ****P < 0.0001 relatively to the control (untreated biofilms). ns, not significant; *P < 0.05, **P < 0.01.

MBEC value was determined after a 24 h treatment. For *S. epidermidis* biofilms, the MBEC value was 0.125 μg mL^{-1}. In the case of *P. aeruginosa* biofilms, the MBEC value was 16 μg mL^{-1}. Due to the high concentration of MOX necessary to eradicate *P. aeruginosa* biofilms, this strain was selected for further studies where the possible synergy between MOX and the developed LNPs was evaluated.

3.7.2. Biofilm Biomass Quantification after Treatment with MOX in Combination with LNPs. To evaluate the potential synergistic effect of combining MOX with LNPs in the treatment of mature biofilms, the biofilm biomass was quantified after a 24 h treatment (Figure 9). MOX alone or in combination with free NAC or LNPs was assessed for three different concentrations below the MBEC value (2, 4, and 8 μg mL^{-1}). For these concentrations, no significant reduction of biofilm biomass was observed when MOX was combined with the formulations or free NAC. These results suggest that under the conditions studied, both developed formulations and free

K https://doi.org/10.1021/acsami.1c05124
ACS Appl. Mater. Interfaces XXXX, XXX, XXX−XXX

ACS Applied Materials & Interfaces www.acsami.org Research Article

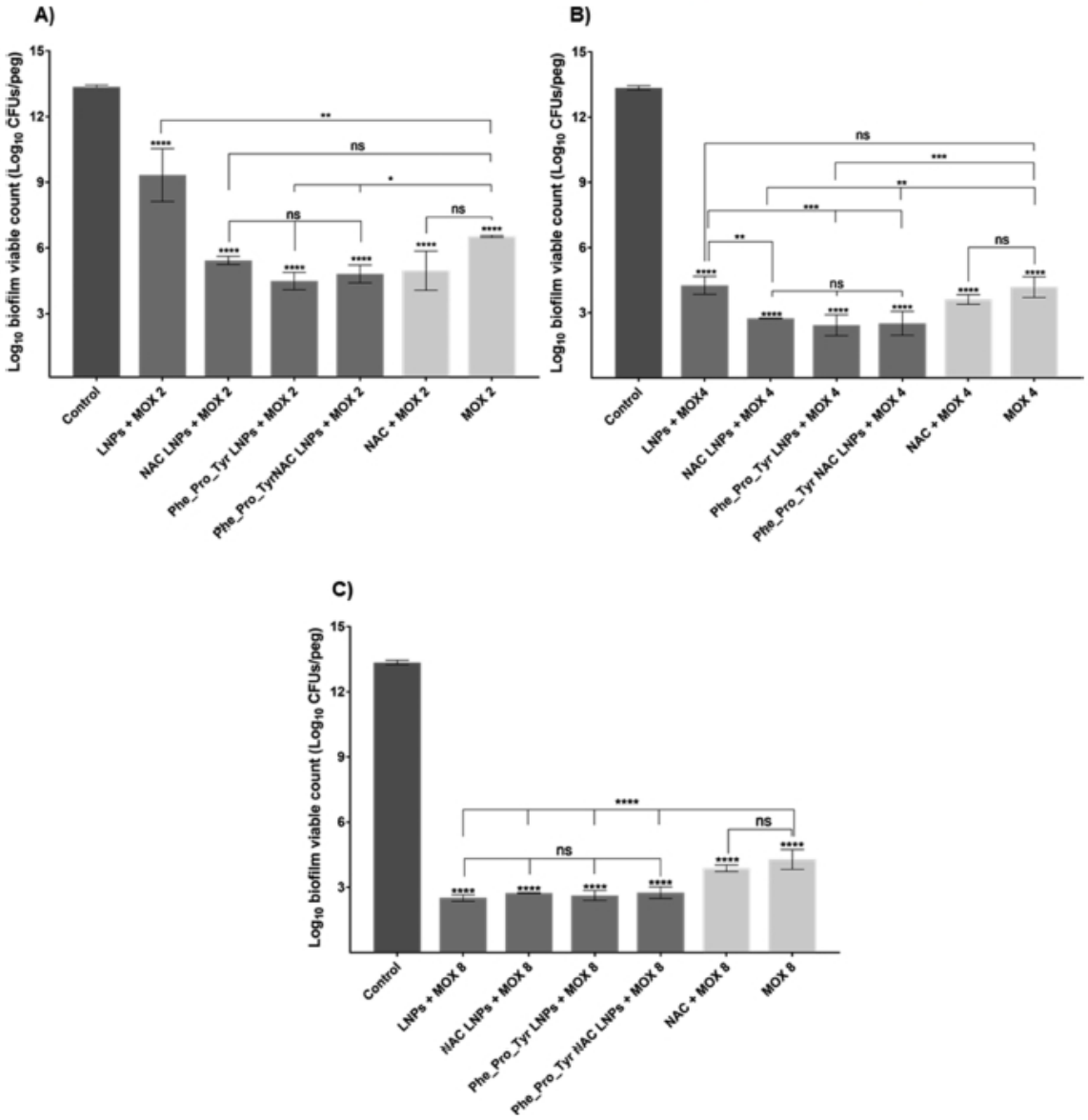


Figure 10. Log_{10} *P. aeruginosa* biofilm viable count of the biofilms untreated (control) and treated for 24 h with LNPs or free NAC in combination with MOX at a concentration of (A) 2 μg mL^{-1}, (B) 4 μg mL^{-1}, and (C) 8 μg mL^{-1}. The LNP suspensions were tested at a solid lipid concentration of 2 mg mL^{-1}. Free NAC was tested at a concentration of 0.9 mg mL^{-1} (amount of NAC corresponding to 2 mg mL^{-1} of solid lipid in the LNPs). Values are represented as the mean ± SD (n = 3). ****P < 0.0001 relatively to the control (untreated biofilms). ns, not significant; *P < 0.05, **P < 0.01, ***P < 0.001, ****P < 0.0001.

NAC do not seem to have a synergistic effect in the reduction of biofilm biomass, when combined with MOX.

3.7.3. Biofilm Viability after Treatment with MOX in Combination with NAC LNPs. Biofilm biomass quantifies not only live bacteria but also the biofilm matrix and death bacteria. To have a better perception regarding the effect of MOX in combination with the developed LNPs, biofilm viability was assessed through the plate count (Figure 10). At a MOX concentration of 2 μg mL^{-1}, functionalized LNPs (Phe_Pro_Tyr LNPs and Phe_Pro_Tyr NAC LNPs) showed a significant reduction in viable count when compared to the treatment with MOX alone (P < 0.05). A similar effect was observed for MOX concentrations of 4 and 8 μg mL^{-1}, with NAC LNPs and functionalized LNPs showing a significant reduction in viability. The formulation LNPs (unloaded and nonfunctionalized) showed lower efficiency than the other formulations because a synergistic effect is only observed when combined with MOX at a concentration of 8 μg mL^{-1}. For all MOX concentrations tested, free NAC (0.9 mg mL^{-1}) does not show a significant decrease in viability when combined

L https://doi.org/10.1021/acsami.1c05124
ACS Appl. Mater. Interfaces XXXX, XXX, XXX−XXX

with this antibiotic, which indicated no synergistic effect at the tested concentrations.

Overall, these results suggest a potential synergistic effect between the developed LNPs and MOX. As mentioned above, NAC and MOX do not show a potential synergistic. Thus, it seems that the reduced viability verified for the combination of functionalized LNPs and MOX (2 $\mu g\ mL^{-1}$) may be attributed to a synergistic effect between the antibiotic and the D-amino acids used as a functionalization of the nanoparticles. In fact, several studies in the literature describe the potential of D-amino acids against biofilms from several types of bacteria.[13,14]

4. CONCLUSIONS

In the present work, functionalized NAC-loaded LNPs were developed with the aim to target and disrupt bacterial biofilms. These particles were produced by the double emulsion technique and were optimized using a three-factor, three-level BBD. The optimized formulations showed a particle hydrodynamic diameter around 200 nm, a low PDI, a high LC, and long-term stability under storage conditions. These properties are suitable not only for intravenous administration but also to reach the biofilm because several studies suggest that nanocarriers with low hydrodynamic diameters have higher potential to penetrate the biofilm matrix and, consequently, deliver their cargo to deeper regions of the biofilm.[43,44]

The biocompatibility of the nanoparticles was evaluated by both cytotoxicity and hemolysis assays. Overall, all formulations showed no cytotoxic effects on the tested L929 cell line and no hemolytic activity was observed for NAC-loaded LNPs. However, for unloaded LNPs (nonfunctionalized and functionalized), hemolysis values between 10 and 25% were observed.

The effect of the developed LNPs was initially assessed in planktonic *S. epidermidis* and *P. aeruginosa*. For both strains, no inhibition was observed at the tested concentration of LNPs (corresponds to 0.9 $mg\ mL^{-1}$ of encapsulated NAC).

The *in vitro* antibiofilm efficacy of the LNPs was evaluated both in *S. epidermidis* and *P. aeruginosa* biofilms. Regarding *S. epidermidis* biofilms, only the unloaded formulations LNPs and Phe_Pro_Tyr LNPs contributed to a significant decrease of the biomass, while both encapsulated and free NAC at the tested concentration (0.9 $mg\ mL^{-1}$) do not seem to efficiently disrupt the biofilm. On the other hand, the developed formulations showed a high potential against *P. aeruginosa* biofilms, revealing that all components of the nanoparticles contribute to an antibiofilm effect observed both in biomass and bacterial viability reduction. The surfactant used to produce the nanosuspensions, Tween80, has reported an inhibitory effect on bacterial biofilms, including *P. aeruginosa* biofilms.[15,16] Furthermore, the functionalization of the nanoparticles may play a role in the observed antibiofilm effect because studies suggest that mixtures of D-amino acids trigger bacterial biofilm disassembly.[14,45] The properties of these components may explain the antibiofilm effect of unloaded formulations (LNPs and Phe_Pro_Tyr LNPs). Despite the functionalized NAC-loaded LNPs (Phe_Pro_Tyr NAC LNPs) do not seem to have a significantly higher antibiofilm effect compared to the functionalized unloaded LNPs (Phe_Pro_Tyr LNPs), it shows a safer profile in hemolytic studies, which is an advantage for *in vivo* applications.

Furthermore, the LNPs were used in combination with the antibiotic MOX to treat mature *P. aeruginosa* biofilms. In this strategy, the developed LNPs aimed to disrupt the biofilm matrix, which facilitates the interaction between the antibiotic and the bacterial cells released from the biofilm structure. This combination showed a potential synergistic effect in the reduction of bacterial viability, at MOX concentrations of 2, 4, and 8 $\mu g\ mL^{-1}$. However, this synergistic effect was not verified on biofilm biomass studies. This incongruity may be due to the fact that the biomass quantification method not only considers the live bacteria and biofilm matrix but also considers dead bacteria entrapped within the biofilm. Nevertheless, the developed nanosystems are a potential therapeutic approach against *P. aeruginosa* mature biofilms, alone or in combination with antibiotics. As an adjuvant therapy, the nanosystem may potentiate the efficacy of antibiotics, allowing for their administration in lower doses and shortening the duration of the treatment. Thus, this combined therapy may benefit commensal bacteria because lower side effects of antibiotics would be possibly observed. In a step forward toward an *in vivo* application, the effect of the developed nanosystem on commensal bacteria and different clinical isolates of *P. aeruginosa* would be important to investigate.

■ ASSOCIATED CONTENT

Supporting Information

The Supporting Information is available free of charge at https://pubs.acs.org/doi/10.1021/acsami.1c05124.

> Correlation between predicted and measured LNP hydrodynamic diameter, PDI, and LC and the correspondent R^2 values for the quadratic model, independent variables (solid lipid, surfactant, and NAC mass) and their corresponding levels, dependent variables (hydrodynamic diameter, PDI, and LC) and their levels of desirability (low, medium, and high), summary of the regression analysis for the hydrodynamic diameter, PDI, and LC, two-dimensional response surface plots for each dependent variable: hydrodynamic diameter, PDI, and LC, and representative SEM images of untreated (control) and treated *P. aeruginosa* biofilms (PDF)

■ AUTHOR INFORMATION

Corresponding Author

Cláudia Nunes − *LAQV, REQUIMTE, Departamento de Ciências Químicas, Faculdade de Farmácia, Universidade do Porto, Porto 4050-313, Portugal*; Present Address: Rua de Jorge Viterbo Ferreira, 228, 4050-313 Porto, Portugal; orcid.org/0000-0002-1502-3710; Phone: +351 220428500; Email: cdnunes@ff.up.pt

Authors

Rita M. Pinto − *LAQV, REQUIMTE, Departamento de Ciências Químicas, Faculdade de Farmácia, Universidade do Porto, Porto 4050-313, Portugal; Laboratory of Molecular Cell Biology, Institute of Botany and Microbiology KU Leuven, Leuven 3001, Belgium; VIB KU Leuven Center for Microbiology, Leuven 3001, Belgium;* orcid.org/0000-0003-0634-2928

Claudia Monteiro − *i3S, Instituto de Investigação e Inovação em Saúde INEB, Instituto de Engenharia Biomédica, Universidade do Porto, Porto 4200-135, Portugal*

Sofia A. Costa Lima − *LAQV, REQUIMTE, Departamento de Ciências Químicas, Faculdade de Farmácia, Universidade*

https://doi.org/10.1021/acsami.1c05124
ACS Appl. Mater. Interfaces XXXX, XXX, XXX−XXX

do Porto, Porto 4050-313, Portugal; orcid.org/0000-0001-8777-5877

Susana Casal − *LAQV, REQUIMTE, Departamento de Ciências Químicas, Faculdade de Farmácia, Universidade do Porto, Porto 4050-313, Portugal;* orcid.org/0000-0002-1686-3850

Patrick Van Dijck − *Laboratory of Molecular Cell Biology, Institute of Botany and Microbiology KU Leuven, Leuven 3001, Belgium; VIB KU Leuven Center for Microbiology, Leuven 3001, Belgium*

M. Cristina L. Martins − *Instituto de Ciências Biomédicas Abel Salazar, Universidade do Porto, Porto 4050-313, Portugal; i3S, Instituto de Investigação e Inovação em Saúde INEB, Instituto de Engenharia Biomédica, Universidade do Porto, Porto 4200-135, Portugal;* orcid.org/0000-0002-6574-4794

Salette Reis − *LAQV, REQUIMTE, Departamento de Ciências Químicas, Faculdade de Farmácia, Universidade do Porto, Porto 4050-313, Portugal;* orcid.org/0000-0002-0736-2835

Complete contact information is available at: https://pubs.acs.org/10.1021/acsami.1c05124

Author Contributions

The manuscript was written through contributions of all authors. All authors have given approval to the final version of the manuscript.

Funding

This work was supported by the project PTDC/NANMAT/31444/2017, financed by FCT/MCTES e FEDER through Programa Operacional Competitividade e Internacionalização—COMPETE 2020.

Notes

The authors declare no competing financial interest.

■ ACKNOWLEDGMENTS

R.M.P. and C.N. are thankful to Fundação para a Ciência e Tecnologia (FCT) for the Ph.D. Grant [SFRH/BD/130319/2017] and the investigator grant [IF/00293/2015], respectively. C.M. would like to acknowledge national funding through Fundação para a Ciência e Tecnologia, I.P. (FCT), provided by the contract program and according to numbers 4, 5, and 6 of art. 23 of Law no. 57/2016 of 29th August, as amended by Law no. 57/2017 of 19th July. S.C.L. thanks funding from FCT/MEC (CEECIND/01620/2017) financed by national funds. P.V.D. is thankful to the Fund for Scientific Research Flanders (FWO grant W000921N). The authors R.M.P., C.N., S.C.L., and S.R. acknowledge to the institution LAQV—Laboratório Associado para a Química Verde (UIDB/50006/2020). R.M.P. also acknowledges the Programa Operacional Capital Humano (POCH), specifically the BiotechHealth Programme (Doctoral Programme on Cellular and Molecular Biotechnology Applied to Health Sciences). The authors acknowledge to Rui Fernandes for his assistance with the transmission electron microscopy from the i3S Scientific Platform Histology and Electron Microscopy (HEMS), member of the PPBI (PPBI−POCI-01-0145-FEDER-022122), to Daniela Silva for her technical assistance to the scanning electron microscopy (CEMUP, Centro de Materiais da Universidade do Porto), and to Rebeca Cruz (LAQV, REQUIMTE) for assistance in the HPLC analyses. The authors also thank Manuela Barros for administrative and technical support.

■ ABBREVIATIONS

BBD, Box−Behnken design
CFUs, colony forming units
D-Phe, D-phenylalanine
D-Pro, D-proline
D-Tyr, D-tyrosine
EE, encapsulation efficiency
FTIR, Fourier transform infrared spectroscopy
HPLC, high performance liquid chromatography
LC, loading capacity
MBC, minimal bactericidal concentration
MBEC, minimal biofilm eradication concentration
MIC, minimal inhibitory concentration
MOX, moxifloxacin
MTT, thiazolyl blue tetrazolium
NAC, *N*-acetyl-L-cysteine
LNPs, lipid nanoparticles
P. aeruginosa, *Pseudomonas aeruginosa*
PDI, polydispersity
PEG, poly (ethylene glycol)
SEM, scanning electron microscopy
S. epidermidis, *Staphylococcus epidermidis*
TEM, transmission electron microscopy

■ REFERENCES

(1) Pinto, R. M.; Lopes-de-Campos, D.; Martins, M. C. L.; Van Dijck, P.; Nunes, C.; Reis, S. Impact of Nanosystems in Staphylococcus aureus Biofilms Treatment. *FEMS Microbiol. Rev.* **2019**, *43*, 622−641.

(2) Samuni, Y.; Goldstein, S.; Dean, O. M.; Berk, M. The Chemistry and Biological Activities of N-Acetylcysteine. *Biochim. Biophys. Acta* **2013**, *1830*, 4117−4129.

(3) Leite, B.; Gomes, F.; Teixeira, P.; Souza, C.; Pizzolitto, E.; Oliveira, R. Combined Effect of Linezolid and N-Acetylcysteine Against Staphylococcus epidermidis Biofilms. *Enferm Infecc Microbiol Clin.* **2013**, *31*, 655−659.

(4) Zhao, T.; Liu, Y. N-Acetylcysteine Inhibit Biofilms Produced by Pseudomonas aeruginosa. *BMC Microbiol.* **2010**, *10*, 140.

(5) Marchese, A.; Bozzolasco, M.; Gualco, L.; Debbia, E. A.; Schito, G. C.; Schito, A. M. Effect of Fosfomycin Alone and in Combination with N-Acetylcysteine on E. coli Biofilms. *Int. J. Antimicrob. Agents* **2003**, *22*, 95−100.

(6) Blasi, F.; Page, C.; Rossolini, G. M.; Pallecchi, L.; Matera, M. G.; Rogliani, P.; Cazzola, M. The Effect of N-Acetylcysteine on Biofilms: Implications for the Treatment of Respiratory Tract Infections. *Respir. Med.* **2016**, *117*, 190−197.

(7) Olofsson, A.-C.; Hermansson, M.; Elwing, H. N-Acetyl-L-Cysteine Affects Growth, Extracellular Polysaccharide Production, and Bacterial Biofilm Formation on Solid Surfaces. *Appl. Environ. Microbiol.* **2003**, *69*, 4814−4822.

(8) Oosterhof, J. J.; Elving, G. J.; Stokroos, I.; van Nieuw Amerongen, A.; van der Mei, H. C.; Busscher, H. J.; van Weissenbruch, R.; Albers, F. W. The Influence of Antimicrobial Peptides and Mucolytics on the Integrity of Biofilms Consisting of Bacteria and Yeasts as Affecting Voice Prosthetic Air Flow Resistances. *Biofouling* **2003**, *19*, 347−353.

(9) Nafee, N. Nanocarriers Against Bacterial Biofilms: Current Status and Future Perspectives. In *Nanotechnology in Diagnosis, Treatment and Prophylaxis of Infectious Diseases*; Kon, K., Ed.; Academic Press: Boston, 2015; Chapter 11, pp 167−189.

(10) Severino, P.; Andreani, T.; Macedo, A. S.; Fangueiro, J. F.; Santana, M. H.; Silva, A. M.; Souto, E. B. Current State-of-Art and

https://doi.org/10.1021/acsami.1c05124
ACS Appl. Mater. Interfaces XXXX, XXX, XXX−XXX

New Trends on Lipid Nanoparticles (SLN and NLC) for Oral Drug Delivery. *J. Drug Delivery* **2012**, *2012*, 750891.
(11) Jokerst, J. V.; Lobovkina, T.; Zare, R. N.; Gambhir, S. S. Nanoparticle PEGylation for Imaging and Therapy. *Nanomedicine (Lond)* **2011**, *6*, 715−728.
(12) Zolnik, B. S.; González-Fernández, A.; Sadrieh, N.; Dobrovolskaia, M. A. Nanoparticles and the Immune System. *Endocrinology* **2010**, *151*, 458−465.
(13) Hochbaum, A. I.; Kolodkin-Gal, I.; Foulston, L.; Kolter, R.; Aizenberg, J.; Losick, R. Inhibitory Effects of D-Amino Acids on Staphylococcus aureus Biofilm Development. *J. Bacteriol.* **2011**, *193*, 5616−5622.
(14) Kolodkin-Gal, I.; Romero, D.; Cao, S.; Clardy, J.; Kolter, R.; Losick, R. D-Amino Acids Trigger Biofilm Disassembly. *Science* **2010**, *328*, 627−629.
(15) Ueda, Y.; Mashima, K.; Miyazaki, M.; Hara, S.; Takata, T.; Kamimura, H.; Takagi, S.; Jimi, S. Inhibitory Effects of Polysorbate 80 on MRSA Biofilm Formed on Different Substrates Including Dermal Tissue. *Sci. Rep.* **2019**, *9*, 3128.
(16) Toutain-Kidd, C. M.; Kadivar, S. C.; Bramante, C. T.; Bobin, S. A.; Zegans, M. E. Polysorbate 80 Inhibition of Pseudomonas aeruginosa Biofilm Formation and its Cleavage by the Secreted Lipase LipA. *Antimicrob. Agents Chemother.* **2009**, *53*, 136−145.
(17) Singh, B.; Kapil, R.; Nandi, M.; Ahuja, N. Developing Oral Drug Delivery Systems Using Formulation by Design: Vital Precepts, Retrospect and Prospects. *Expet Opin. Drug Deliv.* **2011**, *8*, 1341−1360.
(18) Ferreira, S. L. C.; Bruns, R. E.; Ferreira, H. S.; Matos, G. D.; David, J. M.; Brandão, G. C.; da Silva, E. G. P.; Portugal, L. A.; dos Reis, P. S.; Souza, A. S.; dos Santos, W. N. L. Box-Behnken Design: An Alternative for the Optimization of Analytical Methods. *Anal. Chim. Acta* **2007**, *597*, 179−186.
(19) Bezerra, M. A.; Santelli, R. E.; Oliveira, E. P.; Villar, L. S.; Escaleira, L. A. Response Surface Methodology (RSM) as a Tool for Optimization in Analytical Chemistry. *Talanta* **2008**, *76*, 965−977.
(20) Lundstedt, T.; Seifert, E.; Abramo, L.; Thelin, B.; Nyström, Å.; Pettersen, J.; Bergman, R. Experimental Design and Optimization. *Chemometr. Intell. Lab. Syst.* **1998**, *42*, 3−40.
(21) Vestby, L. K.; Grønseth, T.; Simm, R.; Nesse, L. L. Bacterial Biofilm and Its Role in the Pathogenesis of Disease. *Antibiotics* **2020**, *9*, 59.
(22) Siala, W.; Kucharíková, S.; Braem, A.; Vleugels, J.; Tulkens, P. M.; Mingeot-Leclercq, M. P.; Van Dijck, P.; Van Bambeke, F. The Antifungal Caspofungin Increases Fluoroquinolone Activity Against Staphylococcus aureus Biofilms by Inhibiting N-Acetylglucosamine Transferase. *Nat. Commun.* **2016**, *7*, 13286.
(23) Scholar, E. Moxifloxacin. In *xPharm: The Comprehensive Pharmacology Reference*; Enna, S. J., Bylund, D. B., Eds.; Elsevier: New York, 2007; pp 1−6.
(24) Lopes-de-Araújo, J.; Neves, A. R.; Gouveia, V. M.; Moura, C. C.; Nunes, C.; Reis, S. Oxaprozin-Loaded Lipid Nanoparticles Towards Overcoming NSAIDs Side-Effects. *Pharm. Res.* **2016**, *33*, 301−314.
(25) Moghimi, S. M.; Hunter, A. C.; Andresen, T. L. Factors Controlling Nanoparticle Pharmacokinetics: An Integrated Analysis and Perspective. *Annu. Rev. Pharmacol. Toxicol.* **2012**, *52*, 481−503.
(26) INFARMED—National Authority of Medicines and Health Products, I.P *Portuguese Pharmacopoeia 9.0. Health*; Imprensa Nacional: Lisbon, 2008; pp 1380−1381.
(27) Standardization, I. O. F *Biological Evaluation of Medical Devices−Part 5: Tests for in Vitro Cytotoxicity*; International Standard ISO 10993-5: Geneva, Switzerland, 2009.
(28) Guo, Q.; Zhao, Y.; Dai, X.; Zhang, T.; Yu, Y.; Zhang, X.; Li, C. Functional Silver Nanocomposites as Broad-Spectrum Antimicrobial and Biofilm-Disrupting Agents. *ACS Appl. Mater. Interfaces* **2017**, *9*, 16834−16847.
(29) Wiegand, I.; Hilpert, K.; Hancock, R. E. W. Agar and Broth Dilution Methods to Determine the Minimal Inhibitory Concentration (MIC) of Antimicrobial Substances. *Nat. Protoc.* **2008**, *3*, 163.
(30) Allkja, J.; Bjarnsholt, T.; Coenye, T.; Cos, P.; Fallarero, A.; Harrison, J. J.; Lopes, S. P.; Oliver, A.; Pereira, M. O.; Ramage, G.; Shirtliff, M. E.; Stoodley, P.; Webb, J. S.; Zaat, S. A. J.; Goeres, D. M.; Azevedo, N. F. Minimum Information Guideline for Spectrophotometric and Fluorometric Methods to Assess Biofilm Formation in Microplates. *Biofilm* **2020**, *2*, 100010.
(31) Thomas, N.; Thorn, C.; Richter, K.; Thierry, B.; Prestidge, C. Efficacy of Poly-Lactic-Co-Glycolic Acid Micro- and Nanoparticles of Ciprofloxacin Against Bacterial Biofilms. *J. Pharm. Sci.* **2016**, *105*, 3115−3122.
(32) Monteiro, C.; Papenfort, K.; Hentrich, K.; Ahmad, I.; Le Guyon, S.; Reimann, R.; Grantcharova, N.; Römling, U. Hfq and Hfq-Dependent Small RNAs Are Major Contributors to Multicellular Development in Salmonella enterica Serovar Typhimurium. *RNA Biol.* **2012**, *9*, 489−502.
(33) Gomes, R. N.; Borges, I.; Pereira, A. T.; Maia, A. F.; Pestana, M.; Magalhães, F. D.; Pinto, A. M.; Gonçalves, I. C. Antimicrobial Graphene Nanoplatelets Coatings for Silicone Catheters. *Carbon* **2018**, *139*, 635−647.
(34) Blanco, E.; Shen, H.; Ferrari, M. Principles of Nanoparticle Design for Overcoming Biological Barriers to Drug Delivery. *Nat. Biotechnol.* **2015**, *33*, 941−951.
(35) Singh, R.; Lillard, J. W., Jr. Nanoparticle-Based Targeted Drug Delivery. *Exp. Mol. Pathol.* **2009**, *86*, 215−223.
(36) Iqbal, M.; Zafar, N.; Fessi, H.; Elaissari, A. Double Emulsion Solvent Evaporation Techniques Used for Drug Encapsulation. *Int. J. Pharm.* **2015**, *496*, 173−190.
(37) Amin, K.; Dannenfelser, R.-M. In vitro Hemolysis: Guidance for the Pharmaceutical Scientist. *J. Pharm. Sci.* **2006**, *95*, 1173−1176.
(38) Neun, B. W.; Dobrovolskaia, M. A. Method for Analysis of Nanoparticle Hemolytic Properties in vitro. *Methods Mol. Biol.* **2011**, *697*, 215−224.
(39) Kao, L. W.; Kirk, M. A.; Furbee, R. B.; Mehta, N. H.; Skinner, J. R.; Brizendine, E. J. What Is the Rate of Adverse Events After Oral N-Acetylcysteine Administered by the Intravenous Route to Patients with Suspected Acetaminophen Poisoning? *Ann. Emerg. Med.* **2003**, *42*, 741−750.
(40) Sun, H.; Yang, R.; Wang, J.; Yang, X.; Tu, J.; Xie, L.; Li, C.; Lao, Q.; Sun, C. Component-Based Biocompatibility and Safety Evaluation of Polysorbate 80. *RSC Adv.* **2017**, *7*, 15127−15138.
(41) Cacciatore, I.; Di Giulio, M.; Fornasari, E.; Di Stefano, A.; Cerasa, L. S.; Marinelli, L.; Turkez, H.; Di Campli, E.; Di Bartolomeo, S.; Robuffo, I.; Cellini, L. Carvacrol Codrugs: a New Approach in the Antimicrobial Plan. *PloS One* **2015**, *10*, No. e0120937.
(42) Ommen, P.; Zobek, N.; Meyer, R. L. Quantification of Biofilm Biomass by Staining: Non-Toxic Safranin Can Replace the Popular Crystal Violet. *J. Microbiol. Methods* **2017**, *141*, 87−89.
(43) Dong, D.; Thomas, N.; Thierry, B.; Vreugde, S.; Prestidge, C. A.; Wormald, P.-J. Distribution and Inhibition of Liposomes on Staphylococcus aureus and Pseudomonas aeruginosa Biofilm. *PloS One* **2015**, *10*, No. e0131806.
(44) Forier, K.; Messiaen, A.-S.; Raemdonck, K.; Nelis, H.; De Smedt, S.; Demeester, J.; Coenye, T.; Braeckmans, K. Probing the Size Limit for Nanomedicine Penetration Into Burkholderia multivorans and Pseudomonas aeruginosa Biofilms. *J. Controlled Release* **2014**, *195*, 21−28.
(45) Ampornaramveth, R. S.; Akeatichod, N.; Lertnukkhid, J.; Songsang, N. Application of D-Amino Acids as Biofilm Dispersing Agent in Dental Unit Waterlines. *Int. Dent. J.* **2018**, *2018*, 9413925.

https://doi.org/10.1021/acsami.1c05124
ACS Appl. Mater. Interfaces XXXX, XXX, XXX−XXX

Supporting Information

N-Acetyl-$_L$-cysteine-Loaded Nanosystems as a Promising Therapeutic Approach Toward the Eradication of *Pseudomonas aeruginosa* Biofilms

Rita M. Pinto[1,2,3], Claudia Monteiro[5], Sofia A. Costa Lima[1], Susana Casal[1], Patrick Van Dijck[2,3], M. Cristina L. Martins[4,5], Cláudia Nunes[1], Salette Reis[1]*

[1] LAQV, REQUIMTE, Departamento de Ciências Químicas, Faculdade de Farmácia, Universidade do Porto, Porto, Portugal

[2] Laboratory of Molecular Cell Biology Institute of Botany and Microbiology KU Leuven Leuven, Belgium

[3] VIB KU Leuven Center for Microbiology Leuven, Belgium

[4] Instituto de Ciências Biomédicas Abel Salazar, Universidade do Porto, Porto, Portugal

[5] i3S, Instituto de Investigação e Inovação em Saúde INEB, Instituto de Engenharia Biomédica, Universidade do Porto, Porto, Portugal

* Corresponding author: cdnunes@ff.up.pt

1. Experimental Design

For all models (linear, two-factor interactions and quadratic) the correlation between expected and observed values was evaluated (**Figure S1**). The predicted R^2 value was analyzed to evaluate the fitness of each model. According to this information, the quadratic model was selected for all dependent variables.

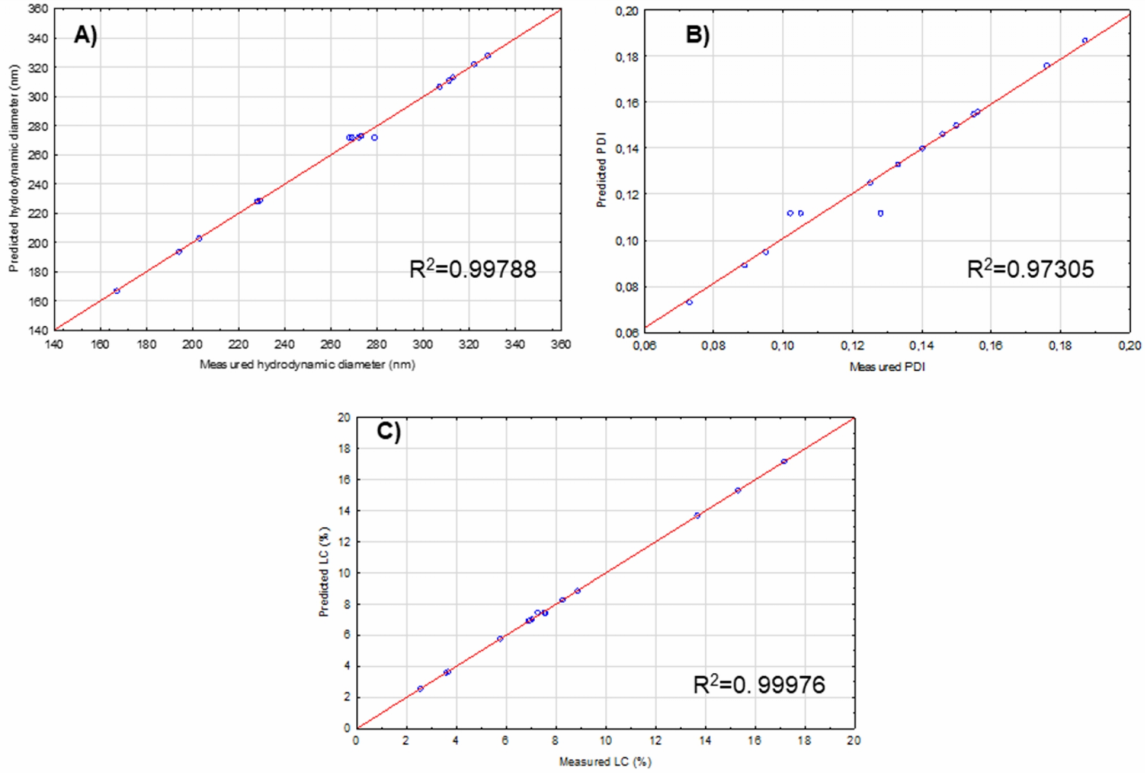


Figure S1. Correlation between predicted and measured **A)** LNPs hydrodynamic diameter, **B)** LNPs PDI, **C)** LNPs LC and the correspondent R^2 values for the quadratic model.

Table S1. Independent variables (solid lipid, surfactant and NAC mass) and their corresponding levels. Dependent variables (hydrodynamic diameter, PDI and LC) and their levels of desirability (low, medium, and high).

	Levels		
	-1	0	1
Independent variables			
X_1 = Cetyl palmitate mass (mg)	50	80	110
X_2 = Surfactant mass (mg)	50	75	100
X_3 = NAC mass (mg)	10	20	30
Dependent variables	**Desirability**		
	Low	**Medium**	**High**
Y_1 = Hydrodynamic diameter (nm)	270	200	100
Y_2 = PDI	0.200	0.150	0.073
Y_3 = LC (%)	5	10	20

The effects of the independent variables and their linear and quadratic interactions on hydrodynamic diameter, PDI and LC can be found in **Table S2**. The polynomial function was validated using ANOVA. Two-dimensional response surface plots (**Figure S2**) were calculated from the quadratic polynomial equation (**Eq. 1**). These plots represent the effect of different factors on each of the observed responses.

Table S2. Summary of the regression analysis for the hydrodynamic diameter, PDI and LC. The values highlighted (grey shade) are statistically significant, with a $P< 0.05$. X_1, X_2 and X_3 represent the solid lipid, surfactant and NAC mass, respectively.

	Hydrodynamic diameter (nm)		**PDI**		**LC (%)**	
	Coefficient	*p*-value	Coefficient	*p*-value	Coefficient	*p*-value
Intercept	262.0833	0.000045	0.135417	0.000918	8.31333	0.000036
X_1 (L)	44.8333	0.002547	-0.010167	0.195159	-3.77750	0.000294
X_1 (Q)	7.9375	0.037538	-0.025896	0.019824	-1.32208	0.001169
X_2 (L)	-40.3333	0.003144	0.003000	0.628477	-0.51750	0.015320
X_2 (Q)	-1.0625	0.571186	0.003104	0.489920	-0.55208	0.006649
X_3 (L)	-3.3333	0.279250	-0.004167	0.514204	3.13917	0.000426
X_3 (Q)	0.5625	0.756282	0.004979	0.310781	1.23917	0.001330
X_1 (L) * X_2 (L)	14.2500	0.042659	-0.014250	0.183014	0.89000	0.009408
X_1 (L) * X_2 (Q)	9.1250	0.051308	-0.001375	0.810185	0.65625	0.008661
X_1 (Q) * X_2 (L)	-3.1250	0.283370	-0.004875	0.434624	0.51375	0.014018
X_1 (L) * X_3 (L)	1.5000	0.670707	-0.009500	0.313353	-1.29250	0.004494
X_1 (Q) * X_3 (L)	-1.2500	0.619857	-0.007750	0.263226	-0.50000	0.014782
X_2 (L) * X_3 (L)	5.5000	0.212274	0.011500	0.247283	0.11750	0.309097

A positive coefficient represents a synergic effect between the independent variables, while a negative coefficient represents an antagonistic effect.

Abbreviations: L, linear; LC, loading capacity; PDI, polydispersity index; Q, quadratic.

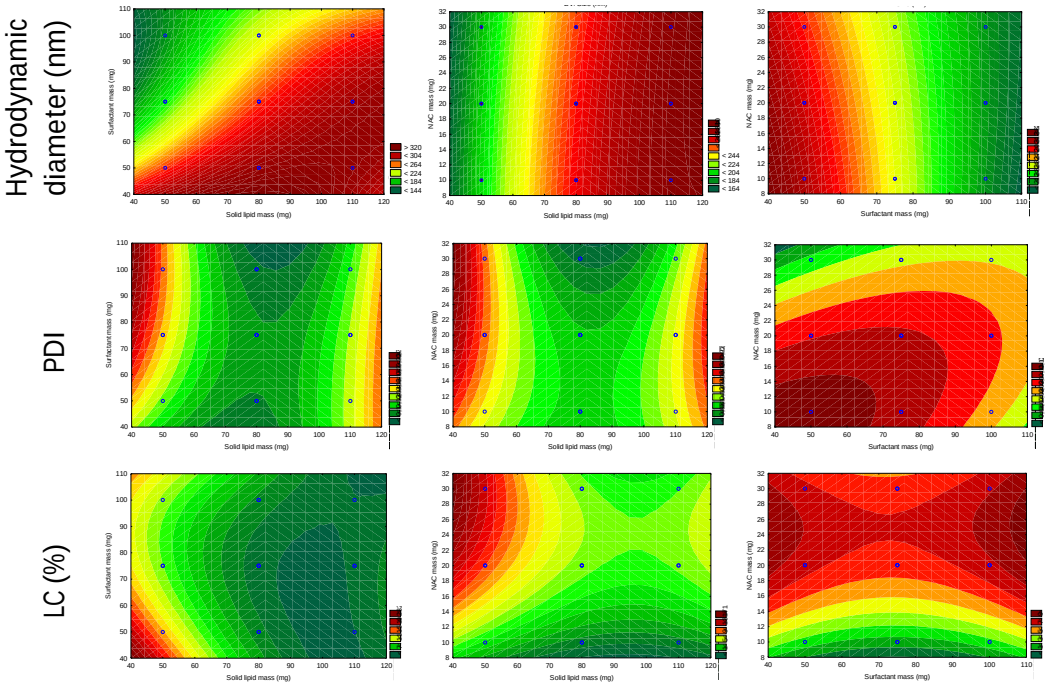


Figure S2. Two-dimension response surface plots for each dependent variable: hydrodynamic diameter, PDI and LC.

The particle hydrodynamic diameter of the formulations was significantly affected by the solid lipid and surfactant mass. The amount of solid lipid revealed a positive effect on the hydrodynamic diameter, both linearly and quadratically. Thus, formulations with higher solid lipid amounts reveal higher particle hydrodynamic diameters. This effect is a consequence of higher quantities of lipid molecules available, which leads to an increased molecular density of the lipid phase [1]. On the other hand, the surfactant amount showed a significant negative linear effect on the hydrodynamic diameter of the LNPs. Increasing quantities of surfactant diminishes the interfacial tension, stabilizing the emulsions. As a consequence, the LNPs hydrodynamic diameter decreases with the increase of surfactant mass [2]. Additionally, a simultaneous increase of solid lipid and surfactant amounts as a positive effect on the LNPs hydrodynamic diameters.

The PDI of all the fifteen formulations characterized remained below 0.2, which suggests they were monodispersed suspensions. The solid lipid amount was the only variable with significant effect on the PDI.

The LC values were affected by all interactions, with exception of the linear interaction between surfactant and NAC amounts. The increasing solid lipid amount leads to a decrease of LC, since the LC is inversely proportional to the amount of lipid. On the opposite, higher amounts of NAC are associated to higher LC values.

2. Scanning Electron Microscopy (SEM) Biofilm Analysis

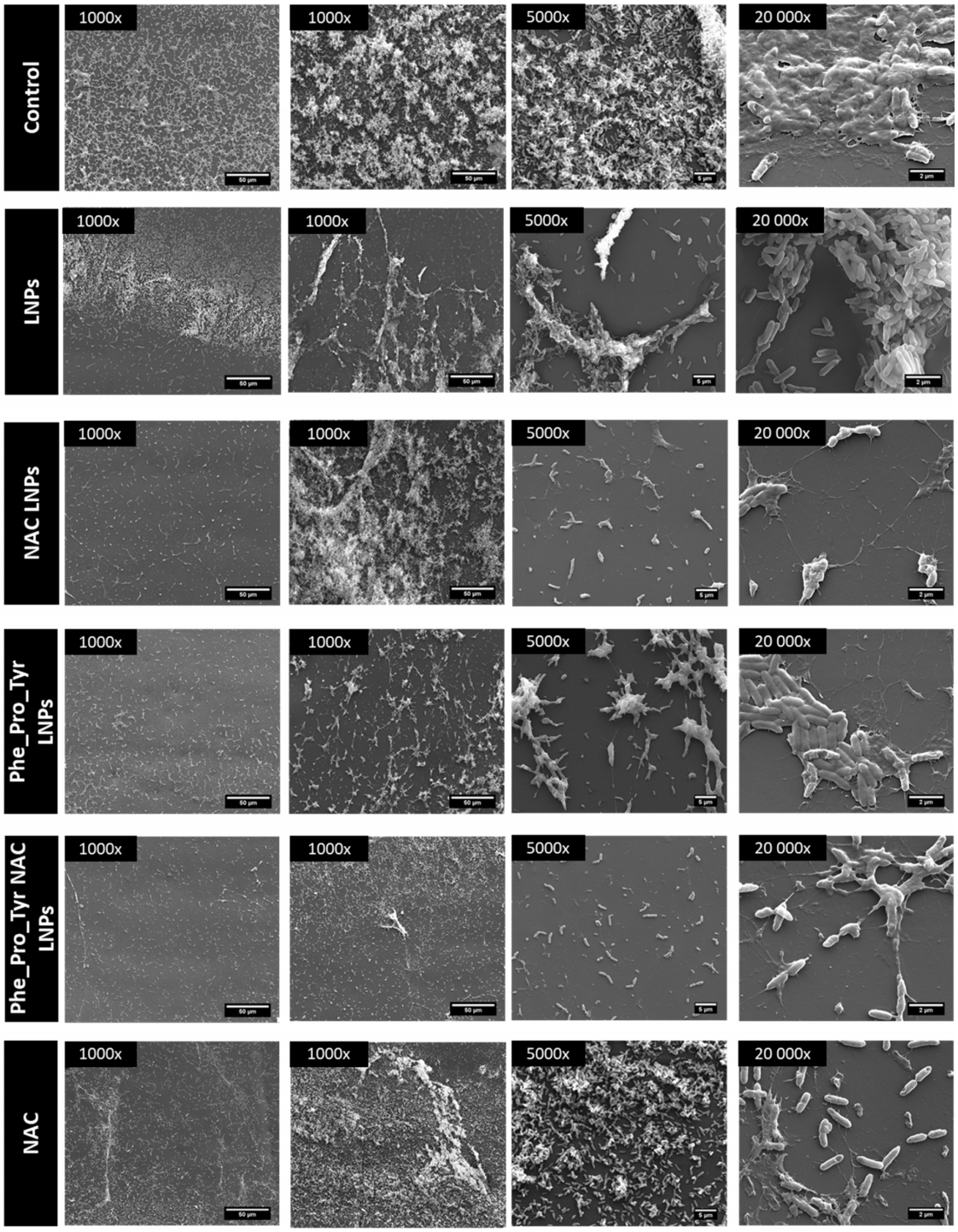


Figure S3. Representative SEM images of untreated (control) and treated *P. aeruginosa* biofilms. The LNPs suspensions were tested at a solid lipid concentration of 2 mg ml^{-1}. Free NAC was tested at a concentration of 0.9 mg ml^{-1} (amount of NAC corresponding to 2 mg ml^{-1} of solid lipid in the LNPs). 1000x, 5000x, and 20 000x (at the top left of each image) indicate the magnification used for the respective image.

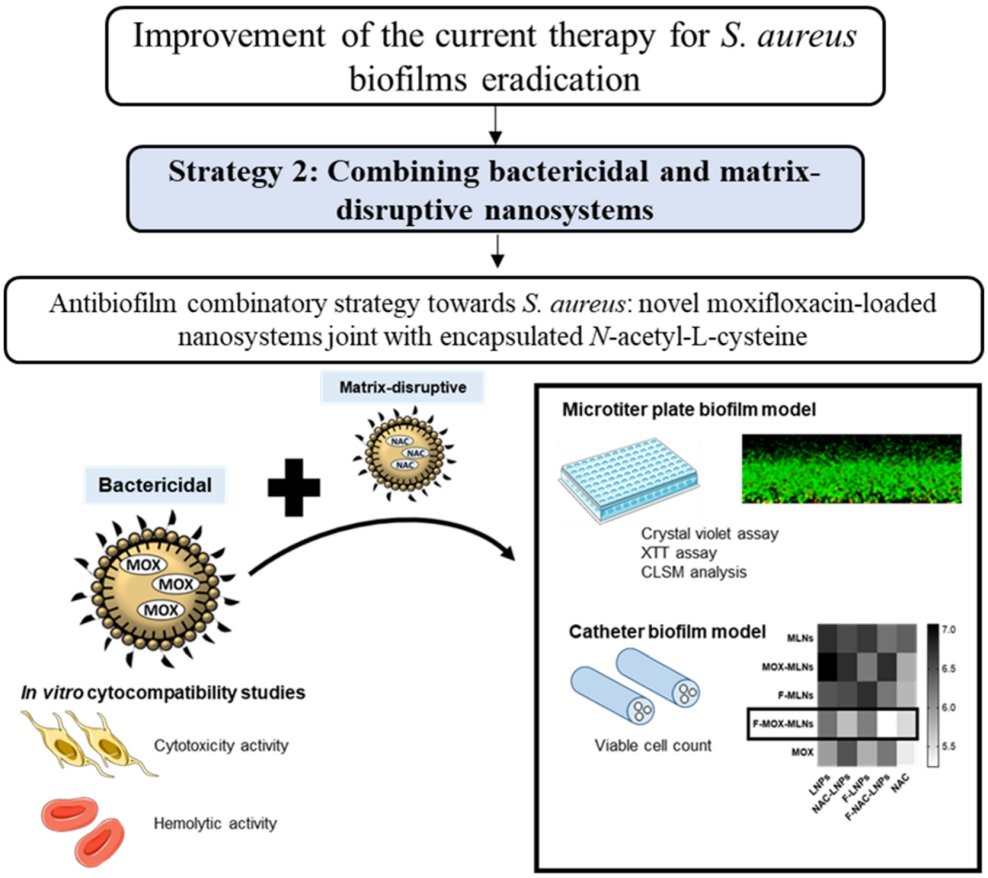
REFERENCES

1. Lopes-de-Campos, D., et al., *Delivering Amoxicillin at the Infection Site - a Rational Design through Lipid Nanoparticles.* Int. J. Nanomedicine, 2019. **14**: p. 2781-2795, 10.2147/ijn.S193992
2. Sahoo, S.K., et al., *Residual Polyvinyl Alcohol Associated with Poly (D,L-Lactide-Co-Glycolide) Nanoparticles Affects Their Physical Properties and Cellular Uptake.* J. Control. Release, 2002. **82**(1): p. 105-114, 10.1016/s0168-3659(02)00127-x

Chapter 6.2.

Antibiofilm combinatory strategy towards *S. aureus*: novel moxifloxacin-loaded nanosystems joint with encapsulated *N*-acetyl-L-cysteine

In the development of an innovative strategy to eradicate *S. aureus* biofilms, it is essential to target both the bacterial cells and the EPS matrix. In this chapter, functionalized lipid nanoparticles loading a broad-spectrum antibiotic, moxifloxacin (MOX), were developed. The formulations were further combined with NAC-loaded nanoparticles previously described (**chapter 6.1.**). The *in vitro* antibiofilm activity of the MOX-loaded and NAC-loaded nanosystems was evaluated in two biofilm models: microtiter plate and polyurethane catheters. The potential synergistic effect between the two nanosystems is a step forward towards the development of a combinatory strategy against S*. aureus* biofilms.



Antibiofilm combinatory strategy towards *S. aureus*: novel moxifloxacin-loaded nanosystems joint with encapsulated *N*-acetyl-L-cysteine

Rita M. Pinto[1,2,3], Catarina Leal Seabra[1], Martine De Jonge[2], M. Cristina L. Martins[4,5], Patrick Van Dijck[2,3], Salette Reis[1], Cláudia Nunes[1*]

[1] LAQV, REQUIMTE, Departamento de Ciências Químicas, Faculdade de Farmácia, Universidade do Porto, Porto, Portugal

[2] Laboratory of Molecular Cell Biology Institute of Botany and Microbiology KU Leuven Leuven, Belgium

[3] VIB KU Leuven Center for Microbiology Leuven, Belgium

[4] Instituto de Ciências Biomédicas Abel Salazar, Universidade do Porto, Porto, Portugal

[5] i3S, Instituto de Investigação e Inovação em Saúde INEB, Instituto de Engenharia Biomédica, Universidade do Porto, Porto, Portugal

*Corresponding author:

Cláudia Nunes: cdnunes@ff.up.pt

Abstract

Bacterial biofilms formed by clinically relevant pathogens, such as *Staphylococcus aureus*, have a massive impact in the increasing figures of antimicrobial resistance phenomena. Biofilms are commonly associated to implantable medical devices, ultimately leading to their failure. The current treatment for biofilm-associated infections is solely based on the administration of conventional antibiotics, failing to target the first physical barrier of biofilms: the extracellular polymeric substances (EPS) matrix. The present work is focused on the development of multiple lipid nanoparticles (MLNs) encapsulating an antibiotic, moxifloxacin (MOX). The nanoparticles were functionalized with D-amino acids to target and disrupt the bacterial biofilms. The produced formulations exhibited a mean hydrodynamic size below 300 nm, a low polydispersity index, and a satisfactorily high encapsulation efficiency (>75%). At a physiological pH of 7.4, the MOX-loaded MLNs showed an initial burst release followed by a controlled release profile. The MLNs were stable under storage conditions up to 12 weeks. *In vitro* cytocompatibility studies revealed that the formulations exhibited a low cytotoxicity effect in fibroblasts and low hemolytic activity. In a complex approach to target both bacterial cells and the EPS matrix, the developed MOX-loaded MLNs were combined with a nanosystem encapsulating a matrix-disruptive agent: *N*-acetyl-L-cysteine (NAC). *In vitro* antibiofilm studies were performed in both methicillin-susceptible and methicillin-resistant *S. aureus* strains. The two nanosystems alone showed a significant reduction of both biofilm viability and biomass, using the microtiter plate biofilm model. Further, biofilms grown in polyurethane catheters were used to assess the effect of combining MOX-loaded and NAC-loaded nanosystems on biofilm viable count. For all tested strains, a potential synergistic effect was observed when combining the functionalized MOX-loaded MLNs and NAC-loaded nanosystems. Thus, nanosystems as carriers of bactericidal and matrix-disruptive agents are a promising combinatory strategy towards the eradication of *S. aureus* biofilms.

1. Introduction

Bacterial biofilms have a massive impact in modern medicine due to the high demand for implantable medical devices. Amongst these, *Staphylococcus aureus* (*S. aureus*) biofilms are the most prevalent and severe, leading to high rates of morbidity and mortality [1]. When a medical device, such as a catheter, enters the human body, it is prone to bacterial colonization and eventual biofilm formation [2]. Biofilms are three-dimensional structures where an extracellular polymeric substances (EPS) matrix surrounds bacterial cells, providing a protective environment against harsh external conditions. The EPS matrix plays a key role in the escalating figures of antimicrobial resistance since it consists in the first barrier encounter by antibiotics. Due to the difficult diffusion and potential interaction of antibiotics with the EPS matrix components, conventional antimicrobial therapies lack efficiency in eradicating biofilm-associated infections [3, 4]. Thus, a therapeutic strategy combining antibiotics with matrix-disruptive agents may be the best approach towards the eradication of bacterial biofilms, targeting both the EPS matrix and bacterial cells within the structure.

Moxifloxacin (MOX) is a well-known fluoroquinolone with a broad antibacterial spectrum against Gram-positive and Gram-negative bacteria [5]. Despite being a promising antibiotic to treat several bacterial infections, it is not highly efficient against biofilms [6]. Thus, MOX in combination with other antimicrobial agents have been reported against bacterial biofilms [7, 8]. More recently, few reports showed the potential of combining MOX with matrix-disruptive agents, such as *N*-acetyl-L-cysteine (NAC) [9]. NAC is a mucolytic agent with antibacterial and antibiofilm properties against several bacterial strains [10-12]. Although the antibiofilm mechanism of NAC is still not fully understood, it shows the potential in inhibiting biofilm formation and even disrupt mature biofilms [13]. Studies suggest that NAC acts on reducing the production of exopolysaccharides and leads to disruption and degradation of EPS matrix components [11]. However, both MOX and NAC are prone to degradation and clearance upon administration. Besides, both show affinity to bound to plasma proteins [14, 15]. Hence, their availability at the biofilm site may be compromised.

Nanotechnology is a powerful tool to improve drug delivery after administration, since nanoparticles protect encapsulated drugs and target them to the biofilm, leading to an increased therapeutic efficacy [16]. Amongst several types of nanoparticles, lipid nanoparticles are highlighted due to their high biocompatibility, cost effectiveness, and controlled drug release [17].

In this work, MOX-loaded multiple lipid nanoparticles (MLNs) were developed to target and eradicate mature *S. aureus* biofilms. The developed nanosystems were functionalized with

D-amino acids (D-Phenylalanine, D-Proline, and D-Tyrosine) covalently linked to poly (ethylene glycol) (PEG). PEG was used to increase circulation time of the nanosystems upon administration, avoiding recognition by the host immune system [18]. The D-amino acids were selected to target and disrupt the biofilms, acting as an adjuvant [19, 20]. The produced formulations were physically characterized, and their *in vitro* cytocompatibility was assessed. The antibiofilm efficacy of the developed MLNs was evaluated alone or in a combinatory therapeutic approach with NAC-loaded nanosystems, which were previously described [9]. In this strategy, NAC would disrupt the biofilm matrix, exposing the dispersed cells to the bactericidal effect of MOX. A schematic overview of the MOX-loaded and NAC-loaded nanosystems used in this work is represented in **Figure 1**.

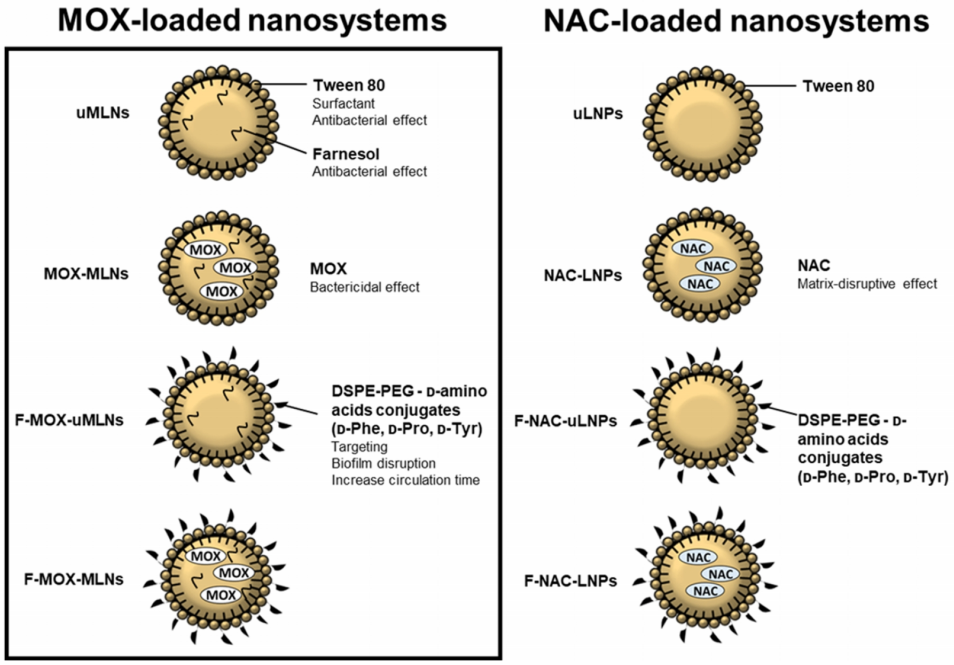


Figure 1: Schematic overview of the antibacterial and antibiofilm components of the nanosystems used for the proposed combinatory strategy. MOX-loaded MLNs were produced by an adapted protocol previously described by Cavalcanti *et al.* (2017), while NAC-loaded nanosystems were produced by the double emulsion method [9]. The MLNs were composed by cetyl palmitate (solid lipid), Miglyol 812 (liquid lipid), farnesol, and the surfactants Tween 80 and Span 80. The LNPs were composed by cetyl palmitate and Tween 80. The surface of the nanoparticles was functionalized with DSPE-PEG-D-amino acid conjugates.

2. Materials and Methods

2.1 Materials

The lipid cetyl palmitate was a kind gift from Gattefossé (Gattefossé, France). DSPE-PEG2000-NH_2 (1,2-distearoyl-*sn*-glycero-3-phosphoethanolamine-N-[amino(polyethylene glycol)-2000] (ammonium salt)) was purchased from Avanti Polar Lipids Inc. (Alabaster, Alabama, USA). D-Phenilalanine (Phe), D-Proline (Pro), D-Tyrosine (Tyr), triethylamine (TEA), dicyclohexylcarbodiimide (DCC), N-hydroxysuccinimide (NHS), sodium hydroxide (NaOH), sodium chloride, moxifloxacin hydrochloride (MOX), farnesol 95%, Tween 80, Triton X-100, thiazolyl blue tetrazolium (MTT), D-(+)-glucose monohydrate >99%, müller-hinton broth cation adjusted (MHB-Ca^{2+}), 2,3-Bis(2-methoxy-4-nitro-5-sulfophenyl)-2H-tetrazolium-5-carboxanilide inner salt (XTT), menadione crystalline, and crystal violet dye were obtained from Sigma-Aldrich (USA). Miglyol 812 and Span 80 were purchased from Acofarma (Spain). *N*-acetyl-L-cysteine (NAC) was purchased to MERK, Milipore Ltd. (Ireland). The FilmTracer™ LIVE/DEATH® Biofilm Viability Kit was acquired from Thermo Fisher Scientific (USA). Chloroform, dimethyl sulfoxide (DMSO), methanol, and acetic acid glacial were obtained from VWR International LLC (USA). Dulbecco's Modified Eagle's Medium (DMEM), trypsin-EDTA (1×), Penicillin-Streptomycin (Pen Strep), Dulbecco's Phosphate Buffered Saline 10x pH 7.4 (PBS), and Fetal Bovine Serum (FBS) were purchased from Gibco by Life Technologies (UK). Lactate dehydrogenase (LDH) Cytotoxicity Detection Kit was obtained from Takara Bio Inc. (Shiga, Japan). L929 cells (ATCC CCL-1TM) were acquired from the American Type Culture Collection (USA). BD Tryptic soy broth (TSB) and Difco Granulated Agar were acquired from Becton Dickinson (USA). All components were used without further purification.

2.2 Bacterial strains

The *S. aureus* strains ATCC 33591 (methicillin-resistant) and ATCC 25923 (methicillin-susceptible) were kindly sent by Prof. Françoise Van Bambeke (UCLouvain). The *S. aureus* strain ATCC 6538 was acquired from ATCC® (USA). The bioluminescent strain *Xen36* (Caliper Life Sciences, Hopkinton, MA, USA) was originally derived from *S. aureus* ATCC 49525 and expresses a stable copy of a modified *Photorhabdus luminescens luxABCDE* operon [21, 22].

2.3 Preparation of the MOX-loaded MLNs

To encapsulate MOX, a new generation of lipid nanoparticles, the MLNs, were produced based on few modifications from a previously reported protocol [23]. Firstly, the lipid phase constituted by the solid lipid cetyl palmitate (135 mg), the lipid liquid Miglyol 812 (305 mg), the lipophilic surfactant Span 80 (115 mg), and farnesol (6 mg) were heated at a temperature above their melting point (60ºC) in a water bath. At the same temperature, 5 mg of MOX dissolved in 650 µl of ultrapure water was pre-heated. Unloaded MLNs were prepared by replacing the drug solution by ultrapure water. Then, the aqueous solution was added to the melted lipid phase and sonicated for 3 mins at 70% amplitude, using a VCX-130 Vibra-Cell™ sonicator (Sonics & Materials Inc, USA), with a CV-18 probe (130 W, 20 kHz). This primary emulsion was left to cool down at room temperature. Further, the hydrophilic surfactant Tween 80 (80 mg) was added to the emulsion. D-amino acids conjugates (D-Phe, D-Pro, and D-Tyr) were also added in the functionalized formulations (1 mg, each conjugate). The synthesis of these conjugates was previously described elsewhere [9]. The emulsion was then heated for 5 mins at 60ºC and sonicated at 80% amplitude during 3 mins.

2.4 Physical characterization of MLNs

The hydrodynamic diameter and polydispersity index (PDI) were determined using a Particle Size Analyzer (Brookhaven Instruments Corporation, Software: Particle Sizing v.5 Brookhaven Instruments, USA). The zeta potential of the MLNs was measured using the Zeta Potential Analyzer (ZetaPALS, Brookhaven Instruments Corporation, Software: PALS Zeta Potential Analyzer v.5 Brookhaven Instruments, USA). The system operated with an incidence light angle of 90˚, at room temperature. Prior to the measurements, 5 µl of MLNs were diluted in 8000 µl of ultrapure water.

2.5 Determination of the encapsulation efficiency and loading capacity

The encapsulation efficiency (EE) was calculated by an indirect method to determine the entrapped MOX. In this method, 5 µl of the MOX-loaded MLNs were diluted in 16 ml of ultrapure water. After, the diluted formulations were transferred to an Amicon Ultra-4 Centrifugal Filter Device 50 kDa (MERCK Milipore, Ltd, Ireland) and centrifuged at 524*g* until complete separation of the MLNs from the supernatant (Allegra X-15R Centrifuge, Beckman Coulter, USA). The supernatant was collected to quantify the non-encapsulated

MOX, using UV-vis spectroscopy (V-660, Jasco Corporation, Software: Spectra Manager V.2, Jasco Corporation, USA) at 288 nm.

The EE was calculated as follows:

$$EE\ (\%) = \frac{Total\ MOX\ amount - unloaded\ MOX\ amount}{Total\ MOX\ amount} \times 100 \quad (1)$$

The LC was calculated using the EE, as follows:

$$LC\ (\%) = \frac{EE \times Total\ MOX\ amount}{Total\ solid\ lipid\ amount} \times 100 \quad (2)$$

2.6 Evaluation of the storage stability

The MLNs formulations were stored at room temperature for 24 weeks. The physicochemical storage stability was assessed over time through the measurements of particle size, PDI, zeta potential, EE, and LC. The measurements were performed using the methods described in the previous sections.

2.7 *In vitro* MOX release study

To assess the MOX release profile from the developed nanoparticles, the dialysis diffusion technique under sink conditions was used [24]. The formulations (MOX-MLNs and F-MOX-MLNs) and free MOX (200 µl diluted in 300 µl of ultrapure water) were added to cellulose dialysis bags (Spectra/Por®1 Dialysis Membrane Standard RC Tubing, MWCO 6-8 kD, SpectrumLabs, USA) and placed into 60 ml of PBS at a physiological pH (7.4), at 37ºC, under agitation, for 48h. At regular intervals, aliquots (1 ml) were collected and replaced with the same volume of fresh medium. The release rate was quantified using UV-vis spectroscopy (V-660, Jasco Corporation, Software: Spectra Manager V.2, Jasco Corporation, USA) at 288 nm.

2.8 *In vitro* cytocompatibility studies

2.8.1 Cytotoxicity and cell viability assessment

The cytotoxicity and cell viability of the developed MLNs was evaluated in a fibroblasts cell line (L929 cell line), as recommended by the ISO international standard 10993–5 for

cytocompatibility assessment studies [25]. These cells were cultured in DMEM supplied with 10% FBS and 1% Penicillin-Streptomycin at 37ºC, 5% CO_2 atmosphere.

The MLNs effect on L929 cells was measured using the MTT and LDH assays [24, 26]. Briefly, the cells were seeded in 96-well plates at a density of 5 x 10^4 cells/well. When cells reach 80 – 90% confluence, MLNs with different concentrations of MOX (2.0, 1.0, 0.5, 0.25, and 0.125 µg ml^{-1}) were added to the wells and incubated for 24h, 37ºC, 5% CO_2. Free MOX was tested at the same concentrations. Triton-100 (1%, v/v) and DMEM were used as negative and positive controls, respectively.

After the incubation time, the medium was collected and centrifuged at 250*g* for 10 mins at room temperature (Centrifuge 5810R, Eppendorf, Germany). Subsequently, the supernatant was collected to quantify the LDH using the LDH cytotoxicity kit, according to the instructions from the manufacturer. The absorbance was read at 490 and 690 nm using a microplate reader (BioTek Instruments Inc., Synergy HT, Software: Gen5 v1.08.4, BioTek Instruments Inc., USA). The latter was used to remove the background interference.

For the MTT assay, after the treatment with the MLNs, the medium was replaced by 100 µl of MTT solution (0.5 mg ml^{-1}) and incubated for 2h at 37ºC, 5% CO_2. Then, the MTT solution was removed, and the formazan crystals were dissolved in 100 µl of DMSO. The absorbance was measured at 550 and 650 nm using a microplate reader (BioTek Instruments Inc., Synergy HT, Software: Gen5 v1.08.4, BioTek Instruments Inc., USA). The reading at 630 nm was used to remove the background interference in the measurements.

2.8.2 Hemolysis activity assessment

The hemolysis assay was conducted using red blood cells isolated from human blood from healthy blood donors, kindly donated by Serviço de Hematologia do Centro Hospitalar do Porto. This procedure was in accordance with the principles of the Declaration of Helsinki. The protocol was adapted from [27]. The samples were centrifuged at 955*g* for 5 mins, at 4ºC (Allegra X-15R Centrifuge, Beckman Coulter, USA), to separate the red blood cells from the remaining components of the blood. The cells were washed three times using saline solution 0.85% (m/v) and further diluted to a volume fraction of 4%. Then, 100 µl of red blood cells were incubated with 100 µl of MLNs for 1h, at 37ºC. The MLNs were tested at a MOX concentration of 512 µg ml^{-1}. Free MOX was tested at the same concentration. After the incubation time, the supernatants were collected and the absorbance of hemoglobin was read at 540 nm and 630 nm, using a microplate reader (BioTek Instruments

Inc., Cytation, Software: Gen5 v1.08.4, BioTek Instruments Inc., USA). The percentage of hemolysis was calculated according to the following:

$$hemolysis\ (\%) = \frac{Abs - Abs\ (-)}{Abs\ (+) - Abs\ (-)} \times 100$$

where Abs, Abs (-) and Abs (+) are the absorbances of the sample, the negative control (saline solution 0.85%) and the positive control (Triton-100, 1%), respectively.

2.9 *In vitro* antibacterial studies

The antibacterial activity of both MOX- and NAC-loaded nanosystems against planktonic bacteria was determined using the micro-broth dilution assay for the four strains of *S. aureus* [28]. Briefly, bacteria were grown overnight at 37ºC in TSB and further diluted to a concentration of 2.0 × 10^5 CFUs ml^{-1} in MHB-Ca^{2+} medium. The bacterial suspension was treated for 24h at 37ºC with the developed nanosystems in a 96-well round bottom polypropylene microtiter plate (Greiner Bio One, Austria). The produced MLNs and free MOX were tested at MOX concentrations from 0.03 to 2 µg ml^{-1}. The unloaded and NAC-loaded LNPs were tested at the solid lipid concentrations of 1 and 2 mg ml^{-1}. Free NAC at the concentrations of 0.45 and 0.9 mg ml^{-1} (corresponding to solid lipid concentrations of 1 and 2 mg ml^{-1}) was also tested. The MIC was recorded as the lowest concentration which inhibited the visual growth of bacteria. The MBC was further determined by spot-plate (10 µl) each well with no visual bacterial growth on TSA plates. The plates were incubated at 37ºC, overnight, followed by CFUs counting. MBC was defined as the lowest concentration resulting in the death of 99.9% of the initial inoculum.

2.10 *In vitro* antibiofilm studies

The potential synergistic effect the developed MLNs with NAC-loaded LNPs was assessed in *S. aureus* biofilms. For this purpose, NAC-loaded LNPs were produced by the double emulsion method according to the protocol described in [9]. The two nanosystems were studied alone using the microtiter plate biofilm model. The effect in bacterial viability of combining both nanosystems was assessed in a more complex model, the catheter biofilm model.

2.10.1 Microtiter plate biofilm model

Biofilm formation and growth conditions were adapted from the literature [29, 30]. Firstly, bacteria were grown overnight at 37ºC on a TSA plate. One or two colonies were collected from the plate and dispersed in TSB 0.6x supplemented with 0.2% glucose to grow overnight at 37ºC, with shaking (240 rpm) (New Brunswick™ Innova® 40/40R, New Brunswick Scientific, USA). The initial inoculum was adjusted to an optical density of 600 nm (OD_{600nm}) of 0.1 and added to the 96-well polystyrene plates for 90 mins, to promote bacterial adhesion. After the incubation time, the non-adhered cells were removed by washing the biofilms twice with 200 µl of PBS 1x. The adhered cells were submerged in 200 µl of fresh TSB 0.6x supplemented with 0.2% glucose and further incubated for 24h, at 37ºC, to allow the growth of a mature biofilm. The 24h-old biofilms were washed twice with PBS 1x and then incubated with the treatment for 24h, at 37ºC. For the treatment with MLNs, the formulations were added at MOX concentrations of 2.0, 1.0, 0.5, 0.25, and 0.125 µg ml^{-1}. Free MOX was tested at the same concentrations. For the NAC-loaded LNPs and respective unloaded LNPs, the formulations at the solid lipid concentration of 1 and 2 mg ml^{-1} (corresponding to 0.45 and 0.9 mg ml^{-1} of NAC) or free NAC (0.45 and 0.9 mg ml^{-1}) were selected. This procedure was used for the following assays.

2.10.1.1 Biofilm biomass study

Biofilm biomass quantification was assessed through the crystal violet assay based on the reported protocol [31]. Briefly, after the treatment incubation time, the biofilms were washed once with 200 µl of PBS 1x. The biofilms were fixed with 200 µl of 99% methanol for 15 mins. After, the methanol was removed, and the wells were left to dry for 15 mins. Then, 200 µl of crystal violet solution (1%, m/v) were added to the biofilms and left to incubate for 5 mins. The stained biofilms were washed with ultrapure water to remove the excess of crystal violet solution. To dissolve the remaining stain in the wells, 200 µl of 33% (v/v) glacial acetic acid was added. Further, the plates were incubated at room temperature for 15 mins, with shaking (250 rpm) (VWR Incubating Microplate Shaker, VWR International LLC, USA). The absorbance was read at 570 nm using a microplate reader (BioTek Instruments Inc., Synergy HT, Software: Gen5 v1.08.4, BioTek Instruments Inc., USA).

2.10.1.2 Biofilm viability study

The metabolic activity of the cells within the biofilm was assessed through the XTT reduction assay [32]. After the treatment, the biofilms were washed once with 200 µl of PBS 1x and

100 µl of XTT solution (1 mg ml^{-1}) supplemented with menadione (1 µM) were added in the absence of light. Then, the plates were incubation at 37ºC for 30 mins, with shaking (250 rpm) (VWR Incubating Microplate Shaker, VWR International LLC, USA). The absorbance was read at 490 nm using a microplate reader (BioTek Instruments Inc., Synergy HT, Software: Gen5 v1.08.4, BioTek Instruments Inc., USA).

2.10.1.3 Confocal laser scanning microscopy (CLSM) biofilm analysis

Xen36 biofilms were formed in µ-Slide 8 Well Glass Bottom (ibidi GmbH, Germany) previously washed once with PBS 1x and once with TSB. After, the biofilms were treated for 24h with the MLNs formulations or free drug at the MOX concentration of 0.5 µg ml^{-1}. For the treatment with unloaded and NAC-loaded LNPs, the suspensions at a solid lipid concentration of 2 mg ml^{-1} (0.9 mg ml^{-1} of NAC) were used. Free NAC at the same concentration was also tested. After treatment, the biofilms were washed once with PBS 1x and further stained with the FilmTracer™ LIVE/DEATH® Biofilm Viability Kit (Thermo Fisher Scientific, USA) according to the instructions provided by the manufacturer. The stained biofilms were analyzed using the inverted confocal laser scanning microscope Leica Stellaris 8 (LeicaMicrosystems, Wetzlar, Germany) equipped with the Leica Application Suite X package (LAS X). The excitation/emission wavelengths were set at 488nm/500-550 nm for Syto9 and 561nm/570-620 nm for propidium iodide. Images were acquired with a resolution of 1024×1024 using a 63X/1.4 oil immersion objective. An area of ~180 µm (X) ×160 µm (Y) was screened in ~1 µm Z-intervals (Z-stack) for 20 µm.

2.10.2 Catheter biofilm model

In the *in vitro* catheter biofilm model, the biofilms were formed inside triple-lumen polyurethane central venous catheters (Certofix duo/trio; B. Braun Melsungen AG, Germany), based on a protocol described in the literature [29]. Firstly, 1 cm long catheter pieces were incubated with 100% FBS overnight, at 37ºC. The bacterial inoculum was adjusted as described in **section 2.10.1**. Then, the catheter pieces were incubated with 1 ml of bacterial inoculum for 90 mins, at 37ºC, to promote adhesion of bacterial cells to the material. After the adhesion period, the biofilms were washed twice with 1 ml of PBS 1x. The adhered cells were submerged in 1 ml of fresh TSB 0.6x supplemented with 0.2% glucose and further incubated for 24h, at 37ºC. The mature biofilms were then treated with MLNs and NAC-loaded LNPs, alone or in combination, for 24h, at 37ºC. The MLNs were tested at a final MOX concentration 0.5 µg ml^{-1}, while NAC-loaded LNPs were added to a

final NAC concentration of 0.9 mg ml^{-1}. The unloaded formulations and the free compounds were also tested at the corresponding concentrations. Catheter pieces were then washed twice with 1 ml of PBS 1x and sonicated (Branson 5510 Ultrasonics bath, Marshall Scientific, USA) for 10 mins in 200 µl of PBS 1x, to disperse the biofilms. The samples were serial diluted in PBS 1x and spot-plated (10 µl) on TSA plates. The plates were incubated overnight at 37ºC, followed by CFUs counting.

2.11 Statistical analysis

Statistical analysis was performed using Graphpad Prism Software (version 7.03; IBM, USA). Data are expressed as mean ± SD and each assay was performed at least three independent times, with the exception of CLSM biofilm analysis, which was repeated two times.

3. Results and Discussion

3.1 Physical characterization of MLNs and storage stability

The developed MLNs were characterized regarding their mean hydrodynamic diameter, PDI, zeta potential, EE, and LC, over a storage period of 24 weeks, at room temperature (**Figure 2**). Both the encapsulation of MOX and the functionalization of the nanoparticles led to an increase in the hydrodynamic diameter compared to the unloaded MLNs (uMLNs) (**Figure 2A**). This outcome may be caused by steric effects inside the lipid matrix and at the surface of the nanoparticles promoted by the drug and the conjugates, respectively. Nevertheless, all formulations showed a mean hydrodynamic diameter below 300 nm, with no significant changes observed in the hydrodynamic size of the formulations over 12 weeks of study. After 24 weeks of storage, significant changes in the hydrodynamic diameter were observed for uMLNs, MOX-MLNs, and F-uMLNs. The low PDI (<0.2) observed for all formulations suggests that they were monodisperse in size and did not tend to form aggregates over time, at the defined storage conditions [33]. This low tendency to aggregate and the high stability of the nanoparticles in suspension was also confirm by their low zeta potential (below -30 mV) (**Figure 2B**) [34].

The EE and the LC of the MLNs were also studied during the 24 weeks of study (**Figure 2 C-D**). For 12 weeks, the EE for both non-functionalized and functionalized MOX-loaded MLNs was satisfactorily high (above 75%), revealing no significant leakage of drug over this time. The LC values were also unaffected during this time. Interestingly, F-MOX-MLNs

showed a significant higher EE and LC compared to MOX-MLNs, which suggests that the surface functionalization improves the entrapment of MOX. It is hypothesized that this increase in EE and LC may be a consequence of the increased steric effects promoted by the functionalization at the nanoparticles surface. After 24 weeks, the EE and LC of both MOX-MLNs and F-MOX-MLNs significantly decreased, revealing a significant drug release. Hence, the developed formulations were stable under storage conditions for 12 weeks.

Overall, the physical characteristics of the developed MLNs are crucial for a safe *in vivo* systemic administration. It is reported that particles entering the bloodstream should be significantly smaller than the diameter of human capillaries (around 5 µm) and with no tendency to form aggregates [34]. Besides particle size, charge may also play a role in the biodistribution and pharmacokinetics of the nanoparticles. Negatively charged nanoparticles have prolonged circulation half-lives than highly positively charged ones [34]. In addition, positively charged nanoparticles are considered more cytotoxic to human cells, due to a higher cellular uptake [35]. Considering these properties and their influence for the *in vivo* fate of the particles, the produced formulations are suitable for a systemic administration.

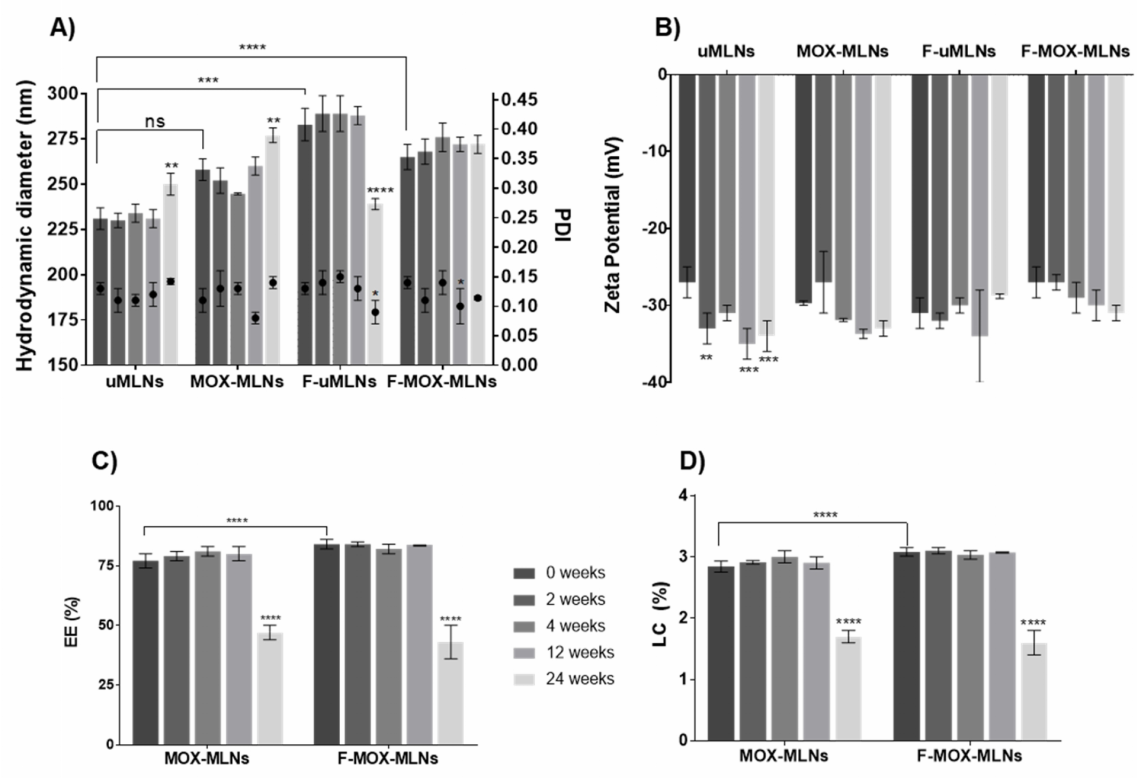


Figure 2: Characterization of the MLNs suspensions over 24 weeks, stored at room temperature. **A)** Hydrodynamic diameter and PDI. The bars represent the hydrodynamic diameter (left y-axis) and the dots represent the PDI (left y-axis). **B)** Zeta potential. **C)** EE. **D)** LC. The parameters were evaluated at different time points (0, 2, 4, 12, and 24 weeks). The values are represented as the

mean ± SD. **P<0.01, ***P<0.001, relatively to 0 weeks. *P<0.05, **P<0.01, ****P<0.0001. Statistical analysis: two-way ANOVA, Tukey's multiple comparisons test.

3.2 *In vitro* MOX release study

The release of MOX from the MLNs was assessed using the dialysis method at a pH 7.4 to simulate the physiological environment [24]. This study is a valuable tool to predict the *in vivo* kinetics of the formulations, once they enter the bloodstream [36]. The release profile of MOX can be found in **Figure S1**. At a physiological pH of 7.4, it is possible to observe an initial burst release (around 40%) after 30 mins of incubation, which indicates the release of non-encapsulated MOX. Besides, drug molecules poorly adsorbed at the surface of the nanoparticles may also contribute to the initial burst profile observed. After this initial burst, both non-functionalized (MOX-MLNs) and functionalized (F-MOX-MLNs) showed a linear profile over 48h, with a total cumulative release below 60%. Interestingly, the functionalized formulation (F-MOX-MLNs) presents a slower release than MOX-MLNs. This may be a consequence of the presence of D-amino acids conjugates at the surface of the nanoparticles, leading to steric effects that promote a slower release of the encapsulated MOX. As expected, MOX free was completely release within the first 3h of incubation.

3.3 *In vitro* cytocompatibility studies

The cytocompatibility of the developed MLNs was assessed using a L929 fibroblast cell line and human red blood cells. The cell viability of fibroblasts after a 24h treatment with both unloaded and MOX-loaded MLNs was not significantly reduced at any of the concentrations tested (**Figure 3A**). However, a significant decrease in cell viability was observed for free MOX at 0.25 µg ml^{-1} and higher concentrations, compared with the untreated cells. At the highest concentrations of MOX (1 and 2 µg ml^{-1}), free MOX revealed a potential toxicity effect, with cell viability values below 70% [37]. The cytotoxicity of the formulations and free MOX was also evaluated through the LDH assay (**Figure 3B**). For this assay, both the developed formulations and free MOX showed cytotoxicity below 4%, which corroborates the results obtained by the MTT assay.

To evaluate the potential effects of the developed MLNs suspensions on red blood cells after a systemic administration, a hemolysis assay was performed (**Figure 3C**). For this assay, the MLNs and free MOX were tested at a MOX concentration of 512 µg ml^{-1}. At this concentration, both the formulations and free drug showed a hemolytic activity below 2.5%. According to the ASTM E2524-08 standard, a hemolysis percentage below 5% does not

cause damage to the red blood cells. Since the developed formulations meet this criterion, they are a potentially safe nanosystem for systemic administration.

From the cytocompatibility studies in both fibroblasts and human red blood cells, it is possible to conclude that the developed MLNs suspensions present a safe profile for further *in vivo* applications.

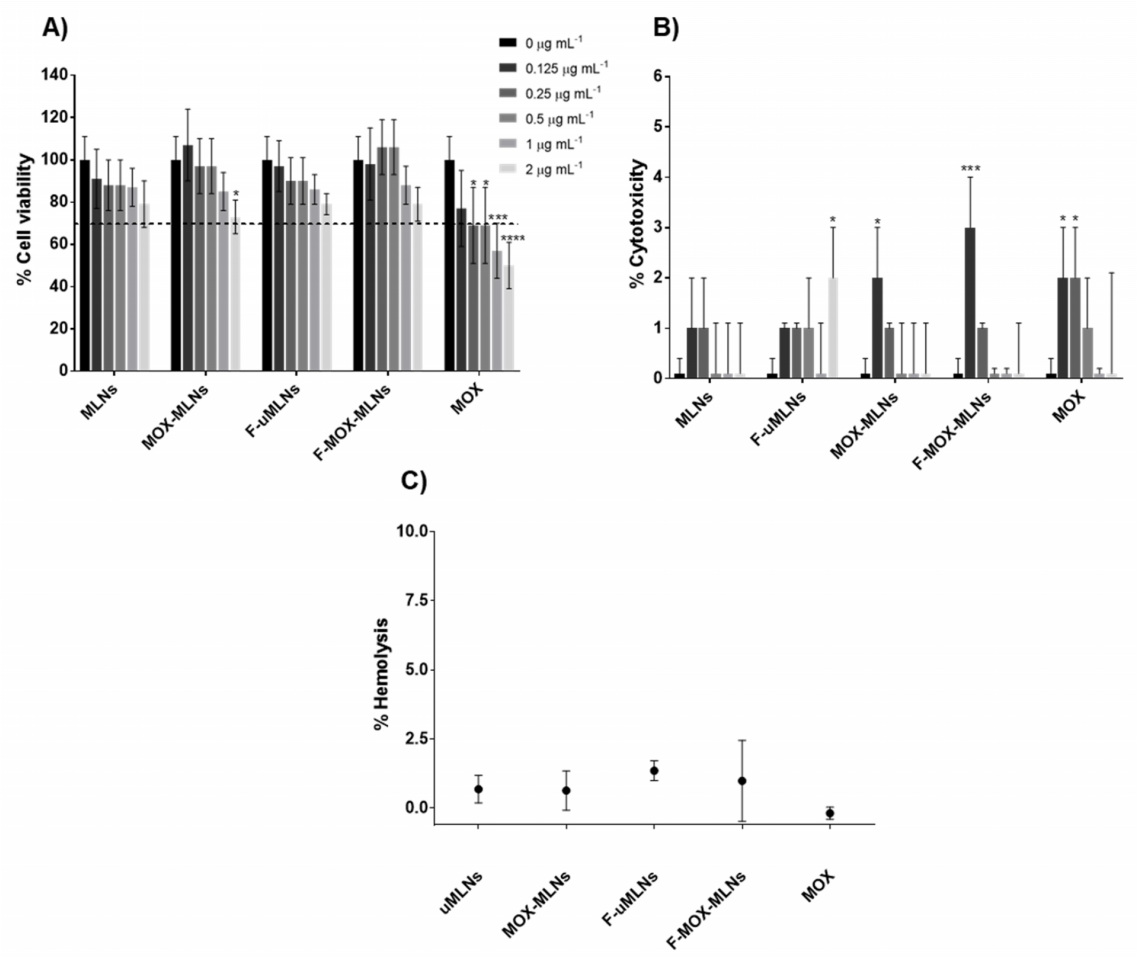


Figure 3: *In vitro* cytocompatibility studies. **A)** MTT and **B)** LDH assays using the fibroblasts L929 cell line. In these assays, different concentrations of encapsulated and free MOX were assessed (2.0, 1.0, 0.5, 0.25, and 0.125 μg ml^{-1}). Triton-100 (1%, v/v) and DMEM were used as negative and positive controls, respectively. **C)** Hemolysis assay. Encapsulated and free MOX at a concentration of 512 μg ml^{-1} were tested. For positive and negative controls, saline solution (0.85%, m/v) and triton-100 (1%, v/v) were used, respectively. All values are represented as mean ± SD. *P<0.05, ***P<0.001, ****P<0.0001, relatively to the positive control. Statistical analysis: two-way ANOVA, Dunnett's multiple comparisons test.

3.4 *In vitro* antibacterial studies

Prior *in vitro* antibiofilm studies, both MOX- and NAC-loaded nanosystems were tested for their antibacterial activity against planktonic bacteria. The efficacy of the developed MOX-loaded nanosystems against planktonic bacterial cells can be found in the Supporting Information (**Table S2, Supporting Information**). At the highest tested concentration, unloaded MLNs showed no inhibition of planktonic bacterial growth for any of the tested strains. The MOX-loaded formulations (MOX-MLNs and F-MOX-MLNs) showed MIC values higher than free MOX. This outcome suggests that not all encapsulated MOX was released from the nanoparticles during the treatment period.

For the NAC-loaded formulations and corresponding unloaded formulations, no bacterial inhibition was found at the highest concentration tested (0.9 mg ml^{-1} of NAC). These results were expected since Drago *et al.* (2013) reported MIC values of NAC for *S. aureus* strains ranging from 12 to 24 mg ml^{-1} [38].

3.5 *In vitro* antibiofilm studies

3.5.1 Biofilm viability and biomass studies

The *in vitro* antibiofilm efficacy of the developed MLNs was initially assessed by quantification of the biofilm viability (**Figure 4 A-C**) and biomass (**Figure 4 D-F**), using the microtiter plate biofilm model for three *S. aureus* strains: MRSA (ATCC 33591), *S. aureus* (ATCC 6538), and the bioluminescent strain *Xen36*. In addition, the antibiofilm activity against the *S. aureus* (ATCC 25923) was also assessed **(Figure S2)**.

For all tested strains, it is possible to observe that MOX-loaded MLNs and free MOX had a higher effect on the biofilm viability compared to the unloaded MLNs (**Figure 4 A-C**). uMLNs did not show any significant reduction of bacterial viability for both MRSA and *S. aureus* (ATCC 6538) strains at any tested concentration. For the *Xen36* strain, this formulation only showed a significant reduction of viability at 0.5 µg ml^{-1} and at higher concentrations. However, the functionalized unloaded MLNs (F-uMLNs) showed a significant reduction of *Xen36* biofilms even at 0.125 µg ml^{-1}. The F-uMLNs also showed a significant effect on MRSA biofilms at 0.25 µg ml^{-1} and concentrations above. These results suggest that the functionalization of the MLNs with D-amino acids (Phe, Pro, and Tyr) may have an impact in bacterial viability of *S. aureus* strains. The effect of a mixture of these three D-amino acids against *S. aureus* biofilm formation and mature biofilms was previously reported [19]. In mature *S. aureus* biofilms, this mixture showed the potential to disassemble the biofilms at concentrations higher than 10 mM [19]. The antibiofilm activity of D-amino acids was also

reported for other relevant pathogens, such as *Pseudomonas aeruginosa* (*P. aeruginosa*), and *Staphylococcus epidermidis* [9]. Unfortunately, the mechanism of action of D-amino acids against biofilms is not completely known [19, 39-41]. Regarding the MOX-loaded MLNs, both non-functionalized (MOX-MLNs) and functionalized (F-MOX-MLNs) nanoparticles showed a significant viability reduction in all strains at a MOX concentration of 0.5 µg ml^{-1}, comparing to the untreated control. At the highest concentration (2 µg ml^{-1}), encapsulated and free MOX revealed a biofilm viability of around 50% for MRSA and *S. aureus* (ATCC 6538) strains, and 25% for the *Xen36* strain.

For the three *S. aureus* strains studied, the crystal violet staining was used to quantify biofilm biomass after a 24h treatment with MLNs or free MOX (**Figure 4 D-F**). For MRSA, only MOX-loaded MLNs and MOX free at the highest concentration (2 µg ml^{-1}) showed a significant reduction in the biofilm biomass compared to the untreated control. Interestingly, for the *S. aureus* strain (ATCC 6538), even at the lowest concentration tested (0.125 µg ml^{-1}), MOX-loaded MLNs (MOX-MLNs and F-MOX-MLNs) and MOX free showed a high effect on the biomass, with a reduction higher than 50%. Finally, for the *Xen36* strain, MOX-loaded MLNs and MOX free showed a significantly high reduction at the two highest concentrations tested, while no effect on reducing biomass was observed for the unloaded MLNs.

Overall, the results from biofilm viability and biomass assays suggest that the MOX-loaded MLNs are more efficient against the methicillin-susceptible (MSSA) strains (ATCC 6538 and *Xen36*) than for the MRSA strain. The efficacy of MOX on mature MRSA biofilms has been previously reported [6]. However, the lower efficacy of MOX-loaded MLNs and free MOX for the MRSA strain may be a consequence of the different phenotype of the MRSA biofilms, compared to the MSSA biofilms [42, 43].

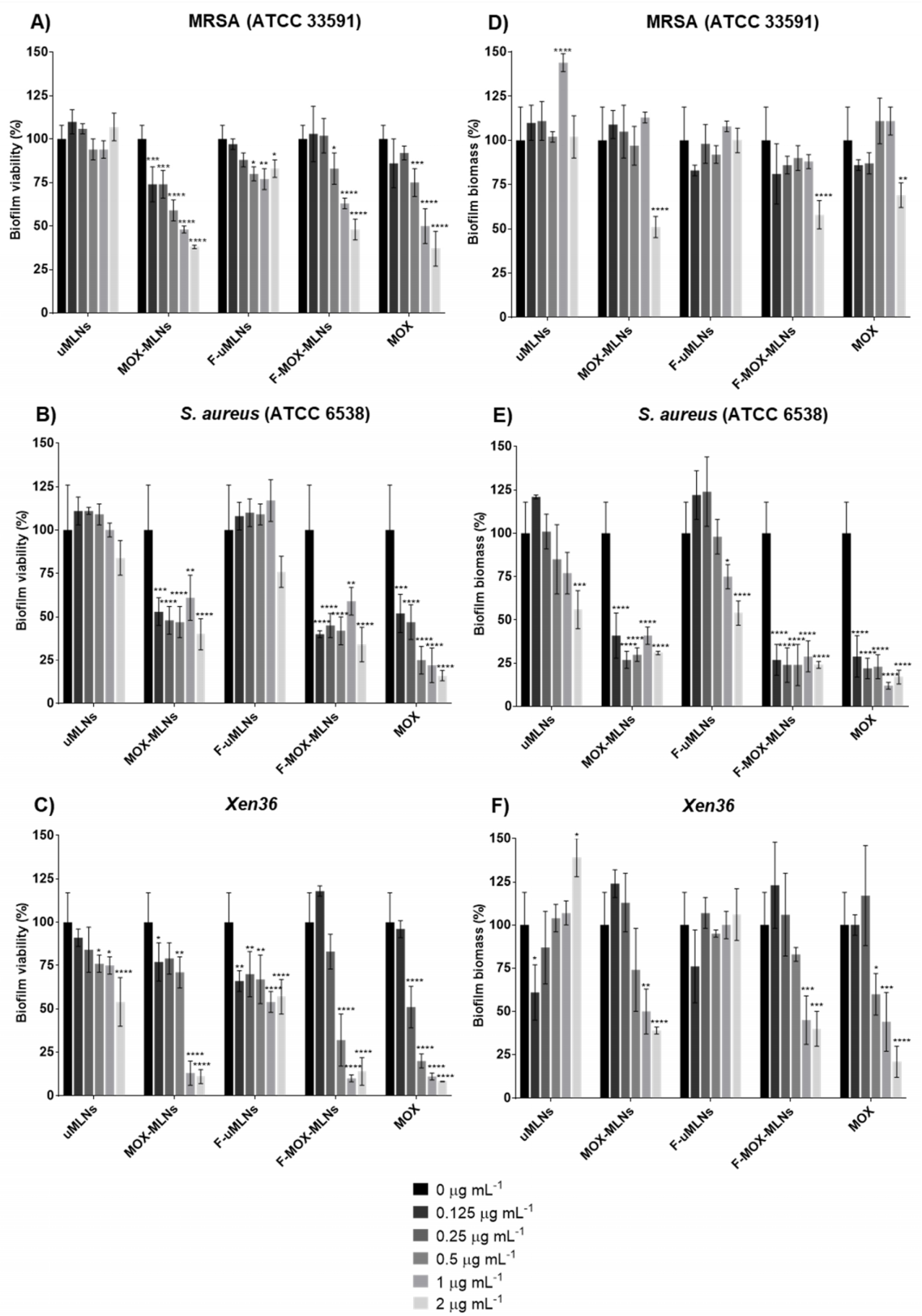


Figure 4: Quantification of **(A-C)** biofilm viability (XTT assay) and **(D-F)** biomass (crystal violet staining) after a 24h treatment with MLNs and free MOX at the concentrations of 0, 0.125, 0.25, 0.5, 1, and 2 µg ml^{-1} of MOX. Unloaded MLNs were tested at the same concentration. The biofilms of **(A, D)** MRSA (ATCC 33591), **(B, E)** *S. aureus* (ATCC 6538), and **(C, F)** the bioluminescent strain *Xen36*

were grown in 96-well plates for 24h prior to the treatment. Untreated biofilms (0 µg ml^{-1} of MOX) were used as a positive control. The values are represented as the mean ± SD. *P<0.05, **P<0.01, ***P<0.001, ****P<0.0001 relatively to 0 µg ml^{-1}. Statistical analysis: two-way ANOVA, Dunnett's multiple comparisons test.

The antibiofilm efficiency of the NAC-loaded LNPs and the respective unloaded formulations was also evaluated using the XTT and crystal violet assays (**Figure 5**). For the three tested strains, all formulations showed a significant reduction of biofilm viability (higher than 50%) at the concentrations of 1 and 2 mg ml^{-1} of solid lipid. However, free NAC only showed a slight reduction of bacterial viability (lower than 25%) for the strain ATCC 6538. For the MRSA and *Xen36* strains, no significant decrease in biofilm viability was observed. These results were expectable since it is reported in the literature that even at a higher concentration (30 mM), NAC alone does not significantly reduce viability in MRSA biofilms [11]. The effect of the unloaded and NAC-loaded LNPs in biofilm biomass was also evaluated. All formulations showed a significant effect on bacterial biomass, which corroborates the results obtained for biofilm viability. Free NAC only at the highest concentration showed a significant reduction in biofilm biomass for the MRSA and *Xen36* strains.

Hence, the reduction of biofilm viability and biomass does not seem to be caused by the encapsulated NAC, but by the vehicle itself. The unloaded LNPs (non-functionalized and functionalized) previously showed a high effect on the viability and biomass of *P. aeruginosa* biofilms [9]. This antibacterial effect is probably due to the use of Tween 80 as a surfactant in the production of the LNPs. This compound is well-known for its antibacterial and antibiofilm properties against a wide range of bacterial strains, including *S. aureus* [44-46].

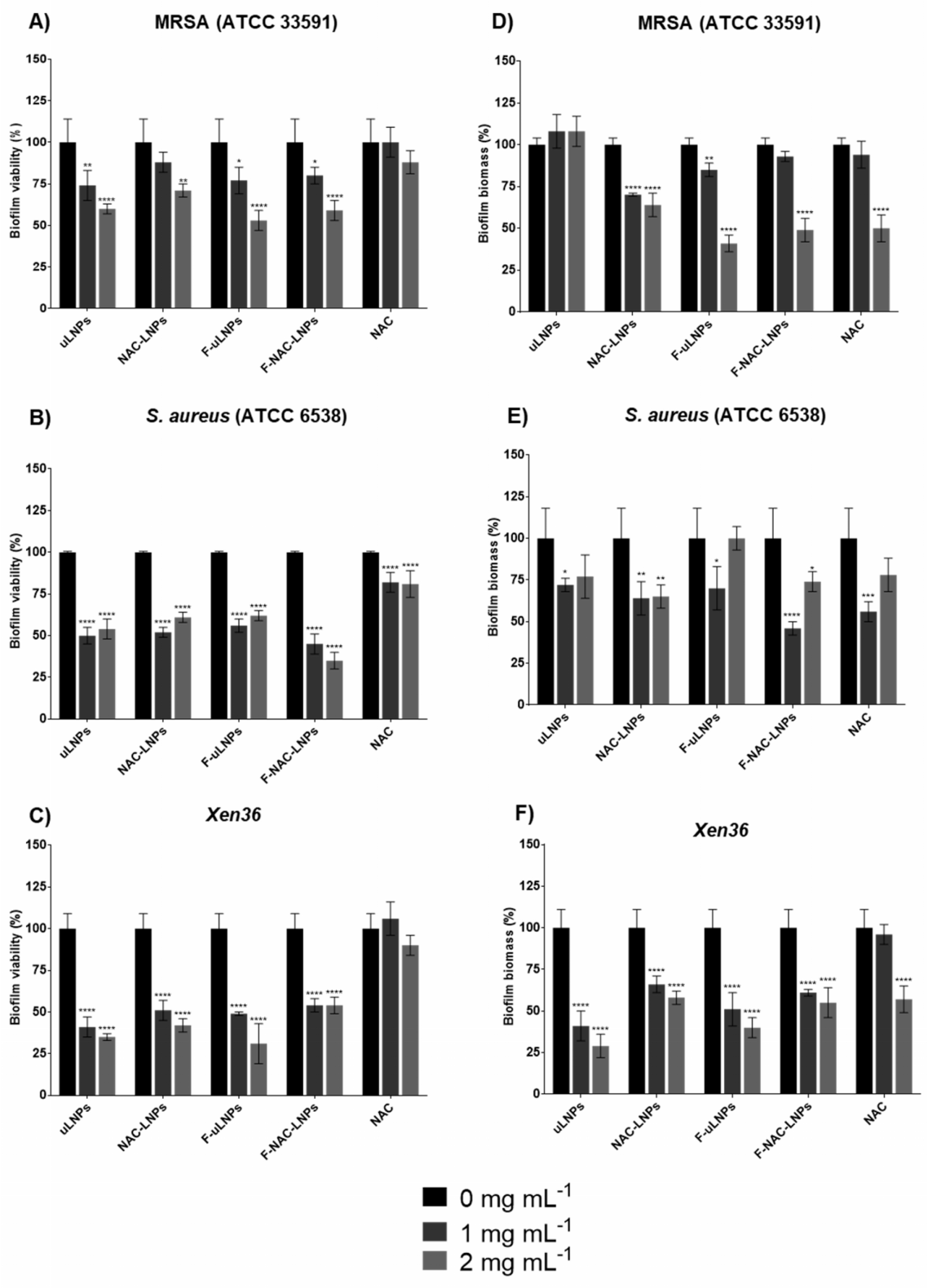


Figure 5: Quantification of **(A-C)** biofilm viability (XTT assay) and **(D-F)** biomass (crystal violet staining) after a 24h treatment with LNPs suspensions at the solid lipid concentrations of 0, 1, and 2 mg ml^{-1}. Free NAC was tested at the concentrations of 0, 0.45, and 0.9 mg ml^{-1}. The biofilms of **(A, D)** MRSA (ATCC 33591), **(B, E)** *S. aureus* (ATCC 6538), and **(C, F)** the bioluminescent strain *Xen36* were grown in 96-well plates for 24h prior the treatment. Untreated biofilms (0 mg ml^{-1} of solid lipid)

were used as a positive control. The values are represented as the mean ± SD. *P<0.05, **P<0.01, ***P<0.001, ****P<0.0001 relatively to 0 mg ml^{-1}. Statistical analysis: two-way ANOVA, Dunnett's multiple comparisons test.

3.5.2 Confocal laser scanning microscopy (CLSM) biofilm analysis

Confocal laser scanning microscopy (CLSM) was used to assess the viability and integrity of the untreated and treated *Xen36* biofilms (**Figure 6**). CLSM images revealed that untreated biofilms were dense and composed mainly of viable bacterial cells. The treatment with unloaded MLNs (non-functionalized and functionalized) showed no visible reduction of bacterial viability. The biofilms treated with F-MOX-MLNs or free MOX, show a slightly higher number of death cells in the deeper regions of the biofilm. Interestingly, the treatment with functionalized MOX-loaded formulation reveals a less dense biofilm comparing to free MOX. This result suggests a possible synergistic effect between the encapsulated antibiotic and the functionalization with D-amino acids. According to the literature, the combination of D-Phe, D-Pro, and D-Tyr not only prevented biofilm formation, but could also disassemble mature *S. aureus* biofilms [19]. In other studies, antibiotics in combination with D-amino acids revealed synergistic potential against *S. aureus* biofilms [20, 47].

The treatment of biofilms with unloaded and NAC-loaded LNPs was also assessed by CLSM (**Figure 6**). Compared to the untreated control, all formulations and free NAC seem to have an effect by reducing the biofilm thickness of the biofilm. These findings are in accordance with the results previously obtained by the biofilm biomass study (**Figure 5F**). Hence, it is hypothesized that both unloaded and NAC-loaded LNPs promote disruption of the biofilm matrix, reducing the biofilm biomass. Additionally, functionalized LNPs (F-uLNPs and F-NAC-LNPs) seem to have an effect in reducing the bacterial viability, since a higher number of dead cells is observable. It seems likely that this outcome may be a consequence of the functionalization, rather than the presence of NAC. Nevertheless, non-functionalized and functionalized NAC-loaded LNPs previously reported a safer profile than the respective unloaded formulations [9].

Overall, CLSM biofilm analysis suggests that the MOX-loaded nanosystems have a bactericidal effect, while the NAC-loaded nanosystems seem to affect mainly the thickness of the biofilms. Thus, a combined nano therapy of the two nanosystems may be a valuable tool toward the eradication of *S. aureus* biofilms.

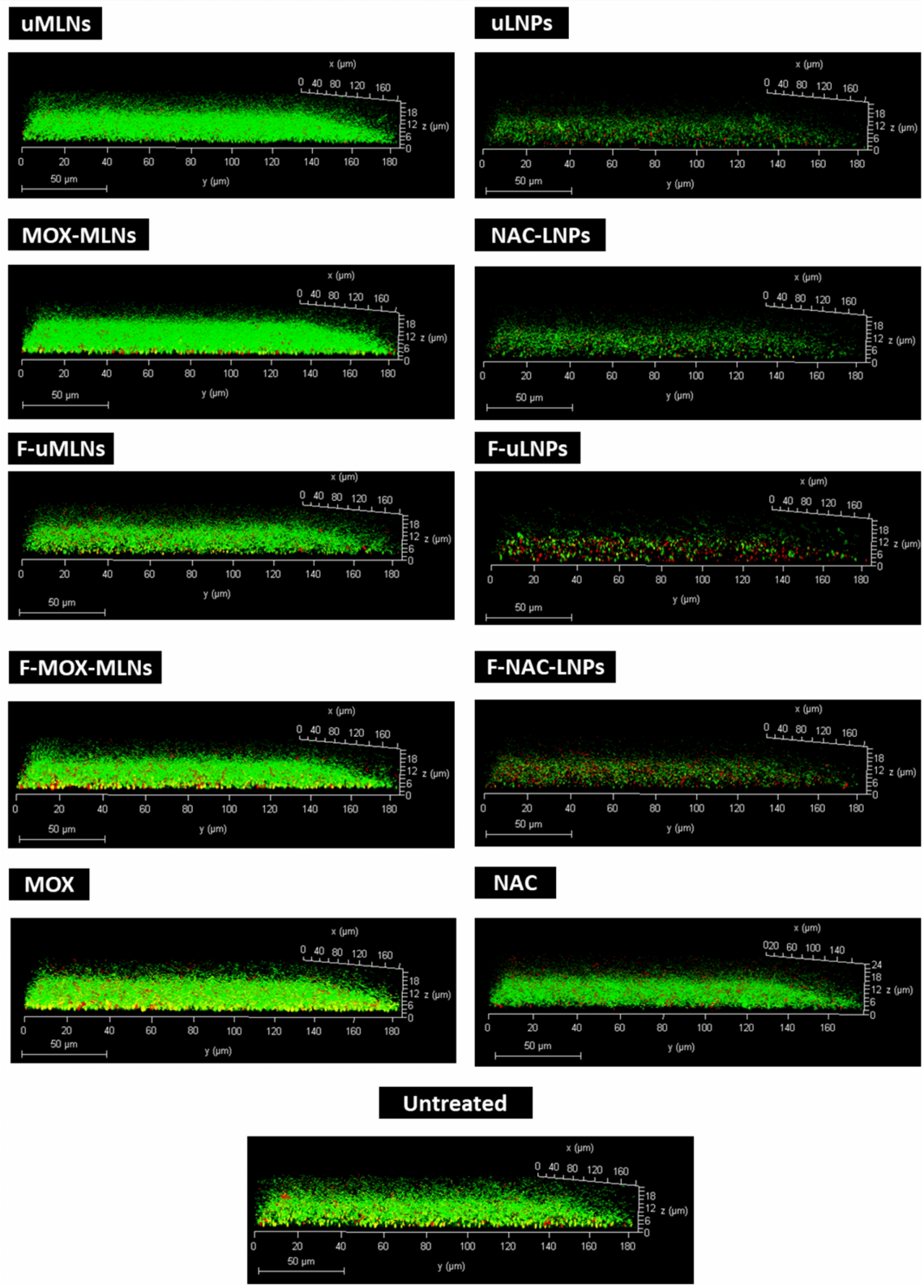


Figure 6: Three-dimensional CLSM images of untreated (control) and treated *Xen36* biofilms. The developed MLNs and free MOX were tested at a MOX concentration of 0.5 µg ml^{-1}. For the biofilms treated with unloaded and NAC-loaded LNPs, a solid lipid concentration of 2 mg ml^{-1} (0.9 mg ml^{-1} of NAC) was used. Free NAC was used at the same concentration. The biofilms were stained with the

LIVE/DEATH kit, where viable and death cells are visualized in green and red, respectively. Untreated biofilms were used as a positive control. Scale bars, 50 µm.

3.5.3 Combined nano therapy of MOX-loaded and NAC-loaded nanosystems

The potential of a nano therapy combining MOX-loaded (bactericidal) and NAC-loaded (matrix disruptive) nanosystems was evaluated using a more complex biofilm model, the *in vitro* catheter model. The biofilms were grown inside polyurethane catheter pieces for 24h and further treated with the nanosystems alone or in combination for additional 24h.

Both unloaded and NAC-loaded LNPs at the solid lipid concentration of 2 mg ml^{-1}, which corresponds to a NAC concentration of 0.9 mg ml^{-1}, showed no effect on the biofilm viability for all the tested strains (**Figure 7A**). Likewise, free NAC at the same concentration did not significantly decrease biofilm viability after a 24h treatment. These results differ from the previously observed in the microtiter plate biofilm model (**Figure 5 A-C**), where the LNPs suspensions showed a biofilm viability reduction between 25 – 75%. Usually, in the microtiter plate model, the biofilm is loosely attached and can be easily detached during the washing steps. Besides, this model is also sensitive to sedimentation, where the biofilm forms mainly from deposition of cells in the bottom of the wells [48]. Thus, it is possible that the different results from the two models are a consequence of the different characteristics of the formed biofilms and the limitations of the microtiter plate biofilm model.

The developed MLNs (unloaded and MOX-loaded) were also tested in the catheter biofilm model (**Figure 7B**). For the MRSA strain, only free MOX at a concentration of 0.5 µg ml^{-1} exhibited a significant decrease in bacterial viability compared to the untreated biofilms. Free MOX also showed a decrease in viability for the strain *Xen36*. These results suggest that maybe not all encapsulated MOX is being released from the nanoparticles during the treatment period. For the *S. aureus* (ATCC 6538), both free and encapsulated MOX had no effect on the cell count. This outcome is probably related to the higher biofilm bacterial load observed in this strain, which is expectable since this is considered a strong biofilm-forming strain [49].

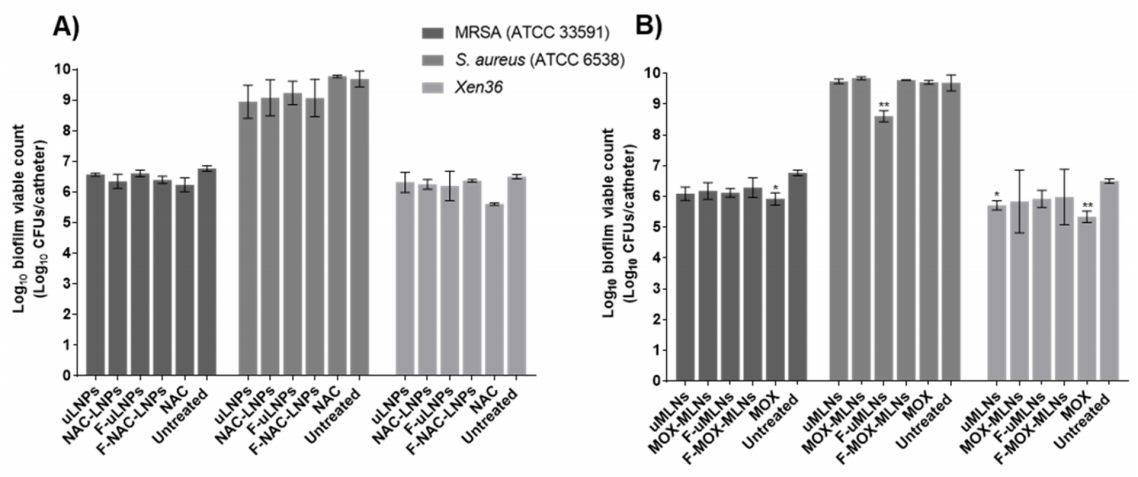


Figure 7: Biofilm viable count of the strains MRSA (ATCC 33591), *S. aureus* (ATCC 6538), and *Xen36* grown *in vitro* for 24h in catheters, after a 24h treatment with different nanosystems. **A)** The unloaded and NAC-loaded LNPs were tested at a concentration of 2 mg ml^{-1} (corresponding to a NAC concentration of 0.9 mg ml^{-1}). Free NAC was tested at the same concentration. **B)** The developed MLNs and free MOX were tested at a MOX concentration of 0.5 µg ml^{-1}. Untreated biofilms were used as a positive control. The values are represented as the mean ± SD for three catheters. *P<0.05, **P<0.01, relatively to the untreated biofilms. Statistical analysis: two-way ANOVA, Dunnett's multiple comparisons test.

In a more complex approach, the MOX- and NAC-loaded nanosystems were combined to assess potential synergistic effects (**Figure 8**). For the MRSA strain (**Figure 8 A-B**), the combination of functionalized particles loaded with MOX (F-MOX-MLNs) and NAC (F-NAC-LNPs) exhibited the highest reduction in cell viability compared to the untreated control. Comparing with F-MOX-MLNs alone, this combination showed a significantly lower viable count (*P<0.05*), revealing a potential synergistic potential. The combination of F-MOX-MLNs and F-NAC-LNPs also revealed a significant effect on bacterial viability for the strain *Xen36*, compared to the untreated control (**Figure 8 E-F**). However, the combination of F-MOX-MLNs with unloaded LNPs (uLNPs) and functionalized unloaded LNPs (F-uLNPs) presented even a higher efficacy against *Xen36* biofilms. In a previously reported study, the unloaded non-functionalized and functionalized LNPs showed a higher potential against mature *P. aeruginosa* biofilms, compared to the NAC-loaded LNPs [9]. This outcome is probably associated with a higher exposition of the biofilms to the surfactant Tween 80 in the unloaded LNPs. Due to the presence of NAC in the loaded LNPs (NAC-LNPs and F-NAC-LNPs), it is believed that this compound is not only encapsulated but partially adsorbed at the surface of the nanoparticles, hindering the interactions between the Tween 80 and the biofilms. Despite the potential of these unloaded formulations, they previously

revealed hemolytic activity against human red blood cells, which was not observed for NAC-loaded nanosuspensions [9]. Therefore, the combination of F-MOX-MLNs with F-NAC-LNPs is a safer therapeutic approach for future *in vivo* application.

For the strain *S. aureus* (ATCC 6538), F-MOX-MLNs and free MOX showed the highest potential to reduce bacterial viability, in combination with the LNPs suspensions (**Figure 8 C-D**). The combination of free MOX with all LNPs suspensions and free NAC showed a significant reduction of viability compared to the untreated control ($P<0.01$). A similar effect was verified in the combination of F-MOX-MLNs and F-NAC-LNPs.

Overall, the combination of the functionalized, loaded nanosystems (F-MOX-MLNs and F-NAC-LNPs) showed a potential synergistic effect in the eradication of mature biofilms formed by the three *S. aureus* strains.

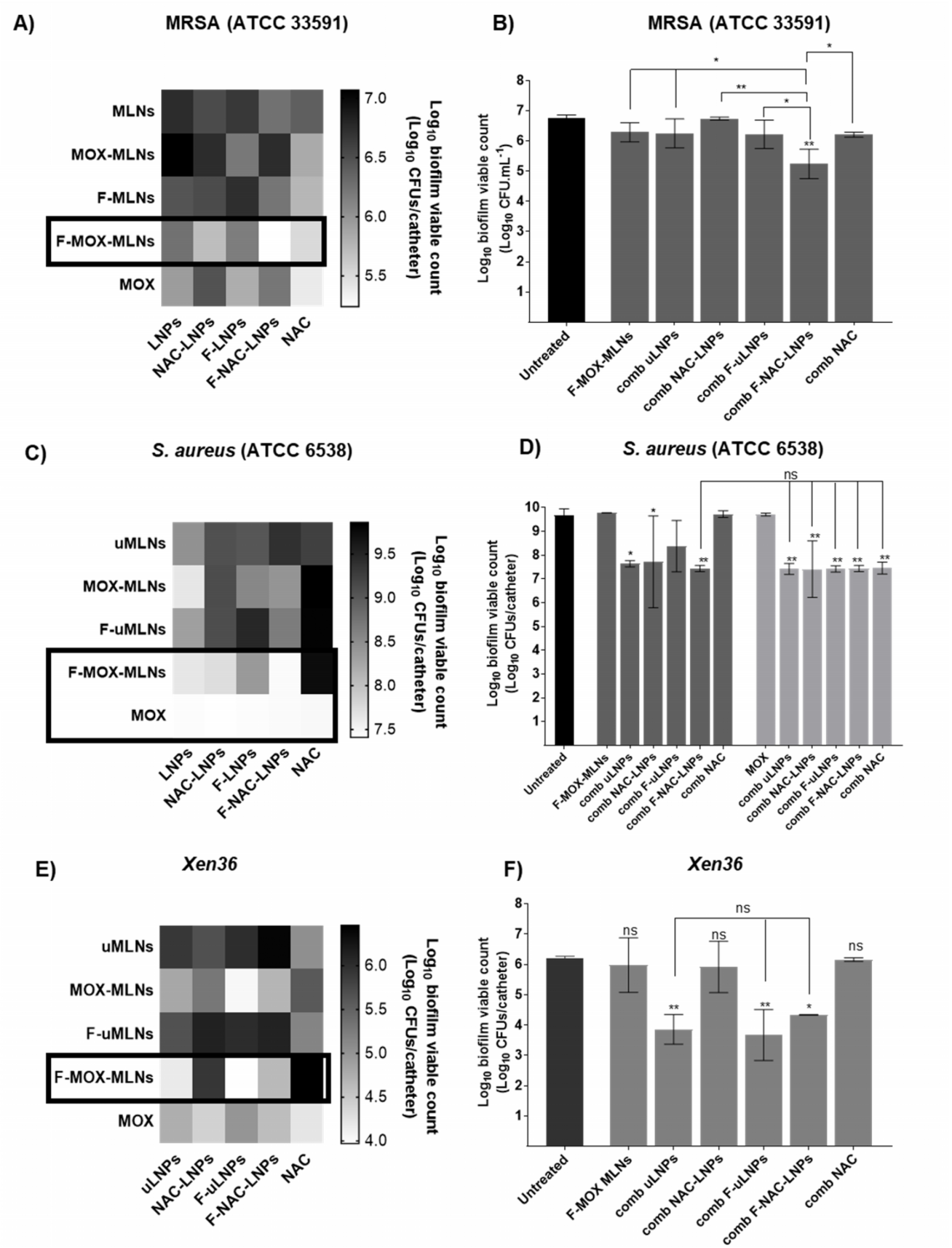


Figure 8: Biofilm viable count of **(A-B)** MRSA (ATCC 33591), **(C-D)** *S. aureus* (ATCC 6538), and **(E-F)** *Xen36* biofilms grown *in vitro* in catheters after treatment with the combined nano therapy. **(A, C, D)** Heat maps represent the effect of the combination of MOX- and NAC-loaded nanosystems on the biofilm viable count. The treatment combinations with lower viable count are highlighted (black squares). **(B, E, F)** F-MOX-MLNs (dark grey) and free MOX (light grey) (0.5 µg ml^{-1}) alone and in combination with NAC-loaded nanosystems (comb uLNPs, comb NAC-LNPs, comb F-uLNPs, and comb F-NAC-LNPs) or free NAC (comb NAC) at a solid lipid concentration of 2 mg ml^{-1}

(corresponding to a NAC concentration of 0.9 mg ml^{-1}). Untreated biofilms were used as a positive control. The values are represented as the mean ± SD for three catheters. *P<0.05, **P<0.01, relatively to the untreated biofilms. ns, not significant; *P<0.05, **P<0.01. Statistical analysis: one-way ANOVA, Tukey's multiple comparisons test.

4. Conclusions

The formulations developed in this work exhibited low hydrodynamic sizes (below 300 nm), low PDI, and highly negative zeta potential values, which reveals a low tendency to form aggregates. The EE and LC were satisfactory, with no drug leakage observed over 12 weeks under storage conditions. Under physiological conditions (pH 7.4), the MOX-loaded MLNs showed an initial burst release followed by controlled release profile. The MLNs showed no cytotoxic effects on fibroblasts and no hemolytic activity against red blood cells at the tested concentrations, revealing a safe profile for further *in vivo* application.

The antibiofilm activity of both the MOX- and NAC-loaded nanosystems was assessed using the microtiter plate biofilm model, in three *S. aureus* strains. Overall, the treatment with MOX-loaded MLNs led to a high reduction of biofilm biomass and viability in all strains tested. However, the formulations were more efficient against MSSA strains, compared to the MRSA. Both unloaded and NAC-loaded nanosystems also exhibited a significant reduction of biofilm viability and biomass, even at the lowest NAC concentration tested (0.45 mg ml^{-1}). Hence, the presence of NAC does not seem to potentiate the antibiofilm effect verified for the vehicle itself. This outcome may be due to the use of Tween 80 as a surfactant, since it has reported antibacterial and antibiofilm activities against several bacterial strains, including *S. aureus* [44, 45, 50]. CLSM analysis of *Xen 36* biofilms after treatment with both MOX- and NAC-loaded nanosystems revealed that the latter affects mainly the thickness of the biofilm, while the treatment with MOX-loaded MLNs increases the population of dead bacterial cells within the structure.

In a more complex approach, the two nanosystems were combined to treat mature *S. aureus* biofilms grown in polyurethane catheters. For all the tested strains, the combination of functionalized nanoparticles encapsulating MOX (F-MOX-MLNs) and NAC (F-NAC-MLNs) revealed a potential synergistic effect in reducing the viable count within the biofilm. For the MRSA strain, the combination of these two formulations was the only condition where a significant reduction of viable count was observed, compared to the untreated control. Thus, the combination of targeted nanosystems loading antibiotics and matrix-disruptive agents is a promising antibiofilm strategy to fight clinically relevant biofilms, such as *S. aureus* biofilms.

Acknowledgements

This work was supported by the project PTDC/NANMAT/31444/2017, financed by FCT/MCTES e FEDER through Programa Operacional Competitividade e Internacionalização - COMPETE 2020. RMP and CN are thankful to Fundação para a Ciência e Tecnologia (FCT) for the Ph.D. Grant [SFRH/BD/130319/2017] and the investigator Grant [IF/00293/2015], respectively. PVD is thankful to the Fund for Scientific Research Flanders (FWO grant WO.009.16N). The authors RMP, CN, and SR acknowledge to the institution LAQV - Laboratório Associado para a Química Verde (UIDB/50006/2020). RMP also acknowledges the Programa Operacional Capital Humano (POCH), specifically the BiotechHealth Programme (Doctoral Programme on Cellular and Molecular Biotechnology Applied to Health Sciences). The authors also thank Manuela Barros for administrative and technical support.

References

1. Otto, M., *Staphylococcal biofilms.* Curr. Top. Microbiol. Immunol., 2008. **322**: p. 207-28,
2. Ribeiro, M., F.J. Monteiro, and M.P. Ferraz, *Infection of orthopedic implants with emphasis on bacterial adhesion process and techniques used in studying bacterial-material interactions.* Biomatter, 2012. **2**(4): p. 176-194, 10.4161/biom.22905
3. Pinto, R.M., et al., *Innovative strategies toward the disassembly of the EPS matrix in bacterial biofilms.* Front. Microbiol., 2020. **11**(952), 10.3389/fmicb.2020.00952
4. Bhattacharya, M., et al., *Prevention and treatment of Staphylococcus aureus biofilms.* Expert Rev. Anti-infect. Ther., 2015. **13**(12): p. 1499-516, 10.1586/14787210.2015.1100533
5. Balfour, J.A.B. and H.M. Lamb, *Moxifloxacin.* Drugs, 2000. **59**(1): p. 115-139, 10.2165/00003495-200059010-00010
6. Bauer, J., et al., *A combined pharmacodynamic quantitative and qualitative model reveals the potent activity of daptomycin and delafloxacin against Staphylococcus aureus biofilms.* Antimicrob Agents Chemother, 2013. **57**(6): p. 2726-37, 10.1128/AAC.00181-13
7. Parra-Ruiz, J., et al., *Activities of high-dose daptomycin, vancomycin, and moxifloxacin alone or in combination with clarithromycin or rifampin in a novel in vitro model of Staphylococcus aureus biofilm.* Antimicrob Agents Chemother, 2010. **54**(10): p. 4329-4334, 10.1128/aac.00455-10
8. Greimel, F., et al., *Efficacy of antibiotic treatment of implant-associated Staphylococcus aureus infections with moxifloxacin, flucloxacillin, rifampin, and combination therapy: an animal study.* Drug design, development and therapy, 2017. **11**: p. 1729-1736, 10.2147/DDDT.S138888
9. Pinto, R.M., et al., *N-acetyl-l-cysteine-loaded nanosystems as a promising therapeutic approach toward the eradication of Pseudomonas aeruginosa biofilms.* ACS Applied Materials & Interfaces, 2021. **13**(36): p. 42329-42343, 10.1021/acsami.1c05124
10. Marchese, A., et al., *Effect of Fosfomycin Alone and in Combination with N-Acetylcysteine on E. coli Biofilms.* Int. J. Antimicrob. Agents, 2003. **22**: p. 95-100, 10.1016/s0924-8579(03)00232-2
11. Manoharan, A., et al., *The effect of N-acetylcysteine in a combined antibiofilm treatment against antibiotic-resistant Staphylococcus aureus.* Journal of Antimicrobial Chemotherapy, 2020. **75**(7): p. 1787-1798, 10.1093/jac/dkaa093

12. Zhao, T. and Y. Liu, *N-Acetylcysteine Inhibit Biofilms Produced by Pseudomonas aeruginosa.* BMC Microbiol., 2010. **10**: p. 140, 10.1186/1471-2180-10-140
13. Olofsson, A.-C., M. Hermansson, and H. Elwing, *N-Acetyl-L-Cysteine Affects Growth, Extracellular Polysaccharide Production, and Bacterial Biofilm Formation on Solid Surfaces.* Appl. Environ. Microbiol., 2003. **69**(8): p. 4814-4822, 10.1128/AEM.69.8.4814-4822.2003
14. Stass, H. and D. Kubitza, *Pharmacokinetics and elimination of moxifloxacin after oral and intravenous administration in man.* Journal of Antimicrobial Chemotherapy, 1999. **43**(suppl_2): p. 83-90, 10.1093/jac/43.suppl_2.83
15. Samuni, Y., et al., *The Chemistry and Biological Activities of N-Acetylcysteine.* Biochim. Biophys. Acta, 2013. **1830**(8): p. 4117-4129, 10.1016/j.bbagen.2013.04.016
16. Nafee, N., *Nanocarriers Against Bacterial Biofilms: Current Status and Future Perspectives*, in *Nanotechnology in Diagnosis, Treatment and Prophylaxis of Infectious Diseases*, K. Kon, Editor. 2015, Academic Press: Boston. p. 167-189.
17. Severino, P., et al., *Current State-of-Art and New Trends on Lipid Nanoparticles (SLN and NLC) for Oral Drug Delivery.* J. Drug Deliv., 2012. **2012**: p. 750891, 10.1155/2012/750891
18. Zolnik, B.S., et al., *Nanoparticles and the Immune System.* Endocrinology, 2010. **151**(2): p. 458-465, 10.1210/en.2009-1082
19. Hochbaum, A.I., et al., *Inhibitory Effects of D-Amino Acids on Staphylococcus aureus Biofilm Development.* J. Bacteriol., 2011. **193**(20): p. 5616-5622, 10.1128/JB.05534-11
20. Sanchez, C.J., et al., *D-Amino Acids Enhance the Activity of Antimicrobials against Biofilms of Clinical Wound Isolates of Staphylococcus aureus and Pseudomonas aeruginosa.* Antimicrobial Agents and Chemotherapy, 2014. **58**(8): p. 4353-4361, doi:10.1128/AAC.02468-14
21. Pribaz, J.R., et al., *Mouse model of chronic post-arthroplasty infection: noninvasive in vivo bioluminescence imaging to monitor bacterial burden for long-term study.* J Orthop Res, 2012. **30**(3): p. 335-340, 10.1002/jor.21519
22. Francis, K.P., et al., *Monitoring bioluminescent Staphylococcus aureus infections in living mice using a novel luxABCDE construct.* Infect Immun, 2000. **68**(6): p. 3594-3600, 10.1128/iai.68.6.3594-3600.2000
23. Cavalcanti, S.M.T., et al., *Multiple Lipid Nanoparticles (MLN), a New Generation of Lipid Nanoparticles for Drug Delivery Systems: Lamivudine-MLN Experimental Design.* Pharm Res, 2017. **34**(6): p. 1204-1216, 10.1007/s11095-017-2136-0

24. Lopes-de-Campos, D., et al., *Delivering Amoxicillin at the Infection Site - a Rational Design through Lipid Nanoparticles.* Int. J. Nanomedicine, 2019. **14**: p. 2781-2795, 10.2147/ijn.S193992
25. Standardization, I.O.f., *International Standard ISO 10993-5*, in *Biological evaluation of medical devices–Part 5: tests for in vitro cytotoxicity*. 2009: Geneva, Switzerland,
26. Granja, A., et al., *EGCG intestinal absorption and oral bioavailability enhancement using folic acid-functionalized nanostructured lipid carriers.* Heliyon, 2019. **5**(7): p. e02020, https://doi.org/10.1016/j.heliyon.2019.e02020
27. Guo, Q., et al., *Functional Silver Nanocomposites as Broad-Spectrum Antimicrobial and Biofilm-Disrupting Agents.* ACS Appl. Mater. Interfaces, 2017. **9**(20): p. 16834-16847, 10.1021/acsami.7b02775
28. Wiegand, I., K. Hilpert, and R.E. Hancock, *Agar and Broth Dilution Methods to Determine the Minimal Inhibitory Concentration (MIC) of Antimicrobial Substances.* Nat. Protoc., 2008. **3**(2): p. 163,
29. Siala, W., et al., *The Antifungal Caspofungin Increases Fluoroquinolone Activity Against Staphylococcus aureus Biofilms by Inhibiting N-Acetylglucosamine Transferase.* Nat. Commun., 2016. **7**: p. 1-15, 10.1038/ncomms13286
30. Vande Velde, G., et al., *Bioluminescence imaging increases in vivo screening efficiency for antifungal activity against device-associated Candida albicans biofilms.* Int J Antimicrob Agents, 2018. **52**(1): p. 42-51, 10.1016/j.ijantimicag.2018.03.007
31. Stepanovic, S., et al., *A modified microtiter-plate test for quantification of staphylococcal biofilm formation.* J Microbiol Methods, 2000. **40**(2): p. 175-179, 10.1016/s0167-7012(00)00122-6
32. Vande Velde, G., et al., *Towards non-invasive monitoring of pathogen-host interactions during Candida albicans biofilm formation using in vivo bioluminescence.* Cell Microbiol, 2014. **16**(1): p. 115-130, 10.1111/cmi.12184
33. Blanco, E., H. Shen, and M. Ferrari, *Principles of Nanoparticle Design for Overcoming Biological Barriers to Drug Delivery.* Nat. biotechnol., 2015. **33**(9): p. 941-951, 10.1038/nbt.3330
34. Singh, R. and J.W. Lillard, Jr., *Nanoparticle-Based Targeted Drug Delivery.* Exp. Mol. Pathol., 2009. **86**(3): p. 215-223, 10.1016/j.yexmp.2008.12.004
35. Frohlich, E., *The role of surface charge in cellular uptake and cytotoxicity of medical nanoparticles.* Int J Nanomedicine, 2012. **7**: p. 5577-5591, 10.2147/ijn.S36111
36. Neves, A.R., J.F. Queiroz, and S. Reis, *Brain-targeted delivery of resveratrol using solid lipid nanoparticles functionalized with apolipoprotein E.* Journal of Nanobiotechnology, 2016. **14**(1): p. 27, 10.1186/s12951-016-0177-x

37. ISO, *10993-5. Biological evaluation of medical devices–Part 5: tests for in vitro cytotoxicity.* Geneva, Switzerland: International Organization for Standardization, 2009,
38. Drago, L., et al., *Activity of N-acetyl-L-cysteine against biofilm of Staphylococcus aureus and Pseudomonas aeruginosa on orthopedic prosthetic materials.* Int J Artif Organs, 2013. **36**(1): p. 39-46, 10.5301/ijao.5000135
39. Kolodkin-Gal, I., et al., *D-Amino Acids Trigger Biofilm Disassembly.* Science, 2010. **328**(5978): p. 627-629, 10.1126/science.1188628
40. Rumbo, C., et al., *Assessment of antivirulence activity of several d-amino acids against Acinetobacter baumannii and Pseudomonas aeruginosa.* J Antimicrob Chemother, 2016. **71**(12): p. 3473-3481, 10.1093/jac/dkw342
41. Aliashkevich, A., L. Alvarez, and F. Cava, *New Insights Into the Mechanisms and Biological Roles of D-Amino Acids in Complex Eco-Systems.* Frontiers in Microbiology, 2018. **9**(683), 10.3389/fmicb.2018.00683
42. Pozzi, C., et al., *Methicillin resistance alters the biofilm phenotype and attenuates virulence in Staphylococcus aureus device-associated infections.* PLoS Pathog, 2012. **8**(4): p. e1002626, 10.1371/journal.ppat.1002626
43. Liesse Iyamba, J.M., et al., *Study of the formation of a biofilm by clinical strains of Staphylococcus aureus.* Biofouling, 2011. **27**(8): p. 811-821, 10.1080/08927014.2011.604776
44. Ueda, Y., et al., *Inhibitory Effects of Polysorbate 80 on MRSA Biofilm Formed on Different Substrates Including Dermal Tissue.* Sci. Rep., 2019. **9**(1): p. 3128, 10.1038/s41598-019-39997-3
45. Toutain-Kidd, C.M., et al., *Polysorbate 80 Inhibition of Pseudomonas aeruginosa Biofilm Formation and its Cleavage by the Secreted Lipase LipA.* Antimicrob. Agents Chemother., 2009. **53**(1): p. 136-145, 10.1128/aac.00500-08
46. Nielsen, C.K., et al., *Effects of Tween 80 on Growth and Biofilm Formation in Laboratory Media.* Frontiers in microbiology, 2016. **7**: p. 1878-1878, 10.3389/fmicb.2016.01878
47. Warraich, A.A., et al., *Evaluation of anti-biofilm activity of acidic amino acids and synergy with ciprofloxacin on Staphylococcus aureus biofilms.* Scientific Reports, 2020. **10**(1): p. 9021, 10.1038/s41598-020-66082-x
48. Azeredo, J., et al., *Critical review on biofilm methods.* Crit Rev Microbiol, 2017. **43**(3): p. 313-351, 10.1080/1040841x.2016.1208146
49. Chen, Q., et al., *Biofilm formation and prevalence of adhesion genes among Staphylococcus aureus isolates from different food sources.* Microbiologyopen, 2020. **9**(1): p. e00946,

50. Sloup, R.E., et al., *Polysorbates prevent biofilm formation and pathogenesis of Escherichia coli O104:H4.* Biofouling, 2016. **32**(9): p. 1131-1140, 10.1080/08927014.2016.1230849

Supporting Information

Antibiofilm combinatory strategy towards *S. aureus*: novel moxifloxacin-loaded nanosystems joint with encapsulated *N*-acetyl-L-cysteine

1. In vitro MOX release study

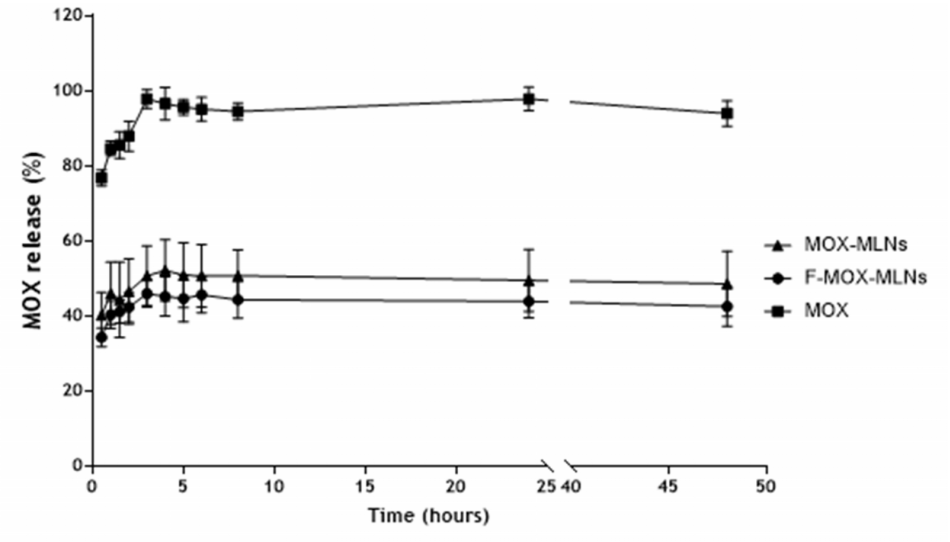


Figure S1: Cumulative MOX release profile of the non-functionalized (MOX-MLNs) and the functionalized (F-MOX-MLNs) formulations. The profile of the free MOX is also represented. The release was assessed in PBS (pH 7.4), at 37ºC. The values are represented as the mean ± SD.

2. Determination of the MIC and MBC values for MOX-loaded nanosystems

Table S1: Activity of the developed MLNs and free MOX against planktonic *S. aureus* strains. MIC and MBC values are expressed in μg ml^{-1} of MOX.

	MRSA (ATCC 33591)		***S. aureus* (ATCC 25923)**		***S. aureus* (ATCC 6538)**		***Xen36***	
	MIC	***MBC***	***MIC***	***MBC***	***MIC***	***MBC***	***MIC***	***MBC***
uMLNs	>2	>2	>2	>2	>2	>2	>2	>2
MOX-MLNs	0.125	0.125	0.06	0.125	0.25	0.25	0.125	0.125
F-uMLNs	>2	>2	>2	>2	>2	>2	>2	>2
F-MOX-MLNs	0.125	0.125	0.06	0.125	0.125	0.125	0.125	0.125
MOX	0.06	0.125	0.03	0.06	0.125	0.125	0.06	0.06

3. In vitro antibiofilm activity: biofilm viability and biofilm biomass study in *S. aureus* (ATCC 25923) biofilms

The antibiofilm efficacy of both MOX- and NAC-loaded nanosystems against the *S. aureus* strain ATCC 25923 was assessed by the XTT and crystal violet assays (**Figure S1**). Similar to the results obtained for the other three tested strains, biofilms treated with both unloaded and NAC-loaded LNPs showed a significant reduction on bacterial viability. However, free NAC does not seem to have a significant effect at the concentrations tested. Regarding biofilm biomass, only formulations or free NAC at the highest concentration (2 mg ml^{-1}) showed a significant reduction compared to the untreated control.

The developed MOX-MLNs and F-MOX-LNPs showed a high effect on reducing bacterial viability at drug concentrations as low as 0.125 µg ml^{-1}, which was not verified for the corresponding unloaded formulations. At the lowest concentration tested, free MOX also exhibited a high effect on viability. These results were further confirmed by the crystal violet assay. In this study, encapsulated and free MOX exhibited a biofilm biomass reduction higher than 50% at the lowest concentration tested. For the unloaded vehicles, only at the highest concentrations it is possible to observe a significant difference in the biofilm biomass, compared to the control.

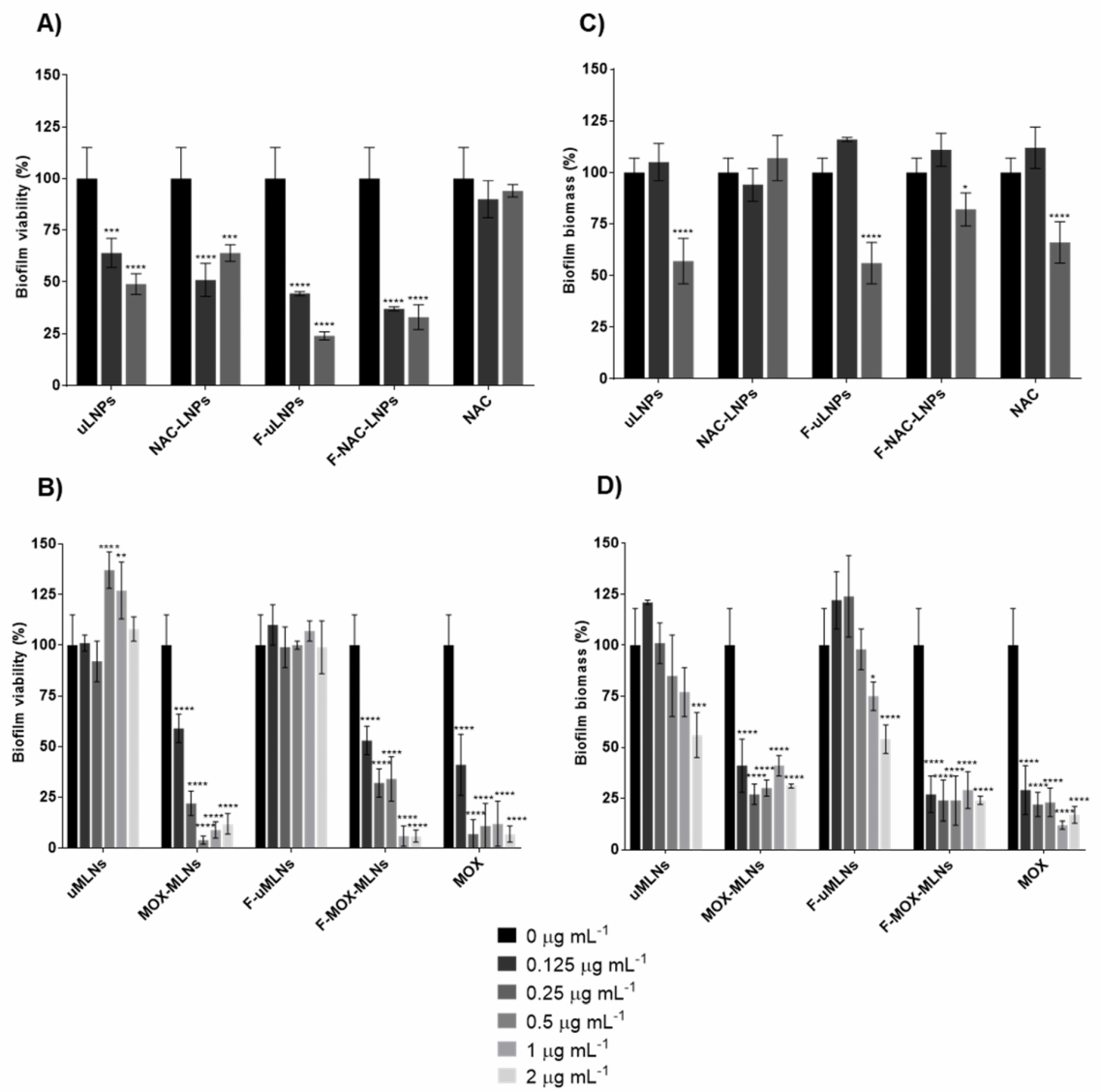
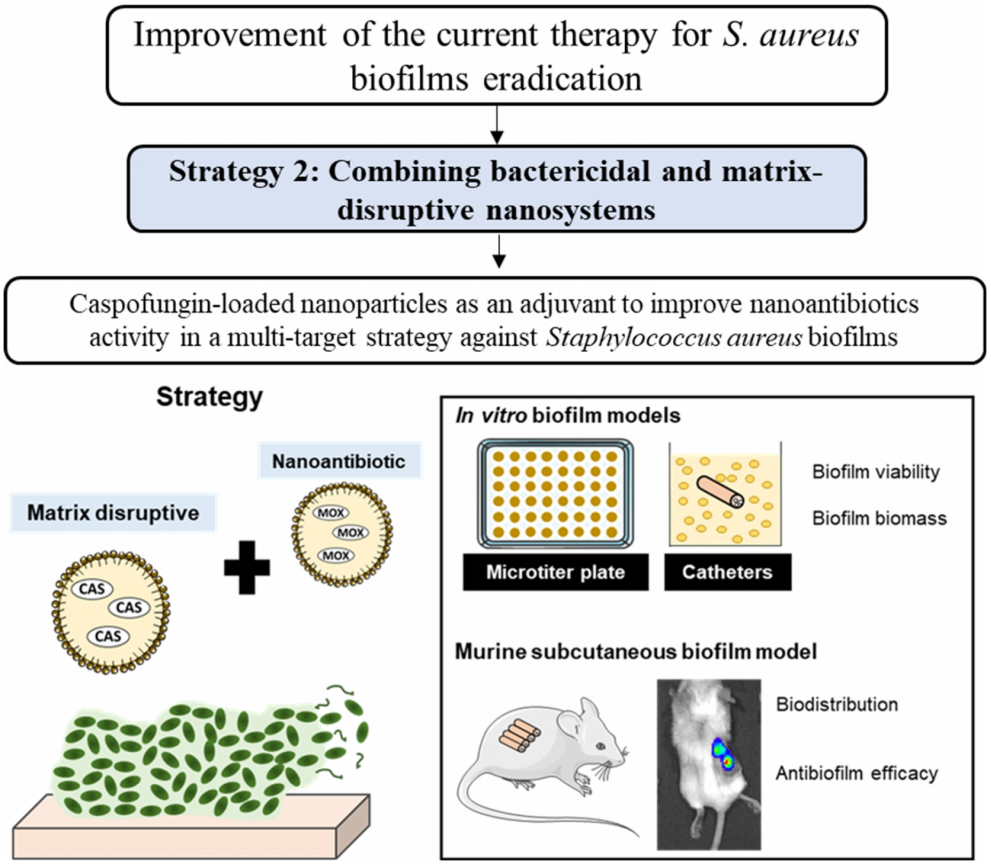


Figure S2: Quantification of **(A, B)** biofilm viability (XTT assay) and **(C, D)** biomass (crystal violet staining) after a 24h treatment of *S. aureus* (ATCC 25923) biofilms. **(A, C)** The biofilms were treated with unloaded and NAC-loaded LNPs at the solid lipid concentrations of 0, 1, and 2 mg ml^{-1}, which corresponds to 0, 0.45, and 0.9 mg ml^{-1} of NAC, respectively. Free NAC was tested at the same concentrations. **(B, D)** The biofilms were treated with the developed MLNs and free MOX at the concentrations of 0, 0.125, 0.25, 0.5, 1, and 2 µg ml^{-1} of MOX. Untreated biofilms (0 µg ml^{-1}) were used as a positive control. The values are represented as the mean ± SD. *P<0.05, **P<0.01, ***P<0.001, ****P<0.0001 relatively to 0 µg ml^{-1}. Statistical analysis: two-way ANOVA, Tukey's multiple comparisons test.

Chapter 6.3.

Caspofungin-loaded nanoparticles as an adjuvant to improve nanoantibiotics activity in a multi-target strategy against *Staphylococcus aureus* biofilms

A strategy involving both antibiotics and matrix disruptive agents has the potential to emerge as a novel therapy towards the eradication of bacterial biofilms. Previously, MOX-loaded nanoparticles were combined with nanoparticles encapsulating a matrix disruptive agent, NAC (**Chapter 6.2.**). In this chapter, we explore the combination of the previously developed MOX-loaded nanosystems with another matrix disruptive agent, caspofungin. With this purpose, caspofungin-loaded nanoparticles were developed as an adjuvant to improve the activity of encapsulated MOX against *S. aureus* biofilms. The potential antibiofilm effect of this multi-target strategy was assessed both *in vitro* and *in vivo*, using different biofilm models.



Caspofungin-loaded nanoparticles as an adjuvant to improve nanoantibiotics activity in a multi-target strategy against *Staphylococcus aureus* biofilms

Rita M. Pinto[1,2,3], Saleh Yazdani[2,3], Catarina Leal Seabra[1], Martine De Jonge[2], Mukaddes Izci[4], Rebeca Cruz[1], Susana Casal[1], Stefaan J. Soenen[4], Salette Reis[1], Patrick Van Dijck[2,3*], Cláudia Nunes[1*]

[1] LAQV, REQUIMTE, Departamento de Ciências Químicas, Faculdade de Farmácia, Universidade do Porto, Porto, Portugal

[2] Laboratory of Molecular Cell Biology Institute of Botany and Microbiology KU Leuven Leuven, Belgium

[3] VIB KU Leuven Center for Microbiology Leuven, Belgium

[4] NanoHealth and Optical Imaging Group, Translational Cell and Tissue Research Unit, Department of Imaging and Pathology, KU Leuven, Leuven, Belgium

*Corresponding authors:

Patrick Van Dijck: patrick.vandijck@kuleuven.be

Cláudia Nunes: cdnunes@ff.up.pt

Abstract

Staphylococcus aureus is considered a high priority pathogen by the World Health Organization due to its high prevalence and the potential to form biofilms. Currently, the available treatments for *S. aureus* biofilm-associated infections do not target the main component of the biofilms: the extracellular polymeric substances (EPS) matrix. This matrix is a physical barrier to bactericidal agents, contributing to the increase in antimicrobial resistance and leading to the failure of several therapeutic approaches. Thus, it is essential to develop strategies that disrupt the EPS, allowing antimicrobial agents to reach the cells within the biofilms. The present work proposes the developed of lipid nanoparticles encapsulating caspofungin (CAS), as a matrix-disruptive nanosystem. The nanoparticles were functionalized with D-amino acids to target the EPS matrix. In a multi-target strategy against *S. aureus* biofilms, CAS-loaded nanoparticles were combined with a nanoantibiotic, as an adjuvant to promote the disruption of the EPS matrix. The synergistic potential between the CAS-loaded nanosystem and nanoparticles encapsulating the antibiotic moxifloxacin (MOX) was assessed. Both in *in vitro* and *in vivo* efficacy studies, biofilm reduction was observed after the combination of functionalized CAS-loaded and MOX-loaded nanosystems. Besides, the combinatory therapy showed no signs of bacterial dissemination into vital organs, while dissemination was observed for the treatment with the free compounds. Additionally, the *in vivo* biodistribution of the two nanosystems revealed the potential of these structures to reach and accumulate in the region of the biofilm, after a systemic administration. Thus, this multi-target strategy based on the nanoencapsulation of matrix-disruptive and antibacterial agents is a promising approach to fight *S. aureus* biofilms.

1. Introduction

Staphylococcus aureus is considered by the World Health Organization as a high priority pathogen since it is a leading cause of nosocomial and community-acquired infections [1, 2]. These bacteria are commonly found in infected implantable medical devices, such as catheters, and are responsible for high morbidity and mortality rates [3]. A virulent factor that highly contributes to the survival of *S. aureus* is the ability to form a biofilm. In these structures, the extracellular polymeric substances (EPS) matrix surrounds bacterial cells, protecting them from the harsh external environment and antibiotics [4]. The EPS matrix is a physical barrier to the diffusion of antimicrobial agents, leading to the failure of conventional therapies that are solely based on the administration of antibiotics [5]. Hence, the EPS matrix highly contributes to antimicrobial resistance phenomena. Novel therapeutic approaches that target not only bacterial cells within the biofilm but also the EPS matrix are critical to eradicate *S. aureus* biofilms.

Caspofungin (CAS) is an echinocandin antifungal agent, used to treat infections caused by *Candida* spp. and *Aspergillus* spp. The mechanism of action of this fungicidal agent consists in inhibiting the synthesis of β-(1,3)-D-glucan, an essential component of the fungal cell wall [6]. However, this compound has been recently highlighted for its antibiofilm activity against bacterial biofilms [7, 8]. Siala *et al.* (2016) reported that CAS inhibited the enzymatic activity of IcaA, which shares homology with β-(1,3)-D-glucan [8]. In *S. aureus*, this enzyme plays a critical role in the production of the EPS matrix component poly-*N*-acetylglucosamine (PNAG) [9]. Due to its matrix-disruptive properties, CAS revealed a potential synergistic effect with moxifloxacin (MOX) against *S. aureus* biofilms [8]. However, both CAS and MOX are prone to degradation, have high affinity to plasma proteins, and present adverse side effects at high doses [10, 11]. Hence, several factors may limit the drugs to reach the biofilm at therapeutic doses.

Nanotechnology is a promising field for drug delivery purposes, improving the efficacy of encapsulated drugs. Besides protecting encapsulated drugs, nanoparticles may also be designed to specifically target a site of interest [12, 13]. Amongst the colloidal carriers described in the literature, lipid nanoparticles (LNPs) have been highlighted for their excellent biocompatibility and biodegradability. Besides, LNPs are highly stable, low cost, and easily functionalized to target a specific region [12].

In this work, functionalized LNPs encapsulating CAS were developed and characterized in a novel approach towards the eradication of *S. aureus* biofilms. The nanosystems were functionalized with a mixture of D-amino acids (D-Phenylalanine, D-Proline, and D-Tyrosine) conjugated with poly (ethylene glycol) (PEG). This mixture of D-amino acids aims to

specifically target and disrupt the biofilm, while PEG was added to the formulation to increase the circulation time of the LNPs, by avoiding recognition by the immune system [14, 15]. The produced formulations were assessed for their *in vitro* cytocompatibility and antibiofilm efficacy. In a step forward towards an efficient antibiofilm treatment against *S. aureus* biofilms, CAS-loaded LNPs were combined with MOX-loaded nanosystems to evaluate potential synergistic effects, both *in vitro* and *in vivo*. Additionally, the *in vivo* biodistribution of these two nanosystems was assessed. In this multi-target strategy, encapsulated CAS (matrix-disruptive agent) would be used as an adjuvant to improve the activity of MOX (bactericidal agent) against the bacterial biofilms. A schematic overview of the nanosystems used in this work is represented in **Figure 1**.

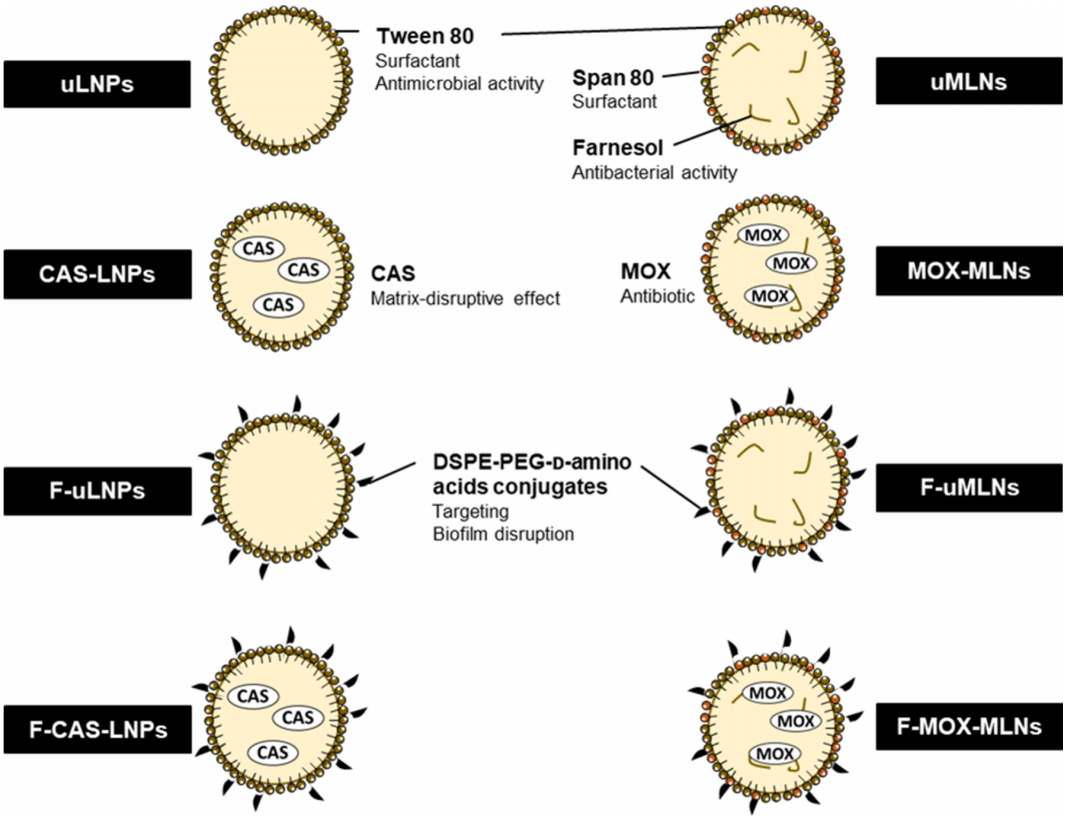


Figure 1: Schematic overview of the CAS-loaded and MOX-loaded nanosystems, and respective unloaded formulations. CAS-loaded LNPs, composed of cetyl palmitate (solid lipid) and Tween 80, were produced by the double emulsion method [16]. The MOX-loaded multiple lipid nanoparticles (MLNs) were composed by cetyl palmitate, Miglyol 812 (liquid lipid), farnesol, and the surfactants, Tween 80 and Span 80 (**chapter 6.2 – section 2.3**). The surface of the nanoparticles was functionalized with DSPE-PEG-D-amino acid conjugates (D-Phenylalanine, D-Proline, and D-Tyrosine).

2. Materials and Methods

2.1 Materials

The lipid cetyl palmitate was a kind gift from Gattefossé (Gattefossé, France). DSPE-PEG2000-NH_2 (1,2-distearoyl-*sn*-glycero-3-phosphoethanolamine-N-[amino(polyethylene glycol)-2000] (ammonium salt)) was purchased from Avanti Polar Lipids Inc. (Alabaster, Alabama, USA). D-Phenilalanine (Phe), D-Proline (Pro), D-Tyrosine (Tyr), triethylamine (TEA), dicyclohexylcarbodiimide (DCC), N-hydroxysuccinimide (NHS), sodium hydroxide (NaOH), sodium chloride, moxifloxacin hydrochloride (MOX), farnesol 95%, Tween 80, trifluoroacetic acid (TFA), Triton X-100, thiazolyl blue tetrazolium (MTT), D-(+)-glucose monohydrate >99%, müller-hinton broth cation adjusted (MHB-Ca^{2+}), 2,3-Bis(2-methoxy-4-nitro-5-sulfophenyl)-2H-tetrazolium-5-carboxanilide inner salt (XTT), menadione crystalline, and crystal violet dye were obtained from Sigma-Aldrich (USA). Miglyol 812 and Span 80 were purchased from Acofarma (Spain). Chloroform, dimethyl sulfoxide (DMSO), methanol, acetonitrile, and acetic acid glacial were obtained from VWR International LLC (USA). Dulbecco's Modified Eagle's Medium (DMEM), trypsin-EDTA (1×), Penicillin-Streptomycin (Pen Strep), Dulbecco's Phosphate Buffered Saline 10x pH 7.4 (PBS), and Fetal Bovine Serum (FBS) were purchased from Gibco by Life Technologies (UK). Lactate dehydrogenase (LDH) Cytotoxicity Detection Kit was obtained from Takara Bio Inc. (Shiga, Japan). L929 cells (ATCC CCL-1TM) were acquired from the American Type Culture Collection (USA). BD Tryptic soy broth (TSB) and Difco Granulated Agar were acquired from Becton Dickinson (USA). Cyanine 7 (Cy7) was purchased to Lumiprobe GmbH (Germany). The isoflurane (Iso-Vet 1000 mg/g) was acquired from Dechra Veterinary Products NV (Belgium). All components were used without further purification.

2.2 Bacterial strains

The *S. aureus* strains ATCC 33591 (methicillin-resistant) and ATCC 25923 (methicillin-susceptible) were kindly provided by Prof. Françoise Van Bambeke (UC Louvain). The bioluminescent strain *Xen36* (Caliper Life Sciences, USA) was derived from the *S. aureus* ATCC 49525. This strain expresses a stable copy of a modified *Photorhabdus luminescens luxABCDE* operon [17, 18]. The *S. aureus* strain ATCC 6538 was acquired from ATCC (USA).

2.3 Preparation of the CAS-loaded LNPs

The formulations were produced by the double emulsion method. In this method, CAS (5 mg) was dissolved in an aqueous solution of NaOH (400 µl of NaOH 1M in 600 µl of ultrapure water). For the unloaded LNPs, CAS was not added to the aqueous solution. The aqueous solution was then added to the solid lipid cetyl palmitate (65 mg), previously dissolved in 2 ml of chloroform. The mixture was sonicated for 30 s at an amplitude of 70%, using a VCX-130 Vibra-Cell sonicator (Sonics & Materials Inc, USA) with a CV-18 probe (130 W, 20 kHz). For the functionalized formulations, 1 mg of each D-amino acids conjugate (D-Phe, D-Pro, and D-Tyr) were dissolved in 100 µl of chloroform and added to the primary emulsion. The synthesis of these conjugates was previously described elsewhere [16]. Then, a solution of Tween 80 (25 mg ml^{-1}, 4 ml) was added, and the emulsion was sonicated for 3 mins at an amplitude of 80%. Finally, a solution of Tween 80 (13.75 mg ml^{-1}, 4 ml) was added, and the final LNPs suspension was placed in a stirring plate at room temperature, under agitation, to evaporate the remaining chloroform.

2.4 Physical characterization of LNPs

The hydrodynamic diameter and polydispersity index (PDI) were measured using a Particle Size Analyzer (Brookhaven Instruments Corporation, Software: Particle Sizing v.5 Brookhaven Instruments, USA). The zeta potential of the developed LNPs was determined using the Zeta Potential Analyzer (ZetaPALS, Brookhaven Instruments Corporation, Software: PALS Zeta Potential Analyzer v.5 Brookhaven Instruments, USA). The system operated with an incidence light angle of 90°, at room temperature. Prior to the measurements, the LNPs were diluted (1:100) in ultrapure water.

The morphology of the produced LNPs was assessed by transmission electron microscopy (TEM). For this purpose, the formulations were diluted (1:100) in ultrapure water. Then, 10 µl of the diluted LNPs were placed onto a copper-mesh grid for 2 min. The excess of LNPs was then removed, and 10 µl of 0.75% (w/v) uranyl acetate solution were added to the grid for 30 s (negative staining). The samples were observed in a JEM-1400 transmission electron microscope (JEOL Ltd., Japan) with an acceleration voltage of 80 kV.

2.5 Determination of the encapsulation efficiency and loading capacity

The encapsulation efficiency (EE) was determined by the HPLC technique, by direct measurement of the entrapped CAS. The diluted LNPs (80 µl of LNPs in 1920 µl of ultrapure

water) were transferred to an Amicon®Ultra-4 Centrifugal Filter Device 50 kDa (MERCK Milipore, Ltd, Ireland) and centrifuged at 524*g* (Allegra X-15R Centrifuge, Beckman Coulter, USA), until complete separation of the LNPs from the supernatant. The pellet was collected and added to 500 µl of acetonitrile, to dissolve the LNPs. The lipids were separated from the dissolved CAS by centrifugation at 30 000*g* for 30 mins. Then, 350 µl of supernatant was added to 650 µl of buffer. The buffer was composed by an aqueous solution of 0.1% of TFA (v/v), adjusted to pH 3 with TEA.

The chromatographic conditions were adapted from the literature [19]. The HPLC system (Jasco, Tokyo, Japan) was composed by one high-pressure pump (PU-4180), a refrigerated automated injector (AS-4050), and a fluorescence detector (FP-4025) set at 220 nm and 304 nm for excitation and emission, respectively. A sample volume of 20 µl was injected. The chromatographic separation was obtained by using a Gemini NX C18 110 Å (150 × 4.60 mm, 5 µm) column from Phenomenex (USA). The isocratic mobile phase consisted of a 65:35 (v/v) mixture of buffer and acetonitrile. At a flow rate of 0.9 ml min^{-1}, the retention time of CAS was 9.5 min. A calibration curve of CAS (0.002 – 0.04 mg ml^{-1}) was used for quantification (data not shown).

The EE was calculated as follows

$$EE\ (\%) = \frac{loaded\ CAS\ amount}{total\ CAS\ amount} \times 100 \quad (1)$$

The loading capacity (LC) was calculated using the EE, as follows

$$LC\ (\%) = \frac{EE \times total\ CAS\ amount}{total\ solid\ lipid\ amount} \times 100 \quad (2)$$

2.6 Evaluation of the storage stability of the LNPs suspensions

The LNPs formulations were stored at 4ºC for 8 weeks. During this time, the physicochemical storage stability was assessed through the measurements of hydrodynamic size, PDI, zeta potential, EE, and LC. The measurements were performed using the methods described in the previous sections.

2.7 *In vitro* CAS release study

The dialysis diffusion technique was used to assess the *in vitro* CAS release profile from the developed LNPs [20]. In this study, CAS-loaded LNPs or free CAS (1 ml) were added

to a cellulose dialysis bag (Spectra/Por®1 Dialysis Membrane Standard RC Tubing, MWCO 12-14 kD, SpectrumLabs, USA) and placed into 60 ml of PBS at a physiological pH (7.4), at 37ºC, under agitation, for 48h. At regular intervals, aliquots (80 µl) were collected from the dialysis membrane. To each aliquot, 500 µl of acetonitrile were added, to dissolve the LNPs. The lipids were separated from the dissolved drug by centrifugation (30 000*g* for 30 mins). Then, 350 µl of the supernatant were added to 650 µl of buffer, which consists of an aqueous solution of 0.1% of TFA (v/v), adjusted to pH 3 with TEA. The chromatographic conditions used to quantify the released CAS are described in detail in **section 2.5**.

2.8 *In vitro* cytocompatibility studies

2.8.1 Cell viability and cytotoxicity assessment

The effect of the developed LNPs in cell viability was evaluated in the L929 cell line (fibroblasts), which is recommended by the ISO international standard 10993–5 for cytocompatibility assessment studies [21]. Briefly, the cells were cultured in DMEM supplemented with 10% FBS and 1% Penicillin-Streptomycin at 37ºC, 5% CO_2 atmosphere. Briefly, after 80 – 90% confluence, cells were seed in 96-well plates at a density of 5 x 10^4 cells/well and let to grow overnight at 37ºC, 5% CO_2 atmosphere. Afterward, the cells were treated with LNPs or free CAS at different CAS concentrations (0, 4, 8, 16, 32, and 64 µg ml^{-1}) for 24h, at 37ºC, 5% CO_2. Cells incubated with DMEM and Triton-100 (1%, v/v) were used as positive and negative controls, respectively.

After the treatment, the medium in each well was replaced by the MTT solution (0.5 mg ml^{-1}, 100 µl) and incubated for 2h, at 37ºC, 5% CO_2. Then, the MTT solution was removed, and the formazan crystals were dissolved in 100 µl of DMSO. The medium collected after the treatment was further centrifuged at 250*g* for 10 mins (Centrifuge 5810R, Eppendorf, Germany). The supernatant was collected to quantify the LDH using the LDH cytotoxicity kit, according to the instructions from the manufacturer. For the MTT assay, the absorbance was measured at 550 and 650 nm, while for the LDH assay it was measured at 490 and 690 nm, using a microplate reader (BioTek Instruments Inc., Synergy HT, Software: Gen5 v1.08.4, BioTek Instruments Inc, USA). The wavelengths 650 and 690 nm were used to remove the background interference in the measurements.

2.8.2 Hemolysis activity assessment

Human red blood cells, kindly donated by Serviço de Hematologia do Centro Hospitalar do Porto, were used to assess the hemolytic activity of the developed LNPs. This procedure was in accordance with the principles of the Declaration of Helsinki. The protocol was adapted from [22]. Briefly, red blood cells were centrifuged at 955*g* for 5 mins, at 4ºC (Allegra X-15R Centrifuge, Beckman Coulter, USA), to separate them from the remaining components of the blood. Afterward, cells were washed three times with saline solution 0.85% (m/v) and diluted to a volume fraction of 4%. Diluted red blood cells (100 µl) were incubated with 100 µl of LNPs or free CAS for 1h, at 37ºC. The LNPs and free CAS were tested at the same CAS concentrations used for the MTT and LDH assays (**section 2.8.1**). Afterward, the supernatant from each well was collected and the absorbance was read at 540 nm and 690 nm, using a microplate reader (BioTek Instruments Inc., Cytation, Software: Gen5 v1.08.4, BioTek Instruments Inc., USA). The percentage of hemolysis was calculated according to the following

$$hemolysis\ (\%) = \frac{Abs - Abs\ (-)}{Abs\ (+) - Abs\ (-)} \times 100 \quad (3)$$

where Abs, Abs (-) and Abs (+) are the absorbances of the sample, the negative control (saline solution 0.85%) and the positive control (Triton-100, 1% v/v), respectively.

2.9 *In vitro* antibacterial studies

The effect of the developed LNPs on planktonic bacteria was assessed using the well-known micro-broth dilution assay [23]. In brief, an overnight bacterial culture was diluted to a concentration of 2.0×10^5 CFUs ml^{-1} in MHB-Ca^{2+} medium. Then, the bacterial suspension was treated with LNPs or free CAS for 24h, at 37ºC, in a 96-well round bottom microtiter plate (Greiner Bio One, Austria). The developed LNPs and free CAS were tested at the same concentrations used for the cytocompatibility studies (**section 2.8**). The MIC was recorded as the lowest concentration which inhibited the visual growth of bacteria, while MBC was defined as the lowest concentration resulting in the death of 99.9% of the initial inoculum. The MBC was further determined by spot-plate (10 µl) each well with no visual bacterial growth on TSA plates. The TSA plates were incubated at 37ºC, overnight, followed by CFUs counting.

2.10 *In vitro* antibiofilm studies

2.10.1 Microtiter plate biofilm model

Biofilm formation and growth conditions were adapted from the literature [8, 24]. Overnight bacterial cultures were adjusted to an optical density of 600 nm (OD_{600nm}) of 0.1 in TSB 0.6x supplemented with 0.2% glucose. Then, 200 µl of the adjusted inoculum were added to each well from a 96-well flat bottom microtiter plate (Greiner Bio One, Austria) and incubated for 90 mins, at 37ºC. Afterward, the medium was removed, and the wells were washed twice with PBS 1x, to remove non-adhered cells. Subsequently to the washing steps, 200 µl of fresh TSB 0.6x supplemented with 0.2% glucose were added to each well. The biofilms were left to grow for 24h, at 37ºC. Prior treatment, the 24h-old biofilms were washed twice with PBS 1x. The developed LNPs and free CAS were tested at several CAS concentrations (0, 4, 8, 16, 32, and 64 µg ml^{-1}). This procedure was used for the following assays.

2.10.1.1 Biofilm metabolic activity assessment

The metabolic activity of the bacterial cells within the biofilm was assessed through the XTT assay [25]. After the treatment, the wells were washed once with PBS 1x and 100 µl of XTT solution (1 mg ml^{-1}, supplemented with 1 µM menadione) were added. Then, the 96-well plates were incubated in the dark, at 37ºC for 30 mins, with shaking (250 rpm) (VWR Incubating Microplate Shaker, VWR International LLC, USA). The absorbance was read at 490 nm using a microplate reader (BioTek Instruments Inc., Synergy HT, Software: Gen5 v1.08.4, BioTek Instruments Inc., USA).

2.10.1.2 Biofilm biomass study

Biofilm biomass quantification was assessed through the crystal violet assay based on the reported protocol [26]. After the treatment with the LNPs, the biofilms were washed once with PBS 1x and fixed with 200 µl of 99% methanol for 15 mins. Then, the methanol was removed from the wells and the biofilms were left to dry until complete evaporation of the organic solvent. To stain the biofilms, 200 µl of crystal violet solution (1%, m/v) were added to the wells for 5 mins, at room temperature. The excess of dye was further removed by washing the stained biofilms with ultrapure water. Finally, 200 µl of glacial acetic acid 33% (v/v) were added to the wells. The plates were incubated at room temperature for 15 mins, with shaking (250 rpm), in an incubating microplate shaker (VWR International LLC, USA).

The absorbance was read at 570 nm using a microplate reader (BioTek Instruments Inc., Synergy HT, Software: Gen5 v1.08.4, BioTek Instruments Inc., USA).

2.10.2 Catheter biofilm model

The potential antibiofilm effect of the developed LNPs in combination with an antibiotic-loaded nanosystem was further evaluated in the catheter biofilm model. For this purpose, MOX-loaded multiple lipid nanoparticles (MLNs) were produced according to a previously reported protocol (**Chapter 6.2. – section 2.3**).

The protocol to grow biofilms using the *in vitro* catheter biofilm model was previously reported [8]. Firstly, triple-lumen polyurethane central venous catheters (Certofix duo/trio; B. Braun Melsungen AG, Germany) were cut into 1 cm long pieces. The pieces were incubated overnight, at 37ºC, with 100% fetal bovine serum. A bacterial overnight culture was adjusted to an OD_{600nm} of 0.1 in TSB 0.6x supplemented with 0.2% glucose. Then, each catheter piece was incubated with 1 ml of the adjusted bacterial inoculum, for 90 mins, at 37ºC, in a 24-well plate for suspension cultures (Greiner Bio One, Austria). After the adhesion step, non-adherent bacteria were removed by two washing steps with 1 ml of PBS 1x. The washed catheters were submerged in 1 ml of fresh TSB 0.6x supplemented with 0.2% glucose and incubated for 24h, at 37ºC, to allow the formation of mature biofilms. Afterward, biofilms were treated for 24h, at 37ºC. For this purpose, the developed LNPs or free CAS were tested at a CAS concentration of 8 µg ml^{-1}. MOX-loaded MLNs and respective unloaded formulations were tested at a MOX concentration of 0.5 µg ml^{-1} (for MRSA ATCC 33591 and *Xen36* strains) and 1.0 µg ml^{-1} (for the strong biofilm-forming ATCC 6538 strain). Free MOX was tested in the same conditions. After the treatment, catheter pieces were washed twice with PBS 1x and sonicated (Branson 5510 Ultrasonics bath, Marshall Scientific, USA) at room temperature for 10 mins in 200 µl of PBS 1x, to disperse the biofilms. The samples were serial diluted in PBS 1x and spot-plated (10 µl) on TSA plates. The plates were incubated overnight at 37ºC to allow CFUs counting.

2.11 *In vivo* studies

2.11.1 Murine subcutaneous biofilm model

Animal experiments were performed under the KU Leuven animal care guidelines and were approved by the KU Leuven Ethics Committee (project number P019/2021). The murine subcutaneous biofilm model used for the *in vivo* studies is detailed in the literature [8, 27].

Female pathogen-free 8-week old BALB/c mice (Janvier Labs, France) were kept in ventilated cages and provided with food and water *ad libitum*. Briefly, serum-coated catheter pieces (1 cm long) were incubated with the bioluminescent strain *Xen36* for 90 mins at 37ºC, to allow adhesion of bacterial cells, as described in **section 2.10.2**. After this incubation time, the catheter pieces were washed twice with PBS 1x and subcutaneously implanted in the back of the mice. For this purpose, the mice were anesthetized with a mixture of isoflurane in oxygen (1.5 to 2%, v/v). Then, the lower back of the mice was shaved and disinfected with ethanol 70%. A small incision in the right side was performed to create a subcutaneous pocket where 4 catheter pieces were placed, per mouse. The incision was closed using surgical glue (3M Vetbond Tissue Adhesive, 3M, USA) and the biofilms were allowed to grow into mature structures for 24h, prior to treatment.

2.11.2 Biodistribution study

2.11.2.1 Preparation of Cyanine7-loaded LNPs and MLNs

LNPs loaded with cyanine7 (Cy7) were prepared according to the protocol described for unloaded LNPs in **section 2.3**. For this purpose, Cy7 at a concentration of 0.2% (w/w) of the solid lipid and surfactant was dissolved in chloroform and added to the lipid phase. Both non functionalized and functionalized Cy7-loaded LNPs were produced.

Cy7-loaded MLNs were prepared according to a previously described protocol (**Chapter 6.2** – **section 2.3**). Briefly, the solid lipid cetyl palmitate (135 mg), the surfactant Span 80 (115 mg), and farnesol (6 mg) were heated at 60ºC in a water bath. Cy7 at a concentration of 0.1% (w/w) of the solid lipid and surfactants was added to the liquid lipid Miglyol 812 (305 mg) and pre-heated. Afterward, the dye solubilized in the liquid lipid was added to the melted lipid phase. Simultaneously, 650 µl of ultrapure water was added and the mixture was sonicated for 3 mins at 70%. The primary emulsion was left to cool down at room temperature. Then, 80 mg of Tween 80 were added. For the functionalized formulation, 1 mg of each D-amino acid conjugate (D-Phe, D-Pro, and D-Tyr) were added. The emulsion was then heated for 5 mins at 60ºC and sonicated at 80% amplitude during 3 mins.

2.11.2.2. Biodistribution imaging

To assess *in vivo* biodistribution, the non-functionalized and functionalized formulations were administered intraperitoneally. Cy7-loaded LNPs were administered at a solid lipid concentration of 52 mg kg^{-1} of body weight, while Cy7-loaded MLNs at a solid lipid

concentration of 135 mg kg^{-1} of body weight. The animals were imaged prior, 1h post- and 24h post-administration of the formulations. For this purpose, mice were anesthetized using a gas mixture of isoflurane in oxygen (1.5 to 2%, v/v) and placed in the *In Vivo* Imaging System (IVIS Spectrum, Perkin-Elmer, USA). Frames were acquired with the fields of view of 23 cm. Bioluminescence imaging was acquired using 40 secs exposure time, binning 2, f/stop=1. Fluorescence images were acquired using an exposure time of 0.3 secs, binning 2, f/stop=2. After 24h, the animals were euthanized by cervical dislocation, and the catheters and organs (liver, spleen, and kidneys) imaged. Frames with fields of view of 6.6 cm and 13 cm were acquired. The signal was quantified in photon flux per second (p s^{-1}) using the Living Image Software (version 4.7.3.20616, Perkin-Elmer) by selecting a rectangular region of interest (ROI) placed over the catheters or organs.

2.11.3 Antibiofilm efficacy study

Mature 24h-old biofilms were treated for 7 days with nanosystems or free compounds. Functionalized CAS-loaded LNPs and free CAS were administered once a day at a CAS dose of 4 mg kg^{-1} of body weight. The functionalized MOX-loaded MLNs and free MOX were administered twice a day at a MOX dose of 5 mg kg^{-1} of body weight. Non infected and untreated infected control groups were treated with sterile ultrapure water. Prior intraperitoneal administration, the mice were anesthetized with a mixture of isoflurane in oxygen (1.5 to 2%, v/v). Mice were imaged on days 1, 2, 5, 7, and 8 after implantation. On day 1 after implantation, the mice were imaging prior to the treatment. Anesthetized animals were placed in the *In Vivo* Imaging System (IVIS Spectrum, Perkin-Elmer, USA). Frames were acquired with the field of view of 23 cm. Bioluminescence imaging was acquired using 40 s exposure time, binning 2, f/stop=1. After the treatment, the animals were sacrificed by cervical dislocation. The catheters were harvested and imaged using frames with the field of view of 13 cm. The signal was quantified in photon flux per second (p s^{-1}) using the Living Image Software (version 4.7.3.20616, Perkin-Elmer) by selecting a rectangular region of interest (ROI) placed over the catheters. Afterward, the catheters were washed twice with PBS 1x and sonicated at room temperature for 10 mins in 200 µl of PBS 1x. The samples were serial diluted in PBS 1x and spot-plated (10 µl) on TSA plates. Spleen, kidneys, and liver were also harvested and further submerged in 500 µl of PBS 1x and homogenized for 40 s (FastPrep-24™; MP Biomedicals, LLC; USA). Then, the samples were serial diluted in PBS 1x and spot-plated (10 µl) on TSA plates. The plates were incubated overnight at 37ºC to allow CFUs counting.

2.12 Statistical analysis

Statistical analysis was performed using Graphpad Prism Software (version 7.03; IBM, USA). All *in vitro* assays were performed at least three independent times. For *in vivo* assays at least three biological replicates were used.

3. Results and Discussion

3.1 Physical characterization of LNPs and storage stability

The produced LNPs were characterized according to their hydrodynamic size, PDI, zeta potential, EE, LC, and morphology (**Figure 2**). All formulations showed a hydrodynamic size below 300 nm, and a relatively low PDI (<0.2). The zeta potential of the LNPs was also measured, revealing values below -30 mV. Both the PDI and zeta potential values suggest that the produced formulations have low tendency to form aggregates [28]. Besides, the encapsulation of CAS does not seem to affect the physical characteristics of the LNPs. The EE and LC of both non-functionalized and functionalized LNPs were measured. CAS-LNPs and F-CAS-LNPs exhibited encapsulation efficiencies of 63% and 83%. Although functionalized LNPs showed a higher EE, it was not significantly different than the EE of non-functionalized nanoparticles. The LC values were also calculated for both formulations, revealing values between 4% and 6.5%. The effect of functionalization in the morphology of the CAS-loaded LNPs was also evaluated (**Figure 2A**). Both non- and functionalized nanoparticles show a spherical shape and no visible aggregation. These results corroborate the measurements determined by dynamic light scattering.

The physical stability of the formulations under storage conditions was also assessed over 8 weeks (**Figure 2 B-E**). The hydrodynamic size of all formulations remained below 300 nm, which is suitable for a systemic administration route [29]. Interestingly, significant changes in the unloaded LNPs (uLNPs and F-uLNPs) were observed over time, while no changes were observed for CAS-loaded LNPs. Thus, these results suggest that the encapsulation of CAS may contribute to a higher stability of the nanoparticles. During the 8 weeks of study, the PDI and zeta potential showed values below 0.2 and -30 mV, respectively. These low values indicate that the developed LNPs do not tend to form aggregates under storage conditions.

The EE and LC of CAS-loaded LNPs were also measured over time. It is possible to observe that EE decreased to values below 10% for both CAS-LNPs and F-CAS-LNPs, after 8 weeks of study. For the latter, a significant decrease in EE was already observed at week 2. Consequently, the LC values observed at week 8 were significantly lower (<1%),

compared with week 0. The release of CAS from the nanoparticles is probably due to the amphipathic nature of this lipopeptide, allowing the molecule to diffuse through the lipidic matrix of the developed LNPs [30].

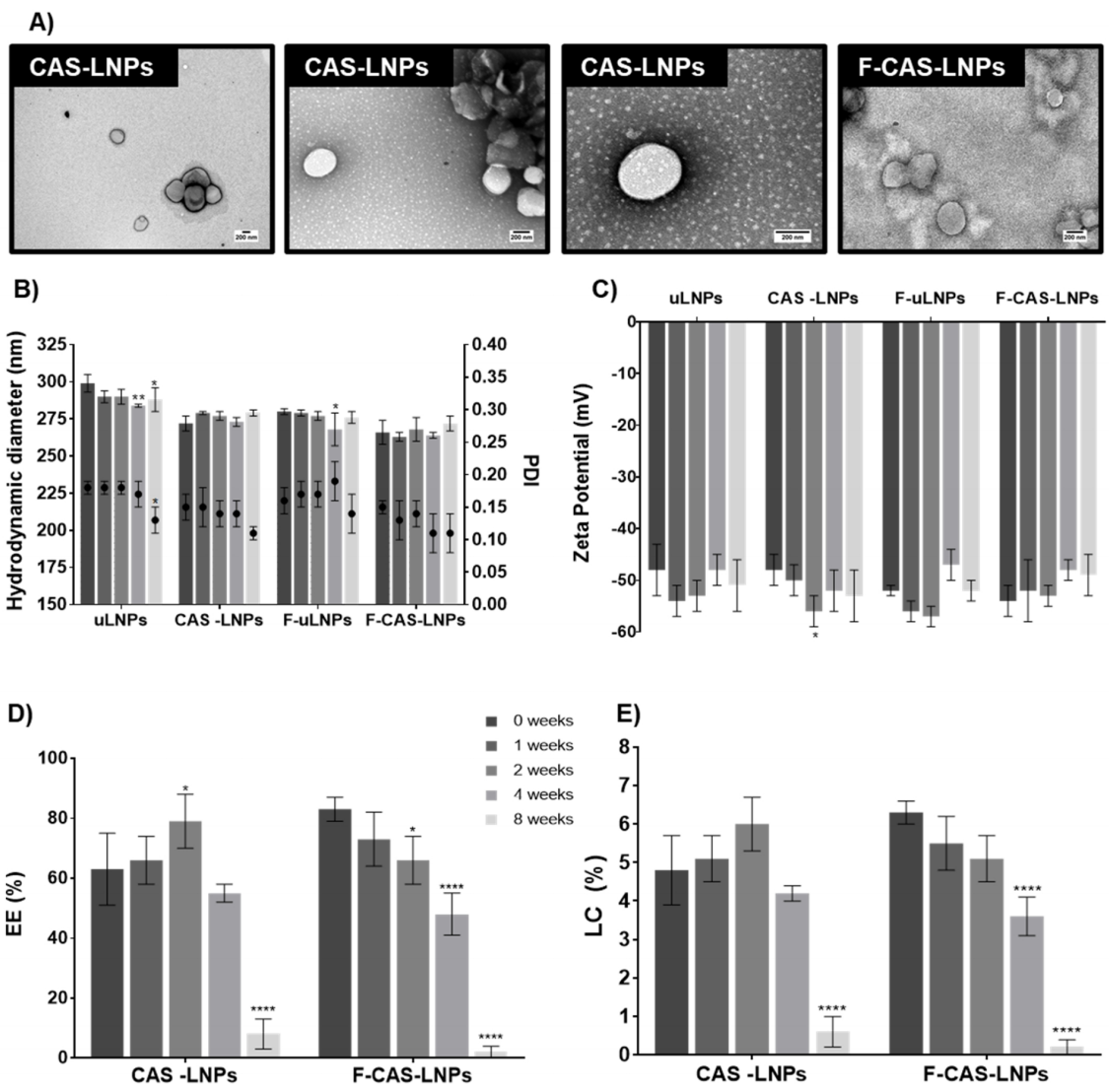


Figure 2: A) TEM images of the CAS-LNPs and the F-CAS-LNPs. CAS-LNPs images were acquired at the magnifications of 25 000× (left) ,50 000× (middle), and 100 000× (right), while F-CAS-LNPs image at 50 000×. **(B–E)** Characterization of the LNPs suspensions over 8 weeks, stored at 4ºC. **B)** Hydrodynamic diameter and PDI. The bars represent the hydrodynamic diameter (left y-axis) and the dots represent the PDI (left y-axis). **C)** Zeta potential. **D)** EE. **E)** LC. The parameters were evaluated at different time points (0, 1, 2, 4, and 8 weeks). The values are represented as the mean ± SD. *P<0.05, **P<0.01, ****P<0.0001, relatively to 0 weeks. Statistical analysis: two-way ANOVA, Dunnett's multiple comparisons test.

3.2 *In vitro* CAS release study

In vitro release studies are essential to give insights regarding to the pharmacokinetics of nanocarriers. The CAS release profile from the LNPs was assessed using the dialysis method at a pH 7.4 to simulate the physiological conditions of the bloodstream [20, 31]. The release profile of CAS-loaded LNPs (CAS-LNPs and F-CAS-LNPs) and free CAS is represented in **Figure S1**. For both non-functionalized and functionalized formulations it is possible to observe an initial burst profile, where around 20% of CAS is release within 30 mins of incubation. This result indicates that the non-encapsulated CAS was released to the dissolution medium during this period. After 5h of incubation, almost 60% of CAS was released, followed by a controlled and sustained release profile over 48h, for both formulations (CAS-LNPs and F-CAS-LNPs). At this time-point, almost 100% of CAS was release by the formulations, with the functionalized LNPs showing a slightly lower release percentage, comparing to the non-functionalized LNPs. This slower release at 48h may be due to steric effects promoted by the D-amino acids conjugates at the surface of the nanoparticles. As expected, 100% of free CAS was released in the first 3h of incubation.

Overall, the release profiles of the CAS-loaded formulations show that the developed LNPs have a controlled and sustained drug release over time, at physiological conditions. Thus, a controlled release profile may contribute to reduce the adverse side effects of CAS.

3.3 *In vitro* cytocompatibility studies

Prior antibacterial and antibiofilm efficacy assays, the cytocompatibility of the developed LNPs was evaluated using a fibroblast cell line and human red blood cells (**Figure 3**). At all tested concentrations, the LNPs and free CAS showed cell viability above 70% (**Figure 3A**), revealing no potential toxicity according to the ISO guidelines [32]. However, the LDH assay (**Figure 3B**) showed that at the two highest concentrations tested (32 and 64 µg ml^{-1} of CAS) both unloaded and CAS-loaded formulations exhibited significantly higher cytotoxicity, compared to the control (0 µg ml^{-1}). At a concentration of 16 µg ml^{-1}, free CAS exhibited cytotoxic effects toward the L929 fibroblast cell line. Hence, encapsulated CAS seems to have lower cytotoxicity than the free compound at the same concentration. This result suggests that not all encapsulated CAS was released from the nanoparticles and, therefore, the fibroblasts were exposed to lower concentrations of CAS over the studied time.

The developed formulations were also evaluated for their potential hemolytic activity (**Figure 3C** and **Figure S2**). At the lowest concentrations tested (4 and 8 µg ml^{-1} of CAS),

all formulations showed no significant differences in the hemolysis values, compared to the free compound. In fact, both free CAS and the developed LNPs showed a mean hemolysis value below 5%, with exception of F-uLNPs. At a CAS concentration of 16 µg ml^{-1}, it is possible to observe that all nanoformulations exhibited a significantly higher hemolytic activity compared to the free drug, with hemolysis values between 20 – 30%. Despite several literature reports claim that hemolysis values between 5 to 25% are of no concern [33, 34], the ASTM E2524-08 standard states that hemolysis percentages above 5% cause some damage to red blood cells. From these results, it seems that the hemolytic potential of the formulations is promoted by the vehicle itself, rather than the encapsulated drug. It is possible that the toxicity presented by the vehicle is due to the use of Tween 80 as a surfactant. This nonionic surfactant is widely used in the pharmaceutical industry. Nevertheless, several adverse side effects of Tween 80, such as hemolysis, have been reported [35].

Overall, the developed LNPs suspensions show a safe profile up to a CAS concentration of 8 µg ml^{-1}, with no observable toxic effects for either human fibroblasts and red blood cells.

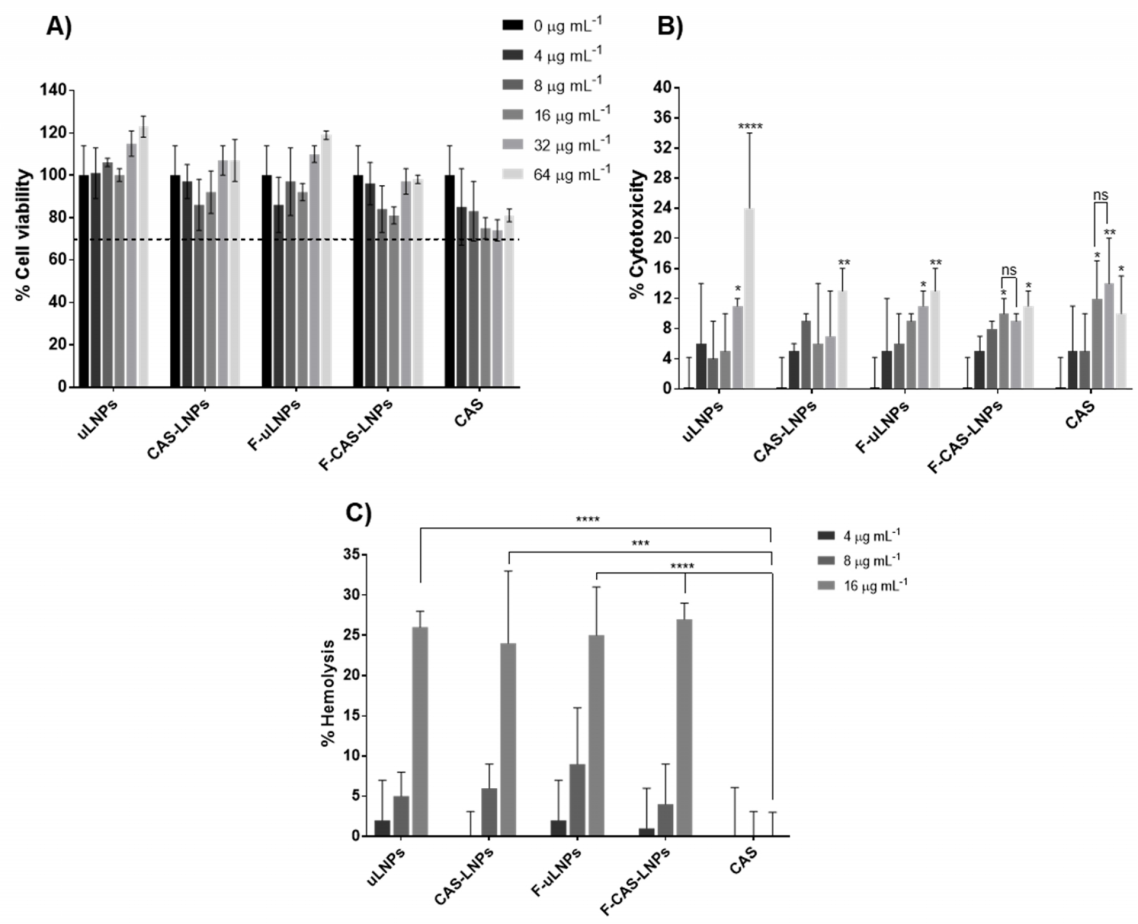


Figure 3: *In vitro* cytocompatibility studies. **A)** MTT and **B)** LDH assays using the fibroblast L929 cell line. In these assays, different concentrations of encapsulated and free CAS were assessed (0, 4, 8, 16, 32, and 64 µg ml^{-1}). Triton-100 (1%, v/v) and DMEM were used as negative and positive controls, respectively. **C)** Hemolysis assay. Encapsulated and free CAS at the CAS concentrations 4, 8, and 16 µg ml^{-1} were tested. For positive and negative controls, saline solution (0.85%, m/v) and triton-100 (1%, v/v) were used, respectively. All values are represented as mean ± SD. *P<0.05, **P<0.01, relatively to the positive control. ns, not significant; ***P<0.001, ****P<0.0001. Statistical analysis: two-way ANOVA, Tukey's multiple comparisons test.

3.4 *In vitro* antibacterial studies

The effect of the formulations on planktonic *S. aureus* was evaluated by determination of the MIC and MBC values for four strains: MRSA (ATCC 33591), ATCC 25923, ATCC 6538, and *Xen36*. At the tested CAS concentrations (0 to 64 µg ml^{-1}), no inhibition of planktonic bacterial growth was observed after treatment with the formulations, for all strains. For the free CAS, the MIC value was 32 µg ml^{-1} for all tested strains. The MBC value corresponded to the MIC, for the four strains. Although commonly used to treat fungal infections, recent studies report antimicrobial activity of CAS against bacterial strains [7, 8]. Siala *et al.* (2016)

reported MIC values between 80 and 160 µg ml^{-1} for several MRSA and MSSA strains [8]. In a more recent study, Sumiyoshi *et al.* (2020) observed that a CAS concentration of 50 µg ml^{-1} was bactericidal for both MRSA and multidrug-resistant *Pseudomonas aeruginosa* [7]. Thus, the MIC and MBC values obtained for free CAS are supported by previously reported studies. Nevertheless, encapsulated CAS did not show an inhibition of bacterial growth at the tested concentrations. This outcome corroborates the hypothesis that not all encapsulated CAS was released from the vehicle at the tested conditions.

3.5 *In vitro* antibiofilm studies

3.5.1 Microtiter biofilm model: biofilm viability study

The antibiofilm efficiency of the developed formulations against *S. aureus* strains was evaluated by determination of the biofilm viability, using the XTT assay (**Figure 4**). For this purpose, the LNPs and free CAS were tested at CAS concentrations between 0 and 64 µg ml^{-1}. At a cytocompatible concentration (8 µg ml^{-1}), only F-CAS-LNPs showed a significant reduction of bacterial viability in MRSA biofilms, compared to the untreated control. However, both unloaded and loaded LNPs showed a higher antibiofilm efficiency against biofilms formed by the remaining three methicillin-susceptible *S. aureus* strains. These results may be a consequence of the increased virulence of MRSA strains, compared to the methicillin-susceptible ones. The presence of resistance genes in MRSA strains promotes their antibiotic resistance, leading to severe infections with high morbidity and mortality rates [36]. Free CAS was also tested against the *S. aureus* biofilms, revealing a significant effect on bacterial viability at the highest concentrations, namely 32 and 64 µg ml^{-1} of CAS. Thus, the main effect of the LNPs suspensions on biofilm viability seems to be associated to the composition of the vehicle. This bactericidal effect may be promoted by the presence of Tween 80 in the formulations, which was used as a surfactant to produce the LNPs. In fact, this compound has antibacterial and antibiofilm properties described against a wide variety of bacterial species, including *S. aureus* strains [37-39]. In addition, biofilm biomass was also assessed for the *S. aureus* strains in study (**Figure S3**). Overall, the crystal violet assay corroborates the results obtained from the XTT assay, with a higher efficacy of the formulations observed for methicillin-susceptible strains.

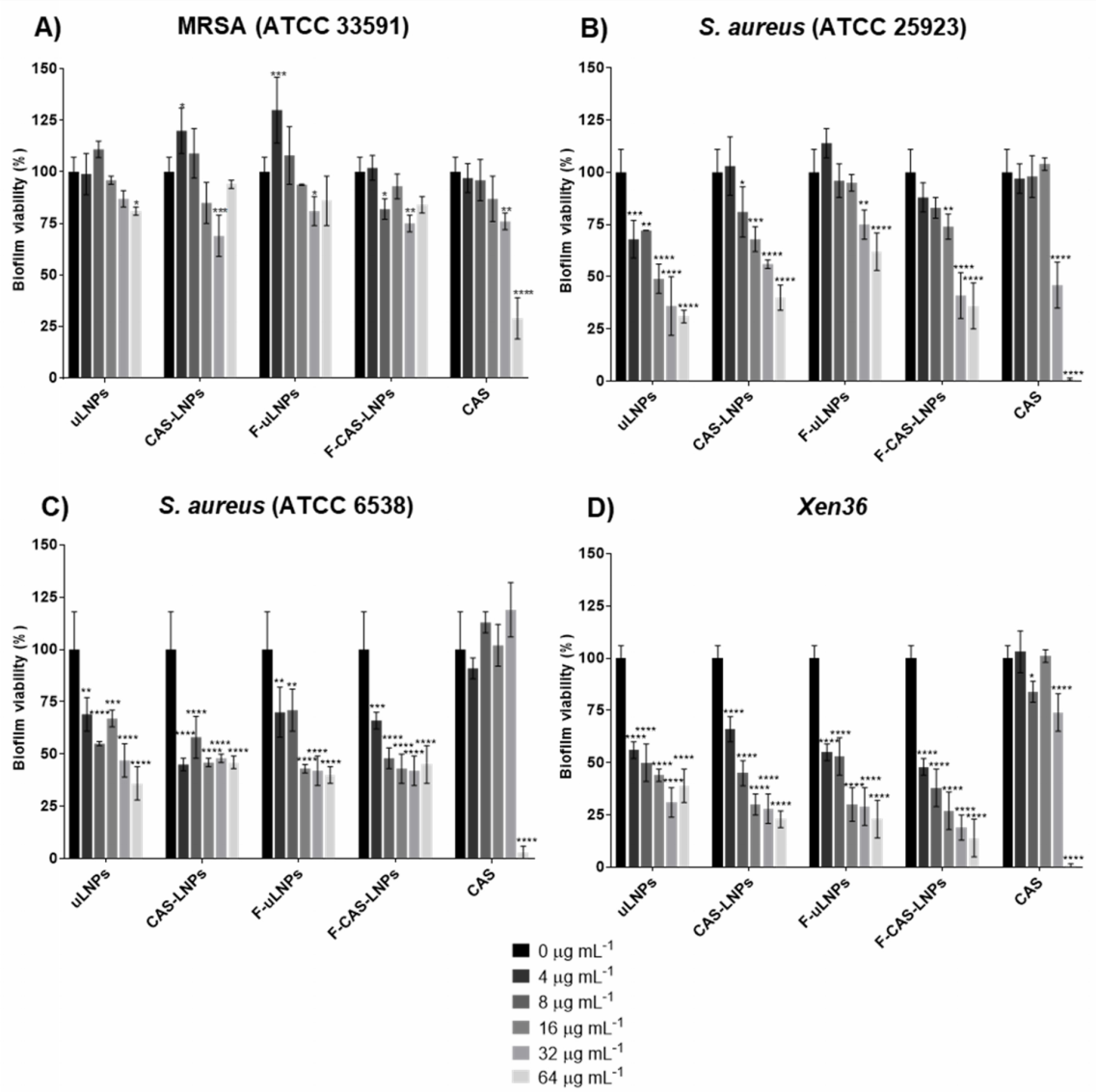


Figure 4: Quantification of biofilm viability by the XTT assay, after a 24h treatment with LNPs or free CAS at the CAS concentrations of 0, 4, 8, 16, 32, and 64 µg ml^{-1}. Prior to the treatment, the biofilms of **A)** MRSA ATCC 33591, **B)** *S. aureus* ATCC 25923, **C)** *S. aureus* ATCC 6538, and **D)** the bioluminescent strain *Xen36*, were grown in 96-well plates for 24h. Untreated biofilms (0 µg ml^{-1} of CAS) were used as a positive control. The values are represented as the mean ± SD. *P<0.05, **P<0.01, ***P<0.001, ****P<0.0001 relatively to 0 µg ml^{-1}. Statistical analysis: two-way ANOVA, Dunnett's multiple comparisons test.

3.5.2 Catheter biofilm model: combined therapy of CAS-loaded and MOX-loaded nanosystems

To evaluate the possible synergistic potential of the developed LNPs with antibiotic-loaded nanoparticles, the catheter biofilm model was used. The combination of the two

nanosystems was evaluated in three *S. aureus* strains (**Figure 5**). For both the MRSA strain and *Xen 36*, the combination of the functionalized loaded nanoparticles (F-CAS-LNPs and F-MOX-MLNs) showed the highest potential in reducing the biofilm viability, compared to the untreated control. This combination suggests potential synergistic effects between the two formulations, since a significant viability reduction is observed, comparing to F-CAS-LNPs and F-MOX-MLNs alone. For the strong *S. aureus* biofilm-forming strain (ATCC 6538), F-MOX-MLNs in combination with F-CAS-LNPs or free CAS showed a very significant reduction of biofilm viability, compared to the untreated control ($P<0.0001$) and the formulations alone ($P<0.001$). For this strain, neither F-MOX-MLNs, F-CAS-LNPs, or free CAS alone showed any statistical difference to the untreated control. This outcome suggests that encapsulated and free CAS may contribute to the disruption of the biofilm matrix, exposing a higher number of bacterial cells to the antibiotic. In fact, the potential synergistic effect of CAS and MOX against *S. aureus* biofilms was previously reported [8]. However, in the reported study, higher concentrations of CAS (40 µg ml^{-1}) and MOX (10 µg ml^{-1}) were required to observe significant biofilm viability reduction compared to the untreated control [8]. The effect of caspofungin against bacterial biofilms is also described in other studies from the literature [7, 40].

Overall, the results showed that a therapeutic approach combining nanosystems loading matrix-disruptive agents, such as caspofungin, and antibiotics, is a step forward toward the eradication of biofilms.

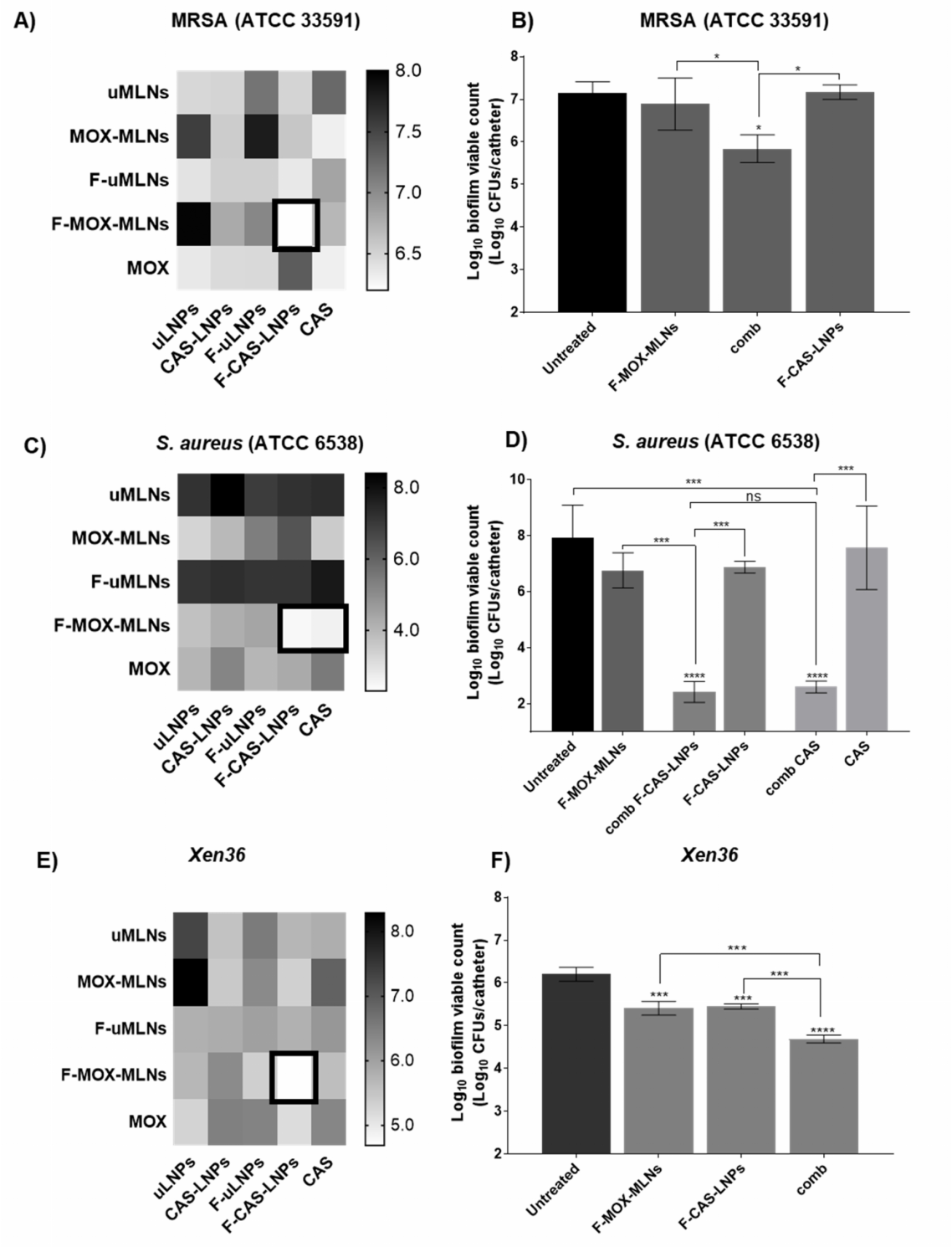


Figure 5: Biofilm viable count of **(A-B)** MRSA ATCC 33591, **(C-D)** *S. aureus* ATCC 6538, and **(E-F)** *Xen36* biofilms grown *in vitro* in catheters after treatment with the combination of lipid nanosystems. **(A, C, D)** Heat maps represent the effect of the combination of CAS- and MOX-loaded nanosystems on the biofilm viable count (represented as Log_{10} CFUs/catheter). The treatment combinations with lower viable count are highlighted (black squares). **(B, F)** F-MOX-MLNs and F-CAS-LNPs alone and in combination (comb). **D)** F-MOX-MLNs alone and in combination with F-CAS-LNPs (comb F-CAS-LNPs) or CAS (comb CAS). F-CAS-LNPs and CAS alone are also represented. The

developed LNPs were assessed at a CAS concentration of 8 µg ml^{-1}. MOX-loaded nanosystems were tested at a MOX concentration of 0.5 µg ml^{-1}, except for the *S. aureus* ATCC 6538 (1 µg ml^{-1} of MOX). Untreated biofilms were used as a positive control. The values are represented as the mean ± SD for three catheters. *P<0.05, ***P<0.001, ****P<0.0001, relatively to the untreated biofilms. ns, not significant; *P<0.05, ***P<0.001. Statistical analysis: one-way ANOVA, Tukey's multiple comparisons test.

3.6 *In vivo* biodistribution study

After intraperitoneal administration of both non-functionalized and functionalized LNPs and MLNs loaded with Cy7, the animals were imaged at two different time points (1h and 24h post-administration) to assess the biodistribution of the formulations. Cy7-loaded LNPs (Cy7-LNPs and F-Cy7-LNPs) have the same lipid composition of CAS-loaded LNPs (CAS-LNPs and F-CAS-LNPs), while Cy7-loaded MLNs (Cy7-MLNs and F-Cy7-MLNs) have the same lipid matrix of MOX-loaded MLNs (MOX-MLNs and F-MOX-MLNs). At 1h post-administration, it is possible to observe that all formulations accumulated in a specific abdominal region that corresponds to the place where the infected catheters were previously placed (**Figure 6A**). The fast diffusion of the lipid nanosystems across the peritoneal membrane has been also recently reported by Mannucci *et al.* (2020), which observed a rapid rise of the fluorescence signal in the whole animal body only 30 mins after intraperitoneal injection [41]. At 24h post-administration, a stronger fluorescent signal in the region of the implanted catheters is observable by optical imaging. For the Cy7-loaded LNPs, it is possible to observe significant differences between functionalized and non-functionalized formulations at both 1h and 24h post-administration, with a higher accumulation of functionalized nanoparticles in the region surrounding the biofilm (**Figure 6B**). Regarding Cy7-loaded MLNs, a significantly higher accumulation of F-Cy7-MLNs compared to Cy7-MLNs is showed in the surroundings of the infected catheters at 1h post-administration (**Figure 6C**). However, this difference is no longer observed after 24h. The higher accumulation of functionalized nanoparticles is partially due to the PEGylation of these carriers, which avoids recognition and clearance by the host immune system, leading to an increased circulation time in the bloodstream [42, 43]. In addition, the use of D-amino acids in the functionalization of the nanoparticles contributes to a higher accumulation in the region of the biofilm [14].

The *ex vivo* acquisition of isolated catheters corroborated the previous results, with a higher accumulation of F-Cy7-LNPs in the catheter pieces comparing to the corresponding non-functionalized formulations (**Figure 6D**). Although F-Cy7-MLNs show a higher fluorescent

signal than Cy7-MLNs, it is not statistically significant. The accumulation of nanoparticles in the spleen, kidneys, and liver was also evaluated *ex vivo* (**Figure S4**). At 24h post-administration, all formulations were mainly accumulated in the kidneys and liver, while a considerably lower signal was observed in the spleen. These findings revealed that after 24h, a high number of nanoparticles was cleared by the reticuloendothelial system (RES), which led to accumulation in the liver [43]. The high intensity of the fluorescence signal in the kidneys also shows that these nanocarriers can be eliminated by the renal clearance pathway, which substantially reduces the potential toxicity of the nanoparticles, compared with the RES clearance. Thus, the high renal clearance observed for the developed LNPs and MLNs may suggest that these nanosystems present a good biocompatibility profile [44].

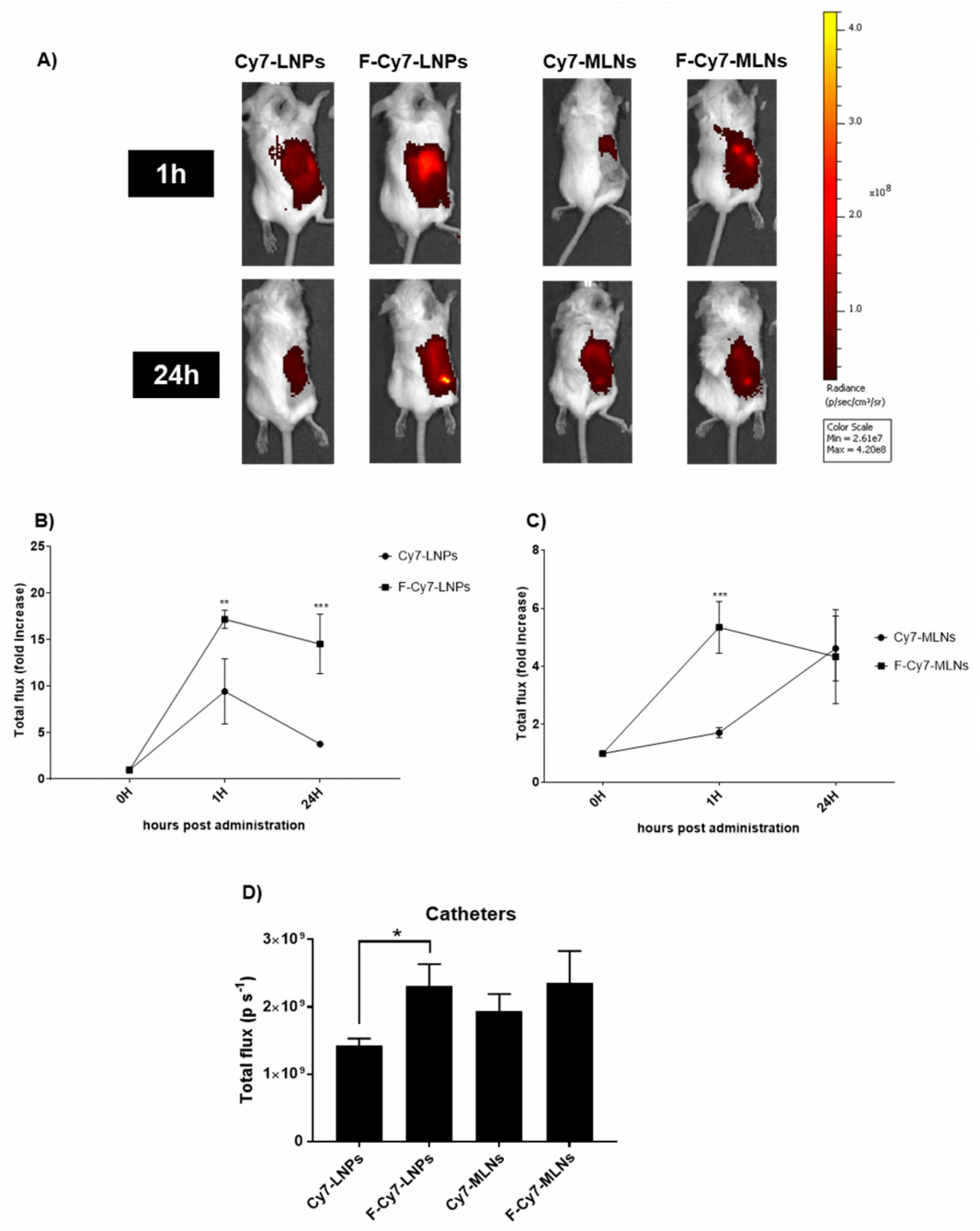


Figure 6: *In vivo* biodistribution study. **A)** Real-time imaging of whole body animals at different time-points (1h and 24h) after intraperitoneal administration of Cy7-loaded LNPs or Cy7-loaded MLNs (non-functionalized or functionalized). Graph of fluorescence signal intensity expressed as *n*-fold increase with respect to 0h (prior administration), at 1h and 24h post-administration of **B)** Cy7-loaded LNPs (Cy7-LNPs and F-Cy7-LNPs) and **C)** Cy7-loaded MLNs (Cy7-MLNs and F-Cy7-MLNs). The values are represented as the mean ± SD for three animals. **P<0.001, ***P<0.001, relatively to 0h. Statistical analysis: two-way ANOVA, Sidak's multiple comparisons test. **D)** Fluorescence signal intensity of the implanted catheters acquired *ex vivo* at 24h post-administration of the Cy7-loaded formulations. Fluorescent signals are expressed in photons per second (p s^{-1}). The values are

represented as the mean ± SD for three animals (each implanted with four catheters). *P<0.05. Statistical analysis: two-way ANOVA, Tukey's multiple comparisons test.

3.7 *In vivo* antibiofilm efficacy study

To evaluate the *in vivo* efficacy of CAS-loaded and MOX-loaded nanosystems alone or in combination, mice were implanted with *Xen36*-infected catheters and further treated for 7 days. The biofilms formed *in vivo* were monitored using bioluminescence imaging from the day 1 (prior treatment) to the day 8 after implantation (**Figure 7 A-B and Figure S5**). Untreated mice showed a signal intensity linear from day 5 to day 8, while mice treated with the combination of F-CAS-LNPs with F-MOX-MLNs, or the combination of the free compounds exhibited a decrease in signal intensity over time. At day 8 post-implantation, a significantly lower bioluminescence intensity signal was observed for both treatments, compared with the untreated control. At this time point, implanted catheters were recovered from sacrificed mice to quantify biofilm viability (**Figure 7C**). Only the combination of both nanosystems (F-CAS-LNPs and F-MOX-MLNs) revealed a significant decrease in the viable count compared to the untreated control. However, the treatment with both nanosystems combined did not show significant difference compared to the treatment with the combination of the free compounds (CAS + MOX).

The potential dissemination of bacterial cells into vital organs after treatment was also assessed, by quantifying the bacterial viability in the spleen, kidneys, and liver (**Figure 7 D-F**). Interestingly, only the mice treated with F-CAS-LNPs in combination with F-MOX-MLNs did not show dissemination in these organs. The nanosystems alone and the free compounds alone or in combination (CAS + MOX) promoted dissemination of bacterial cells into the three organs, with a higher bacterial load observed in the liver. The dissemination of bacteria to these organs is highly concerning since it may contribute to the survival of the pathogen. When *S. aureus* cells reach the liver, they are rapidly phagocyted by Kupffer cells. However, it is reported that part of the bacterial cells may survive and proliferate intracellularly, remaining undetected by neutrophils [45, 46]. Additionally, intracellular *S. aureus* are protected from antibiotic activity, since most antibiotics do not reach the intraphagocyte niche [45]. Eventually, Kupffer cells lyse, leading to the release of bacteria into the circulation. This process promotes the dissemination of *S. aureus* to other organs, such as kidneys, where they can form abscesses [45, 46].

Overall, these results suggest that the combination of F-CAS-LNPs with F-MOX-MLNs is a potentially safe antibiofilm therapeutic approach, which does not promote the dissemination of bacterial cells from the biofilm into vital organs.

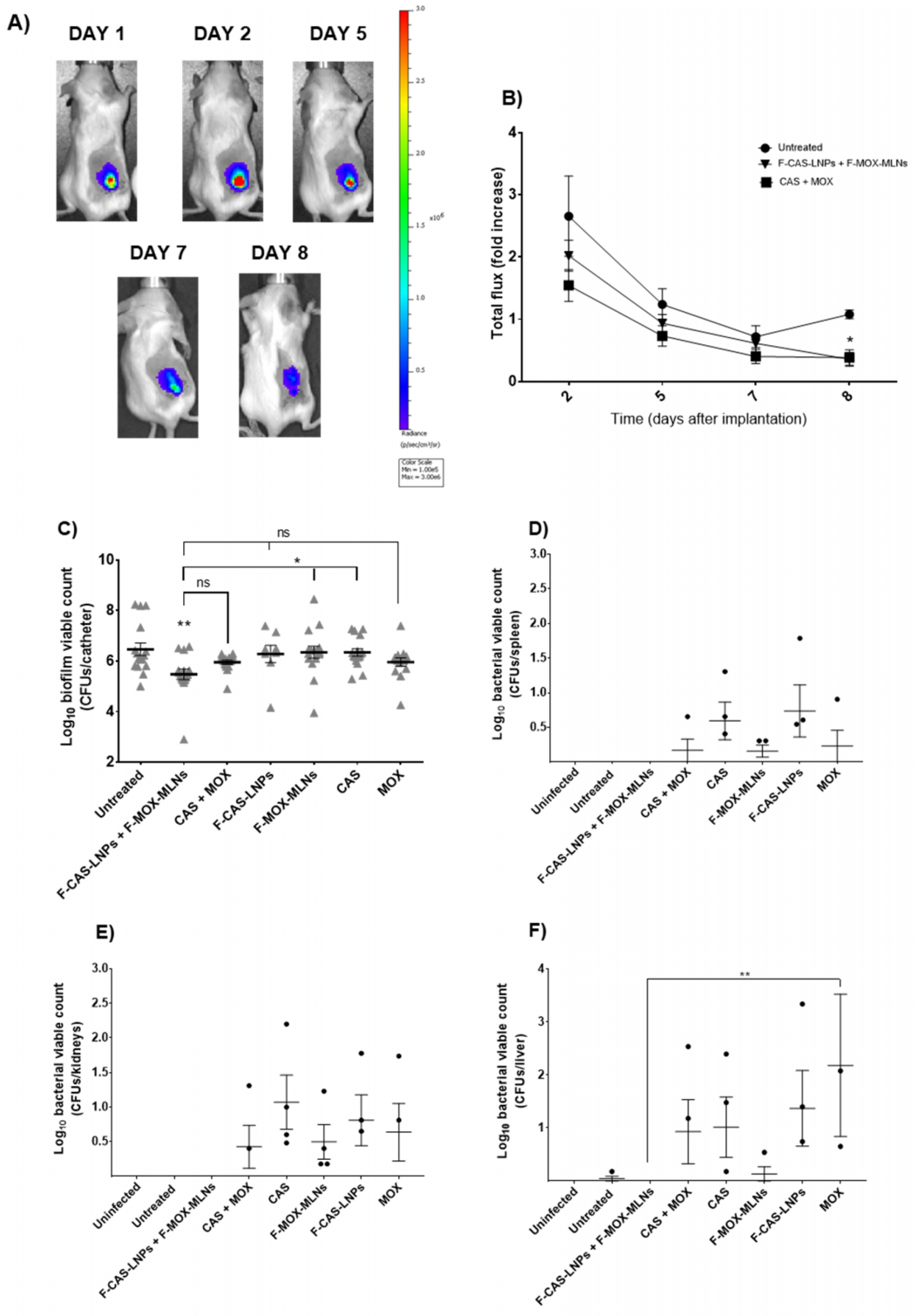


Figure 7: *In vivo* antibiofilm activity of the combination of CAS-loaded and MOX-loaded nanosystems against the bioluminescent strain *Xen36*. Infected catheters were implanted at day 0 in the back of mice treated 24h after implantation and for the following 7 days. **A)** Representative bioluminescence images at different time points (1, 2, 5, 7, and 8 days after implantation) of the group treated with the combination of F-CAS-LNPs with F-MOX-MLNs. At day 1, mice were imaged prior to the treatment. **B)** Graph of bioluminescence signal intensity expressed as *n*-fold increase with respect to day 1 after

implantation (prior treatment), at different time points (2, 5, 7, and 8 days after implantation). The values are represented as the mean ± SEM for four animals. *P<0.05 relatively to the untreated control at the same time point. Statistical analysis: one-way ANOVA, Dunnett's multiple comparisons test. **C)** Biofilm viable count retrieved from implanted catheters after 7 days of treatment. The catheters were recovered after sacrifice on day 8 after implantation. The values are represented as the mean ± SEM for four animals (each implanted with four catheters). **P<0.01, relatively to the untreated control. ns, not significant; *P<0.05. Statistical analysis: one-way ANOVA, Tukey's multiple comparisons test. Bacterial viable count in **D)** spleen, **E)** kidneys, and **F)** liver of mice. The organs were collected at day 8 after implantation. ** P<0.01. Statistical analysis: two-way ANOVA, Tukey's multiple comparisons test.

4. Conclusions

The CAS-loaded LNPs developed in this work presented a spherical morphology, with a mean hydrodynamic size below 300 nm, a low PDI (<0.2), and a highly negative zeta potential, which reveals a low tendency to form aggregates. The EE and LC were satisfactorily high during 2 weeks of storage, with values above 60% and 4%, respectively. At 8 weeks under storage conditions (4ºC), most of the encapsulated CAS was released from the nanoparticles by diffusion. In addition, the CAS-loaded formulations showed a controlled and sustained release profile under physiological conditions (pH 7.4).

The cytocompatibility of the developed LNPs was evaluated against fibroblasts (L929 cell line) and human red blood cells. Cell viability studies revealed that the formulations did not exhibit cytotoxic effects against fibroblasts up to a CAS concentration of 16 μg ml^{-1}. However, at this concentration, the formulations showed a significantly higher hemolytic activity compared to the free compound. Hence, the developed LNPs showed a safe profile up to a CAS concentration of 8 μg ml^{-1}.

The *in vitro* antibiofilm activity of the CAS-loaded LNPs was firstly evaluated using the microtiter plate biofilm model. At a cytocompatible concentration (8 μg ml^{-1} of CAS), only the functionalized CAS-loaded formulation (F-CAS-LNPs) showed a significant biofilm viability reduction against MRSA. However, for the methicillin-susceptible strains, all formulations significantly reduced the viability at the same concentration. It is hypothesized that this difference between the strains is mainly due to the increased virulence of the MRSA strain, compared to the remaining studied strains, leading to lower efficiency of the LNPs. The biofilm viability after treatment with CAS-loaded LNPs alone or in combination with MOX-loaded MLNs was further evaluated in an *in vitro* catheter biofilm model. Interestingly, for the three strains studied, the combination of functionalized loaded nanoparticles (F-CAS-

LNPs and F-MOX-MLNs) showed the highest reduction in the biofilm viable count. The potential synergistic effect between these two nanosystems was further confirmed by *in vivo* efficacy studies. The combination of F-CAS-LNPs with F-MOX-MLNs showed a decrease in the biofilm viable count of implanted catheters recovered from mice, compared to the untreated control. Besides, the treatment with this combination showed no signs of dissemination of bacterial cells into vital organs, such as spleen, kidneys, and liver. Additionally, *in vivo* biodistribution studies showed that the two nanosystems reached the targeted site, accumulating in the region of the biofilm, even 24h post-administration. Besides, a high renal clearance observed for the developed nanosystems suggests a good biocompatibility profile. Overall, this work presents a novel multi-target strategy combining functionalized nanosystems encapsulating matrix-disruptive (CAS) and bactericidal (MOX) agents, as a tool towards the improvement of a therapy against *S. aureus* biofilms.

Acknowledgements

This work was supported by the project PTDC/NANMAT/31444/2017, financed by FCT/MCTES e FEDER through Programa Operacional Competitividade e Internacionalização - COMPETE 2020. RMP and CN are thankful to Fundação para a Ciência e Tecnologia (FCT) for the Ph.D. Grant [SFRH/BD/130319/2017] and the investigator Grant [IF/00293/2015], respectively. PVD is thankful to the Fund for Scientific Research Flanders (FWO grant WO.009.16N). The authors RMP, CN, and SR acknowledge to the institution LAQV - Laboratório Associado para a Química Verde (UIDB/50006/2020). RMP also acknowledges the Programa Operacional Capital Humano (POCH), specifically the BiotechHealth Programme (Doctoral Programme on Cellular and Molecular Biotechnology Applied to Health Sciences). The authors also thank Manuela Barros for administrative and technical support.

References

1. Otto, M., *Staphylococcal biofilms.* Curr. Top. Microbiol. Immunol., 2008. **322**: p. 207-28,
2. Tacconelli, E., et al., *Discovery, research, and development of new antibiotics: the WHO priority list of antibiotic-resistant bacteria and tuberculosis.* Lancet. Infect. Dis., 2018. **18**(3): p. 318-27, 10.1016/s1473-3099(17)30753-3
3. Pinto, R.M., et al., *Impact of Nanosystems in Staphylococcus aureus Biofilms Treatment.* FEMS Microbiol. Rev., 2019. **43**(6): p. 622-641, 10.1093/femsre/fuz021
4. Pinto, R.M., et al., *Innovative strategies toward the disassembly of the EPS matrix in bacterial biofilms.* Front. Microbiol., 2020. **11**(952), 10.3389/fmicb.2020.00952
5. Bhattacharya, M., et al., *Prevention and treatment of Staphylococcus aureus biofilms.* Expert Rev. Anti-infect. Ther., 2015. **13**(12): p. 1499-516, 10.1586/14787210.2015.1100533
6. McCormack, P.L. and C.M. Perry, *Caspofungin.* Drugs, 2005. **65**(14): p. 2049-2068, 10.2165/00003495-200565140-00009
7. Sumiyoshi, M., et al., *Novel and potent antimicrobial effects of caspofungin on drug-resistant Candida and bacteria.* Scientific Reports, 2020. **10**(1): p. 17745, 10.1038/s41598-020-74749-8
8. Siala, W., et al., *The Antifungal Caspofungin Increases Fluoroquinolone Activity Against Staphylococcus aureus Biofilms by Inhibiting N-Acetylglucosamine Transferase.* Nat. Commun., 2016. **7**: p. 1-15, 10.1038/ncomms13286
9. O'Gara, J.P., *ica and beyond: biofilm mechanisms and regulation in Staphylococcus epidermidis and Staphylococcus aureus.* FEMS Microbiol Lett, 2007. **270**(2): p. 179-188, 10.1111/j.1574-6968.2007.00688.x
10. Bellmann, R. and P. Smuszkiewicz, *Pharmacokinetics of antifungal drugs: practical implications for optimized treatment of patients.* Infection, 2017. **45**(6): p. 737-779, 10.1007/s15010-017-1042-z
11. Stass, H. and D. Kubitza, *Pharmacokinetics and elimination of moxifloxacin after oral and intravenous administration in man.* Journal of Antimicrobial Chemotherapy, 1999. **43**(suppl_2): p. 83-90, 10.1093/jac/43.suppl_2.83
12. Duan, Y., et al., *A brief review on solid lipid nanoparticles: Part and parcel of contemporary drug delivery systems.* RSC Advances, 2020. **10**(45): p. 26777-26791,
13. Nafee, N., *Nanocarriers Against Bacterial Biofilms: Current Status and Future Perspectives*, in *Nanotechnology in Diagnosis, Treatment and Prophylaxis of Infectious Diseases*, K. Kon, Editor. 2015, Academic Press: Boston. p. 167-189.

14. Hochbaum, A.I., et al., *Inhibitory Effects of D-Amino Acids on Staphylococcus aureus Biofilm Development.* J. Bacteriol., 2011. **193**(20): p. 5616-5622, 10.1128/JB.05534-11
15. Zolnik, B.S., et al., *Nanoparticles and the Immune System.* Endocrinology, 2010. **151**(2): p. 458-465, 10.1210/en.2009-1082
16. Pinto, R.M., et al., *N-acetyl-l-cysteine-loaded nanosystems as a promising therapeutic approach toward the eradication of Pseudomonas aeruginosa biofilms.* ACS Applied Materials & Interfaces, 2021. **13**(36): p. 42329-42343, 10.1021/acsami.1c05124
17. Pribaz, J.R., et al., *Mouse model of chronic post-arthroplasty infection: noninvasive in vivo bioluminescence imaging to monitor bacterial burden for long-term study.* J Orthop Res, 2012. **30**(3): p. 335-340, 10.1002/jor.21519
18. Francis, K.P., et al., *Monitoring bioluminescent Staphylococcus aureus infections in living mice using a novel luxABCDE construct.* Infect Immun, 2000. **68**(6): p. 3594-3600, 10.1128/iai.68.6.3594-3600.2000
19. Schwartz, M., W. Kline, and B. Matuszewski, *Determination of a cyclic hexapeptide (L-743 872), a novel pneumocandin antifungal agent in human plasma and urine by high-performance liquid chromatography with fluorescence detection.* Analytica chimica acta, 1997. **352**(1-3): p. 299-307,
20. Lopes-de-Campos, D., et al., *Delivering Amoxicillin at the Infection Site - a Rational Design through Lipid Nanoparticles.* Int. J. Nanomedicine, 2019. **14**: p. 2781-2795, 10.2147/ijn.S193992
21. Standardization, I.O.f., *International Standard ISO 10993-5*, in *Biological evaluation of medical devices–Part 5: tests for in vitro cytotoxicity*. 2009: Geneva, Switzerland,
22. Guo, Q., et al., *Functional Silver Nanocomposites as Broad-Spectrum Antimicrobial and Biofilm-Disrupting Agents.* ACS Appl. Mater. Interfaces, 2017. **9**(20): p. 16834-16847, 10.1021/acsami.7b02775
23. Wiegand, I., K. Hilpert, and R.E. Hancock, *Agar and Broth Dilution Methods to Determine the Minimal Inhibitory Concentration (MIC) of Antimicrobial Substances.* Nat. Protoc., 2008. **3**(2): p. 163,
24. Vande Velde, G., et al., *Bioluminescence imaging increases in vivo screening efficiency for antifungal activity against device-associated Candida albicans biofilms.* Int J Antimicrob Agents, 2018. **52**(1): p. 42-51, 10.1016/j.ijantimicag.2018.03.007
25. Vande Velde, G., et al., *Towards non-invasive monitoring of pathogen-host interactions during Candida albicans biofilm formation using in vivo bioluminescence.* Cell Microbiol, 2014. **16**(1): p. 115-130, 10.1111/cmi.12184

26. Stepanovic, S., et al., *A modified microtiter-plate test for quantification of staphylococcal biofilm formation.* J Microbiol Methods, 2000. **40**(2): p. 175-179, 10.1016/s0167-7012(00)00122-6
27. Kucharíková, S., et al., *Candida albicans biofilm development on medically-relevant foreign bodies in a mouse subcutaneous model followed by bioluminescence imaging.* Journal of visualized experiments : JoVE, 2015(95): p. 52239-52239, 10.3791/52239
28. Blanco, E., H. Shen, and M. Ferrari, *Principles of Nanoparticle Design for Overcoming Biological Barriers to Drug Delivery.* Nat. biotechnol., 2015. **33**(9): p. 941-951, 10.1038/nbt.3330
29. Singh, R. and J.W. Lillard, Jr., *Nanoparticle-Based Targeted Drug Delivery.* Exp. Mol. Pathol., 2009. **86**(3): p. 215-223, 10.1016/j.yexmp.2008.12.004
30. Deresinski, S.C. and D.A. Stevens, *Caspofungin.* Clin Infect Dis, 2003. **36**(11): p. 1445-1457, 10.1086/375080
31. Neves, A.R., J.F. Queiroz, and S. Reis, *Brain-targeted delivery of resveratrol using solid lipid nanoparticles functionalized with apolipoprotein E.* Journal of Nanobiotechnology, 2016. **14**(1): p. 27, 10.1186/s12951-016-0177-x
32. ISO, *10993-5. Biological evaluation of medical devices–Part 5: tests for in vitro cytotoxicity.* Geneva, Switzerland: International Organization for Standardization, 2009,
33. Amin, K. and R.M. Dannenfelser, *In vitro Hemolysis: Guidance for the Pharmaceutical Scientist.* J. Pharm. Sci., 2006. **95**(6): p. 1173-1176, 10.1002/jps.20627
34. Neun, B.W. and M.A. Dobrovolskaia, *Method for Analysis of Nanoparticle Hemolytic Properties in vitro.* Methods Mol. Biol., 2011. **697**: p. 215-224, 10.1007/978-1-60327-198-1_23
35. Sun, H., et al., *Component-Based Biocompatibility and Safety Evaluation of Polysorbate 80.* RSC Adv., 2017. **7**(25): p. 15127-15138,
36. Turner, N.A., et al., *Methicillin-resistant Staphylococcus aureus: an overview of basic and clinical research.* Nature Reviews Microbiology, 2019. **17**(4): p. 203-218, 10.1038/s41579-018-0147-4
37. Ueda, Y., et al., *Inhibitory Effects of Polysorbate 80 on MRSA Biofilm Formed on Different Substrates Including Dermal Tissue.* Sci. Rep., 2019. **9**(1): p. 3128, 10.1038/s41598-019-39997-3
38. Toutain-Kidd, C.M., et al., *Polysorbate 80 Inhibition of Pseudomonas aeruginosa Biofilm Formation and its Cleavage by the Secreted Lipase LipA.* Antimicrob. Agents Chemother., 2009. **53**(1): p. 136-145, 10.1128/aac.00500-08

39. Sloup, R.E., et al., *Polysorbates prevent biofilm formation and pathogenesis of Escherichia coli O104:H4.* Biofouling, 2016. **32**(9): p. 1131-1140, 10.1080/08927014.2016.1230849
40. Fernandes, L., et al., *Caspofungin and Polymyxin B Reduce the Cell Viability and Total Biomass of Mixed Biofilms of Carbapenem-Resistant Pseudomonas aeruginosa and Candida spp.* Frontiers in Microbiology, 2020. **11**(3177), 10.3389/fmicb.2020.573263
41. Mannucci, S., et al., *A correlative imaging study of in vivo and ex vivo biodistribution of solid lipid nanoparticles.* Int J Nanomedicine, 2020. **15**: p. 1745-1758, 10.2147/ijn.S236968
42. Jokerst, J.V., et al., *Nanoparticle PEGylation for Imaging and Therapy.* Nanomedicine (Lond), 2011. **6**(4): p. 715-728, 10.2217/nnm.11.19
43. Ernsting, M.J., et al., *Factors controlling the pharmacokinetics, biodistribution and intratumoral penetration of nanoparticles.* J Control Release, 2013. **172**(3): p. 782-794, 10.1016/j.jconrel.2013.09.013
44. Du, B., M. Yu, and J. Zheng, *Transport and interactions of nanoparticles in the kidneys.* Nature Reviews Materials, 2018. **3**(10): p. 358-374, 10.1038/s41578-018-0038-3
45. Pidwill, G.R., et al., *The role of macrophages in Staphylococcus aureus infection.* Frontiers in immunology, 2021. **11**: p. 620339-620339, 10.3389/fimmu.2020.620339
46. Surewaard, B.G., et al., *Identification and treatment of the Staphylococcus aureus reservoir in vivo.* J Exp Med, 2016. **213**(7): p. 1141-1151, 10.1084/jem.20160334

Supporting Information

Caspofungin-loaded nanoparticles as an adjuvant to improve the nanoantibiotics activity against *Staphylococcus aureus* biofilms

1. In vitro CAS release study

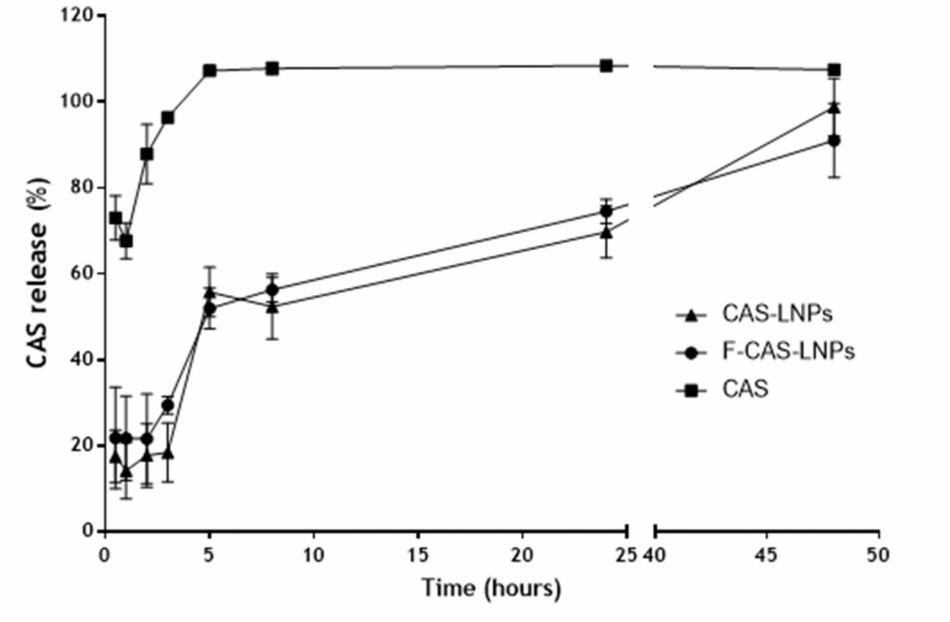


Figure S1: Cumulative CAS release profile of the non-functionalized (CAS-LNPs) and the functionalized (F-CAS-LNPs) formulations. The profile of the free CAS is also represented. The release was assessed in PBS (pH 7.4), at 37ºC. The values are represented as the mean ± SD.

2. *In vitro* biocompatibility studies: hemolysis assay

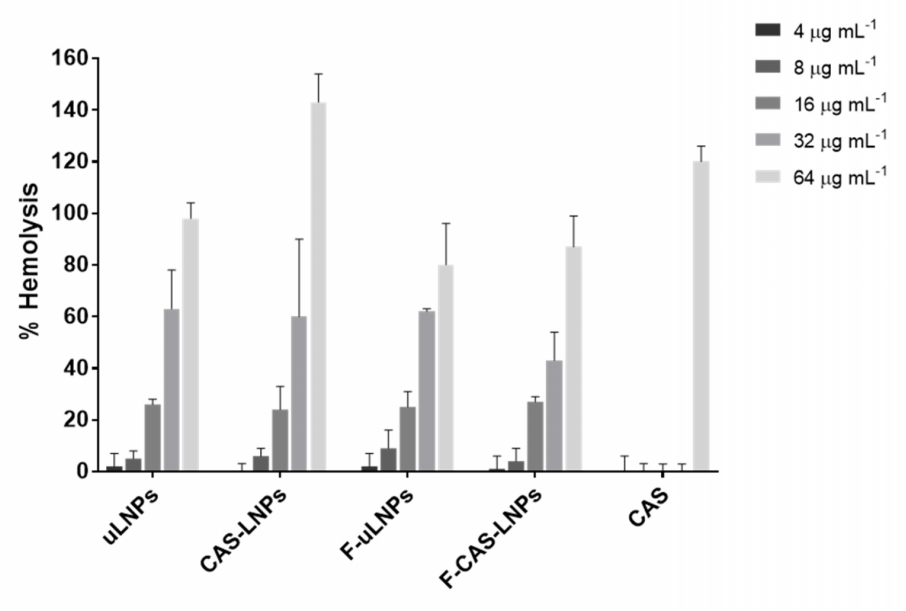


Figure S2: Evaluation of the hemolytic activity of the developed LNPs and free CAS. The LNPs and free compound at the CAS concentrations 4, 8, 16, 32, and 64 μg ml^{-1} were tested. For positive and negative controls, saline solution (0.85%, m/v) and triton-100 (1%, v/v) were used, respectively.

3. In vitro antibiofilm activity: biofilm biomass study

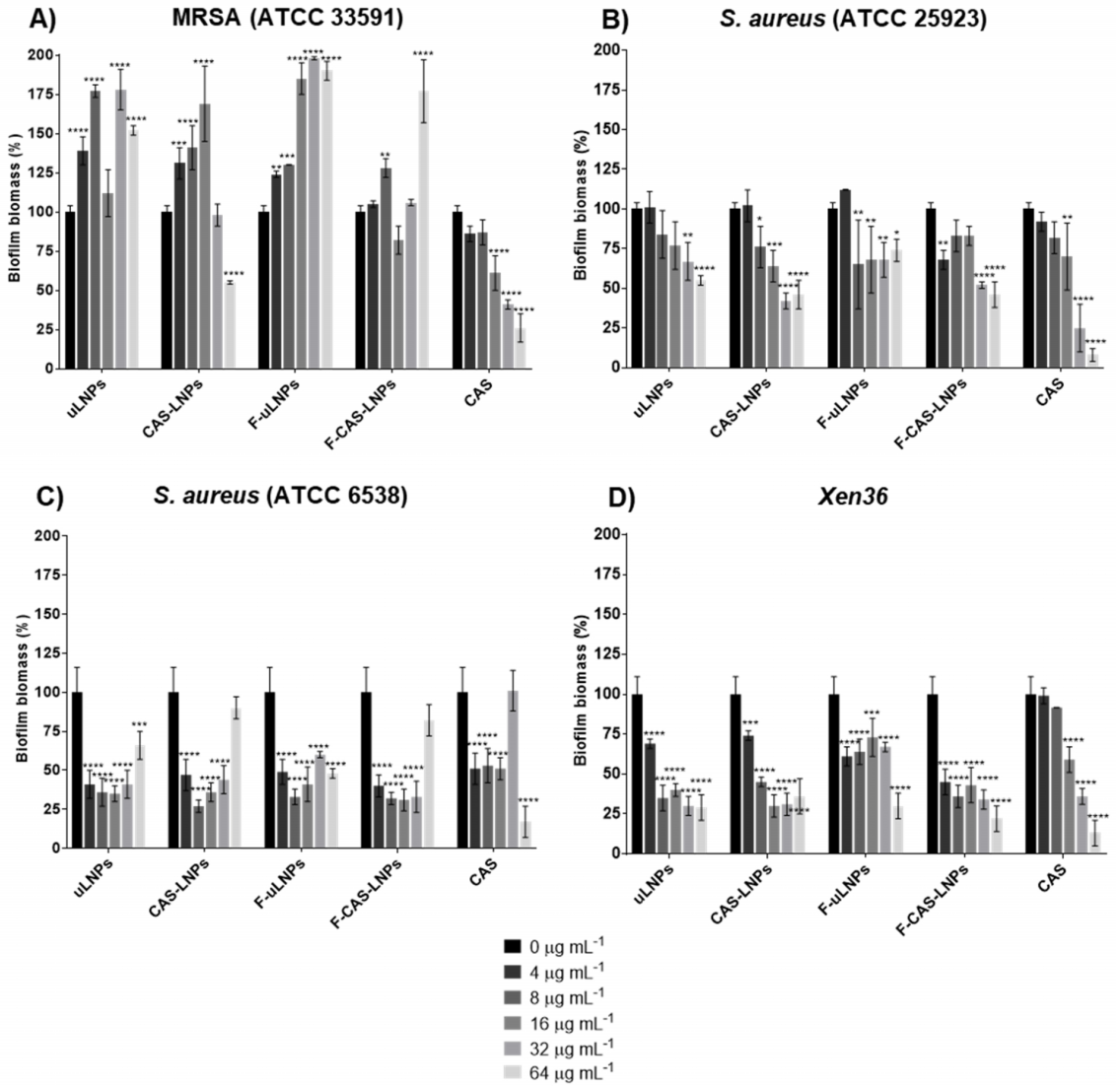


Figure S3: Quantification of biofilm biomass (crystal violet staining) after a 24h treatment with LNPs or free CAS at the CAS concentrations of 0, 4, 8, 16, 32 and 64 µg ml^{-1}. Prior to the treatment, the biofilms of **A)** MRSA ATCC 33591, **B)** *S. aureus* ATCC 25923, **C)** *S. aureus* ATCC 6538, and **D)** the bioluminescent strain *Xen36*, were grown in 96-well plates for 24h. Untreated biofilms (0 µg ml^{-1}) were used as a positive control. The values are represented as the mean ± SD. *P<0.05, **P<0.01, ***P<0.001, ****P<0.0001 relatively to 0 µg ml^{-1}. Statistical analysis: two-way ANOVA, Dunnett's multiple comparisons test.

4. In vivo biodistribution study

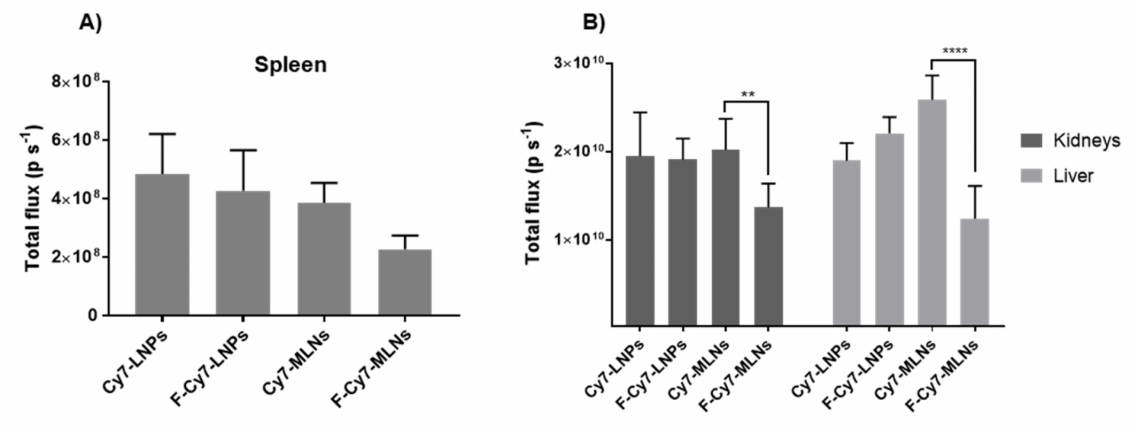


Figure S4: *In vivo* biodistribution study. Fluorescence signal intensity of **A)** spleen and **B)** kidneys and liver. The organs were acquired *ex vivo* at 24h post-administration of the Cy7-loaded formulations. Fluorescent signals are expressed in photons per second (p s^{-1}). The values are represented as the mean ± SD for three animals (each implanted with four catheters). **P<0.001, ****P<0.0001. Statistical analysis: two-way ANOVA, Tukey's multiple comparisons test.

5. In vivo antibiofilm efficacy study

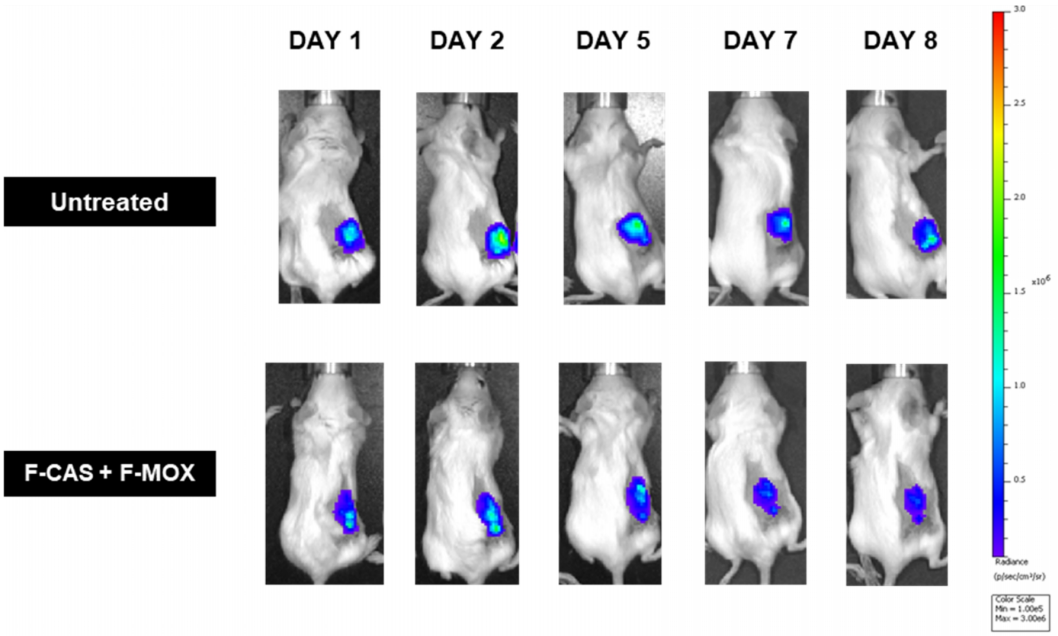
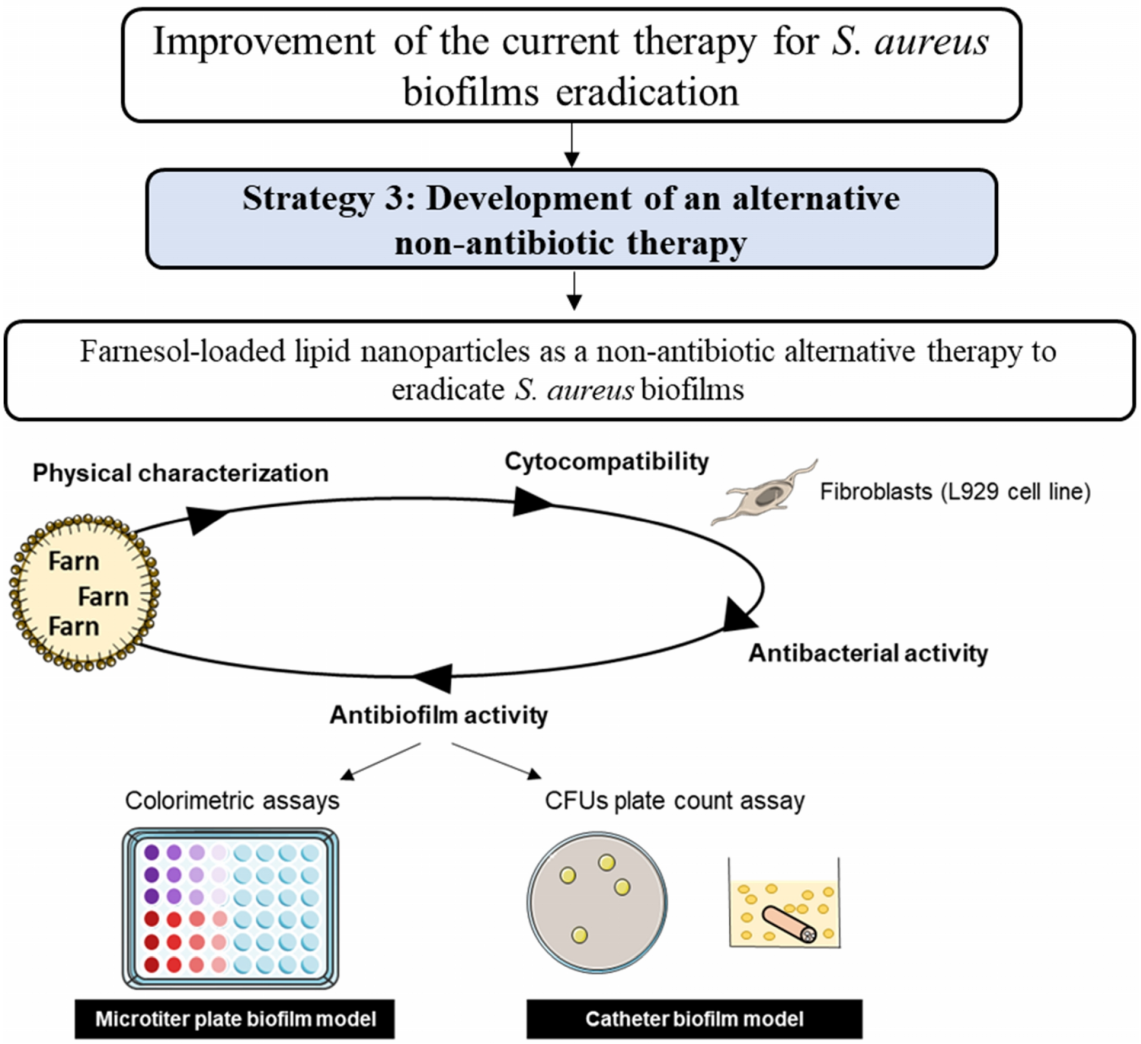


Figure S5: Representative bioluminescence images of *Xen36* biofilms at different timepoints (1, 2, 5, 7, and 8 days after implantation) for the groups untreated and treated with the combination of F-CAS-LNPs with F-MOX-MLNs. At day 1, mice were imaged prior to the treatment.

Chapter 6.4.

Farnesol-loaded lipid nanoparticles as a non-antibiotic alternative therapy to eradicate *S. aureus* biofilms

The increasing antimicrobial resistance towards conventional antibiotics prompted research for alternative compounds with antibacterial and antibiofilm activities, such as farnesol. In this chapter, we developed farnesol-loaded lipid nanoparticles as an alternative formulation to the use of nanoantibiotics, for a future combination with matrix-disruptive nanosystems.



Farnesol-loaded lipid nanoparticles as a non-antibiotic alternative therapy to eradicate *S. aureus* biofilms

Rita M. Pinto[1,2,3], Durgasruthi Pully[2], Catarina Leal Seabra[1], Salette Reis[1], Cláudia Nunes[1], Patrick Van Dijck[2,3*]

[1] LAQV, REQUIMTE, Departamento de Ciências Químicas, Faculdade de Farmácia, Universidade do Porto, Porto, Portugal

[2] Laboratory of Molecular Cell Biology Institute of Botany and Microbiology KU Leuven Leuven, Belgium

[3] VIB KU Leuven Center for Microbiology Leuven, Belgium

*Corresponding author:

Patrick Van Dijck: patrick.vandijck@kuleuven.be

Abstract

Staphylococcus aureus is the leading pathogen associated with nosocomial infections. One of the key virulent factors of *S. aureus* consists in its ability to adhere to human tissues and medical devices and form a biofilm. Biofilm structures are well known to promote antimicrobial resistance to conventional antibiotics, commonly leading to failure of the available therapies. Herein, an innovative nonantibiotic therapeutic approach based on the encapsulation of farnesol (Farn) in solid lipid nanoparticles (SLNs) is proposed. Farn is a quorum-sensing molecule with antimicrobial and antibiofilm potential against several bacterial strains. The developed formulations showed suitable physical characteristics for a systemic administration, with a mean hydrodynamic diameter below 300 nm, a low polydispersity index, and low zeta potential. Under storage conditions, the formulations were stable for up to 5 months. *In vitro* cytocompatibility studies showed that suspensions at a Farn concentration of 12.5 µM presented low cytotoxicity potential towards fibroblasts. The *in vitro* antibiofilm activity was assessed using the microtiter plate biofilm model and the catheter biofilm model, against MRSA ATCC 33591, *S. aureus* ATCC 6538, and *Xen36*. In the microtiter biofilm model, Farn-loaded SLNs (at a Farn concentration of 12.5 µM) exhibited a higher effect on biofilm biomass and viability for all studied strains, compared to the unloaded SLNs and free Farn. In the more complex catheter biofilm model, this synergistic potential between the vehicle and the encapsulated Farn was observed for the *Xen 36* strain. Overall, Farn-loaded SLNs present a potential nonantibiotic therapeutic approach against mature *S. aureus* biofilms, with different degrees of antimicrobial resistance

1. Introduction

Staphylococcus aureus is a gram-positive bacterium, well known to be the leading pathogen in nosocomial infections, causing high rates of morbidity and mortality. This microorganism has several virulent factors that promote bacteria adhesion to human tissues or implantable medical devices [1]. Consequently, a biofilm community is established, where an extracellular polymeric substances (EPS) matrix surrounds and protects the bacterial cells from the harsh external environment. Currently, the standard therapy against biofilm-associated infections consists in the administration of high doses of antibiotics, which commonly fails in a complete biofilm eradication. Ultimately, the administration of antibiotics may promote antimicrobial resistance phenomena [2]. Hence, alternative nonantibiotic treatments to fight *S. aureus* biofilms are currently in demand.

Farnesol (Farn), a quorum-sensing molecule commonly found in the genus *Candida* and in the composition of essential oils of some plant species, has been highlighted for its antimicrobial and antibiofilm properties [3-5]. This compound acts as a virulence-repressing factor in *Candida* spp., preventing the morphological transition from yeast to hyphae, which compromises biofilm formation [3]. Although the effect of Farn in bacterial species is not yet fully understood, several studies indicate that this compound may interact with the bacterial cell membrane, leading to its damage [6-8]. Particularly, Farn showed potential antibiofilm effects against *S. aureus* biofilms, including methicillin-resistant *S. aureus* (MRSA), alone or in combination with antibiotics [9, 10].

The EPS matrix is the first barrier that compounds such as farnesol encounter when in contact with the biofilm. This barrier may interact with the compounds and usually avoids their penetration into deeper layers of the structure, highly contributing to their inefficiency in eradicating the biofilms [2]. In recent decades, nanocarriers have been emerging as a tool to overcome this limitation. Nanoparticles as drug delivery carriers contribute to a higher penetration within the biofilm structure, leading to a controllable release of their contents closer to bacterial cells [11]. Therefore, lower doses of compound are required to achieve a therapeutic dose.

In this work, Farn-loaded solid lipid nanoparticles (SLNs) were developed as a therapeutic nonantibiotic strategy to eradicate mature *S. aureus* biofilms. Both the unloaded (SLNs) and the Farn-loaded (Farn-SLNs) formulations were characterized according to their hydrodynamic diameter, polydispersity index (PDI), and zeta potential. The stability of the formulations under storage conditions was evaluated for 20 weeks and *in vitro* cytocompatibility studies were also performed. Moreover, the *in vitro* antibacterial and

antibiofilm efficacy of the developed SLNs were assessed in methicillin-susceptible *S. aureus* (MSSA) and MRSA strains.

2. Materials and Methods

2.1 Materials

The solid lipid cetyl palmitate was a kind gift from Gattefossé (Gattefossé, France). Sodium hydroxide (NaOH), sodium chloride (NaCl), Tween 80, Triton X-100, thiazolyl blue tetrazolium (MTT), müller-hinton broth cation adjusted (MHB-Ca^{2+}), crystal violet dye, farnesol 95%, D-(+)-glucose monohydrate >99%, 2,3-Bis(2-methoxy-4-nitro-5-sulfophenyl)-2H-tetrazolium-5-carboxanilide inner salt (XTT), and menadione crystalline were obtained from Sigma-Aldrich (USA). Lactate dehydrogenase (LDH) Cytotoxicity Detection Kit was obtained from Takara Bio Inc. (Shiga, Japan). Dulbecco's Modified Eagle's Medium (DMEM), trypsin-EDTA (1×), Penicillin-Streptomycin (Pen Strep), Dulbecco's Phosphate Buffered Saline 10x pH 7.4 (PBS), and Fetal Bovine Serum (FBS) were purchased from Gibco by Life Technologies (UK). Dimethyl sulfoxide (DMSO), methanol, and acetic acid glacial were obtained from VWR International LLC (USA). BD Tryptic soy broth (TSB) and Difco Granulated Agar were acquired from Becton Dickinson (USA). L929 cells (ATCC CCL-1TM) were acquired from the American Type Culture Collection (USA). All components were used without further purification.

2.2 Bacterial strains

The strains ATCC 33591 (methicillin-resistant) and ATCC 25923 (methicillin-susceptible) were kindly provided by Prof. Françoise Van Bambeke (UC Louvain). The bioluminescent strain *Xen36* was acquired from Caliper Life Sciences (USA) and the strain ATCC 6538 from ATCC (USA).

2.3 Preparation of the Far-loaded SLNs

The SLNs were prepared by the modified free organic-solvent emulsification/sonication method [12]. Briefly, 250 mg of solid lipid (cetyl palmitate), and 50 mg of Tween 80 were melted in a hot bath at a temperature above their melting point (60ºC). For the Farn-loaded SLNs, 30 µl of Farn were added to the lipid phase. The lipid phase was then dispersed in 6 ml of pre-heated ultrapure water at the same temperature. Then, the mixture was sonicated

at 70% for 5 mins, using a VCX-130 Vibra-Cell™ sonicator, with a CV-18 probe (Sonics & Materials Inc, USA) (130 Watt, 20 kHz).

2.4 Physical characterization and storage stability of SLNs suspensions

The hydrodynamic diameter and polydispersity index (PDI) were measured using the VASCO particle size analyzer (Cordouan Technologies, France). The zeta potential of the developed SLNs was determined using the WALLIS zeta potential analyzer (Cordouan Technologies, France). Prior to the measurements, the SLNs were diluted (1:100) in ultrapure water. To evaluate their stability under storage conditions, the LNPs were kept at 4ºC for 20 weeks. The storage stability was assessed through the measurements of hydrodynamic size, PDI, and zeta potential.

2.5 *In vitro* cell viability and cytotoxicity studies

The effect of the developed SLNs in the viability of human fibroblasts was evaluated, using the L929 cell line [13]. Firstly, the cells were cultured in DMEM supplemented with 10% FBS and 1% Penicillin-Streptomycin at 37ºC, 5% CO_2 atmosphere. When cells reached 80 – 90% confluence, they were seed in flat bottom 96-well plates at a density of 5 x 10^4 cells per well and incubated overnight (37ºC, 5% CO_2). After this incubation period, the cells were treated with Farn-SLNs suspensions or free compound at farnesol concentrations ranging from 12.5 µM to 200 µM. The unloaded formulations were tested at the same concentrations. The cells were incubated with the treatment for 24h, at 37ºC, 5% CO_2. DMEM and 1% Triton-100 (v/v) were used as positive and negative controls, respectively. To assess cell viability after treatment, the medium from the wells was replaced by the MTT solution (0.5 mg ml^{-1}, 100 µl). The plates were incubated for 2h, at 37ºC, 5% CO_2. Afterward, the solution was removed, and 100 µl of DMSO were added to the wells. In the meantime, the medium collected from the wells after the treatment was centrifuged at 250*g* for 10 mins (Centrifuge 5810R, Eppendorf, Germany). The supernatant was collected and the LDH cytotoxicity kit was used according to the instructions of the manufacturer. The absorbance was measured at 490 nm and 690 nm for both the LDH assay and at 550 nm and 650 nm for the MTT assay, using a microplate reader (BioTek Instruments Inc, Synergy HT, Software: Gen5 v1.08.4, BioTek Instruments Inc, USA). The measurements at 690 nm and 650 nm were used to remove background interference.

2.6 Micro-broth dilution assay

The micro-broth dilution assay was used to evaluate the effect of the developed SLNs on planktonic bacteria [14]. In this assay, a bacterial overnight culture was diluted to a concentration of 2.0×10^5 CFUs ml^{-1} in MHB- Ca^{2+} medium. The diluted inoculum was treated with SLNs or free Farn at several Farn concentrations (12.5, 25, 50, 100, and 200 µM), for 24h, at 37ºC, in round bottom 96-well plates (Greiner Bio One, Austria). Both the MIC and MBC values were determined. The MIC was recorded at the lowest concentration that visually inhibited bacterial growth, while the MBC was determined by spot-plate (10 µl) the wells with no visual bacterial growth on TSA plates. These plates were incubated overnight, at 37ºC.

2.7 *In vitro* antibiofilm activity studies

2.7.1 Crystal violet assay

The crystal violet assay was used to evaluate the effect of the developed SLNs on the biofilm biomass. For this assay, biofilm formation and growth conditions were adapted from the literature [15, 16]. Briefly, bacterial cultures were adjusted to an optical density at 600 nm (OD_{600nm}) of 0.1 in TSB 0.6x supplemented with 0.2% glucose. From this inoculum, 200 µl were added to each well from a flat bottom 96-well plate (Greiner Bio One, Austria) and incubated for 90 mins, at 37ºC, to allow adherence of bacterial cells. Afterward, the cells were washed twice with PBS 1x, and 200 µl of fresh TSB 0.6x supplemented with 0.2% glucose were added to each well. The biofilms were incubated at 37ºC for 24h, to reach a mature state. After this incubation time, the biofilms were washed twice with PBS 1x and further treated for 24h, at 37ºC. The SLNs suspensions and free Farn were used at the same concentrations described in the previous sections. After the treatment, the medium was removed, and the wells were washed once with PBS 1x. The biofilms were fixed for 15 mins at room temperature with 200 µl of 99% methanol. The methanol was then removed, and the biofilms were left to dry until complete evaporation of the solvent. A 1% (w/v) crystal violet solution (200 µl) was added to the wells for 5 mins. The biofilms were washed with ultrapure water to remove the excess of dye and then 200 µl of 33% (v/v) glacial acetic acid were added to each well. The plate was incubated for 15 mins at room temperature, under agitation (250 rpm), in a microplate shaker (VWR International LLC, USA). The absorbance was read at 570 nm using a microplate reader (Synergy HT, BioTek Instruments Inc, USA).

2.7.2 XTT assay

For this assay, the biofilms were grown in the conditions described in **section 2.7.1**. After the treatment, the biofilms were washed once with PBS 1x and 100 µl of XTT solution (1 mg ml^{-1}, supplemented with 1 µM menadione) were added to each well. The plates were incubated for 30 mins, in the dark, at 37ºC, with shaking (250 rpm) (VWR Incubating Microplate Shaker, VWR International LLC, USA). The absorbance was read at 490 nm using a microplate reader (Synergy HT, BioTek Instruments Inc, USA).

2.7.3 CFU assay

Biofilm viability was also tested through the CFU assay, using the *in vitro* catheter biofilm model [16]. Polyurethane catheters (Certofix duo/trio; B. Braun Melsungen AG, Germany) were firstly cut in 1 cm long pieces and incubated with 100% FBS at 37ºC, overnight. Bacterial overnight cultures were adjusted with TSB 0.6x (supplemented with 0.2% glucose) to an OD_{600nm} of 0.1. The catheters were submerged in 1 ml of the adjusted inoculum and incubated for 90 mins, at 37ºC, in 24-well plates for suspension cultures (Greiner Bio One, Austria). Then, the catheters were washed twice with PBS 1x and incubated with fresh medium for 24h, at 37ºC, to allow the formation of mature biofilms. After this incubation period, the catheters were washed twice with PBS 1x and treated with SLNs or free compound at the Farn concentration of 25 µM, for 24h, at 37ºC. Afterward, catheter pieces were washed twice with PBS 1x and sonicated (Branson 5510 Ultrasonics bath, Marshall Scientific, USA) for 10 mins at room temperature in 200 µl of PBS 1x. The samples were then serial diluted in PBS 1x and spot-plated (10 µl) on TSA plates. The plates were incubated overnight at 37ºC to allow CFUs counting.

2.8 Statistical analysis

Statistical analysis was performed using the GraphPad Prism Software (v7.03, GraphPad Software Inc, USA). The data are expressed as mean ± SD and each assay was performed at least three independent times.

3. Results and Discussion

3.1 Physical characterization of the SLNs under storage conditions

The developed SLNs were characterized according to their hydrodynamic size, polydispersity index (PDI), and zeta potential over 20 weeks of study, under storage conditions (4ºC) (**Figure 1**). After production, both unloaded and Farn-loaded SLNs showed a mean hydrodynamic size below 300 nm, with the encapsulation of Farn revealing no significant changes in the particles size. Over the 20 weeks of study, the mean hydrodynamic diameters of both formulations did not change significantly. The low PDI value (below 0.2) was also evaluated, revealing that the suspensions were monodisperse, with uniform homogenous populations [17]. Besides, the highly negative zeta potential (< -30 mV) indicated that the formulations were physically stable, with no tendency to form aggregates due to the electrostatic repulsion between the charged particles [18]. Despite few significant changes over time, the zeta potential values were always below -30 mV, which reflects the high stability of the SLNs.

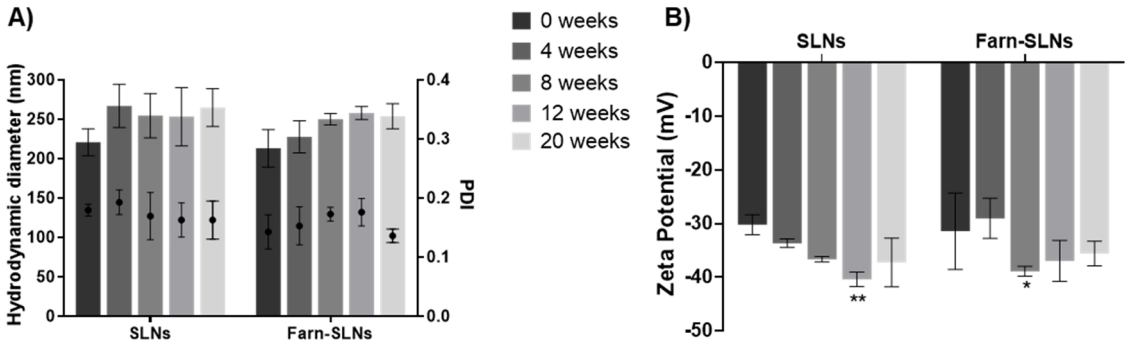


Figure 1: Characterization of the SLNs suspensions over 20 weeks at storage conditions (4ºC). **A)** Hydrodynamic diameter and PDI. The bars represent the hydrodynamic diameter (left y-axis) and the dots represent the PDI (left y-axis). **B)** Zeta potential. The parameters were evaluated over time (0, 4, 8, 12, and 20 weeks). The values are represented as the mean ± SD. *P<0.05, **P<0.01, relatively to 0 weeks. Statistical analysis: two-way ANOVA, Dunnett's multiple comparisons test.

3.2 *In vitro* cell viability and cytotoxicity studies

The possible toxicity of the SLNs against human cells was evaluated by the MTT and LDH assays (**Figure 2**). For this purpose, the fibroblast cell line L929 was used [13]. The ISO international standard 10993–5 considers a cytotoxic effect when cell viability is below 70% of the blank [13]. According to this standard, both unloaded and Farn-loaded formulations

do not seem to affect L929 cells up to a Farn concentration of 100 µM, with cell viability values above 70% (**Figure 2A**). For a concentration of 200 µM, the cell viability after the treatment with Farn-SLNs drops to around 40%. At the tested conditions, free Farn revealed a very high effect on cell viability, showing toxicity towards human fibroblasts. These results were corroborated by the LDH assay, where all concentrations of free Farn tested induced high cytotoxicity in L929 cells (**Figure 2B**). The potential cytotoxic effect of Farn against fibroblasts has been previously reported in several studies [19, 20]. In fact, Kim *et al.* (2017) observed that Farn concentrations as low as 5 µM promoted a cell viability reduction of 50% in 3T3-L1 cells [21].

Overall, the results from both MTT and LDH assays show that encapsulated Farn has a much safer profile than the compound in the free form. It is hypothesized that in the Farn-SLNs, Farn is incorporated in the lipid matrix due to its lipophilicity, being less exposed to the human cells.

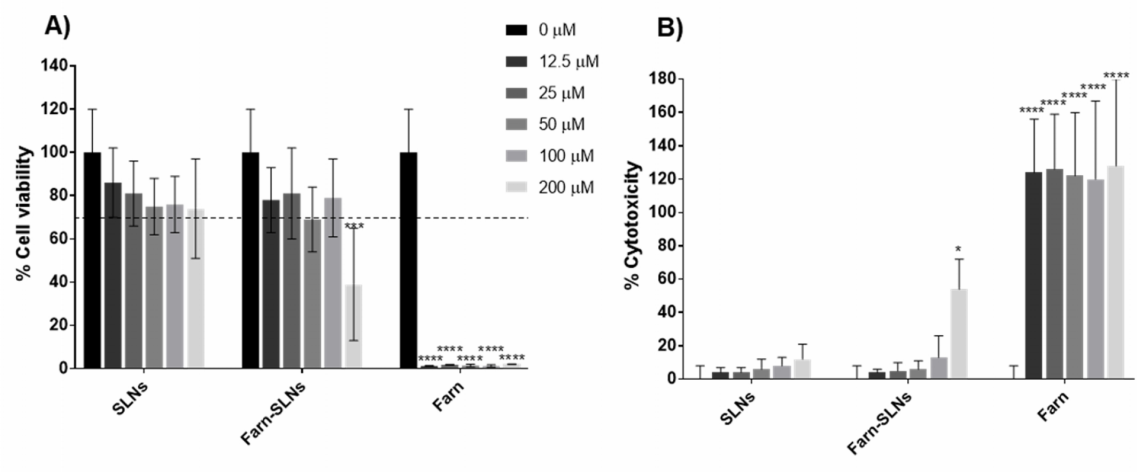


Figure 2: *In vitro* cell viability and cytotoxicity studies. **A)** MTT and **B)** LDH assays using the fibroblasts L929 cell line. The cells were treated with the developed SLNs or free Farn, at the Farn concentrations 0, 12.5, 25, 50, 100, and 200 µM. DMEM and 1% (v/v) Triton-100 were used as controls. All values are represented as mean ± SD. *P<0.05, ***P<0.001, ****P<0.0001 relatively to 0 µM. Statistical analysis: two-way ANOVA, Dunnett's multiple comparisons test.

3.3 Antibacterial activity

The antibacterial activity of the developed formulations was assessed in several *S. aureus* strains (**Table 1**). For all tested strains, the unloaded formulation did not inhibit planktonic bacteria at the highest concentration used. Farn-SLNs showed a MIC value of 100 µM for the four strains. However, the MBC for this SLNs suspension was higher than 200 µM. Regarding free Farn, no inhibition of planktonic bacteria was observed for the four strains

tested. This outcome is in agreement with the literature, which reports higher MIC values for several *S. aureus* strains (around 5 mM) [6].

Table 1: Antibacterial activity of the unloaded and Farn-loaded SLNs against planktonic *S. aureus*. Free Farn was tested at the same conditions. MIC and MBC values are expressed in μM of Farn.

	MRSA (ATCC 33591)		***S. aureus* (ATCC 25923)**		***S. aureus* (ATCC 6538)**		***Xen36***	
	MIC	***MBC***	***MIC***	***MBC***	***MIC***	***MBC***	***MIC***	***MBC***
SLNs	>200	>200	>200	>200	>200	>200	>200	>200
Farn-SLNs	100	>200	100	>200	100	>200	100	>200
Farn	>200	>200	>200	>200	>200	>200	>200	>200

3.4 *In vitro* antibiofilm activity studies

The antibiofilm activity of the developed SLNs was assessed through quantification of the biofilm biomass and biofilm viability.

The quantification of biofilm biomass removal after treatment with the developed SLNs or free Farn was evaluated by the crystal violet assay (**Figure 3**). For the concentrations tested, both unloaded and Farn-loaded nanoparticles showed a significantly higher biomass removal, compared to the free compound at the same concentration. Free Farn showed a low biofilm biomass removal (< 20%), even at the highest concentration tested (200 μM), in the three *S. aureus* strains studied. Regarding the Farn-SLNs at the lowest concentration tested (12.5 μM), a significantly higher biofilm biomass reduction was observed, compared to the unloaded SLNs.

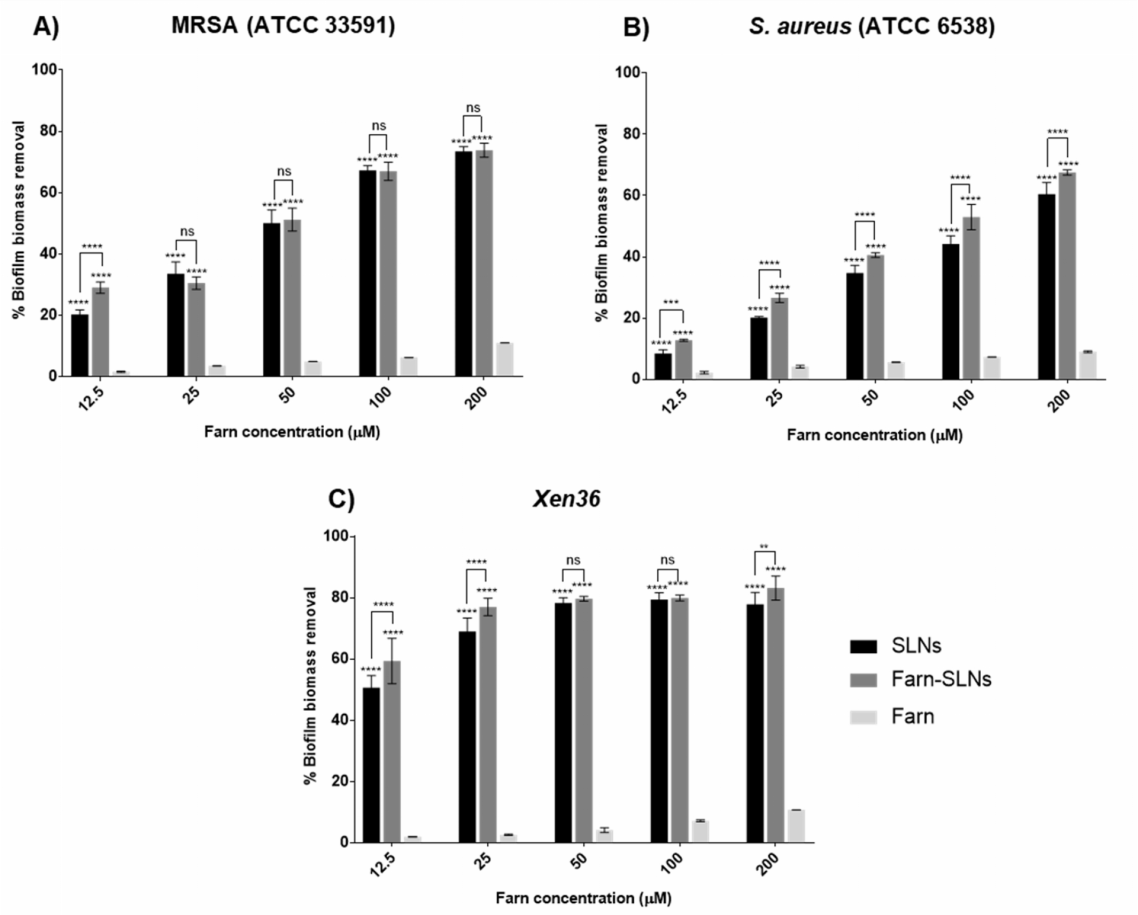


Figure 3: Quantification of biofilm biomass removal by the crystal violet assay for **A)** MRSA ATCC 33591, **B)** *S. aureus* ATCC 6538, and **C)** *Xen36*. The biofilms were grown for 24h and then treated with the developed formulations or free Farn at the Farn concentrations of 12.5, 25, 50, 100, and 200 µM. Untreated biofilms were used as a positive control. The values are represented as the mean ± SD. ****P<0.0001 relatively to free Farn at the same concentration. ns, not significant; **P<0.01, ***P<0.001, ****P<0.0001. Statistical analysis: two-way ANOVA, Tukey's multiple comparisons test.

The results of biofilm biomass were further corroborated by the XTT assay (**Figure 4**). In this assay, the biofilm viability was quantified for the strains MRSA ATCC 33591, *S. aureus* ATCC 6538, and *Xen36*. In accordance with the previous results, Farn alone does not seem to have an impact on the biofilm viability, even at the highest concentration tested (200 µM). In fact, the effect of Farn on 24h-old *S. aureus* biofilms has been previously reported, with significant biofilm viability reduction observed at a much higher concentration (30 mM) [9]. Thus, it is likely that the high biofilm biomass and viability reduction observed in Farn-SLNs is mainly due to the antibiofilm activity of the vehicle. The use of Tween 80 as a surfactant may contribute to this outcome, since it is reported in the literature that this compound has antibiofilm activity against several bacterial strains, including MRSA [22, 23]. Nevertheless,

Farn-SLNs show a significantly higher biofilm viability and biomass reduction at the lowest concentrations, compared to the unloaded SLNs. These findings suggest a potential synergistic effect between the vehicle and encapsulated Farn. Hence, Farn-SLNs may be a potential therapy against *S. aureus* biofilms, even at a Farn concentration as low as 12.5 µM.

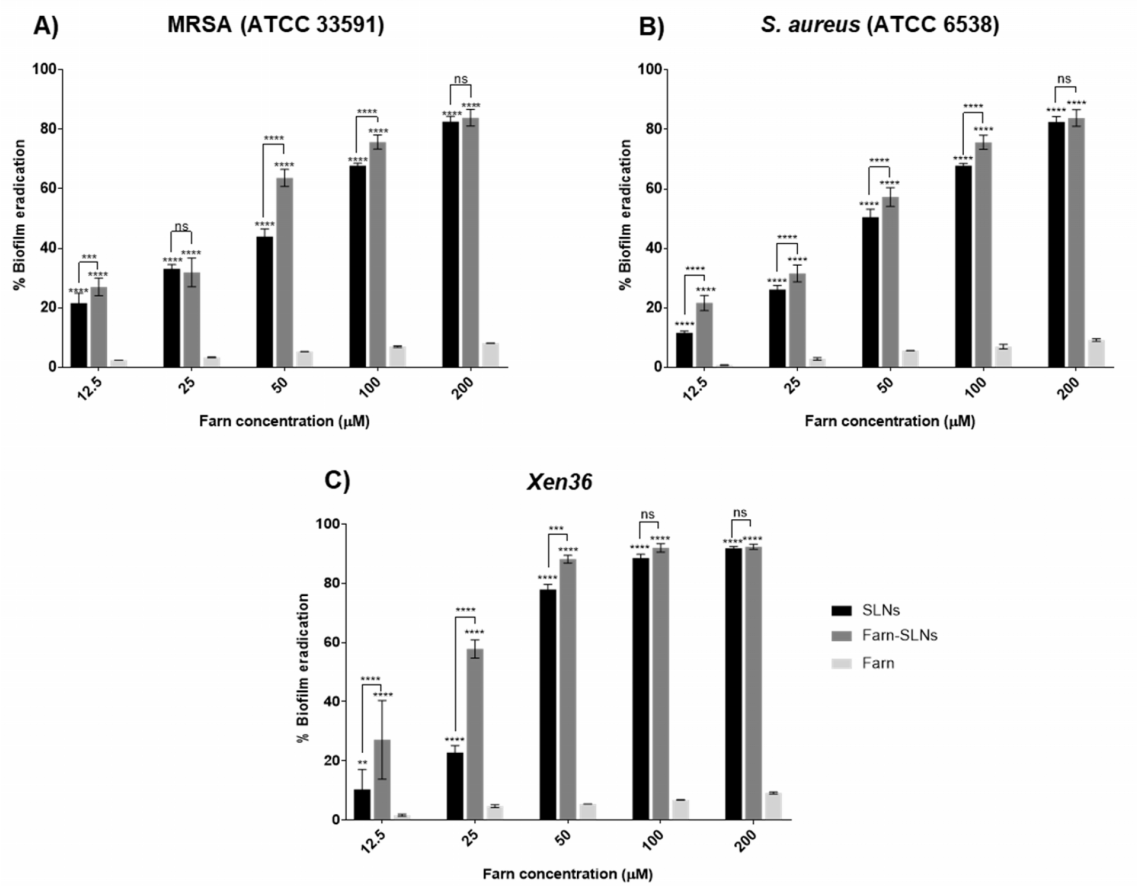


Figure 4: Assessment of biofilm eradication for 24h-old biofilms of **A)** MRSA ATCC 33591, **B)** *S. aureus* ATCC 6538, and **C)** *Xen36*. The biofilm viability was quantified using the XTT assay. The biofilms were treated with the developed SLNs or free Farn at 12.5, 25, 50, 100, and 200 µM of Farn. Untreated biofilms were used as a positive control. The values are represented as the mean ± SD. **P<0.01, ****P<0.0001, relatively to free Farn at the same concentration. ns, not significant; ***P<0.001, ****P<0.0001. Statistical analysis: two-way ANOVA, Tukey's multiple comparisons test.

The biofilm viability was also evaluated using an *in vitro* catheter biofilm model, through CFUs count (**Figure 5**). For the MRSA and *S. aureus* ATCC 6538 strains, both formulations and free Farn (at the concentration of 25 µM) showed a significant reduction of biofilm viable count, compared to the untreated control. Nonetheless, unloaded and Farn-loaded SLNs

showed no significant differences. For *Xen 36*, Farn-SLNs exhibited the highest reduction in viable count, which was significantly different to the effect of the SLNs alone (*P<0.0001*). Interestingly, for this strain free Farn did not show a significant difference from the untreated control. Thus, the results seem to suggest a synergistic effect of Farn and the vehicle in the Farn-SLNs, for this strain.

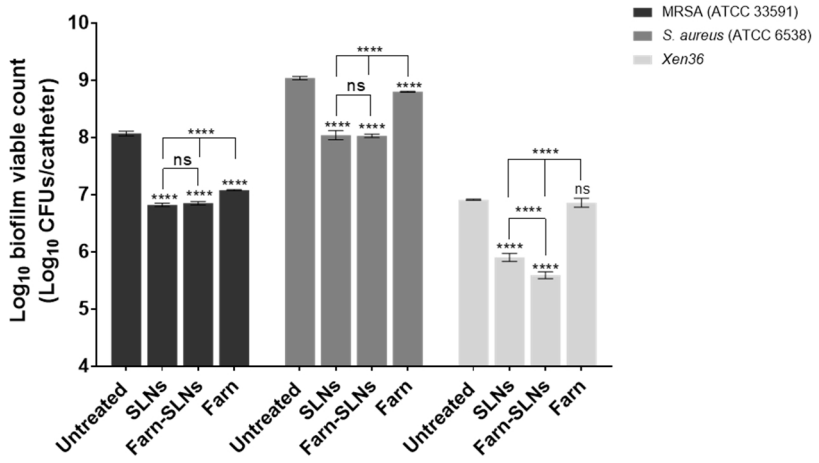


Figure 5: Biofilm viable count for three strains tested: MRSA ATCC 33591, *S. aureus* ATCC 6538, and *Xen36*. The biofilms were grown *in vitro* in catheters and after treated with the developed formulations or free Farn (25 µM of Farn). Untreated biofilms were used as a positive control. The values are represented as the mean ± SD for three catheters. ns, not significant; ****P<0.0001, relatively to the untreated biofilms. ns, not significant; ****P<0.0001. Statistical analysis: two-way ANOVA, Tukey's multiple comparisons test.

4. Conclusions

In this work, Farn-loaded lipid nanoparticles were developed as a potential antibiofilm strategy towards the eradication of *S. aureus* mature biofilms. The produced formulations exhibited a hydrodynamic diameter below 300 nm, low PDI, and a low zeta potential, over 20 weeks of study, under storage conditions. *In vitro* cell viability studies in fibroblasts revealed that the formulations up to a concentration of 100 µM of Farn, did not show cytotoxic effects.

The *in vitro* antibiofilm activity of the developed SLNs was evaluated in different *S. aureus* strains using the microtiter plate and the catheter biofilm models. In the microtiter plate model, at a cytocompatible concentration (12.5 µM of Farn), the Farn-SLNs showed a significantly higher effect on biofilm biomass and viability than SLNs and Farn alone. These

findings suggest a potential synergistic effect between the encapsulated Farn and the vehicle. It is hypothesized that the antibiofilm activity of the vehicle may be due to the presence of Tween 80, which is known to have antibacterial and antibiofilm properties [22]. In the more complex catheter biofilm model, treatment with Farn-SLNs only showed a lower viable count compared with SLNs alone for the *Xen36* strain. For the remaining strains tested, no significant differences in viable count between unloaded and Farn-loaded SLNs were observed. This outcome may be a consequence of the low concentration of Farn tested in this model (12.5 µM), however, higher concentrations would compromise the safety profile of the formulations. Nevertheless, Farn-loaded SLNs alone showed potential to be used as an alternative nonantibiotic therapy against *S. aureus* biofilms. In a step forward towards an *in vivo* application, an antibiofilm strategy combining the developed Farn-loaded SLNs with matrix disruptive agents would be important to investigate.

Acknowledgements

RMP and CN are thankful to Fundação para a Ciência e Tecnologia (FCT) for the Ph.D. Grant [SFRH/BD/130319/2017] and the investigator Grant [IF/00293/2015], respectively. PVD is thankful to the Fund for Scientific Research Flanders (FWO grant WO.009.16N). The authors RMP, CN, and SR acknowledge to the institution LAQV - Laboratório Associado para a Química Verde (UIDB/50006/2020). RMP also acknowledges the Programa Operacional Capital Humano (POCH), specifically the BiotechHealth Programme (Doctoral Programme on Cellular and Molecular Biotechnology Applied to Health Sciences).

References

1. Otto, M., *Staphylococcal biofilms.* Curr. Top. Microbiol. Immunol., 2008. **322**: p. 207-28,
2. Pinto, R.M., et al., *Innovative strategies toward the disassembly of the EPS matrix in bacterial biofilms.* Front. Microbiol., 2020. **11**(952), 10.3389/fmicb.2020.00952
3. Yu, L.H., et al., *Possible inhibitory molecular mechanism of farnesol on the development of fluconazole resistance in Candida albicans biofilm.* Antimicrob Agents Chemother, 2012. **56**(2): p. 770-775, 10.1128/aac.05290-11
4. Langford, M.L., A.L. Atkin, and K.W. Nickerson, *Cellular interactions of farnesol, a quorum-sensing molecule produced by Candida albicans.* Future Microbiol, 2009. **4**(10): p. 1353-1362, 10.2217/fmb.09.98
5. Weber, K., B. Schulz, and M. Ruhnke, *The quorum-sensing molecule E,E-farnesol-its variable secretion and its impact on the growth and metabolism of Candida species.* Yeast, 2010. **27**(9): p. 727-739, 10.1002/yea.1769
6. Akiyama, H., et al., *Actions of farnesol and xylitol against Staphylococcus aureus.* Chemotherapy, 2002. **48**(3): p. 122-128, 10.1159/000064916
7. Brehm-Stecher, B.F. and E.A. Johnson, *Sensitization of Staphylococcus aureus and Escherichia coli to antibiotics by the sesquiterpenoids nerolidol, farnesol, bisabolol, and apritone.* Antimicrob Agents Chemother, 2003. **47**(10): p. 3357-3360, 10.1128/aac.47.10.3357-3360.2003
8. Gomes, F.I., et al., *Effect of farnesol on planktonic and biofilm cells of Staphylococcus epidermidis.* Curr Microbiol, 2009. **59**(2): p. 118-122, 10.1007/s00284-009-9408-9
9. Unnanuntana, A., et al., *The effects of farnesol on Staphylococcus aureus biofilms and osteoblasts. An in vitro study.* J Bone Joint Surg Am, 2009. **91**(11): p. 2683-2692, 10.2106/jbjs.H.01699
10. Jabra-Rizk, M.A., et al., *Effect of farnesol on Staphylococcus aureus biofilm formation and antimicrobial susceptibility.* Antimicrobial agents and chemotherapy, 2006. **50**(4): p. 1463-1469, 10.1128/AAC.50.4.1463-1469.2006
11. Fulaz, S., et al., *Nanoparticle-biofilm interactions: the role of the EPS matrix.* Trends Microbiol, 2019. **27**(11): p. 915-926, 10.1016/j.tim.2019.07.004
12. Lopes-de-Campos, D., et al., *Delivering Amoxicillin at the Infection Site - a Rational Design through Lipid Nanoparticles.* Int. J. Nanomedicine, 2019. **14**: p. 2781-2795, 10.2147/ijn.S193992

13. ISO, *10993-5. Biological evaluation of medical devices–Part 5: tests for in vitro cytotoxicity.* Geneva, Switzerland: International Organization for Standardization, 2009,
14. Wiegand, I., K. Hilpert, and R.E. Hancock, *Agar and Broth Dilution Methods to Determine the Minimal Inhibitory Concentration (MIC) of Antimicrobial Substances.* Nat. Protoc., 2008. **3**(2): p. 163,
15. Vande Velde, G., et al., *Bioluminescence imaging increases in vivo screening efficiency for antifungal activity against device-associated Candida albicans biofilms.* Int J Antimicrob Agents, 2018. **52**(1): p. 42-51, 10.1016/j.ijantimicag.2018.03.007
16. Siala, W., et al., *The Antifungal Caspofungin Increases Fluoroquinolone Activity Against Staphylococcus aureus Biofilms by Inhibiting N-Acetylglucosamine Transferase.* Nat. Commun., 2016. **7**: p. 1-15, 10.1038/ncomms13286
17. Danaei, M., et al., *Impact of Particle Size and Polydispersity Index on the Clinical Applications of Lipidic Nanocarrier Systems.* Pharmaceutics, 2018. **10**(2), 10.3390/pharmaceutics10020057
18. Müller, R.H., C. Jacobs, and O. Kayser, *Nanosuspensions as particulate drug formulations in therapy. Rationale for development and what we can expect for the future.* Adv Drug Deliv Rev, 2001. **47**(1): p. 3-19, 10.1016/s0169-409x(00)00118-6
19. Wu, G.X., et al., *Evaluation of the UVB-screening capacity and restorative effects exerted by farnesol gel on UVB-caused sunburn.* Environ Toxicol, 2018. **33**(4): p. 488-507, 10.1002/tox.22535
20. Chávez-Andrade, G.M., et al., *Cytotoxicity, genotoxicity and antibacterial activity of poly(vinyl alcohol)-coated silver nanoparticles and farnesol as irrigating solutions.* Arch Oral Biol, 2017. **84**: p. 89-93, 10.1016/j.archoralbio.2017.09.028
21. Kim, H.L., et al., *Farnesol Has an Anti-obesity Effect in High-Fat Diet-Induced Obese Mice and Induces the Development of Beige Adipocytes in Human Adipose Tissue Derived-Mesenchymal Stem Cells.* Front Pharmacol, 2017. **8**: p. 654, 10.3389/fphar.2017.00654
22. Ueda, Y., et al., *Inhibitory Effects of Polysorbate 80 on MRSA Biofilm Formed on Different Substrates Including Dermal Tissue.* Sci. Rep., 2019. **9**(1): p. 3128, 10.1038/s41598-019-39997-3
23. Toutain-Kidd, C.M., et al., *Polysorbate 80 Inhibition of Pseudomonas aeruginosa Biofilm Formation and its Cleavage by the Secreted Lipase LipA.* Antimicrob. Agents Chemother., 2009. **53**(1): p. 136-145, 10.1128/aac.00500-08

Chapter 7 – Concluding remarks and future perspective

Bacterial biofilms are a major health concern, mainly due to their contribution to the escalating figures of antimicrobial resistance to conventional antibiotics. These structures are commonly associated to implantable medical devices, such as catheters, ultimately leading to their failure [1]. Amongst several bacterial species, *S. aureus*, *S epidermidis*, and *P. aeruginosa* are the most frequently isolated from infected implants [2, 3]. Current therapies to eradicate bacterial biofilms lack efficiency since they are solely focused on the administration of conventional antibiotics and fail to target the EPS matrix, the first physical barrier encounter on bacterial biofilms [4].

The current work was developed as an innovative strategy towards the eradication of bacterial biofilms, by focusing not only in killing bacterial cells, but also targeting and disrupting the EPS matrix to achieve a higher antibiofilm efficiency. For this purpose, lipid nanoparticles encapsulating matrix-disruptive agents (NAC and CAS) and bactericidal agents (MOX and Farn) were developed. The nanosystems were characterized according to their physical properties, cytocompatibility, and antibiofilm efficacy. The four developed nanosystems showed suitable hydrodynamic diameters for intravenous administration, and low values of PDI and zeta potential. Besides, the nanoparticles presented low toxicity to both fibroblasts (L929 cell line) and human red blood cells.

NAC-loaded nanoparticles were firstly evaluated for their *in vitro* antibiofilm potential against *S. epidermidis* and *P. aeruginosa* biofilms (**Chapter 6.1.**). These nanoparticles showed no effect against *S. epidermidis* biofilms however, a great potential was observed alone or in combination with an antibiotic, MOX. In a combinatory strategy with MOX, the designed nanoparticles improved the therapeutic efficacy of the antibiotic.

This combination was further investigated in *S. aureus* biofilms, due to the high prevalence of this pathogen in implant-associated biofilms. To overcome limitations associated with the administration of MOX, such as adverse side effects and potential *in vivo* degradation, multiple lipid nanoparticles were used to encapsulate this drug (**Chapter 6.2**). MOX-loaded nanosystems were evaluated alone or in combination with the NAC-loaded nanoparticles using an *in vitro* catheter biofilm model. A synergistic effect was observed between MOX-loaded and NAC-loaded nanoparticles functionalized with D-amino acids conjugates. However, the synergistic potential was also observed between the unloaded lipid nanoparticles and the MOX-loaded nanoparticles.

To investigate the potential of combining the developed MOX-loaded nanosystems with other matrix-disruptive agents, CAS-loaded nanoparticles were developed by the double emulsion technique (**Chapter 6.3.**). In this work, encapsulated CAS and MOX showed synergistic potential at much lower concentrations than previously reported for the free drugs [5]. The *in vitro* antibiofilm efficacy of the two nanosystems combination was further assessed *in vivo*, using a murine subcutaneous catheter model. This combinatory strategy exhibited antibiofilm activity while avoiding dissemination of bacterial cells to vital organs. Besides, *in vivo* biodistribution studies showed that the nanosystems accumulated in the target site and have a high renal clearance, which suggests a good biocompatible profile.

Although NAC-loaded nanoparticles have an excellent biocompatibility, their combination with the MOX nanosystem showed less efficiency than when the CAS nanosystem was used. Nevertheless, the use of CAS in patients that are not infected by fungi can negatively affect the fungal flora [5].

Due to the increase of antimicrobial resistance to antibiotics, an alternative nonantibiotic strategy focused on the encapsulation of farnesol into lipid nanoparticles was investigated (**Chapter 6.4.**). The encapsulation of farnesol improved its antibiofilm activity against *S. aureus* biofilms grown in both the microtiter plate biofilm model and the *in vitro* catheter biofilm model. However, the encapsulation of farnesol does not seem to improve the efficacy of the unloaded vehicle, which indicates that further optimization of the nanoparticles is required. Besides, it would have been interesting to study the combination of Farn-loaded nanoparticles in combination with the matrix disruptive nanosystems developed in this work.

Limitations and future perspectives

One of the main limitations of this work is associated to the different methods of production of each nanosystem, which influenced their antibiofilm activity. In the NAC nanosystem, the presence of encapsulated NAC does not seem to improve the antimicrobial efficiency of the vehicle alone. This is likely due to the high amount of Tween 80 present in the NAC-loaded nanoparticles, which has antibiofilm activity against both *P. aeruginosa* and *S. aureus* [6, 7]. These particles were produced by the double emulsion technique, which requires high amounts of surfactant to stabilize the nanoemulsion. CAS-loaded nanoparticles were also produced by this method. Similarly to the NAC-loaded nanosystem, the unloaded vehicles revealed an effect against biofilms grown in the microtiter plate model. However, the effect of F-CAS-LNPs in combination with the F-MOX-MLNs showed the highest antibiofilm potential. In the Farn-loaded nanoparticles produced by the modified free organic-solvent

emulsification/sonication method, the effect of Tween 80 was also observed. The unloaded formulation exhibited a high antibiofilm effect against *S. aureus* biofilms for both the microtiter plate and the catheter biofilm models. Although MOX-loaded nanoparticles also have Tween 80, unloaded formulations did not show a significant antibiofilm activity against *S. aureus* biofilms. In the production method of multiple lipid nanoparticles (MOX-loaded nanoparticles), a lower amount of Tween 80 is required, due to the addition of another surfactant, Span 80. Due to the differences between the production methods for each nanosystem, a comparison between the effect of the different encapsulated compounds is difficult to achieve.

The work presented in this thesis is far from achieving its full potential. The combination of the three nanosystems developed in this thesis could be further investigated to evaluate a potentially higher antibiofilm efficacy. Besides, a prolonged *in vivo* treatment (e.g., 14 days) would be also important to assess, since it may increase the efficacy of the therapeutic approach. The developed nanosystems should be investigated against not only reference strains, but also clinical isolates with different resistance levels. In addition, it would be interesting to investigate the nanosystems against other pathogens commonly found associated to medical devices, such as *Klebsiella* pneumoniae, *Enterococcus* spp., and *Candida* spp. [1, 8]. Also, the potential of these nanosystems should be investigated in polymicrobial biofilms, where fungal-bacterial interactions pose a major challenge due to enhanced virulence and increased drug tolerance [9]. Particularly, in fungal-bacterial biofilms, it would be valuable the use of the MOX and CAS nanosystems in combination to target both the bacterial and fungal cells.

The *in vitro* evaluation of the nanosystems could be further improved by using dynamic systems, such as flow cells. In this thesis, the *in vitro* antibiofilm activity of the nanocarriers was solely assessed using static systems (Calgary device, microtiter plate, and catheter biofilm models), which are simple methods that allow high throughput screening. However, these models have limited nutrient flow and aeration, which impact biofilm growth. In dynamic systems, there is a continuous replacement of nutrients and removal of dead cells and metabolic byproducts. Despite the advantages, these systems were not used as a first approach in this work due to their lack of high throughput screening and the requirement of specialized equipment [1, 10].

In this work, we mainly focused on the treatment of biofilms grown in catheters. However, biofilms associated to orthopedic implants have even higher economic and health impacts [11]. The removal of infected orthopedic implants commonly requires surgery, which

represents high costs for the Healthcare systems. Besides, the removal of orthopedic implants may impair the life quality of the patients. Thus, it would be valuable to evaluate the potential of the developed nanosystems in *in vivo* models that represent these infections [12, 13]. For instance, Niska *et. al* (2013) described a model of prosthetic joint infection where a medical-grade stainless steel wire is placed into the femur of mice to study the combinatory effect of vancomycin and rifampin [12].

Implant-associated biofilms can be found in different places of the human body and caused by different pathogens. The choice of antibiotics to treat these biofilms largely depends on the condition to treat. The MOX nanosystem was developed and studied in this work as a proof of concept due to a previous report that showed the effect of this antibiotic in combination with CAS against *S. aureus* biofilms [5]. However, the study of other antibiotics (e.g., vancomycin, daptomycin) in combination with matrix disruptive agents should be further evaluated to treat different clinical conditions.

Nanoparticles as tools to prevent bacterial adhesion to medical devices have been highly investigated [14, 15]. The nanosystems developed in this work could also be used in a preventive strategy as coatings of implants, since all encapsulated compounds have also impact in inhibiting the biofilm formation process.

References

1. Pinto, R.M., et al., *Impact of Nanosystems in Staphylococcus aureus Biofilms Treatment.* FEMS Microbiol. Rev., 2019. **43**(6): p. 622-641, 10.1093/femsre/fuz021
2. Otto, M., *Staphylococcal biofilms.* Curr. Top. Microbiol. Immunol., 2008. **322**: p. 207-28,
3. Srivastava, S. and A. Bhargava, *Biofilms and human health.* Biotechnol Lett, 2016. **38**(1): p. 1-22, 10.1007/s10529-015-1960-8
4. Pinto, R.M., et al., *Innovative strategies toward the disassembly of the EPS matrix in bacterial biofilms.* Front. Microbiol., 2020. **11**(952), 10.3389/fmicb.2020.00952
5. Siala, W., et al., *The Antifungal Caspofungin Increases Fluoroquinolone Activity Against Staphylococcus aureus Biofilms by Inhibiting N-Acetylglucosamine Transferase.* Nat. Commun., 2016. **7**: p. 1-15, 10.1038/ncomms13286
6. Toutain-Kidd, C.M., et al., *Polysorbate 80 Inhibition of Pseudomonas aeruginosa Biofilm Formation and its Cleavage by the Secreted Lipase LipA.* Antimicrob. Agents Chemother., 2009. **53**(1): p. 136-145, 10.1128/aac.00500-08
7. Ueda, Y., et al., *Inhibitory Effects of Polysorbate 80 on MRSA Biofilm Formed on Different Substrates Including Dermal Tissue.* Sci. Rep., 2019. **9**(1): p. 3128, 10.1038/s41598-019-39997-3
8. Flores-Mireles, A.L., et al., *Urinary tract infections: epidemiology, mechanisms of infection and treatment options.* Nature Reviews Microbiology, 2015. **13**(5): p. 269-284, 10.1038/nrmicro3432
9. Van Dyck, K., et al., *Microbial Interkingdom Biofilms and the Quest for Novel Therapeutic Strategies.* Microorganisms, 2021. **9**(2): p. 412,
10. Lebeaux, D., et al., *From in vitro to in vivo models of bacterial biofilm-related infections.* Pathogens, 2013. **2**(2): p. 288-356, 10.3390/pathogens2020288
11. Ribeiro, M., F.J. Monteiro, and M.P. Ferraz, *Infection of orthopedic implants with emphasis on bacterial adhesion process and techniques used in studying bacterial-material interactions.* Biomatter, 2012. **2**(4): p. 176-194, 10.4161/biom.22905
12. Niska, J.A., et al., *Vancomycin-rifampin combination therapy has enhanced efficacy against an experimental Staphylococcus aureus prosthetic joint infection.* Antimicrob Agents Chemother, 2013. **57**(10): p. 5080-6, 10.1128/aac.00702-13
13. Bernthal, N.M., et al., *A mouse model of post-arthroplasty Staphylococcus aureus joint infection to evaluate in vivo the efficacy of antimicrobial implant coatings.* PLoS One, 2010. **5**(9): p. e12580, 10.1371/journal.pone.0012580
14. Zhang, Y., et al., *Dental implant nano-engineering: advances, limitations and future directions.* Nanomaterials, 2021. **11**(10): p. 2489,

15. Zhu, T., et al., *Coronary stents decorated by heparin/NONOate nanoparticles for anticoagulant and endothelialized effects.* Langmuir, 2020. **36**(11): p. 2901-2910, 10.1021/acs.langmuir.0c00112

Appendix

microorganisms

MDPI

Review

Microbial Interkingdom Biofilms and the Quest for Novel Therapeutic Strategies

Katrien Van Dyck [1,2], Rita M. Pinto [1,2,3], Durgasruthi Pully [1] and Patrick Van Dijck [1,2,*]

[1] Laboratory of Molecular Cell Biology, Institute of Botany and Microbiology, Department of Biology, KU Leuven, 3001 Leuven, Belgium; katrien.vandyck@kuleuven.be (K.V.D.); anaritaoliveiramacedo.pinto@kuleuven.be (R.M.P.); durgasruthi.pully@student.kuleuven.be (D.P.)
[2] VIB—KU Leuven Center for Microbiology, 3001 Leuven, Belgium
[3] LAQV, REQUIMTE, Departamento de Ciências Quimicas, Faculdade de Farmácia, Universidade Do Porto, 4050-313 Porto, Portugal
* Correspondence: patrick.vandijck@kuleuven.vib.be

Abstract: Fungal and bacterial species interact with each other within polymicrobial biofilm communities in various niches of the human body. Interactions between these species can greatly affect human health and disease. Diseases caused by polymicrobial biofilms pose a major challenge in clinical settings because of their enhanced virulence and increased drug tolerance. Therefore, different approaches are being explored to treat fungal–bacterial biofilm infections. This review focuses on the main mechanisms involved in polymicrobial drug tolerance and the implications of the polymicrobial nature for the therapeutic treatment by highlighting clinically relevant fungal–bacterial interactions. Furthermore, innovative treatment strategies which specifically target polymicrobial biofilms are discussed.

Keywords: polymicrobial; biofilm; *Candida*; biofilm matrix; quorum sensing; antimicrobial peptides; essential oils; nanoparticles; probiotics

check for updates

Citation: Van Dyck, K.; Pinto, R.M.; Pully, D.; Van Dijck, P. Microbial Interkingdom Biofilms and the Quest for Novel Therapeutic Strategies. *Microorganisms* **2021**, *9*, 412. https://doi.org/10.3390/microorganisms9020412

Academic Editor: Adolfo J. Martinez-Rodriguez

Received: 29 January 2021
Accepted: 15 February 2021
Published: 17 February 2021

Publisher's Note: MDPI stays neutral with regard to jurisdictional claims in published maps and institutional affiliations.

Copyright: © 2021 by the authors. Licensee MDPI, Basel, Switzerland. This article is an open access article distributed under the terms and conditions of the Creative Commons Attribution (CC BY) license (https://creativecommons.org/licenses/by/4.0/).

1. Introduction

Within the human body, microorganisms mostly exist in complex communities, including bacteria, fungi, and viruses [1]. In various niches of the host, interactions between fungi and bacteria frequently occur during infections [2]. The most diverse polymicrobial niches are the oral cavity and gastrointestinal tract; however, polymicrobial diseases may be located throughout the human body [1]. Both mucosal tissues and abiotic surfaces, such as catheters, dentures, and implants, are ideal surfaces for polymicrobial biofilm formation. Although it is widely accepted that the human body contains tremendous microbial diversity, most research was focused on bacteria while the fungal species, referred to as the mycobiome, were neglected [2]. *Candida* species, of which *Candida albicans* is the most prevalent, are commensal fungal species often involved in biofilm-related infections [3]. *C. albicans* is an opportunistic pathogen able to cause a variety of infections mainly in immunocompromised patients [4]. Other *Candida* species, including *Candida glabrata*, *Candida tropicalis*, *Candida parapsilosis*, *Candida krusei*, and *Candida auris*, are emerging as important causes of fungal infections as well [5]. These *Candida* species exhibit varying degrees of intrinsic resistance to the commonly used antifungal agents. The shift toward intrinsically resistant species, such as *C. krusei* and *C. auris*, in the epidemiology of *Candida* infections poses an additional medical concern [6,7]. *Candida* biofilm-associated infections are also a major challenge in clinical settings due to their intrinsic resistance to antifungals and the host immune response [8]. However, interactions of *Candida* species with bacteria in polymicrobial biofilms are an even bigger hurdle as they greatly impact the efficiency of the treatment strategy and the disease outcome [9]. *C. albicans* co-exists with commensal bacteria in several niches of the host and some of these fungal–bacterial interactions have a clear synergistic interaction, enhancing the pathogenicity of one or both species.

Staphylococcus aureus is a Gram-positive commensal bacterium of healthy humans, but is also an opportunistic pathogen able to cause disease [10]. Among the wide variety of diseases ranging from superficial to life-threatening, methicillin-resistant *S. aureus* (MRSA) is an important cause of nosocomial infections [11,12]. *C. albicans* and *S. aureus* are often co-isolated from a variety of biofilm-associated diseases, including periodontitis, cystic fibrosis, and denture stomatitis, and they display a specific increased pathogenicity and enhanced drug tolerance [13–15]. A similar synergistic interaction is observed for *C. albicans* with *Staphylococcus epidermidis*, a Gram-positive commensal bacterium often involved in implant-associated infections [16]. Another bacterium often isolated together with *C. albicans*, especially from cystic fibrosis patients, is a Gram-negative bacterium *Pseudomonas aeruginosa* [17]. In contrast to the obviously synergistic interaction with *S. aureus*, the nature of the interaction with *P. aeruginosa* is not completely clear, and highly depends on the host and model system used to establish co-infection [18]. Streptococcal bacteria including *Streptococcus oralis*, *Streptococcus mutans*, *Streptococcus gordonii*, and *Streptococcus sanguinis* are the primary colonizers of the oral cavity. Interactions between oral bacteria and *C. albicans* tend to be mostly synergistic, stimulating the colonization and pathogenic potential of one or more microorganisms [19]. Several diseases of the oral cavity, including dental caries, endodontic infections, periodontal diseases, and denture-related infections, are associated with the formation of polymicrobial biofilms [20]. In addition, *C. albicans* provides a hypoxic microenvironment that supports the growth of anaerobic bacteria as well [21].

In clinical settings, polymicrobial diseases are increasingly recognized and are often accompanied with altered infection outcomes and therapeutic problems. The most obvious challenge in the treatment of interkingdom biofilms is the evolutionary distance between the disease-causing microorganisms, since the majority of antimicrobials target only one causative agent [22]. Standard treatment strategies for interkingdom polymicrobial infections, therefore, involve a combination of an antibacterial and antifungal drug. However, this approach has a poor efficacy, resulting in high chances of treatment failure [23,24]. The main reason is the specific increased drug tolerance and enhanced pathogenicity when the nature of the biofilm is polymicrobial, caused by a variety of factors including the biofilm matrix and quorum sensing [9]. Therefore, novel treatment strategies in which a sole agent can be used to prevent or eradicate polymicrobial biofilms are urgently needed. In this regard, alternative treatment strategies including antimicrobial peptides, plant-derived components, quorum quenchers, probiotics, and the use of nanoparticles are being explored for the treatment of fungal–bacterial biofilm infections.

In this review, the main mechanisms that underlie this specific polymicrobial pathogenicity and drug tolerance and the implications of the polymicrobial nature for the therapeutic treatment and infection outcome are described, using clinically relevant fungal–bacterial interactions. Furthermore, drawbacks of existing therapeutic strategies are raised, and novel treatment strategies are highlighted.

2. The Challenges of Targeting Interkingdom Biofilms

2.1. Enhanced Pathogenicity and Altered Infection Outcome

The synergistic interaction between fungal and bacterial species often leads to an altered infection outcome related with higher morbidity and mortality rates. For example, *C. albicans* and *S. aureus* display a synergistic interaction leading to enhanced drug resistance and increased mortality in different mouse models [23,25,26]. The most common fungal biofilm-like infection of the oral cavity is oropharyngeal candidiasis (OPC), predominantly caused by *C. albicans* [27]. Since *S. aureus* is also commonly isolated from the oral cavity, a mouse model of oral *C. albicans–S. aureus* co-infection was developed [28–30]. Using this model, it was found that co-infected mice had both a higher oral colonization of *S. aureus* and were susceptible to a systemic *S. aureus* infection, whilst this was not the case for mono-infected mice [29,30]. Afterwards, research was focused on figuring out the mechanism of *S. aureus* dissemination when co-infected with *C. albicans*. Thereby, two important

requirements for bacterial dissemination were identified: the physical interaction between both species via *C. albicans* agglutinin-like sequence (Als) 1 and 3 and the host immune response [31–33]. This increased mortality and morbidity was also observed in other animal models. In a peritoneal infection mouse model, an infection with both *C. albicans* and *S. aureus* was lethal whilst the corresponding mono-microbial infections were not [26,34]. A similar synergistic interaction is observed for *C. albicans* with *S. epidermidis*, the most commonly co-isolated bacteria from *C. albicans* bloodstream infections [16]. Using a polymicrobial biofilm model in *Caenorhabditis elegans*, increased mortality was observed for a *C. albicans–S. epidermidis* co-infection compared to mono-microbial infections [35].

Regarding *P. aeruginosa*, the nature of the interaction with *C. albicans* is not completely clear. Several studies suggested that *P. aeruginosa* inhibits growth of *C. albicans* in vitro, thereby defining the interaction as antagonistic [18]. The physical interaction between the two species, mediated by type IV pili, appeared to be required for killing of *C. albicans* hyphae [36,37]. Similar effects were observed in co-infection mouse models of lung infections where prior colonization of *C. albicans* resulted in increased *P. aeruginosa* clearance [38,39]. However, in a zebrafish infection model, increased *C. albicans* pathogenicity was observed in a co-infection with *P. aeruginosa*, and also in a mouse burn wound model, higher mortality rates were observed in co-infected mice [40,41]. In addition, clinical observations also indicate a potential synergistic interaction as *Candida* colonization in the respiratory tract of critically ill patients receiving mechanical ventilation increased the risk of *P. aeruginosa* ventilator-associated pneumonia [42].

The interaction of *C. albicans* with oral streptococcal bacteria tends to be mostly synergistic. Biofilm formation of oral streptococcal bacteria including *S. gordonii*, *S. sanguinis*, and *S. oralis*, was promoted by *C. albicans* on the surface of an oral mucosa analogue [43]. The physical interaction of *C. albicans* with *S. gordonii* was shown to be mediated by streptococcal surface proteins SspA and SspB and the *Candida* adhesin Als3 [44–46]. The oral opportunistic pathogen *S. oralis* was found to colonize better in the presence of *C. albicans* in an oral infection mouse model [43,47]. Clearly, numerous animal studies confirm the increased persistence, severity, and mortality of fungal–bacterial co-infections. Additionally, in clinical settings, diseases including infections of the oral cavity, cystic fibrosis, and diabetic foot wound infections are recognized as polymicrobial infections and the composition of the microbial population can predict the disease severity and outcome of the infection [1].

2.2. The Biofilm Matrix: A Protective Shield

Biofilms are embedded in a matrix consisting of extracellular polysaccharides (EPS), proteins, and extracellular DNA (eDNA). Interestingly, more matrix material is produced in polymicrobial biofilms [23]. In *C. albicans–S. aureus* or *S. epidermidis* polymicrobial biofilms, the enhanced tolerance towards antibiotics originates from the extracellular matrix of the biofilm which limits drug penetration [10]. One of the main polysaccharides of the *C. albicans* biofilm matrix, β-1,3-glucan, was shown to be the key constituent for *S. aureus*-enhanced drug tolerance to vancomycin [48]. Likewise, extracellular polymers produced by *S. epidermidis* protected *C. albicans* against fluconazole by inhibiting penetration of the drug in a polymicrobial biofilm [49]. In addition, increased eDNA was observed in *C. albicans–S. epidermidis* or *S. aureus* mixed biofilms, and degradation of this eDNA significantly increased the sensitivity of *C. albicans* to miconazole [50,51].

C. albicans extracellular matrix components also play an important role in enhancing drug resistance of *P. aeruginosa* [52]. It was recently shown that *C. albicans* α-mannan and β-glucan polysaccharides increased the tolerance of *P. aeruginosa* to meropenem, directly impacting the treatment of co-infected cystic fibrosis patients [52]. In *P. aeruginosa–C. albicans* mixed biofilms, *C. albicans* enhances *P. aeruginosa* EPS production by increasing alginate-producing genes, *AlgU* and *mucA*. Thus, the synergy between these two microorganisms leads to thicker biofilms with an easier bacterial dissemination [53]. However, this effect seems to be attenuated in the presence of *N*-acetyl-L-cysteine both in vitro and

in an in vivo catheter-subcutaneous implantation model. This thiol-containing cysteine derivative is commonly known to disrupt disulfide bonds and cysteine utilization, exhibiting antimicrobial activity [54]. Hence, *N*-acetyl-L-cysteine may be a promising agent to prevent biofilm formation and to attenuate catheter-related sepsis due to its ability to inhibit matrix production on *P. aeruginosa–C. albicans* biofilms [53].

In *C. albicans–S. mutans* polymicrobial biofilms, bacterial EPS can bind and sequester fluconazole, thereby reducing the uptake and intracellular transport of the drug and enhancing *C. albicans* tolerance to this widely used azole drug [55]. In polymicrobial *C. albicans–S. gordonii* biofilms, the biofilm matrix components produced by *C. albicans* protected *S. gordonii* against antimicrobial treatment with clindamycin [56]. The polymicrobial biofilm architecture and composition of the biofilm matrix can be modified in several ways, thereby greatly influencing the drug susceptibility of the polymicrobial community [57]. Further research into the biofilm matrix components is crucial for the development of improved treatment strategies with a better penetration into the biofilm structure.

2.3. Quorum Sensing: Communication is the Key

Communication within microbial communities, referred to as quorum sensing (QS), is mediated by the secretion of small metabolites and plays an important role in biofilm formation. However, QS might play an even bigger role in polymicrobial biofilms [58]. In *C. albicans–P. aeruginosa* mixed biofilms, the QS molecule 3-oxo-C12 homoserine lactone was found to induce *C. albicans* resistance to fluconazole [59]. This is accomplished by facilitation of the ergosterol synthesis which is the target of fluconazole. In addition, upregulation of drug efflux and maintenance of cell wall integrity further contribute to this phenomenon. Other studies, however, indicated that this QS molecule is able to inhibit *C. albicans* filamentation without affecting fungal growth rates [60]. Interestingly, this QS molecule structurally resembles an important *C. albicans* QS molecule, farnesol, which also inhibits the morphological shift from yeast to hyphae [59,61]. In *C. albicans–S. aureus* mixed biofilms, farnesol is partly responsible for the enhanced tolerance of *S. aureus* to vancomycin, by inducing oxidative stress which in turn triggers the upregulation of drug efflux pumps [62]. In contrast, mixed biofilm formation of *C. albicans* with *S. mutans* was reduced in the presence of farnesol [63]. Farnesol treatment reduced the total biomass, metabolic activity, and cell viability. In addition, the treatment of *C. albicans–S. aureus* biofilms with a combination of farnesol and gentamicin enhanced the antimicrobial efficacy of gentamicin, demonstrating the synergy between these compounds [64]. A second important QS molecule in *C. albicans* is tyrosol, which stimulates *C. albicans* hyphal formation [65]. Similar to farnesol, an antibiofilm effect was observed for tyrosol against mixed biofilms consisting of *C. albicans*, *C. glabrata*, and *S. mutans* on acrylic resin and hydroxyapatite surfaces [66]. Farnesol and tyrosol were also investigated in the context of *C. albicans–P. aeruginosa* biofilms. Tyrosol was found to exert antibacterial activity against *P. aeruginosa* by inhibiting bacterial growth and inhibiting the production of virulence factors hemolysin and protease [67]. However, there was no effect on the antibiotic resistance of *P. aeruginosa*. Farnesol inhibited bacterial growth and hemolysin production to a lesser extent. In the case of *S. gordonii*, autoinducer 2 (AI-2), a group of molecules that promotes cross-communication between bacteria, was found to enhance *C. albicans* hyphal formation during polymicrobial biofilm growth [44].

Prostaglandin E_2, produced by *C. albicans*, is an oxygenated metabolite of arachidonic acid which is upregulated during biofilm formation. Prostaglandin E_2 functions as a regulator of host immune responses by stimulating the activation, maturation, and migration of immune-related host cells [68]. This molecule was found to stimulate growth and biofilm formation of *S. aureus* in *C. albicans–S. aureus* mixed biofilms [69]. The accessory gene regulator (*agr*) QS system in *S. aureus* controls the expression of different virulence factors including α-toxin, which mediates hemolytic activity and inflammasome activation, and reduces macrophages phagocytic killing. Significantly elevated levels of both Prostaglandin E_2 and α-toxin were observed during *C. albicans–S. aureus* co-infection in a mouse model of

intraabdominal infection, while there was no difference in bacterial burden [70]. Further research should reveal the role of interspecies communication in fungal–bacterial biofilms and the possibility to target these QS systems in the treatment of co-infections. A major advantage of interfering with QS mechanisms is that it will control virulence and biofilm formation without causing a selective pressure.

3. Novel Treatment Strategies

Polymicrobial biofilms are usually more tolerant compared to their corresponding single species biofilms thereby limiting the possibility to use conventional drugs. However, voriconazole, a second-generation antifungal drug, was found to inhibit the interaction between *C. albicans* and *Actinomyces viscosus*, a Gram-positive bacterium associated with root caries, by inhibiting the ergosterol biosynthesis pathway [71]. In addition, the antifungal and antibacterial agents caspofungin and polymyxin B were able to reduce both the cell viability and total biomass of mixed biofilms consisting of *P. aeruginosa* with *C. albicans*, *C. parapsilosis*, *C. tropicalis* or *C. glabrata* [72]. The treatment of polymicrobial infections by using a combination of antibacterial and antifungal drugs is generally associated with a poor efficacy; however, combination therapy can also result in desirable outcomes. For example, in an intraabdominal catheter infection model in mice, it was found that anidulafungin acts synergistically with tigecycline against *C. albicans–S. aureus* mixed biofilms [73]. Similarly, an antimicrobial lock solution containing micafungin, doxycycline, and ethanol, used to sterilize infected catheters or medical devices, inhibited *C. albicans–S. aureus* mixed biofilms [74]. In addition, povidone iodine enhances the efficacy of fluconazole against mixed *C. albicans–S. mutans* biofilms by functioning as an EPS inhibitor through inhibition of α-glucan synthesis [55]. However, alternative approaches are being explored to treat fungal–bacterial biofilm infections and are discussed below and summarized in Table 1.

Table 1. Summary of alternative treatment strategies for fungal–bacterial biofilms.

Treatment	Strengths	Limitations	Examples	Biofilm Target	Ref.
Antimicrobial peptides	Broad-spectrum activity Low toxicity Low probability of resistance Rapid Efficient	Chemical instability High production cost Pharmacokinetic properties	gH625 analogues	*C. tropicalis–S. aureus–S. marcescens* *C. albicans–K. pneumoniae*	[75,76]
			cholic acid-peptide conjugates	*C. albicans–S. aureus*	[77]
			guanylated polymethacrylates	*C. albicans–S. aureus*	[78]
			ε-poly-L-lysine in chitosan hydrogel	*P. aeruginosa–S. aureus–C. albicans*	[79]
Quorum quenchers	Selective pressure only under QS conditions Low probability of resistance	May disturb microbiota homeostasis May cause enhanced virulence	thiazolidinedione-8	*C. albicans–S. mutans*	[80,81]
			QQ-5 and QQ-7	*C. albicans–S. epidermidis*	[82]
Plant-derived components	Wide variety of pharmaceutical and biological activities Low toxicity	High volatility Low stability Low bioavailability Small scale production	citral and nepodine	*C. albicans–S. aureus*	[83,84]
			citrus EOs and limonene	*P. aeruginosa–A. fumigatus or S. apiospermum*	[85]
			eugenol	*C. albicans–S. mutans*	[86]
			curcumin	*C. albicans–S. aureus* *C. albicans–A. baumannii*	[87,88]
			carvacrol	*C. albicans–S. aureus*	[89]
			Rhamnus prinoides stem extract	*C. albicans–S. mutans*	[90]

Table 1. *Cont.*

Treatment	Strengths	Limitations	Examples	Biofilm Target	Ref.
Photodynamic therapy	Broad-spectrum activity No toxicity Low probability of resistance	Limited effect against biofilms in vitro studies rarely translate into animal models	erythrosine—green light	*C. albicans–S. sanguinis*	[91]
			acrylic resins doped with *Undaria pinnatifida*—blue light	*C. albicans–S. sanguinis–S. mutans–L. acidophilus*	[92]
			Zn(II)chlorin e6 methyl ester—red light	*C. albicans–E. faecalis*	[93]
Chitosan	No toxicity BiodegradableLow cost Good accessibility Low immunogenicity	Poor solubility in water	carboxymethyl chitosan	*C. albicans–C. tropicalis–S. epidermidis–S. salivarius–R. dentocariosa–L. gasseri*	[94,95]
				C. tropicalis–S. epidermidis	[96]
Nanoparticles	Enhanced bioavailability of loaded drugs Targeted delivery Easier penetration inside biofilm Protection of drugs from external environment	Possible toxicity to mammalian cells Unknown processes of in vivo metabolism clearanceLong-term toxicity Difficult scale-up High-cost	polymeric NPs magnetic NPs mesoporous silica NPs silver NPs	cf. Table 2	[97,98]
Probiotics	Restores and maintains the balance of microbiota Good accessibility Easy to use	Limited survival of viable probiotic cells Lack of clinical studies and mode-of-action studies	*S. boulardii–L. acidophilus–L. rhamnosus–B. breve* with amylase	*C. albicans* or *C. tropicalis–E. coli–S. marcenscens*	[99]
			supernatant probiotic *Lactobacillus*	*C. albicans–C. tropicalis–S. salivarius–R. dentocariosa–S. epidermidis*	[100]
			L. salivarius	*C. albicans–S. mutans*	[101]

3.1. Antimicrobial Peptides

Antimicrobial peptides (AMPs) are short positively-charged molecules with an amphipathic character which are being explored as promising antimicrobial and antibiofilm compounds [102]. In nature, AMPs belong to the innate immunity of organisms to react against various pathogens and are, therefore, promising candidates in the development of new antibiotics. The main advantages are broad-spectrum activity, relatively low toxicity, rapid mechanism of action, and low probability of antimicrobial resistance. Several studies showed that AMPs can target bacteria and fungi by interacting with microbial membranes and disrupting the physical integrity [103,104]. However, the potential to use AMPs against polymicrobial infections has only been explored recently.

The membranotropic peptide gH625 (HGLASTLTRWAHYNALIRAF), derived from the herpes simplex virus type I, is a twenty-residue peptide which was shown to interact with and destroy membrane bilayers [105]. Later, this peptide was adapted by adding a sequence of lysine residues (gH625-GCGKKKK) which promotes both the interaction with negative charges of bacterial membranes and crossing of membrane bilayers and, therefore, interferes with biofilm formation [106]. The activity of the native and adapted peptide was assessed against monomicrobial and polymicrobial biofilms of *C. tropicalis*, *S. aureus*, and *Serratia marcescens* grown on silicone platelets. Although gH625 was not able to prevent *C. tropicalis* biofilm formation, the modified peptide displayed 90% inhibition. Similarly, for polymicrobial biofilms, the modified peptide showed a greater inhibition on biofilm formation compared to the native peptide. Both peptides appeared to be potent in the eradication of mature polymicrobial biofilms, likely due to the cell-penetrating capacity [75]. Recently, the antibiofilm activity of an analogue of the gH625 peptide, gH625-M (gH625-GGGKKKK), was evaluated against polymicrobial *C. albicans–Klebsiella pneumoniae* biofilms

in vitro and in vivo [76]. Subminimal inhibitory concentrations of gH625-M were able to inhibit the formation of both mono- and polymicrobial in vitro biofilms, as well as to eradicate them. Furthermore, the in vivo antimicrobial activity of gH625-M was evaluated for the first time using *Galeria mellonella* larvae infected with *C. albicans* and *K. pneumoniae* isolates. The mortality of larvae co-infected with *C. albicans* and *K. pneumoniae* was slightly higher compared to single species infections. gH625-M was nontoxic for the larvae and the administration of gH625-M after and, especially, before infection greatly improved larvae survival rates. In addition, gH625-M treatment before infection significantly reduced the expression of *C. albicans* biofilm-associated genes *HWP1* and *ALS3* [76].

Unfortunately, the high production cost of AMPs and the chemical instability and pharmacokinetic properties hampers the development of AMP-based treatments. Therefore, alternative studies are using the characteristics of AMPs as an inspiration to develop small molecules which target bacterial or fungal membranes. In this regard, cholic acid was recently investigated for its activity against bacterial, fungal, and polymicrobial biofilms [77]. Cholic acid is a naturally-occurring bile acid with an amphiphilic nature. By adapting this molecule to better resemble the amphiphilic and cationic characteristics of AMPs, nonpeptide compounds referred to as "ceragenins" were developed [107]. Subsequently, cholic acid–peptide conjugates (CAPs), in which dipeptide units are conjugated on a cholic acid backbone, were shown to effectively interact with lipopolysaccharides and the valine–glycine dipeptide-derived CAP 3 was shown to be the most effective against Gram-negative bacteria [108]. Recently, CAP 3 was also tested against *C. albicans*, *S. aureus*, and polymicrobial biofilms [77]. Treatment with CAP 3 degraded preformed polymicrobial biofilms, and the formation of polymicrobial biofilms on CAP 3-coated catheters was prevented. In addition, CAP 3 was shown to be effective in polymicrobial wound and catheter infection models in mice. In a wound infection model, mice treated three times daily with CAP 3 showed approximately 2-log decreases in both *S. aureus* and *C. albicans* colonies. In a catheter infection model, CAP 3-coated catheters showed significant reductions in both bacterial and fungal loads [77].

Furthermore, AMP-mimicking synthetic polymers are under investigation for their anti-polymicrobial biofilm properties. These molecules have some considerable advantages as they are cheap and easy to produce and they can be chemically manipulated and integrated into drug delivery systems [109]. In this regard, guanylated polymethacrylates were synthesized, which are random copolymers of 2-guanidinoethyl methacrylate and methyl methacrylate, respectively, mimicking the cationic amino acid arginine and the lipophilic amino acid alanine. These molecules were recently shown to eradicate *C. albicans–S. aureus* polymicrobial biofilms in vitro [78]. Interestingly, when comparing the use of guanylated polymethacrylates with the use of different antimicrobial combinations, guanylated polymethacrylates were much more effective, with killing rates of >94% for *S. aureus* and >80% for *C. albicans* in the polymicrobial biofilm.

Finally, an ex vivo porcine wound biofilm model was developed to study the treatment of *P. aeruginosa*, *S. aureus*, and *C. albicans* polymicrobial biofilms [79]. As a treatment strategy, the natural peptide epsilon-poly-L-lysine was incorporated in a chitosan hydrogel and the antibiofilm efficiency was evaluated against mature polymicrobial biofilms ex vivo. The hydrogel was especially effective against *P. aeruginosa* when applied ex vivo to 24 h old polymicrobial wound biofilms; however, the activity was lower against *S. aureus*, and the hydrogel was ineffective against *C. albicans*. When the hydrogel was topically applied within 5 h after inoculation for 2 to 3 days, the biofilm thickness was reduced by at least 96% compared to untreated biofilms. Likewise, topical application of the hydrogel for 24 h to mature biofilms at 24 and 48 h after inoculation reduced biofilm thickness by >70%.

3.2. Quorum Quenchers

As described earlier, QS is a crucial process in polymicrobial biofilm formation and is, therefore, an interesting target for the development of novel treatment strategies. Interference in the process of QS, for example by inhibiting the synthesis or interaction of

QS molecules, is referred to as quorum quenching. Quorum-quenching molecules have already been used as novel therapeutic agents combating bacterial or fungal biofilms; however, the possibility to use them against polymicrobial biofilms should be investigated further. Derivatives of thiazolidinediones, which are inhibitors of QS in the Gram-negative bacterium *Vibrio harveyi*, were developed as antibiofilm agents against *C. albicans* [110,111]. One of these derivatives, thiazolidinedione-8, profoundly affected *C. albicans* biofilm formation and was able to destroy preformed biofilms [111,112]. To further increase its therapeutic potential as a drug against oral candidiasis, thiazolidinedione-8 was incorporated in a sustained-release membrane, thereby allowing a prolonged release of the drug in the oral cavity [113]. This inhibited *C. albicans* in vitro biofilm formation in a time-dependent manner and significantly eradicated mature biofilms. Additionally, it was shown that thiazolidinedione-8 decreases the biomass of *C. albicans–S. mutans* mixed biofilms in vitro, although no effect was observed against *S. mutans*, resulting in a favorable effect for *S. mutans* [80]. This was further investigated using a model system with constant flow conditions to mimic *C. albicans–S. mutans* mixed biofilm formation in the oral cavity [81]. Thiazolidinedione-8 incorporated in a sustained-release membrane allowed better penetration of the compound in the mixed species biofilm, thereby affecting both pathogens by decreasing the biofilm metabolic activity and the production of EPS and altering the morphology of both pathogens.

Other quorum-quenching molecules were identified through functional screening of metagenomic large insert libraries. Two naturally-occurring quorum-quenching enzymes (QQ-5 and QQ-7) were found to potentially interfere with *C. albicans* and *S. epidermidis* biofilm formation [82]. QQ-5 and QQ-7 were able to prevent in vitro *C. albicans* biofilm formation by inhibiting the process of morphogenesis. Inhibition of *S. epidermidis* biofilm formation was likely due to the induction of a repressor for polysaccharide intracellular adhesin (PIA), which plays a key role in *S. epidermidis* biofilm formation. These findings highlight the potential of using such quorum-quenching molecules in targeting fungal–bacterial biofilms. Non antibiotic pharmacological agents can be assessed for QS inhibition to identify new quorum-quenching molecules [114]. This drug development strategy is referred to as drug repurposing and offers some valuable advantages, as the toxicity and pharmacokinetic profile of these drugs are already established.

3.3. Plant-Derived Components

Plants protect themselves from microbial infections by the production of different types of antimicrobial molecules, including essential oils (EOs) and essential oil components. A large number of studies have been published where such compounds were tested for their antimicrobial or antibiofilm activity against either bacterial or fungal species [115–118]. More recently, several such molecules have also been tested in mixed fungal–bacterial settings. An example is citral, that shows strong activity against MRSA, where it targets biofilm specific pathways and also shows activity against different *Candida* species [119–121]. Recently, citral, as well as lemongrass, which is rich in citral and nepodin, were shown to have strong activity against dual-species *C. albicans–S. aureus* biofilms [83,84]. Citral resulted in lower biofilm biomass as well as in the number of viable cells of both species. The authors also showed that citral was interfering with the expression of *Candida* adhesins, as well as downregulating the expression of genes involved in the production of QS molecules, peptidoglycan, and fatty acids in *S. aureus* [84]. Nepodin, isolated from *Rumex crispus*, was shown to reduce the expression of hypha-specific genes and upregulated the expression of several transport genes [83]. Whereas citral was only tested in vitro, nepodin also affected *C. albicans* virulence in a nematode infection model system, but dual-species infections were not performed.

Citrus EOs obtained from pompia and grapefruit, and their major compound, limonene, were tested for their activity against mixed *P. aeruginosa–Aspergillus fumigatus* or *Scedosporium apiospermum* biofilms, which are relevant species in cystic fibrosis patients [85]. After a 24-h treatment, biofilms composed of *P. aeruginosa* and *A. fumigatus* were completely inhib-

ited, and biofilms composed of *P. aeruginosa* and *S. apiospermum* were significantly reduced. Interestingly, these EOs showed the ability to interfere with the QS system of *P. aerugonisa* and to cause *Candida* membrane damage.

Eugenol, the major component of EOs from the *Syzygium aromaticum* plant (clove), was tested for its antibiofilm activity in the management of oral diseases [86]. A concentration-dependent antibiofilm activity was observed against polymicrobial *C. albicans–S. mutans* biofilms with a reduction in biofilm formation of 52% at a subminimal inhibitory concentration of eugenol. In addition, the cell viability was significantly reduced, and cell membranes and matrix structures were disrupted. Moreover, eugenol is nontoxic and safe for human use and should, therefore, be further evaluated in vivo. A combination therapy of conventional drugs with geranium, citronella, and clove EOs was also assessed against *C. albicans–S. aureus* biofilms [122]. Treatment of these preformed polymicrobial biofilms with fluconazole or mupirocin in combination with clove oil was the most effective and resulted in a 10-fold and 4-fold increase in antibiofilm activity of fluconazole and mupirocin, respectively.

Curcumin is a polyphenol isolated from the spice *Curcuma longa* (turmeric) with a wide range of pharmacological activities, including antibacterial and antifungal effects [123]. However, the antibiofilm activity against polymicrobial *C. albicans–S. aureus* biofilms was only explored recently. Curcumin significantly reduced the formation of both mono- and polymicrobial biofilms and was effective against preformed biofilms, although the effect was smaller [87]. Interestingly, the effect was enhanced when curcumin was combined with 2-aminobenzimidazole. The antimicrobial effect of curcumin was also evaluated against mixed biofilms of *C. albicans* with *Acinetobacter baumannii*, a Gram-negative bacterium responsible for a variety of nosocomial infections [88]. Curcumin was able to reduce mixed biofilm formation by >85% and reduced *A. baumannii* virulence in a *C. elegans* model without exhibiting toxicity; however, the in vivo activity against mixed biofilms was not assessed. Unfortunately, the therapeutic application of curcumin is hindered due to its instability and low bioavailability [124].

The phenolic essential oil component carvacrol has broad spectrum antimicrobial properties and was already proved to be effective against oral and vaginal candidiasis in vivo [125,126]. However, carvacrol has a poor solubility and high volatility, which limits the application potential. Therefore, drug delivery systems using electrospun nanofibers were explored to improve the stability and prolong the activity [89]. Carvacrol-containing polylactic acid electrospun nanofibrous membranes were evaluated against *C. albicans–S. aureus* biofilms. Carvacol was gradually released from the membrane which ensured an antimicrobial activity up to 144 h. Both the formation of polymicrobial biofilms and metabolic activity, vitality, and biomass of preformed biofilms were reduced, indicating the potential of this compound for skin and wound infections [89]. Finally, a stem extract from the small *Rhamnus prinoides* tree (gesho) was able to inhibit *S. mutans–C. albicans* biofilm formation by 98%, likely by reducing the EPS production [90].

3.4. Photodynamic Therapy

Photodynamic therapy involves the combination of visible light with nontoxic dyes, called photosensitizers, to kill microbial cells including bacteria, fungi, and viruses [127]. The photosensitizers are irradiated by light of the wavelength, which they are able to absorb to generate oxidized products and singlet oxygen capable of damaging essential cell components. Photodynamic therapy appears to be very promising within various subspecialties of dentistry by offering a minimally-invasive antimicrobial treatment modality. In addition, several photosensitizers are already approved for safe use in dentistry and there is no threat of antibiotic resistance against photodynamic therapy [128].

By using erythrosine as a photosensitizer and a green light-emitting diode, significant microbial reduction of both *C. albicans* and *S. sanguinis* in a mixed in vitro biofilm was observed [91]. However, mixed biofilms of *C. albicans* with *S. sanguinis*, *S. mutans*, or *S. aureus* were still more resistant to photodynamic inactivation compared to single species

biofilms, likely due to the more complex biofilm matrix [91,129,130]. Erythrosine is already approved for use in dentistry and was used because of its nontoxic effect to the host. In addition, green LED light has some noteworthy advantages compared to other lasers, such as the cost, smaller size, and broader emission bands.

Furthermore, acrylic resins doped with *Undaria pinnatifida*, a brown seaweed microalga which contains the natural photoactive pigment chlorophyll-a, were used as photosensitizers in combination with blue light to target multispecies biofilms [92]. This study showed a dose-dependent reduction of viable microbial cells in biofilms of *C. albicans*, *S. sanguinis*, *S. mutans*, and *Lactobacillus acidophilus* and inhibition of biofilm formation of all microorganisms by 99%.

Finally, photodynamic therapy was evaluated for the eradication of endodontic biofilms by using the photosensitizer Zn(II)chlorin e6 methyl ester, obtained from chlorophyll-a, in combination with red light [93]. In an in vitro model of endodontic *C. albicans–Enterococcus faecalis* biofilm, the photodynamic therapy was able to remove 60% of the biofilm mass and was, therefore, more efficient compared to other photosensitizers. In the endodontic field, a microbial infection in the root canal system caused by multispecies biofilms remains a common problem, which led to the emergence of photodynamic therapy in this field.

3.5. Carboxymethyl Chitosan

Chitosan is a natural polysaccharide polymer that has received increasing attention in the medical world because of its antimicrobial activity combined with a low cost, good accessibility, and low toxicity [131]. However, chitosan has a poor solubility in water, which has been resolved by carboxymethylation, yielding carboxymethyl chitosan (CMC). Chitosan is active on the cell surface of fungi and bacteria via electrostatic interactions, resulting in permeabilization of the cells. The antibiofilm effect of CMC was assessed against mixed fungal–bacterial biofilms developed on silicone plates, often used for the construction of medical devices and voice prostheses [94,95]. Mixed biofilms consisted of *C. albicans*, *C. tropicalis*, *S. epidermidis*, *Streptococcus salivarius*, *Rothia dentocariosa*, and *Lactobacillus gasseri*, all isolated from voice prostheses of laryngectomized patients. Treatment with CMC inhibited biofilm formation by approximately 73% and significantly decreased the biofilm metabolic activity. In addition, CMC inhibited *Candida* morphogenesis and adhesion of both fungi and bacteria. Furthermore, CMC could effectively inhibit both mono- and polymicrobial biofilms of *C. tropicalis* and *S. epidermidis* in microplates and on silicone surfaces [96]. Polymicrobial biofilms were inhibited by 56.2% and 54.7% on microtiter plates and on silicone surfaces, respectively. Although CMC itself displays antimicrobial activity, the effect of CMC can also be further enhanced with the use of various nanoparticles. In addition, further animal model studies are crucial for the evaluation of CMC in vivo.

3.6. Nanoparticles

A promising solution to overcome the limitations of conventional therapies is to employ the use of nanoparticles (NPs). Nanomaterials behavior is different from the bulk material, mainly due to their high surface area-to-volume ratio [132]. Consequently, nanostructures have mechanical, electrical, chemical, and magnetic properties that can be an advantage for drug delivery purposes. The small size of nanocarriers facilitates their penetration into the biofilm, ensuring the release of their antimicrobial contents locally. In addition, the small size allows efficient interaction with the microbial membrane and, eventually, with the nuclear content of the pathogen, thereby interfering with cellular processes [133]. The surface charge of the NPs also plays a role in the interaction with the biofilm, since positively-charged NPs bind to the negatively-charged EPS through electrostatic interactions, which allows them to reach deeper regions. Besides being a valuable tool as nanocarriers, NPs may also show intrinsic antimicrobial properties, such as silver and gold NPs [134]. These particles inhibit QS and generate reactive oxygen species

(ROS), leading to cell damage [132,135]. Due to these unique characteristics, NPs have been explored to target polymicrobial biofilms (Table 2).

Table 2. Summary of nanoparticles developed as a therapeutic approach against interkingdom biofilms.

Nanoparticles	Formulation and Associated Compounds	Applications	Mechanism of Action	Ref.
Polymeric NPs	chitosan sodiumtripolyphosphate curcumin	Medical devices-associated infections *C. albicans–S. aureus*	Increase bioavailability Enhanced antimicrobial activity	[124]
	polylactic acid, dextran sulfate, CTAB (cationic) curcumin	Oral biofilms *S. mutans–C. albicans*–MRSA	Increase bioavailability Improve water solubility Decrease cytotoxicity Improve photodynamic effect	[136]
	chitosan sodiumtriphosphate Functionalization: CDH, DNase I	Medical devices-associated infections *C. albicans–S. aureus*	Disrupt EPS Enhanced antimicrobial activity Improve physical stability	[137]
	chitosan NPs ozonated olive oil	Endodontic infections *E. faecalis–S. mutans–C. albicans*	Synergy between ozonated olive oil and chitosan NPs	[138]
	chitosan tripolyphosphate	Early childhood caries *S. mutans–C. albicans*	Enhanced antimicrobial activity	[139]
	alginate, copper Solvents: EtOAc, DMC *A. platensis* lipid extract	*C. albicans–C. acnes*	Increase bioavailability	[140]
Magnetic NPs	iron chloride salts ammonium hydroxide Coating: aminosilane chlorhexidine	Oral biofilms *C. albicans*–MRSA–*P. aeruginosa–E. faecalis*	Decrease effective dosage Enhanced bioavailability Enhanced biocompatibility Enhanced antimicrobial activity	[141]
	iron oxide NPs Coating: chitosan chlorhexidine	Oral biofilms *C. albicans–S. mutans*	Decrease effective dosage Enhanced bioavailability	[142]
	iron oxide NPs Coating: chitosan miconazole	Caries, dentures, gingivitis *C. albicans–F. nucleatum–F. nucleatum vincentii–V. dispar–A. naeslundii*–Streptococci–*L. zeae–L. casei–R. dentocariosa*	Increase bioavailability	[143,144]
Mesoporous silica NPs	CTAB, tetraethoxysilane Functionalization: phenazine-1-carboxamide	Infections associated to urethral catheters *C. albicans–S. aureus*	Increase bioavailability Lower effective dosage Controlled drug release	[145]
Silver NPs	silver nitrate	Infections associated with catheters *C. albicans*–MRSA	Enhanced antimicrobial activity Prevent surface colonization	[146,147]
	branched polyethylenimine silver nitrate	Biofilm-based nosocomial infections *C. albicans–P. aeruginosa–S. aureus*	Prevent surface colonization	[148]
	polyamide, silver nitrate *Eucalyptus citriodora* leaves extract	Ventilator-associated pneumonia *C. albicans–P. aeruginosa–S. aureus*	Prolonged antimicrobial activity	[149]

NPs: nanoparticles; CTAB: cetyltrimethylammonium bromide; MRSA: methicillin-resistant *S. aureus*; CDH: cellobiose dehydrogenase; DNaseI: deoxyribonuclease I; EPS: extracellular polysaccharides; EtOAc: ethyl acetate; DMC: dimethyl carbonate.

Several studies reported the use of NPs as drug delivery systems of natural compounds with antimicrobial properties. Taking advantage of the antimicrobial activity of curcumin, curcumin-loaded chitosan NPs were developed and tested against *S. aureus* and *C. albicans* mono- and polymicrobial biofilms [124]. The ability of these NPs to penetrate biofilms was evaluated, and NPs were observed both at the surface and deeper regions of the biofilm, which is likely a consequence of the NPs' positive charge, promoting its interaction with negatively-charged biofilm components and microbial cells. Thus, the low diffusion of free curcumin into the biofilm is overcome by encapsulation into NPs [124]. Curcumin-loaded NPs were more effective against preformed biofilms compared to free curcumin, with a biofilm reduction of 84.36%. In a more complex approach, curcumin-loaded chitosan NPs were designed for antimicrobial photodynamic therapy, where the antimicrobial properties of the photosensitizer curcumin would be potentiated in the presence of light by ROS production [150,151]. The efficiency of anionic and cationic curcumin-loaded NPs was evaluated against mono-, dual-, and triple-species biofilms of MRSA, *S. mutans*, and *C. albicans*. For the anionic formulation, only *S. mutans* in mono-species biofilms was susceptible, possibly due to the repulsion between the NPs and the anionic components of the biofilm matrix [136]. Therefore, cetyltrimethylammonium bromide (CTAB) was further incorporated into the nanoformulation to produce cationic curcumin-loaded NPs. Both unloaded and curcumin-loaded cationic NPs showed a reduction of microbial viability in multi-species biofilms, even in the absence of light. This effect may be attributed to their positive charge, which promotes interactions with the microbial cell membrane [136]. Additionally, CTAB has been demonstrated to promote cell lysis of *S. aureus*, *E. faecalis*, and *Escherichia coli* [152]. Despite their potential, these cationic NPs are not safe systems for in vivo applications due to their cytotoxicity towards mammalian cells [136].

The previous studies showed the potential of nanocarriers to encapsulate antimicrobial agents. However, the biofilm matrix plays an important role in protecting microbial cells, thus, it is important to combine an approach that not only kills microbial cells but also disrupts matrix components [153]. In a combinatory strategy, cellobiose dehydrogenase (CDH) and deoxyribonuclease I (DNase I) were co-immobilized on chitosan NPs to target both microbial cells and the biofilm matrix [137]. CDH is widely used as an antimicrobial agent, while DNase I is able to degrade eDNA in the matrix of biofilms [154–156]. CDH–DNase NPs inhibited *C. albicans–S. aureus* mixed biofilm formation by 90.5% [137]. For preformed biofilms, the formulation showed a disruption higher than 80%. Both CDH and DNase I were also immobilized separately into NPs (CDH NPs and DNase NPs, respectively) [137]. As expected, DNase NPs had no effect on biofilm since it is not able to kill microbial cells, which allows biofilms to be constantly formed even after dispersal. However, CDH–DNase NPs showed a higher antibiofilm activity than CDH NPs, indicating a synergistic effect of DNase I by improving NPs penetration into the biofilm. Therefore, the developed nanosystem may present a safe therapeutical strategy to eradicate polymicrobial biofilms [137]. In another study, the synergy between chitosan NPs and olive oil in the treatment of oral biofilms was assessed [138]. For this purpose, an ex vivo premolar teeth model was used to grown mature mixed biofilms of *E. faecalis*, *S. mutans*, and *C. albicans*. The combinatory treatment of olive oil and chitosan NPs led to a 6-log reduction of viable cells in only two days, while chitosan NPs or olive oil alone needed at least one week to provide acceptable viability reduction [138].

Despite their advantages as nanocarriers, chitosan NPs alone have been investigated as a therapeutical strategy against polymicrobial biofilms. The in vitro efficiency of chitosan NPs was assessed against *C. albicans–S. mutans* biofilm formation. A decreasing trend of remaining biofilm biomass and a significant cell viability decrease with the increase of concentration of chitosan NPs was observed [139]. Besides chitosan, other biocompatible polymers have been used in nanosystems for antibiofilm purposes. Recently, alginate-based nanocarriers loaded with lipid extracts from cyanobacteria *Arthrospira platensis* were developed. The activity of the extracted lipids was assessed in dual-species *C. albicans–Cutibacterium acnes* biofilms. The lipid-loaded alginate NPs were successful in inhibiting

biofilm growth and disrupting preformed single-species *C. albicans* biofilms, which was not verified for the free lipid extracts. However, limited efficiency was observed when these NPs were tested in dual-species biofilms [140].

Recently, NPs with magnetic properties were explored as nanocarriers to eradicate polymicrobial biofilms. These NPs generate ROS and have, therefore, intrinsic antimicrobial activity [157]. Besides, magnetic NPs are advantageous for a targeted delivery to a specific site, since it is possible to guide them using an external magnetic field [157]. Chlorhexidine (CHX) was immobilized onto the magnetic NPs surface to enhance its antimicrobial activity [141]. Both free CHX and CHX-loaded magnetic NPs were tested in the presence of human saliva for its efficiency against multi-species oral biofilms. It was observed that immobilized CHX had an increased ability to restrict biofilm growth compared to free CHX at the same concentration. Additionally, the immobilized CHX did not exhibit cytotoxic effects against human osteoblast cells, while the free agent induced significant toxic effects [141]. To improve its biocompatibility and stability, CHX-loaded magnetic NPs were coated with chitosan [142]. The developed particles showed a significant reduction in biofilm biomass of dual-species *C. albicans–S. mutans* biofilms. The in vitro efficiency of the formulation was also assessed against preformed biofilms. The nanocarrier and the free CDX showed a metabolic activity reduction of 94.4% and 89.7% against dual-species biofilms, respectively. Thus, CDX-loaded nanocarriers may promote a higher antibiofilm effect of the drug, while lowering its toxicity toward human cells [142]. Magnetic NPs coated with chitosan were also used to load miconazole, a drug with both antibacterial and antifungal properties [143,158]. This formulation was further tested on three representative interkingdom oral biofilms (caries, denture, and gingivitis) [143]. In all three models, nanocarriers containing miconazole significantly reduced the number of viable cells. Interestingly, the formulation also promoted changes in the predominance of the different species composing the biofilm, with bacterial cells showing higher susceptibility to the treatment. In addition, fewer hyphae were observed in the presence of the designed NPs, which suggests an inhibition of *C. albicans* hyphal form during treatment. Consequently, the support provided by hyphae to bacteria is partially lost, explaining the lower numbers of bacterial cells [143].

The potential of NPs for the development of antimicrobial surface coatings to avoid biofilm formation has been also highly explored in the past years. Mesoporous silica NPs functionalized with phenazine-1-carboxamide (PCN) were produced to coat silicone urethral catheters. The authors assessed the antibiofilm activity of PCN extracted from *P. aeruginosa* and hypothesized that this metabolite induces ROS accumulation and reduction of ergosterol content. The NPs showed a controlled release of PCN over a 40-h period, which contributed to an inhibition higher than 88% of *C. albicans–S. aureus* biofilms. In fact, PCN-loaded NPs were able to inhibit mixed biofilms at a very low concentration compared to unloaded PCN [145]. In a distinct approach to inhibit formation of *C. albicans–S. aureus* biofilms in catheters, silicone elastomers were functionalized with silver NPs. The silver NPs effectively prevented mixed biofilm formation; however, the study lacks cytotoxicity assessment of the developed coating, which may hinder in vivo applications [147]. Silver NPs were also reported as a surface coating to avoid formation of *C. albicans–P. aeruginosa* biofilms [148]. Polyethylene and silicon substrates functionalized with silver NPs efficiently inhibited biofilm formation in *P. aeruginosa* monocultures, however this effect was not verified for mixed biofilms. It is believed that limited efficiency of silver NPs in coatings may be a consequence of a fast silver release from the NPs and moisture intake [148,149]. To overcome this drawback, a coating composed of silver NPs and polyamide was developed to decrease microbial adherence to endotracheal tubes [149].

3.7. Probiotics

Another strategy to target polymicrobial fungal–bacterial biofilms is the use of probiotics, which are defined as live microorganisms with beneficial effects on health when administered in adequate amounts. In patients with Crohn's disease, an inflammatory

disease of the bowel, an increase in the abundance of *C. albicans*, *C. tropicalis*, *E. coli*, and *S. marcescens* was observed [159]. Therefore, probiotics which target these pathogenic microorganisms and support beneficial microorganisms are being explored in the setting of Crohn's disease [160]. A novel probiotic formulation was developed consisting of *Saccharomyces boulardii*, *L. acidophilus*, *Lactobacillus rhamnosus*, and *Bifidobacterium breve* combined with amylase for its antibiofilm activity. This probiotic formulation possessed antibiofilm activity against polymicrobial biofilms grown on silicone elastomer discs consisting of *C. albicans* or *C. tropicalis* in combination with *E. coli* and *S. marcenscens* by reducing the polymicrobial biofilm matrix and thickness and inhibiting *Candida* hyphal formation [99]. Polymicrobial biofilm growth of *C. albicans*, *C. tropicalis*, *S. salivarius*, *R. dentocariosa*, and *S. epidermidis* on silicone medical devices, such as voice prostheses, increases the risk of infection and limits the lifetime of the prosthesis. Therefore, the supernatant of probiotic *Lactobacillus*, containing exometabolites with antimicrobial activity, was tested as a treatment for these fungal–bacterial biofilms on silicone material [100]. This *Lactobacilli* supernatant was able to inhibit the adhesion and biofilm formation and reduce the polymicrobial biofilm metabolic activity. In addition, this probiotic treatment was able to inhibit *Candida* hyphal formation. The beneficial effects of probiotics were also explored in the context of early childhood caries, of which *S. mutans* is the main etiological agent [101]. Coexistence of *S. mutans* with *C. albicans* appears to be involved in dental caries progression and recurrence. A probiotic containing *Lactobacillus salivarius* was shown to decrease the biofilm mass and inhibit *Candida* hyphal formation in dual-species biofilms of *S. mutans* with *C. albicans*, thereby weakening its pathogenic potential.

3.8. Other Treatment Strategies

A series of compounds based on a 2-aminoimidazole scaffold were constructed and tested for their antibiofilm capacity against *Salmonella* Typhimurium and *P. aeruginosa* [161]. The nontoxic N1- and 2N-substituted 5-acryl-2-aminoimidazoles compounds were screened for antibiofilm activity against polymicrobial biofilms as well [162]. These compounds showed a strong activity against polymicrobial biofilm formation by Gram-positive bacteria and *C. albicans*; however, there was no activity against Gram-negative bacteria.

Dentures are an ideal surface for polymicrobial biofilm formation and can, therefore, lead to denture-related stomatitis. The possibility to reduce biofilm formation on polymethyl methacrylate denture material by incorporating antimicrobials into the material is being investigated [163]. The antimicrobial properties against mixed biofilms consisting of *C. albicans*, *Lactobacillus casei*, and *S. mutans* of a novel fluoride-releasing material were compared with a non-fluoridated copolymer. This study showed that the fluoride release significantly reduced the cell densities of all three species, highlighting the potential to include fluoride in dentures to control biofilm growth and subsequent diseases.

Bacteriophages are viruses which are able to infect bacteria and reproduce inside. The use of bacteriophages in phage therapy is a promising strategy against pathogenic bacterial infections and was shown to be effective against biofilm-related infections as well [164]. A few studies also investigated the activity of phages and the synergistic activity of phages with antibiotics against bacterial polymicrobial biofilms [165,166]. In addition, the possibilities of phage therapy are being explored in the context of nonbacterial infections [167]. In this context, it was shown that a bacteriophage of *P. aeruginosa* is not only able to inhibit *P. aeruginosa* biofilms, but also *A. fumigatus* and *C. albicans* biofilms [168]. Both biofilm formation and preformed biofilms of *C. albicans* were inhibited, likely by iron denial [169]. The drug repurposing strategy to use such phages for the treatment of mixed fungal–bacterial infections has not yet been explored but could have a lot of potential.

4. Conclusions

Polymicrobial diseases are increasingly being recognized in clinical settings and effective treatment strategies are lacking. Therefore, understanding the molecular mechanisms of the interactions between fungal and bacterial species in different niches of the host

are of great importance. However, fungal–bacterial infections have been studied most extensively in the context of the oral microbial flora, and there is still a lack of research on these interactions in other anatomical areas or pathologies.

Although several promising techniques are highlighted here, the development of innovative therapeutic strategies to prevent interkingdom biofilms is still in its infancy. Several studies indicated the in vitro potential of antimicrobial peptides, plant-derived components, quorum quenchers, and probiotics, however, there remain hurdles to be overcome. The in vivo evaluation of the activity of these new therapeutic strategies in animal models and the assessment of possible toxicity are crucial but currently rather limited. Nanotechnology has also been highlighted as a promising tool to fight polymicrobial biofilms. Nanoparticles can be used as drug delivery systems to improve their antimicrobial effect, while decreasing their toxicity toward human cells. Besides, due to their small size, nanoparticles can reach deeper layers of the biofilm structure, leading to a higher concentration of antimicrobial agents in these regions. The intrinsic antimicrobial properties of nanoparticles have been also explored to overcome resistance phenomena and to avoid biofilm formation on medically relevant substrates. Although the reported studies showed in vitro efficacy against mixed biofilms, in vivo studies to evaluate the antibiofilm efficacy are lacking.

On a concluding note, the clinical need for the development of new strategies to target fungal–bacterial biofilm infections is high, and requires a good understanding of the interactions within these biofilms. In addition, some important properties of new drugs including broad-spectrum activity, no toxicity, and availability for oral administration should always be taken into account during the development [170]. Therefore, new components only rarely succeed from the preclinical to the clinical phase, and the quest for novel therapeutic strategies remains extremely challenging.

Author Contributions: Conceptualization: K.V.D. and P.V.D.; writing—original draft preparation: K.V.D., R.M.P., D.P., and P.V.D.; writing—review and editing: K.V.D., R.M.P., and P.V.D.; funding acquisition: P.V.D. All authors have read and agreed to the published version of the manuscript.

Funding: K.V.D. was supported by a personal research grant (1181818N) from the FWO (Fund for Scientific Research Flanders). R.M.P. is thankful to Fundação para a Ciência e Tecnologia (FCT) for her PhD grant (SFRH/BD/130319/2017). Work in the lab is supported by the FWO research community on biofilms (W000921N) and by the National Institute of Allergy and Infectious Diseases of the NIH under award number R01AI130170 (NIAID).

Data Availability Statement: The data presented in this study are available upon request from the corresponding author.

Conflicts of Interest: The authors declare no conflict of interest.

References

1. Peters, B.M.; Jabra-Rizk, M.A.; O'May, G.A.; Costerton, J.W.; Shirtliff, M.E. Polymicrobial Interactions: Impact on Pathogenesis and Human Disease. *Clinical. Microbiol. Rev.* **2012**, *25*, 193–213. [CrossRef] [PubMed]
2. Huseyin, C.E.; O'Toole, P.W.; Cotter, P.D.; Scanlan, P.D. Forgotten fungi-the gut mycobiome in human health and disease. *FEMS Microbiol. Rev.* **2017**, *41*, 479–511. [CrossRef]
3. Nobile, C.J.; Johnson, A.D. *Candida albicans* biofilms and human disease. *Annu. Rev. Microbiol.* **2015**, *69*, 71–92. [CrossRef]
4. Kim, J.; Sudbery, P. *Candida albicans*, a major human fungal pathogen. *J. Microbiol.* **2011**, *49*, 171–177. [CrossRef] [PubMed]
5. Deorukhkar, S.C.; Saini, S.; Mathew, S. Non-*albicans Candida* infection: An emerging threat. *Interdiscip. Perspect. Infect. Dis.* **2014**, *2014*, 615958. [CrossRef] [PubMed]
6. Arendrup, M.C.; Patterson, T.F. Multidrug-resistant *Candida*: Epidemiology, molecular mechanisms, and treatment. *J. Infect. Dis.* **2017**, *216*, S445–S451. [CrossRef] [PubMed]
7. Ksiezopolska, E.; Gabaldon, T. Evolutionary emergence of drug resistance in *Candida* opportunistic pathogens. *Genes* **2018**, *9*, 461. [CrossRef]
8. Gulati, M.; Nobile, C.J. *Candida albicans* biofilms: Development, regulation, and molecular mechanisms. *Microbes Infect.* **2016**, *18*, 310–321. [CrossRef]
9. Harriott, M.M.; Noverr, M.C. Importance of *Candida*-bacterial polymicrobial biofilms in disease. *Trends Microbiol.* **2011**, *19*, 557–563. [CrossRef]

10. Carolus, H.; van Dyck, K.; van Dijck, P. *Candida albicans* and *Staphylococcus* species: A threatening twosome. *Front. Microbiol.* **2019**, *10*, 2162. [CrossRef]
11. Kong, E.F.; Johnson, J.K.; Jabra-Rizk, M.A. Community-associated methicillin-resistant *Staphylococcus aureus*: An enemy amidst us. *PLoS Pathog.* **2016**, *12*, e1005837. [CrossRef]
12. Gajdacs, M. The continuing threat of methicillin-resistant *Staphylococcus aureus*. *Antibiotics* **2019**, *8*, 52. [CrossRef]
13. Baena-Monroy, T.; Moreno-Maldonado, V.; Franco-Martinez, F.; Aldape-Barrios, B.; Quindos, G.; Sanchez-Vargas, L.O. *Candida albicans*, *Staphylococcus aureus* and *Streptococcus mutans* colonization in patients wearing dental prosthesis. *Med. Oral. Patol. Oral. Cir. Bucal.* **2005**, *10*, E27–E39.
14. Valenza, G.; Tappe, D.; Turnwald, D.; Frosch, M.; Konig, C.; Hebestreit, H.; Abele-Horn, M. Prevalence and antimicrobial susceptibility of microorganisms isolated from sputa of patients with cystic fibrosis. *J. Cyst. Fibros.* **2008**, *7*, 123–127. [CrossRef] [PubMed]
15. Cuesta, A.I.; Jewtuchowicz, V.; Brusca, M.I.; Nastri, M.L.; Rosa, A.C. Prevalence of *Staphylococcus* spp and *Candida* spp in the oral cavity and periodontal pockets of periodontal disease patients. *Acta Odontol. Latinoam.* **2010**, *23*, 20–26.
16. Klotz, S.A.; Chasin, B.S.; Powell, B.; Gaur, N.K.; Lipke, P.N. Polymicrobial bloodstream infections involving *Candida* species: Analysis of patients and review of the literature. *Diagn. Microbiol. Infect Dis.* **2007**, *59*, 401–406. [CrossRef] [PubMed]
17. Fourie, R.; Ells, R.; Swart, C.W.; Sebolai, O.M.; Albertyn, J.; Pohl, C.H. *Candida albicans* and *Pseudomonas aeruginosa* interaction, with focus on the role of eicosanoids. *Front. Physiol.* **2016**, *7*, 64. [CrossRef] [PubMed]
18. Fourie, R.; Pohl, C.H. Beyond antagonism: The interaction between *Candida* species and *Pseudomonas aeruginosa*. *J. Fungi* **2019**, *5*, 34. [CrossRef] [PubMed]
19. Kruger, W.; Vielreicher, S.; Kapitan, M.; Jacobsen, I.D.; Niemiec, M.J. Fungal-bacterial interactions in health and disease. *Pathogens* **2019**, *8*, 70. [CrossRef]
20. O'Donnell, L.E.; Millhouse, E.; Sherry, L.; Kean, R.; Malcolm, J.; Nile, C.J.; Ramage, G. Polymicrobial Candida biofilms: Friends and foe in the oral cavity. *FEMS Yeast Res.* **2015**, *15*, fov077. [CrossRef]
21. Fox, E.P.; Cowley, E.S.; Nobile, C.J.; Hartooni, N.; Newman, D.K.; Johnson, A.D. Anaerobic bacteria grow within *Candida albicans* biofilms and induce biofilm formation in suspension cultures. *Curr Biol.* **2014**, *24*, 2411–2416. [CrossRef] [PubMed]
22. Brogden, K.A.; Guthmiller, J.M.; Taylor, C.E. Human polymicrobial infections. *Lancet* **2005**, *365*, 53–55. [CrossRef]
23. Harriott, M.M.; Noverr, M.C. *Candida albicans* and *Staphylococcus aureus* form polymicrobial biofilms: Effects on antimicrobial resistance. *Antimicrob. Agents Chemother.* **2009**, *53*, 3914–3922. [CrossRef]
24. Kim, S.H.; Yoon, Y.K.; Kim, M.J.; Sohn, J.W. Risk factors for and clinical implications of mixed *Candida*/bacterial bloodstream infections. *Clin. Microbiol. Infect.* **2013**, *19*, 62–68. [CrossRef]
25. Harriott, M.M.; Noverr, M.C. Ability of *Candida albicans* mutants to induce *Staphylococcus aureus* vancomycin resistance during polymicrobial biofilm formation. *Antimicrob. Agents Chemother.* **2010**, *54*, 3746–3755. [CrossRef] [PubMed]
26. Carlson, E. Synergistic effect of *Candida albicans* and *Staphylococcus aureus* on mouse mortality. *Infect. Immun.* **1982**, *38*, 921–924. [CrossRef]
27. Swidergall, M.; Filler, S.G. Oropharyngeal Candidiasis: Fungal invasion and epithelial cell responses. *PLoS Pathog.* **2017**, *13*, e1006056. [CrossRef]
28. McCormack, M.G.; Smith, A.J.; Akram, A.N.; Jackson, M.; Robertson, D.; Edwards, G. *Staphylococcus aureus* and the oral cavity: An overlooked source of carriage and infection? *Am. J. Infect. Control.* **2015**, *43*, 35–37. [CrossRef]
29. Kong, E.F.; Kucharikova, S.; van Dijck, P.; Peters, B.M.; Shirtliff, M.E.; Jabra-Rizk, M.A. Clinical implications of oral candidiasis: Host tissue damage and disseminated bacterial disease. *Infect. Immun.* **2015**, *83*, 604–613. [CrossRef] [PubMed]
30. Schlecht, L.M.; Peters, B.M.; Krom, B.P.; Freiberg, J.A.; Hansch, G.M.; Filler, S.G.; Jabra-Rizk, M.A.; Shirtliff, M.E. Systemic *Staphylococcus aureus* infection mediated by *Candida albicans* hyphal invasion of mucosal tissue. *Microbiology* **2015**, *161*, 168–181. [CrossRef] [PubMed]
31. Allison, D.L.; Scheres, N.; Willems, H.M.E.; Bode, C.S.; Krom, B.P.; Shirtliff, M.E. The host immune system facilitates disseminated *Staphylococcus aureus* disease due to phagocytic attraction to *Candida albicans* during coinfection: A case of bait and switch. *Infect. Immun.* **2019**, *87*, e00137-19. [CrossRef] [PubMed]
32. Peters, B.M.; Ovchinnikova, E.S.; Krom, B.P.; Schlecht, L.M.; Zhou, H.; Hoyer, L.L.; Busscher, H.E.; van der Mei, H.C.; Jabra-Rizk, M.A.; Shirtliff, M.E. *Staphylococcus aureus* adherence to *Candida albicans* hyphae is mediated by the hyphal adhesin Als3p. *Microbiol. SGM* **2012**, *158*, 2975–2986. [CrossRef]
33. Van Dyck, K.; Viela, F.; Mathelié-Guinlet, M.; Demuyser, L.; Hauben, E.; Jabra-Rizk, M.A.; Vande Velde, G.; Dufrêne, Y.F.; Krom, B.P.; Van Dijck, P. Adhesion of *Staphylococcus aureus* to *Candida albicans* during co-infection promotes bacterial dissemination through the host immune response. *Front. Cell. Infect. Microbiol.* **2021**, *10*, 916. [CrossRef]
34. Carlson, E. Effect of strain of *Staphylococcus aureus* on synergism with *Candida albicans* resulting in mouse mortality and morbidity. *Infect. Immun.* **1983**, *42*, 285–292. [CrossRef]
35. Holt, J.E.; Houston, A.; Adams, C.; Edwards, S.; Kjellerup, B.V. Role of extracellular polymeric substances in polymicrobial biofilm infections of *Staphylococcus epidermidis* and *Candida albicans* modelled in the nematode *Caenorhabditis elegans*. *Pathog. Dis.* **2017**, *75*, ftx052. [CrossRef]
36. Hogan, D.A.; Kolter, R. *Pseudomonas-Candida* interactions: An ecological role for virulence factors. *Science* **2002**, *296*, 2229–2232. [CrossRef] [PubMed]

37. Grainha, T.; Jorge, P.; Alves, D.; Lopes, S.P.; Pereira, M.O. Unraveling *Pseudomonas aeruginosa* and *Candida albicans* communication in coinfection scenarios: Insights through network analysis. *Front. Cell Infect. Microbiol.* **2020**, *10*, 550505. [CrossRef] [PubMed]
38. Ader, F.; Jawhara, S.; Nseir, S.; Kipnis, E.; Faure, K.; Vuotto, F.; Chemani, C.; Sendid, B.; Poulain, D.; Guery, B. Short term *Candida albicans* colonization reduces *Pseudomonas aeruginosa*-related lung injury and bacterial burden in a murine model. *Crit Care* **2011**, *15*, R150. [CrossRef]
39. Faure, E.; Bortolotti, P.; Kipnis, E.; Faure, K.; Guery, B. Studying microbial communities in vivo: A model of host-mediated interaction between *Candida Albicans* and *Pseudomonas Aeruginosa* in the airways. *J. Vis. Exp.* **2016**, *107*, e53218.
40. Bergeron, A.C.; Seman, B.G.; Hammond, J.H.; Archambault, L.S.; Hogan, D.A.; Wheeler, R.T. *Candida albicans* and *Pseudomonas aeruginosa* interact to enhance virulence of mucosal infection in transparent zebrafish. *Infect. Immun.* **2017**, *85*, e00475-17. [CrossRef] [PubMed]
41. Neely, A.N.; Law, E.J.; Holder, I.A. Increased susceptibility to lethal *Candida* infections in burned mice preinfected with *Pseudomonas aeruginosa* or pretreated with proteolytic enzymes. *Infect Immun.* **1986**, *52*, 200–204. [CrossRef]
42. Azoulay, E.; Timsit, J.F.; Tafflet, M.; de Lassence, A.; Darmon, M.; Zahar, J.R.; Adrie, C.; Garrouste-Orgeas, M.; Cohen, Y.; Mourvillier, B.; et al. *Candida* colonization of the respiratory tract and subsequent *pseudomonas* ventilator-associated pneumonia. *Chest* **2006**, *129*, 110–117. [CrossRef]
43. Diaz, P.I.; Xie, Z.; Sobue, T.; Thompson, A.; Biyikoglu, B.; Ricker, A.; Ikonomou, L.; Dongari-Bagtzoglou, A. Synergistic interaction between *Candida albicans* and commensal oral *streptococci* in a novel in vitro mucosal model. *Infect Immun.* **2012**, *80*, 620–632. [CrossRef] [PubMed]
44. Bamford, C.V.; d'Mello, A.; Nobbs, A.H.; Dutton, L.C.; Vickerman, M.M.; Jenkinson, H.F. *Streptococcus gordonii* modulates *Candida albicans* biofilm formation through intergeneric communication. *Infect. Immun.* **2009**, *77*, 3696–3704. [CrossRef] [PubMed]
45. Hoyer, L.L.; Oh, S.H.; Jones, R.; Cota, E. A proposed mechanism for the interaction between the *Candida albicans* Als3 adhesin and streptococcal cell wall proteins. *Front. Microbiol.* **2014**, *5*, 564. [CrossRef] [PubMed]
46. Silverman, R.J.; Nobbs, A.H.; Vickerman, M.M.; Barbour, M.E.; Jenkinson, H.F. Interaction of *Candida albicans* cell wall Als3 protein with *Streptococcus gordonii* SspB adhesin promotes development of mixed-species communities. *Infect. Immun.* **2010**, *78*, 4644–4652. [CrossRef]
47. Xu, H.; Sobue, T.; Thompson, A.; Xie, Z.; Poon, K.; Ricker, A.; Cervantes, J.; Diaz, P.I.; Dongari-Bagtzoglu, A. Streptococcal co-infection augments *Candida* pathogenicity by amplifying the mucosal inflammatory response. *Cell. Microbiol.* **2014**, *16*, 214–231. [CrossRef]
48. Kong, E.F.; Tsui, C.; Kucharikova, S.; Andes, D.; van Dijck, P.; Jabra-Rizk, M.A. Commensal protection of *Staphylococcus aureus* against antimicrobials by *Candida albicans* Biofilm Matrix. *mBio* **2016**, *7*, e01365-16. [CrossRef] [PubMed]
49. Adam, B.; Baillie, G.S.; Douglas, L.J. Mixed species biofilms of *Candida albicans* and *Staphylococcus epidermidis*. *J. Med. Microbiol.* **2002**, *51*, 344–349. [CrossRef]
50. Kean, R.; Rajendran, R.; Haggarty, J.; Townsend, E.M.; Short, B.; Burgess, K.E.; Lang, S.; Millington, O.; Mackay, W.G.; Williams, C.; et al. *Candida albicans* mycofilms support *Staphylococcus aureus* colonization and enhances miconazole resistance in dual-species interactions. *Front. Microbiol.* **2017**, *8*, 258. [CrossRef]
51. Pammi, M.; Liang, R.; Hicks, J.; Mistretta, T.A.; Versalovic, J. Biofilm extracellular DNA enhances mixed species biofilms of *Staphylococcus epidermidis* and *Candida albicans*. *BMC Microbiol.* **2013**, *13*, 257. [CrossRef] [PubMed]
52. Alam, F.; Catlow, D.; di Maio, A.; Blair, J.M.A.; Hall, R.A. *Candida albicans* enhances meropenem tolerance of *Pseudomonas aeruginosa* in a dual-species biofilm. *J. Antimicrob. Chemother.* **2020**, *75*, 925–935. [CrossRef]
53. Phuengmaung, P.; Somparn, P.; Panpetch, W.; Singkham-In, U.; Wannigama, D.L.; Chatsuwan, T.; Leelahavanichkul, A. Coexistence of *Pseudomonas aeruginosa* with *Candida albicans* enhances biofilm thickness through alginate-related extracellular matrix but is attenuated by N-acetyl-l-cysteine. *Front. Cell Infect. Microbiol.* **2020**, *10*, 594336. [CrossRef] [PubMed]
54. Olofsson, A.C.; Hermansson, M.; Elwing, H. N-Acetyl-l-Cysteine affects growth, extracellular polysaccharide production, and bacterial biofilm formation on solid surfaces. *Appl. Environ. Microbiol.* **2003**, *69*, 4814–4822. [CrossRef]
55. Kim, D.; Liu, Y.; Benhamou, R.I.; Sanchez, H.; Simon-Soro, A.; Li, Y.; Hwang, G.; Fridman, M.; Andes, D.R.; Koo, H. Bacterial-derived exopolysaccharides enhance antifungal drug tolerance in a cross-kingdom oral biofilm. *ISME J.* **2018**, *12*, 1427–1442. [CrossRef] [PubMed]
56. Montelongo-Jauregui, D.; Saville, S.P.; Lopez-Ribot, J.L. Contributions of *Candida albicans* Dimorphism, Adhesive Interactions, and Extracellular Matrix to the Formation of Dual-Species Biofilms with *Streptococcus gordonii*. *mBio* **2019**, *10*, e01179-19. [CrossRef]
57. Orazi, G.; O'Toole, G.A. "It Takes a Village": Mechanisms Underlying antimicrobial recalcitrance of polymicrobial biofilms. *J. Bacteriol.* **2019**, *202*, e00530-19. [CrossRef]
58. Dixon, E.F.; Hall, R.A. Noisy neighbourhoods: Quorum sensing in fungal-polymicrobial infections. *Cell. Microbiol.* **2015**, *17*, 1431–1441. [CrossRef]
59. Bandara, H.; Wood, D.L.A.; Vanwonterghem, I.; Hugenholtz, P.; Cheung, B.P.K.; Samaranayake, L.P. Fluconazole resistance in *Candida albicans* is induced by *Pseudomonas aeruginosa* quorum sensing. *Sci. Rep.* **2020**, *10*, 7769. [CrossRef]
60. Hogan, D.A.; Vik, A.; Kolter, R. A *Pseudomonas aeruginosa* quorum-sensing molecule influences *Candida albicans* morphology. *Mol. Microbiol.* **2004**, *54*, 1212–1223. [CrossRef]
61. Rodrigues, C.F.; Cernakova, L. Farnesol and Tyrosol: Secondary metabolites with a crucial quorum-sensing role in *Candida* Biofilm Development. *Genes* **2020**, *11*, 444. [CrossRef]

62. Kong, E.F.; Tsui, C.; Kucharikova, S.; van Dijck, P.; Jabra-Rizk, M.A. Modulation of *Staphylococcus aureus* response to antimicrobials by the *Candida albicans* quorum sensing molecule farnesol. *Antimicrob. Agents Chemother.* **2017**, *61*, e01573-17. [CrossRef]
63. Fernandes, R.A.; Monteiro, D.R.; Arias, L.S.; Fernandes, G.L.; Delbem, A.C.; Barbosa, D.B. Biofilm formation by *Candida albicans* and *Streptococcus mutans* in the presence of farnesol: A quantitative evaluation. *Biofouling* **2016**, *32*, 329–338. [CrossRef]
64. Jabra-Rizk, M.A.; Meiller, T.F.; James, C.E.; Shirtliff, M.E. Effect of farnesol on *Staphylococcus aureus* biofilm formation and antimicrobial susceptibility. *Antimicrob. Agents Chemother.* **2006**, *50*, 1463–1469. [CrossRef]
65. Chen, H.; Fujita, M.; Feng, Q.; Clardy, J.; Fink, G.R. Tyrosol is a quorum-sensing molecule in *Candida albicans*. *Proc. Natl. Acad. Sci. USA* **2004**, *101*, 5048–5052. [CrossRef]
66. Arias, L.S.; Delbem, A.C.; Fernandes, R.A.; Barbosa, D.B.; Monteiro, D.R. Activity of tyrosol against single and mixed-species oral biofilms. *J. Appl. Microbiol.* **2016**, *120*, 1240–1249. [CrossRef] [PubMed]
67. Abdel-Rhman, S.H.; El-Mahdy, A.M.; El-Mowafy, M. Effect of tyrosol and farnesol on virulence and antibiotic resistance of clinical isolates of *Pseudomonas aeruginosa*. *Biomed. Res. Int.* **2015**, *2015*, 456463. [PubMed]
68. Erb-Downward, J.R.; Noverr, M.C. Characterization of prostaglandin E2 production by *Candida albicans*. *Infect. Immun.* **2007**, *75*, 3498–3505. [CrossRef] [PubMed]
69. Krause, J.; Geginat, G.; Tammer, I. Prostaglandin E2 from *Candida albicans* stimulates the growth of *Staphylococcus aureus* in mixed biofilms. *PLoS ONE* **2015**, *10*, e0135404. [CrossRef]
70. Todd, O.A.; Fidel, P.L., Jr.; Harro, J.M.; Hilliard, J.J.; Tkaczyk, C.; Sellman, B.R.; Noverr, M.C.; Peters, B.M. *Candida albicans* augments *Staphylococcus aureus* virulence by engaging the staphylococcal *agr* quorum sensing system. *mBio* **2019**, *10*, e00910-19. [CrossRef]
71. Deng, L.; Zou, L.; Wu, J.; Liu, H.; Luo, T.; Zhou, X.; Li, W.; Ren, B. Voriconazole inhibits cross-kingdom interactions between *Candida albicans* and *Actinomyces viscosus* through the ergosterol pathway. *Int. J. Antimicrob. Agents* **2019**, *53*, 805–813. [CrossRef]
72. Fernandes, L.; Fortes, B.N.; Lincopan, N.; Ishida, K. Caspofungin and polymyxin B reduce the cell viability and total biomass of mixed biofilms of carbapenem-resistant *Pseudomonas aeruginosa* and *Candida* spp. *Front. Microbiol.* **2020**, *11*, 573263. [CrossRef]
73. Rogiers, O.; Holtappels, M.; Siala, W.; Lamkanfi, M.; van Bambeke, F.; Lagrou, K.; Van Dijck, P.; Kucharikova, S. Anidulafungin increases the antibacterial activity of tigecycline in polymicrobial *Candida albicans/Staphylococcus aureus* biofilms on intraperitoneally implanted foreign bodies. *J. Antimicrob. Chemother.* **2018**, *73*, 2806–2814. [CrossRef] [PubMed]
74. Lown, L.; Peters, B.M.; Walraven, C.J.; Noverr, M.C.; Lee, S.A. An optimized lock solution containing micafungin, ethanol and doxycycline inhibits *Candida albicans* and mixed, *C. albicans-Staphylococcus aureus* biofilms. *PLoS ONE* **2016**, *11*, e0159225. [CrossRef] [PubMed]
75. De Alteriis, E.; Lombardi, L.; Falanga, A.; Napolano, M.; Galdiero, S.; Siciliano, A.; Carotenuto, R.; Guida, M.; Galdiero, E. Polymicrobial antibiofilm activity of the membranotropic peptide gH625 and its analogue. *Microb Pathog.* **2018**, *125*, 189–195. [CrossRef] [PubMed]
76. Maione, A.; de Alteriis, E.; Carraturo, F.; Galdiero, S.; Falanga, A.; Guida, M.; Di Cosmo, A.; Maselli, V.; Galdiero, E. The membranotropic peptide gH625 to combat mixed *Candida albicans/Klebsiella pneumoniae* biofilm: Correlation between in vitro anti-biofilm activity and in vivo antimicrobial protection. *J. Fungi* **2021**, *7*, 26. [CrossRef] [PubMed]
77. Gupta, S.; Thakur, J.; Pal, S.; Gupta, R.; Mishra, D.; Kumar, S.; Yadav, K.; Saini, A.; Yavvari, P.S.; Vedantham, M.; et al. Cholic acid-peptide conjugates as potent antimicrobials against interkingdom polymicrobial biofilms. *Antimicrob. Agents Chemother.* **2019**, *63*, e00520-19. [CrossRef]
78. Qu, Y.; Locock, K.; Verma-Gaur, J.; Hay, I.D.; Meagher, L.; Traven, A. Searching for new strategies against polymicrobial biofilm infections: Guanylated polymethacrylates kill mixed fungal/bacterial biofilms. *J. Antimicrob. Chemother.* **2016**, *71*, 413–421. [CrossRef]
79. Pati, B.A.; Kurata, W.E.; Horseman, T.S.; Pierce, L.M. Antibiofilm activity of chitosan/epsilon-poly-L-lysine hydrogels in a porcine ex vivo skin wound polymicrobial biofilm model. *Wound Repair Regen.* **2021**. [CrossRef] [PubMed]
80. Feldman, M.; Ginsburg, I.; Al-Quntar, A.; Steinberg, D. Thiazolidinedione-8 alters symbiotic relationship in *C. albicans-S. mutans* dual species biofilm. *Front. Microbiol.* **2016**, *7*, 140. [CrossRef]
81. Feldman, M.; Shenderovich, J.; Lavy, E.; Friedman, M.; Steinberg, D. A sustained-release membrane of thiazolidinedione-8: Effect on formation of a *Candida*/bacteria mixed biofilm on hydroxyapatite in a continuous flow model. *Biomed. Res. Int.* **2017**, *2017*, 3510124. [CrossRef] [PubMed]
82. Weiland-Brauer, N.; Malek, I.; Schmitz, R.A. Metagenomic quorum quenching enzymes affect biofilm formation of *Candida albicans* and *Staphylococcus epidermidis*. *PLoS ONE* **2019**, *14*, e0211366. [CrossRef]
83. Lee, J.H.; Kim, Y.G.; Khadke, S.K.; Yamano, A.; Watanabe, A.; Lee, J. Inhibition of biofilm formation by *Candida albicans* and polymicrobial microorganisms by nepodin via hyphal-growth suppression. *ACS Infect. Dis.* **2019**, *5*, 1177–1187. [CrossRef]
84. Gao, S.; Liu, G.; Li, J.; Chen, J.; Li, L.; Li, Z.; Zhang, X.; Zhang, S.; Thorne, R.F.; Zhang, S. Antimicrobial activity of lemongrass essential oil (Cymbopogon flexuosus) and its active component citral against dual-species biofilms of *Staphylococcus aureus* and *Candida* species. *Front. Cell Infect. Microbiol.* **2020**, *10*, 603858. [CrossRef]
85. Pekmezovic, M.; Aleksic, I.; Barac, A.; Arsic-Arsenijevic, V.; Vasiljevic, B.; Nikodinovic-Runic, J.; Senerovic, L. Prevention of polymicrobial biofilms composed of *Pseudomonas aeruginosa* and pathogenic fungi by essential oils from selected Citrus species. *Pathog Dis.* **2016**, *74*, ftw102. [CrossRef] [PubMed]

86. Jafri, H.; Khan, M.S.A.; Ahmad, I. In vitro efficacy of eugenol in inhibiting single and mixed-biofilms of drug-resistant strains of *Candida albicans* and *Streptococcus mutans*. *Phytomedicine* **2019**, *54*, 206–213. [CrossRef] [PubMed]
87. Tan, Y.; Leonhard, M.; Moser, D.; Ma, S.; Schneider-Stickler, B. Antibiofilm efficacy of curcumin in combination with 2-aminobenzimidazole against single- and mixed-species biofilms of *Candida albicans* and *Staphylococcus aureus*. *Colloids Surf. B Biointerfaces* **2019**, *174*, 28–34. [CrossRef] [PubMed]
88. Raorane, C.J.; Lee, J.H.; Kim, Y.G.; Rajasekharan, S.K.; Garcia-Contreras, R.; Lee, J. Antibiofilm and antivirulence efficacies of flavonoids and curcumin against *Acinetobacter baumannii*. *Front. Microbiol.* **2019**, *10*, 990. [CrossRef] [PubMed]
89. Scaffaro, R.; Lopresti, F.; D'Arrigo, M.; Marino, A.; Nostro, A. Efficacy of poly(lactic acid)/carvacrol electrospun membranes against *Staphylococcus aureus* and *Candida albicans* in single and mixed cultures. *Appl. Microbiol. Biotechnol.* **2018**, *102*, 4171–4181. [CrossRef]
90. Campbell, M.; Fathi, R.; Cheng, S.Y.; Ho, A.; Gilbert, E.S. *Rhamnus prinoides* (gesho) stem extract prevents co-culture biofilm formation by *Streptococcus mutans* and *Candida albicans*. *Lett. Appl. Microbiol.* **2020**, *71*, 294–302. [CrossRef]
91. Palma, A.; Paula-Ramos, L.; Domingues, N.; Back-Brito, G.N.; de Oliveira, L.D.; Pereira, C.A.; Jorge, A.O.C. Biofilms of *Candida albicans* and *Streptococcus sanguinis* and their susceptibility to antimicrobial effects of photodynamic inactivation. *Photodiagnosis Photodyn. Ther.* **2018**, *24*, 95–101. [CrossRef]
92. Pourhajibagher, M.; Ghorbanzadeh, R.; Bahador, A. Antimicrobial properties of acrylic resins doped with *Undaria pinnatifida* exposed to light-emitting diode: In silico and in vitro assessments on multispecies biofilm-producing microbiota. *Photodiagnosis Photodyn. Ther.* **2019**, *27*, 210–215. [CrossRef] [PubMed]
93. Diogo, P.; Fernandes, C.; Caramelo, F.; Mota, M.; Miranda, I.M.; Faustino, M.A.F.; Neves, M.G.P.M.S.; Uliana, M.P.; de Oliveira, K.T.; Santos, J.M. Antimicrobial photodynamic therapy against endodontic *Enterococcus faecalis* and *Candida albicans* mono and mixed biofilms in the presence of photosensitizers: A comparative study with classical endodontic irrigants. *Front Microbiol.* **2017**, *8*, 498. [CrossRef]
94. Tan, Y.; Leonhard, M.; Moser, D.; Ma, S.; Schneider-Stickler, B. Long-term antibiofilm activity of carboxymethyl chitosan on mixed biofilm on silicone. *Laryngoscope* **2016**, *126*, E404–E408. [CrossRef]
95. Tan, Y.; Leonhard, M.; Moser, D.; Ma, S.; Schneider-Stickler, B. Inhibition of mixed fungal and bacterial biofilms on silicone by carboxymethyl chitosan. *Colloids Surf. B Biointerfaces* **2016**, *148*, 193–199. [CrossRef]
96. Tan, Y.; Leonhard, M.; Ma, S.; Moser, D.; Schneider-Stickler, B. Efficacy of carboxymethyl chitosan against *Candida tropicalis* and *Staphylococcus epidermidis* monomicrobial and polymicrobial biofilms. *Int. J. Biol. Macromol.* **2018**, *110*, 150–156. [CrossRef] [PubMed]
97. Ramasamy, M.; Lee, J. Recent nanotechnology approaches for prevention and treatment of biofilm-associated infections on medical devices. *BioMed Res. Int.* **2016**, *2016*, 1851242. [CrossRef] [PubMed]
98. Yetisgin, A.A.; Cetinel, S.; Zuvin, M.; Kosar, A.; Kutlu, O. Therapeutic nanoparticles and their targeted delivery applications. *Molecules* **2020**, *25*, 2193. [CrossRef] [PubMed]
99. Hager, C.L.; Isham, N.; Schrom, K.P.; Chandra, J.; McCormick, T.; Miyagi, M.; Ghannoum, M.A. Effects of a novel probiotic combination on pathogenic bacterial-fungal polymicrobial biofilms. *mBio* **2019**, *10*, e00338-19. [CrossRef]
100. Tan, Y.; Leonhard, M.; Moser, D.; Schneider-Stickler, B. Inhibition activity of *Lactobacilli* supernatant against fungal-bacterial multispecies biofilms on silicone. *Microb. Pathog.* **2017**, *113*, 197–201. [CrossRef]
101. Krzysciak, W.; Koscielniak, D.; Papiez, M.; Vyhouskaya, P.; Zagorska-Swiezy, K.; Kolodziej, I.; Bystrowska, B.; Jurczak, A. Effect of a *Lactobacillus salivarius* probiotic on a double-species *Streptococcus mutans* and *Candida albicans* caries biofilm. *Nutrients* **2017**, *9*, 1242. [CrossRef]
102. Mahlapuu, M.; Hakansson, J.; Ringstad, L.; Bjorn, C. Antimicrobial peptides: An emerging category of therapeutic agents. *Front. Cell. Infect. Microbiol.* **2016**, *6*, 194. [CrossRef] [PubMed]
103. Buda De Cesare, G.; Cristy, S.A.; Garsin, D.A.; Lorenz, M.C. Antimicrobial peptides: A new frontier in antifungal therapy. *mBio* **2020**, *11*, e02123-20. [CrossRef] [PubMed]
104. Marr, A.K.; Gooderham, W.J.; Hancock, R.E. Antibacterial peptides for therapeutic use: Obstacles and realistic outlook. *Curr. Opin. Pharmacol.* **2006**, *6*, 468–472. [CrossRef] [PubMed]
105. Galdiero, S.; Falanga, A.; Morelli, G.; Galdiero, M. gH625: A milestone in understanding the many roles of membranotropic peptides. *Biochim. Biophys. Acta* **2015**, *184*, 16–25. [CrossRef]
106. Falanga, A.; Valiante, S.; Galdiero, E.; Franci, G.; Scudiero, O.; Morelli, G.; Galdiero, S. Dimerization in tailoring uptake efficacy of the HSV-1 derived membranotropic peptide gH625. *Sci. Rep.* **2017**, *7*, 9434. [CrossRef]
107. Lai, X.Z.; Feng, Y.; Pollard, J.; Chin, J.N.; Rybak, M.J.; Bucki, R.; Epand, R.F.; Epand, R.M.; Savage, P.B. Ceragenins: Cholic acid-based mimics of antimicrobial peptides. *Acc. Chem. Res.* **2008**, *41*, 1233–1340. [CrossRef] [PubMed]
108. Yadav, K.; Kumar, S.; Mishra, D.; Asad, M.; Mitra, M.; Yavvari, P.S.; Gupta, S.; Vendantham, M.; Ranga, P.; Komalla, V.; et al. Deciphering the role of intramolecular networking in cholic acid-peptide conjugates on the lipopolysaccharide surface in combating gram-negative bacterial infections. *J. Med. Chem.* **2019**, *62*, 1875–1886. [CrossRef]
109. Locock, K.E.; Michl, T.D.; Valentin, J.D.; Vasilev, K.; Hayball, J.D.; Qu, Y.; Traven, A.; Griesser, H.J.; Meagher, L.; Haeussler, M. Guanylated polymethacrylates: A class of potent antimicrobial polymers with low hemolytic activity. *Biomacromolecules* **2013**, *14*, 4021–4031. [CrossRef] [PubMed]

110. Brackman, G.; Al Quntar, A.A.; Enk, C.D.; Karalic, I.; Nelis, H.J.; van Calenbergh, S.; Srebnik, M.; Coenye, T. Synthesis and evaluation of thiazolidinedione and dioxazaborocane analogues as inhibitors of AI-2 quorum sensing in *Vibrio harveyi*. *Bioorg. Med. Chem.* **2013**, *21*, 660–667. [CrossRef]
111. Kagan, S.; Jabbour, A.; Sionov, E.; Alquntar, A.A.; Steinberg, D.; Srebnik, M.; Nir-Paz, R.; Weiss, A.; Polacheck, I. Anti-*Candida albicans* biofilm effect of novel heterocyclic compounds. *J. Antimicrob. Chemother.* **2014**, *69*, 416–427. [CrossRef] [PubMed]
112. Feldman, M.; Al-Quntar, A.; Polacheck, I.; Friedman, M.; Steinberg, D. Therapeutic potential of thiazolidinedione-8 as an antibiofilm agent against *Candida albicans*. *PLoS ONE* **2014**, *9*, e93225. [CrossRef] [PubMed]
113. Feldman, M.; Shenderovich, J.; Al-Quntar, A.A.; Friedman, M.; Steinberg, D. Sustained release of a novel anti-quorum-sensing agent against oral fungal biofilms. *Antimicrob. Agents Chemother.* **2015**, *59*, 2265–2272. [CrossRef]
114. Gajdacs, M.; Spengler, G. The role of drug repurposing in the development of novel antimicrobial drugs: Non-antibiotic pharmacological agents as quorum sensing-inhibitors. *Antibiotics* **2019**, *8*, 270. [CrossRef]
115. Horvath, G.; Acs, K. Essential oils in the treatment of respiratory tract diseases highlighting their role in bacterial infections and their anti-inflammatory action: A review. *Flavour. Fragr. J.* **2015**, *30*, 331–341. [CrossRef] [PubMed]
116. Feyaerts, A.F.; Mathe, L.; Luyten, W.; de Graeve, S.; van Dyck, K.; Broekx, L.; Van Dijck, P. Essential oils and their components are a class of antifungals with potent vapour-phase-mediated anti-*Candida* activity. *Sci. Rep.* **2018**, *8*, 3958. [CrossRef]
117. Trifan, A.; Luca, S.V.; Greige-Gerges, H.; Miron, A.; Gille, E.; Aprotosoaie, A.C. Recent advances in tackling microbial multidrug resistance with essential oils: Combinatorial and nano-based strategies. *Crit. Rev. Microbiol.* **2020**, *46*, 338–357. [CrossRef]
118. D'Agostino, M.; Tesse, N.; Frippiat, J.P.; Machouart, M.; Debourgogne, A. Essential oils and their natural active compounds presenting antifungal properties. *Molecules* **2019**, *24*, 3713. [CrossRef]
119. Zouhir, A.; Jridi, T.; Nefzi, A.; Ben Hamida, J.; Sebei, K. Inhibition of methicillin-resistant *Staphylococcus aureus* (MRSA) by antimicrobial peptides (AMPs) and plant essential oils. *Pharm. Biol.* **2016**, *54*, 3136–3150. [CrossRef]
120. de Silva, C.B.; Guterres, S.S.; Weisheimer, V.; Schapoval, E.E. Antifungal activity of the lemongrass oil and citral against *Candida* spp. *Braz. J. Infect. Dis.* **2008**, *12*, 63–66. [CrossRef]
121. Valliammai, A.; Sethupathy, S.; Ananthi, S.; Priya, A.; Selvaraj, A.; Nivetha, V.; Aravindraja, C.; Mahalingam, S.; Pandian, S.K. Proteomic profiling unveils citral modulating expression of IsaA, CodY and SaeS to inhibit biofilm and virulence in methicillin-resistant *Staphylococcus aureus*. *Int. J. Biol. Macromol.* **2020**, *20*, 33095–33096. [CrossRef]
122. Budzynska, A.; Rozalska, S.; Sadowska, B.; Rozalska, B. *Candida albicans/Staphylococcus aureus* dual-species biofilm as a target for the combination of essential oils and fluconazole or mupirocin. *Mycopathologia* **2017**, *182*, 989–995. [CrossRef]
123. Chattopadhyay, I.; Biswas, K.; Bandyopadhyay, U.; Banerjee, R.K. Turmeric and curcumin: Biological actions and medicinal applications. *Curr. Sci.* **2004**, *87*, 44–53.
124. Ma, S.; Moser, D.; Han, F.; Leonhard, M.; Schneider-Stickler, B.; Tan, Y. Preparation and antibiofilm studies of curcumin loaded chitosan nanoparticles against polymicrobial biofilms of *Candida albicans* and *Staphylococcus aureus*. *Carbohydr. Polym.* **2020**, *241*, 116254. [CrossRef] [PubMed]
125. Chami, F.; Chami, N.; Bennis, S.; Trouillas, J.; Remmal, A. Evaluation of carvacrol and eugenol as prophylaxis and treatment of vaginal candidiasis in an immunosuppressed rat model. *J. Antimicrob. Chemother.* **2004**, *54*, 909–914. [CrossRef] [PubMed]
126. Chami, N.; Chami, F.; Bennis, S.; Trouillas, J.; Remmal, A. Antifungal treatment with carvacrol and eugenol of oral candidiasis in immunosuppressed rats. *Braz. J. Infect. Dis.* **2004**, *8*, 217–226. [CrossRef] [PubMed]
127. Huang, L.; Dai, T.; Hamblin, M.R. Antimicrobial photodynamic inactivation and photodynamic therapy for infections. *Methods Mol. Biol.* **2010**, *635*, 155–173.
128. Stajer, A.; Kajari, S.; Gajdacs, M.; Musah-Eroje, A.; Barath, Z. Utility of photodynamic therapy in dentistry: Current concepts. *Dent. J.* **2020**, *8*, 43. [CrossRef]
129. Pereira, C.A.; Romeiro, R.L.; Costa, A.C.; Machado, A.K.; Junqueira, J.C.; Jorge, A.O. Susceptibility of *Candida albicans, Staphylococcus aureus*, and *Streptococcus mutans* biofilms to photodynamic inactivation: An in vitro study. *Lasers Med. Sci.* **2011**, *26*, 341–348. [CrossRef]
130. Tome, F.M.; Paula Ramos, L.; Freire, F.; Pereira, C.A.; de Oliveira, I.C.B.; Junqueira, J.C.; Jorge, A.O.C.; Oliveira, L.D. Influence of sucrose on growth and sensitivity of *Candida albicans* alone and in combination with *Enterococcus faecalis* and *Streptococcus mutans* to photodynamic therapy. *Lasers Med. Sci.* **2017**, *32*, 1237–1243. [CrossRef]
131. Shariatinia, Z. Carboxymethyl chitosan: Properties and biomedical applications. *Int. J. Biol. Macromol.* **2018**, *120*, 1406–1419. [CrossRef]
132. Hajipour, M.J.; Fromm, K.M.; Ashkarran, A.A.; Jimenez de Aberasturi, D.; de Larramendi, I.R.; Rojo, T.; Serpooshan, V.; Parak, W.J.; Mahmoudi, M. Antibacterial properties of nanoparticles. *Trends Biotechnol.* **2012**, *30*, 499–511. [CrossRef] [PubMed]
133. Hoseinzadeh, E.; Makhdoumi, P.; Taha, P.; Hossini, H.; Stelling, J.; Kamal, M.A.; Ashraf, G.M. A review on nano-antimicrobials: Metal nanoparticles, methods and mechanisms. *Curr. Drug. Metab.* **2017**, *18*, 120–128. [CrossRef]
134. Lopes, D.; Nunes, C.; Martins, M.C.; Sarmento, B.; Reis, S. Eradication of *Helicobacter pylori*: Past, present and future. *J. Control. Release* **2014**, *189*, 169–186. [CrossRef]
135. Masurkar, S.A.; Chaudhari, P.R.; Shidore, V.B.; Kamble, S.P. Effect of biologically synthesised silver nanoparticles on *Staphylococcus aureus* biofilm quenching and prevention of biofilm formation. *IET Nanobiotechnol.* **2012**, *6*, 110–114. [CrossRef] [PubMed]

136. Trigo Gutierrez, J.K.; Zanatta, G.C.; Ortega, A.L.M.; Balastegui, M.I.C.; Sanitá, P.V.; Pavarina, A.C.; Barbugli, P.A.; Mima, E.G.O. Encapsulation of curcumin in polymeric nanoparticles for antimicrobial ohotodynamic therapy. *PLoS ONE* **2017**, *12*, e0187418. [CrossRef]
137. Tan, Y.; Ma, S.; Leonhard, M.; Moser, D.; Ludwig, R.; Schneider-Stickler, B. Co-immobilization of cellobiose dehydrogenase and deoxyribonuclease I on chitosan nanoparticles against fungal/bacterial polymicrobial biofilms targeting both biofilm matrix and microorganisms. *Mat. Sci. Eng. C Mater. Biol. Appl.* **2020**, *108*, 110499. [CrossRef] [PubMed]
138. Elshinawy, M.I.; Al-Madboly, L.A.; Ghoneim, W.M.; El-Deeb, N.M. Synergistic effect of newly introduced root canal medicaments; ozonated olive oil and chitosan nanoparticles, against persistent endodontic pathogens. *Front. Microbiol.* **2018**, *9*, 1371. [CrossRef]
139. Ikono, R.; Vibriani, A.; Wibowo, I.; Saputro, K.E.; Muliawan, W.; Bachtiar, B.M.; Mardliyati, E.; Bachtiar, E.W.; Rochman, N.; Kagami, H.; et al. Nanochitosan antimicrobial activity against *Streptococcus mutans* and *Candida albicans* dual-species biofilms. *BMC Res. Notes* **2019**, *12*, 383. [CrossRef]
140. Lemoine, V.; Bernard, C.; Leman-Loubiere, C.; Clement-Larosiere, B.; Girardot, M.; Boudesocque-Delaye, L.; Munnier, E.; Imbert, C. Nanovectorized microalgal extracts to fight *Candida albicans* and *Cutibacterium acnes* biofilms: Impact of dual-species conditions. *Antibiotics* **2020**, *9*, 279. [CrossRef]
141. Tokajuk, G.; Niemirowicz, K.; Deptuła, P.; Piktel, E.; Cieśluk, M.; Wilczewska, A.Z.; Dabrowski, J.R.; Bucki, R. Use of magnetic nanoparticles as a drug delivery system to improve chlorhexidine antimicrobial activity. *Int. J. Nanomed.* **2017**, *12*, 7833–7846. [CrossRef]
142. Vieira, A.P.M.; Arias, L.S.; de Souza Neto, F.N.; Kubo, A.M.; Lima, B.H.R.; de Camargo, E.R.; Pessan, J.P.; Delbem, A.C.B.; Monteiro, D.R. Antibiofilm effect of chlorhexidine-carrier nanosystem based on iron oxide magnetic nanoparticles and chitosan. *Coll. Surfaces B Biointerfaces* **2019**, *174*, 224–231. [CrossRef]
143. Arias, L.S.; Brown, J.L.; Butcher, M.C.; Delaney, C.; Monteiro, D.R.; Ramage, G. A nanocarrier system that potentiates the effect of miconazole within different interkingdom biofilms. *J. Oral Microbiol.* **2020**, *12*, 1771071. [CrossRef]
144. Arias, L.S.; Pessan, J.P.; de Souza Neto, F.N.; Lima, B.H.R.; de Camargo, E.R.; Ramage, G.; Delbem, A.C.B.; Monteiro, D.R. Novel nanocarrier of miconazole based on chitosan-coated iron oxide nanoparticles as a nanotherapy to fight *Candida* biofilms. *Coll. Surf. B Biointerfaces* **2020**, *192*, 111080. [CrossRef] [PubMed]
145. Kanugala, S.; Jinka, S.; Puvvada, N.; Banerjee, R.; Kumar, C.G. Phenazine-1-carboxamide functionalized mesoporous silica nanoparticles as antimicrobial coatings on silicone urethral catheters. *Sci. Rep.* **2019**, *9*, 6198. [CrossRef] [PubMed]
146. Romero-Urbina, D.G.; Lara, H.H.; Velázquez-Salazar, J.J.; Arellano-Jiménez, M.J.; Larios, E.; Srinivasan, A.; Lopez-Ribot, J.L.; Yacaman, M.J. Ultrastructural changes in methicillin-resistant *Staphylococcus aureus* induced by positively charged silver nanoparticles. *Beilstein. J. Nanotechnol.* **2015**, *6*, 2396–2405. [CrossRef] [PubMed]
147. Lara, H.H.; Lopez-Ribot, J.L. Inhibition of mixed biofilms of *Candida albicans* and methicillin-resistant *Staphylococcus aureus* by positively charged silver nanoparticles and functionalized silicone elastomers. *Pathogens* **2020**, *9*, 784. [CrossRef] [PubMed]
148. Hůlková, M.; Soukupová, J.; Carlson, R.P.; Maršálek, B. Interspecies interactions can enhance *Pseudomonas aeruginosa* tolerance to surfaces functionalized with silver nanoparticles. *Coll. Surf B Biointerfaces* **2020**, *192*, 111027. [CrossRef]
149. Lethongkam, S.; Daengngam, C.; Tansakul, C.; Siri, R.; Chumpraman, A.; Phengmak, M.; Voravuthikunchai, S.P. Prolonged inhibitory effects against planktonic growth, adherence, and biofilm formation of pathogens causing ventilator-associated pneumonia using a novel polyamide/silver nanoparticle composite-coated endotracheal tube. *Biofouling* **2020**, *36*, 292–307. [CrossRef] [PubMed]
150. Dovigo, L.N.; Pavarina, A.C.; Ribeiro, A.P.; Brunetti, I.L.; Costa, C.A.; Jacomassi, D.P.; Bagnato, V.S.; Kurachi, C. Investigation of the photodynamic effects of curcumin against *Candida albicans*. *Photochem. Photobiol.* **2011**, *87*, 895–903. [CrossRef]
151. Hamblin, M.R. Antimicrobial photodynamic inactivation: A bright new technique to kill resistant microbes. *Curr. Opin. Microbiol.* **2016**, *33*, 67–73. [CrossRef] [PubMed]
152. Salton, M.R. The adsorption of cetyltrimethylammonium bromide by bacteria, its action in releasing cellular constituents and its bactericidal effects. *J. Gen. Microbiol.* **1951**, *5*, 391–404. [CrossRef] [PubMed]
153. Pinto, R.M.; Soares, F.A.; Reis, S.; Nunes, C.; Van Dijck, P. Innovative strategies toward the disassembly of the EPS matrix in bacterial biofilms. *Front. Microbiol.* **2020**, *11*, 952. [CrossRef]
154. Ma, S.; Preims, M.; Piumi, F.; Kappel, L.; Seiboth, B.; Record, E.; Kracher, D.; Ludwig, R. Molecular and catalytic properties of fungal extracellular cellobiose dehydrogenase produced in prokaryotic and eukaryotic expression systems. *Microb. Cell Factories* **2017**, *16*, 37. [CrossRef] [PubMed]
155. Linley, E.; Denyer, S.P.; McDonnell, G.; Simons, C.; Maillard, J.Y. Use of hydrogen peroxide as a biocide: New consideration of its mechanisms of biocidal action. *J. Antimicrobial Chemother.* **2012**, *67*, 1589–1596. [CrossRef]
156. Tetz, G.V.; Artemenko, N.K.; Tetz, V.V. Effect of DNase and antibiotics on biofilm characteristics. *Antimicrob. Agents Chemother.* **2009**, *53*, 1204–1209. [CrossRef]
157. Rodrigues, G.R.; López-Abarrategui, C.; de la Serna Gómez, I.; Dias, S.C.; Otero-González, A.J.; Franco, O.L. Antimicrobial magnetic nanoparticles based-therapies for controlling infectious diseases. *Int. J. Pharm.* **2019**, *555*, 356–367. [CrossRef]
158. Nenoff, P.; Koch, D.; Krüger, C.; Drechsel, C.; Mayser, P. New insights on the antibacterial efficacy of miconazole in vitro. *Mycoses* **2017**, *60*, 552–557. [CrossRef]

159. Hoarau, G.; Mukherjee, P.K.; Gower-Rousseau, C.; Hager, C.; Chandra, J.; Retuerto, M.A.; Neut, C.; Vermeire, S.; Clemente, J.; Colombel, J.F.; et al. Bacteriome and mycobiome interactions underscore microbial dysbiosis in familial Crohn's disease. *mBio* **2016**, *7*, e01250-16. [CrossRef]
160. Hager, C.L.; Ghannoum, M.A. The mycobiome: Role in health and disease, and as a potential probiotic target in gastrointestinal disease. *Dig. Liver. Dis.* **2017**, *49*, 1171–1176. [CrossRef]
161. Steenackers, H.P.; Ermolat'ev, D.S.; Savaliya, B.; De Weerdt, A.; De Coster, D.; Shah, A.; Van der Eycken, E.V.; De Vos, D.E.; Vanderleyden, J.; De Keersmaecker, S.C.J. Structure-activity relationship of 4(5)-aryl-2-amino-1H-imidazoles, N1-substituted 2-aminoimidazoles and imidazo[1,2-a]pyrimidinium salts as inhibitors of biofilm formation by *Salmonella typhimurium* and *Pseudomonas aeruginosa*. *J. Med. Chem.* **2011**, *54*, 472–484. [CrossRef] [PubMed]
162. Peeters, E.; Hooyberghs, G.; Robijns, S.; Waldrant, K.; De Weerdt, A.; Delattin, N.; Liebens, V.; Kucharikova, S.; Tournu, H.; Verstraeten, N.; et al. Modulation of the substitution pattern of 5-aryl-2-aminoimidazoles allows fine-tuning of their antibiofilm activity spectrum and toxicity. *Antimicrob. Agents Chemother.* **2016**, *60*, 6483–6497. [CrossRef] [PubMed]
163. Yassin, S.A.; German, M.J.; Rolland, S.L.; Rickard, A.H.; Jakubovics, N.S. Inhibition of multispecies biofilms by a fluoride-releasing dental prosthesis copolymer. *J. Dent.* **2016**, *48*, 62–70. [CrossRef]
164. Pires, D.P.; Melo, L.; Vilas Boas, D.; Sillankorva, S.; Azeredo, J. Phage therapy as an alternative or complementary strategy to prevent and control biofilm-related infections. *Curr. Opin. Microbiol.* **2017**, *39*, 48–56. [CrossRef]
165. Tkhilaishvili, T.; Wang, L.; Perka, C.; Trampuz, A.; Gonzalez Moreno, M. Using bacteriophages as a trojan horse to the killing of dual-species biofilm formed by *Pseudomonas aeruginosa* and methicillin resistant *Staphylococcus aureus*. *Front. Microbiol.* **2020**, *11*, 695. [CrossRef] [PubMed]
166. Akturk, E.; Oliveira, H.; Santos, S.B.; Costa, S.; Kuyumcu, S.; Melo, L.D.R.; Azeredo, J. Synergistic Action of Phage and Antibiotics: Parameters to Enhance the Killing Efficacy Against Mono and Dual-Species Biofilms. *Antibiotics* **2019**, *8*, 103. [CrossRef] [PubMed]
167. Gorski, A.; Bollyky, P.L.; Przybylski, M.; Borysowski, J.; Miedzybrodzki, R.; Jonczyk-Matysiak, E.; Weber-Dabrowska, B. Perspectives of Phage Therapy in Non-bacterial Infections. *Front. Microbiol.* **2018**, *9*, 3306. [CrossRef]
168. Penner, J.C.; Ferreira, J.A.G.; Secor, P.R.; Sweere, J.M.; Birukova, M.K.; Joubert, L.M.; Haagensen, J.A.J.; Garcia, O.; Malkovskiy, A.V.; Kaber, G.; et al. Pf4 bacteriophage produced by *Pseudomonas aeruginosa* inhibits *Aspergillus fumigatus* metabolism via iron sequestration. *Microbiology* **2016**, *162*, 1583–1594. [CrossRef] [PubMed]
169. Nazik, H.; Joubert, L.M.; Secor, P.R.; Sweere, J.M.; Bollyky, P.L.; Sass, G.; Cegelski, L.; Stevens, D.A. *Pseudomonas* phage inhibition of *Candida albicans*. *Microbiology* **2017**, *163*, 1568–1577. [CrossRef]
170. Gajdacs, M. The Concept of an Ideal Antibiotic: Implications for Drug Design. *Molecules* **2019**, *24*, 892. [CrossRef]